National Research FLAGSHIPS Wealth from Oceans

CSIRO

WAMSI NODE 1 PROJECT 1

FINAL REPORT

Southwest Australian Coastal Biogeochemistry

ANNEXURE A – RESEARCH CHAPTERS

Editor: John K. Keesing
Chapter senior authors: Peter D Craig, Ming Feng, Jim Greenwood, Martin Lourey, Peter A. Thompson, John K. Keesing, Graham Symonds and Mat A Vanderklift
30 June 2011

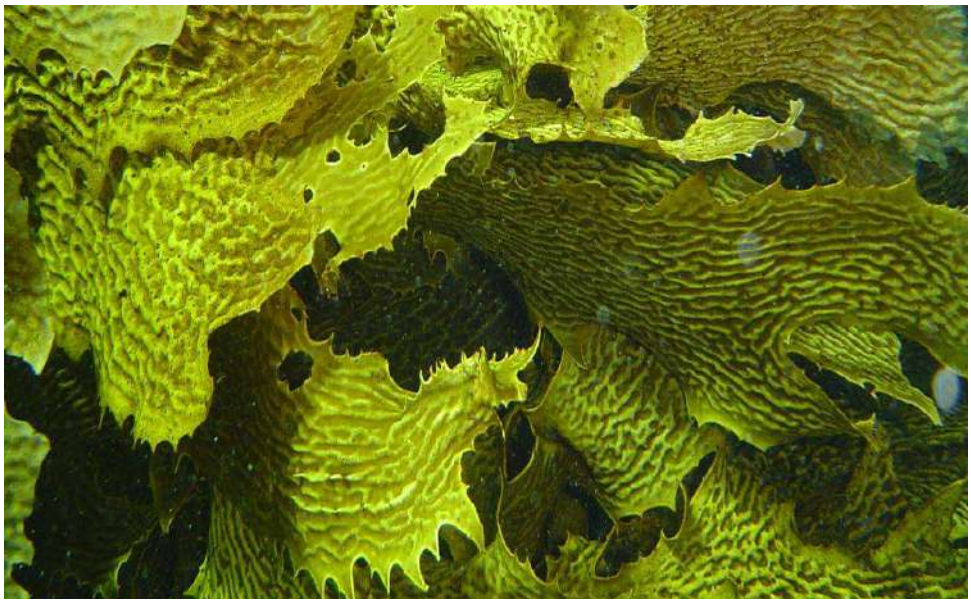

This is an unpublished report for the
Western Australian Marine Science Institution [WAMSI]
It should not be cited without permission of the authors.
Enquiries should be addressed to:

Dr John Keesing, CSIRO Private Bag 5, Wembley, Australia 6913

john.keesing@csiro.au

Important Disclaimer

Acknowledgements

The editor and authors would like to thank WAMSI and its staff for financial support for, and assistance on, this project, the vessels and crews of the RV Southern Surveyor, RV Linnaeus and RV BF Ryan especially Stelios Kondylas and Ryan Crossing, Leonie Wyld, Toni Cannard, Lucy Kay and Mizue Iijima for helping prepare the report and the following people who assisted with field and laboratory work and sample and data analyses: Phil Adams, Pru Bonham, Geordie Clapin, Leslie Clementson, Kylie Cook, Gabrielle Cummins, Claudio Del Deo, Quinton Dell, Peter Dunn, Blake Edmunds, Christine Hanson, David Holliday, Peter Hughes, Neale Johnston, Hiski Kippo, Andrew Limbourn, Ian McLeod, Hector Lozano-Montes, Natalie Millar, Stephane Pesant, Richard Pillans, Janelle Ritchie, Ellen Smith, Luke Twomey, Ted Wassenberg, Oliver Wells and Sharon Yeo. In addition we thank our colleagues for partnering with us in this exploration of Western Australian marine science and their roles in supervising WAMSI Node 1 students, especially: Lynnath Beckley, Gary Kendrick, Di Walker, Alan Pearce, Nick Caputi, Tony Koslow, Anya Waite, Chari Pattiaratchi, Mike van Keulen, Thomas Wernberg, Carolyn Oldham, Euan Harvey, Glenn Hyndes and Paul Lavery.

Contents

1. DOWNSCALED HYDRODYNAMIC MODELS

Peter Craig, Ming Feng, Graham Symonds, Liejun Zhong, Nick Mortimer and Dirk Slawinski
CSIRO Marine and Atmospheric Research

Objective 1: Downscaled hydrodynamic models to explore influences on benthic habitat, and the cross-shore and longshore exchange of water, nutrients and particles between the lagoon and shelf regions.

1.1 Introduction

WAMSI Node 1 has been focused on the Western Australian coastline from North West Cape to Cape Leeuwin, on waters from the upper continental slope into the shore. This is an open coastline exposed to the influence of the Indian and Southern Oceans and also, via the Indonesian Throughflow, to the Pacific. Any description of the biophysical dynamics on this Western Australian shelf must account for the influence of dynamics occurring at ocean-basin scales.

The present chapter describes the physical oceanography at successively smaller scales, from that of the eastern Indian Ocean, to the shelf from NW Cape to Cape Leeuwin, down to the Marmion lagoon. At the largest scale, the primary tool is the global Ocean Forecasting Australia Model (OFAM), that has coarse (>2 degree) resolution distant from Australia, but has 0.1 degree (~10 km) resolution in the Australasian region. Being global, OFAM simulates the longshore pressure gradient, largely due to the Indonesian Throughflow, that drives the Leeuwin Current southward along the shelf break of the WA coast. The model provides good qualitative representation of the Leeuwin Current and its associated eddies but, at 10 km resolution, tends to underestimate the current speeds on the shelf and cross-shore fluxes.

OFAM output has been corrected with observations (in a separate CSIRO project) and archived to provide nearly 2 decades of ocean conditions. As a prelude to later biological investigations, it is used to investigate the longshore connectivity of shelf waters, demonstrating that the shelf can be classified into several sections of alternating low and high retention. At this scale, open-ocean swells are important, with biological particles near the surface being driven north-east under their influence.

At the next level, the Rutgers Ocean Modelling System (ROMS) is nested inside OFAM, covering the southern west shelf, with resolution down to 2 km near the coast. ROMS produces similar patterns of circulation to OFAM, but the Leeuwin Current and inshore wind-driven currents are narrower and stronger. The ROMS model is used primarily to drive a model of primary productivity over the shelf (see Chapter 2). ROMS produces eddies that correspond well with those observed in sea-surface temperature images, and also shows instances of intermittent upwelling along the shelf break. Upwelling and eddy transport prove to be significant mechanisms for moving nutrients and phytoplankton on and off the shelf, respectively. As shown in chapter 2, surface waves, in addition to currents, again prove to be important to the biology across the shelf.

At the scale of the Marmion lagoon, surface waves breaking on the reefs drive currents in the lagoon. The present study incorporated a year-long measurement program to quantify the reef and lagoon circulation. At low wave heights, the lagoonal circulation is driven primarily by longshore winds. However, when the incoming waves are higher than about 1.5 m, they break on the reef, carrying water into the lagoon, and causing currents to the north and south out of the lagoon. Modelling of reef dynamics requires very high resolution, down to tens of metres, and a model that includes both waves and currents. Two model configurations have been used in the present study: ROMS together with the wave model SWAN, and XBeach, a littoral-zone model still under development at Delft University. XBeach accurately represents the lagoonal dynamics. In the following chapter, ROMS is used under lower wave conditions to investigate the nutrient distributions observed during the measurement program.

1.2 Eastern Indian Ocean Scale

1.2.1 Model verification

The shelf-scale circulation on the Western Australian coast is dominated by the Leeuwin Current that flows along the shelf-edge from the Northwest Cape around the southern capes. The Leeuwin Current is primarily a response to a north-south pressure gradient in the eastern Indian Ocean that is established mainly as a result of the flow of water from the Pacific to the Indian Ocean through the Indonesian Archipelago. As the Leeuwin Current flows southward, its volume increases, as it entrains water from the Indian Ocean. It is impossible to describe the oceanography of Australia's western shelf without accounting for the large scale ocean circulation patterns of the eastern Indian Ocean and the Indonesian Throughflow.

For WAMSI modelling, the primary source of large-scale information is the global ocean model, OFAM (Ocean Forecasting Australia Model), developed as part of the BLUElink partnership between CSIRO, the Bureau of Meteorology, and the Royal Australian Navy (Schiller *et al*., 2008). In particular, OFAM has been run, within the BLUElink project, to create a 1993-2008 archive of daily values of ocean properties including ocean currents, salinity and temperature in 3 dimensions, resolved at 10 km horizontally and 10 m vertically (in the upper ocean) in the Australian region. There are two versions of the archive: one is a free run, and the second utilises data assimilation, that is, continuous correction by satellite (including altimeter) and in-situ data (Oke *et al*., 2008). These runs are referred to as the "Spinup" and "BRAN" (for Bluelink ReANalysis), respectively.

A second source of global model data, referenced in this section for comparison with BRAN, is HYCOM, the Hybrid Coordinate Ocean Model, with a vertical coordinate that is isopycnal (i.e. following density surfaces) in the open, stratified ocean, but smoothly reverts to a terrain-following coordinate in shallow coastal regions, and to z-level coordinates in the mixed layer and/or unstratified seas (Bleck and Boudra 1981; Bleck and Benjamin 1993). The HYCOM hindcast system is configured for the global ocean with HYCOM 2.2 as the dynamical model. Computations are carried out on a Mercator grid between 78°S and 47°N (1/12° equatorial resolution). Daily output from the model was downloaded from (http://hycom.rsmas.miami.edu/hycom-model/overview.html).

The present section is devoted to a comparison of BRAN and HYCOM with existing data sets off the WA coast. Monthly climatology of horizontal currents from BRAN is consistent with observations in the southeast Indian Ocean region (Figure 1.1). The seasonal cycles of the Indonesian Throughflow, South Equatorial Current, and the Leeuwin Current are well reproduced by BRAN (Schiller *et al*., 2008). Similar climatology can be derived from HYCOM (not shown).

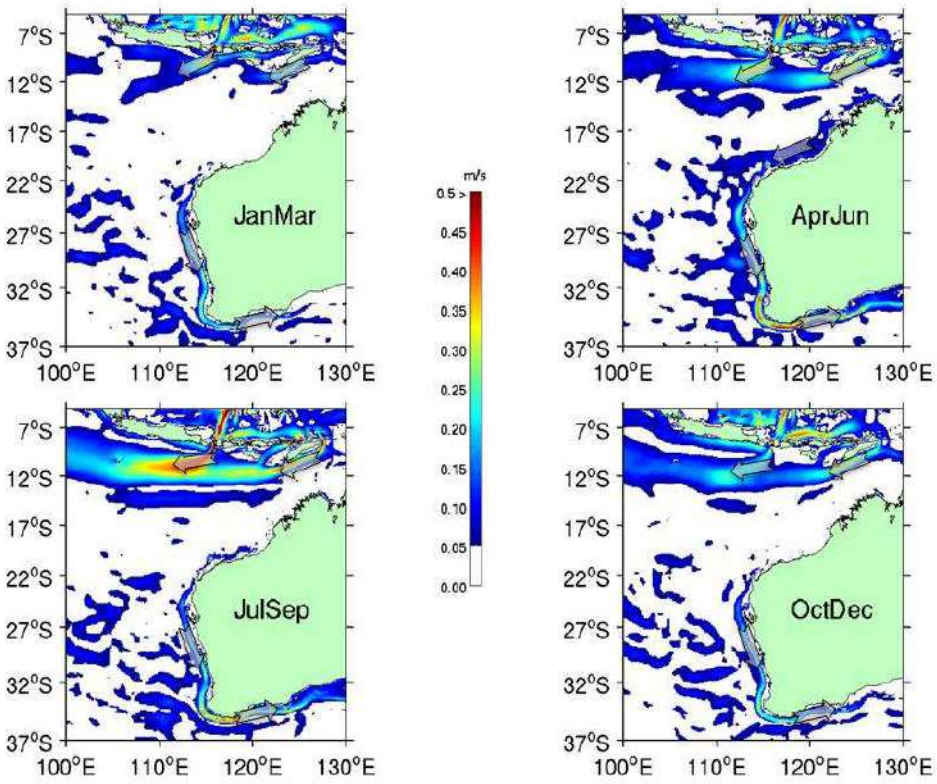

Figure 1.1. Seasonaly climatology of horizontal current speed (shading), averaged over the top 150 m, from BRAN. The broad arrows denote the direction of major ocean boundary currents. Visual comparison of BRAN and HYCOM near-surface ocean current velocities measured with ADCP from Southern Surveyor cruise SS200704 in May-June 2007 shows that there are agreements in broad-scale features of the Leeuwin Current and eddies off the west coast, although the model outputs tend to lack of some of the sub-mesoscale variability in the observation (Figure 1.2).

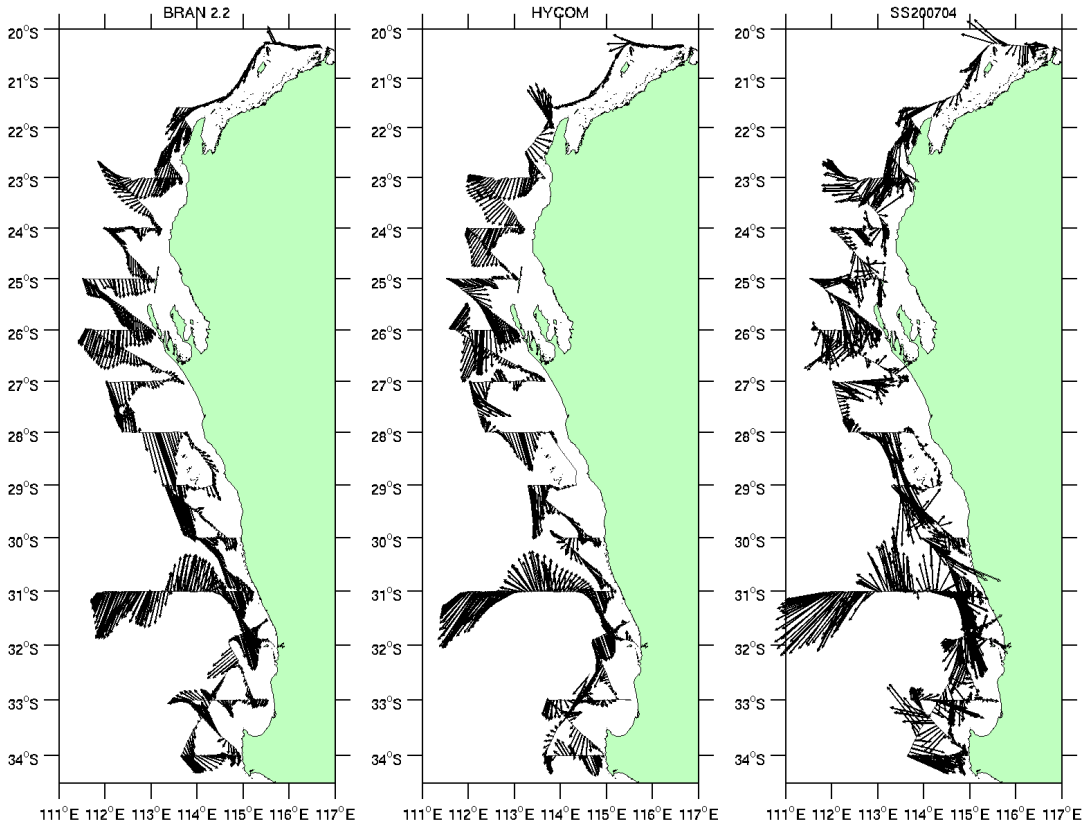

Figure 1.2. Comparison of horizonal current velocities derived from BRAN, HYCOM and SS200704 shipboard measurements at 95 metres depth.

The eastward and northward components of current velocity can be approximately regarded as cross-shelf and alongshore off the west coast. Figure 1.3 shows comparisons of the two components of the velocity fields from models and observations during the SS200704 cruise. As is also apparent in Figure 1.2, both BRAN and HYCOM clearly underestimate the cross-shelf velocities. This is quantified in the linear regression between the cruise data and the BRAN data (interpolated to the cruise data locations and times) (Figure 1.3). The linear correlations are generally between 0.6-0.7, and the slopes of the linear regressions are slightly lower.

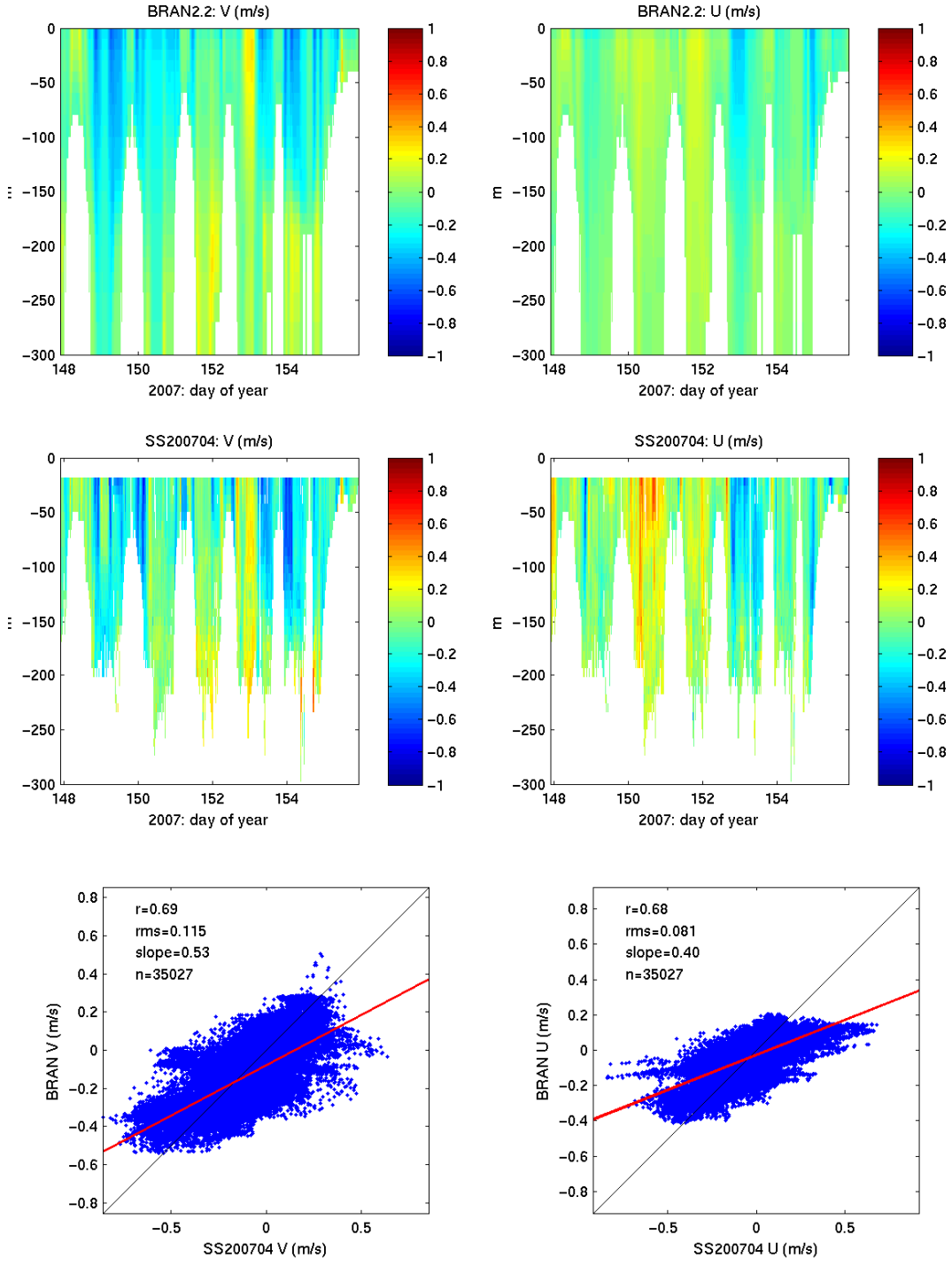
BRAN2.2: V (m/s)
BRAN2.2: U (m/s)
SS200704: V (m/s)
SS200704: U (m/s)
m
2007: day of year
r=0.69
rms=0.115
slope=0.53
n=35027
BRAN V (m/s)
SS200704 V (m/s)
r=0.68
rms=0.081
slope=0.40
n=35027
BRAN U (m/s)
SS200704 U (m/s)

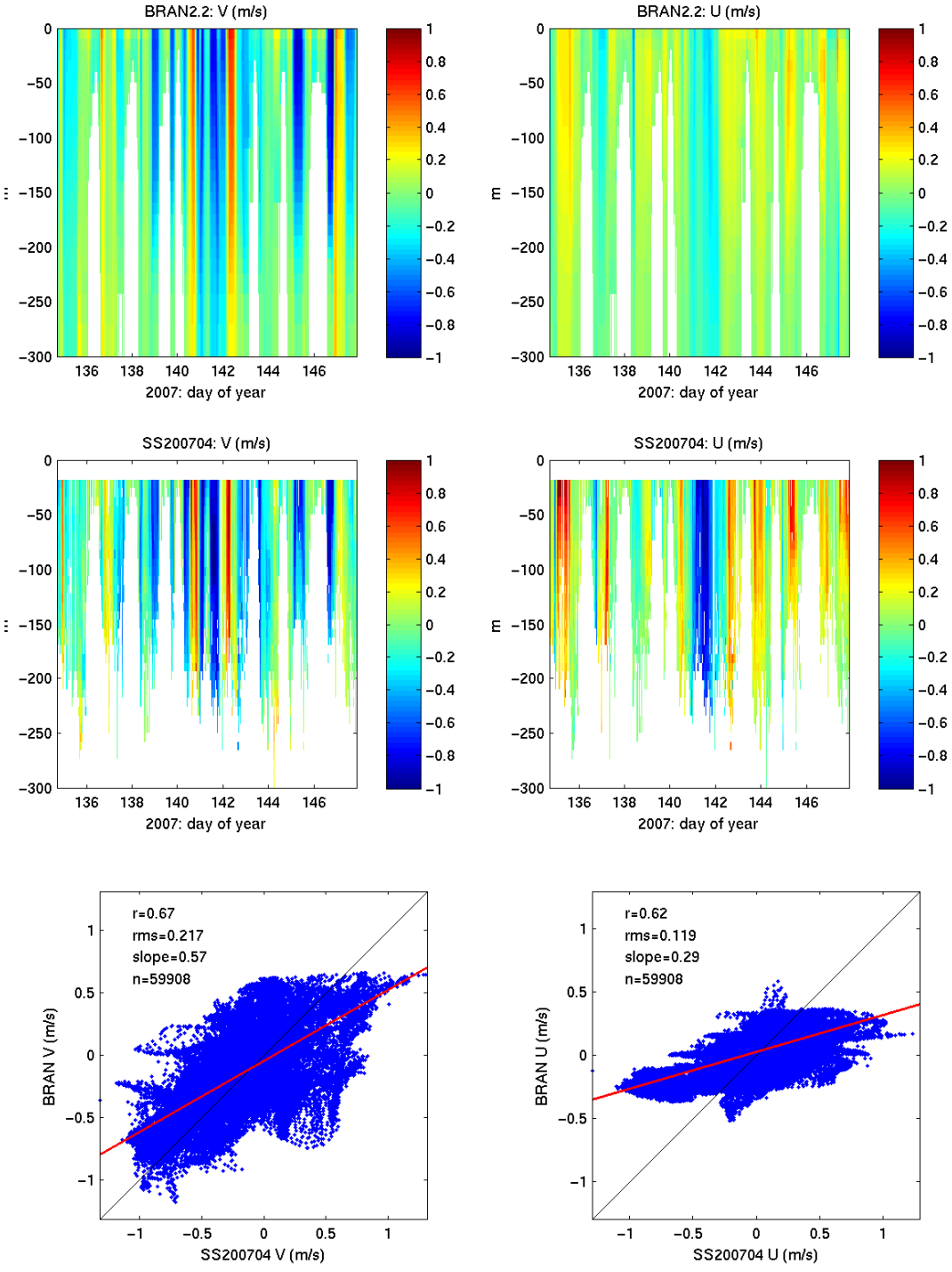

Figure 1.3. Cruise track comparison of eastward (U) and northward (V) velocity components and BRAN data.

The daily binned SS200704 CTD temperature data compare well with BRAN data with a linear correlation and slope of linear regression close to 1 (Figure 1.4). The CTD salinities are also well correlated with the BRAN data, except that BRAN tends to underestimate the high salinity

values and overestimate the low salinity values. The comparison with HYCOM is similar although the underestimation of high salinity values is greater than that of BRAN (Figure 1.5).

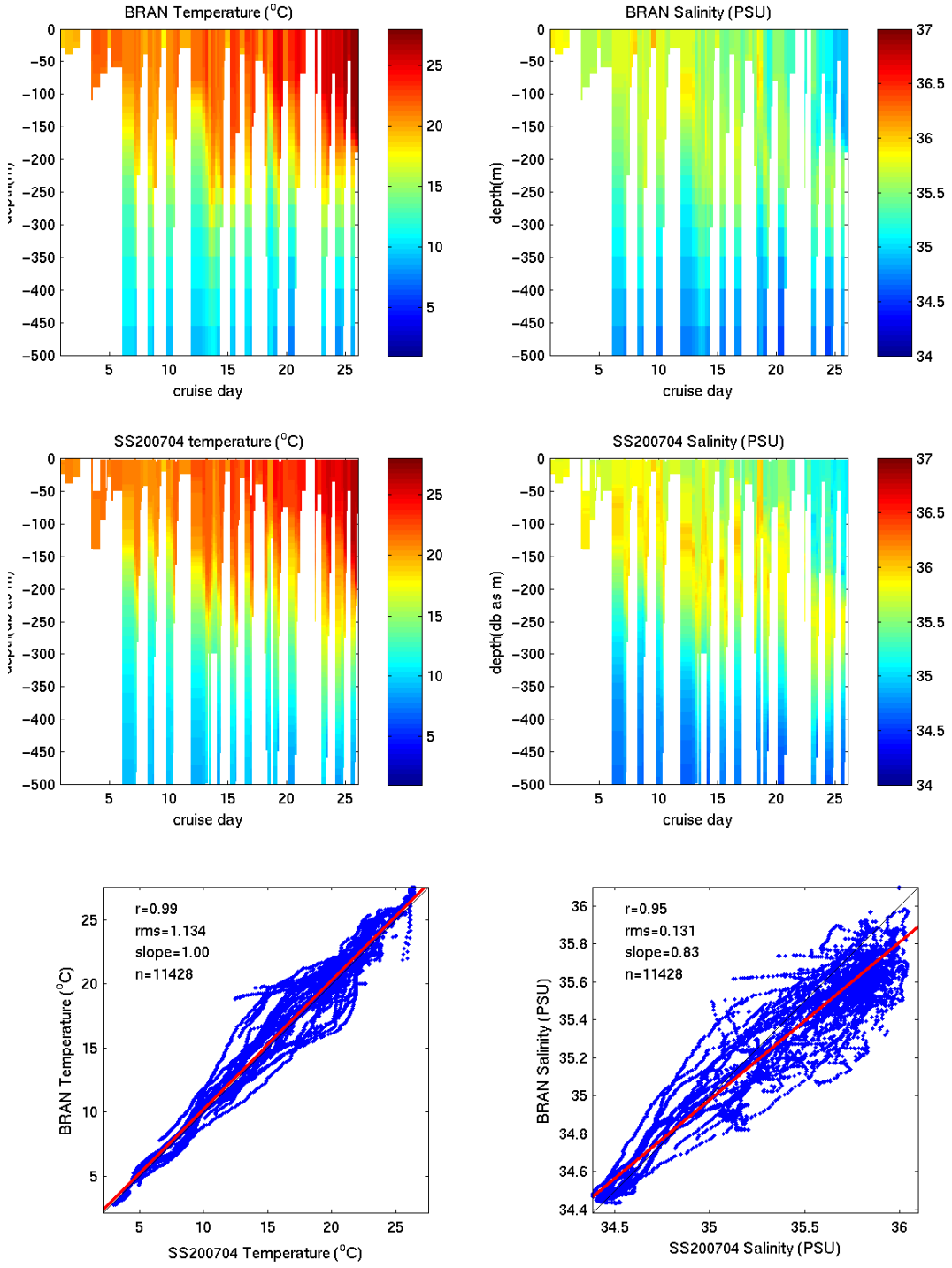

Figure 1.4. Comparison between daily binned SS200704 cruise CTD temperatures and salinities and BRAN data.

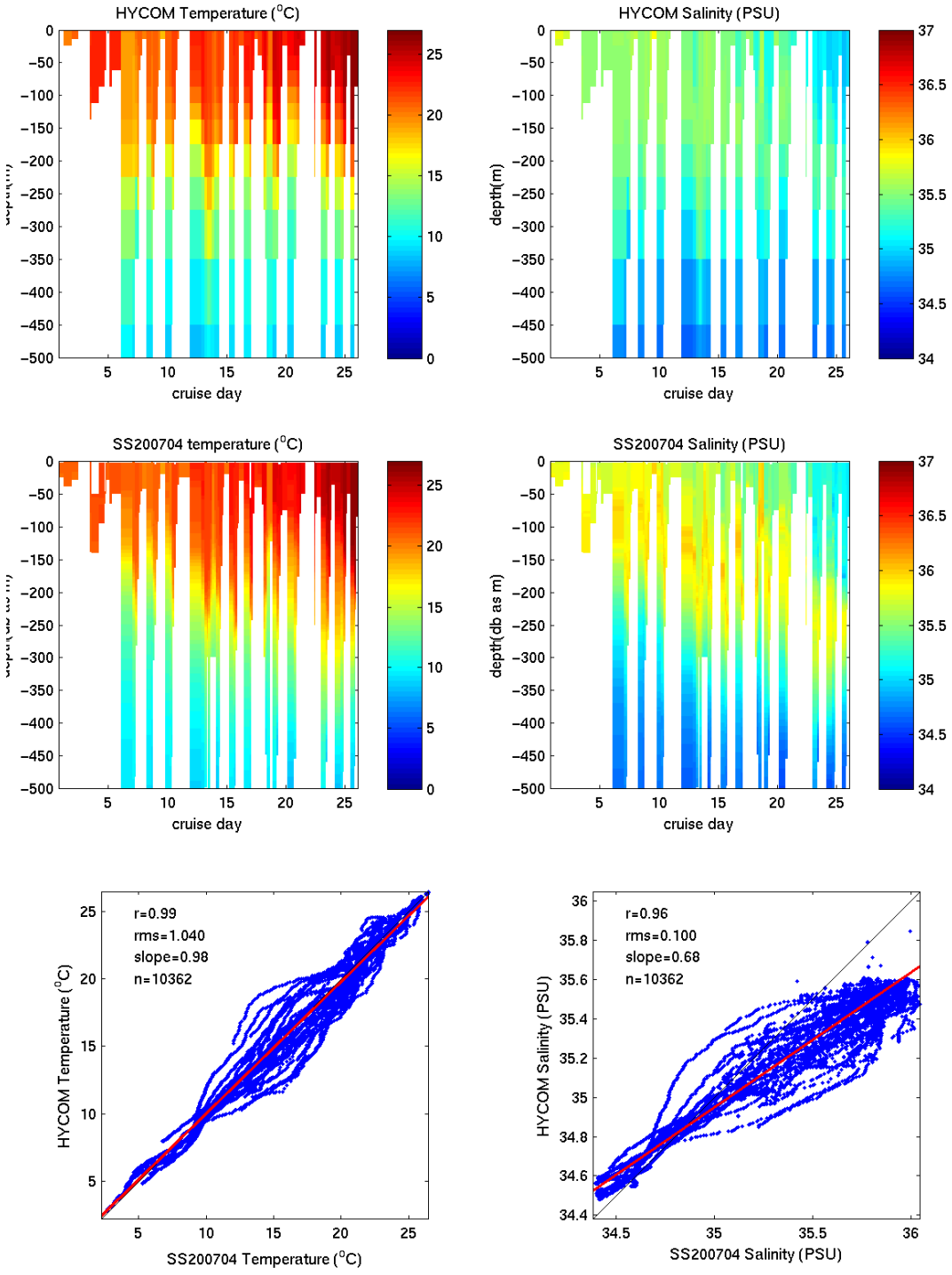

Figure 1.5. Daily binned cruise temperatures and salinities compared with HYCOM data.

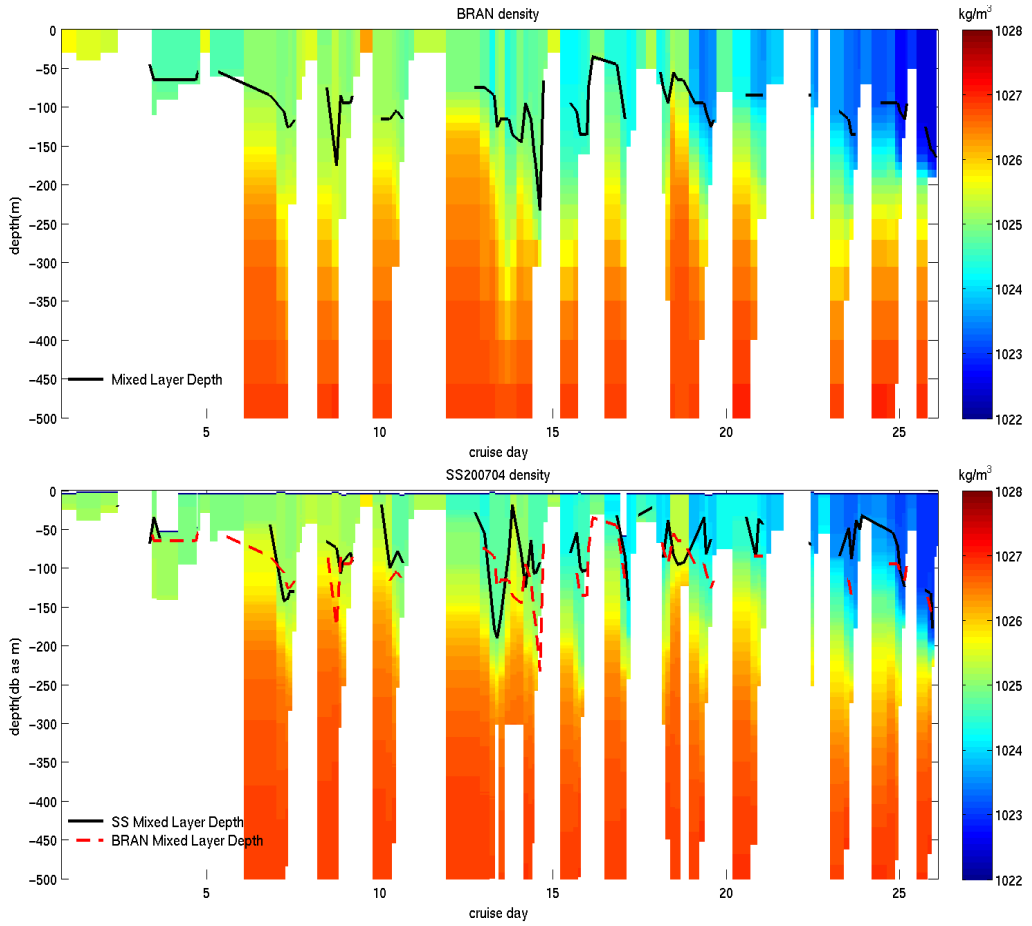

Figure 1.6. Comparison of mixed layer depth and potential density between the SS200704 cruise data and BRAN

For the temperature and salinity from both the cruise and BRAN data, mixed-layer depths were calculated as the depth at which the density is 0.125 kg/m^3 higher than that at the surface (10m). Figure 1.6 shows the calculated mixed-layer depths and potential density from individual CTD profiles. The comparison is visually reasonable, but the correlation between the mixed layer depths is only 0.34.

BRAN data off Ningaloo Reef are compared with current metre data collected as part of the WOCE program in 1995 and 1996. Figure 1.7 shows the locations of the moorings near Ningaloo Reef (Domingues *et al*., 1999). Only moorings m61 (1995/1996), m62 (1995/1996) and m63 (1995) had data that were suitable for comparison.

As with the cruise data, the comparison of the alongshore current is much better than that for the cross-shore. This confirms that BRAN underestimates cross-shore currents near the shelf break. Overall the correlation in the meridional flow is around 0.6 or better if extremes are removed (Figure 1.8, Figure 1.9 and Figure 1.10).

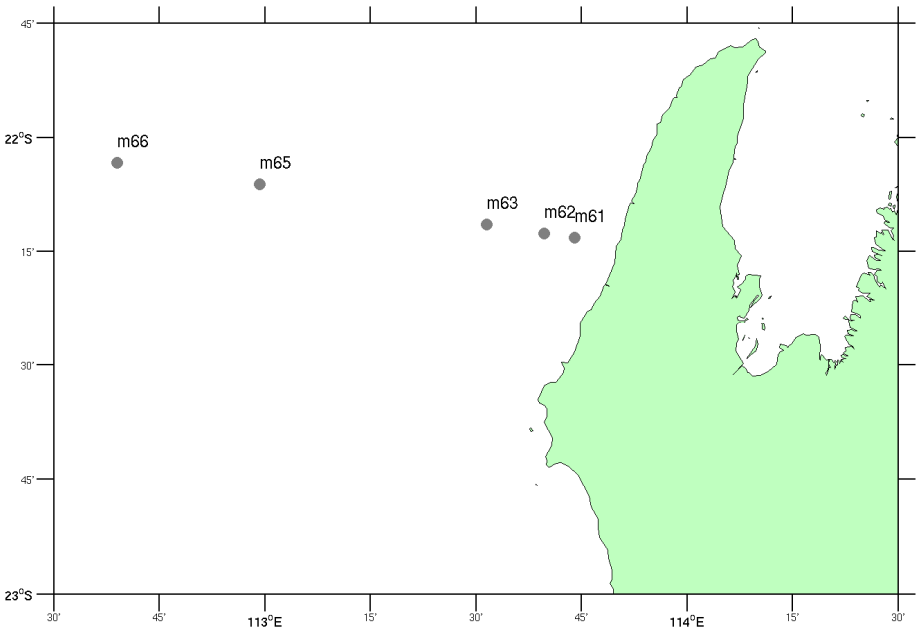

Figure 1.7. WOCE mooring locations.

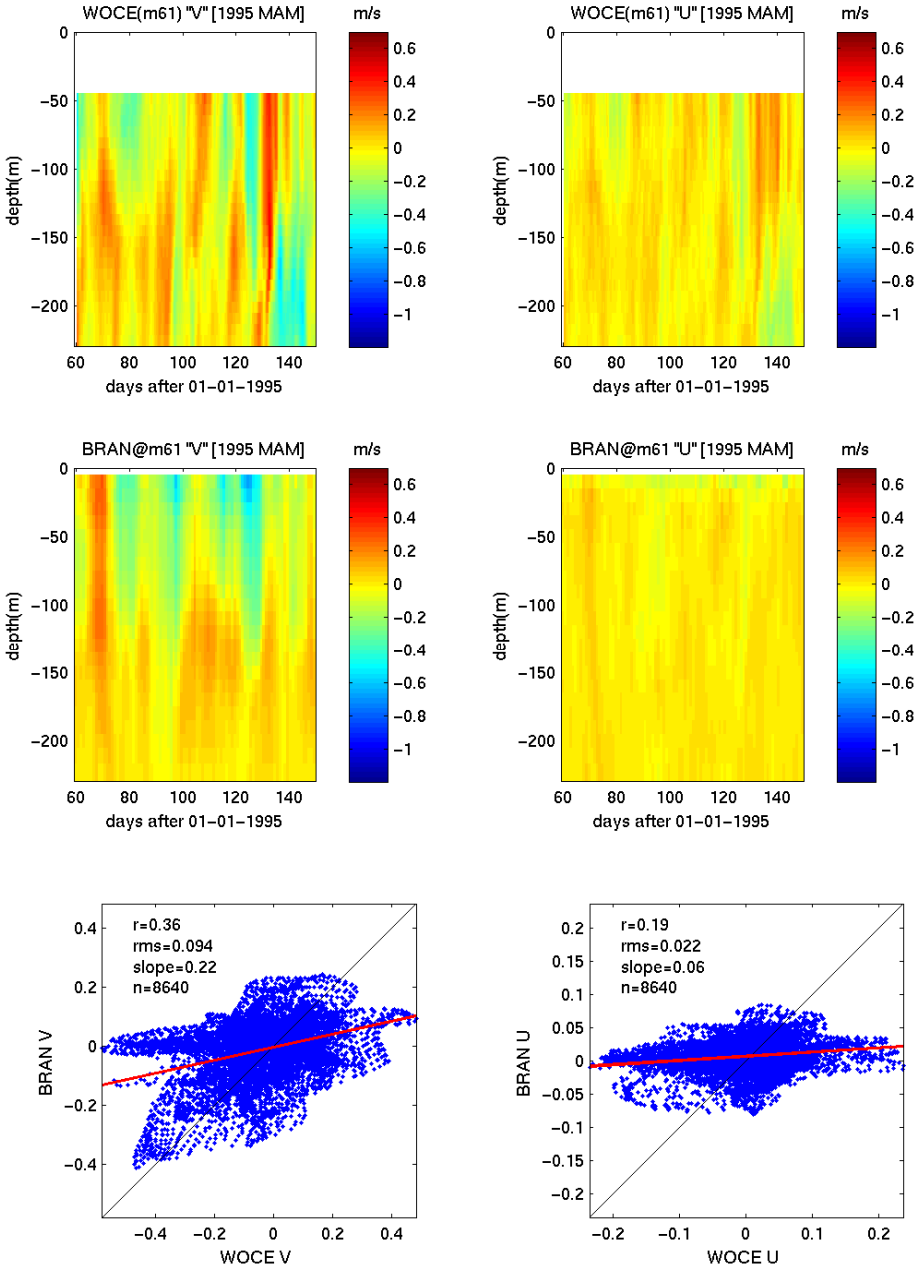
WOCE(m61) "V" [1995 MAM]
m/s
depth(m)
days after 01−01−1995
WOCE(m61) "U" [1995 MAM]
BRAN@m61 "V" [1995 MAM]
BRAN@m61 "U" [1995 MAM]
r=0.36
rms=0.094
slope=0.22
n=8640
BRAN V
WOCE V
r=0.19
rms=0.022
slope=0.06
n=8640
BRAN U
WOCE U

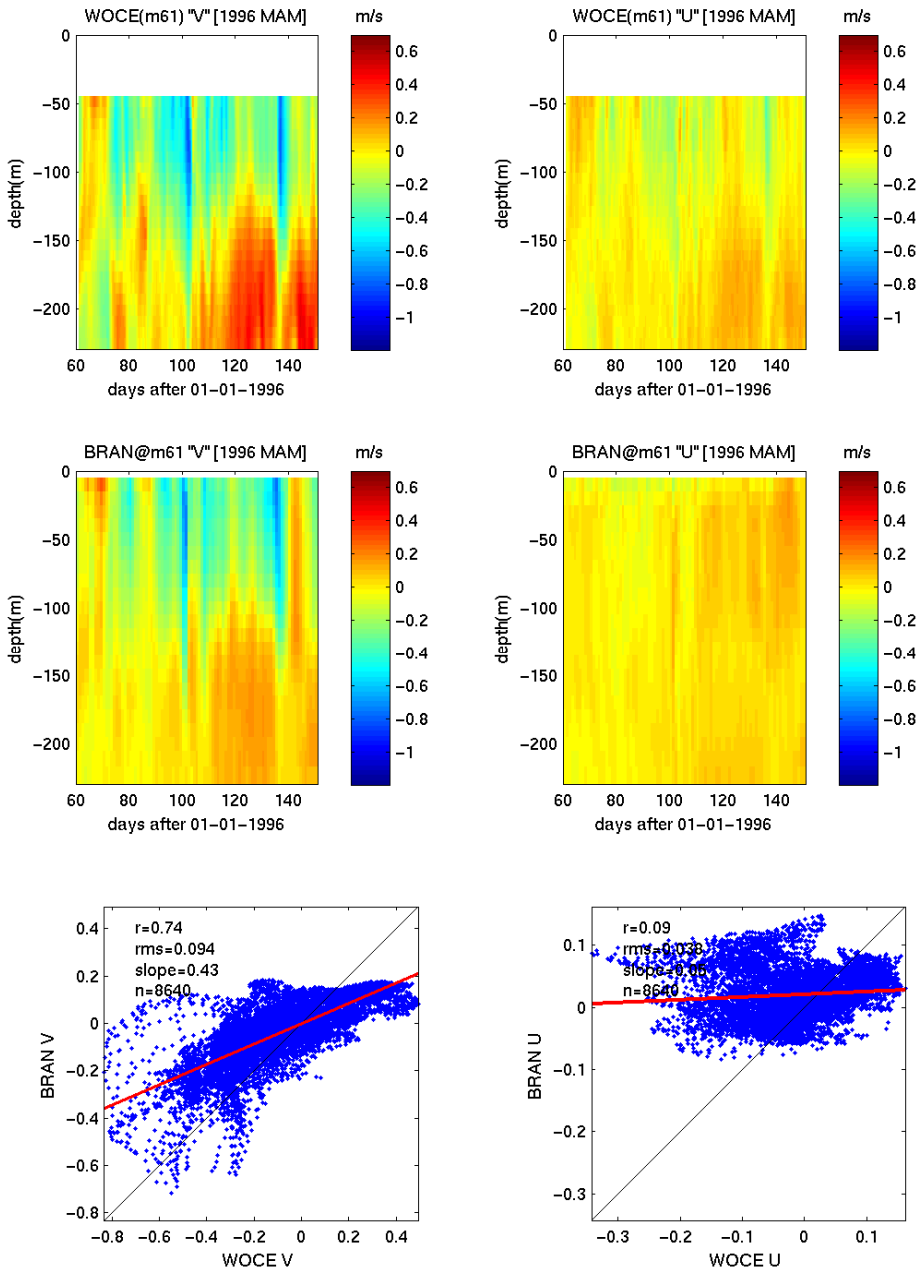

Figure 1.8. Comparison of northward (V) and eastward (U) components of velocity at the WOCE mooring m61 with BRAN data for March to May in 1995 (upper panel) and 1996 (lower panel).

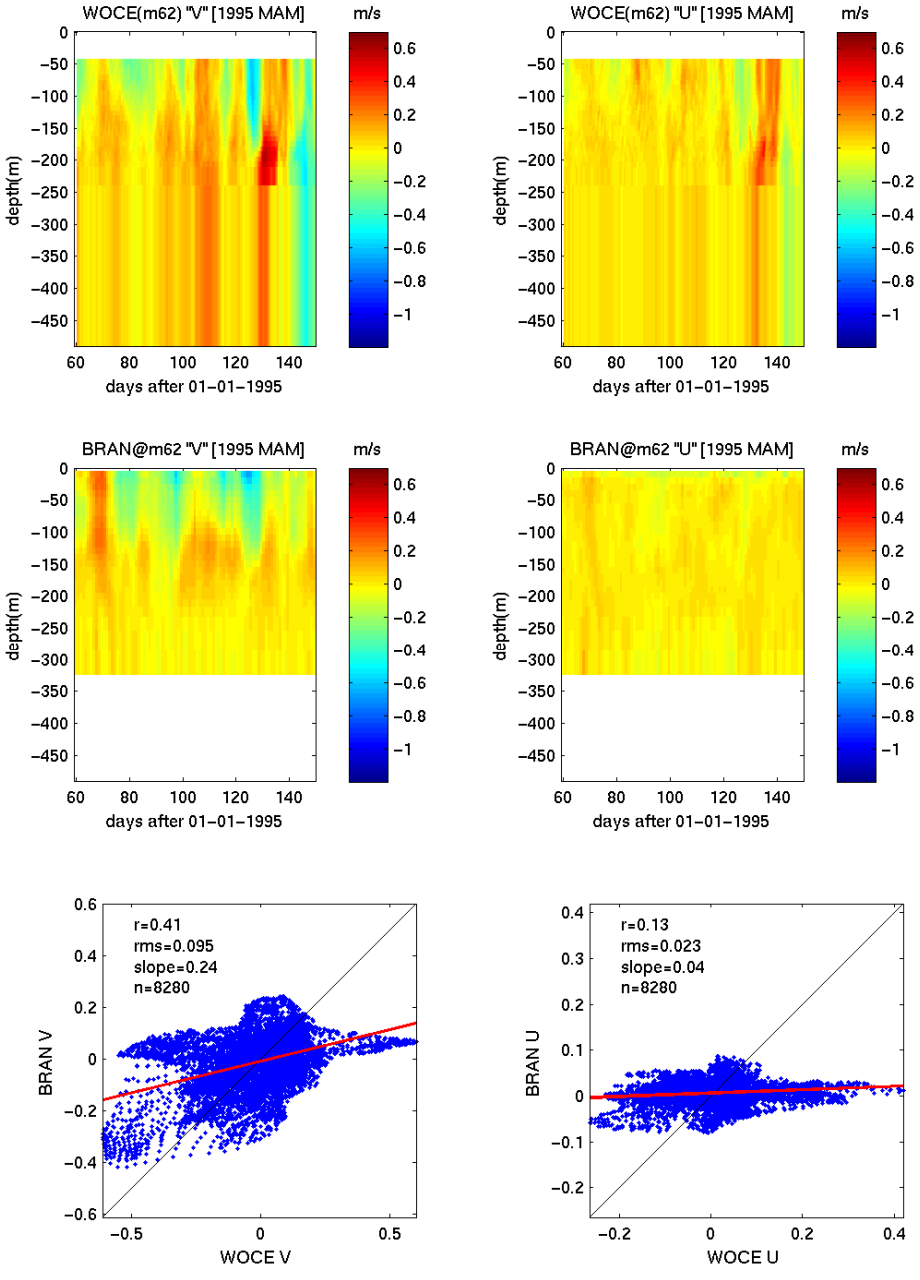
WOCE(m62) "V" [1995 MAM]
m/s
depth(m)
days after 01−01−1995
WOCE(m62) "U" [1995 MAM]
m/s
depth(m)
days after 01−01−1995
BRAN@m62 "V" [1995 MAM]
m/s
depth(m)
days after 01−01−1995
BRAN@m62 "U" [1995 MAM]
m/s
depth(m)
days after 01−01−1995
r=0.41
rms=0.095
slope=0.24
n=8280
BRAN V
WOCE V
r=0.13
rms=0.023
slope=0.04
n=8280
BRAN U
WOCE U

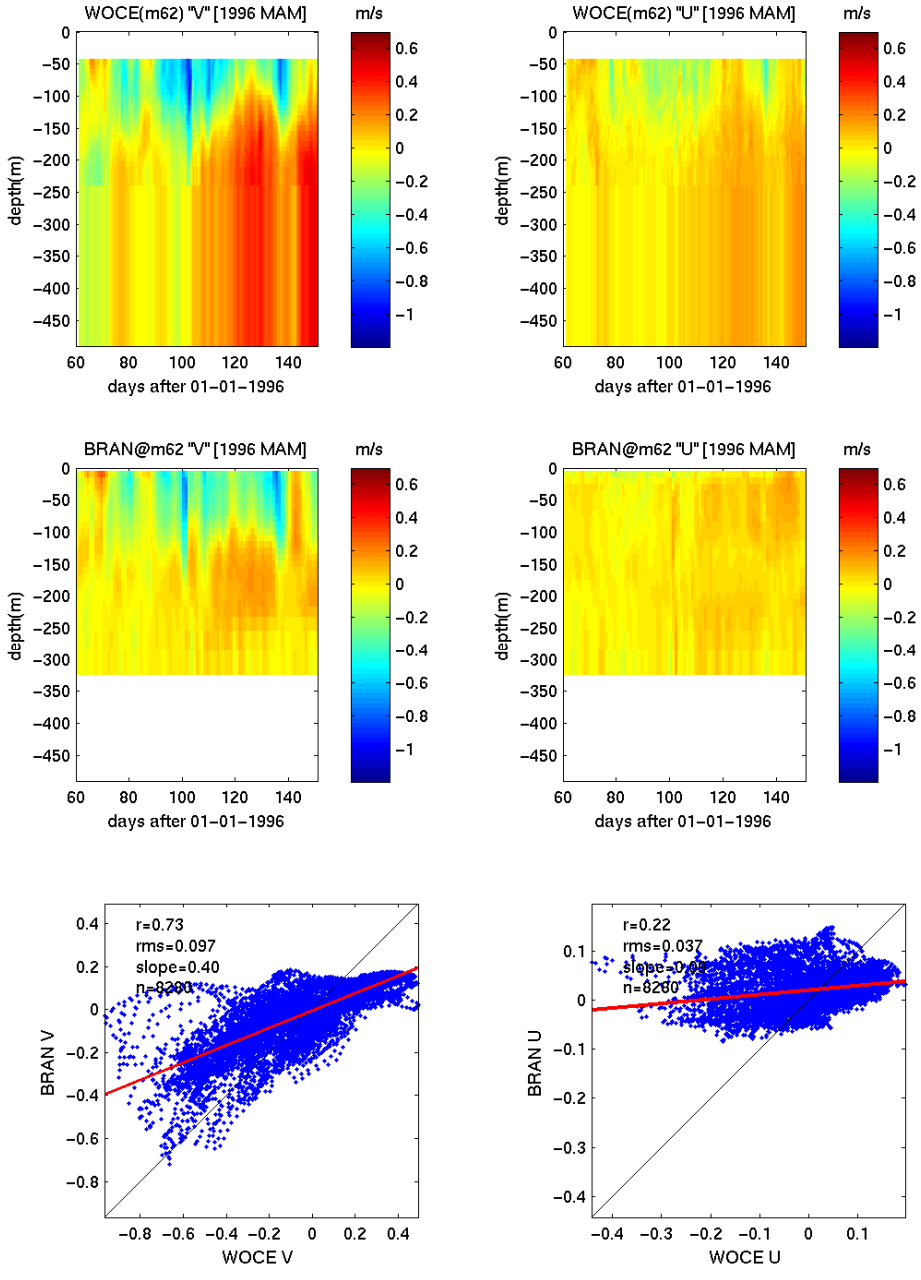

Figure 1.9. Comparison of northward (V) and eastward (U) components of velocity at the WOCE mooring m62 with BRAN data for March to May in 1995 (upper panel) and 1996 (lower panel).

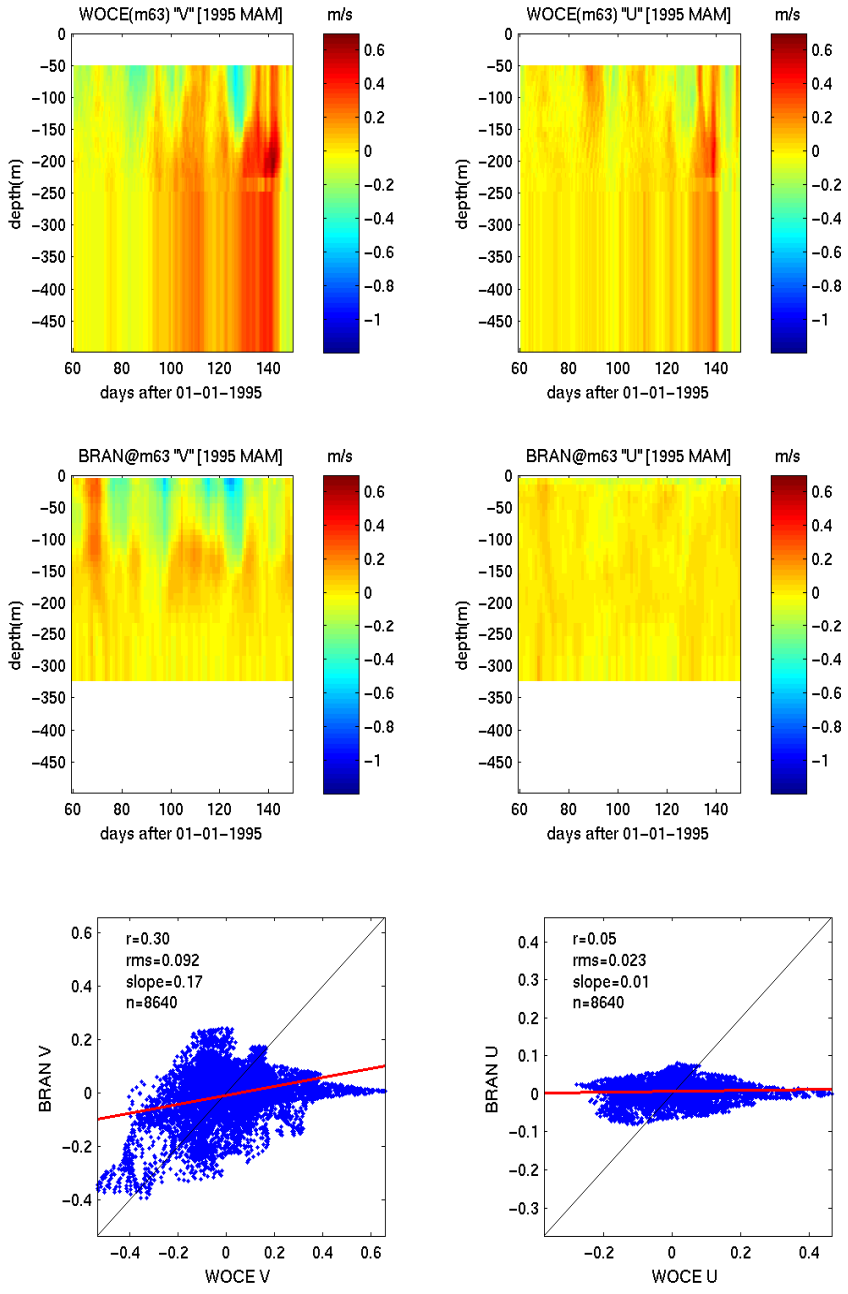

Figure 1.10. Comparison of northward (V) and eastward (U) components of velocity at the WOCE mooring m63 with BRAN data for March to May in 1995.

The SRFME current measurements off Two Rocks in 2004-2005 are used to validate the output from BRAN simulates the current system along the lower west Western Australian continental shelf (Pearce *et al.*, 2009). Full-column ADCP current meters were deployed for a year (with gaps) at SRFME sites A (20m) and C (100m), while a single-point current meter was moored at mid-depth at Site B for part of 2005 (Fandry *et al.*, 2006). Temperature was also measured at fixed depths at all 3 sites for varying periods. The original current records were at 15-minute intervals and Fandry *et al*. (2006) derived hourly current components using 5-point moving

averages. Because the temporal resolution of the BRAN model is daily in 10 m depth layers, daily vector-averaged currents have been derived from the ADCP measurements in 10 m depth bins for this analysis and monthly current statistics have been calculated. Only the surface layer currents and temperatures at sites A and C are discussed.

At the shallow inshore site A, the BRAN daily alongshore components closely matched the measured currents in the surface layer (Figure 1.11**,** upper). Both the average current velocity and the daily variability were very similar, with a correlation coefficient of 0.61 over the year-long period. Agreement was not as good for the cross-shelf flow (Figure 1.11**,** lower) where the observed currents were much lower than the modelled values (especially in the first half of the record); the correlation coefficient was only 0.21. The isolated southward/offshore "spike" in the measured currents (>50 cm/s) in August 2004 was not reproduced by the model. For the deeper layer (not shown here), the alongshore correlation between the model and the observations was 0.68, while the cross-shelf correlation of 0.30 was also higher than that near the surface.

For the 3 successful deployment periods at site C, the BRAN near-surface alongshore currents were generally weaker than the observed flow (Figure 1.12 upper), particularly during the 2nd deployment in summer 2005, although the few-day variability matched reasonably well. The correlation coefficient was 0.56 (over 107 days). Again, the cross-shelf agreement was poorer (Figure 1.12 lower) with a correlation of -0.22. Down the water column, the alongshore correlations decreased marginally to 0.49, but the cross-shelf correlations improved substantially to +0.44 near the seabed.

The modelled 10 m temperatures at site A agreed moderately well with the measurements during the summer period, but were too high (by 2 to 3 °C) in winter (Figure 1.13 upper). Nevertheless, because of the strong seasonal signal, the correlation was overall quite high at 0.84. As would be expected in such shallow water, the correlation at 20 m was similar at 0.85.

Further offshore at site C, the comparison between the modelled and observed temperatures was better than at site A, with a correlation of 0.91 near the surface (Figure 1.13 lower), but dropped to 0.74 in the deepest layer.

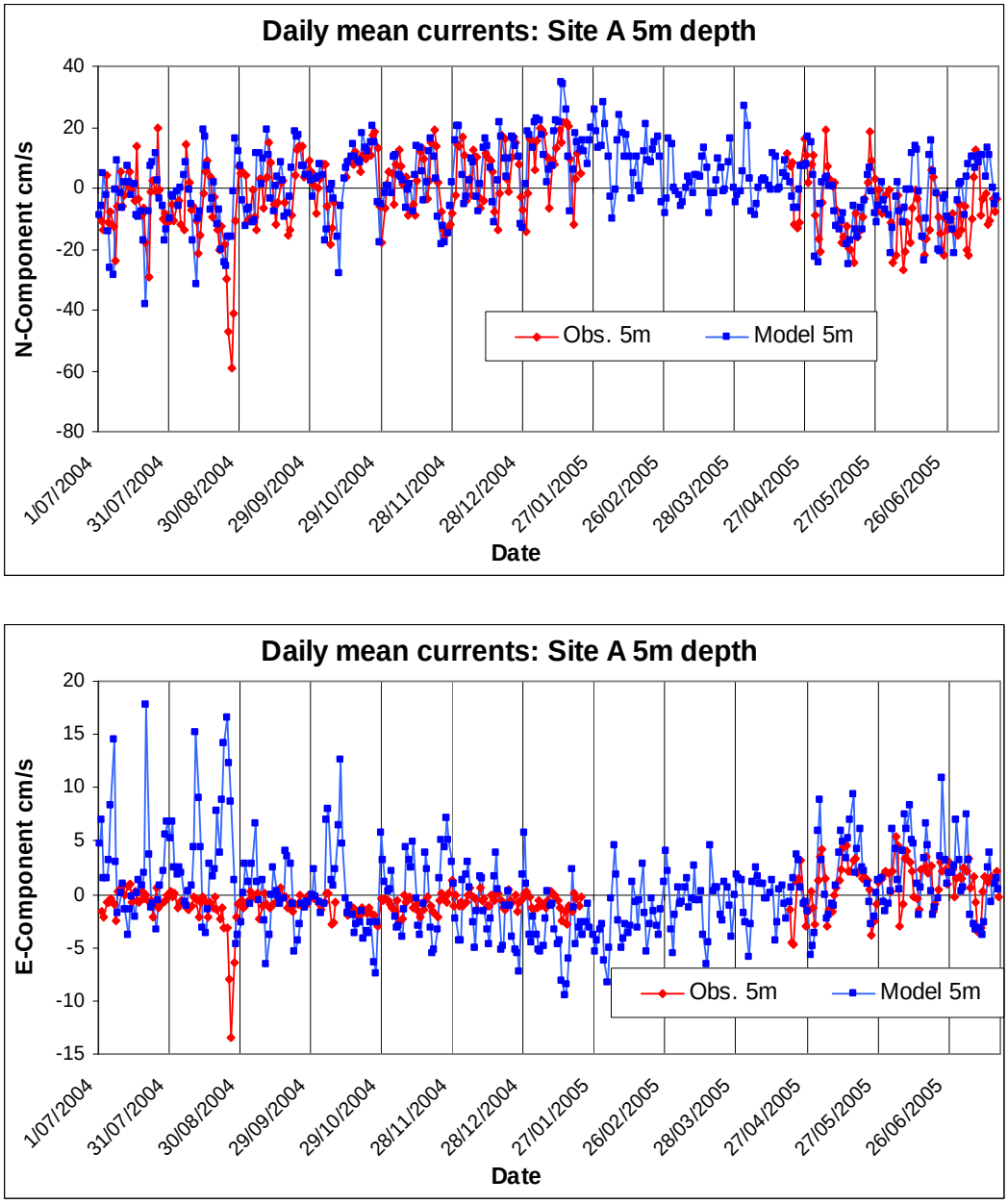

Figure 1.11. Daily alongshore (upper) and cross-shelf (lower) current components at 5 m depth at Two Rocks Transect site A in 2004/2005; red represents the observed ADCP currents and blue the BRAN simulation.

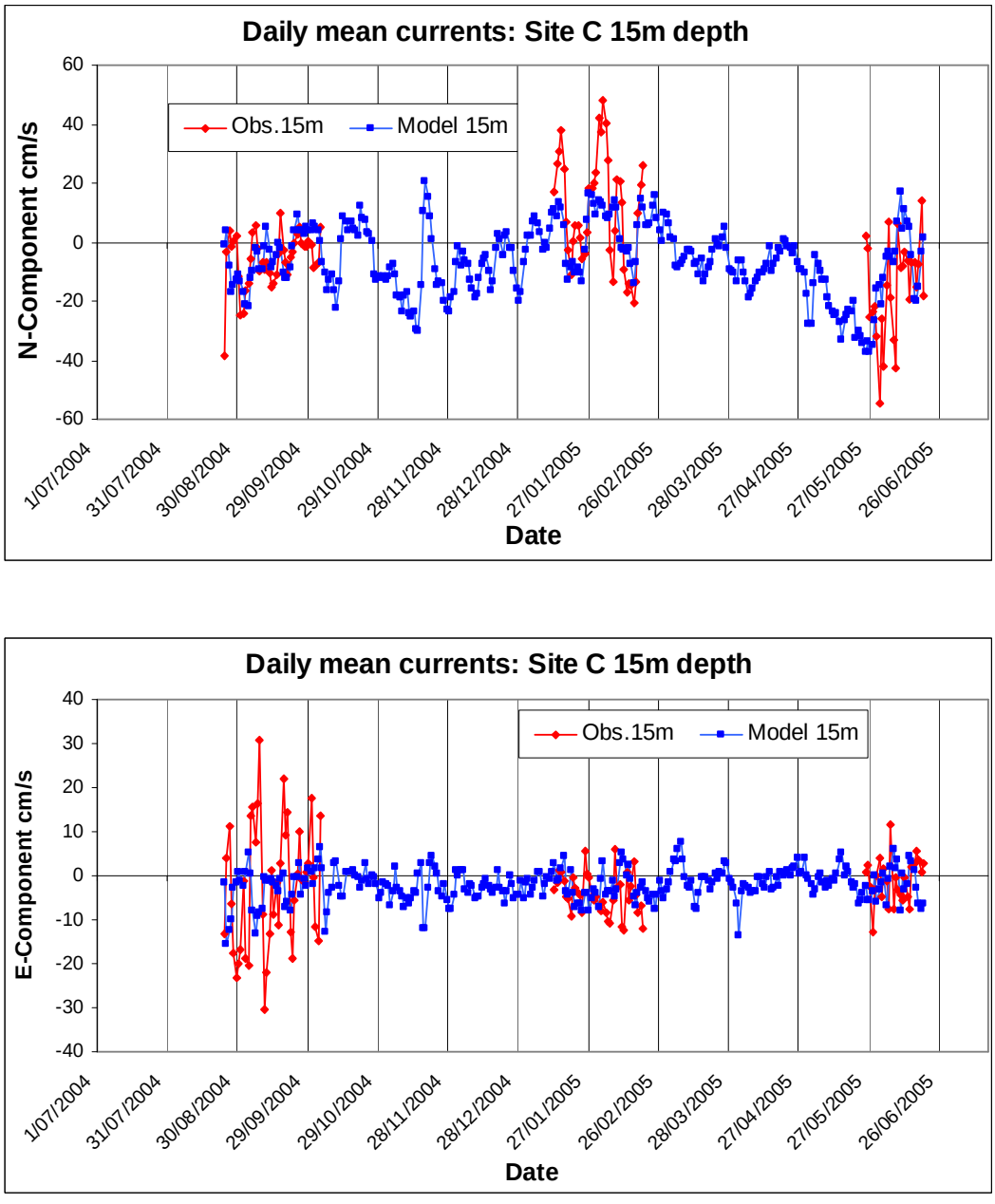

Figure 1.12. Daily alongshore (upper) and cross-shelf (lower) current components at 15 m depth at Two Rocks Transect site C in 2004/2005; red represents the observed ADCP currents and blue the BRAN simulation.

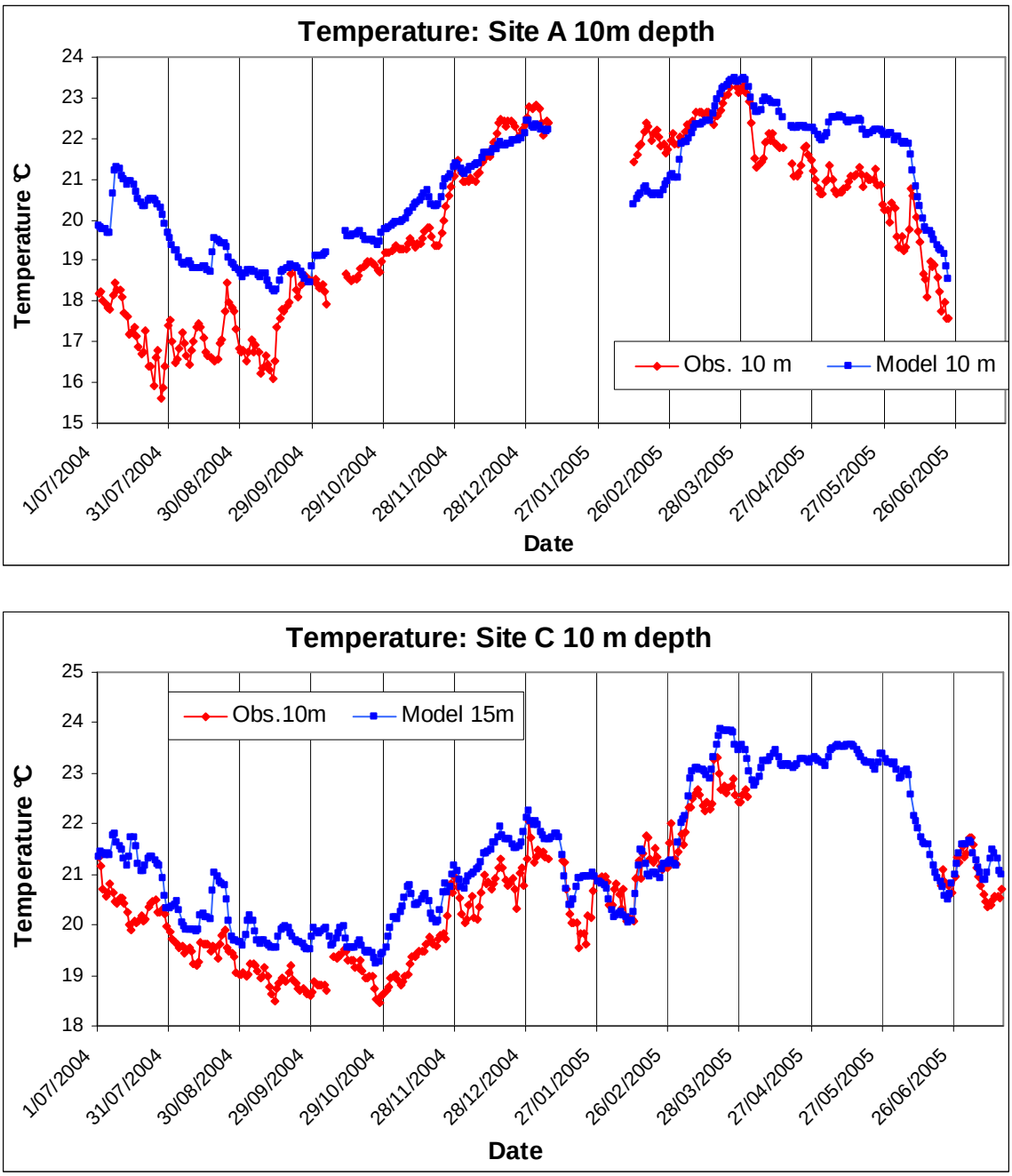

Figure 1.13. Daily mean near-surface temperatures from observations (red) and BRAN (blue) at site A (upper) and site C (lower) in 2004/2005.

In summary, BRAN has captured the broad scale features of the boundary current systems, the Indonesian Throughflow and the Leeuwin Current off the coast of Western Australia. BRAN has also well simulated the structure and variability of upper ocean temperature off the coast. For shelf currents, BRAN does reasonably well with longshore current variability, but tends to underestimate currents speeds by a factor between 0.2 and 0.6. This may be the constraint to use BRAN data for the near-shore current studies.

1.2.2 Long-shore connectivity

Marine species that have a pelagic larval phase have the potential to be widely dispersed alongshore by the Leeuwin Current. Modelled currents from BRAN can be used to predict the trajectories of larvae from their spawning point to there settling destination. Given the underestimation of the cross-shelf current on the inner shelf, the connectivity calculation may be only applicable for larvae released in the outer shelf.

Growth, survival, and dispersal of marine planktonic larvae rely strongly on their behaviour. Larval fish change their vertical positioning due to strong vertical gradients in light, temperature, predation pressure, and prey availability. In some circumstances, they also use vertical migration to take advantage of the prevailing ocean currents. In this project, we have used individual-based (particle-tracking) models (IBM) of the western rock lobster and abalone larvae off the west coast as examples to demonstrate how larval behaviours may affect recruitment processes of different marine species.

The western rock lobster has a long larval phase (~10 months) in the open ocean, and exhibits significant variations in post-larval puerulus settlement correlated with oceanic factors (Caputi et al. 2001). The first IBM developed to investigate the larval phase of the western rock lobster incorporated satellite-based ocean currents and larval behaviour and was capable of moving significant numbers of early-stage larvae (phyllosoma) offshore from breeding areas along the continental shelf and returning them to the west coast as puerulus some 9-11 months later (Griffin *et al*. 2001). This model was a major step forward in the oceanographic sense, but the authors noted that their model involved a number of simplifications and was not able to fully replicate the observed geographic distribution of puerulus settlement or the interannual variability in settlement.

The IBM model is based on a Lagrangian particle-tracking method. The advection scheme is 4th-order Runge-Kutta, in which the position of a particle at time step *n+1* in one direction, x_{n+1}, is given by

$$x_{n+1} = x_n + u_{n+1/2}\Delta t + R\left[2r^{-1}K_m\Delta t\right]^{1/2},$$

where x_n is the position of the particle at the previous time step, Δt is the time step, and $u_{n+1/2}$ is velocity at the predicted position at time $(n+½)\ \Delta t$. The third term on the right-hand side represents sub-grid scale processes unresolved by the archived BRAN data. It is a model of diffusion by random-walk, with R a random number having zero mean and variance of 1, and K_m the horizontal diffusivity (r=1 is a scaling factor).

The selection of K_m is dependent on the length and time scales of the unresolved processes. It is often specified by comparing the statistics of surface drifters and modelled particles. Most studies suggest that the source-sink relationship of particles is not strongly related to the choice of K_m, and commonly used K_m values range from 0 to100 m^2/s (Table 1.1).

Table 1.1. Summary of diffusivity used in different particle tracking models.

Hydrodynamic Model Grid Size	Diffusivity (m^2/s)	"Ocean Scape"	Reference
Analytical domain	10, 100	Coastal	Parslow and Gabric 1989
0.5 km x 0.5 km	10, 50	Shelf/Open Ocean	Hannah et al. 1998
500 m x 500 m	10	Coastal	Ommundsen 2002
0.25^o x 0.25^o	100	Shelf/Open Ocean	Thorpe et al. 2004
0.25^o x 0.25^o	0	Shelf/Open Ocean	Murphy et al. 2004
1.4 to 47.3 km (non-uniform grid)	60	Shelf	Ribergaard et al. 2004
3 m to 4 km (non-uniform grid)	1, 10	Coastal	Bilgili et al. 2005
2.5^o x 2.5^o	100	Shelf/Coastal	Marinone 2006
3 km to 5 km (curvilinear grid)	20, 200, 400	Shelf/Open Ocean	Xue et al. 2008
4 km x 4 km	~33	Shelf/Coastal	Mitarai et al. 2008

Figure 1.14 and Figure 1.15 show results to test K_m selections in the particle tracking based on BRAN off the WA coast. Particles were released in the surface layer in a 50 by 50 km box about 300 km offshore of the Abrolhos Islands on 1 January and 1 July 2000, and were followed for 30 days. The particles were advected by the horizontal current at the sea-surface. Results show that the particles experience long-distance excursions during the 30 days from their release site, mostly due to the mean current and eddy activity. By comparing the simulations using different K_m, it is confirmed that the random walk plays only a minor role in the spatial dispersion of the particles and the dispersion patterns are not sensitive to the K_m selection in the range of 10 – 50 m^2/s.

We emphasise that it is important to seed a large number of particles for tracking, to properly represent the flow variability and range of possible outcomes, and thus achieve correct statistics.

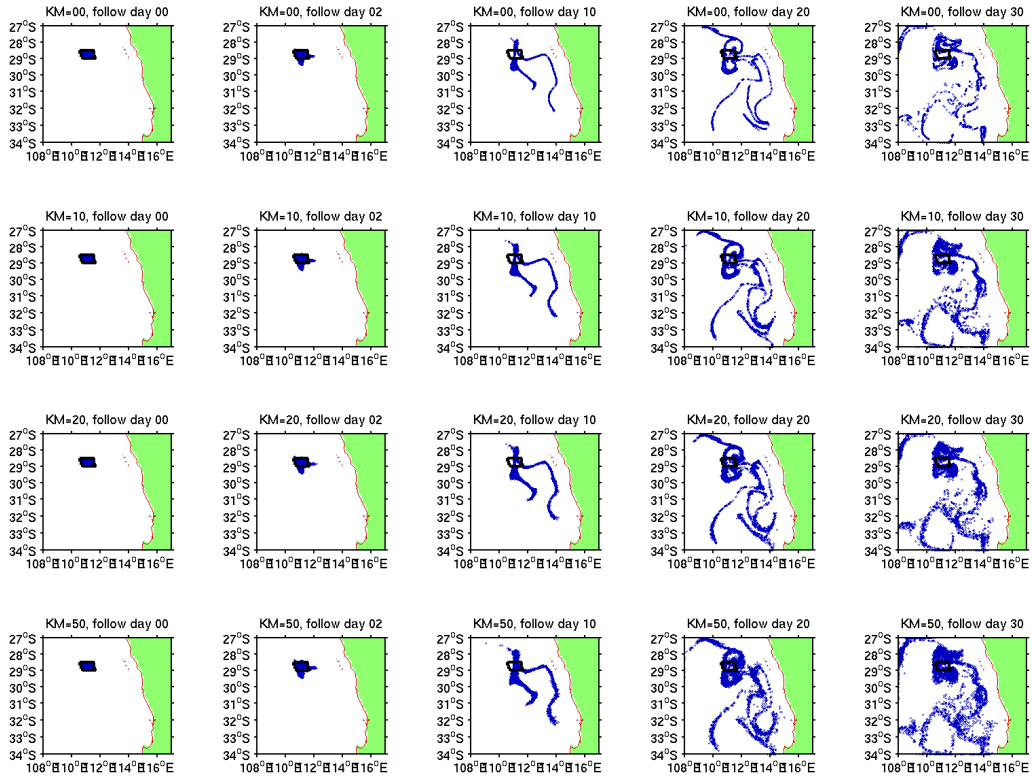

Figure 1.14. Distribution patterns of 4997 particles released on 01 January 2000. The particles were advected for one month using the BRAN velocity field. Particle locations at 0, 2, 10, 20 and 30 days after release are shown. Each row represents a realization using a different diffusivity coefficient (K_m) of 0, 10, 20 and 50 m^2/s, respectively.

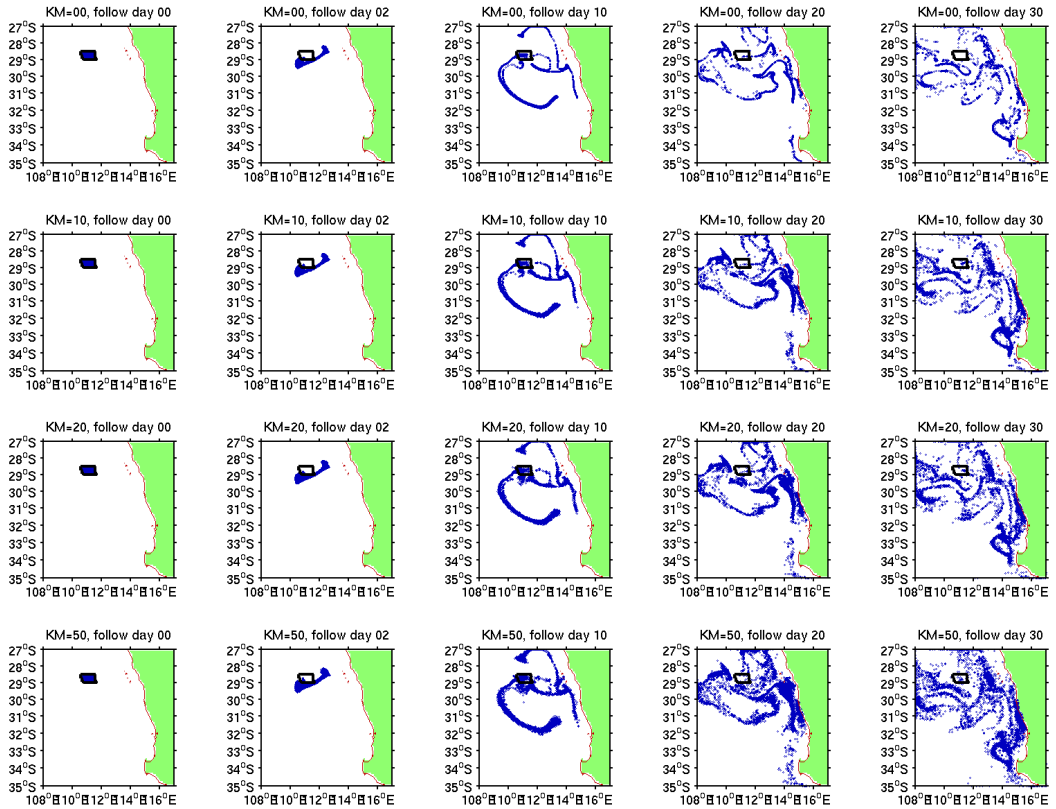

Figure 1.15. Same as Figure 1.1. Seasonaly climatology of horizontal current speed (shading), averaged over the top 150 m, from BRAN. Except for particles released on 01 July 2000.

Source of the Leeuwin Current waters

As a further preliminary example of the use of particle tracking, the technique has been used to identify the source and fate of Leeuwin Current waters. Particles were seeded in the upper 200 m along 22 °S, offshore of the Ningaloo Reef, in the region generally regarded as the start of the Leeuwin Current. From there, the particles were back-tracked using the 3-dimensional BRAN velocity field. Over the 10-year period, 1997 – 2006, about 500 particles were released on the 1st of each month, and then back-tracked for 6 months. The back-tracking uses only advection, with no random walk component.

The modelled seasonal variations of the source regions of the LC seem to be consistent with those identified in earlier studies (e.g. Domingues *et al.*, 2007): in spring and summer the LC waters tend to have a western source, while in autumn and winter they seem to have a more northern source (Figure 1.16). Most of the particles arrive from the region between 15-25 °S off the northwest Australia.

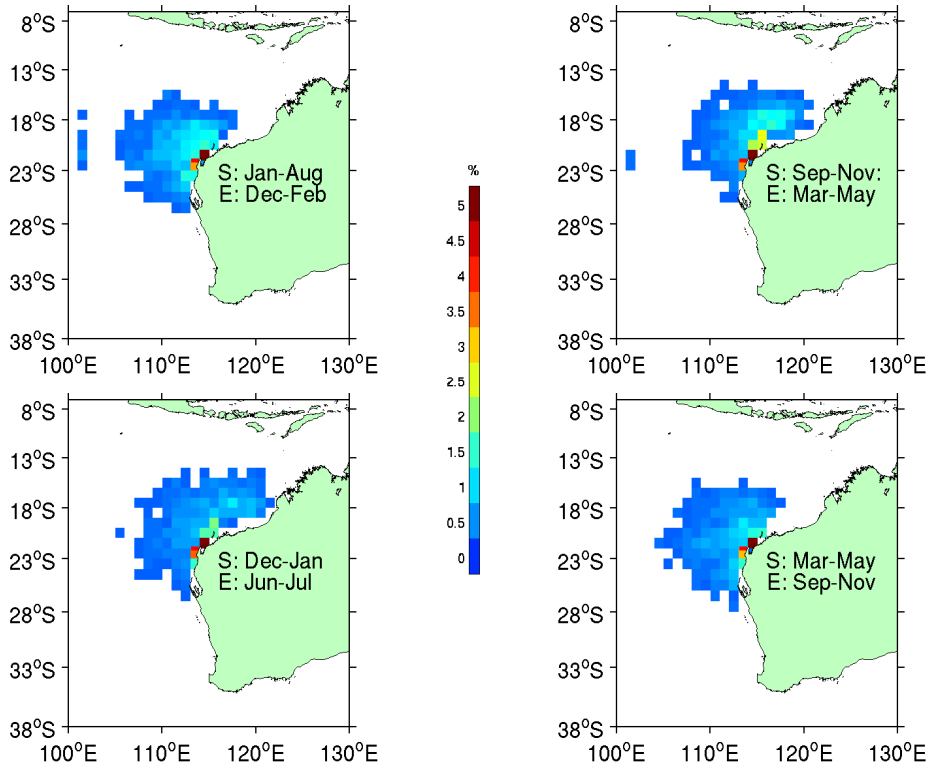

Figure 1.16. Average distributions of likely source regions of backtracked particles released at 22 °S in the Leeuwin Current for 1997 – 2006. The pa rticles are tracked for 6 months.

Retention rates

As already noted, the shelf circulation off the coast is strongly influenced by the poleward-flowing Leeuwin Current all year round, interrupted by episodic, wind-driven, northward, inshore surface transport during the austral summer (Figure 1.17). This section describes a 2-dimensional implementation of the Lagrangian particle tracking model, in which particle movements were passively advected by the 0–20 m depth-averaged, daily velocity field from BRAN. Particle locations were updated every 6 hours (by linearly interpolating velocity from daily fields), and random effects were included by perturbing the initial particle seeding. A reflection scheme, based on geometric intersections of boundaries, was added to the 2D particle tracking code to prevent particles from stranding on land.

The continental shelf between 22º and 35°S off the west coast of Australia was divided into 26 half-degree (55 km) latitudinal segments (Figure 1.17). The offshore boundary of each segment was determined by the 200 m isobath, except for the Ningaloo segment where the 1000 m isobath was used because the narrow shelf (< 10 km) is unresolved by BRAN off Ningaloo. 5000 particles were randomly seeded in each segment daily for model years 1996 through 2000 and the particles were tracked for one month. Sensitivity tests showed that the results from this study were robust if the number of particles released at each segment was halved.

The retention rate of a segment is defined as the percentage of particles initially seeded there that remained in the segment at the end of a certain tracking period. The dispersal rates from a

segment were defined as the percentage of particles seeded in the initial segment that subsequently had entered any of the other segments at the end of a certain tracking period.

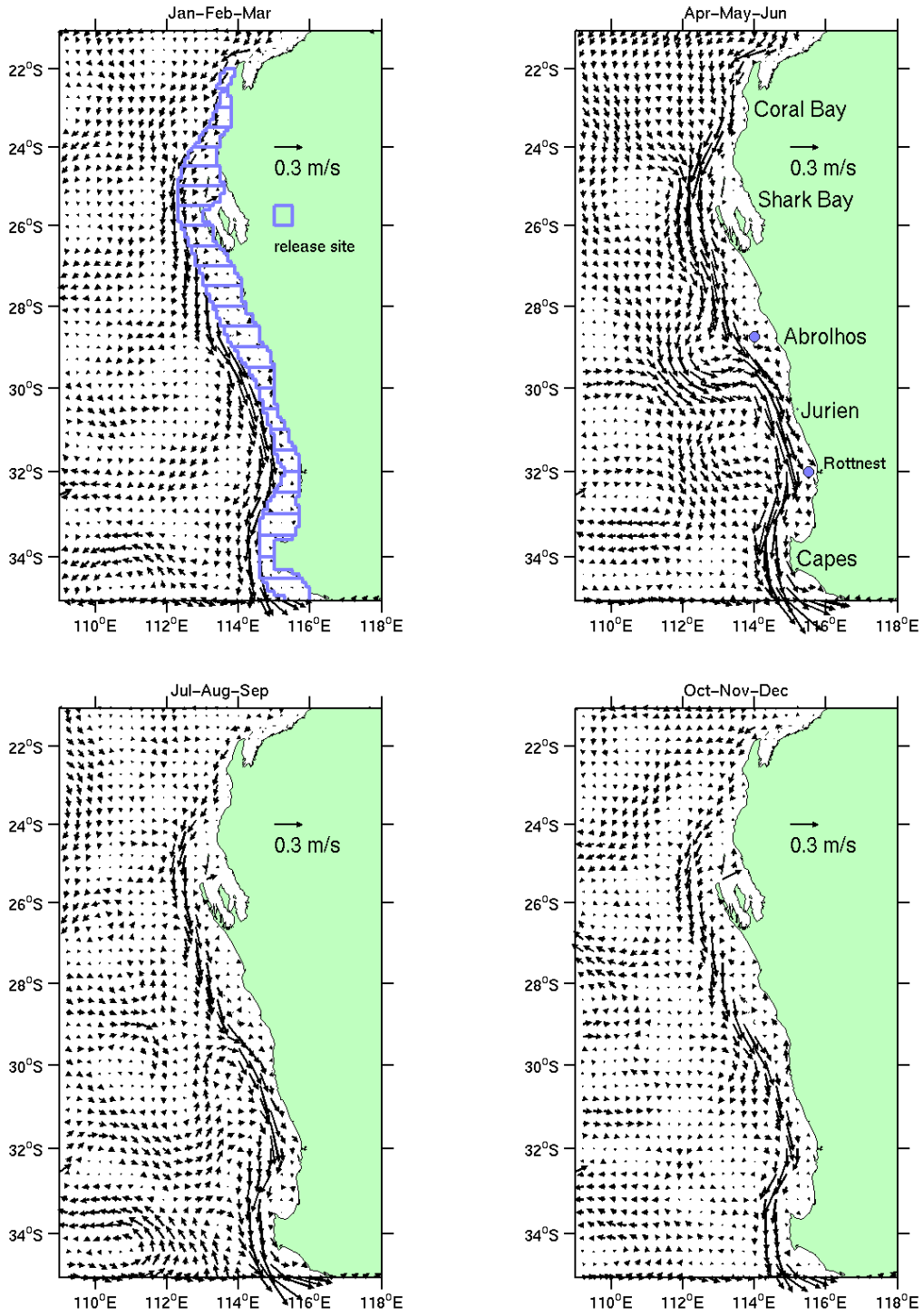

Figure 1.17. Seasonally averaged 0-20m BRAN velocity field for 1997 to 2006. The blue boxes in the upper left panel represent particle release sites.

Retention rates of surface waters have significant spatial variations on the continental shelf off the west coast of Australia (Figure 1.18). Based on a 5-year average, the lowest retention rate of

less than 3% occurs off North West Cape (Ningaloo, ~22ºS), and the highest retention rate of more than 40% occurs at Geographe Bay, 14 days after particle release. Shelf regions identified to have significantly higher retention rates than their standard deviations were: Carnarvon (24º-25.5ºS), the broad Abrolhos region (26.5º-29.5ºS), between Perth and Geographe Bay (32-33.5°S), and south of Cape Leeuwin (34.5-35ºS). In addition to North West Cape, low retention shelf regions were identified off Shark Bay (~26°S), near Jurien Bay (30-31°S), and off Cape Leeuwin (~34ºS).

The spatial inhomogeneity of shelf-water retention rates is to a large extent determined by the magnitude of alongshore velocity, and to a lesser extent by the width of the continental shelf. Shelf regions of low retention tend to experience stronger alongshore currents: the narrow shelves off North West Cape and Cape Leeuwin tend to be more influenced by the Leeuwin Current; the shelf region off Shark Bay has protruding coastal geography and is more exposed to the Leeuwin Current; and the formation of mesoscale eddies near Jurien Bay caused significant cross-shelf exchanges of waters (Feng *et al.* 2005; 2007). By contrast, most shelf regions with higher retention rates are sheltered from the direct influence of the Leeuwin Current by coastal geography and have weaker alongshore currents: the region south of Abrolhos is sheltered by the island chain; the Leeuwin Current is diverted offshore upstream of Geographe Bay; and the region south of Cape Leeuwin is located in the shadow of the Cape.

The saucer scallop, *Amusium balloti* is an Indo-Pacific species that is abundant in four shelf regions off the west coast, centred on the Shark Bay area, the Abrolhos, the south-west near Fremantle and Geographe Bay (Figure 1.18; Harris *et al.* 1999; Caputi *et al.* 1998). Between the Abrolhos and Fremantle, *A. balloti* spawning occurs from July to March (Joll and Caputi 1995), with a pelagic larval phase of 10-14 days (Rose *et al*. 1988). Thus, with the exception of the Shark Bay fishery (which occurs inside the shelter of an almost continuous island chain), the shelf areas with sufficient scallop populations to support commercial fisheries occur in close association with regions with high levels of particle retention rates (Figure 1.18).

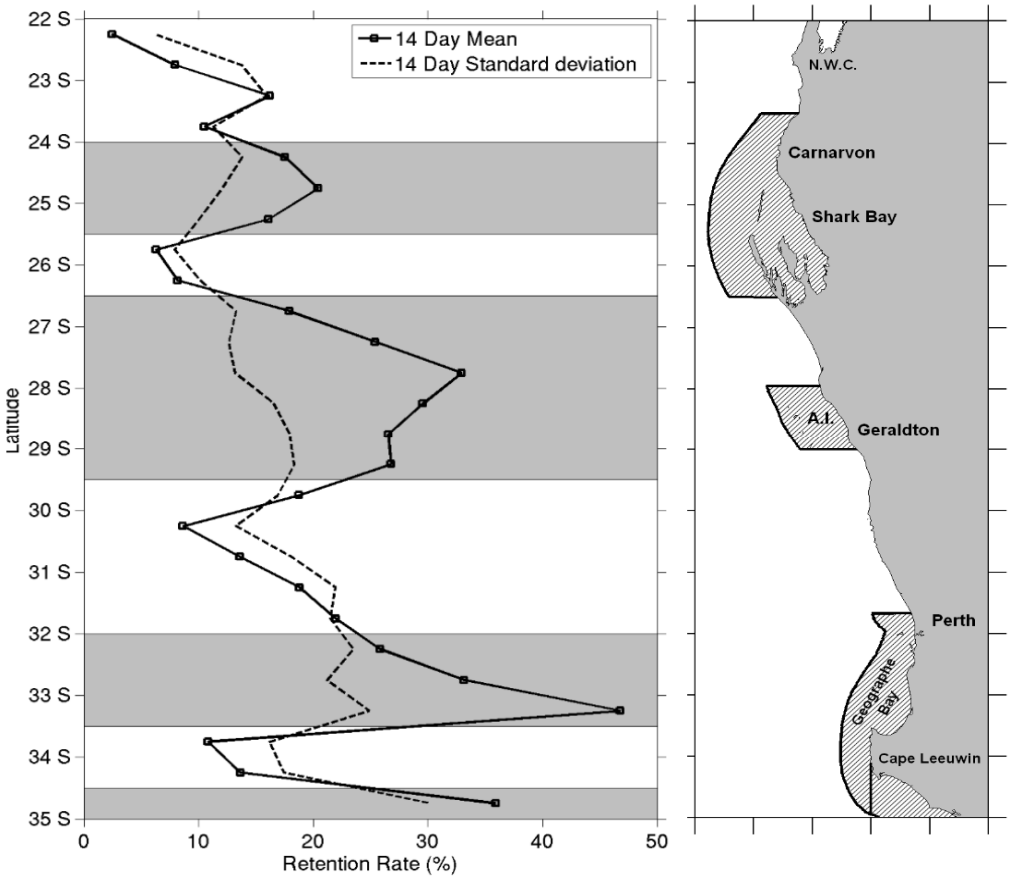

Figure 1.18. (left panel) Retention rates off the west coast of Australia after two weeks of particle tracking and their standard deviations, and (right panel) the boundaries of the saucer scallop fisheries in Western Australia (source: Harris et al. 1999).

Alongshore dispersal is more symmetrical in October-December, whereas dominantly southward dispersal occurs in April-June when the Leeuwin Current is strong (Figure 1.19). However, spatial inhomogeneity of dispersal patterns was also evident: whereas in most high retention regions the alongshore dispersals were similar to that of the southern Abrolhos, there were more southward excursions for particles released off North West Cape, Shark Bay, and Jurien Bay during April-June; and there was more northward alongshore movement of particles released from Jurien Bay during October-December. Further study is needed to determine how the inhomogeneity of alongshore dispersal is linked to interaction between the Leeuwin Current and coastal geometry. The sensitivity of local retention and alongshore dispersal to timing and location of spawning, as well as larval duration, are potentially important determinants of the patterns of distribution and abundance of marine organisms that have a pelagic larval phase.

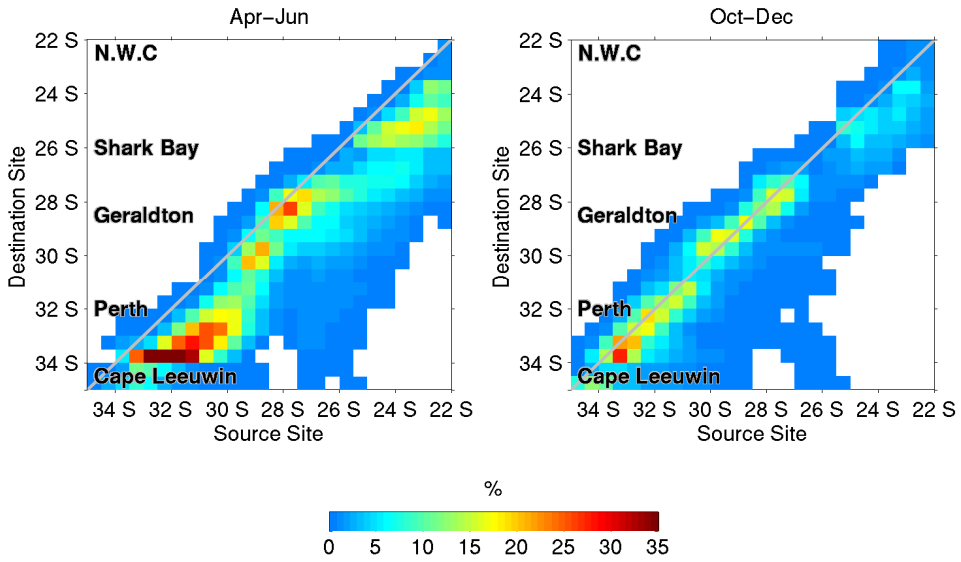

Figure 1.19. Alongshore connectivity matrix along the west coast of Australia after four weeks of particle tracking in April-June and September-December. Only values with particle density of greater than 0.1% of original releases are plotted.

Stokes Drift

Larvae often float at the surface, or migrate on a daily basis to spend significant time at the surface. As an example, western rock lobster larvae through their phyllosoma and puerulus stages have been observed to have extensive vertical migration. At the surface, particles are subject to a net drift, called the Stokes drift, due to the action of waves (swells), which is not included in standard hydrodynamic models like BRAN. For an open coastline, like Western Australia's, with a persistent swell from the south to southwest, Stokes drift may have a significant influence on the larval dispersion.

The Stokes drift velocity in the direction of wave propagation can be calculated as

$$U_s = \frac{(ak)^2 C_P \cosh[2k(z+H)]}{2\sinh^2(kH)}$$

Here, $C_P = \sigma / k$, is the phase speed of the waves, $\sigma^2 = gk\tanh(kH)$, where a is the wave height, k is the wavenumber, z is the depth which is zero at sea surface and positive upward, and H is the water depth. For significant wave height H_S, and significant wave period T_S, derived from a wave model or observations, $a = H_S/2$, and $\sigma = 2\pi/T_S$, (Monismith and Fong 2004).

Significant wave height, wave period and direction from Wave Watch 3 model (WW3) data (http://polar.ncep.noaa.gov/waves/wavewatch.shtml; Tolman et al. 2002) were used to derive a Stokes drift velocity for the particle tracking. Eight-hourly global WW3 data at 1-degree longitude by 1.25-degree latitude resolution from 1997 to present were downloaded. The WW3 data are converted to daily means, and then interpolated onto the ~10km x ~10km BRAN velocity grid between 90E – 130E and 1N – 61S.

In addition, QuikScat (http://winds.jpl.nasa.gov/missions/quikscat/index.cfm) wind data derived from satellite data are also used in the particle tracking, to correct the surface Ekman drift. Underestimate the surface Ekman drift is likely to be one of causes of the underestimation of surface current in BRAN. The twice daily global data at ¼ degree by ¼ degree resolution from 1999 to present were downloaded. The data are averaged into daily values, and then interpolated onto the BRAN ~10km by ~10km velocity grid.The correction may be calculated as 2-3% of the wind speed, 20-30 degrees to the left of wind direction in the southern hemisphere (Jenkins 1987). Note that the wind correction is used in addition to the wave-driven Stokes drift effect.

Figure 1.20 shows an example of the effect of including Stokes drift in the model calculations. With Stokes drift, the latitudinal distributions of model particles in June-July are centred around 22-33°S, largely consistent with late stage [VI to IX] phyllosoma spatial distributions (Rimmer and Phillips 1979). Without Stokes drift, they have a more southern distribution, skewed toward 30-32°S. The average latitudes of all late-stage particles during this period are 27.6°S and 28.6°S for the IBM simulations with and without Stokes drift, respectively, so that the net effect of Strokes drift is to shift the particle population by about a 100 km northward, and retain the particle population off the west coast.

As a consequence of the northward shift of particle distribution due to Stokes drift, the mean latitude of settling particles is at 29.7°S, more than 150 km north of the settling location without Stokes drift. With the Stokes drift effect, the central region of the settlements is located between the Abrolhos and Fremantle and the settlements in the southern Capes region are significantly reduced. These model outputs are consistent with the puerulus collector data and the location of catches by the western rock lobster fishery, and overcomes one of the significant issues of settlement being too far south in the previous model (Griffin *et al.*, 2001).

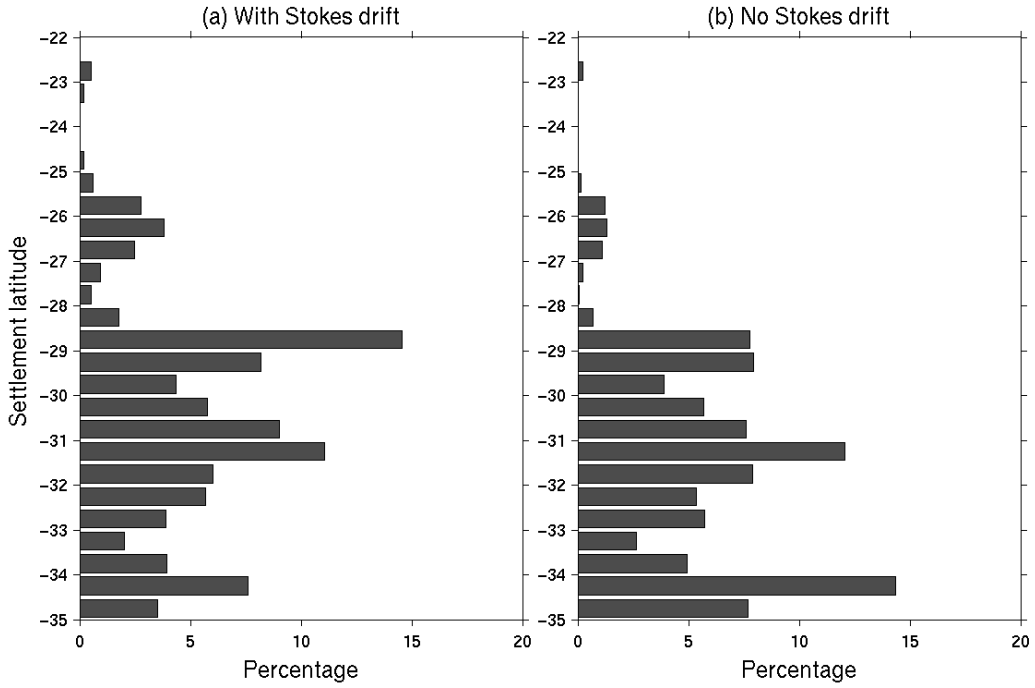

Figure 1.20. Latitudinal distribution of successfully settled IBM particles averaged over the 9 years modelled (a) with Stokes drift incorporated in the IBM and (b) without Stokes drift effect.

The improvement of the IBM of the western rock lobster larvae has been utilised in a joint FRDC project with the WA Department of Fisheries to better understand the source-sink relationship of the western rock lobster puerulus recruitments.

1.3 Western Australian Continental Shelf Scale

1.3.1 Introduction

A shelf-scale model with resolution down to around 2km, centred on Perth and extending from the coast to the continental slope, is nested within a regional scale model. Its primary task is to simulate seasonal changes in phytoplankton chlorophyll concentrations and help quantify seasonal fluxes of nitrogen on and off the shelf. The model should be capable of resolving sub-mesoscale processes (e.g. Leeuwin Current System and eddies) on time scales ranging from days to seasonal cycles. The shelf-scale model is downscaled from a global model archive from CSIRO's BRAN (BLUElink ReANalysis), which has 10km resolution in the Australian region and is based on a data-assimilation model (Oke et al., 2008).

1.3.2 Methodology

A coupled hydrodynamic-biogeochemical model (ROMS) has been configured for the southwest shelf off Western Australia. ROMS solves the incompressible, hydrostatic, primitive-equation model with a free surface, horizontal curvilinear coordinate, and a generalised terrain-following vertical coordinate (Haidvogel et al., 2000). The model domain extends from the coast to offshore 108^{o}E and from 35^{o}S (Cape Leeuwin) to 21^{o}S (the North West Cape). The horizontal resolution in cross-shore direction varies between 2 km and 4 km from the coast to the 1000 m isobath and then increases to 8 km at the oceanic boundary. The alongshore resolution varies from 3 km to 8 km. There are 30 vertical levels with refinement in the top 200 m. The ROMS model is one-way nested in BRAN, a global model with 10 km resolution in the Australian region. The BRAN archive provides the initial field and physical boundary data, including sea level, velocities, temperature and salinity. At the surface, the ROMS model is forced by 3-hourly atmospheric fields from the ERA-interim archive of the ECMWF obtained from the ECMWF data server, which includes wind stresses, heat and freshwater fluxes, and solar radiation. At the three lateral open boundaries, an oblique radiation condition (Marchesiello et al., 2001) was used with a nudging term for tracers and 3d velocities. A Flather boundary condition (Flather 1976) is used for the depth-averaged velocity and zero gradient condition for sea surface level. There are sponge layers and weak nudging layers in the outermost 6 grid cells of the model.

The model was integrated for 4 years from January 2000 to December 2003 and the solution for 2003 is selected to represent the typical conditions of the Leeuwin Current System in the study region. The model performance is assessed as follows.

1.3.3 Results

Annual mean sea-surface height and sea surface temperature

Annual mean sea-surface height (SSH) and sea-surface temperature (SST) simulated by ROMS in 2003 are compared with results from the BRAN model, satellite imagery and the CARS06 dataset (Figure 1.21). SSH looks similar in ROMS, BRAN and CARS06 in terms of both pattern and magnitude. As shown in Figure 1.21 sea level is high in the north and low in the south. This north-south pressure difference plays an important role in driving the pole-ward flowing Leeuwin Current, bringing a high pressure tongue along the shelf break.

The spatial distribution of SST has a similar pattern to SSH. Temperature decreases as the Leeuwin Current moves towards the South Pole and there exists a warm-water tongue along the shelf break, where SST is a couple of degrees higher than ambient offshore and inshore waters.

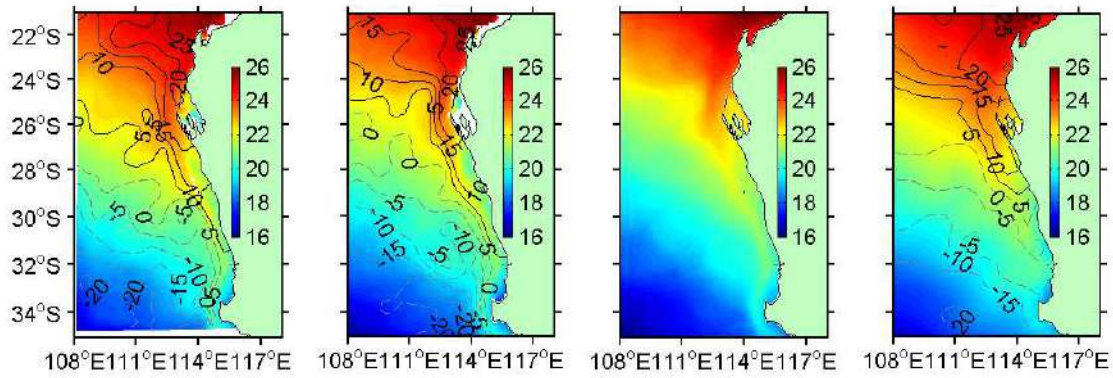

Figure 1.21. Maps of annual mean sea surface temperature (in colour) and sea surface height (contour lines, units in centimetre) in 2003 from the ROMS model, BRAN model, satellite sea-surface temperature imagery (no sea-surface height contours) and CARS06 dataset (CSIRO Atlas of Regional Seas - 2006).

Surface eddy kinetic energy (EKE)

A common feature associated with the Leeuwin Current is mesoscale eddies, whose activities can be measured by surface eddy kinetic energy (EKE). As shown in Figure 1.22, mesoscale eddies in ROMS develop preferentially offshore of the continental shelf break between 27°S and 33°S, consistent with previous studies based on satellite altimeter data (Fang and Morrow, 2003; Feng et al., 2005 and Feng et al., 2009).

Figure 1.22 also compares the seasonal variation of EKE between the ROMS model and the climatological EKE derived from satellite altimeter data (Feng et al. 2009). Both show a clear seasonal cycle of EKE, with eddy activity stronger in austral winter and weaker in austral summer.

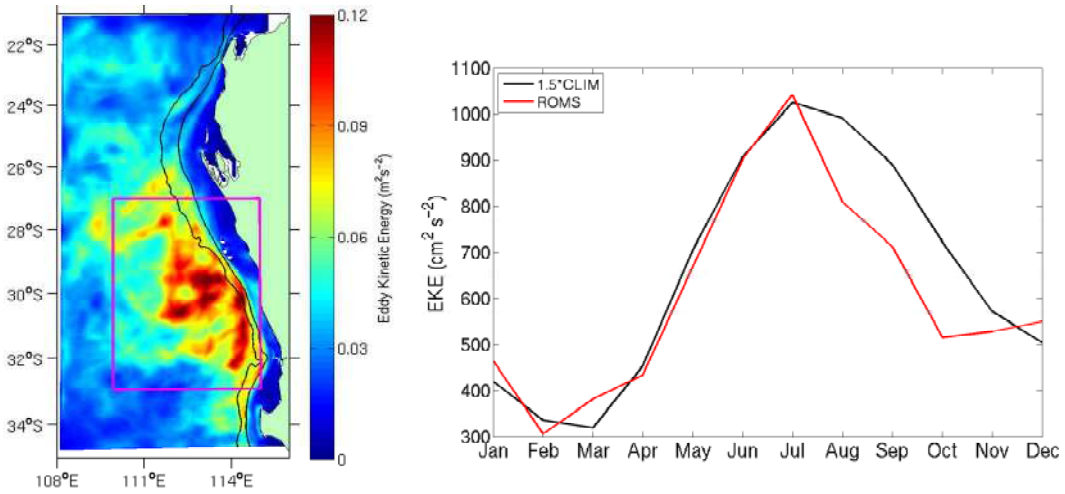

Figure 1.22. Map of annual mean surface eddy kinetic energy in ROMS (left) and comparison of seasonal EKE between ROMS model and climatological EKE derived from satellite altimetry by Feng et al. (2009).

Seasonal variability of the Leeuwin Current and its transport

The Leeuwin Current and its seasonal variation is illustrated at three transects at 23°S, 27°S and 31°S (Figure 1.23). In the model the Leeuwin Current is about 100 km wide on the surface and shallower than 300m. In austral winter, the Leeuwin Current can reach to 0.5 m/s, and becomes stronger as it moves toward the south. The Leeuwin Current is much weaker in austral summer; however, the northward Capes Current is developed inshore due to the prevailing southerly wind. The temperature stratification also shows seasonal variation. The surface mixing layer is deeper in austral winter than in summer due to stronger heat flux loss from the ocean.

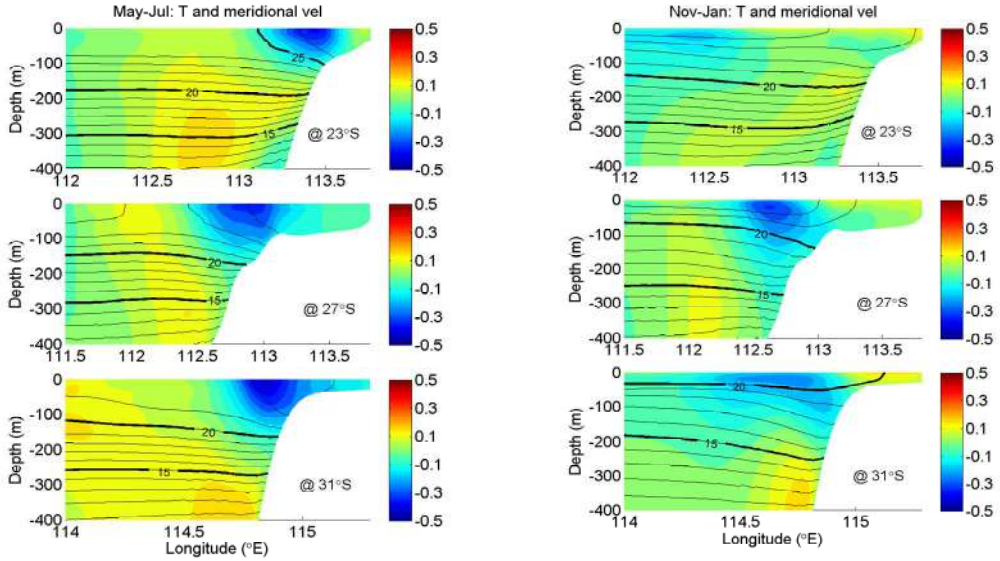

Figure 1.23. Meridional velocity (in colour) and temperature (contour lines in black) averaged in austral winter (left panel) and summer (right panel) along three transects at 23°S, 27°S and 31°S. The Leeuwin Current is represented by negative current in blue colour while the Leeuwin Undercurrent is represented by positive current in yellow. The Capes Current near the shore moves northward in austral summer.

Warm water volume transported by the Leeuwin Current is calculated from ROMS results and then compared with BRAN model and geostrophic transport calculated by Feng et al. 2003 (Figure 1.24). There is a distinct seasonal cycle in the transport of Leeuwin Current, with transport maximised in austral winter and minimised in austral summer. Monthly mean transport can reach up to 4.6 Sv ($10^6 m^3/s$) in austral winter, which is consistent in all three calculations. In austral summer the transport calculated from ROMS and BRAN is about 1 Sv higher than the geostrophic transport.

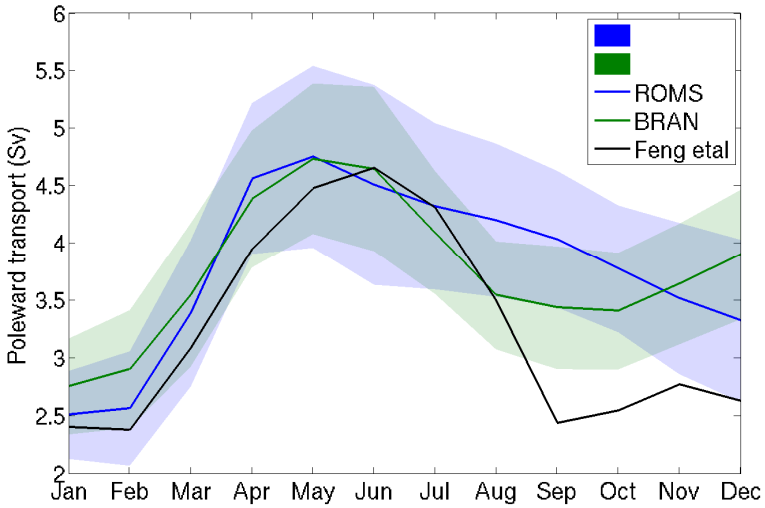

Figure 1.24. Comparison of Leeuwin Current transport between ROMS, BRAN and geostrophic transport at 32°S calculated by Feng et al., 2003. C olour patches show the standard deviation of transport in ROMS and BRAN.

Upwelling in austral summer

The wind along the Western Australia coast is predominantly southerly in austral summer, and drives the Capes Current flowing equatorward on the shelf. The Capes Current is cooler water due to coastal upwelling. ROMS model captured the coastal upwelling in austral summer that we examine along two transects on 27°S and 31°S (Figure 1.25).

Figure 1.25 shows temperature stratification, longshore, cross-shore and vertical velocity at the two transects. At these two transects the Capes Current locates inshore of the Leeuwin Current and moves in the opposite direction. Below 100m water depth, temperature contours tilt down toward the coast, which is typical of the temperature stratification (Figure 1.25); however, temperature contours tilt up toward the coast in the surface layer, an indicator of upwelling. Moreover, the water in and below the Leeuwin Current is uplifted, bringing cold water to the surface.

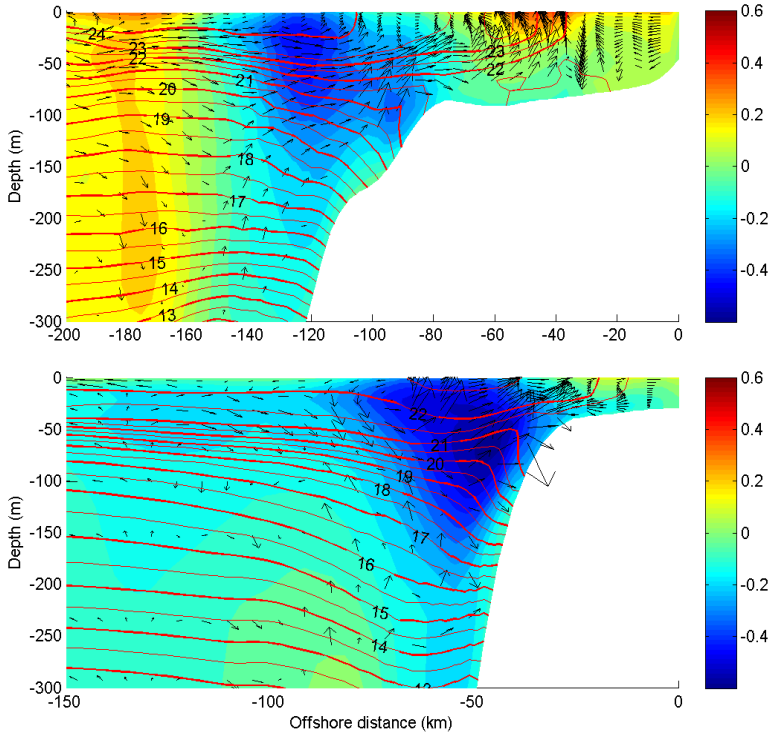

Figure 1.25. Meridional current (in colour), temperature (contour lines in red), and cross-shore and vertical currents (vectors in black) along transects at 27°S (upper panel) and 31°S (lower panel) on 11 February 2003. The Leeuwin Current is represented by negative current in blue colour and the inshore Cape Current is represented by positive current in yellow. Note vertical velocity (in the order of 10^{-5} m/s and 10^{4} times smaller than horizontal velocity) in the vectors is greatly exaggerated to illustrate vertical movement of water masses.

Particle tracking

Particle tracking using ROMS is compared with that using BRAN model (see the previous section). The ROMS model simulation captures a much stronger Capes Current compared with BRAN (Figure 1.26). Particles released in the Cape region have more persistent northward movements compared to BRAN when using the 0-20 m averaged velocities to advect the particles (Figure 1.27). Simulations using the fine resolution ROMS model are being applied to fisheries recruitment (FRDC project proposal on Dhufish fish larvae dispersal).

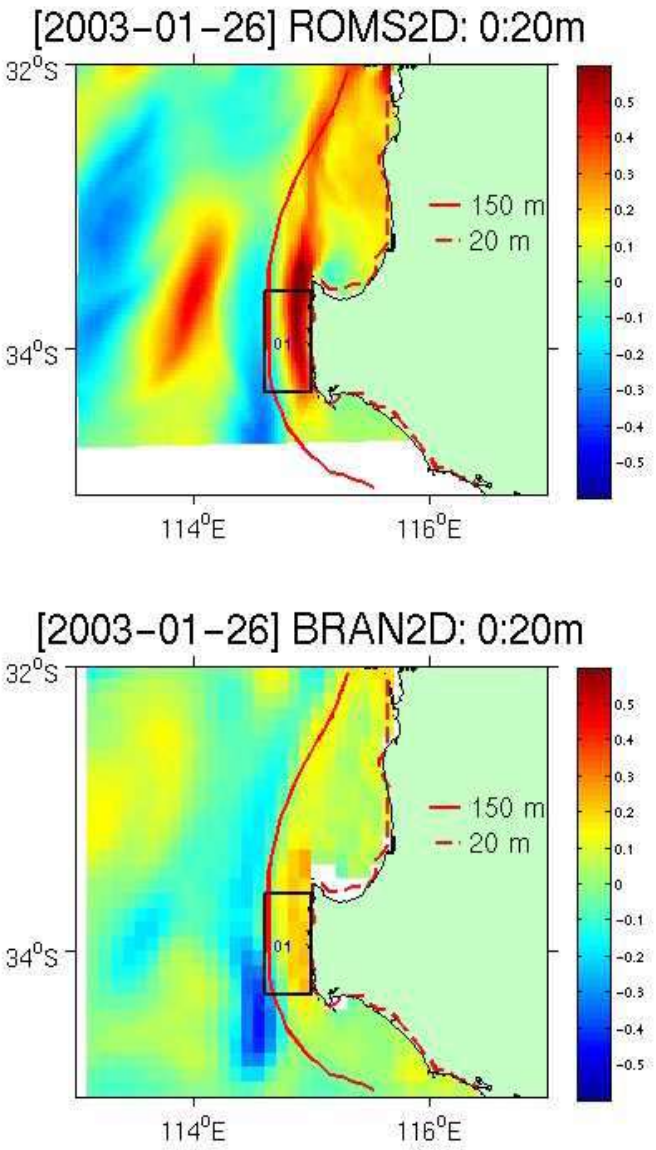

Figure 1.26. Comparison of meridional flows near Cape Mentelle between ROMS and BRAN model simulations. Note that the Capes Current (in black boxes) is much stronger in ROMS simulation compared to BRAN.

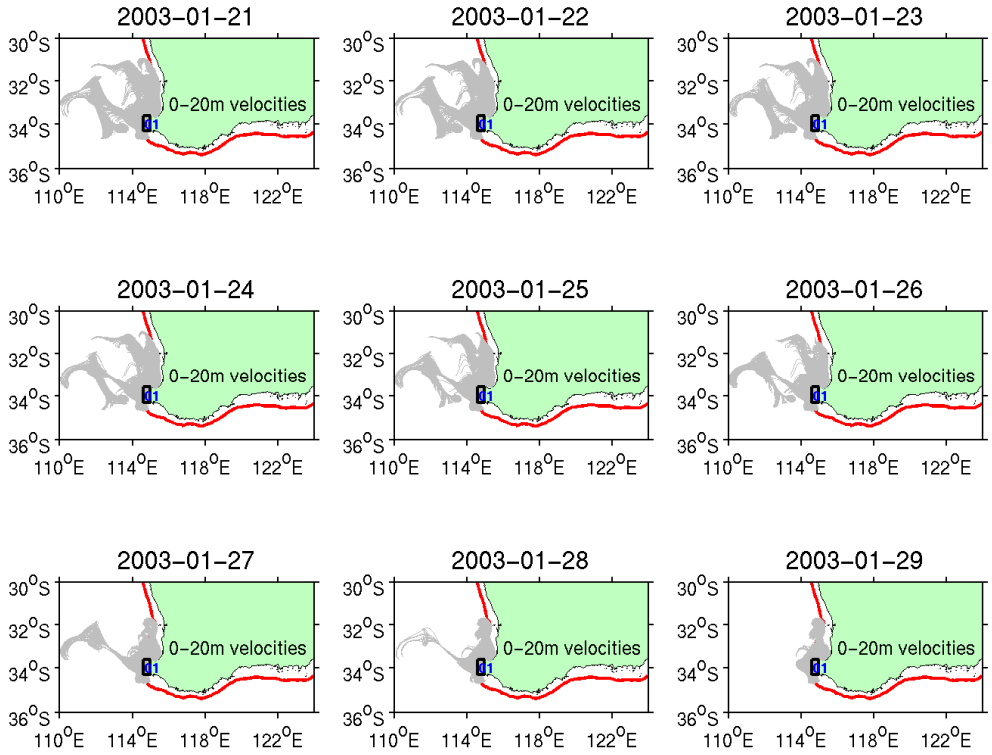

Figure 1.27. 30-day trajectories of particles released off the Capes (within the black boxes) on different days in January 2003 using ROMS model output.

1.3.4 Discussion

The fine-resolution ROMS model is downscaled from a regional model. It is driven by the same air-sea flux forcing as the Bluelink model and uses BRAN model outputs as open boundary conditions. It is expected to reproduce the Leeuwin Current System with more detailed structures. The general features of the Leeuwin Current System and its seasonal variability simulated in the shelf-scale model agree reasonably well with the mother model BRAN and observations. However, the fine resolution model indeed captures different circulations from the coarse resolution model. For example, the shelf-scale model produces a much stronger northward Capes Current compared with BRAN (Figure 1.26). Both models have distinct seasonal cycle of EKE, that is, higher EKE in austral winter and lower EKE in austral summer; however, EKE is higher in ROMS than in BRAN (figure not shown), which seems reasonable since flows tend to be more intense in ROMS with higher resolution.

The ROMS implementation described in this section is primarily required to drive a biogeochemical model of the southwestern shelf region (section 2). Based on the present comparisons with data, ROMS appears to reproduce faithfully the spatial structure and seasonal variability of the hydrodynamics, particularly of the Leeuuwin Current, its eddies, and the inshore wind-driven currents. ROMS, at resolutions down to 2 km inshore, produces stronger, and more realistic currents than the coarser (10 km) BRAN model in which it is nested. Accurate representation of the currents is important to the success of the biogeochemical model, in which the advection nutrients, phytoplankton and other constituents, determines the strength and distribution of primary productivity along this WA shelf region.

1.4 Lagoon scale (Marmion Lagoon)

1.4.1 Introduction

Coastal waters off South West Western Australia are unusual, supporting high benthic biomass and a winter phytoplankton bloom, while the poleward flowing Leeuwin Current is nutrient poor. The region is micro-tidal, dominated by diurnal tides with a spring range of about 0.7m, exposed to long period southern ocean swell (8s<T<20s), and a strong sea-breeze cycle during summer months. A feature of the coastal zone is a series of limestone reefs dotted along the coast for about 700km between 3-10km offshore (Pattiaratchi et al, 1995). The distribution of the reefs is very patchy, individual reefs have relatively small areal extent and are often shallow enough for waves to break over them. Mean currents on the inner shelf, inshore of the Leeuwin Current but offshore of the reefs, are largely wind driven (Pattiaratchi et al, 1995; Zaker et al, 2007) and Feng et al (2006) report the alongshore current at 20m depth is 2.5-3% of the wind speed with a correlation of .87. In the lagoon, shorewards of the reefs, the correlation between wind and current is less and Pattiaratchi et al (1995) report periods during winter months when the current and wind are in opposing directions. However, Zaker et al (2007), using the same data described by Pattiaratchi et al (1995) report the currents inside the lagoon are dominated by wind forcing for most of the year. The site of the study described by Pattiaratchi et al (1995) and Zaker et al (2007) is a few kilometers north where the distribution of reefs is more patchy than our site.

Breaking waves have the potential to drive strong currents over the shallow reefs (Symonds et al, 1995) and, during high wave events, the wave-driven currents may dominate over wind forced currents. These cross-reef currents are due to a body force associated with gradients in the radiation stress defined as the excess momentum due to the presence of the waves (Longuet-Higgins and Stewart, 1964). Due to the greater mass under the wave crest, relative to the trough, the depth integrated forward momentum flux under the wave crest is greater than the opposite momentum flux under the trough. Averaged over a wavelength there is a net flux of momentum in the direction of the waves known as radiation stress and is proportional to wave energy (Longuet-Higgins and Stewart, 1964). Horizontal gradients in radiation stress, due to gradients in wave energy, cause a body force which on a beach can force alongshore currents (Bowen, 1969; Longuet-Higgins, 1970a,b; Thornton and Guza, 1986) and cross-shore setup (Bowen et al, 1968; Guza and Thornton, 1981). In the latter case the shoreline prevents any cross-shore flow, resulting in an increase in sea surface elevation at the shoreline, known as wave setup, such that the cross-shore gradient in radiation stress is balanced by an offshore directed pressure gradient. In the presence of wave breaking on a shallow reef cross-reef, currents can also result since, unlike a beach, there is no shoreline to constrain the flow or support wave setup (Symonds et al, 1995).

These wave forced mean flows are known to be important on coral reefs (Roberts and Suhayda, 1983; Kraines et al, 1998; Kraines et al, 1999; Tartinville and Rancher, 2000; Callaghan et al, 2006; Monismith, 2007; Lowe et al, 2009) and can have a significant impact on nutrient uptake in coral communities (Atkinson et al, 1994; Bilger and Atkinson, 1992; Atkinson and Bilger, 1992; Hearn et al, 2001). However, fringing coral reefs typically have long, continuous stretches of reef of order several kilometres punctuated by narrow gaps of order hundreds of metres, while the limestone reefs off the Western Australian coast are more scattered and the

gaps between the reefs are often considerably greater than the scale of the individual reefs. In coral reef systems wave setup behind the reef limits the cross reef flow, the magnitude of the setup depending on the wave forcing and cross sectional areas of the lagoon and gaps. Wave-driven flows over more isolated reefs may not be limited to the same extent and Mulligan et al (2008) showed local wave forcing on a relatively small reef in the middle of a much larger bay affected circulation over a considerable fraction of the bay area. In an earlier study just a few kilometers north of the current work Pattiaratchi et al (1995) speculated the effects of waves may influence the circulation in the immediate vicinity of the reefs, though no observations were available to support this, and across the wider lagoon they conclude the effects of wave forcing could be neglected. Using the same data Zaker et al (2007) conclude the momentum balance in the lagoon is dominated by wind stress and bottom friction with a smaller but significant contribution from an alongshore pressure gradient. In contrast to these earlier studies this paper reports observations of wave-forced currents in the vicinity of the reefs and, during periods of large waves, the effects of wave forcing dominate and are felt across the lagoon.

1.4.2 Methodology

Between July 2007 and May 2008 in situ measurements of waves, currents and water properties were made on and around a series of reefs off Perth, Western Australia. The field site is characterised by a series of shallow limestone reefs about 3km offshore, the depth over the top of the reefs varies between 1 to 4m. The bathymetry is shown in Figure 1.28 where the filled areas represent depths less than 4m showing the distribution of shallow reefs.

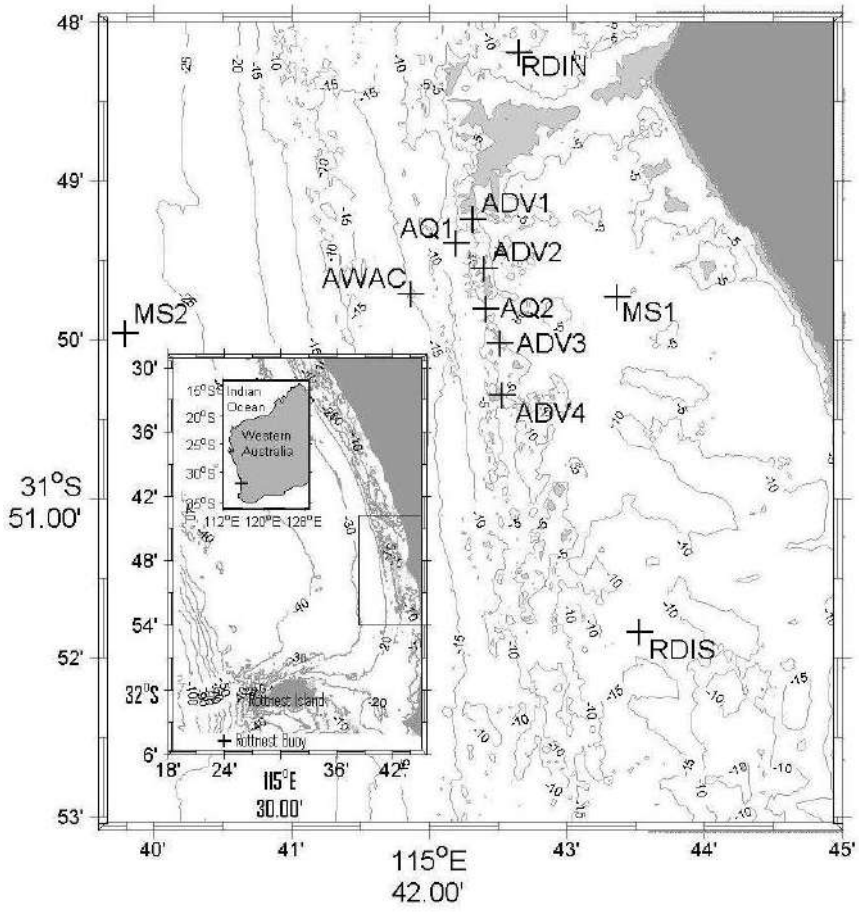

Figure 1.28. Site location and instrument array. The contours are bathymetry. The filled light gray areas are where the shallow reefs are located with a water depth of less than 4m.

The field program consisted of in situ measurements of waves, currents and water properties at 11 sites shown in Figure 1.28 using a variety of point current meters and profiling ADCPs, wave gauges and multi-sensors measuring temperature, salinity, oxygen, Photosynthetically Active Radiation (PAR), and fluorescence. The array was deployed four times throughout the year-long program, each deployment being 6-8 weeks duration. A summary of the deployment schedule and measured parameters is shown in Table 1.2. A CTD survey, including surface and bottom nutrient and chlorophyll measurements, on a grid of 30 stations was completed at approximately monthly intervals at the times shown at the bottom of Table 1.2. These data are described elsewhere in this report.Nortek Vector Velocimeters (sites ADV1, ADV2, ADV3, and ADV4 in Figure 1.28) were deployed on the shoreward edge of the reefs in depths of 4-6m with Nortek Aquadopps (Acoustic Doppler Current Profilers) in the channels between the reefs (sites AQ1, AQ2 in Figure 1.28). Two multi-sensors were also deployed; one inside the lagoon and one further offshore (sites MS1 and MS2 respectively in Figure 1.28). MS1 was deployed in about 8m water depth with a Seabird SBE19plus measuring near bottom temperature, salinity, depth, PAR, oxygen and fluorescence. MS1 was also equipped with a Seabird SBE26 measuring waves and tides and an RDI ADCP measuring vertical profiles of mean currents. MS2 was deployed approximately 4km seawards of the reef line in 25m water depth and was equipped with a Seabird SBE19plus 15m above the bottom measuring the same parameters as MS1. Below the SBE19plus were four Seabird SBE37 Microcats measuring conductivity, temperature and depth at 5, 7.5, 10 and 12.5 m above the bottom. Also at MS2 was a Seabird

SBE26 measuring waves and tides. A Nortek AWAC with Acoustic Surface Tracking was deployed just seawards of the reef line (site AWAC in Figure 1.28) measuring wave height and direction and mean current profiles in 15m water depth. Finally two RDI ADCP's were deployed in the lagoon to the north and south of MS1 measuring mean current profiles at sites RDIN and RDIS in Figure 1.28.

An aim of the measurement program was to identify the role of waves and storm events in driving the circulation and exchange between the lagoon and offshore so, where possible, the instruments were set to resolve water motion associated with surface waves, requiring sampling rates of 1Hz or more. Table 1.3 summarises the instrument setup. The Vectors were set to measure 2048 samples at 1Hz every 2 hours. Cell size in Table 1.3 refers to the size of the depth bins used in the ADCP profiles. In addition to the estimated limits in battery power and memory usage bio-fouling is also a major problem in these shallow waters. To ensure the highest quality data the array was deployed for approximately 6 weeks and then recovered to download data, replace batteries and clean sensors and mooring frames. During the first deployment a number of instruments were buried in sand to varying degrees, though only one (ADV4) was completely buried. On all subsequent deployments the moorings were deployed on reef or seagrass beds to avoid burial. The data return is shown in Table 1.2. In summary, no data are available at ADV4 for deployments 1 and 2 and at ADV1 for deployments 3 and 4. At ADV2 data from deployments 1 and 4 have been discarded and at ADV3 data from deployment 1 have not been used. The pressure data from all the ADV sites during deployment 1 appears to be good, the pressure sensor continuing to measure the wave induced pressure even after it was buried. Data from AQ1 for deployment one were also suspect due to partial burial, and the ADCP at MS1 failed in deployment one.

Table 1.2. Deployment schedule according to site name (column 1), the instruments deployed at each site (column 2) and the parameters measured (column 3); *u,v,w* horizontal and vertical velocity components, *T* temperature, *S* salinity, chl-a chlorophyll, PAR Photsynthetically active radiation, *P* mean pressure, *Pw* wave resolving pressure.

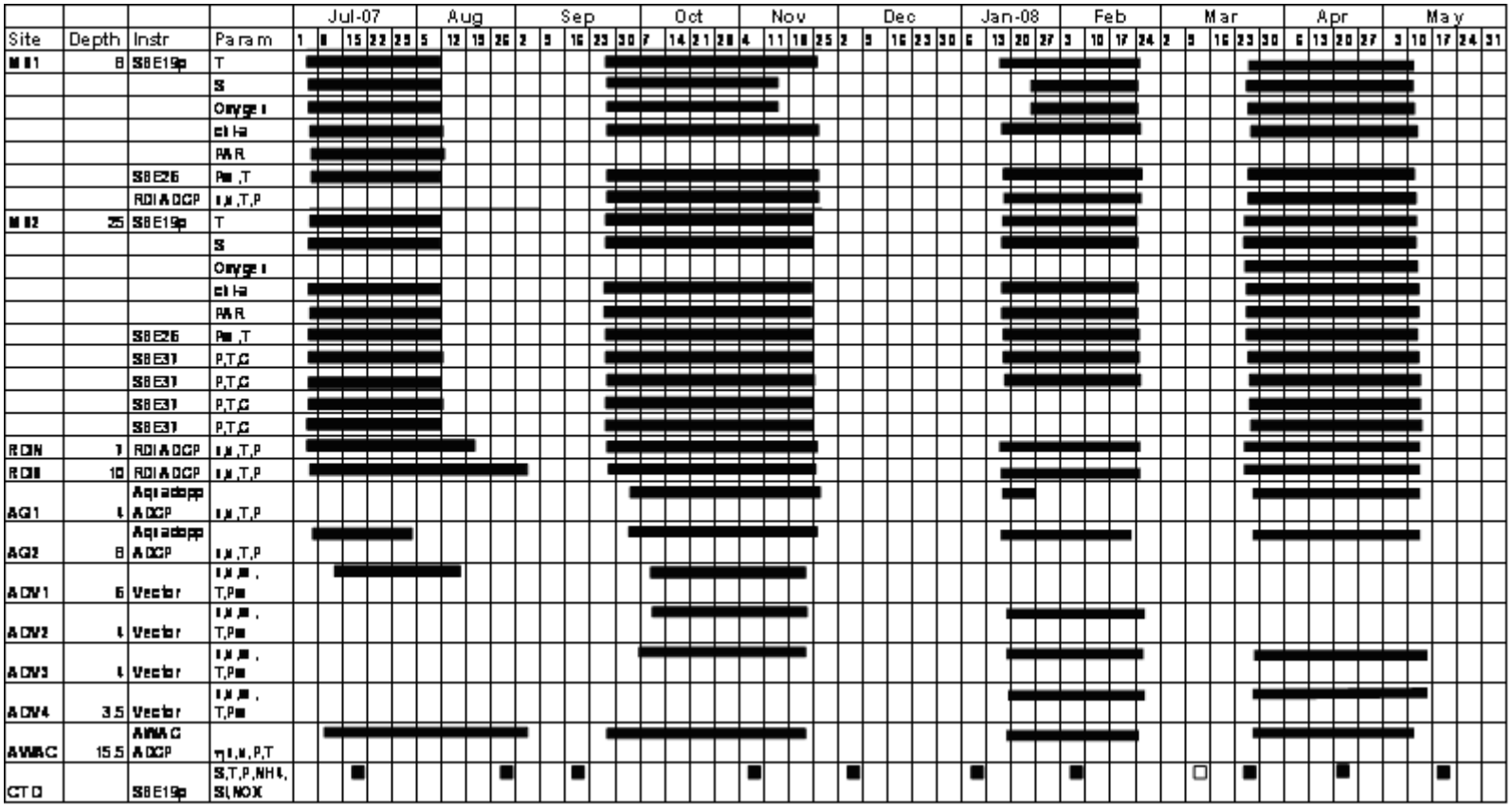

Table 1.3. Sampling parameters.

Site ID	Instrument	Sampling rate (Hz)	Burst length (s)	Measurement Interval (hours)	Cell size (m)
RDIN	RDI ADCP 300kHz	2	300	1	0.5
MS1	SBE26				
	Tides	4		0. 5	
	Waves	2	1200	6	
	RDI(600kHz)	2	300	1	0.5
RDIS	RDI ADCP 300kHz	2	300	1	0.5
MS2	SBE26				
	Tides	4		0.5	
	Waves	2	1200	6	
AQ1	Aquadopp 600kHz	6	1800	1	1
AQ2	Aquadopp 1MHz	6	600	1	0.5
ADV1	Vector	1	2048	2	
ADV2	Vector	1	2048	2	
ADV3	Vector	1	2048	2	
ADV4	Vector	1	2048	2	
AWAC	AWAC				
	Profile		600	1	0.5
	Waves	1	2048	2	

1.4.3 Results

In addition to the observations at the sites described in the previous section a permanent directional wave buoy is maintained off Rottnest Island about 40 km south west of the field site at 32°05’39’’S, 115°24’28’’E in a depth of 48m (see Figure 1.28). Data from the wave buoy for the duration of the field program are shown in Figure 1.29. The study site is exposed to long period (T ~ 12s) Southern Ocean swell with maximum wave heights peaking at over 5m in winter. The biggest storm events occurred during the first deployment with a couple during the second and fourth deployments. As the waves propagate towards the coast the wave height is reduced due to refraction and partial shadowing from Rottnest Island. Linear regression between the root-mean-square wave heights at the AWAC (*Hrms(AWAC))* and Rottnest Island (*Hrms(RI)*) gives

$$Hrms\,(AWAC\,) = .6\,Hrms\,(RI\,) \tag{1}$$

with a correlation r=0.93. A further reduction in root-mean-square wave height occurs between the AWAC and MS1 sites due to wave breaking over the reefs and bottom friction, the linear regression given by

$$Hrms\,(MS1) = .42\,Hrms\,(AWAC\,) \tag{2}$$

with r=0.95. In the remaining text, unless otherwise stated, *Hrms* refers to the root-mean-square wave height at the AWAC.

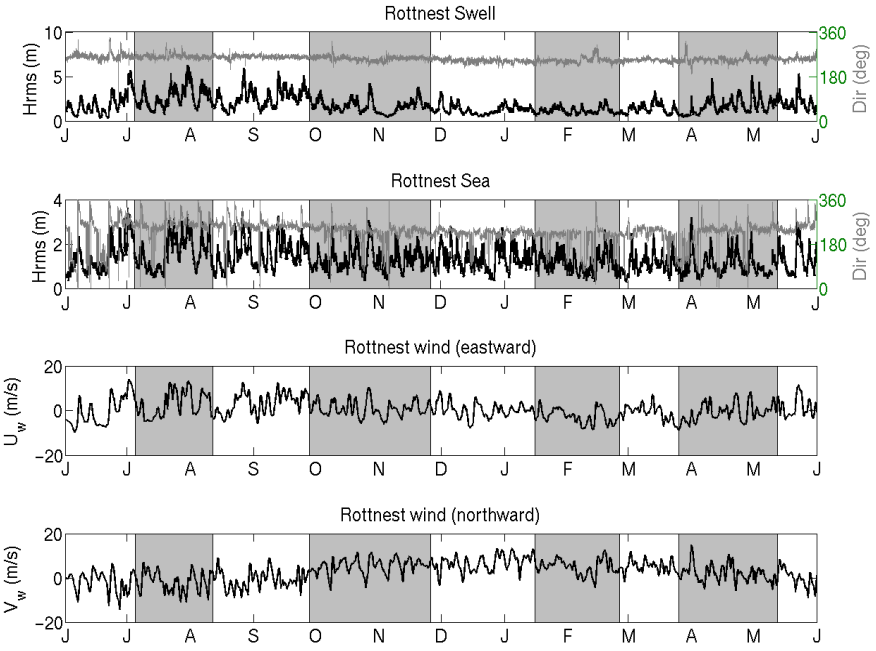

Figure 1.29. Rottnest wave and wind data. The grey shaded blocks mark the periods of the four deployments.

Previous studies in this region have concluded the nearshore alongshore currents are wind driven and the current speed is reasonably predicted using 2.5-3% of the wind speed (Feng et

al, 2006; Zaker et al, 2007). In Figure 1.30 the depth averaged alongshore currents at the AWAC from all four deployments are plotted against the alongshore wind.

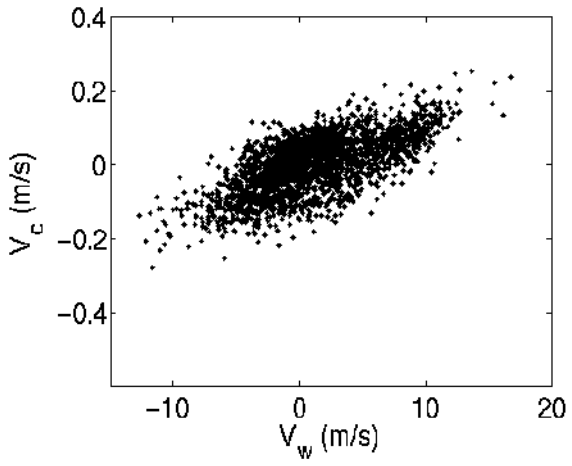

Figure 1.30. Depth averaged alongshore current (Vc) at the AWAC versus alongshore wind (Vw).

The alongshore currents are correlated with the alongshore wind, r=0.67, and the corresponding regression is given by,

$$V_c = -.01 + .01 V_w \tag{3}$$

where V_c is the alongshore depth averaged current at the AWAC and V_w is the alongshore wind. Shorewards of the reef line at RDIS there is considerably more scatter between the depth averaged alongshore currents and the alongshore wind as shown in Figure 1.31.

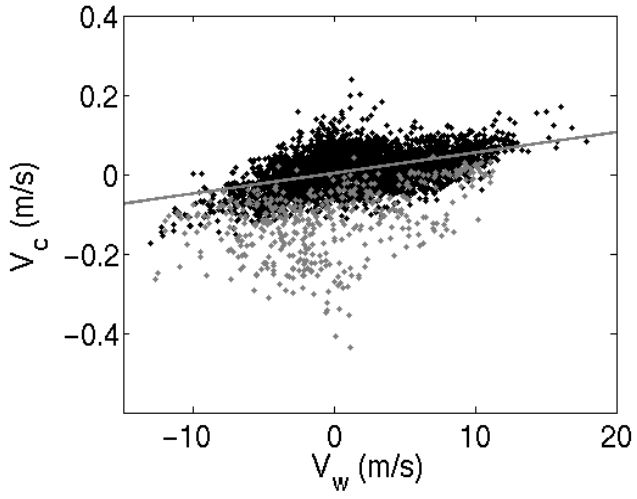

Figure 1.31. Depth averaged alongshore current (Vc) at RDIS versus alongshore wind (Vw). Black dots at times when Hrms <1.5m and grey dots when Hrms >1.5m.

The grey and black points in Figure 1.31 correspond to times when *Hrms* at the AWAC is greater than 1.5 m and less than 1.5 m respectively. The strongest currents are towards the

south when *Hrms* >1.5m, often occurring when the wind speed is small, and at times are opposed to the wind. After discarding data at times when *Hrms*>1.5m the correlation is 0.5 and the linear regression given by

$$V_c = .003 + .005 V_w \tag{4}$$

where V_c is the depth averaged alongshore current at RDIS.

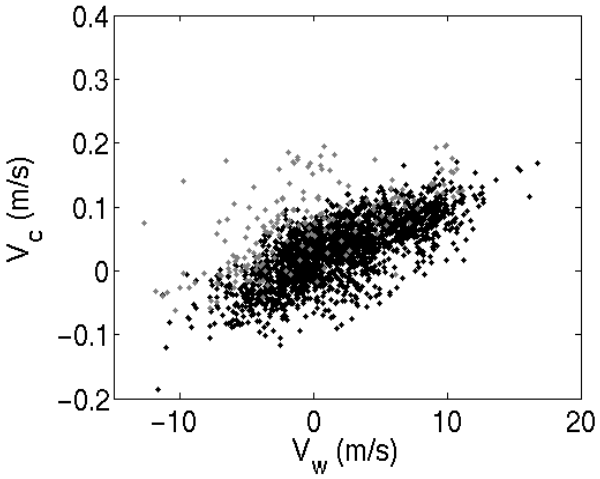

Figure 1.32. Depth averaged alongshore current (Vc) at RDIN versus alongshore wind (Vw). Black dots at times when Hrms <1.5m and grey dots when Hrms >1.5m.

Similarly, at RDIN the scatter between the depth averaged alongshore current and the alongshore wind, shown in Figure 1.32, is reduced by discarding data at times when *Hrms* >1.5m. In this case the correlation is 0.72 and the regression given by

$$V_c = .02 + .008 V_w \tag{5}$$

where V_c is the depth averaged alongshore current at RDIN. Using (4) and (5) the wind driven component of the alongshore currents can be subtracted from the depth averaged alongshore currents at RDIS and RDIN respectively. The resulting residual currents at RDIN and RDIS are plotted against *Hrms* for all four deployments in Figure 1.33a and Figure 1.33b respectively. During periods of low waves there is little correlation but when *Hrms* exceeds about 1.5m the correlation improves, with northward currents at RDIN and southward at RDIS. During deployment 1 RDIN was recovered earlier than RDIS, missing a storm event during which time RDIS recorded some of the strongest southward currents.

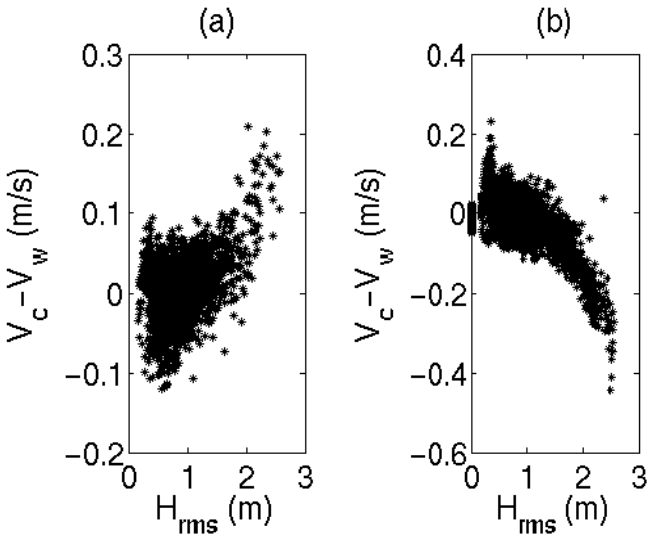

Figure 1.33. Depth averaged alongshore current (Vc) minus the wind forced component (Vw) at (a) RDIN and (b) RDIS plotted against Hrms at the AWAC from all four deployments.

ADCP's were located in channels between reefs at sites AQ1 and AQ2 (see Figure 1.28) where the mean wave-driven flows are offshore. At these sites a wind driven component was present in both the alongshore and cross-shore currents and was subtracted using a linear regression derived using data from periods of low waves as above. The residual cross-shore flows are shown in Figure 1.34 plotted against *Hrms* at the AWAC. At both sites offshore flows are associated with larger waves. At AQ2 strong offshore currents up to 0.5 m/s are associated with larger waves. Note that data at AQ1 for deployment one is not used due to the partial burial of the instrument frame.

At the reef sites where the four ADV instruments were deployed, the cross-reef flows are often shorewards, into the lagoon, during periods of high waves. There was little correlation with the cross-shore wind at these sites and we have not attempted to remove a wind forced component from the currents which are shown in Figure 1.35 plotted against *Hrms* at the AWAC.

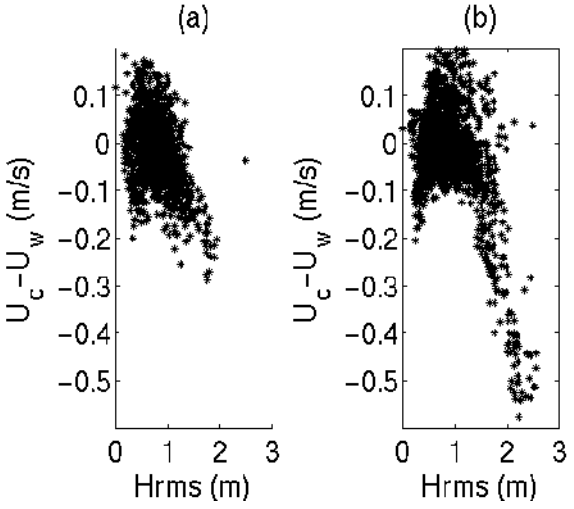

Figure 1.34. Depth averaged cross-shore currents (Uc) minus wind forced component (Uw) at (a) AQ1 and (b) AQ2 plotted against Hrms at the AWAC for all deployments.

After discarding data, as discussed in the previous section, positive cross-reef currents (directed into the lagoon) are associated with larger waves at all the ADV sites. At sites ADV3 and ADV4 the cross-reef currents are reasonably well correlated with wave height, even under quite small waves at ADV3. At ADV1 the currents are weaker and only start to show a correlation with wave height when *Hrms* >2m. At ADV2 the currents are also weak but are correlated with wave height when *Hrms*>1m.

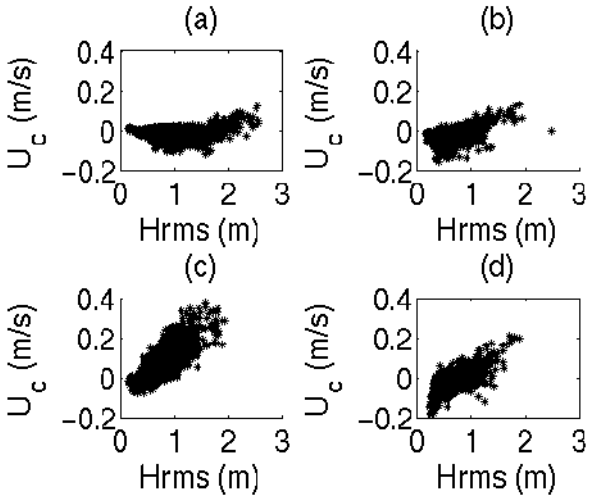

Figure 1.35. Cross-shore currents at sites ADV1,…,4 plotted against Hrms at the AWAC; (a) ADV1 (deployments 1 and 2 only); (b) ADV2 (deployments 2 and 3 only); (c) ADV3 (deployments 1, 2 and 3 only); (d) ADV4 (deployments 3 and 4 only).

During periods of high waves we also observe an increase in sea level shorewards of the reef line relative to offshore. Shown in Figure 1.36 is the difference in sea level between MS1 and MS2 plotted against *Hrms* at the AWAC showing a significant increase in mean sea level at MS1 relative to MS2 when *Hrms*>1.5 m.

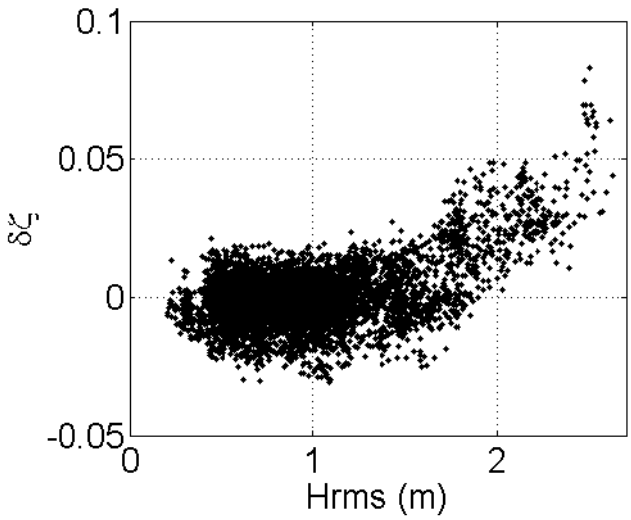

Figure 1.36. Difference in sea level δζ between MS1 and MS2, versus root-mean-square wave hieght at the AWAC.

The data presented here demonstrates that wave forcing becomes important in driving mean currents shorewards of the reef line when *Hrms* at the AWAC reaches about 1.5m. As discussed in the introduction, to force significant mean flows across the reefs the waves must be big enough to break causing a cross reef gradient in the radiation stress. A measure of depth-induced wave breaking is obtained by comparing root-mean-square wave height in front of the reefs (at the AWAC) with wave height at the back reef locations (at the ADV sites), as shown in Figure 1.37. The root-mean-square wave heights at the ADV sites were calculated from the frequency spectra of bottom pressure, converted to surface wave height using linear wave theory. For low waves the root-mean-square wave heights are similar at the AWAC and ADV sites. However, as the offshore wave height increases we begin to see a reduction in wave height at the ADV sites relative to the AWAC. The point at which the ADV observations begin to diverge varies for the different sites; at ADV3 the data diverge when *Hrms*>0.5m at the AWAC, while the other sites begin to deviate when *Hrms*>1.5m. The reduction in wave heights at the ADV sites reflects depth induced wave breaking over the reefs, and the onset of breaking at ADV3 at a lower wave height can be attributed to shallower water over the reef crest at ADV3. The earlier onset of breaking at ADV3 also accounts for the correlation between cross-reef current and quite small waves at ADV3 shown in Figure 1.35. Given the observations at RDIS and RDIN presented previously, the wave height seawards of the reef line needs to be greater than 1.5m before the effects of wave forcing are felt across the lagoon between the reefs and the shoreline.

1.4.4 Modelling

The numerical model XBeach has been use to simulate the depth-averaged wave-driven circulation (Roelvink et al, 2009). The wave field is obtained using a simplified time dependent wave action balance equation to give the directional distribution of the frequency

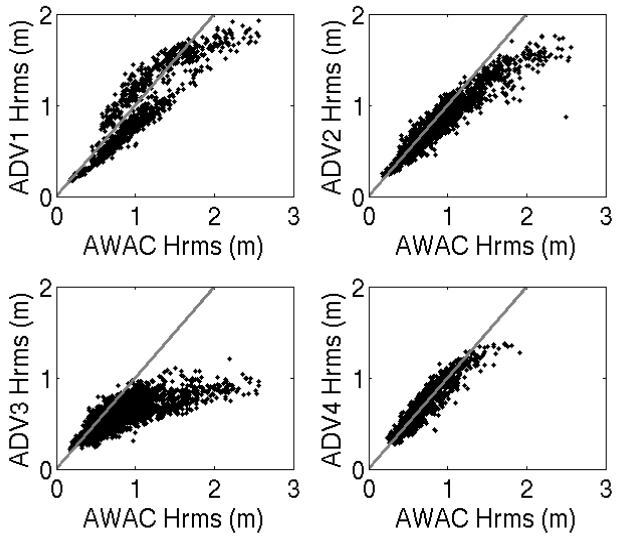

Figure 1.37. Root-mean-square wave heights at ADV1…4 versus Hrms at the AWAC for the four deployments. The straight line has a slope of one.

integrated wave action density (Holthuijsen et al, 1989). This time varying wave action balance includes refraction, shoaling, current refraction, bottom friction and wave breaking. The model forcing can accommodate non-stationary, time varying incident wave energy and the

corresponding bound long wave (van Dongeren et al, 2003), but in this study the model has been run in stationary mode, forced at the offshore boundary with observed *Hrms*, wave period and direction from the AWAC. In the current application the model domain is 269x440 cells and the grid size is 30x30 m. The wave model provides the spatial distribution of wave action, and therefore wave energy, which is then used to evaluate the radiation stress terms in the depth averaged, shallow water equations to obtain the mean flows. To account for higher bottom roughness over the reefs we introduced a depth dependent drag coefficient following Daily and Harleman (1966),

$$C_D = \frac{25g}{C^2} \tag{6}$$

where g is gravitational acceleration and C is given by,

$$C = \frac{h^{\alpha}}{0.02} \tag{7}$$

where h is the water depth and α=1/3.

In the absence of wind, gradients in the radiation stress provide the primary forcing. While the direct forcing due to depth-induced wave breaking is confined to the relatively small and patchy reefs the effects on the circulation are seen across the model domain. In Figure 1.38 the eastward and northward velocities are plotted for the case where wave forcing at the offshore boundary is given by *Hrms*=2.2m, *T*=14s and direction=266^{o}. In the vicinity of the reefs the circulation is spatially variable with onshore flow over the reef crests (sites ADV1…4) and offshore flow in the channels (sites AQ1 and AQ2). At RDIS the flow is southward and at RDIN the flow is generally weaker and towards the northeast, all of which is in general agreement with the observations. The corresponding sea level is shown in Figure 1.39.

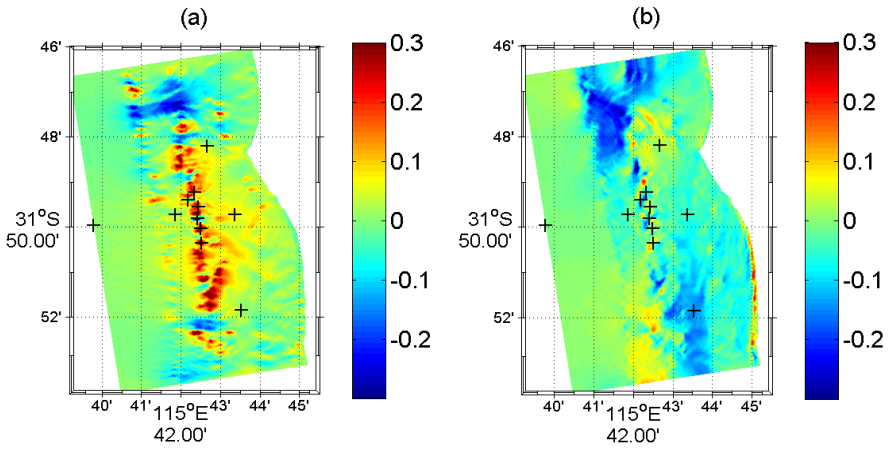

Figure 1.38. (a) Eastward, (b)Northward velocity components from XBeach with offshore wave forcing of Hrms=2.2m, T=14s and direction=266o. + indicate instrument locations (see Figure 1.28 for site names)

The onshore flow over the reefs causes an increase in mean sea level between the reefs and shoreline which in turn produces alongshore pressure gradients which drive the southward flow at RDIS and northward flow at RDIN. In this case (*Hrms*=2.2m) the maximum lagoon setup is

approaching 20cm and about 8cm at the MS1 site compared with about 4 cm in the observations for the same wave height from Figure 1.36. The corresponding velocity vectors in the vicinity of the reefs are shown in Figure 1.40 showing the spatial variability with local recirculation around the reefs and general southerly flow between the reefs and shore.

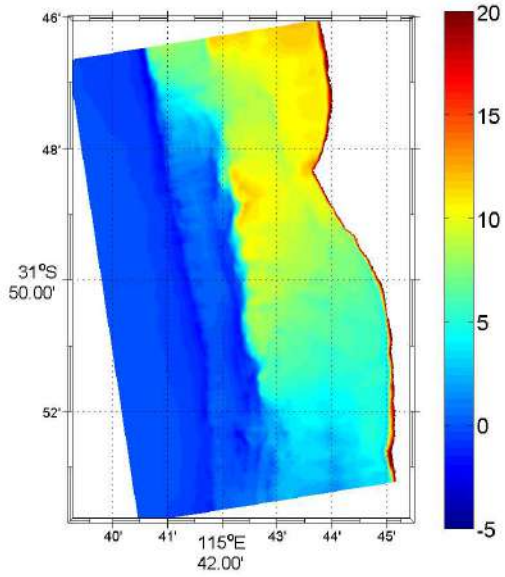

Figure 1.39. Mean sea surface elevation from XBeach with the same offshore wave forcing as Figure 1.38.

Qualitatively the model results are similar to the observations; a more quantitative assessment is made by comparing modelled and observed currents at the measurement sites. To investigate the wave-driven currents we focus on the high wave events, most of which occurred during deployment one.

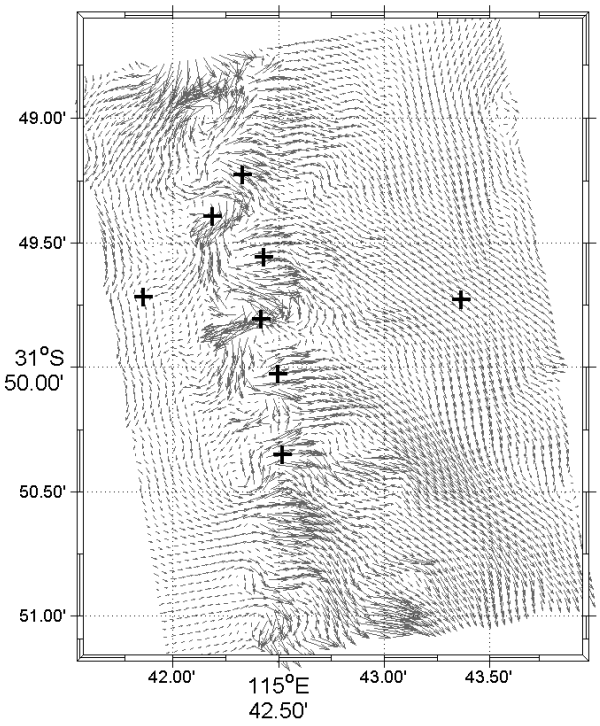

Figure 1.40. Velocity vectors from XBeach in the vicinity of the reefs, with the same offshore wave forcing as Figure 1.40.

In Figure 1.41 model data comparisons for deployment 1 are shown at RDIS, RDIN, and AQ2 (data at other sites during deployment one are not usable for reasons discussed previously). The selected period covers several high wave events. The ADCP at RDIS was left in the water for considerably longer than the other instruments and captured a bigger wave event on August 26-27. The model does quite poorly predicting wave heights at MS1 during periods of low waves, being almost constant with offshore wave height. This might suggest the model wave height at MS1 is depth-limited due to too much breaking over the reefs, although attempts to reduce the breaking led to poorer model/data comparisons elsewhere. At RDIS and RDIN the model and data are in good agreement though the modeled currents at RDIN are relatively weak. At AQ2 the model tends to overestimate the offshore flow when the waves are low, but during the high wave event fromJuly 30 to August 1, the agreement is good. The strongest currents were observed at RDIS and AQ2; at both sites the model agrees well with the observations.

Model data comparisons for deployment 2 at three ADV sites (ADV1, ADV2, and ADV 3) and AQ1 are shown in Figure 1.42. At ADV3 the model does exceptionally well, but not so good at the other sites. At ADV2 there is very good correlation between model and data, but the model consistently overestimates the currents by about 0.1m/s. This discrepancy remains unexplained.

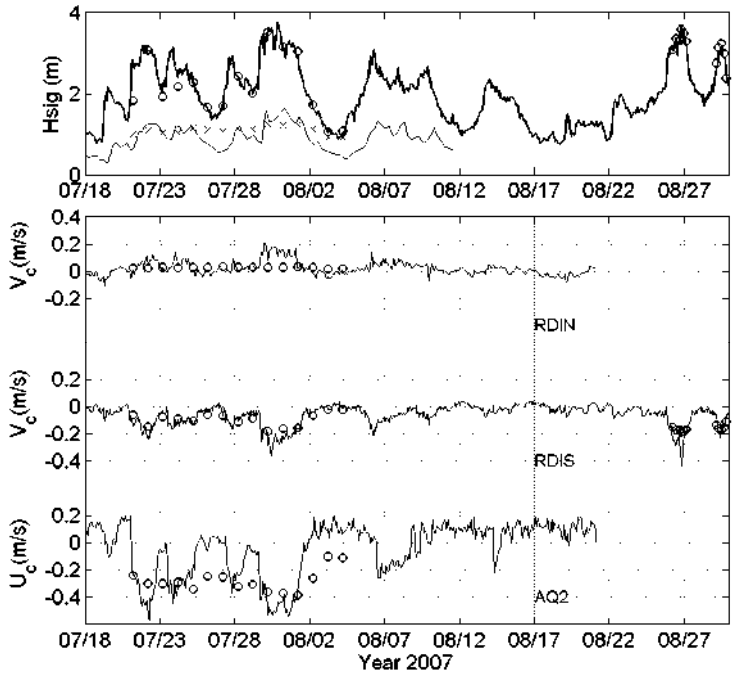

Figure 1.41. Model (circles and crosses) and observations from deployment one. At top significant wave height (Hsig) at the AWAC and MS1 sites, in bold and thin lines respectively. Below are the corresponding alongshore currents (Vc) at RDIN, RDIS and cross-shore currents (U_c) at AQ2.

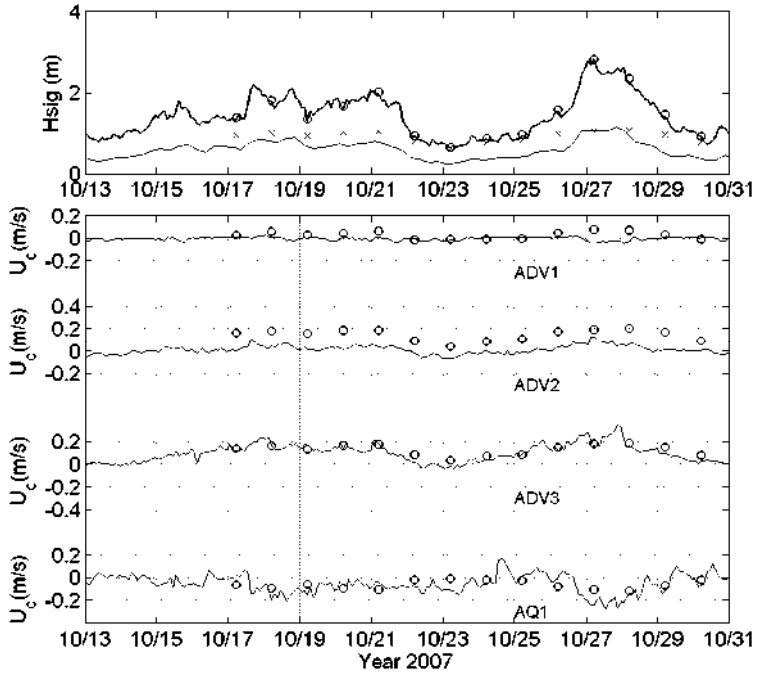

Figure 1.42. Model (circles and crosses) and observations from deployment two. At top significant wave height (Hsig) at the AWAC and MS1 sites, in bold and thin lines respectively. Below are the corresponding cross-shore currents (Uc) at sites ADV1, ADV2, ADV3 and A.

1.4.5 Discussion

The temperate reefs considered in this study are patchy, narrow with little or no reef flat, deep such that only larger waves break over them, and separated from land by a deep (~10m) and wide (~3km) lagoon. In comparison coral reefs are often more continuous, have wide reef flats, the reef crest is usually very shallow so that even small waves break, and the lagoons are often quite shallow. In both cases high dissipation over the reefs causes locally large gradients in radiation stress which can drive strong currents in the direction of wave propagation. Away from the reefs the dissipation is low and the radiation stress gradients are no longer sufficient to drive the flow and, in the absence of any other forcing, continuity constraints cause the pressure field to adjust to accommodate the flow across the reefs. Analytic solutions reported by Symonds et al (1995) and Gourlay (1996a,b) show how the balance between the radiation stress gradients forcing the cross reef current and the corresponding adjustment in the pressure field vary with reef geometry and wave forcing over an idealised one dimensional reef. In the two dimensional case the pressure field must also adjust to accommodate the alongshore flow (Lowe et al, 2009) as shown in Figure 1.39 where the north-south pressure gradient at the RDIS site is responsible for the observed southerly flow. Similarly a south-north pressure gradient drives a northerly flow at RDIN. Through this adjustment of the pressure field the effect of wave forcing due to depth-induced breaking over the very patchy reefs, with relatively small areal extent, is felt across the lagoon several kilometers removed from the reefs. In Figure 1.40 it is also apparent that there is considerable local recirculation in the immediate vicinity of the reefs. The high spatial variability associated with the local recirculation around the reefs might explain some of the discrepancies between model and data. Zaker at al (2002) modeled the circulation in a region just north of our study site and concluded that wind forcing was dominant through most of the year. The results presented here show, during large wave events ($Hrms$>1.5m), wave forcing dominates over local wind producing spatially variable currents with onshore flow over the reefs, offshore flow between the reefs and alongshore flow in the lagoon behind the reefs.

1.5 Acknowledgements

The authors would like to thank the following for their invaluable support in all field operations; Stelios Kondylas, Jim Greenwood, James McLaughlin, Martin Lowrey, Ryan Downey, Andy Limbourne, Phil Adams, Ted Wassenberg, Ian McLeod and Quinton Dell. We also thank iVEC (http://www.ivec.org/) for providing supercomputing capacity. This work was supported with funding through the Western Australian Marine Science Institution.

1.6 References

Atkinson, M.J., and Bilger, R.W. (1992). Effects of water velocity on phosphate uptake in coral reef-flat communities, *Limnol. Oceanogr*., 37, 273-279.

Atkinson, M.J., Kotler, E., and Newton, P. (1994). Effects of water velocity on respiration, calcification and ammonium uptake of a porites compressa community, *Pacific Science*, 48, 296-303.

Bilger, R.W., and Atkinson, M.J. (1992). Anomolous mass transfer of phosphate on coral reef flats, *Limnol. Oceanogr*., 37, 261-272.

Bilgili, A., Proehl, J.A., Lynch, D.R, Smith, K.W., and Swift, R.M. (2005). Estuary/ocean exchange and tidal mixing in a Gulf of Maine Estuary: A Lagrangian modeling study, *Estuarine, Coastal and Shelf Science* 65, 607-624.

Bleck, R., and Boudra, D. (1981). Initial testing of a numerical ocean circulation model using a hybrid (quasi-isopycnic) vertical coordinate. *J. Phys. Oceanogr.*, 11, 755-770.

Bleck, R., and Benjamin S. (1993). Regional weather prediction with a model combining terrain-following and isentropic coordinates. Part I: Model description. *Mon. Wea. Rev*., 121, 1770-1785.

Bowen, A.J. (1969). The generation of longshore currents on a plane beach, *J. Mar. Res*., 27(2), 206-215.

Bowen, A.J., Inman, D.I., and Simmons, V.P. (1968), Wave set-down and set-up, *J. Geophys. Res*., 73(8), 2569-2577.

Callaghan, D.P., Nielsen, P., Cartwright, N., Gourlay, M.R., and Baldock, T.E. (2006). Atoll lagoon flushing forced by waves, *Coastal Eng.*, 53, 691-704.

Caputi, N., Penn, J.W., Joll, L.M., and Chubb, C.F. (1998). Stock-recruitment-environment relationships for invertebrate species of Western Australia. In Jamieson, G.S. and Campbell A. Proceedings of the North Pacific Symposium on Invertebrate Stock Assessment and Management. *Canadian Special Publication on Fisheries and Aquatic Sciences* 125. pp 247-255.

Cowen, R., Paris, C., and Srinivasan, A. (2006). Scaling of connectivity in marine populations. *SCIENCE* 311(5760), 522-527.

Daily, J.W., and Harleman, D.R.F. (1966). *Fluid Dynamics*. Addison-Wesley, Reading, MA, pp. 297–298.

Domingues, C.M., Tomczak, M., Wijffels, S., Beggs, H., and Church, J.A. (1999). Direct observations of the Leeuwin Current at 22 °S (Augast 1994 - June 1996). *CSIRO Marine Laboratories Report* 235.

Domingues, C.M., Maltrud, M.E., Wijffels, S.E., Church, J.A., and Tomczak, M. (2007). Simulated Lagrangian pathways between the Leeuwin Current system and the upper-ocean circulation of the southeast Indian Ocean, *Deep-Sea Research II*, 54, 797-817.

Fandry, C.B., Slawinski, D., and Pender, L. (2006). Two-Rocks moorings data report. *CSIRO Marine and Atmospheric Research Paper* 005, January 2006, 26pp.

Fang, F., and Morrow, R. (2003). Evolution, movement and decay of warm-core Leeuwin Current eddies. *Deep-Sea Research II* 50, 2245-2261.

Feng, M., Craig, P., Fandry, C., Greenwood, J., Margvelashvili, N., Pearce, A., and Symonds, G. (2006). Physical Oceanography of the South Western Australian Shelf, pp 11-54. In: Keesing, J.K., Heine, J.N., Babcock, R.C., Craig, P.D., and Koslow, J.A.. *Strategic Research Fund for the Marine Environment Final Report, Volume 2: the SRFME core projects* 274p. Strategic Research Fund for the Marine Environment, CSIRO, Australia.

Feng, M., Meyers, G., Pearce, A., and Wijffels, S. (2003). Annual and interannual variations of the Leeuwin Current at 32S. *Journal of Geophysical Research* 108 (C11), 3355, doi:10.1029/2002JC0001763.

Feng, M., Waite, A., and Thompson, P.A. (2009). Climate variability and ocean production in the Leeuwin Current system off the west coast of Western Australia. *Journal of the Royal Society of Western Australia* 92, 67-81.

Feng, M., Wijffels, W., Godfrey, S., and Meyers, G. (2005). Do eddies play a role in the Momentum Balance of the Leeuwin Current? *Journal of Physical Oceanography* 35, 964-975.

Flather, R.A. (1976). A tidal model of the north-west European continental shelf, *Memoires dela Societe Royale des Sciences de Liege* 6 (10), pp. 141-164.

Gourlay, M.R. (1996a). Wave set-up on coral reefs. 1. Set-up and wave generated flow on an idealized two dimensional horizontal reef. *Coastal Eng*., 27, 161-193.

Gourlay, M.R. (1996b). Wave set-up on coral reefs. 2. Set-up on reefs with various profiles. *Coastal Eng*., 28, 17-55.

Haidvogel, D.B., Arango, H., Hedstrom, K., Beckmann, A., Malanotte-Rizzoli, P., Shchepetkin, A.F. (2000). Model evaluation experiments in the North Atlantic Basin: simulations in non-linear terrain following coordinates. *Dynamics of Atmospheres and Oceans* 32, 239-281.

Harris, D.C., Joll, L.M. and Watson, R.A. (1999). The Western Australian scallop industry. *Fisheries Research Report, Fisheries Western Australia* No 114 p1-30.

Hannah, C. G., Naimie, C. E., Loder, J. W., and Werner, F.E. (1998). Upper-ocean transport mechanisms from the Gulf of Maine to Georges Bank, with implications for Calanus supply, *Continental Shelf Research* 17, 1887-1911.

Hearn, C.J., Atkinson, M.J. and Falter, J.L. (2001). A physical derivation of nutrient-uptake rates in coral reefs: effects of roughness and waves. *Coral Reefs*, doi 10.1007/s00338-001-0185-6.

Holthuijsen, L.H., Booij, N., and Herbers, T.H.C. (1989). A prediction model for stationary, short-crested waves in shallow water with ambient currents, *Coastal Eng*., 13, 23-54.

Jenkins, A. D. (1987), A Lagrangian model for wind- and wave-induced near-surface currents. *Coastal Engineering*, 11, 513-526.

Joll, L.M., and Caputi, N. (1995) geographic variation in the reproductive cycle of the saucer scallop, *Amusium balloti* (Bernardi, 1861) (Mollusca:Pectinidae), along the Western Australian coast. *Marine and Freshwater Research* 46: 779-92.

Kraines, S.B., Yanagi, T., Isobe, M., and Komiyama, H. (1998). Wind-wave-driven circulation on the Coral reef at Bora Bay. Miyako Island, *Coral Reefs*, 17, 133-143.

Kraines, S.B., Suzuki, A., Yanagi, T., Isobe, M., Guo, X., and Komiyama, H. (1999). Rapid water exchange between the lagoon and the open ocean at Majuro Atoll due to wind, waves and tide. *J. Geophys. Res*., 104(C7), 15,635-15,653.

Longuet-Higgins, M.S. (1970a). Longshore Currents Generated by Obliquely Incident Sea Waves, 1. *J. Geophys. Res*., 75(33), 6778-6789.

Longuet-Higgins, M.S. (1970b). Longshore Currents Generated by Obliquely Incident Sea Waves, 2. *J. Geophys. Res*., 75(33), 6790-6801.

Longuet-Higgins, M.S., and Stewart, R.W. (1964). Radiation stresses in water waves; a physical discussion, with applications. *Deep Sea Res*., 11, 529-562.

Lowe, R.J., Falter, J.L., Monismith, S.G., and Atkinson, M.J. (2009). Wave-driven circulation of a coastal reef-lagoon system. *J. Phys. Oceanogr*., 39, 873-893.

Marchesiello, P., McWilliams, J.C., Shchepetkin, A. (2001). Open boundary conditions for long-term integration of regional oceanic models. *Ocean Modelling* 3, 1-20.

Marinone, S. G. (2006). A numerical simulation of the two- and three-dimensional Lagrangian circulation in the northern Gulf of California. *Estuarine, Coastal and Shelf Science* 68, 93-100.

Mitarai, S., Siegel, D.A. and Winters, K.B. (2008): A numerical study of stochastic larval settlement in the California Current system. *Journal of Marine Systems* 69, 295–309.

Monismith, S.G. (2007). Hydrodynamics of coral reefs. *Ann Rev. Fluid Mech*, 39, 37-55.

Monismith S.G. and Fong, D.A. (2004): A note on the potential transport of scalars and organisms by surface waves. *Limnology and Oceanography* 49, 1214-1217.

Mulligan, R.P., Hat, A.E., and Bowen, A.J. (2008). Wave-driven circulation in a coastal bay during the landfall of a hurricane. *J. Geophys. Res*., 113, C05026, doi: 10.1029/2007JC004500.

Murphy, E. J., Thorpe, S.E., Watkins, J.L. and Hewitt, R. (2004). Modeling the krill transport pathways in the Scotia Sea: spatial and environmental connections generating the seasonal distribution of krill. *Deep-Sea Research II* 51, 1435–1456.

Ommundsen, A. (2002). Models of cross shelf transport introduced by the Lofoten Maelstrom. *Continental Shelf Research* 22, 93–113.

Oke, P.R., Brassington, G.B., Griffin, D.A. and Schiller, A. (2008). The Bluelink Ocean Data Assimilation System (BODAS). *Ocean Modelling*, 20, 46-70, doi:10.1016/j.ocemod.2007.11.002.

Parslow J.S. and Gabric, A.J. (1989). Advection, Dispersal and Plankton Patchiness on the Great Barrier Reef. *Aust. J. Mar. Freshwater Res*. 40, 403-19.

Pattiaratchi, C., Imberger, J., Zaker, N., and Svenson, T. (1995). Perth Coastal Waters Study, Project P2: Physical Measurements. *Centre for Water Research Report* WP 958 CP, University of Western Australia.

Pearce, A.F., Feng, M., Slawinski, D., and Hutchins, B. (2009, in prep). Modelling the transport of tropical fish larvae in the Leeuwin Current. To be submitted to *Continental Shelf Research*.

Ribergaard, M., Pedersen, S.A., Adlandsvik, B., and Kliem, N. (2004). Modelling the ocean circulation on the West Greenland shelf with special emphasis on northern shrimp recruitment, *Continental Shelf Research* 24, 1505–1519.

Roberts, H.H., and Suhayda, J.N. (1983). Wave-Current Interactions on a shallow reef (Nicaragua, Central America). *Coral Reefs*, 1, 209-214.

Roelvink, D., Reniers, A., Van Dongeren, A., Van Thiel de Vries, J., McCall, R., and Lescinski, J. (2009). Modelling storm impacts on beaches, dunes and barrier islands. *Coastal Eng*., 56, 133-1152.

Rose, R.A., Campbell, G.R. and Saunders, S.G. (1988). Larval development of the scallop *Amusium balloti* (Bernardi)(Mollusca:Pectinidae). *Australian Journal of Marine and Freshwater Research* 39: 153-160.

Schiller, A., Oke, P.R., Brassington, G.B., Entel, M., Fiedler, R., Griffin, D.A. and Mansbridge, J. (2008). Eddy-resolving ocean circulation in the Asian-Australian region inferred from an ocean reanalysis effort. *Progress in Oceanography*, doi:10.1016/j.pocean.2008.01.003.

Symonds, G., Black, K.P. and Young, I.R. (1995). Wave driven flow over shallow reefs. *J. Geophys. Res.* 100(C2), 2639-2648.

Tartinville, B., and Rancher, J. (2000). Wave induced flow over Mururoa Atoll reef, J. *Coastal Res*., 16(3), 776-781.

Thornton, E.B., and Guza, R.T. (1986). Surf Zone Longshore Currents and Random Waves: Field Data and Models. *J. Phys. Oceanogr*., 16,1165-1178.

Thorpe, S. E., Heywood, K.J., Stevens, D.P. and Brandon, M.A. (2004). Tracking passive drifters in a high resolution ocean model: implications for interannual variability of larval krill transport to South Georgia. *Deep-Sea Research I* 51, 909–920.

Tolman, H. L., Balasubramaniyan, B., Burroughs, L.D., Chalikov, D.V., Chao, Y.Y., Chen, H.S. and Gerald, V.M. (2002). Development and implementation of wind generated ocean surface wave models at NCEP. *Weather and Forecasting*, 17, 311-333.

Van Dongeren, A., Reniers, A., Battjes, J., and Svendsen, I. (2003). Numerical modelling of infragravity wave response during DELILAH, *J. Geophys. Res*., 108(C9), 3288 doi:10.1029/2002JC001332.

Xue, H., Incze, L., Xu, D., Wolff, N., and Pettigrew, N. (2008). Connectivity of lobster populations in the coastal Gulf of Maine Part I: Circulation and larval transport potential. *Ecological Modelling* 210, 193-211.

Zaker, N.H., Imberger,J., and Pattiaratchi, C. (2002). Numerical simulation of a coastal boundary layer off Perth, Western Australia, *J. Coastal Res*., 18(3), 470-485.

Zaker, N.H., Imberger,J., and Pattiaratchi, C. (2007). Dynamics of the coastal boundary layer off Perth, Western Australia. *J. Coastal Res.*, 23(5), 1112-1130.

2. COUPLED HYDRODYNAMIC AND BIOGEOCHEMICAL MODELS

Jim Greenwood, Liejun Zhong, Peter Craig, Ming Feng and Karen Wild-Allen

CSIRO Marine and Atmospheric Research

Objective 2: Coupled hydrodynamic and biogeochemical models and a quantitative nutrient budget for coastal waters at shelf and lagoon scales.

2.1 Shelf-scale

2.1.1 Introduction to shelf-scale biogeochemical modelling

The seasonal dynamic of chlorophyll *a* on the continental shelf along the south west WA coast is characterised by a surface minimum during the summer and a surface maximum during the winter, which coincides with a peak in pelagic primary production (Koslow et al. 2008), and a peak in zooplankton biomass and grazing (Koslow, pers. com.). The lack of strong wind-driven upwelling along this coast severely limits nitrogen in the pelagic ecosystem, accounting for the low summer primary production on the shelf. There have been various suggestions to explain the cause of the shelf-wide winter increase in chlorophyll *a* (Lourey et al. 2006, Koslow et al. 2008, Thompson et al. 2011).

The work presented in this section is designed to improve understanding of the shelf biogeochemical dynamics, and quantify the fluxes of nitrogen on and off the shelf that, in turn, define the observed patterns of primary production and chlorophyll biomass. The results from a number of different model experiments are described. Collectively, they provide valuable new information about the influence of upwelling, mesocale eddies and convective mixing on biological production. The work also highlights the importance of the recycling of nutrients on the shelf, and introduces a new hypothesis about the role of waves in mediating the release of nutrients from the shelf sediment.

2.1.2 Background/Settings

The dynamics of the seasonal evolution of chlorophyll *a* at the continental shelf break around 32 degrees south has been investigated using a one-dimensional numerical BGC model. The results show that a combination of vertical mixing associated with the Leeuwin Current and surface cooling during the winter months is responsible for the wintertime increase in chlorophyll a concentration at the shelf break (Greenwood and Soetaert, 2008). In addition, variation in the timing and magnitude of the winter increase in chlorophyll is shown, for the first time, to relate to the strength of the Leeuwin Current (Figure 2.1). It is important to establish how these shelf-break processes relate to the seasonal chlorophyll dynamics on the

mid- and inner-shelf. This challenge is taken up in Section 2.1.4 by using a three-dimensional model to try and simulate the seasonal shelf chlorophyll dynamics.

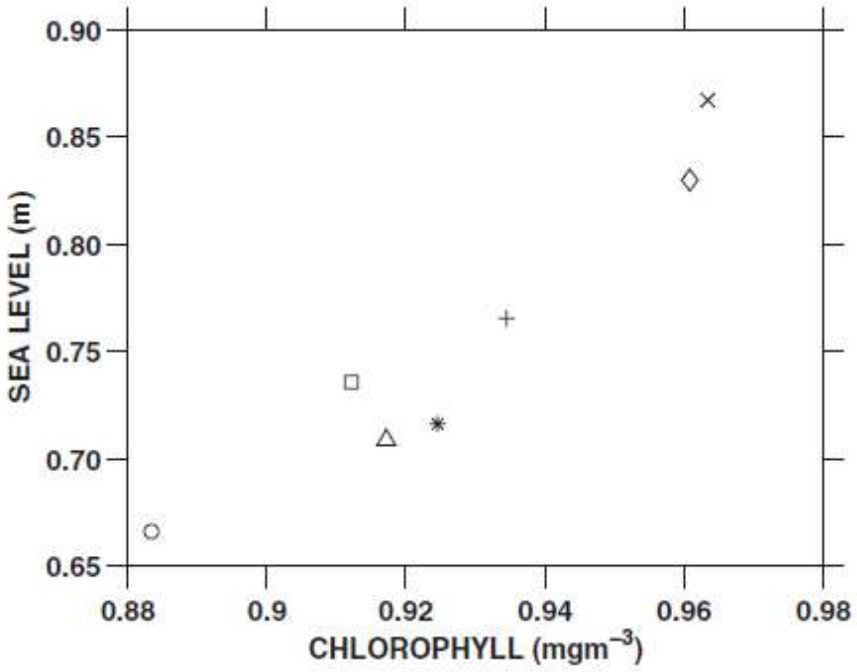

Figure 2.1. Increase in the magnitude of the autumn chlorophyll a signal in the Leeuwin Current at 32S between 1998 and 2005 in response to increased Leeuwin Current strength (indicated by Fremantle sea level). Reproduced from Greenwood and Soetaert (2008).

A nitrogen budget has also been constructed for the Western Australian shelf from Shark Bay to Cape Leeuwin based on a range of observations throughout the region (Feng and Wild-Allen, 2010) (Figure 2.2). The budget has provided some important basic findings. The budget shows that terrestrial and atmospheric inputs to the continental shelf off western WA are small (<1%) compared to preliminary estimates of nitrogen derived from Leeuwin Current advection and eddy activity (8%) and seasonal upwelling along the shelf (7%). By closure, the budget suggests that 84% of primary production is recycled on the shelf, suggesting that even considering the uncertainties in the flux estimates, the continental shelf off the west coast of WA is primarily a recycling system. Elsewhere in the world similarly narrow shelves are typically export systems, while this preliminary budget suggested that just 7% of the shelf productivity off WA was transported offshore and 5% exported to the deep ocean. The importance of the sediment nutrient flux to the overall shelf nutrient budget suggests that it plays a leading role in fuelling the phytoplankton production on the shelf. This implies that production may peak in the winter in response to a peak in the sediment nutrient flux. In Section 2.1.3, a mechanism is proposed to support this hypothesis. The idea is further tested in the context of a three-dimensional model in Section 2.1.4.

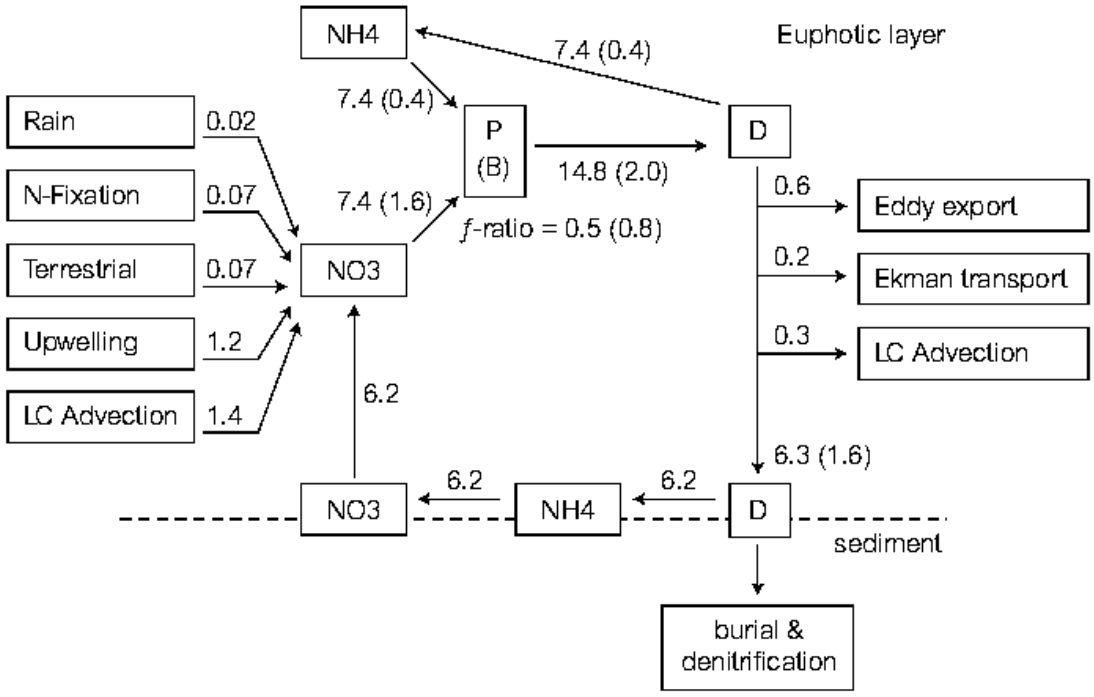

Figure 2.2. Preliminary shelf nitrogen budget derived from observations (unit: gN $m^{-2}y^{-1}$) (reproduced from Feng & Wild-Allen, 2010). P denotes pelagic production and the contributions from benthic production (B) are given in brackets. D denotes organic detritus.

2.1.3 A 1-D shelf model to test seasonal variation in the sediment nutrient flux

The flux of nutrients from shelf sediments has been identified as a major component of the shelf nutrient budget (Figure 2.2). The sediment nutrient flux is likely to vary seasonally (e.g. as a result of changes in temperature or hydrodynamic forcing) and may explain in part the seasonal pattern of plankton in shelf waters. The relative influence of temperature and passing surface-waves on the seasonality of this flux is examined here with the use of a one-dimensional coupled physical biogeochemical model.

The mineralisation rate, and the flux of nutrients from shelf sediments to the overlying water column, is strongly affected by the circulation of pore water, which transports substrates and reactive solutes to and from microorganisms that are attached to the sand grains. Pore-water circulation within permeable sediments is known to be enhanced by the passage of surface gravity waves over a seabed, especially when it is rippled (Webb and Theodor, 1968; Riedl *et al.*, 1972; Webster and Taylor, 1992; Webster, 2003). An increase in wave energy can therefore increase the mineralisation of organic matter (Shum and Sundby, 1996), releasing dissolved nutrients and stimulating enhanced algal production (Marinelli *et al.*, 1998). The southwest WA shelf is covered in coarse-grained, highly permeable, sandy sediment that is strongly rippled making it highly susceptible to hydrodynamic forcing associated with surface waves. We explore whether the flux of dissolved nitrogen from the sediment, and pelagic algal production, are impacted by changes in the surface wave conditions. Evidence presented here in support of this hypothesis is based on the analysis of seasonal and inter-annual variations in chlorophyll *a* and wave height on the inner shelf, and results from a 1-D model (Greenwood, 2010).

Chlorophyll *a* and wave height display similar seasonal variation, and the monthly averages of wave height and chlorophyll *a* are strongly correlated (n=84; r=0.8; p<0.001) (Figure 2.3A). This high correlation is partly due to the similarity in the phase of the seasonal cycle of the two variables. Accordingly, when the data is filtered to remove the seasonal correlation, the strength of the correlation is reduced. Even so, a linear relationship between waves and chlorophyll *a* remains statistically significant (n=84; r=0.42; p<0.001), with more than 70% of the positive (negative) chlorophyll anomalies above (below) 0.1 mg Chl*a* m^{-3} associated with positive (negative) wave height anomalies (Figure 2.3B).

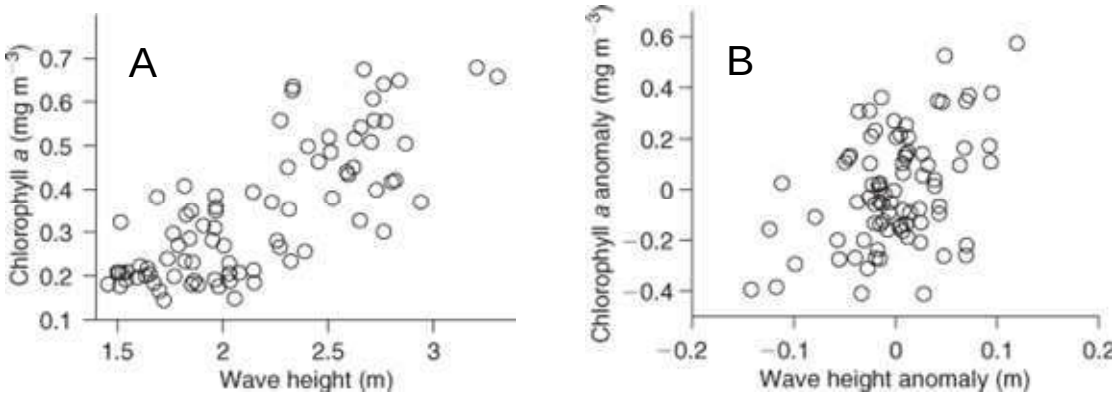

Figure 2.3. Comparison of monthly averages (A) and monthly anomalies (B) of chlorophyll and wave height. Reproduced from Greenwood, 2010.

The 1-D model used here considers aspects of water column and sediment nitrogen cycling (see Greenwood, 2010 for full details). Various temperature and wave-dependent parameterisations of the sediment mineralisation rate have been tested with the model. Only those which included wave-forcing were able to reproduce the correct seasonal and inter-annual variations in water-column chlorophyll (Greenwood, 2010). The best results were obtained when the sediment mineralisation rate was parameterised as the square of the wave-height (Figure 2.4). This result is consistent with theory on the variation in pore-water flow with changing wave height for rippled seabeds (Shum, 1993).

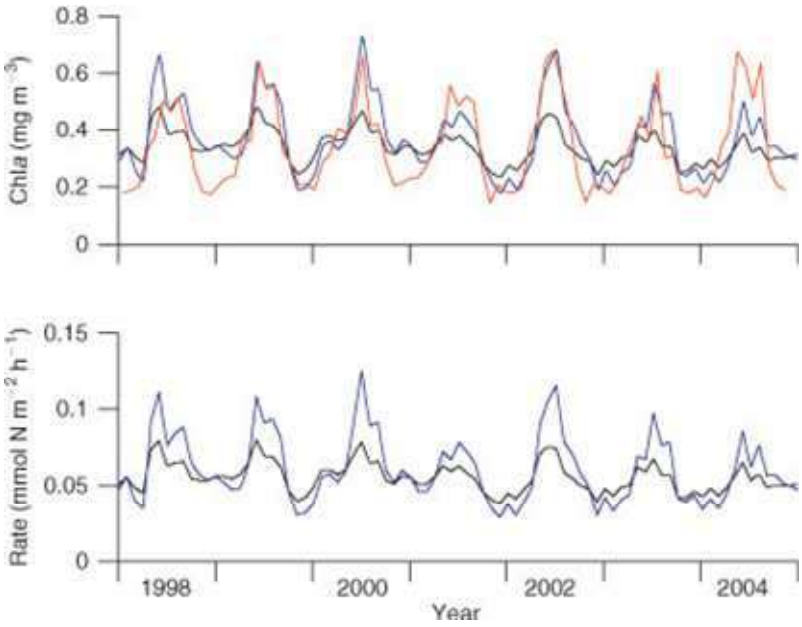

Figure 2.4. Comparison between satellite (red line) and model simulated surface chlorophyll when sediment mineralisation is parameterised in the model either as a linear (black line) or quadratic (blue line) function of wave height (upper panel). The lower panel shows the corresponding modelled variation in sediment mineralisation rate. Reproduced from Greenwood, 2010.

2.1.4 A 3-D model simulation of phytoplankton production and nitrogen cycling on the shelf

Model description

A coupled three-dimensional hydrodynamic-biogeochemical model (ROMS) has been configured for the southwest shelf off Western Australia. The primary task of the model is to simulate seasonal changes in phytoplankton chlorophyll concentrations and help quantify seasonal fluxes of nitrogen on and off the shelf. The model domain extends from the coast to offshore 108^{o}E and from 35^{o}S (Cape Leeuwin) to 21^{o}S (the North West Cape). The horizontal resolution in cross-shore direction varies between 2 km and 4 km from the coast to the 1000 m isobath and then increases to 8 km at the oceanic boundary. The alongshore resolution varies from 3 km to 8 km. There are 30 vertical levels with refinement in the top 200 m. Full details of the hydrodynamic model are given in chapter 1.

The biogeochemical model describes pelagic and benthic aspects of nitrogen cycling. The pelagic model is NPZD in nature following Fasham et al. (1990), and includes seven state variables: phytoplankton (PHY), zooplankton (ZOO), nitrate (NO3), ammonium (NH4), small and large detritus (SDET and LDET), and phytoplankton chlorophyll (CHL) (Figure 2.5). In previous applications of this model, the sediment has typically been parameterised as a reflective lower boundary condition (Soetaert et al., 2000), where the flux of sinking detritus is returned instantly to the bottom water-column layer as an ammonium flux (Fennel et al., 2006). In the present study however, the lower boundary influx of ammonium is uncoupled from the lower boundary deposition flux of detritus, to allow a time-dependence for the mineralisation of

organic matter in the sediment to be imposed. In this case, the imposed ammonium influx is depth dependent and confined to the inner shelf (<50m). The flux is also seasonally adjusted, using a basic sine function, and arranged to reach a maximum during mid-June. This approach was employed to approximate the link between the release of nitrogen from the sediment and wave height established by Greenwood (2010) (see previous section). The annual seabed influx of ammonium is nominally balanced by sinking of phytoplankton and detritus that is allowed to leave the model domain at the lower boundary. Following the 1-D model results (Greenwood, 2010), it is hypothesised that net release of nitrogen from the sediment during the winter will be balanced by net accumulation of nitrogen during the summer.

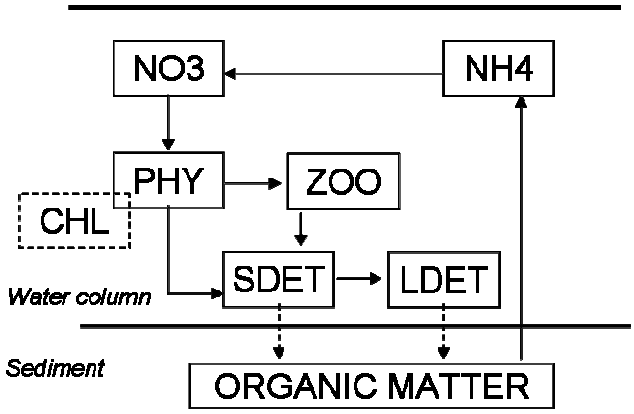

Figure 2.5. Biogeochemical model schematic (used in 4-D simulations) showing main compartments and fluxes.

Initial and boundary conditions for nitrate are taken from the CSIRO Atlas of Regional Seas climatology (Ridgway et al., 2002). All other biological variables are set initially, and at the boundaries, to a homogenous small value of 0.1 mmol N m^{-3}. All biological variables are allowed to evolve freely throughout the model interior. The model was integrated for 4 years from January 2000 to December 2003 and the solution for 2003 is compared with observations.

Large-scale features

The performance of the biogeochemical model is assessed by comparison with satellite or ship-based observations of surface and sub-surface chlorophyll distributions. The modelled nitrate field is also compared with the CARS nitrate climatology. The annual mean modelled distribution of chlorophyll on the shelf generally agrees well with satellite observations (Figure 2.6). However the model tends to underestimate the chlorophyll on the shelf north of the Abrolhos Islands, and does not reproduce the relatively high signal, that is seen in the satellite data, in the immediate vicinity of the Abrolhos Islands (Figure 2.6). The model reproduces the seasonal peak of chlorophyll in August, and the subsequent decay during September and October (Figure 2.7). However, the model gets the timing of the onset of the winter increase late by about 1 month and underestimates chlorophyll concentrations throughout the year (Figure 2.7). The timing of the winter increase of shelf chlorophyll in the model is primarily associated with the shape of the sine function that is used to impose the seasonally biased sediment nutrient flux. The 1 month lag in the model result suggests that either the sine

function is not an adequate representation of the true wave signal, or that there are other processes responsible for chlorophyll production during the autumn that are not captured by the model. The exact cause of the underestimation of chlorophyll concentrations is unknown, but may result either from inaccuracies in the growth and loss rates of phytoplankton, or an under-estimation in the supply of dissolved nitrogen to the shelf.

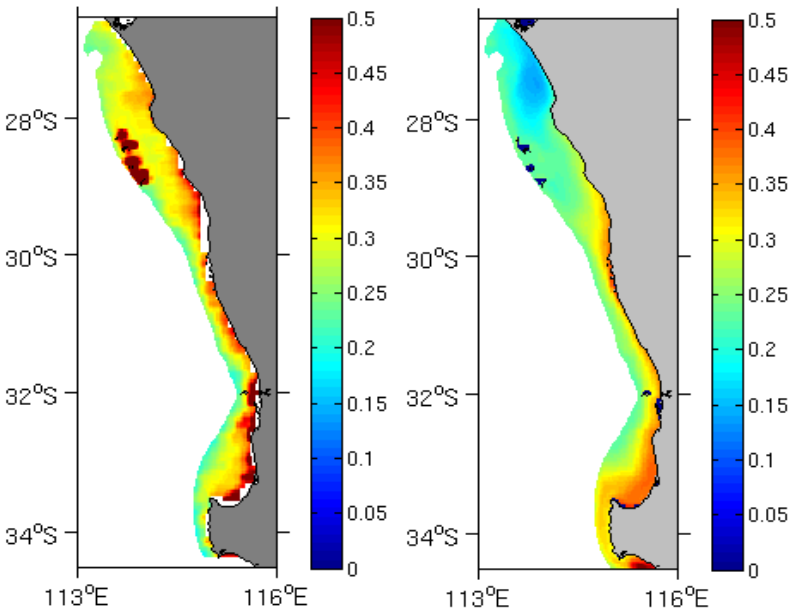

Figure 2.6. Annual mean chlorophyll (mg m^{-3}) simulated by the model (right) and estimated from SeaWiFS (left).

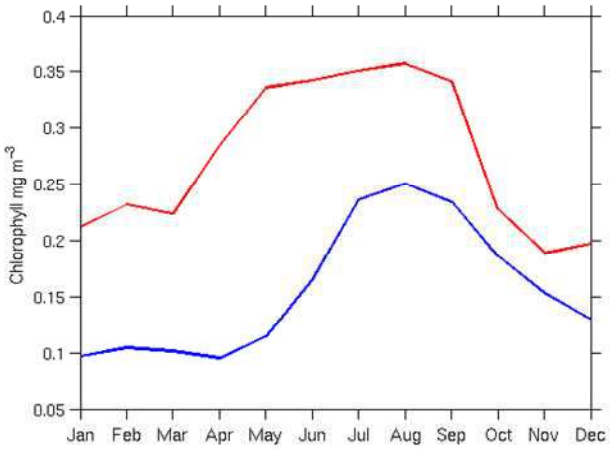

Figure 2.7. Mean monthly surface chlorophyll (mg m^{-3}) simulated by the model (blue line) and estimated from SeaWiFs (red line) for shelf region shown in Figure 2.6.

The model accurately simulates the depth and steepness of the nitracline in offshore waters compared with climatology (Figure 2.8). The characteristic downward tilting of the >1 mmol N m^{-3} contours against the shelf-edge during the autumn and winter, is also well reproduced by the model. However, the model does not show the upward sloping of the 0.5 mmol N m^{-3} contour seen in the climatology during autumn and winter. This suggests that the model may be

underestimating the flux of nitrate onto the shelf. Since this occurs during the autumn and winter it may have important implications for the winter increase in chlorophyll on the shelf.

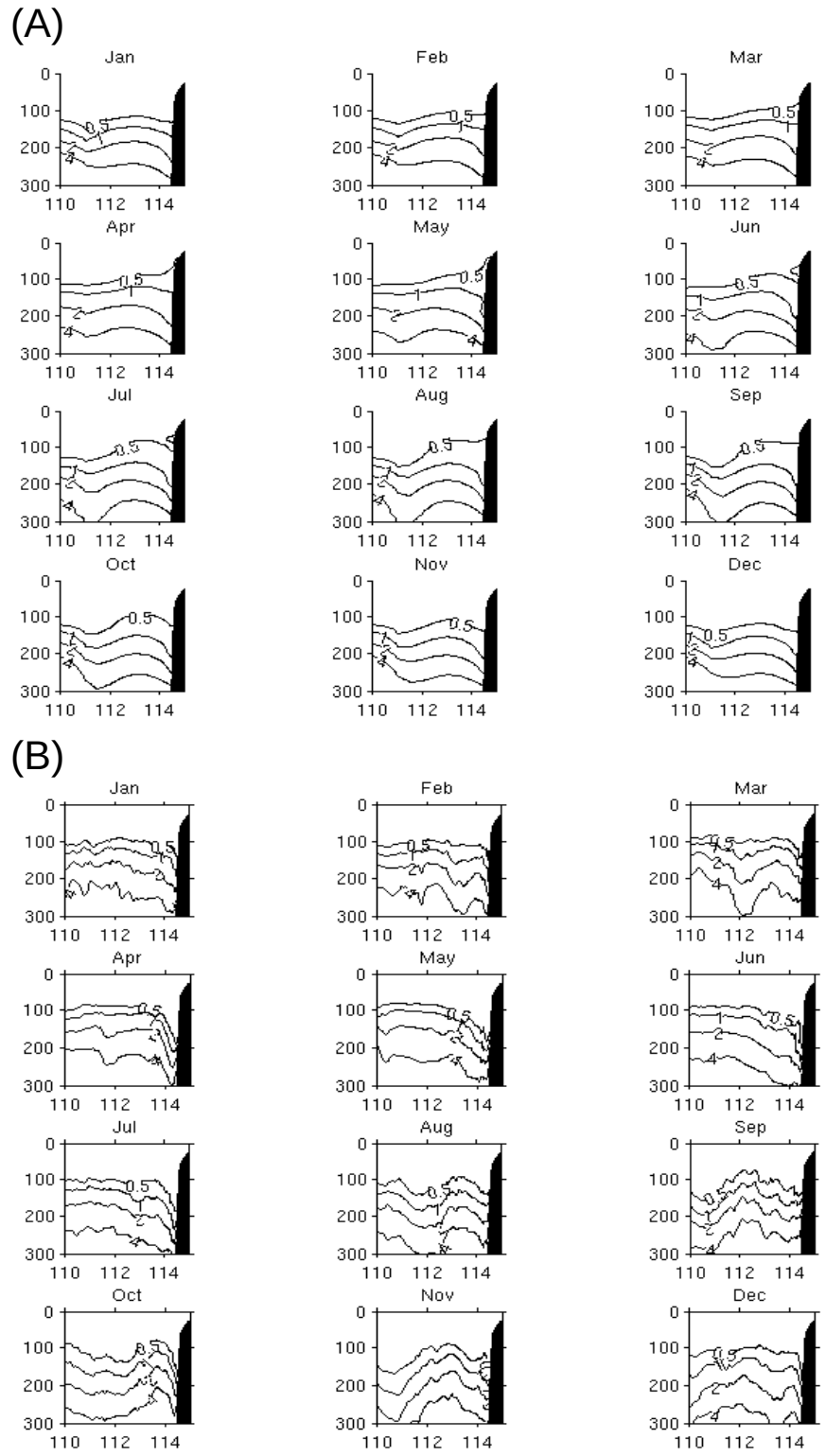

Figure 2.8. Monthly nitrate climatology (A) and model simulated mean monthly nitrate (B) along 30°S (mmol N m^{-3}). The same contour intervals are used in all panels.

Sub-surface chlorophyll and upwelling

A deep chlorophyll maximum (DCM) is frequently observed in offshore and outer-shelf waters along the southwest WA coast (Hanson et al., 2005; 2007, Twomey et al., 2007; Koslow et al., 2008). For example, Twomey et al. (2007) observed an extensive DCM across the study region between 24 October and 9 November 2003 that is compared here with the model. The DCM observed by Twomey et al. (2007) resulted in an increase in depth-averaged chlorophyll at the shelf edge that is accurately reproduced in the model simulations (Figure 2.9). The vertical structure of the DCM is also well reproduced by the model (Figure 2.10).

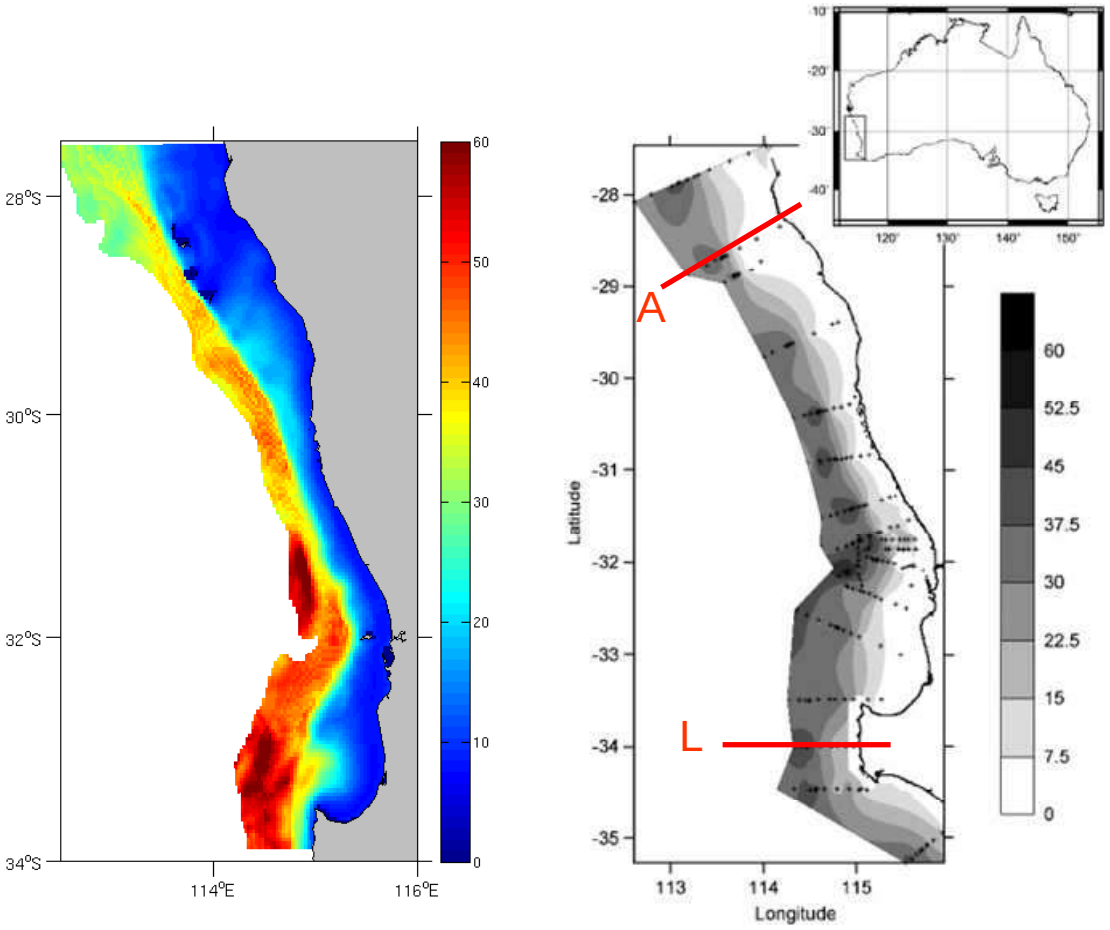

Figure 2.9. Depth integrated chlorophyll (mg m^{-2}) simulated by the model (left hand panel) and reproduced from Twomey et al. (2007) (right hand panel). Model output is averaged over exactly the same period as the data was collected by Twomey et al. (2007). Concentration range is the same in both panels.

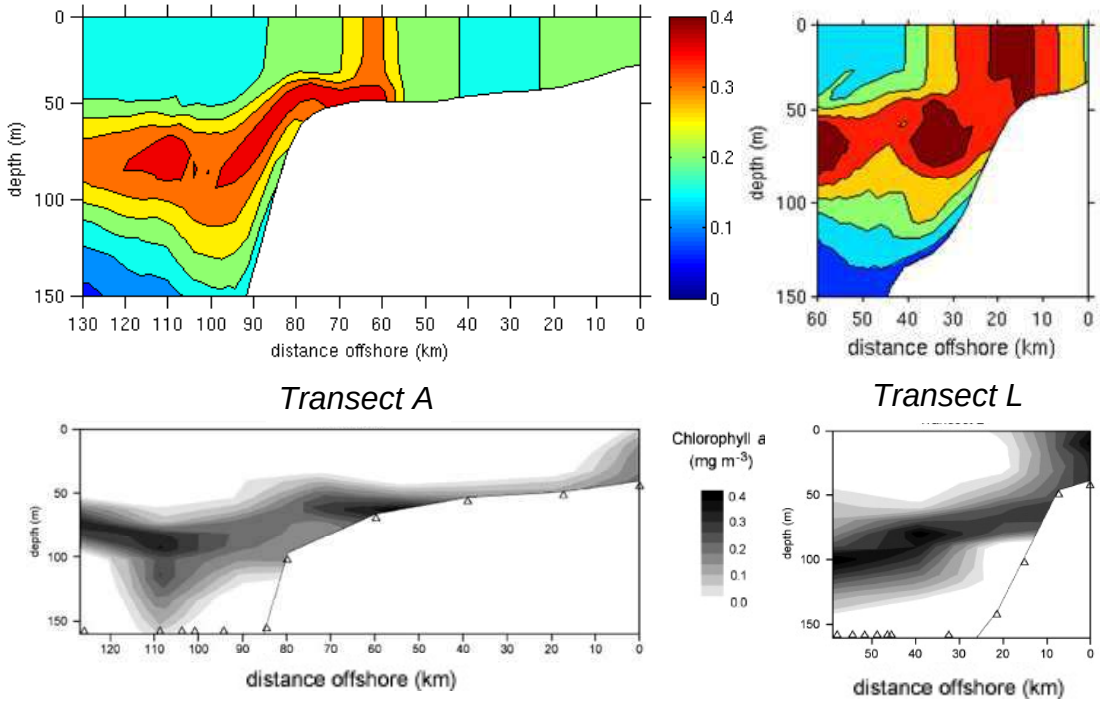

Figure 2.10. Vertical structure of the DCM along sections 'A' and 'L' (shown in Fig 2.9) simulated by the model (upper colour panels) and reproduced from Twomey et al. (2007) (lower panels). Model output is averaged over the five days before (and including) the day that the data were collected by Twomey et al. (2007). Concentration range (mg m^{-3}) is the same in all 4 panels.

The plots shown in Figure 2.10 show evidence of upwelling (particularly along 'Transect L'). This is consistent with earlier reports of wind-driven upwelling at 34°S (Gersbach et al. 1999). Upwelling in the model is intermittent and extends throughout the summer months at many locations along the southwest WA shelf in response to wind-forcing. This is evident in surface maps of chlorophyll that show elevated chlorophyll concentrations either along the shelf edge or at the coast (Figure 2.11), and in cross-sections of nitrate and chlorophyll (Figure 2.12). The model gives information for the first time about the spatial extent and temporal nature of the biological response to wind-driven upwelling along this coast.

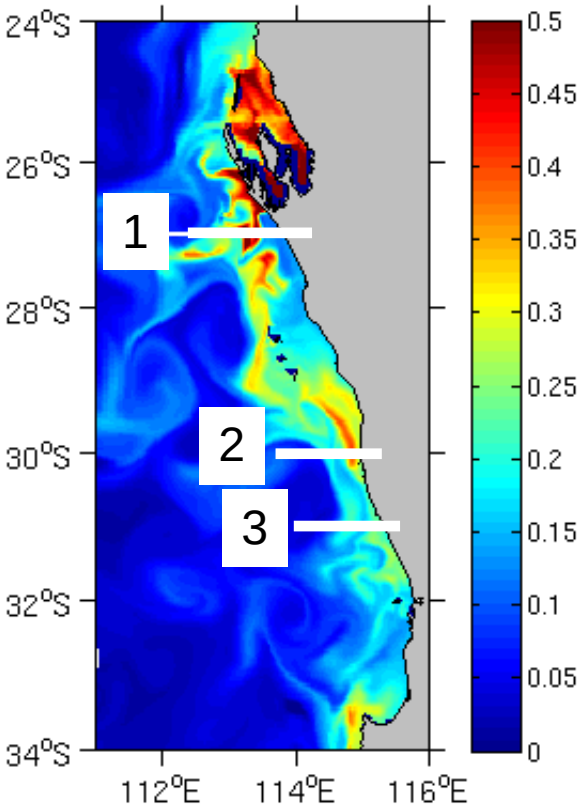

Figure 2.11. Map of modelled surface chlorophyll (mg m^{-3}) on 11th Feb. Transects 1, 2 and 3 are plotted in Fig 2.12.

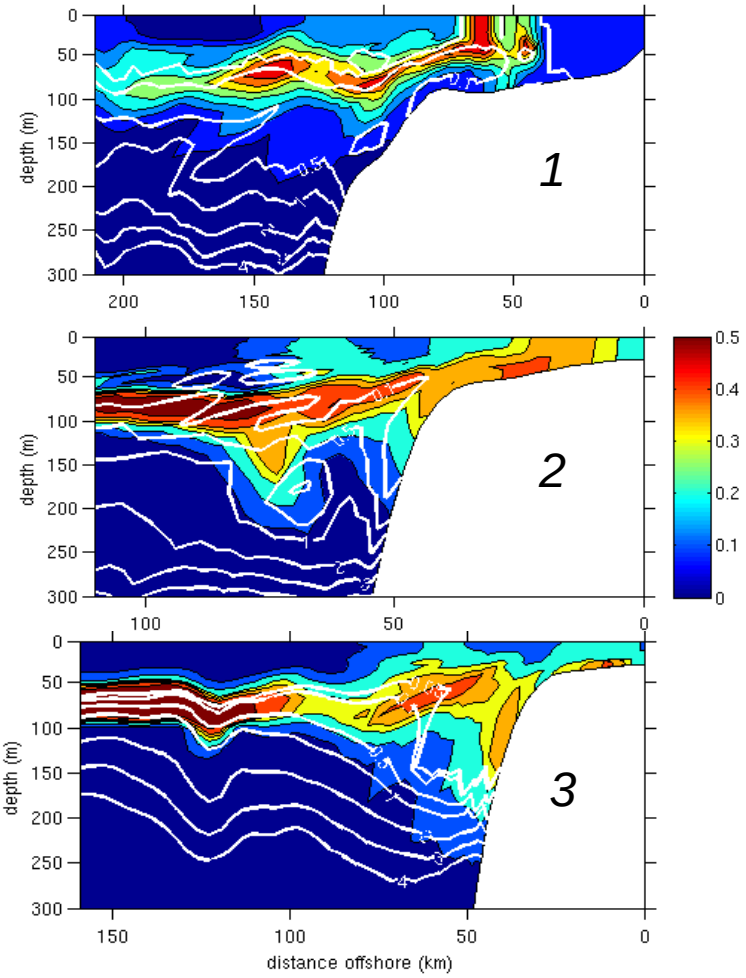

Figure 2.12. Chlorophyll (mg m^{-3}) (in colour) and nitrate concentration (mmol N m^{-3}) (white contour lines) along transects at 27 ºS (upper panel , #1), 30 ºS (middle panel, #2) and 31 ºS (lower panel, #3) on 11 Feb 2003. Location of transects 1, 2 and 3 are shown in Figure 2.11.

Meso-scale features

Phytoplankton concentrations are known to be higher in anticyclonic (warm-core) eddies than in cyclonic (cold-core) eddies along the west coast of Australia. The elevated phytoplankton concentrations observed in the anticyclonic eddies are thought to be the result of the entrainment of nitrogen-rich shelf-water during eddy formation (Greenwood et al., 2007; Dietze et al., 2009). This entrainment is often seen in satellite chlorophyll images as thin filaments of chlorophyll that extend offshore. As the eddies mature, detach from the Leeuwin Current, and move westward, they take with them a surface signature of chlorophyll resulting in isolated ‘patches’ of chlorophyll in offshore water. Evidence of this is seen in maps of surface chlorophyll from both the satellite, and the model (Figure 2.13). Sequential images from the model reveal the complete entrainment and export process (Figure 2.14).

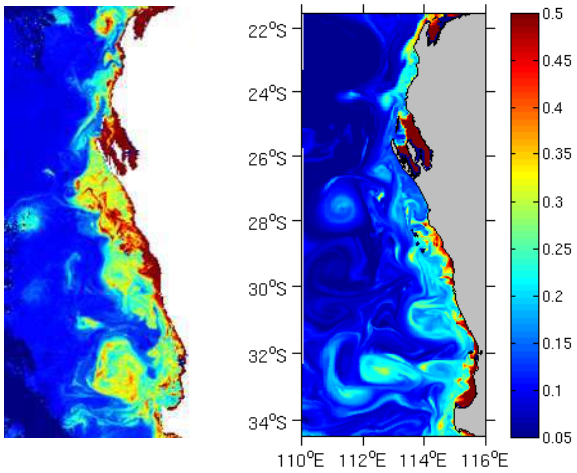

Figure 2.13. Comparison of surface chlorophyll (mg m^{-3}) estimated from SeaWiFS (left) and simulated by the model (right) on 28th May 2003. Concentration scales are the same in both panels.

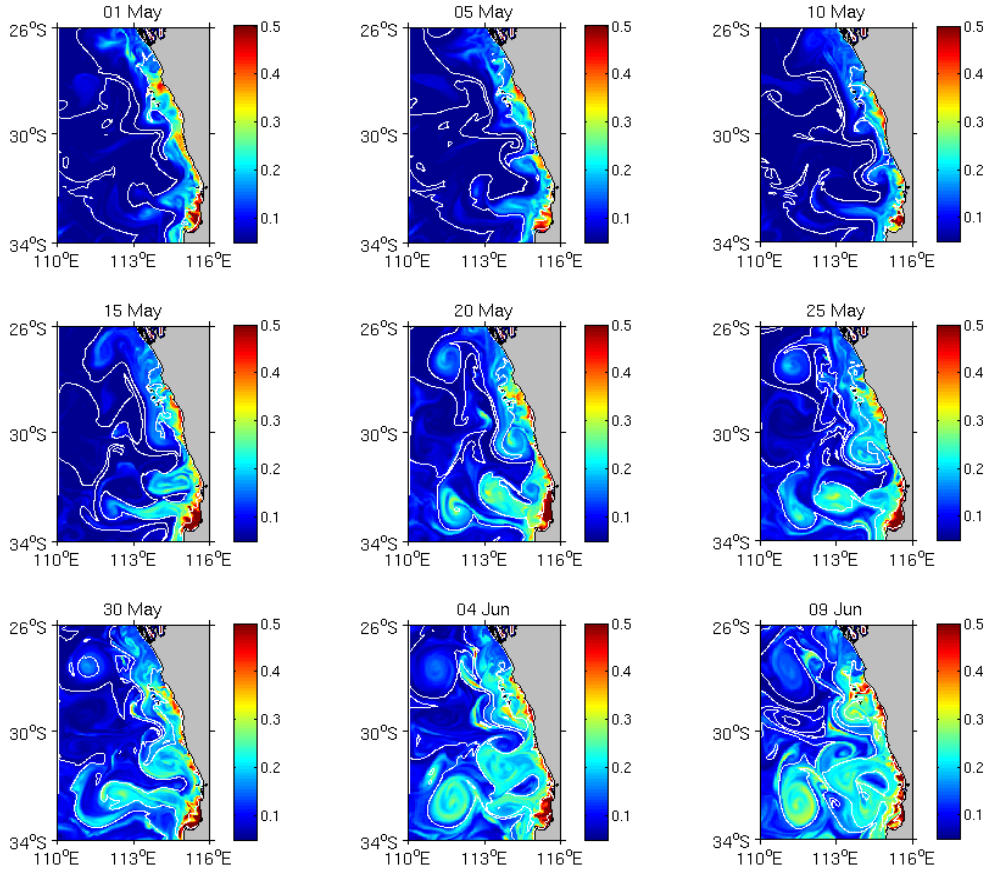

Figure 2.14. Surface maps of model simulated surface chlorophyll (mg m^{-3}) (colour map) and sea surface temperature (°C) (white contour lines) every 5 days from 1st May until the 9th June 2003, between 26 ℃ and 34 ℃.

2.1.5 Discussion

1-D modelling

Following from the 1-D model results (Section 2.1.3), it is proposed that enhanced sediment pore-water flow associated with large amplitude surface waves during the winter increases the sedimentary mineralisation rate of nitrogen in the sediment, which releases dissolved nitrogen to the overlying water column. This seasonal increase in sediment nitrogen flux drives pelagic phytoplankton production, accounting for the observed correlation between chlorophyll *a* concentration and surface-wave height (Figure 2.3). Finally, during the summer months the sediment mineralisation lowers again, allowing organic matter to accumulate in the sediment and balancing the annual sediment nitrogen budget.

3-D modelling

A nitrogen budget for the southwest WA shelf has been derived by diagnosing the simulated fluxes of particulate and dissolved nitrogen from the 3-D model across the shelf boundaries (across two cross-shelf transects at 27S and 34.5S and across the 100 m isobath) as well as deposition and release of nitrogen at the seafloor (Figure 2.15). Inputs of dissolved nitrogen are at the seafloor and across the shelf break, and losses of particulate nitrogen result from gravitational settling and horizontal advection.

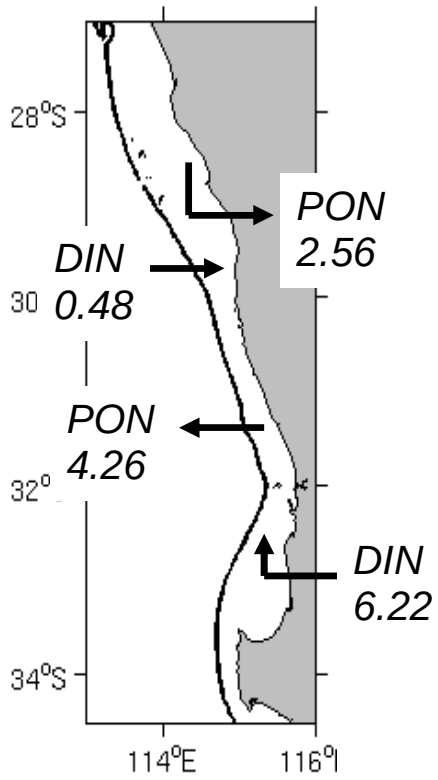

Figure 2.15. Nitrogen budget for the southwest WA shelf. Fluxes are in 10^9 mol N yr^{-1}.

The dissolved flux across the shelf break is the result of intermittent upwelling during the summer months (Figure 2.16). The upwelling events are short-lived and coincide with the appearance of chlorophyll in surface waters along the shelf-break and coast as seen, for example, in Figure 2.11. The annual flux of dissolved nitrogen across the shelf break estimated here is equivalent to 0.1 g N m^{-2} yr^{-1} (based on a shelf area of $6.23x10^{10}$ m^2) which is 10 times smaller than the annual areal upwelling flux estimated by Feng and Wild-Allen (2010). Feng and Wild-Allen (2010) considered a much larger shelf area, and based their upwelling flux on an estimate of offshore Ekman transport between North West Cape and the Abrolhos (assuming that no upwelling occurs south of the Abrolhos), and a deep compensation inflow nitrogen concentration of 1μM. Analysis of upwelling events simulated by the present model between Shark Bay and Cape Leeuwin (Figure 2.12), suggest that the compensation inflow is fairly shallow with a nitrogen concentration of between 0.1-0.2 μM. Concentrations of 0.2 μM nitrate have typically been observed in upwelled waters between Shark Bay and Cape Leeuwin (Gersbach et al., 1999; Twomey et al., 2007). It is likely that the estimate made by Feng and Wild-Allen (2010) is not applicable for the region between Shark Bay and Cape Leeuwin.

The main loss of particulate nitrogen from the shelf occurs across the shelf-break and the southern boundary as a result of eddy export and Leeuwin Current advection (Figure 2.16). Most of this loss occurs during the autumn and winter months when the Leeuwin Current transport and eddy kinetic energy are greatest. The annual flux of particulate nitrogen is equivalent to 1.0 g N m^{-2} yr^{-1} which matches the estimate made by Feng and Wild-Allen (2010). However, this represents a much larger proportion of the overall shelf production than in the budget of Feng and Wild-Allen (2010) (Figure 2.2), and contradicts their earlier assertion that the WA shelf, despite being narrow, exports very little fixed carbon into the offshore.

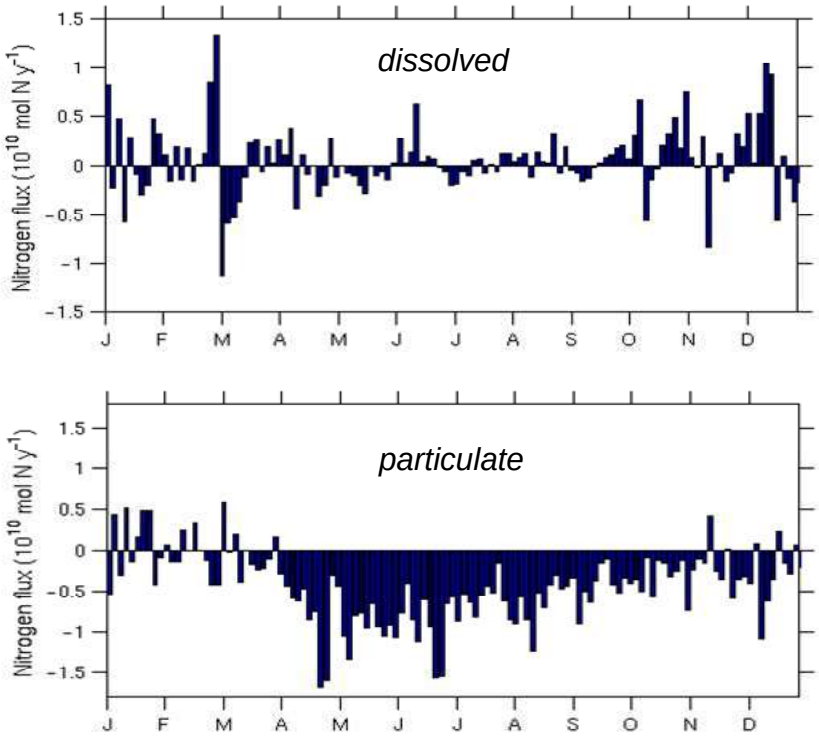

Figure 2.16. Modelled seasonal input (positive) and removal (negative) of dissolved and particulate nitrogen for the southwest WA shelf. Each bar represents a 3-day mean.

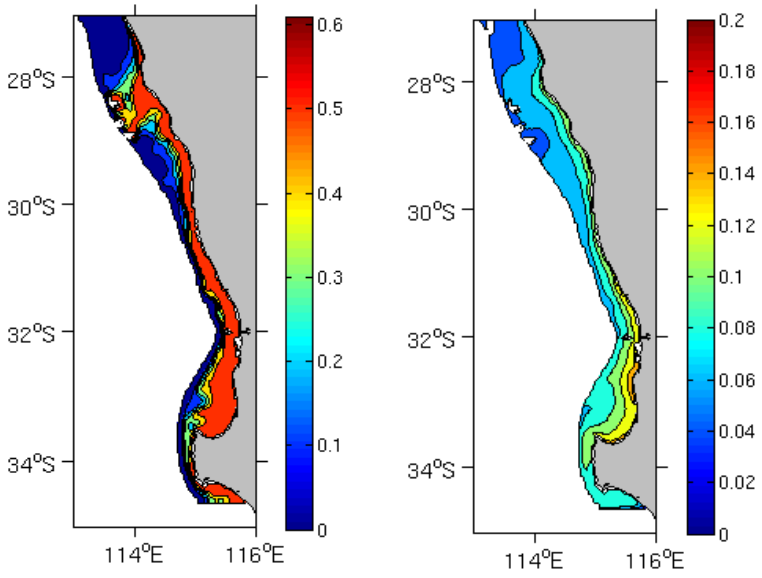

Figure 2.17. Modelled annual mean efflux (left) and deposition (right) of nitrogen at the seafloor (mmol N m^{-2} d^{-1}).

The flux of dissolved nitrogen at the seabed has previously been estimated between 0.5 and 2.0 mmol N m^{-2} d^{-1} (Rosich et al. 1994). The flux imposed in the model varies seasonally and spatially with a maximum annual mean in the nearshore region of 0.5 mmol N m^{-2} d^{-1} (Figure 2.17) representing a conservative estimate compared with the measured fluxes. The total annual flux for the southwest WA shelf amounts to 1.4 g N m^{-2} y^{-1} which is about 4 times smaller than the flux estimated by Feng and Wild-Allen (2010) by closure of their model. Roughly 40% of this seafloor input of dissolved nitrogen is balanced by deposition of particulate nitrogen at the seafloor (Figure 2.17) with the remaining 60% being advected off the shelf. This result is contrary to the behaviour of the 1-D model (Section 2.1.3) where winter release of nitrogen from the sediment is balanced by summer accumulation. It is essential that the two balance if the theory of wave-driven nutrient supply from the sediment is to hold.

That more than half of the phytoplankton biomass in the model, fuelled by nutrients from the seabed, is advected off the shelf rather than being deposited back to the seafloor, may indicate that the settling velocities of particulate nitrogen in the model are too small. Higher settling velocities would have the effect of retaining more of the nitrogen biomass on the shelf. There is much uncertainty concerning the settling velocities that should be used in biogeochemical models with estimates ranging from 0.009 to 25 m d^{-1} (Lima and Doney, 2004). Since there is no data on sinking velocities available for the WA shelf, the values used in the present model were taken from a recent modelling study for the Middle Atlantic Bight (Fennel et al., 2006) and are at the low end of the global range (0.1 to 1.0 m d^{-1}). Model sensitivity to sinking velocity is currently an active area of research.

The release of nutrients from the sediment has been shown both in the box model (Section 2.1.1) and in both the numerical models (Sections 2.1.3 and 2.1.4) to be an important aspect of the shelf nutrient dynamics. In addition, the inclusion of seasonal variation in the supply of dissolved nitrogen from the sediment has proved to be important in the 1-D and 4-D numerical simulations. Wave forcing has been proposed to explain the source of this seasonal variation. When this effect was included, both models (1-D and 4-D) captured the seasonal peak in

chlorophyll on the shelf (Figure 2.4 and Figure 2.7). Without it, neither model was able to simulate increased chlorophyll on the shelf during winter. This suggests that the sediment play an important role in mediating seasonal phytoplankton production on the shelf. However, until the 4-D model can be shown to balance release of dissolved nitrogen from the sediment during winter with deposition of particulate nitrogen during the summer (as in the 1-D model), attribution remains an open question.

Key Findings

- Variation in the timing and magnitude of the winter increase of chlorophyll at the shelf break is related to the strength of the Leeuwin Current.
- Primary production on the continental shelf off the west coast of WA appears to be largely fuelled by recycled nitrogen.
- Evidence has been found that the flux of dissolved nitrogen from the sediment, and pelagic production on the inner shelf, are linked to surface wave conditions.
- Model results suggest that short-lived wind-driven upwelling events occur throughout the region between Shark Bay and Cape Leeuwin during summer months bringing deep-water nitrate to the surface.
- Model results confirm the role of warm-core eddies in the entrainment and export of particulate nitrogen from the shelf.

2.2 Lagoon-scale

2.2.1 Introduction to lagoon-scale BGC modelling

During the biophysical sampling of the Marmion Lagoon (Figure 1.28), high nitrate concentrations were repeatedly observed in the vicinity of the limestone reef in both surface and bottom water (see chapter 3). Four contrasting examples of this are shown in Figure 2.18. A major question concerns the source of the nitrate seen in each of these maps. A sewage outfall located to the north of Marmion Lagoon is known to be the cause of elevated concentrations of surface nitrate in surrounding waters (Thompson & Waite, 2003). However, this cannot explain finding high nitrate at the bottom (as well as the top) of the water column in Marmion Lagoon (since the sewage effluent is buoyant). This has led investigation into alternative explanations for the high levels of nitrate around the reef. The observed variation in concentration and spatial distribution of nitrate between surveys (for example, between the 8th Nov 2007 and the 6th Feb 2008 (Figure 2.18)) must also be explained. These questions are the main subject of this section of the report.

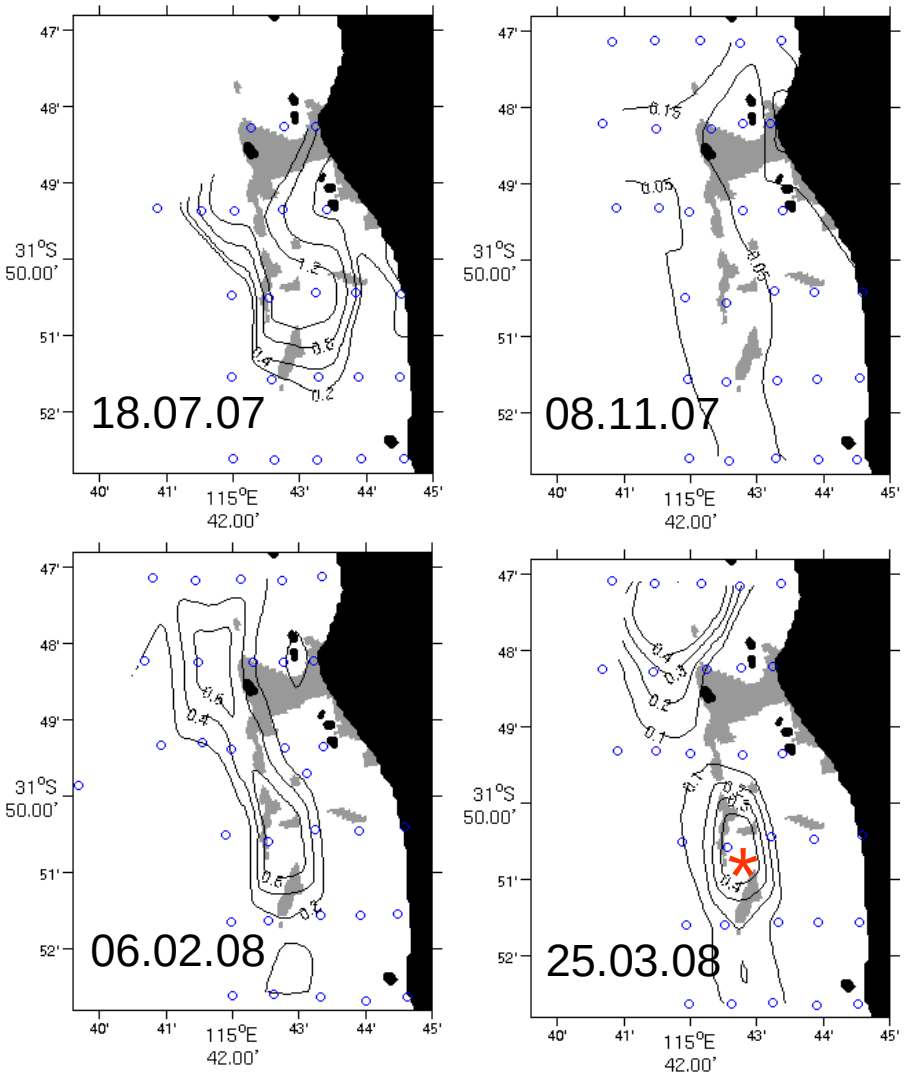

Figure 2.18. Distribution of nitrate (mmol m^{-3}) in the Marmion Lagoon on four separate occasions. Where samples were collected for surface and bottom water, the two values have been averaged. Blue circles show the sample locations. The red asterisk in the bottom right panel marks the location used for the box model calculations presented in section 2.2.3.

2.2.2 Passive tracer experiments using a 4-D model

To help identify the source of the nitrate observed in the vicinity of the Marmion reefs, a series of simulated dye release experiments have been conducted using a high resolution version of the ROMS hydrodynamic model configured for Marmion Lagoon. The hydrodynamic model was found to produce good agreement with measured currents during periods of low waves (not shown).

In the simulated dye-release experiments, a flux of dye with a magnitude of 8.0×10^{-4} Kg m^{-2} s^{-1} is added at two specified locations on the seabed (Figure 2.19). The dye flux is added constantly across a single 50×50 m model cell. The resulting depth-averaged distributions of dye are compared with depth averaged measured distributions of nitrate. The model is run for

four separate periods corresponding to the instrument deployments described in chapter 1 (see Table 1.2).

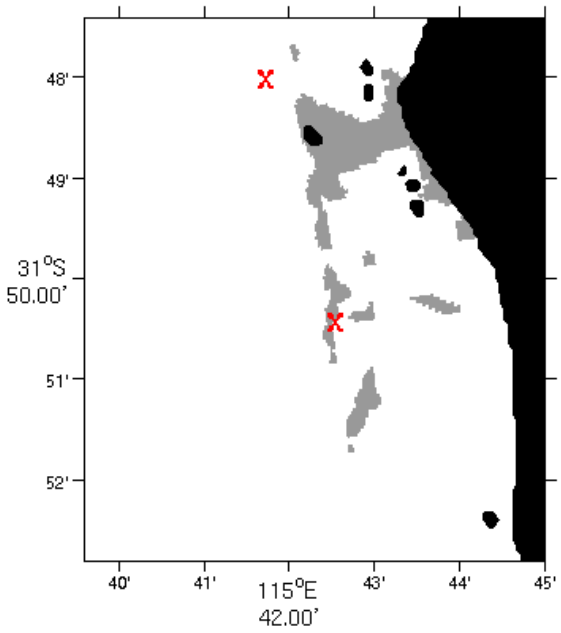

Figure 2.19. Location of seabed dye flux used in the model simulations.

The four nitrate distributions shown in Figure 2.18 were collected on separate days during each of the four deployments, providing one map of nitrate for each deployment. These four maps of nitrate are compared with modelled dye distributions calculated on the same day (Figure 2.20 and Figure 2.21). For each comparison depth-averaged hourly values of the modelled dye field are averaged, in time, for the hours (usually about 6 hours in total) over which the measurements were made. The model data is then re-sampled at the same spatial resolution as the field samples, and interpolated onto the same grid that is used to contour the observations.

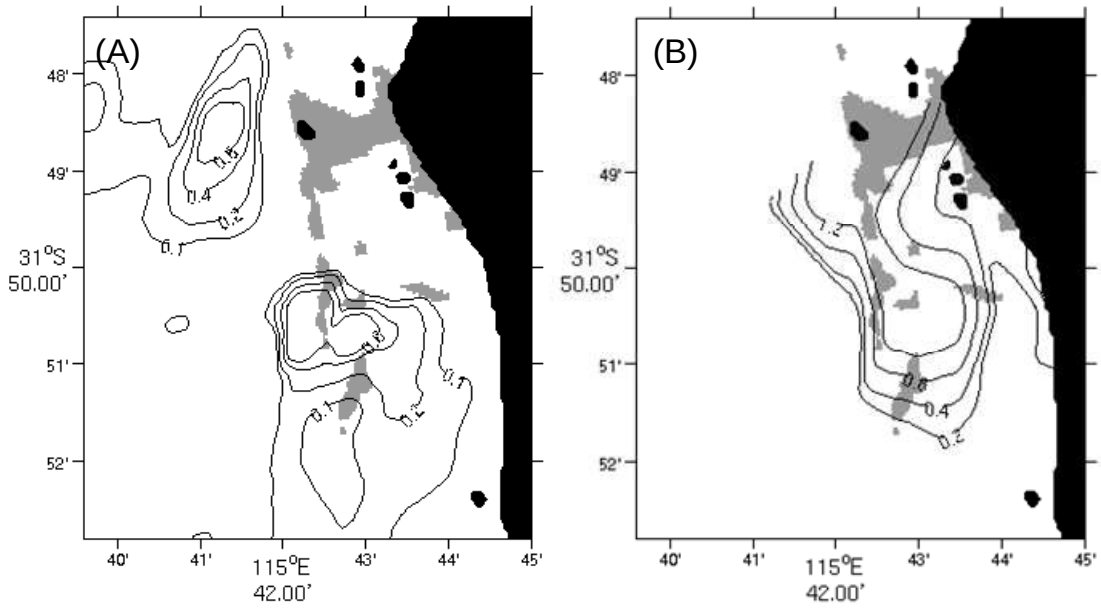

Figure 2.20. Comparison of modelled dye (Kg m^{-3}) (A) and measured nitrate (mmol N m^{-3}) (B) fields on 18th July 2007 (during deployment 1). Note that the measured nitrate concentrations are a factor of 2 bigger than the modelled dye concentrations.

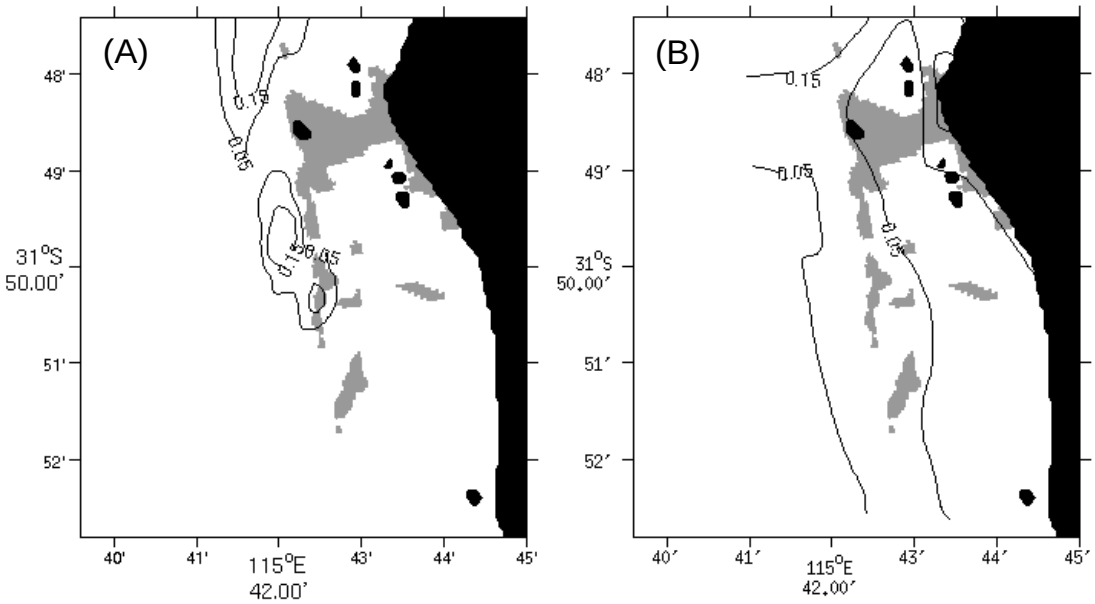

Figure 2.21. Comparison of modelled dye (Kg m^{-3}) (A) and measured nitrate (mmol N m^{-3}) (B) fields on 8th November 2007 (during deployment 2).

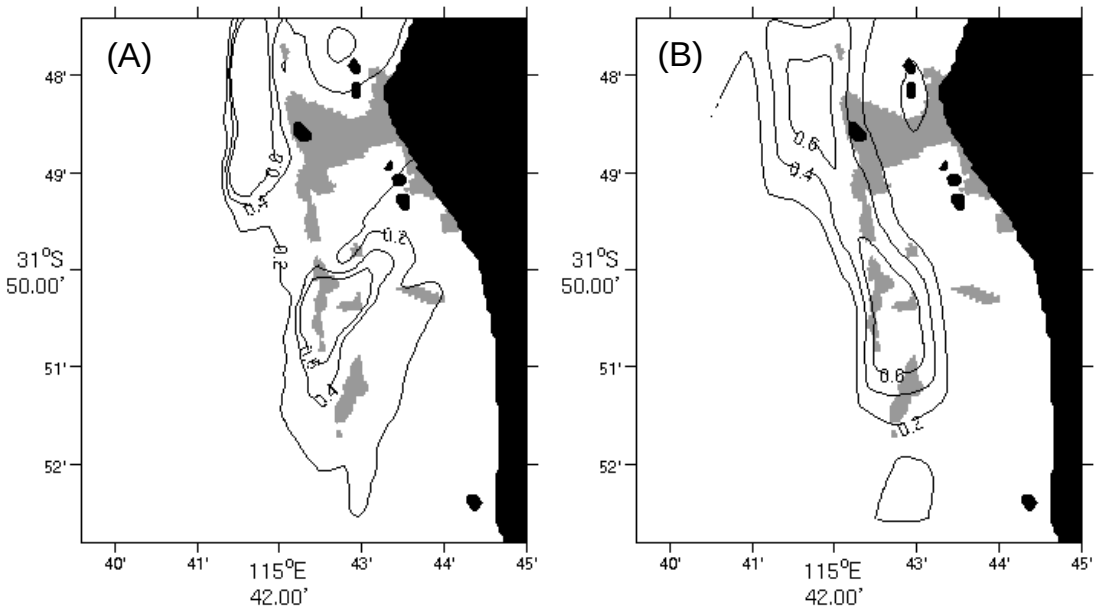

Figure 2.22. Comparison of modelled dye (Kg m^{-3}) (A) and measured nitrate (mmol N m^{-3}) (B) fields on 6th February 2008 (during deployment 3).

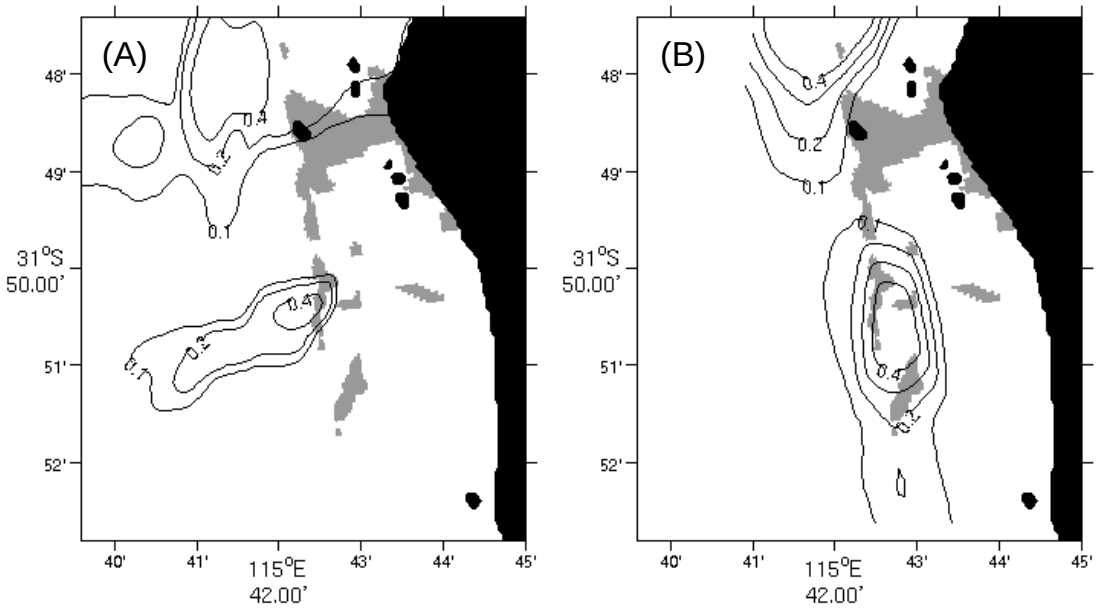

Figure 2.23. Comparison of modelled dye (Kg m^{-3}) (A) and measured nitrate (mmol N m^{-3}) (B) on 25th March 2008 (during deployment 4).

The results show general similarity between modelled surface dye and measured nitrate fields (Figure 2.20 to Figure 2.23) suggesting that the various observed nitrate distributions are consistent with the release of nitrate from two separate locations on the seabed. The best overall agreement between the modelled dye and measured nitrate fields are obtained for deployment 3 (Figure 2.22).

Evidence that the lagoon circulation is the primary factor in determining the concentration and spatial pattern of nitrate in the lagoon is provided by the unusually low concentrations of nitrate measured during deployment 2 (75% less than during deployment 3) which are closely reflected in the modelled surface dye field (Figure 2.21). In the model these reduced dye concentrations result from strong wind-driven flow to the north.

Simulation of deployment 1 shows some agreement in terms of the spatial distribution of modelled dye and measured nitrate, but the dye concentrations are a factor of 2 smaller than the measured nitrate concentrations (Figure 2.20). This particular nitrate survey (July 18th 2007) was conducted during mid-winter and represents some of the highest nitrate concentrations recorded (1-2 mmol N m^{-3}) suggesting that the magnitude of the seabed nitrate flux may be higher during the winter. The spatial distribution of dye for deployment 4 (Figure 2.23) indicates some offshore transport in the southern reef section that is not evident in the measured nitrate distribution, suggesting that the modelled currents were inaccurate.

The modelled dye release experiments reveal rapid changes in the surface dye field in response to changes in the lagoon circulation. This is best demonstrated for deployment 3 by comparison of 6 consecutive days of dye distribution (Figure 2.24). The implication of the high temporal variability in the modelled dye fields is that the measured nitrate distributions are themselves rather transient features. In fact, many of the features of the four nitrate distributions shown in Figure 2.18 are mirrored in the 6-day sequence of dye distributions. This further implies that the location and to some extent the magnitude of the nitrate source is relatively constant in time, but that the distribution of surface nitrate differs primarily because of changes in lagoon circulation.

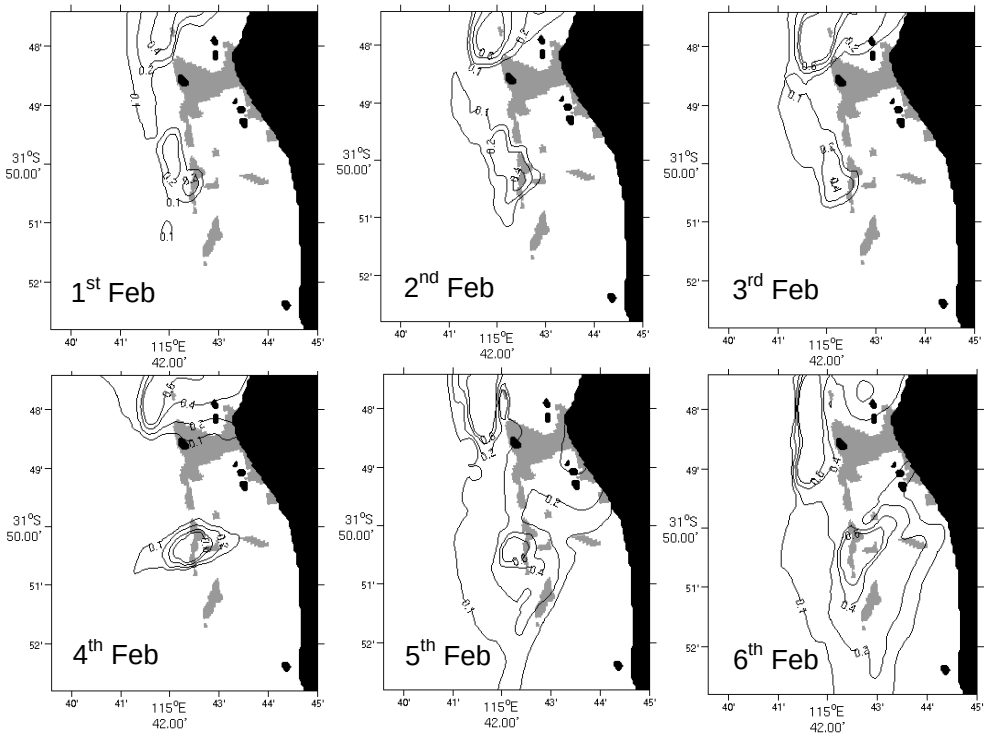

Figure 2.24. Daily variation in modelled surface dye (Kg m^{-3}) distribution (averaged between 9am and 3pm) between the 1st and 6th February 2008 (during deployment 3).

2.2.3 Discussion of Lagoon modelling results

The results of the dye release experiments indicate that the observed nitrate distributions in Marmion Lagoon are consistent with the release of nitrate from two separate locations on the seabed. Rapid change in the surface dye fields, in response to changes in circulation, suggests that the observed nitrate fields are highly transient features. Knowledge about the temporal variability in the dye fields, and the similarity between the spatial distributions of depth-averaged dye and nitrate (especially during deployments 2 and 3), provides good evidence that the nitrate is originating from the seabed. The process responsible for the release of nitrate from the seabed is more difficult to determine.

One hypothesis is that the nitrate originates from biologically mediated nitrification of organic matter on the reef. For example, there is evidence from elsewhere in the world that sponges (in association with cyanobacteria) can be a significant source of nitrate in both temperate and tropical shallow water (Diaz and Ward, 1997; Jiménez & Ribes, 2007; Southwell et al., 2008). Sponge mediated nitrification rates can be relatively large. Estimates range from 0.3×10^{-4} to 1.5×10^{-4} mmol N m^{-2} s^{-1} (Diaz and Ward, 1997; Jiménez & Ribes, 2007; Southwell et al., 2008). At these rates a reef area of 50,000 m^2 would probably provide enough nitrate to account for the concentrations measured in Marmion. However, this would represent a much more diffuse source than the two point sources used in the present model, and it is likely that the resultant distributions would look quite different. Since it is yet to be established whether sponge mediated nitrification is occurring on the Marmion reefs, this idea has not been pursued here any further.

Another hypothesis is that the nitrate originates from the submarine discharge of ground-water. Since, significant nitrate inputs to Marmion Lagoon from groundwater have already been established to occur along the beach (Johannes & Hearn, 1985), this idea is examined in more detail. For this hypothesis to be valid, nitrate-rich ground water would need to be transported beneath the seabed, via conduits in the limestone, and discharge along the offshore reef line. This type of artesian aquifer is common along many coasts (Zektzer et al. 1973), and it is hypothesised that it may also be a feature of the Marmion geology. Submarine ground-water nitrate concentrations in the Marmion area were reported in 1980 to be about 30 mmol N m^{-3} (Johannes, 1980). More recently the groundwater nitrate levels in this area have reportedly increased to about 200 mmol N m^{-3} (average of 4 sites) as a result of urbanisation (Appleyard, 1995). This includes nitrate levels as high as 400 mmol N m^{-3}, throughout the saturated aquifer, measured at a nearby bore in the Whitfords area (a few km's to the north of Marmion) (Appleyard, 1995). A flux of 1×10^{-3} mmol m^{-2} s^{-1} (roughly equivalent to the magnitude of the flux used in the dye release experiments for the southern section of reef by converting Kg dye into mmol of nitrate), and a groundwater nitrate concentration of 200 mmol N m^{-3} would suggest a ground water flow rate of about 5×10^{-6} m s^{-1}. This is similar to an estimated flow rate of groundwater for the Swan coastal plain of 3×10^{-6} m s^{-1} (Allen, 1981).

A box model approach is used to check the validity of the groundwater hypothesis and also to calculate the change in salinity that would be expected with this kind of input of freshwater. A 50×50 m box (equivalent to one grid cell in the 4-D model) centred on a sample location in the southern reef section (shown on the bottom right panel of Figure 2.18 by the red asterisk) is considered with an average water depth of 5m. This point coincides with the highest nitrate concentration measured at the southern reef section during deployment 4 with a depth averaged

nitrate value of 0.52 mmol N m^{-3}. Mass and volume conservation is assumed so that influx (from long-shore advection and groundwater) and efflux (into the lagoon) of volume, nitrate and salt are balanced. The conceptual model is shown in Figure 2.25.

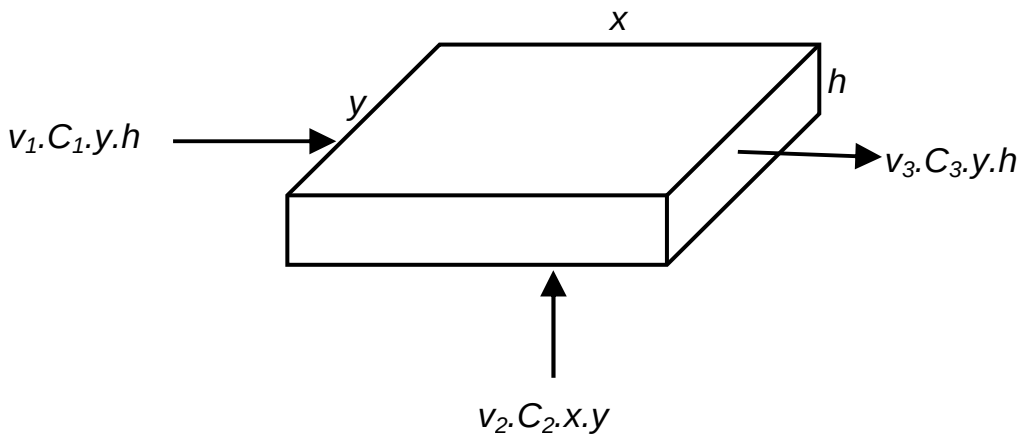

Figure 2.25. Schematic of the box model showing input and output fluxes, where x, y and h are the dimensions of the box (m), V indicates a velocity (m s^{-1}) and C indicates a tracer concentration (e.g. mmol N m^{-3} for nitrate)

Assuming conservation of volume,

$$v_1.y.h + v_2.x.y - v_3 y.h = 0$$

$$v_3 = v_1 + v_2 \frac{x}{h}$$

And conservation of tracer (nitrogen or salinity), a value for C_3 can be obtained:

$$c_3 = \frac{v_1 c_1 + v_2 c_2 \frac{x}{h}}{v_1 + v_2 \frac{x}{h}}$$

The long-shore velocity (v_1) is taken to be 0.05 ms^{-1} (the approximate long-shore velocity measured during deployment 4 around the time of the nitrate survey) and the upstream concentration of nitrate and salt (C_1) are set at 0.1 mmol N m^{-3} and 35 respectively. Ground water velocity (v_2) and nitrate concentration (C_2) are taken to be 5×10^{-6} m s^{-1} and 200 mmol N m^{-3}. Ground water salinity (C_2) is assumed to be zero (i.e. freshwater). From these velocity and tracer concentration estimates, and the use of the above equation, a mean nitrate concentration of 0.3 mmol N m^{-3} and a mean salinity of 34.97 (a drop of 0.03) is calculated for the area considered. The box-model surface nitrate estimate is 0.2 mmol N m^{-3} less than the depth averaged concentration of nitrate measured during deployment 4. The estimated drop in salinity is very small compared with the range of variation typically seen in the surface salinity fields across the lagoon (Figure 2.26). This may partly explain why the observed salinity distribution

does not clearly mirror the nitrate distribution (Figure 2.26). It is also possible that the box model has overestimated the impact on salinity by assuming that the inflowing groundwater has a salinity of zero. Saltwater intrusion is a common feature of submarine groundwater dynamics, and often results in salty groundwater discharge.

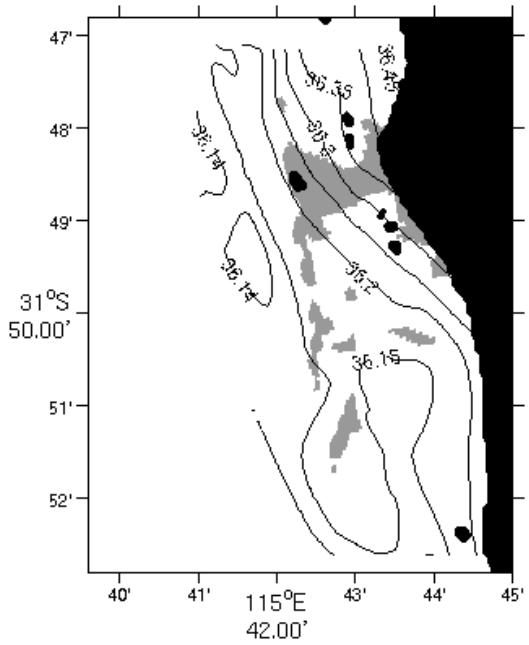

Figure 2.26. Distribution of depth averaged salinity (colour contours) measured in Marmion Lagoon on 25th March 2008. Depths less than 5 m are shaded grey to show the position of the sub-merged limestone reef.

Overall, the modelled dye experiments, and box-model calculations, provide some support to the groundwater hypothesis. The dye experiments show that the observed nitrate fields are generally consistent with the continuous addition of nitrate at 2 fixed locations on the reef (although the exact location of these inputs is unknown). The box model calculations show that the results are consistent with a groundwater velocity of 5×10^{-6} ms^{-1} and a groundwater nitrate concentration of 200 mmol N m^{-3} , in approximate agreement with field estimates of groundwater flow rate (Allen, 1981) and nitrate concentration (Appleyard, 1995). If this is true then submarine groundwater discharge of dissolved nitrogen may be playing a crucial role in supporting the reef ecosystem right the way along the Perth coast-line. This in turn would have important implications for the management of groundwater in the Perth metropolitan area. Meanwhile, biological sources of nitrate cannot be ruled-out.

Key Findings:

Model simulations show that elevated nitrate concentrations measured in the vicinity of limestone reefs in Marmion Marine Park are consistent with the release of nitrate from two separate locations on the seabed.

Calculations suggest that the discharge of nitrate-rich submarine groundwater at these two locations offers one possible explanation for the observations.

2.3 Acknowledgments

The ROMS simulations were run on an iVEC supercomputer at the Australian Research Centre in Technology Park, Kensington. Liejun Zhong helped in the set-up and running of ROMS. Peter Craig and Graham Symonds helped in the design of the model experiments.

2.4 References

Allen, A.D. (1981). Groundwater resources of the Swan coastal plain, near Perth, Western Australia. In Groundwater Resources of the Swan Coastal Plain (Whelan, B.R., ed.). CSIRO, Perth. Pp29-74.

Appleyard, S. (1995). The impact of urban development on recharge and groundwater quality in a coastal aquifer near Perth, Western Australia. Hydrogeology Journal, 3 (2), 65-75.

Dietze, H., Matear, R., Moore, T. (2009). Nutrient supply to anticyclonic meso-scale eddies off Western Australia estimated with artificial tracers released in a circulation model. Deep-Sea Res. I, 56, 1440-1448.

Fasham, M.J.R., Ducklow, H.W., McKelvie, S.M. (1990). A nitrogen-based model of plankton dynamics in the oceanic mixed layer. Journal of Marine Research, 48, 591-639.

Feng, M., and Wild-Allen, K. (2010). The Leeuwin Current. In ‘Carbon and Nutrient Fluxes in Continental Margins: A Global Synthesis’. (Eds K-K. Liu, L. Atkinson, R. Quinones, L. Talaue-McManus.) pp 197-210. (Springer-Verlag, New York.)

Fennel, K., Wilkin, J., Levin, J., Moisan, J., O’Reilly, J., and Haidvogel, D. (2006). Nitrogen cycling in the Middle Atlantic Bight: Results from a three-dimensional model and implications for the North Atlantic nitrogen budget. Global Biogeochemical Cycles 20, GB3007, doi:10.1029/2005GB002456.

Gersbach, G.H., Pattiaratchi, C.B., Ivey, G.N. and Cresswell, G.R. (1999). Upwelling on the south-west coast of Australia – source of the Capes Current. Continental Shelf Research, 19 (3), 363-400.

Greenwood, J.E., Feng, M., Waite, A.M. (2007). A 1-dimensional simulation of biological production in two contrasting mesoscale eddies in the south eastern Indian Ocean. Deep-Sea Res. II, 54, 1029-1044.

Greenwood, J., Soetaert, K. (2008). Interannual variability in the seasonal cycle of chlorophyll within the Leeuwin Current off the southwest Western Australian coast. Journal of Marine Research, 66 (3), pp. 373-390

Greenwood, J. (2010). Evidence that increased nitrogen efflux from wave-influenced marine sediment enhances pelagic phytoplankton production on the inner continental shelf of Western Australia. Marine and Freshwater Research, 61, 625-632.

Hanson, C.E., Pattiaratchi C.B. and Waite, A.M. (2005). Sporadic upwelling on a downwelling coast: phytoplankton responses to spatially variable nutrient dynamics off the Gascoyne region of Western Australia. Continental Shelf Research, 25, 1561-1582.

Hanson, C.E., Peasant, S., Waite, A.M. and Pattiaratchi C.B. (2007). Assessing the magnitude and significance of deep chlorophyll maxima of the coastal eastern Indian Ocean. Deep-Sea Research II, 54, 884-901.

Johannes, R. (1980). The ecological significance of the submarine discharge of groundwater. Marine Ecology Progress Series, 3, 365-373.

Johannes, R.E. and Hearn C.J. (1985). The effect of submarine groundwater discharge on nutrient and salinity regimes in a coastal lagoon off Perth, Western Australia. Estuarine, Coastal and Shelf Science 21, 789-800.

Koslow, J.A., Pesant, S., Feng, M., Pearce, A., Fearns, P., Moore, T., Matear, R. and Waite, A. (2008). Structure and dynamics of the pelagic ecosystem off southwestern Western Australia, 2002 – 2004: phytoplankton biomass and productivity. Journal of Geophysical Research 113, C07050, doi:10.1029/2007JC004102.

Lima, I.D. and Doney, S.C. (2004) A three-dimensional, multi-nutrient and size-structured ecosystem model for the North Atlantic. Global Geochemical Cycles, 18, GB3019, doi:10.1029/2003GB002146.

Lourey, M., Dunn, J., and Waring, J. (2006). A mixed-layer nutrient climatology of Leeuwin Current and Western Australian Shelf waters: Seasonal nutrient dynamics and biomass. Journal of Marine Systems 59, 25-51.

Marinelli, R.L., Jahnke, R.A., Craven, D.B., Nelson, J.R., and Eckman, J.E. (1998). Sediment nutrient dynamics on the South Atlantic Bight continental shelf. Limnology and Oceanography 43, 1305-1320.

Riedl, R.J., Huang, N., and Machan, R. (1972). The subtidal pump: a mechanism of interstitial water exchange by wave action. Marine Biology 13, 210-221.

Ridgway, K.R., Dunn, J.R., Wilkin, J.L. (2002). Ocean interpolation by four-dimensional least squares-application to the waters around Australia. Journal of Atmospheric and Oceanographic Technology 19, 1357-1375.

Rosich, R.S., Bastyan, G.R., Pailing, E.I., and Van Senden, D.C. (1994). Sediment nutrient processes. Perth Coastal Water Study, project E3.4 (phase 2) report no. SSB 15/94. p468. Water Authority Perth Western Australia.

Shum, K.T. (1993). The effects of wave-induced pore water circulation on the transport of reactive solutes below a rippled sediment bed. Journal of Geophysical Research 98, 10,289-10,301.

Shum, K.T. and Sundby, B. (1996). Organic matter processing in continental shelf sediments – the subtidal pump revisited. Marine Chemistry 53, 81-87.

Soetaert, K., Middelburg, J.J., Herman, P.M.J., Buis, K. (2000). On the coupling of benthic and pelagic biogeochemical models. Earth Science Reviews 51, 173-201.

Thompson, P. and Waite, A. (2003). Phytoplankton responses to wastewater discharges at two sites in Western Australia. Marine and Freshwater Research 54, 721-735.

Thompson, P.A., Wild-Allen, K., Lourey, M., Rousseaux, C., Waite, A.M., Feng, M. and Beckley, L.E. (2011). Nutrients in an oligotrophic boundary current: Evidence of a new role for the Leeuwin Current. Progress in Oceanography, in press

Twomey, L.J., Waite, A.M., Pez, C.B. and Pattiaratchi, C.B. (2007). Variability in nitrogen uptake and fixation in the oligotrophic waters off the south west coast of Australia. Deep-Sea Research II, 54, 925-942.

Webb, J.E., and Theodor, J. (1968). Irrigation of submerged marine sands through wave action. Nature 220, 682-683.

Webster, I.T. (2003). Wave enhancement of diffusivities within surficial sediments. Environmental Fluid Mechanics 3, 269-288.

Webster, I.T., and Taylor, J.H. (1992). Rotational dispersion in porous media due to fluctuating flows. Water Resources Research 28(1), 109-119.

Zekter, I.S., Ivanov, V.A. and Meskheteli, A.V. (1973). The problem of direct groundwater discharge to the seas. Journal of Hydrology 20, 1-36.

3. IMPROVED DESCRIPTIONS AND CONCEPTUAL MODELS

Objective 3: Improved descriptions and conceptual biogeochemical models for shelf and lagoon waters incorporating seasonal and interannual variability and improved representation of benthic primary production and bentho-pelagic coupling.

3.1 Lagoon Observations

Mat Vanderklift, Martin Lourey, Joanna Strzelecki, Doug Bearham, Fiona Graham, Damian Thomson, James Mclaughlin, Ryan Downie, John Keesing and Russ Babcock.

CSIRO Marine and Atmospheric Research

3.1.1 Introduction

Shallow nearshore ecosystems along the lower west coast of Australia are characterised by a high biomass of benthic autotrophs. Seagrasses form extensive meadows in soft sediments, while macroalgae, especially large brown macroalgae such as kelp, dominate rocky surfaces. The annual biomass production of these autotrophs can be very high, with both seagrasses and macroalgae capable of producing several kilograms of biomass (dry weight) in a single square metre of seafloor each year. This biomass production does not occur evenly over the year, but appears to be somewhat seasonal.

This high production occurs in a system with typically high light and water movement, but also low nutrients. The factors that allow high rates of benthic production to be favoured over pelagic production, and those that lead to seasonal patterns in production, were therefore key foci of this project. Previous studies of production have been typically limited to a few sites at a time. However, spatial variation in production can be large, so that results obtained from some places do not apply elsewhere – potentially leading to over- or underestimates of the importance of production to an ecosystem. An additional focus was on quantifying and understanding the causes of this spatial variation. As part of the research towards addressing these questions, we undertook a comprehensive survey program to measure spatial and temporal patterns in temperature, salinity and nutrients (which included re-analysis of historical datasets), and laboratory- and field-based measurements of primary production by key benthic autotrophs. Part of this program included measurements of environmental variables (such as light) that might help explain the observed patterns in production.

Seasonal patterns in production can also provide some insights into the ways in which production is transferred through the ecosystem. For example, seasonal decreases in biomass suggest that detritus might be an important source of nutrition for higher trophic levels. This possibility is supported by observations that little of the seagrass or macroalgae production is directly grazed, and that exchange of material among habitats is considerable. Suspension- and deposit-feeding invertebrates are also an important link between benthic and planktonic food webs, and they might play an important role in cycling of this detritus. However, the

ecosystem-level role of herbivores, filter feeders and deposit feeders are quite poorly understood. We investigated these potential pathways in several ways. First, we surveyed the biomasses of the different functional groups of invertebrates in reef, seagrass and sand habitats; this involved re-analysis of extensive historical data on the biomass of suspension feeders in Marmion Lagoon. Second, we attempted to evaluate the role of plant detritus in secondary production by measuring the importance of different sources of production to suspension feeders, using blue mussels *Mytilus edulis* as a model. Third, we extended this investigation to encompass measurements of rates of direct grazing on macroalgae, and rates of filtering by suspension feeders.

The high rates of benthic primary production, coupled with the low rates of direct grazing of this production, suggests that suspension feeders and detrital food webs are sustaining higher trophic levels. However, the magnitude of the importance of the links is quite unknown. We therefore investigated how much of this production might in turn flow to higher trophic levels by measuring predation on one group of suspension feeders. Like the investigation into the sources of production sustaining filter feeders, we selected the common blue mussel *Mytilis edulis* as a model.

3.1.2 Lagoon Biophysical Measurements

Methods

30 sampling stations were distributed along six east – west transects across Marmion Lagoon. Conductivity, temperature and depth (CTD) profiles of the whole water column were obtained at each station using a calibrated Seabird SBE 911. Fluorescence profiles were collected using a separate fluorometer. Bottle samples were collected from the surface and bottom and analyzed for nitrate+nitrite, ammonium, silicate and phosphate using a LACHAT® flow injection instrument. Chlorophyll a samples for calibration of the Flourometer were collected at 3 stations on each transect by filtering 1 litre of water onto a Whatman GF/F™ filter. Filters were stored frozen until extracted in 90% acetone and analysed for chlorophyll *a* on a calibrated Turner Designs model 10 AU fluorometer.

Results

Temperature

The lowest temperatures (17.2°C) were observed on the July survey (Figure 3.1). The highest (up to 24.8°C) were observed on the February cruise (Figure 3.1). This temperature range is similar to those observed in this area previously (Lourey & Kirkman 2009). During winter (May - August) inshore waters were cooler than those outside the reef, while in summer (December –March) the shallower areas (and particularly the shallow bank in the north of our domain was warmer than further off shore reflecting the smaller volume of water in the lagoon and limited exchange. Inshore temperature ranged between 17.2 and 24.8°C, outside the reef it range from 18.2 to 24.2 (Figure 3.1).

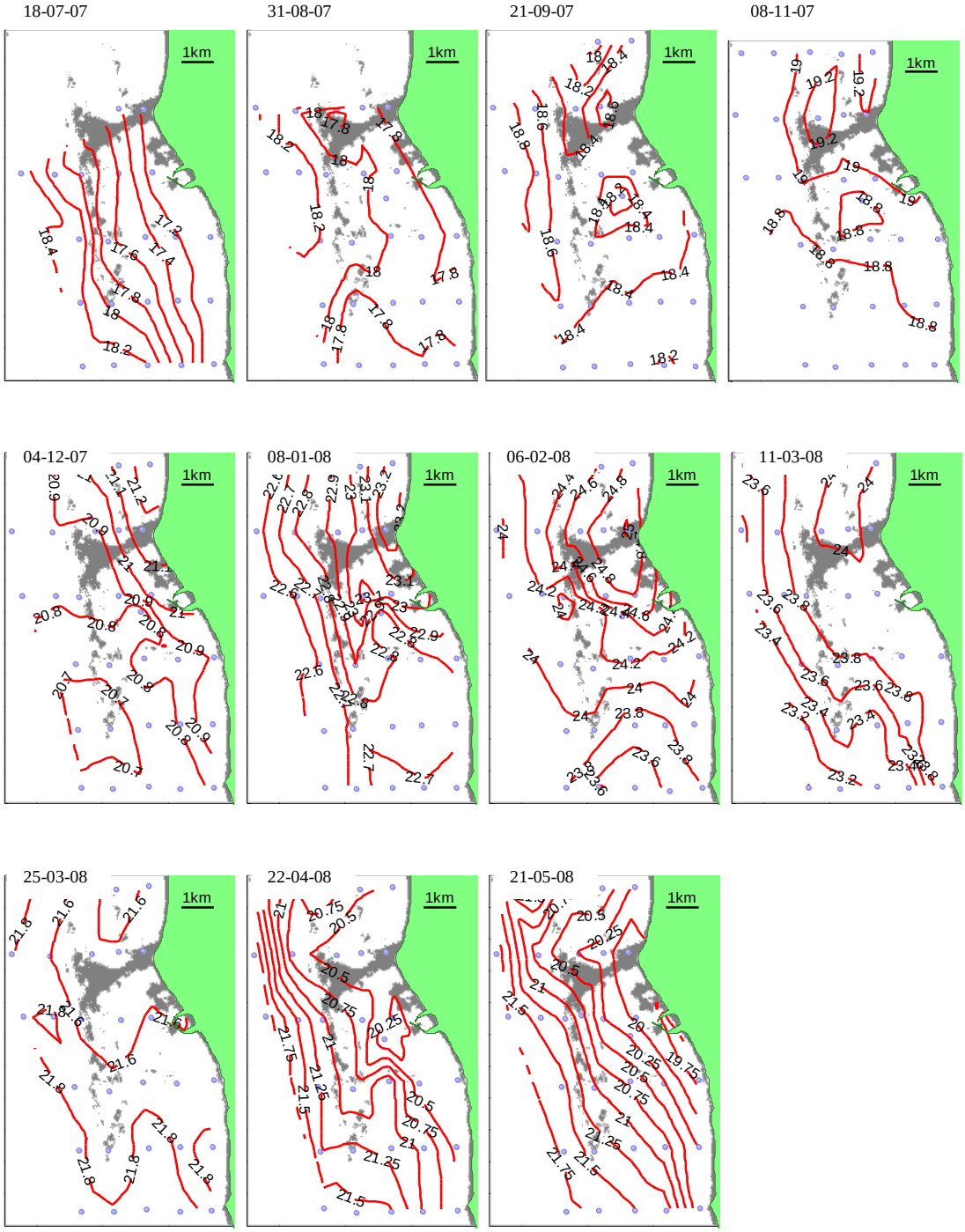

Figure 3.1. Spatial variations in temperature (ºC) collected on 11 monthly cruises in Marmion Lagoon. Sampling stations are represented by the blue points

Salinity

Salinity patterns were variable (Figure 3.2). There were instances where salinity was lower outside the reef than in the lagoon (i.e., July, and March) while in other instances it was fresher in the lagoon (November and May) possibly reflecting recent regional variations in

precipitation/ground water discharge and evaporation (Figure 3.2). In addition a north to south gradient was also common with the isobars tending off shore in the north in October, March and May possible reflecting greater input of freshwater to the north (Figure 3.2). An isolated patch of fresh water was observed over the reefs in August and may indicate the input of ground water (Figure 3.2).

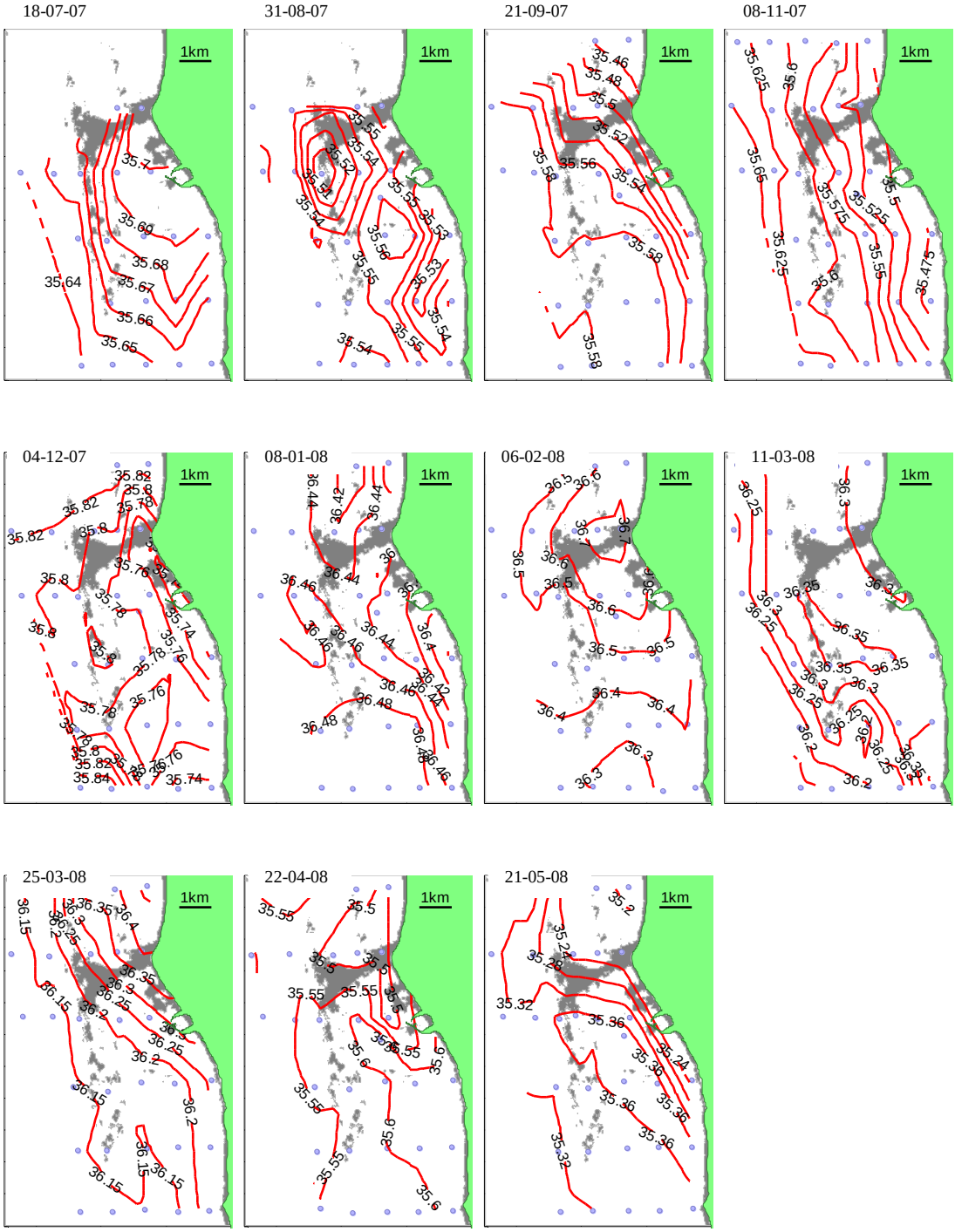

Figure 3.2. Spatial variations in salinity collected on 11 monthly cruises in Marmion Lagoon.

Nitrate

Nitrate concentrations tended to be highest over the reef areas (Figure 3.3). The area of elevated nitrate was distributed over both the northern and southern reefs (Figure 3.3). The highest nitrate concentrations (i.e. >2μM) were universally in the north of our domain, either as a contained patch of high nitrate water over reef (i.e. August and September) or as a gradient potentially indicating a source further north (May) (Figure 3.3) . The reefs typically have a high biomass of macroalgae (Kirkman 1981) and abraded plant material (particularly small pieces of seaweed tips) and may be a source of labile organic matter for remineralisation and release of constituent nutrients. Filter feeders have been recognised as important recyclers of pelagic particulate organic matter (POM) in hard bottom habitats (Ribes 2005) and substantial assemblages of filter feeding organisms are common on local reef systems (Hatcher 1989). An association between nitrifying bacteria and some species of sponge results in them excreting nitrate rather than ammonium (Jiménez 2007). Limestone reefs may be conduits of contaminated groundwater which is generally high in nitrate (Johannes 1980). We would expect groundwater discharge to appear as a patch of low salinity water immediately above the reef and this was evident in August along with a patch of high nitrate (~2 μM) in the same area (Figure 3.3). Similar high nitrate patches over reefs did not coincide with areas of low salinity so the influence of groundwater as a nitrate source remains speculative. In some cases there is a north south gradient and it is possible that there is advection of nutrient rich water into our study area from the north. While it is possible that this nitrate source is the sewerage outfall located to the north of our domain, its influence is thought not to extend this far from the discharge point (Thompson 2003).

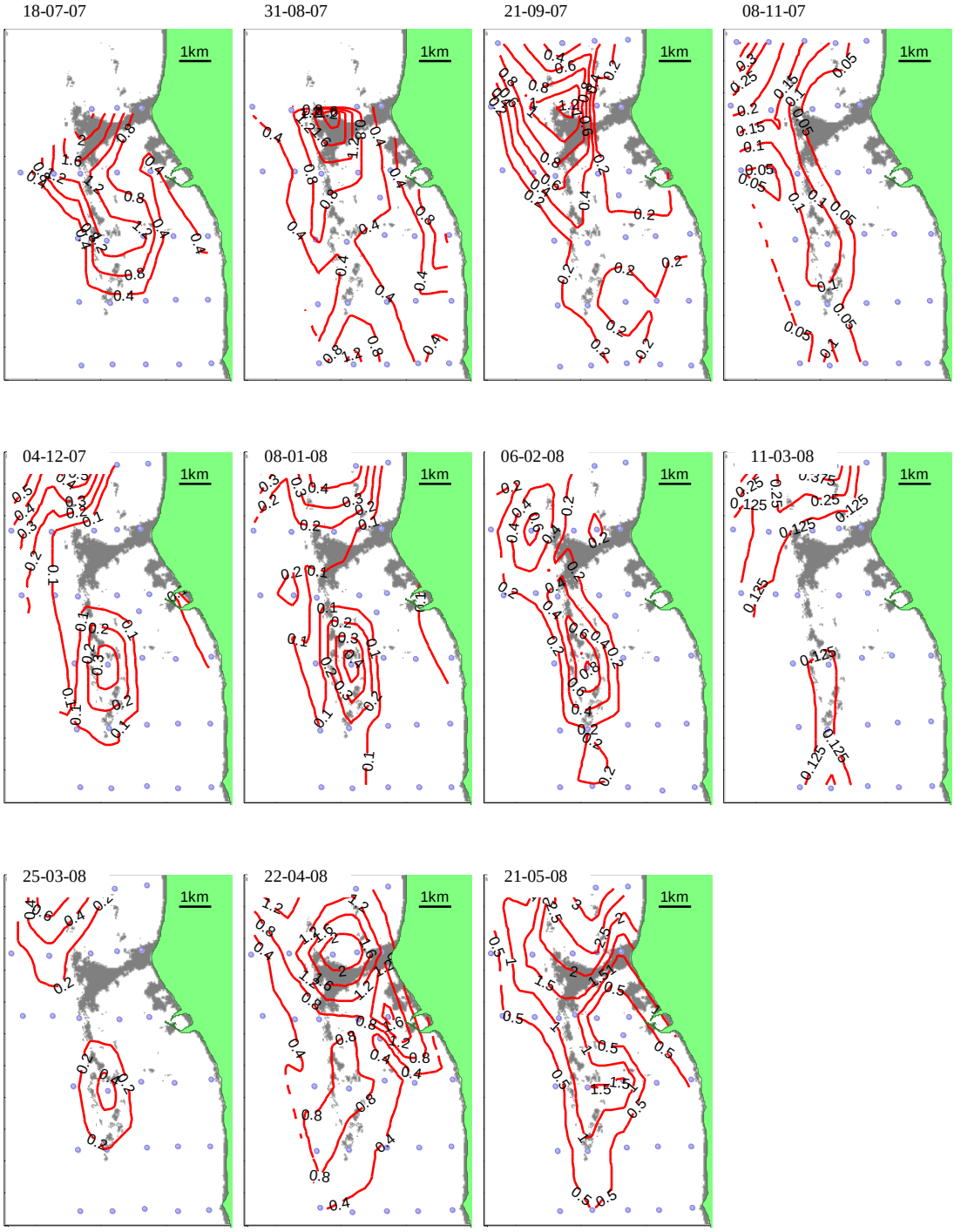

Figure 3.3. Spatial variations in nitrate (µM) collected on 11 monthly cruises in Marmion Lagoon.

Ammonium

Ammonium concentrations were generally low (<0.1μM) (Figure 3.4). However, slightly elevated ammonium concentrations (0.2 – 0.4μM) were observed particularly over southern reefs in February, May and September (Figure 3.4). Ammonium is a direct product of remineralisation by bacteria or excretion and elevated levels over reefs suggest a reef based, biotic nutrient source such as filter feeders.

Phosphate

Phosphate distributions were similar to nitrate in May June, July and August (Figure 3.5). In November – February phosphate levels were a little higher inshore than expected based on nitrate (Figure 3.5). Phosphate is not limiting in these waters and the reduced demand compared to nitrate explains the difference in distribution (Lourey et al. 2006).

Silicate

Silicate levels were generally highest inshore near the coast indicative of land based sources and near shore runoff (Figure 3.6). Consistent with runoff (or ground water) being the dominant source of silicate in the lagoon, winter levels were higher than those measured in summer (Figure 3.6).

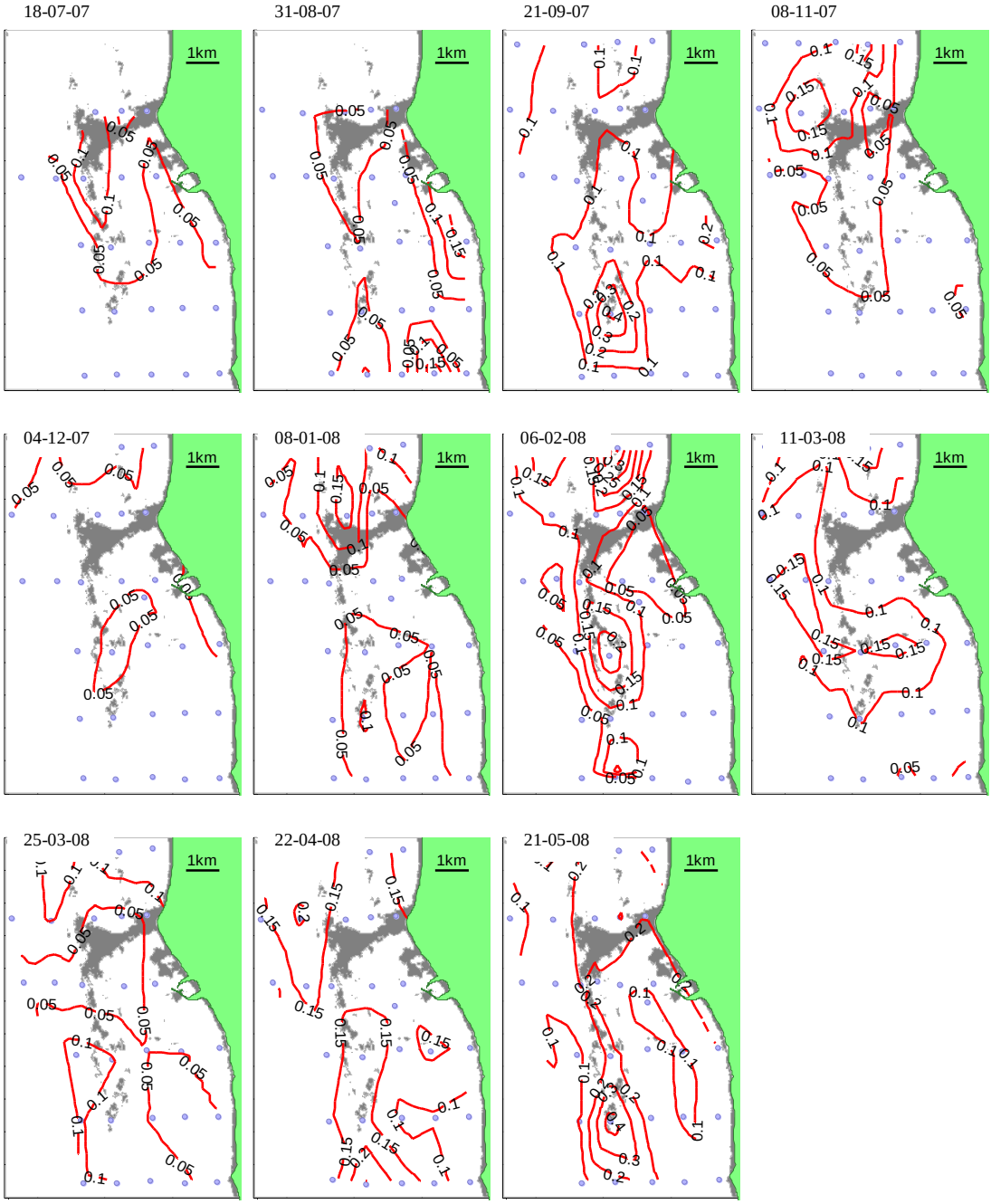

Figure 3.4. Spatial variations in ammonium (µM) collected on 11 monthly cruises in Marmion Lagoon.

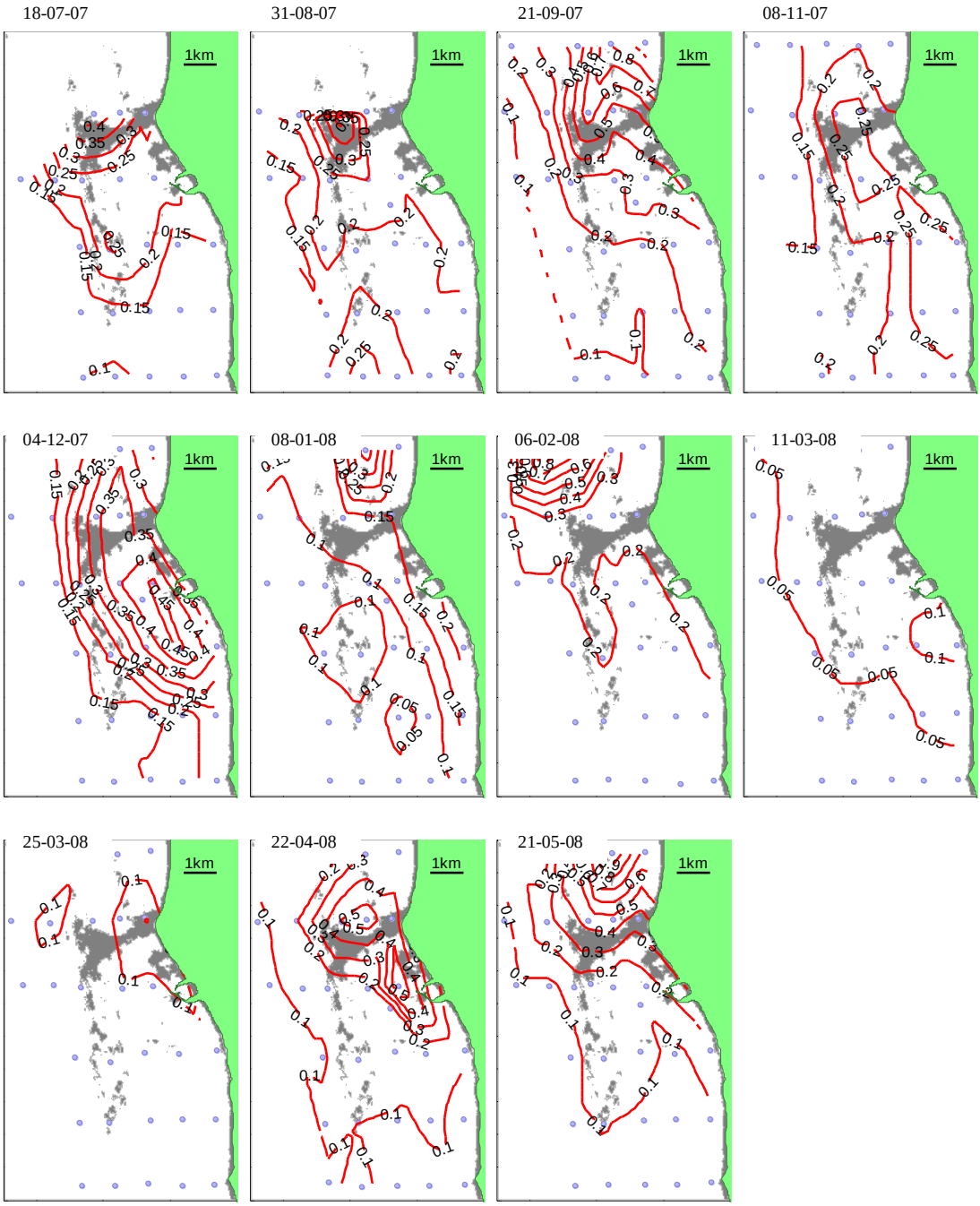

Figure 3.5. Spatial variations in phosphate (µM) collected on 11 monthly cruises in Marmion Lagoon.

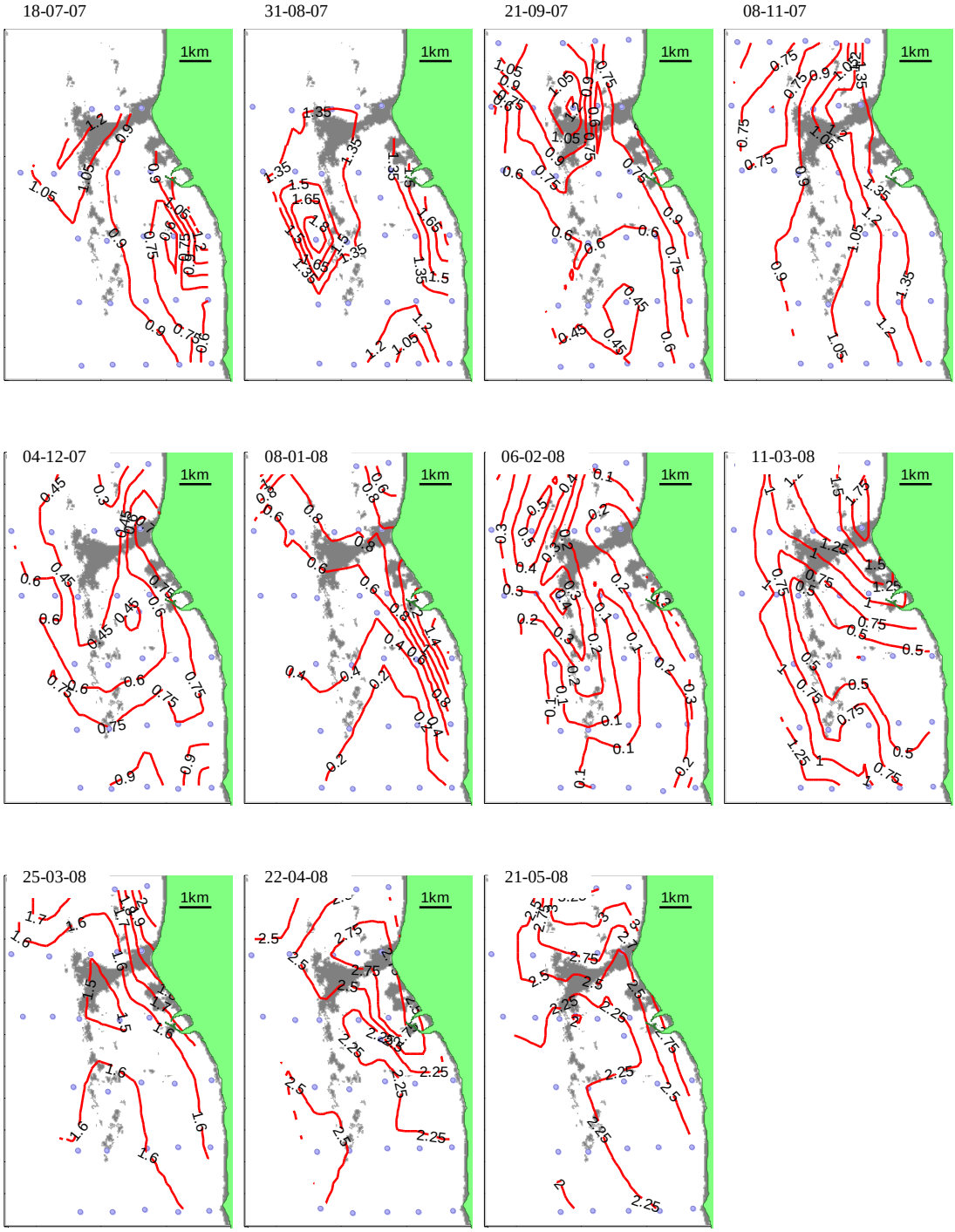

Figure 3.6. Spatial variations in silicate (µM) collected on 11 monthly cruises in Marmion Lagoon.

3.1.3 Historical nitrate analysis

Methods

Study area

We present historical surface water nitrate data collected at a range of temporal scales (weekly to hourly) with the aim of better understanding nutrient resupply mechanisms to Marmion Lagoon (Figure 3.7). The study area is offshore from Mullaloo Point, with one station located in about 6 m of water outside the reef (station A); a station approximately 50 m east of Station A located 10 m inside the reef in 7 m of water (station B); and a station 30 m from the beach (station C) (Figure 3.7). Comparison with samples collected from similar habitats suggest each station is representative of similar areas within the lagoon (Lourey and Kirkman 2009). Samples were taken at least weekly during fine weather (less than 25 knots) at station A and C between March 1980 and June 1984 (Figure 3.7). A more intensive sampling regime (daily) was conducted at all three stations during September 1983 and at stations B and C from June until August 1984 (Figure 3.7). On two occasions (from 27th–28th of July and 2nd–7th August 1985) an ISCO automatic water sampler was used to collect hourly water samples at station B.

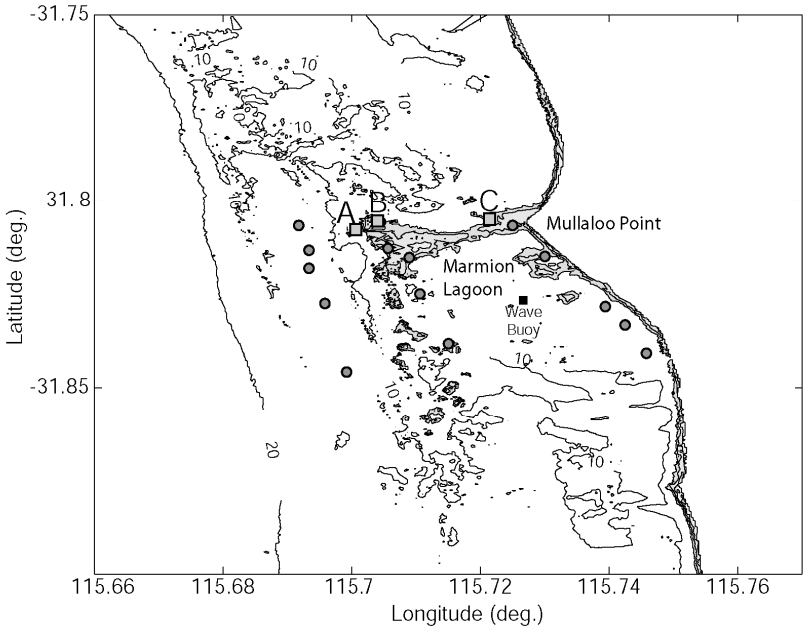

Figure 3.7. Map of the study. The three main stations, A, B and C are labelled (grey squares), as is the location of the wave rider buoy (black square). The grey circles are the three north-south transects occupied to examine spatial variations.

At each station, a 20 L bucket of surface seawater was collected from the seaward side of the boat and a 250 mL sample taken from the bucket for analysis. The samples were filtered (0.4 µm Millipore membrane) and analysed i for dissolved nitrate and nitrite by the method of Strickland and Parsons (1972). Wave height data (H1, the most probable value of the height of the highest wave) were collected between the 7th of June 1984 and the 17th of October 1984

from a Wave Rider buoy situated within Marmion Lagoon around 500 m south of the shore (station C) site (Figure 3.7).

Results

Nitrate concentrations varied considerably between weekly (Figure 3.8), daily (Figure 3.9 Figure 3.10) and even hourly (Figure 3.11) sampling events. Not surprisingly, in an area such as this where the surface waters are strongly nitrogen limited, large nitrate increases between sampling trips were equally rapidly depleted. Although not necessarily "new" nitrogen, these nitrate pulses appear to make a considerable contribution to maintaining primary producers in Marmion Lagoon. Over the course of each of the daily sampling periods, nitrate accumulation during the periods where nitrate increased between sampling trips was 6.2 µM (average of 0.26 µM day^{-1} for the period) in September 1983 (Figure 3.9) and 18.7 µM (an average 0.35 µM day^{-1} for the period) from June to August in 1984 (Figure 3.10). Annually, the average of the two daily flux measurements would correspond to an effective flux of around 111.5 µM for the year or, in 7 m of water, 7.8 x 10^5 µM m^{-2} yr^{-1} (10.9 gN m^{-2} yr^{-1}).

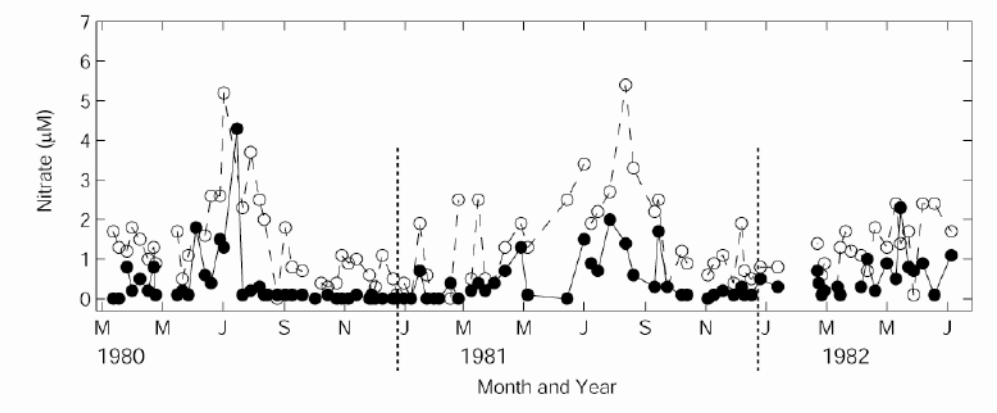

Figure 3.8. Mean weekly dissolved nitrate concentrations (µM) of station A, reef (open circles) and station C, shore (closed circles) sites.

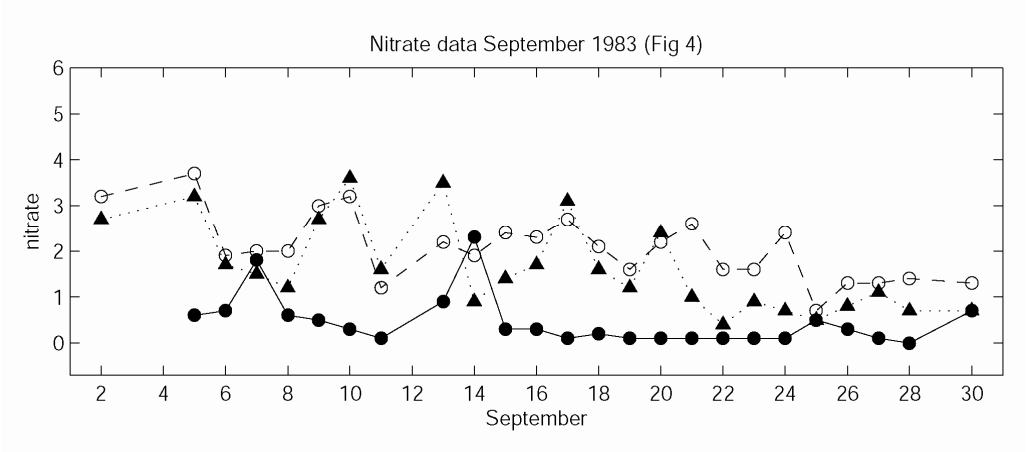

Figure 3.9. Top: Daily nitrate concentration (µM) in September 1983 taken at two reef sites (stations A located outside and B located inside, open circles and closed triangles, respectively) and the shore (station C, closed circles) site.

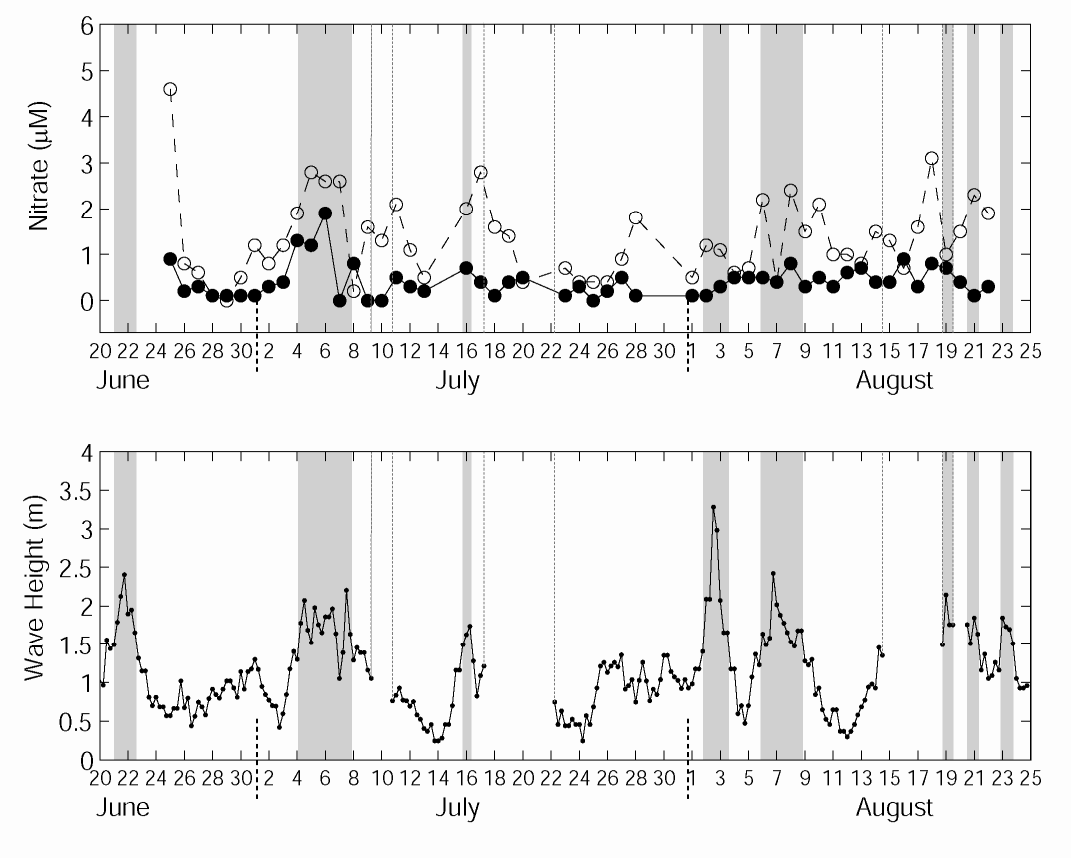

Figure 3.10. Top: Daily nitrate concentration (µM) from late June until late August (winter) 1984 at reef (station B, open circles) and shore (station C) sites. Bottom. Six-hourly average wave height in the Lagoon for the period from late June until late August (winter) 1984. The shaded areas in both upper and lower plots are periods where measured wave heights are over 1.5m.

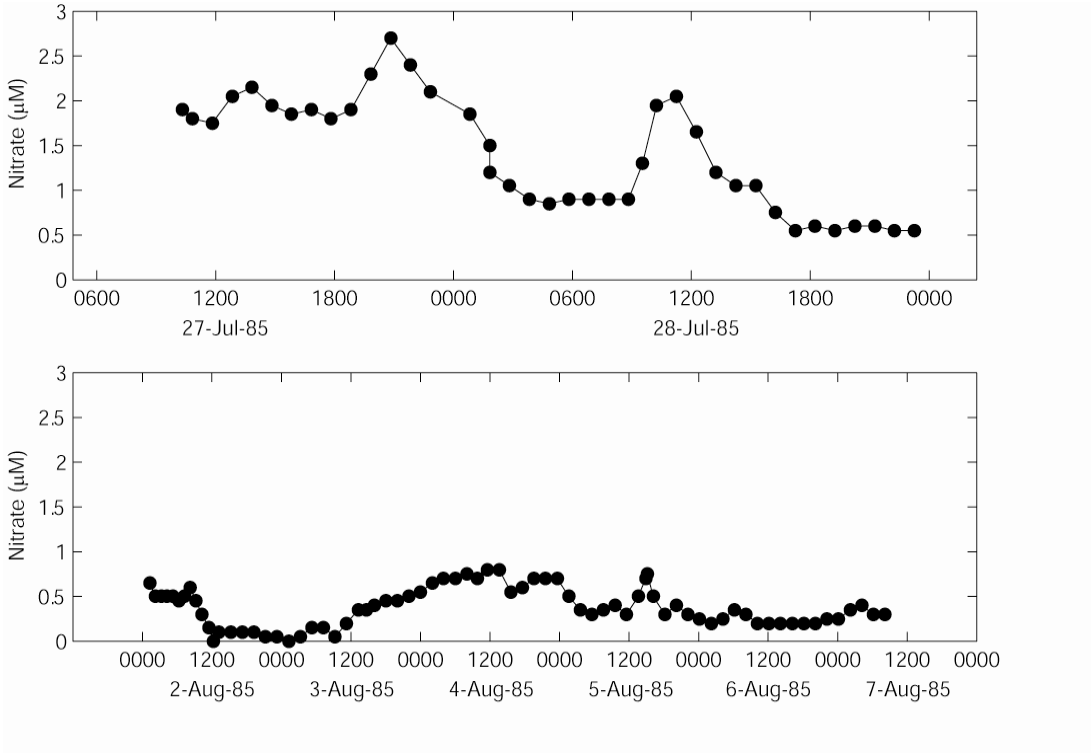

Figure 3.11. Four hourly means of nitrate concentration of hourly samples taken by ISCO automatic water samplers on two occasions.

This annualised nitrate flux is comparable with the estimated nitrate recycling flux required to balance the whole-of-shelf nutrient budget (6.2 gN m^{-2} yr^{-1}) and our flux estimates are likely to be conservative as the calculations only consider the flux attributable to observable increases in nitrate and do not consider the depletion due to uptake by phytoplankton during and between the periods of accumulation. The observed flux calculated above combined with the unquantified uptake during periods of accumulation suggest that on an areal basis, shallow areas such as Marmion Lagoon may make a particularly important contribution to the overall shelf nutrient budget.

Generally, ammonium is the direct product of the decomposition of organic material. Nitrate, the compound measured here is derived from this ammonium by bacterial nitrification. In this system, rapid ammonium consumption by autotrophs would leave little scope for conversion of significant amounts to nitrate. It is perhaps more likely that the remineralisation and nitrification processes that generate the nitrate observed here are isolated from the autotrophic biota. Porewaters trapped by surface sediment layers may provide the conditions required for nitrification of ammonium to nitrate.

The short lived pulses of nitrate suggest that the mechanism that generates them is dynamic. On average, nitrate concentrations were highest in winter (although there was considerable interannual variability in the timing and magnitude of the winter maxima) between June and August (Figure 3.12). Winter is the high wave energy period and physical processes may generate the nitrate pulses observed here and as such sustain primary production. Wave data coinciding with the collected nitrate data are limited and only coincide with daily samples collected between late June and August in 1984 (Figure 3.10). There is a general correlation

between periods of increased wave activity and elevated nitrate concentration (see Figure 3.13) although the correlation between them is not statistically significant (p = 0.17).

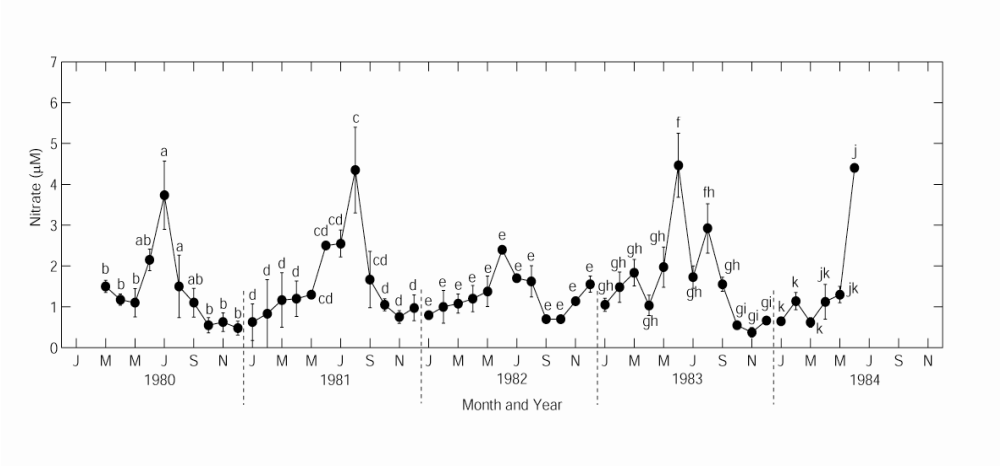

Figure 3.12. Mean monthly (upper) dissolved nitrate concentrations at the reef site (station A) for five years. The error bars are 1 standard error about the mean. The number of samples each month varies. Significant differences for individual comparisons within each year are denoted by letters. Months in any one year with differing letters are significantly different from one another.

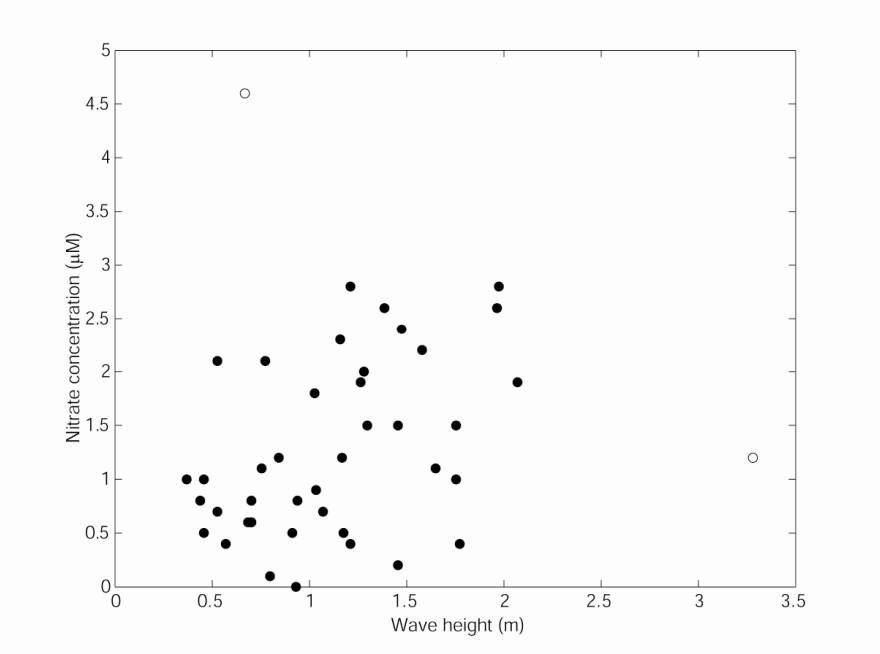

Figure 3.13. The relationship between nitrate concentrations (µM) measured daily between late June and late August (winter) in 1984 at reef station B, and the corresponding wave height (from six-hourly measurements). The open circles are outliers.

Physical processes may may release nutrients that have accumulated in the sediment porewaters between wave events. It may promote the remineralisation and release of nutrients bound up in organic carbon accumulated in rock crevices or between reefs, or large pieces of detritus lying on the bottom or fine grained material trapped within the surface sediments. Alternatively, the organic carbon could also be derived from living tissue, such as attached macroalgae and seagrass whose tips are physically abraded during storms. Finally it is possible that wave driven

variations in pressure on uneven (ridges and troughs) permeable sediments enhances pore water circulation within the sediments and drives it across the sediment-water interface.

Nitrate concentrations measured outside the reef were significantly higher than those measured inside the reefs which, in turn, were higher than those measured inshore (Figure 3.14). This is not particularly surprising as the Lagoon stations (B and C) are sheltered somewhat by a series of offshore reefs (Figure 3.7) which dissipate some of the wave energy encountered at the outer station. It is possible that rates of macroalgal erosion or sediment resuspension are lower inside the reef due to the reduced physical forcing. The high concentrations at stations nearest the reef suggest that the reefs themselves may act as nutrient point sources. The reefs typically have a high biomass of macroalgae and abraded plant material and may be a more important source of labile biomass to surface waters. If most of the small organic matter decomposes on or near the reef or is incorporated into the sediments close by, then the reefs would appear to be a nutrient source. In contrast the inner station (the site with the lowest pelagic nitrate concentrations) is well removed from this abrading macroalgae and could be limited by a reduced fresh detrital supply. However, the inshore site is very shallow, disturbance is omnipresent, and the sediments are likely to be resuspended more often than in deeper areas and this continuous disturbance may not allow detritus to accumulate to an extent sufficient to generate the nitrate peaks observed further offshore.

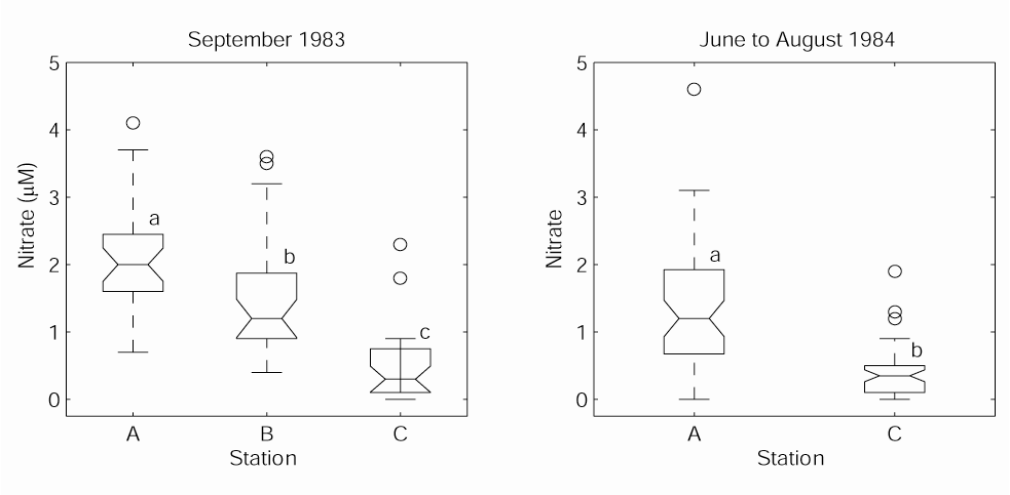

Figure 3.14. Box plots comparing the distribution of nitrate concentrations (µM), measured daily during September 1983 (left) and between late June and late August 1984 (right) at three positions across the Lagoon. Station A located outside the Lagoon near a reef, Station B located inside the Lagoon and station C located near shore in the Lagoon. The centre line is the median. The notched area is the uncertainty about the medians for box-to-box comparison (boxes whose notches do not overlap indicate that the medians of the two groups differ at the 5% significance level). Stations with differing letters are significantly different from one another. The top and bottom of the box represent the 25th and 75th percentiles (the distance between the upper and lower percentiles is the interquartile range). The error bars bound the rest of the data except for outliers (open circles which are data that are more than 1.5 times the interquartile range outside the 25th or 75th percentiles).

3.1.4 Benthic nutrient exchange

Methods

Sediment nutrient fluxes were quantified twice once in winter (August 2008) and once in summer (January 2009). At six stations within or near Marmion Lagoon (Cow Rock, AA, BB, MM4, MM1 and M3MRS see Figure 3.15) we collected twenty four 9.3cm ID sediment cores. The cores were selected from a restricted location to reduce the small scale spatial variability. However, if sand ridges were present cores were evenly distributed between the ridge peaks and troughs to average out this potential source of variability. Cores were returned to the laboratory and distributed into four tubs (i.e. 6 cores per tub) with a continuous flow of clean ambient seawater (6 litres per minute). The cores in each tub represent replicates of an experimental treatment. In all, there were 8 experimental treatments for each station (7 different light intensities and one dark incubation) achieved by conducting incubations on sequential days using the same cores.

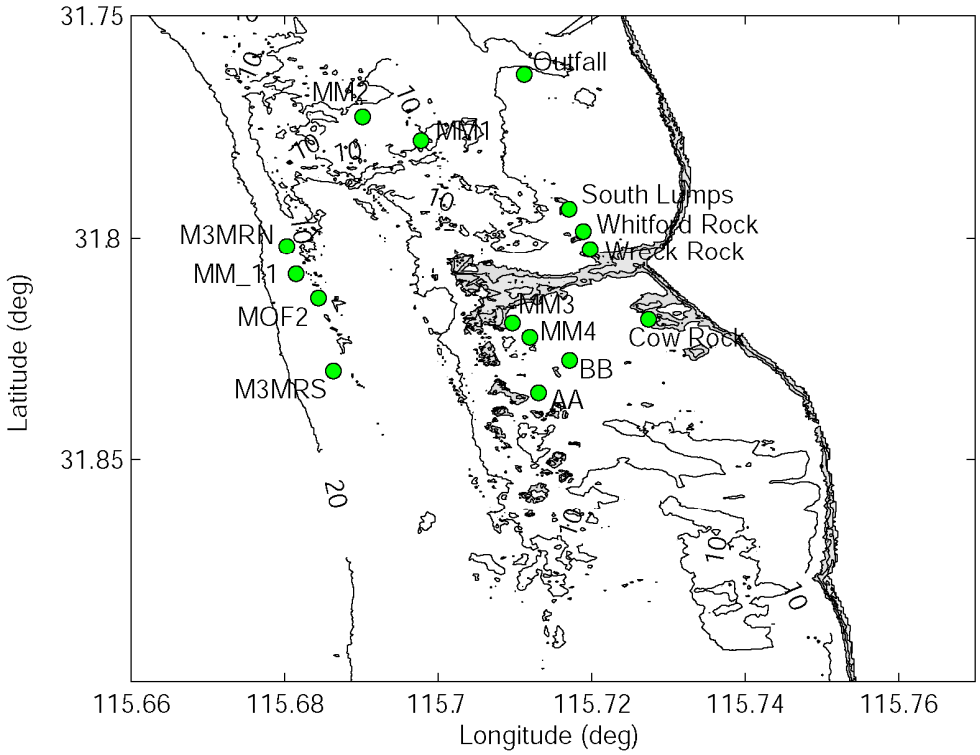

Figure 3.15. Map of Marmion Lagoon sampling stations.

Each experimental aquarium was illuminated by a metal halide lamp. Light exposure was varied using neutral density film sufficient to achieve a range of nominal light intensities up to 1200 µmol quanta m^{-2} s^{-1}. Light readings were taken with a Licor PAR meter equipped with at two pi PAR sensor at the beginning and end of the incubation and the irradiance used in the calculations represents the average of these two measurements. Heavy black plastic was wrapped around the bin containing the cores for the dark treatment.

At the beginning of the incubation, each of the cores was sealed with a clear acrylic lid. The lid has two ports, one for sampling and the other to allow the resupply of surrounding water as each sample is collected. The water inside the core is stirred gently by a 4 cm Teflon coated magnetic stirrer bar suspended under the lid and driven by a small electric motor. Soon after each core was sealed a 30 ml sample of water was collected for dissolved oxygen analysis and a further 35 ml sample of water was collected from each core for dissolved nutrient analyses. This initial sampling serves as a starting reference for the incubation. Two further samples were collected from each core at regular intervals during the incubation. After the incubation was complete the lids were removed and the cores left until the next morning when the same routine was practiced for the remaining light intensity treatments. After the final sampling, the length of the sediment plug and overlying water column were measured and the sediment stored frozen for later geochemical analysis (chlorophyll a, sediment grain size, sediment moisture content, and sediment POC/PON).

Rates of production and nutrient fluxes were calculated as the slope of the solute versus time relationship, normalised by the overlying water volume. Corrections were made for the replacement water from the ambient tank. Illuminated flux rates are the average of all illuminated treatments.

Results

Even in dark respiration dominated treatments, nutrient flux data is dominated by consumption. On average, nitrate, ammonium and for the most part silicate were consumed in both the dark and light treatments at each of the stations (see summer silicate fluxes at Cow Rock for the exception) (Figure 3.16). This is to be expected in situations where oxygen is being produced as photosynthesis consumes any nutrients produced by remineralisation in addition to any present in the water column. However, in this case there was also dark uptake of nutrients. Assuming rates of denitrification are low (Forehead 2009), we expect bacterial processes to release nutrients and in the absence of photosynthesis (dark incubations).

In general, ammonium, nitrate and silicate consumption was higher in the summer than the winter (Figure 3.16), presumably reflecting temperature related constraints on photosynthesis during winter (Colijn & Vanbuurt 1975).

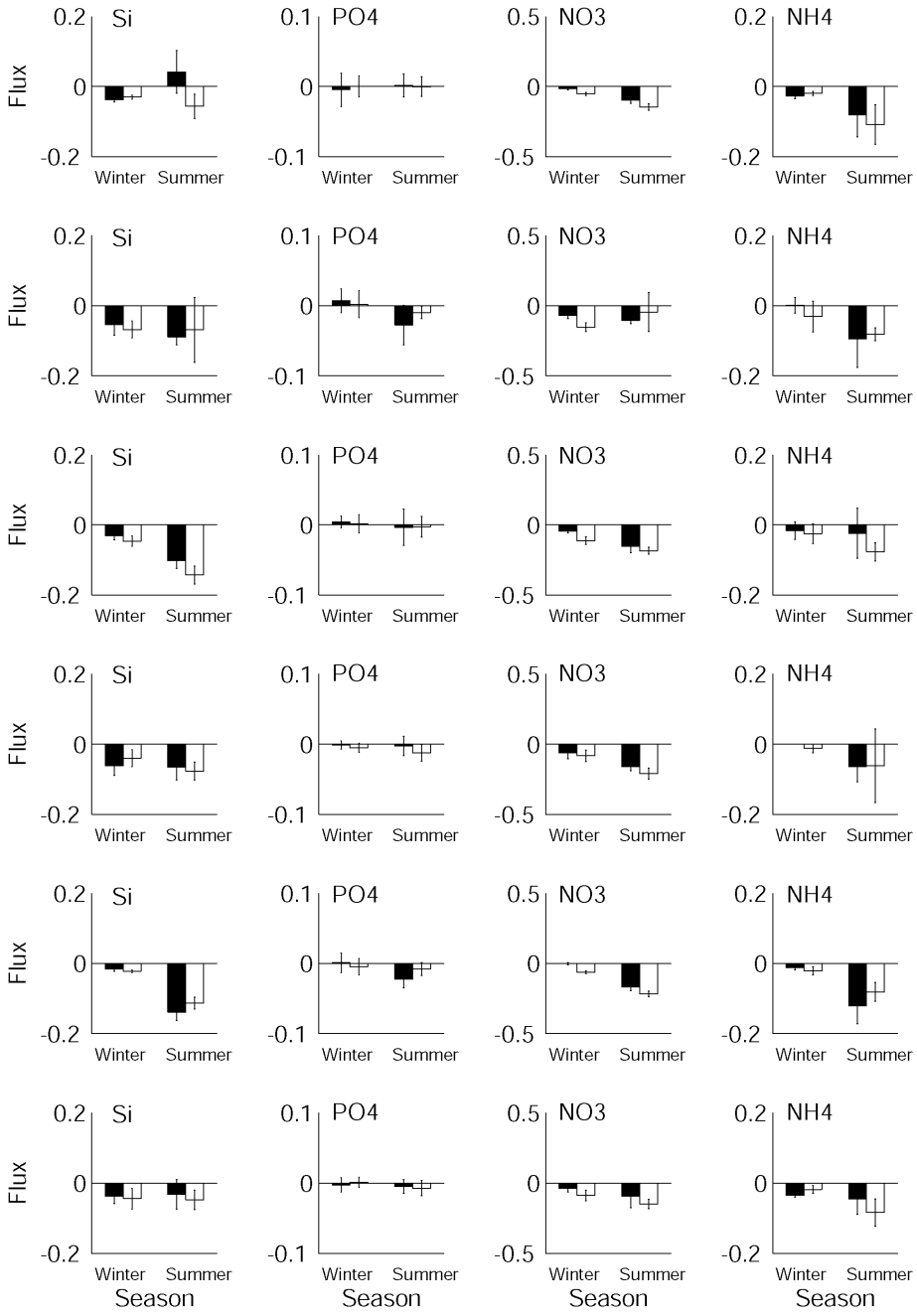

Figure 3.16. Summer and winter sediment nutrient fluxes (mmol nutrients m-2 hr-1) at six stations im Marmion lagoon. The stations arranged from top to bottom are Cow Rocks (inner shelf), AA (mid shelf in Marmion Lagoon), BB (mid shelf in Marmion Lagoon), MM4 (mid shelf in Marmion lagoon), MM1 (Mid shelf to the north of Marmion Lagoon) and M3MRS (outer shelf). The dark bars are dark fluxes (respiration) and the light bars represent the average of all the irradiated treatments.

Dark uptake of nutrients is also evident in Figure 3.17 where the majority of silicate, nitrate and ammonium fluxes were negative (nutrient consumption), despite many situations where respiration appears to dominate production and oxygen was consumed. The result is that the range of nutrient fluxes was small compared to the equivalent DO fluxes and the fluxes are a small proportion of what would be expected from the rates of oxygen production and Redfield

requirements of phytoplankton. This disconnection between the observed nutrient fluxes and what we would expect based on redfield stochiometry suggests that rapid uptake by microphytobenthos dominates the nutrient flux dynamics in these sediments.

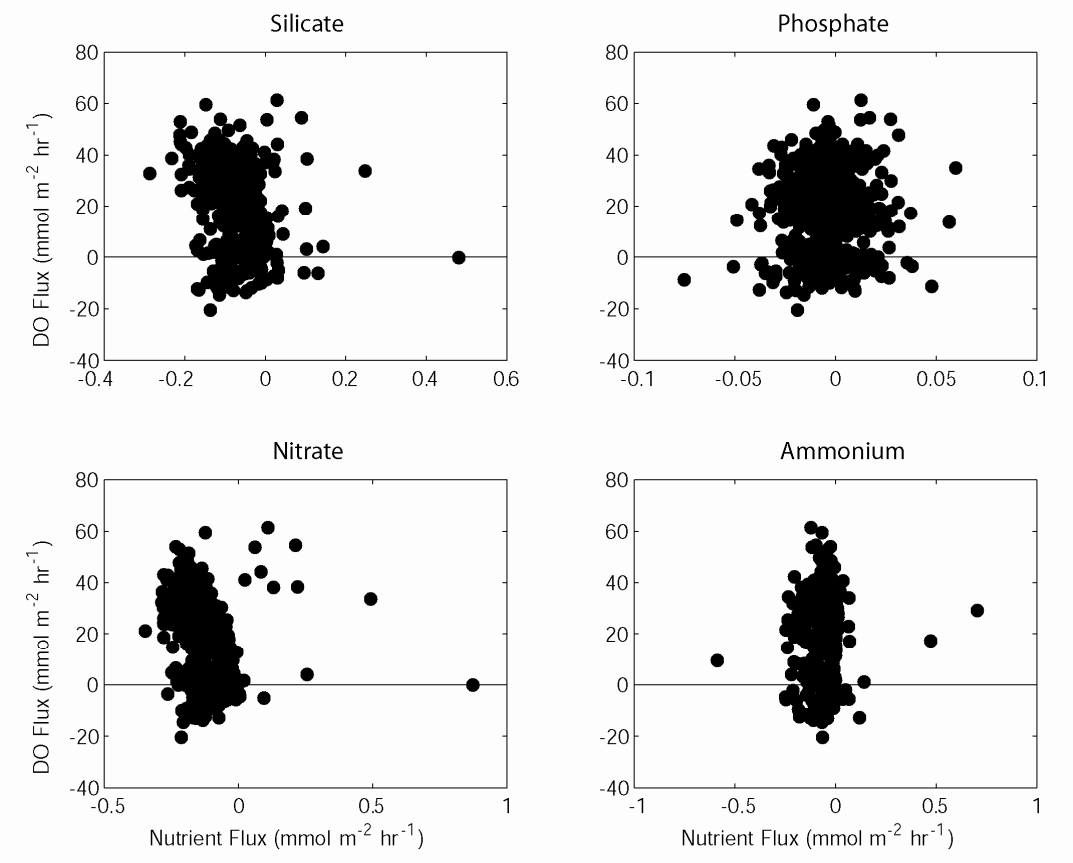

Figure 3.17. Relationship between oxygen production/consumption and sediment nutrient flux.

3.1.5 Abundance and diet of Zooplankton

Methods

Zooplankton was sampled in 6 stations and in MS1, MS2 and AWAC stations (Figure 3.18, Table 1.1). Samples for biomass analysis were collected by oblique tows of Bongo nets with 50 cm diameter opening and 100 and 355 µm mesh nets towed from depth of the station to the surface. Biomass of zooplankton was determined using Ash-Free Dry Weight which is a measurement of the weight of organic material. Samples were immediately preserved in 5 % borax buffered formalin (2 g of borax to 98 ml of 40% formaldehyde). In the lab samples from 100 µm mesh net were size fractionated on precombusted and pre-weighted Whatman GFC filters. Filters were pre-combusted at 500º C for 2 hours. Samples were dried at 60º C for 48 h in Qualtex Solidstat oven. Samples were transferred to a desiccator and allowed to cool to room temperature. Next the dry samples were weighted on balance Sartorius MC1. The resulting dry weight was the weight of both the organic and inorganic contents of the sample. The weighted samples on glass fiber filters were combusted in a muffle furnace (Heraeus Electronic) starting at room temperature and reaching 500 ºC for 12 hours to determine ash weight. The AFDW (the organic content of the sample) was obtained by subtracting the weight of the ash (inorganic contents only) from dry weight (inorganic and organic contents).

Chlorophyll a was used as a measure of phytoplankton biomass. Water for chlorophyll *a* was collected using Niskin's bottles from surface and chlorophyll maximum layers. Water samples were filtered under low vacuum (<100 mm Hg) onto 25 mm diameter glass fiber filters (Whatman GF/F™; nominal mesh size = 0.7 µ) (total phytoplankton) and 5 µm Nitex™ mesh (large phytoplankton). Pigments were extracted overnight in 90% acetone over night in the dark at 4 ºC and measured using a Turner Designs model TD 700™ fluorometer and chlorophyll a was calculated following standard methods (Parsons et al., 1984). For the analysis we averaged the measurements from surface and chlorophyll maximum layers. Small phytoplankton biomass was obtained by subtracting large fraction biomass from total phytoplankton.

Zooplankton for fatty acid analysis was sampled with Bongo nets 355 and 100 µm, 50 cm diameter towed obliquely from depth of the station to the surface. Zooplankton was size fractionated immediately. Samples from 355 µm net were sieved through 1 mm size mesh and organisms retained on that mesh were discarded leaving 1 mm to 355 µm fraction. Content of 100 µm mesh were sieved through 355, 250, 150, and 100 µm mesh. Organisms retained on 355 µm were discarded and the rest of the fractions were frozen in cryotubes in liquid nitrogen creating the following size fractions: 355-1000, 250-355, 150-250 and 100-150 µm. Upon arrival on shore samples were transferred to - 80 ºC until fatty acid analysis. Fatty acids were a mixture of fatty acids from the food in the guts and fatty acids assimilated into the mesozooplankton body tissues. Lipids were quantitatively extracted from the samples by a single-phase chloroform/methanol method, which was modified by substituting dichloromethane for the chloroform. Each sample was added to 20 ml of a 3:6:1 v/v/v dichloromethane/methanol/water solution and held at room temperature overnight. Samples were then centrifuged at 10,000rpm (Orbital 420). After centrifugation, 10 ml of the solution was taken, with 10 ml of dichloromethane, followed by 10 ml of water, added and the mixture centrifuged again. The bottom dichloromethane solution was then concentrated using a rotatory evaporator under vacuum. The resulting sample was mixed with 2% sodium hydroxyl in

methanol refluxing for 10 minutes. Borotrifluoride-methanol complex was then added into the samples and mixed for 2 minutes. Finally, hexane was added. The upper hexane solution was transferred to a gas chromatography (GC) vial for fatty acid analysis by GC analysis. Gas chromatography (GC) was initially performed using a HP 5890 GC system equipped with FID detector and Agilent 6890 Series injector. The gas chromatograph was equipped with a 60 m x 0.25 mm i.d. and 0.25 um BPX 70 (SGE) with hydrogen (ultra pure) as the carrier gas. The initial oven temperature was set for 100°C, increasing at a rate of 2.5°C/minute to 150°C (held for 2 minutes). Temperature was then increased at 1.5°C/minute to 220°C (held for 1 minute). Finally, the temperature increased at 12°C/minute to 250°C (held for 8 minutes). The peak areas were determined with an integrator (Hewlett-Packard 5890). Peak identifications were based on comparison of retention times with authentic and laboratory standards and subsequent gas chromatographic-mass spectrometric (GC-MS) analysis using an Agilent Technologies 6890N network GC System and 5973 Network Selective Detector. Data were acquired and peak area quantified using ChemStation chromatography software. The abbreviated fatty acid nomenclature used within this paper is A:Bn-X, where A designates the total number of carbon atoms, B the number of double bonds, and X the position of the double bond closest to the terminal methyl group. Based on the fatty acid composition different biomarkers and biomarker ratios were used (Table 3.1).

Figure 3.18. Location of sampling stations.

Table 3.1. Sampling stations and dates.

stations	sampling times
AWAC	28/11/2007, 9/01/2008, 6/03/2008, 8/04/2008
MS1	13/08/2007, 28/11/2007, 9/01/2008, 6/03/2008, 8/04/2008
MS2	13/08/2007, 28/11/2007, 9/01/2008, 6/03/2008, 8/04/2008
S1	3/08/2007, 2/05/2008, 8/10/2008
S2	19/02/2007, 3/08/2007, 6/05/2008,17/10/2008
S3	19/02/2007, 3/08/2007, 6/05/2008, 17/10/2008
S4	21/02/2007, 3/08/2007, 6/05/2008, 17/10/2008
S5	21/02/2007, 3/08/2007, 28/04/2008, 10/10/2008
S6	3/08/2007, 2/05/2008, 8/10/2008

Results

The average biomass of zooplankton (AFDW) was 0.02 g m^{-3} (±S.D. 0.01) and varied in time and space (Figure 3.19, Figure 3.20). Biomass was highest in autumn and lowest in summer, however the difference was not statistically significant (ANOVA, P=0.066). Zooplankton biomass was not correlated with total biomass, large or small phytoplankton biomass (Figure 3.21, Figure 3.22, Figure 3.23). The biomass of zooplankton in Marmion lagoon was comparable to biomass in other coastal waters (Table 3.2). The temporal pattern was the same as in Two Rocks transect with lowest biomass in summer. Parallel increase in phytoplankton biomass during May to October was observed in western Australian coastal waters (Koslow 2008). This increase could be due to increased flow of the Leeuwin Current and influx of regenerated nutrients from sediments or advection of the nutrients from the north (Koslow 2008). The 355 µm size fraction comprised most of the zooplankton biomass in stations S1 to S6 and AWAC. In MS1and MS2 1000 µm size dominated (Figure 3.24). It is important to note that small zooplankton < 150 µm formed an important part of biomass ranging from 40 to 30 % in most stations.

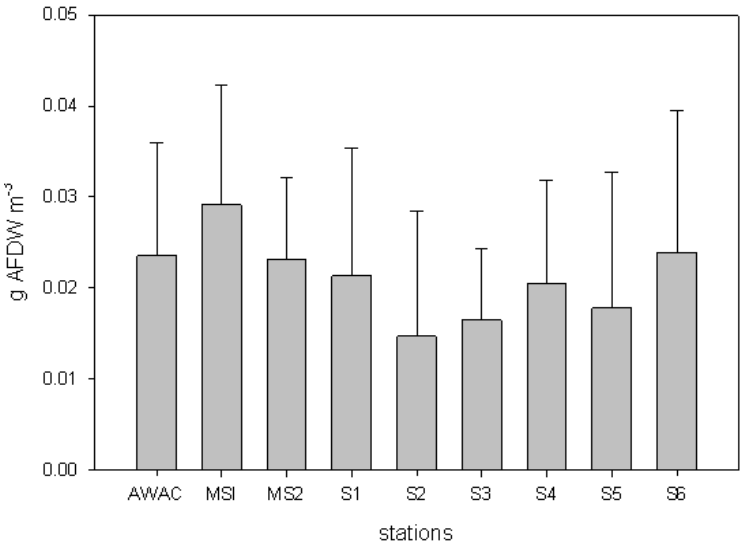

Figure 3.19. Biomass of zooplankton in Marmion Lagoon in different stations (error bars are s.d. of means)

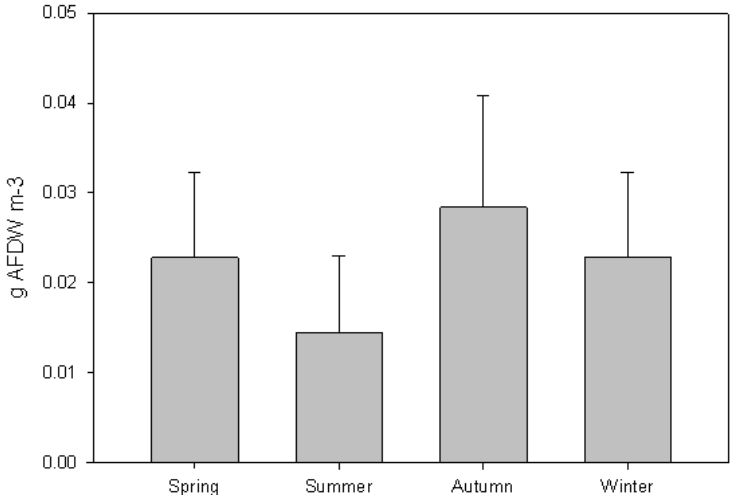

Figure 3.20. Biomass of zooplankton in different seasons (error bars are s.d. of means).

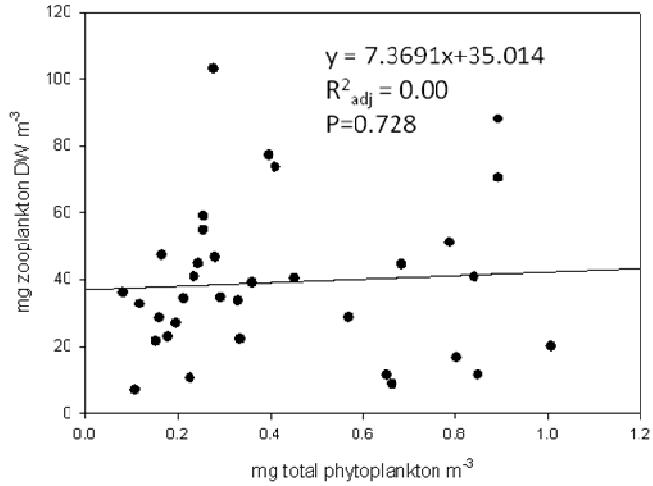

Figure 3.21. Correlation between zooplankton biomass and total phytoplankton biomass.

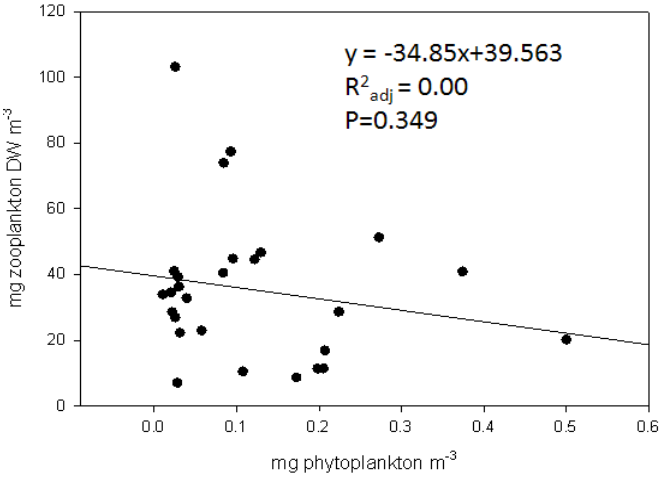

Figure 3.22. Correlation between zooplankton biomass and large phytoplankton biomass.

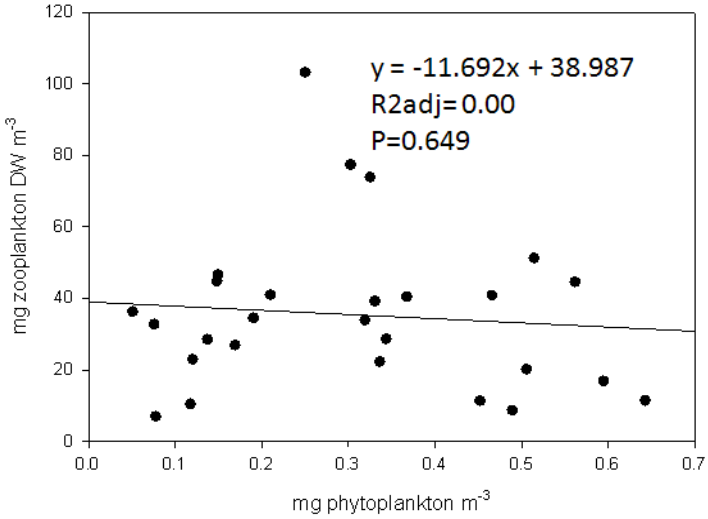

Figure 3.23. Correlation between zooplankton biomass and small phytoplankton biomass.

Table 3.2. Comparison of dry weight zooplankton biomass from different coastal zones.

Biomass of zooplankton mg Dwt m-3	Region	Reference
7-60	Kariega estuary, South Africa	Froneman, P.W. 2001 Seasonal changes in zooplankton biomass and grazing in a temperate estuary, South Africa. Estuarine, Coastal and Shelf Science, 52, 543-553
9.9	Florida coast	Hopkins, T.L. 1966 The plankton of the St. Andrew Bay System, Florida. Publ. Inst. Mar. Sci. Texas 11, 12-64.
60-300	Southeastern Gulf of Mexico	De la Cruz, A. 1972 Investigaciones del plancton de la Plataforma sur de Cuba. Investigaciones Pesqueras Sovietico-Cubanas. VNIRO-CIP. Moscu. Fasciculo 2, 58-73
0.3 - 7.5	Mexican Caribbean coast (Chetumal Bay)	Gasca, R. and Castellanos, I 1993. Zooplancton de la Bahia de Chetumal, Mar Caribe, Mexico. Rev. Biol. Trop. 41(3) 291-297.
6-37.5	Mexican Caribbean coast (Ascencion Bay)	Suarez E. and Gasca, R. 1994 Zooplankton Biomass Fluctuations in a Mexican Caribbean Bay (Bahia de la Ascencion) during a year cycle. Caibbean Journal of Science, 30 (1-2) 116-123
2.6-231	Gulf of Tehuantepec, Mexico	Ayala-Duval, 1996, Spatial and Temporal Distribution of Zooplankton Biomass in the Gulf of Tehuantepec, Mexico. Pacific Science, 50(4), 415-426
15-55	Two Rocks, Western Australia	Strzelecki, J., Koslow, .A., 2006. Mesoplankton. In: Keesing, J.K., Heine, J.N., Babcock, R.C., Craig, P.D., Koslow, J.A. (Eds.), Strategic Research Fund for the Marine Environment Final Report. The SRFME Core Projects. Strategic Research Fund for the Marine Environment, vol. 2. CSIRO, Australia, pp. 88–102. 274pp.
14-167	Coastal waters off Western Australia	Strzelecki, unpublished data
7-103	Marmion lagoon	this study

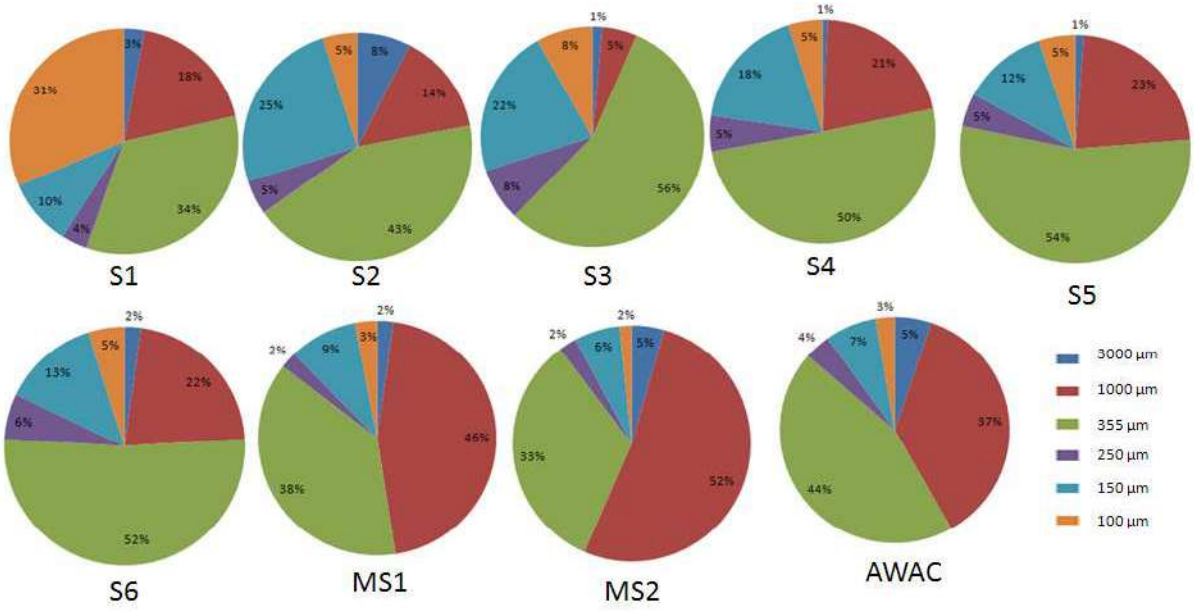

Figure 3.24. Size structure of zooplankton based on AFDW.

The ratio of EPA to DHA of <1 indicated that zooplankton of all sizes was feeding mostly on microzooplankton except large zooplankton in MS2 (Figure 3.25) since diatoms are rich in EPA and dinoflagellates are rich in DHA (Dalsgaard et al, 2003). This is not unexpected in low nutrients waters where phytoplankton is too small to be grazed directly by zooplankton. In such systems microzooplankton is the main grazer of phytoplankton and they are main prey of zooplankton. Main food items of zooplankton were dinoflagellates, followed by diatoms, bacterivorous ciliates. The observed lack of 18:5 n-3 which is a marker for dinoflagellates suggested that zooplankton was feeding on heterotrophic dinoflagellates (i.e. lacking photosynthetic pigment) since only photosynthetic dinoflagellates contain this fatty acid. Alternatively this dinoflagellate marker was metabolised by zooplankton. However, photosynthetic dinoflagellates were found only infrequently in coastal waters and not found at all at stations further offshore during monthly surveys from 2002 to 2004 along the Two Rocks transect north of Perth, Western Australia yet high proportion of heterotrophic dinoflagellates especially in offshore waters were identified in cell counts from that region throughout the study. Carnivory represented relatively small part of the total diet. Carnivory markers off Western Australian coast increased with the distance offshore while diatom markers were higher in zooplankton caught inshore during Southern Surveyor cruise in 2007 (Strzelecki unpublished data).

Table 3.3. Food biomarkers used in this study.

Fatty Acid	Marker	Reference
∑16:1n-7, 16:4n-1, 20:5n-3	Diatoms	Graeve, M., Kattner, G. and Hagen, W. (1994). Diet-induced changes in the fatty acid composition of Arctic herbivorous copepods: Experimental evidence of trophic markers. Journal of Experimental Marine Biology and Ecology 182, 97-l 10. Bugde et al 2001 Fatty acid composition of phytoplankton settling particulate matter and sediments at a shelter bivalve aquaculture site Marine Chemistry 76 285-303
∑18:5n-3, 22:6n-3	Dinoflagellates	Dalsgaard, J., St John, M., Kattner, G., Müller-Navarra, D., Hagen, W. 2003 Fatty acids trophic markers in the pelagic marine environment. Advances in marine Biology, 46, 225-340
18:3n-3	Dinoflagellate, Prymnesiophytes (sometimes), non diatom algae, cryptophytes, haptophytes, flagellates	Graeve, M., Kattner, G. and Hagen, W. (1994). Diet-induced changes in the fatty acid composition of Arctic herbivorous copepods: Experimental evidence of trophic markers. Journal of Experimental Marine Biology and Ecology 182, 97-l 10. Dalsgaard, J., St John, M., Kattner, G., Müller-Navarra, D., Hagen, W. 2003 Fatty acids trophic markers in the pelagic marine environment. Advances in marine Biology, 46, 225-340 Mayzaud, P., Laureilard, J., Merien, D., Brinis, A., Godard, C., Razouls, S., Labat, J-P. 2007. Zzooplankton nutrition, storage and fecal lipid composition in different water masses associated with the Agulhas and subtropical fronts Marine Chemistry 107, 202-213 Brett, M.T., Müller-Navarra, Person, J. 2009. Crustacean zooplankton fatty acid composition. in: Lipids in Aquatic Ecosystems, Arts, M.T., Brett, M.T., Kainz, M.J. eds.Springer Dordrech Heidelberg London, New York. P 124
18:1n-9	carnivory	G. Kattner, G., Albers, C., Graeve, M., Schnack-Schiel S. B. 2003. Fatty acid and alcohol composition of the small polar copepods, *Oithona* and *Oncaea* : indication on feeding modes. Polar Biology, 26, 666-671
18:1n-7	Bacterivorous	Ederington, M. C. McManus, G. B. and Harvey, H. R. (1995). Trophic transfer of fatty acids, sterols, and a

Fatty Acid	**Marker**	**Reference**
	ciliates	triterpenoid alcohol between bacteria, a ciliate, and the copepod *Acartia onsa* Limnology and Oceanography 40, 860-867.
15:0, 17:0, iso and anteiso	Bacteria	Budge, S. M. and Parrish, C. C. (1998). Lipid biogeochemistry of plankton, settling matter and sediments in Trinity Bay, Newfoundland. II. Fatty acids. Organic Geochemistry 29, 1547-1559. Budge, S. M., Parrish, C. C. and Mckenzie, C. H. (2001). Fatty acid composition of phytoplankton, settling particulate matter and sediments at a sheltered bivalve auaculture site. Marine Chemistry 2001, 285-303
∑18:1n-9, 18:4n-3	Hapthophytes	Desvilettes, C.H, Bourdier, G., Amblard, C.H, Barth, B., 1997 Use of Fatty acids for the assessment of zooplankton grazing on bacteria, protozoans and microalgae Viso, A-C., Marty, J-C., 1993 Fatty acids from 28 marine microalgae. Phytochemistry, 34, 1521-1533
16:1n-7/16:0	Low ratio >1 indicated diatom food web	Kharlamenko, V. I., Zhukova, N. V., Khotimchenko, S. V., Svetashev. V. I. and Kamenev, G. M. (1995). Fatty acids as markers of food sources in a shallow-water hydrothermal ecosystem (Kraternaya Bight, Yankich Island, Kurile Islands). Marine Ecology Progress Series 120, 231-241. St. John, M. A. and Lund, T. (1996). Lipid biomarkers: linking the utilization of frontal plankton biomass to enhanced condition of juvenile North Sea cod. Marine Ecology Progress Series 131, 75-85.

Table 3.4. Fatty acids in size fractionated zooplankton.

	Site name	MS1	MS1	MS1	MS1	MS2	MS2	MS2	MS2	AWAC	AWAC	AWAC	AWAC
	Size fraction (µm)	1000 - 355	355-250	250-150	150-100	1000 - 355	355-250	250-150	150-100	1000-355	355-250	250 - 150	150 - 100
Saturated		%	%	%	%	%	%	%	%	%	%	%	%
Myristic	C14:0	6.6	6.0	4.1	6.8	15.5	6.1	5.3	2.9	3.3	12.5	6.1	**7.7**
Pentanoic	C15:0	1.1	0.7	0.6	1.0	2.3	0.8	0.7	0.9	0.6	1.1	0.6	0.8
Palmitic	C16:0	17.5	17.5	18.0	29.8	29.9	17.1	15.1	8.0	15.4	31.0	17.7	24.0
Margaric	C17:0	1.3	0.9	0.3	0	1.8	0.9	1.1	1.6	1.2	1.5	1.0	1.3
Stearic	C18:0	6.2	5.7	7.3	10.3	8.8	5.5	6.8	3.7	7.1	10.0	6.3	**7.9**
Nonadecanoic	C19:0	0.2	0.2	1.9	2.2	0.2	0.2	0.2	0.2	0.2	0.2	0.2	0.2
Arachidic	C20:0	0.3	0.4	0.4	0.0	0.0	0.3	0.2	0.1	0.4	0.5	0.3	0.4
Heneicosanoic	C21:0	0.2	0.2	0.0	0.0	0.3	0.1	0.1	1.0	0.1	0.0	0.2	0.1
Behenic	C22:0	0.5	0.8	0.3	0.0	0.2	0.9	0.9	0.4	0.2	0.3	0.8	0.0
Tricosanoic	C23:0	0.0	0.1	0.0	0.0	0.2	0.2	0.1	0.3	0.1	0.0	0.1	0.0
Lignoceric	C24:0	0.9	1.2	1.4	1.8	0.0	1.1	1.5	0.8	1.2	0.3	1.2	0.8
Cerotic	C26:0	0.0	0.0	0.3	0.0	0.0	0.2	0.0	0.0	0.0	0.0	0.0	0.0
Heptacosanoic	C27:0	0.0	0.1	0.0	0.0	0.5	0.1	0.2	0.0	0.0	0.0	0.1	0.1
Triacontanoic	C30:0	0.1	0.0	0.0	0.0	0.3	0.0	0.0	0.0	0.0	0.0	0.0	0.0
	sum	**34.9**	**33.8**	**34.7**	**52.0**	**60.1**	**33.5**	**32.2**	**19.9**	**29.8**	**57.5**	**34.5**	**43.4**
Branched	i-C15:0	0.6	0.4	0.3	0.0	0.8	0.2	0.2	0.2	0.2	0.4	0.2	0.4
	i-C16:0	0.5	0.2	0.3	0.0	0.2	0.0	0.0	1.0	0.2	0.0	0.1	0.1
	i-C17:0	0.6	0.5	0.5	0.0	0.7	0.4	0.4	0.2	0.3	0.6	0.4	0.4
	sum	**1.6**	**1.0**	**1.1**	**0.0**	**1.7**	**0.6**	**0.6**	**1.4**	**0.8**	**1.0**	**0.7**	**1.0**
Monounsaturated													
Palmitelaidic	C16:1n-7t	0.3	0.4	0.0	0.0	0.4	0.3	0.3	0.2	0.1	0.5	0.3	0.4
Palmitoleic	C16:1n-7c	3.7	6.9	4.6	8.3	5.1	5.8	2.8	1.7	2.7	10.8	4.2	5.1
	c16.1	0.8	0.2	0.0	0.0	2.6	0.3	0.3	0.1	0.2	0.3	0.2	0.3
Heptadecenoic	C17:1n-7c	0.6	0.2	0.0	0.0	0.5	0.2	0.1	0.2	0.6	0.2	0.4	0.6
Petroselaidic	C18.1 t-6	0.1	0.1	0.0	0.0	0.0	0.1	0.1	0.0	0.1	0.0	0.1	0.3
Petroselenic	C18:1 c-6	0.0	0.2	0.0	0.0	0.0	0.2	0.0	0.0	0.0	0.0	0.2	0.1
Oleic	C18:1n-9c	4.8	3.1	3.6	5.8	12.7	3.6	3.9	2.1	5.0	5.7	4.1	6.0
Vaccenic	C18:1n-7c	3.0	1.4	1.9	3.5	3.9	1.1	1.1	0.9	2.4	2.2	1.2	1.7
Gadoleic	C20:1n-10c	0.0	0.0	0.8	0.9	0.2	0.0	0.4	0.3	0.5	0.3	0.3	0.8
Gondoic	C20:1n-8c	0.5	0.2	0.4	1.9	0.3	0.5	0.0	2.1	0.5	0.4	0.0	0.6
Eicosenoic	C20:1n-6c	0.1	0.6	0.3	0.0	0.0	0.3	0.1	0.2	0.1	0.5	0.3	0.1
Brassidic	C22:1n-9t	0.1	0.0	0.0	1.4	0.0	0.1	0.1	0.0	0.2	0.2	0.1	0.2
Erucic	C22:1n-9c	0.0	0.1	0.3	0.0	0.5	0.0	0.0	0.0	0.0	0.0	0.1	0.1
Nervonic	C24:1n-7c	0.3	0.4	0.0	0.0	0.3	0.9	0.2	26.9	0.5	0.4	0.3	0.3
	sum	**14.0**	**13.4**	**11.9**	**21.8**	**26.1**	**12.4**	**9.3**	**7.9**	**12.6**	**21.1**	**11.5**	**16.4**
Polyunsaturated													
Linoleic	C18:2n-6c	3.1	1.8	0.0	0.0	3.8	2.3	2.3	1.1	2.0	1.6	2.0	2.2
Linolenelaidic	C18:3n-3t	0.2	0.2	0.0	0.0	0.0	0.2	0.2	0.0	0.1	0.0	0.2	0.2
	C18.3 t9,t12,c15	0.3	0.3	0.3	0.0	0.2	0.3	0.2	0.0	0.3	0.0	0.2	0.3
Linolenic	C18:3n-3c	2.5	1.4	2.4	3.3	0.0	1.5	1.5	1.1	1.0	0.7	1.3	1.5
gamma-Linolenic	C1:3n-6c,	0.0	0.0	0.0	0.0	0.7	0.0	0.0	0.0	0.0	0.0	0.0	0.0
Stearidonic	C18:4n-3c	1.2	1.6	1.4	0.0	0.3	2.3	2.1	1.0	1.1	0.8	2.0	1.8

	Site name	**MS1**	**MS1**	**MS1**	**MS1**	**MS2**	**MS2**	**MS2**	**MS2**	**AWAC**	**AWAC**	**AWAC**	**AWAC**
	Size fraction (µm)	**1000 - 355**	**355-250**	**250-150**	**150-100**	**1000 - 355**	**355-250**	**250-150**	**150-100**	**1000-355**	**355-250**	**250 - 150**	**150 - 100**
Eicosadienoic	C20:2n-6c	0.4	0.2	0.5	0.0	0.4	0.2	0.4	0.3	0.6	0.2	0.4	0.5
Arachidonic	C20:4n-6c, AA	3.5	2.3	3.0	2.8	0.5	2.1	1.7	1.3	3.7	1.2	2.0	2.4
Eicosatrienoic	C20:3n-3c	0.2	0.1	0	0.0	0.0	0.1	0.15	0.2	0.16	0	0.1	0.2
Eicosatetraenoic	C20:4n-8c	0.2	0.3	0.0	0.0	0.0	0.2	0.1	0.0	0.0	0.0	0.2	0.3
Eicosapentanoic	C20:5n-3, EPA	15.1	13.6	12.8	5.9	1.4	12.7	12.0	5.5	14.8	4.8	12.3	8.0
Docostetraenoic	C22:4n-6c	0.0	0.0	0.0	1.3	0.4	0.0	0.0	1.1	0.1	0.0	0.0	0.2
Docasapentenoic	C22:5n-3c	0.8	0.9	1.0	0.0	0.0	0.8	0.8	0.6	1.0	0.3	0.8	1.0
Docosahexenoic	C22:6n-3, DHA	18.3	25.7	26.4	8.0	0.8	24.1	32.8	14.0	27.9	7.3	28.3	14.8
	Sum	**45.8**	**48.3**	**47.9**	**21.2**	**8.4**	**46.7**	**54.4**	**26.4**	**52.8**	**16.9**	**49.7**	**33.4**
	Sum n-3	23.5	30.2	31.6	11.3	1.3	29.2	37.8	17.0	31.6	9.0	33.0	19.8
	sum n-6	7.1	5.1	3.8	4.0	5.7	5.1	4.6	4.1	6.5	3.6	4.7	5.6
	n-3:n-6	3.3	5.9	8.2	2.8	0.2	5.7	8.2	4.1	4.8	2.5	7.0	3.5

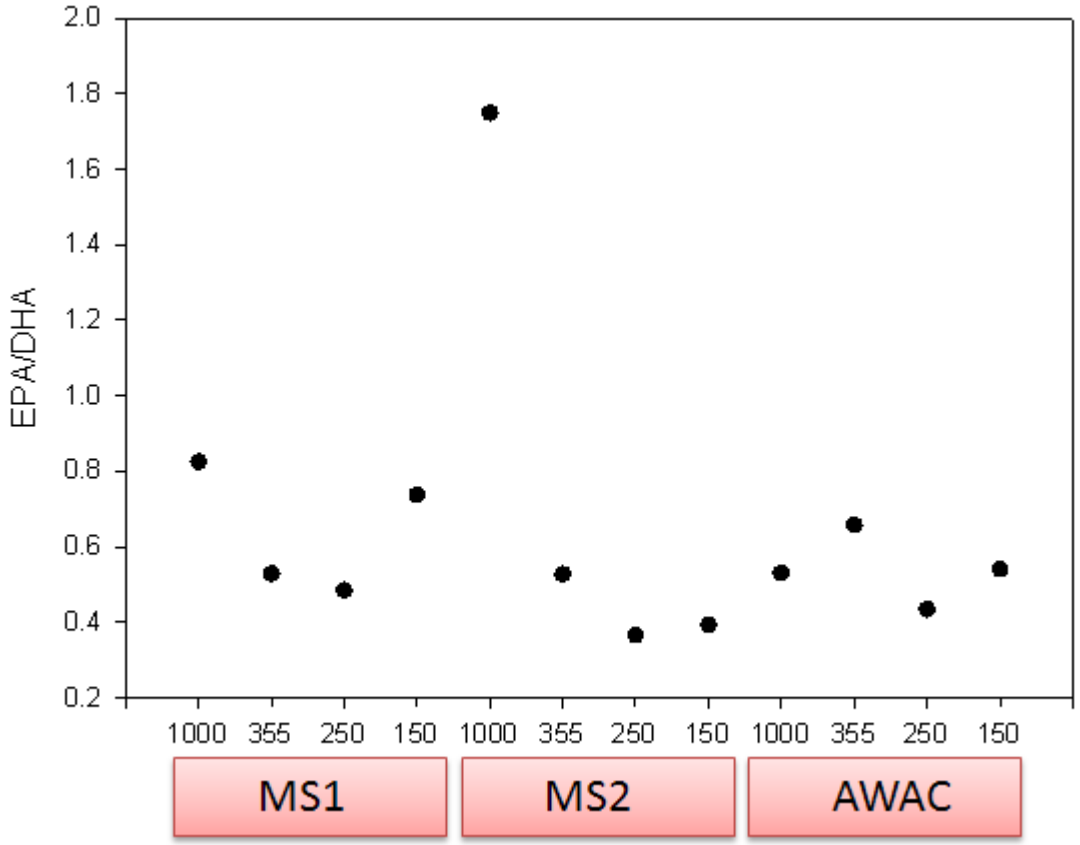

Figure 3.25. Ratio of EPA to DHA in size fractionated zooplankton from three stations.

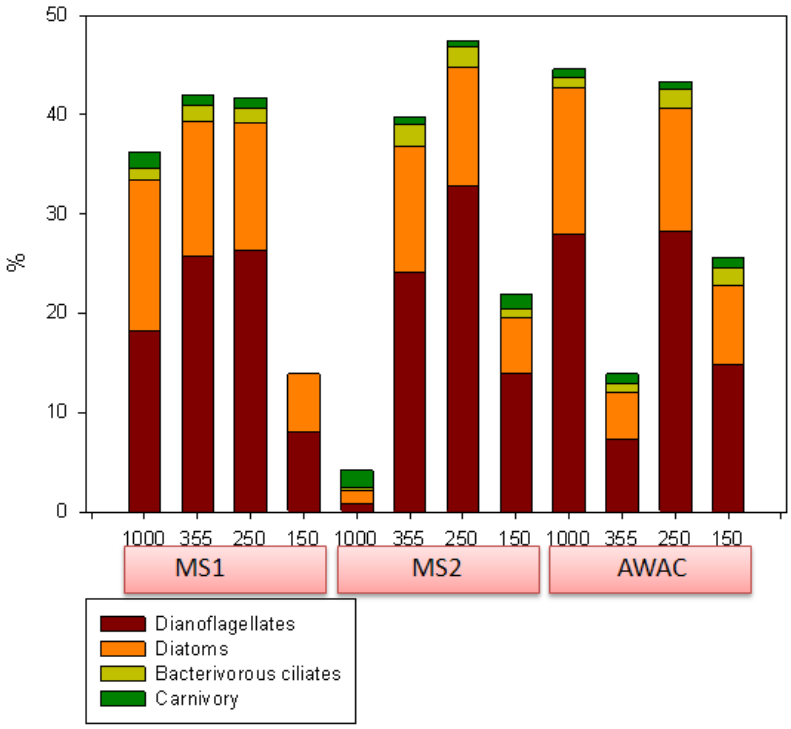

Figure 3.26. Main food items of zooplankton based on fatty acid markers.

3.1.6 Biomass: mobile benthic invertebrates

Methods

Surveys

The density (number of individuals) and biomass of benthic invertebrates were surveyed in three habitats: rocky reef, seagrass and unvegetated sand. These three habitats were surveyed at each of five sites in both Marmion Lagoon and Jurien Bay. The surveys were done by SCUBA divers, who searched five 5 × 1 m transects at each site. Searches in the unvegetated sand habitat were done by raking the sand, while searches in the rocky reef and seagrass habitats were done by visual and tactile inspection of the surface. Large (> 1 cm) invertebrates were identified to lowest taxonomic level (usually species) and sizes (in cm) were estimated. In some cases individuals were also collected and subsequently measured for biomass in the laboratory, in other cases biomass was estimated from size-weight regressions (see below).

We used statistical analyses to test for the presence of patterns in density or biomass among Habitats (3 levels, fixed factor), locations (2 levels, random factor), and sites (10 levels, random and nested in location). Because the data contained many zeros, parametric statistics were unsuitable and so data were analysed using permutational multivariate ANOVA (PERMANOVA; Anderson 2001), which uses permutation to test for statistical significance. Euclidean distances were calculated from untransformed data, and the permutation tests used 9,999 permutations of residuals under a reduced model. Biomass data were typically highly skewed, a characteristic that can lead to high dispersion, and so biomass data were log-transformed (x+1) prior to analysis. Densities and biomasses of species were combined into the following broad taxonomic and functional groups: asteroids, crinoids, echinoids, holothuroids, herbivorous gastropods and predatory gastropods (Table 3.5).

Biomass estimation

During the surveys some individuals were collected for measurements in the laboratory. These were supplemented by additional collections in cases for which there were not enough intervals to establish reliable size-weight relationships. Sizes (in mm) were measured with callipers, and weights (wet weight, in g) were measured on a laboratory balance.

Size weight relationships were determined from regressions of the form log(weight) ~ log(size). To test whether species within a taxonomic or functional group could be pooled, we first used ANCOVA to test whether the slope of the regressions varied significantly among species. In each case the slopes varied significantly among species, and so species-specific regressions were calculated (Table 3.6).

Table 3.5. Species recorded during the surveys of benthic invertebrates, with the total number of individuals recorded in each habitat at each location.

		Reef		Sand		Seagrass		Total
Class	Species	Jurien	Marmion	Jurien	Marmion	Jurien	Marmion	
Anthozoa	*Actinernidae* sea anemones		217				7	224
Asteroidea	*Archaster angulatus*				98			98
	Coscinasterias muricata		5					5
	Fromia polypora		3					3
	Goniodiscaster seriatus						4	4
	Luidia australiae						2	2
	Nectria saoria		1					1
	Patiriella brevispina		8				246	254
	Patiriella gunni				3			3
	Pentagonaster dubeni	2	1					3
	Petricia vernicina	1	3					4
Bivalvia	*Circe sp. Rough cockle*				3			3
	Mactra sp. Smooth cockle				13			13
	Pinna bicolor						5	5
Crinoidea	*Cenolia trichoptera*		57					57
	Comatula purpurea		57				155	212
Echinoidea	*Amblypneustes leucoglobus*					1	13	14
	Ammotrophus arachnoides				14			14
	Clypeaster cf. telurus			2	1			3
	Goniocidaris tubaria						6	6
	Heliocidaris erythrogramma	56	77					133
	Phyllacanthus irregularis	7	24					31
Gastropoda (herbivorous)	*Astralium squamiferum*	2	5					7
	Australium tentoriformis	1	1			1		3
	Campanile symbolicum	6				2		8
	Haliotis scalaris		2					2
	Scutus antipodes	1						1
	Bulla quoyii				7			7

Table 3.5. Species recorded during the surveys of benthic invertebrates, with the total number of individuals recorded in each habitat at each location.

		Reef		Sand		Seagrass		Total
Class	Species	Jurien	Marmion	Jurien	Marmion	Jurien	Marmion	
	Turbo intercostalis	1						1
	Turbo jourdani	1						1
	Turbo torquatus	2	5					7
Gastropoda (predatory)	*Cymbiola nivosa*				1			1
	Oliva australis				3			3
	Thais orbita	1	5					6
Holothuroidea	*Stichopus mollis*	2	8			2		12
	Stichopus sp						1	1
TBA	Echinoderm T2-EA				1			1
	Echinoderm T5-EA				1			1
	Mollusc T1-A			4	7			11
	Mollusc T1-B				3			3
	Mollusc T1-C				2			2
	Mollusc T1-D				5			5
	Mollusc T1-E				1			1
	Mollusc T2-A			1	2			3
	Mollusc T2-B			2	1			3
	Mollusc T2-C			1				1
	Mollusc T3-A			3	3			6
	Mollusc T3-B			1	2			3
	Mollusc T3-C				1			1
	Mollusc T4-A			1	4			5
	Mollusc T4-B				3			3
	Mollusc T4-C				1			1
	Mollusc T4-D				1			1
	Mollusc T5-A			3	7			10
	Mollusc T5-B				10			10
	Mollusc T5-C				3			3

Table 3.5. Species recorded during the surveys of benthic invertebrates, with the total number of individuals recorded in each habitat at each location.

		Reef		Sand		Seagrass		Total
Class	Species	Jurien	Marmion	Jurien	Marmion	Jurien	Marmion	
	Mollusc T5-D				3			3
	Mollusc T5-E				4			4
	Mollusc T5-F				2			2

Table 3.6. Regression equations for the relationship between size (in mm) and weight (in g wet weight). n= number of individuals.

Species	n	Size range (mm)	Equation
Echinodermata			
Echinoidea			
Amblypneustes leucoglobus	18	27 - 41	log(Weight) ~ -3.098 + 1.624*log(Size)
Ammotropus arachnoides	21	52 - 152	log(Weight) ~ -9.629 + 2.846*log(Size)
Goniocidaris tubaria	10	33 - 43	log(Weight) ~ -5.800 + 2.586*log(Size)
Heliocidaris erythrogramma	15	32 - 95	log(Weight) ~ -5.175 + 2.348*log(Size)
Holopneustes inflatus	19	30 - 65	log(Weight) ~ -6.171 + 2.587*log(Size)
Holopneustes porosissimus	11	30 - 66	log(Weight) ~ -6.294 + 2.642*log(Size)
Peronella lesueuri	139	53 - 154	log(Weight) ~ -8.476 + 2.665*log(Size)
Phyllacanthus irregularis	19	64 - 119	log(Weight) ~ -5.545 + 2.593*log(Size)
Asteroidea			
Archaster angulatus	149	32 - 240	log(Weight) ~ -3.030 + 1.496*log(Size)
Coscinasterias muricata	19	59 - 247	log(Weight) ~ -8.332 + 2.324*log(Size)
Fromia polypora	14	57 - 123	log(Weight) ~ -4.642 + 1.634*log(Size)
Goniodiscaster seriatus	13	88 - 149	log(Weight) ~ -9.183 + 2.789*log(Size)
Patiriella brevispina	10	24 - 87	log(Weight) ~ -6.523 + 2.313*log(Size)
Patiriella gunnii	21	26 - 85	log(Weight) ~ -2.935 + 1.265*log(Size)
Pentagonaster dubeni	6	55 - 122	log(Weight) ~ -7.549 + 2.417*log(Size)
Petricia vernicina	10	118 - 175	log(Weight) ~ -2.428 + 1.387*log(Size)
Crinoidea			
Cenolia trichoptera	6	54-141	log(Weight) ~ -4.542 + 1.401*log(Size)
Comatula purpurea	6	67 - 144	log(Weight) ~ -7.012 + 1.883*log(Size)
Holothuroidea			
Stichopus spp	6	110 - 150	log(Weight) ~ -4.168 + 1.715*log(Size)
Cercodemas anceps	44	39 - 93	log(Weight) ~ -3.825 + 1.650*log(Size)
Mollusca			
Gastropoda			
Australium squamifera	23	15 - 34	log(Weight) ~ -9.793 + 3.494*log(Size)
Bedeva paivae	6	21 - 26	log(Weight) ~ 1.637 + -0.275*log(Size)
Turbo torquatus	87	21 - 62	log(Weight) ~ -7.347 + 2.799*log(Size)
Bivalvia			
“Large scallop”	5	44 - 75	log(Weight) ~ -4.018 + 1.848*log(Size)
“Scallop”	6	23 - 80	log(Weight) ~ -8.814 + 3.001*log(Size)

Results

Analyses of density indicated that in almost all cases densities differed between habitats, but the magnitude of the differences were not consistent at each site (significant Habitat × Site interactions in Table 3.24). The only exception was predatory gastropods, for which the only pattern detected was differences among sites – although densities of predatory gastropods were typically low everywhere. In general, qualitative differences in density among habitats were also not present. The single exception was echinoids, for which densities were typically higher on reef habitat (Table 3.24, Figure 3.59). There were also qualitative differences in the distribution of crinoids, which were only recorded in Marmion Lagoon (Table 3.24, Figure 3.59).

Analyses of biomass indicated that differences among habitats existed for echinoids, crinoids and holothurians, but that the nature of the differences varied among sites (significant Habitat × Site interactions in Table 3.8). These differences did not exist for asteroids, herbivorous gastropods or predatory gastropods; for two of these three taxa (asteroids and predatory gastropods) there were significant differences in biomass among sites. Qualitative differences in the distribution of biomass were present for echinoids, for which biomasses were almost always higher on reefs (Table 3.8, Figure 3.28) – Boyinaboat Reef, where the biomass of echinoids was higher in sand, was the only exception.

In addition to the trends in overall densities and biomasses of taxonomic and functional groups, there were strong differences in the identity of species recorded in each habitat (Table 3.5). Species that were only recorded in abundance on rocky reefs included the Asteroidea *Coscinasterias muricata, Fromia polypora* and *Petricia vernicina,* the Echinoidea *Heliocidaris erythrogramma* and *Phyllacanthus irregularis,* the Crinoidea *Cenolia trichoptera* and the Gastropoda *Australium squamiferum, Turbo torquatus* and *Thais orbita*. Species that were only recorded in abundance in sand included the Asteroidea *Archaster angulatus,* the Echnoidea *Ammotrophus arachnoids* and the Gastropoda *Bulla qouyi*. Species that were only recorded in seagrass included the Asteroidea *Goniodiscasetr seriatus* and the Echinoidea *Goniocidaris tubaria* and *Amblypneustes leucoglobus*.

Table 3.7. Results of PERMANOVA testing for differences in density of each taxonomic or functional group.

Asteroidea						
Source	df	MS	Pseudo-F	P	Permutations	MC-P
Habitat	2	313.61	0.93	0.605	30	0.528
Location	1	636.54	2.51	**0.016**	54	0.153
Site (Location)	8	253.95	23.43	**0.000**	9940	**0.000**
H x L	2	337.22	1.53	0.250	9952	0.241
H x S(L)	16	219.96	20.30	**0.000**	9912	**0.000**
Residual	120	10.84				
Echinoidea						
Source	df	MS	Pseudo-F	P	Permutations	MC-P
Habitat	2	119.89	106.41	0.203	60	**0.010**
Location	1	18.73	2.27	0.193	37	0.167
Site (Location)	8	8.25	2.37	**0.022**	9951	**0.022**
H x L	2	1.13	0.17	0.849	9949	0.853
H x S(L)	16	6.63	1.90	**0.024**	9913	**0.026**
Residual	120	3.48				
Crinoidea						
Source	df	MS	Pseudo-F	P	Permutations	MC-P
Habitat	2	125.93	1.00	0.709	10	0.493
Location	1	457.63	10.05	**0.008**	16	**0.013**
Site (Location)	8	45.53	2.46	**0.006**	9924	**0.018**
H x L	2	125.93	1.79	0.202	9955	0.197
H x S(L)	16	70.33	3.81	**0.000**	9899	**0.000**
Residual	120	18.48				
Holothuroidea						
Source	df	MS	Pseudo-F	P	Permutations	MC-P
Habitat	2	0.53	1.84	0.363	30	0.348
Location	1	0.17	0.85	0.479	7	0.379
Site (Location)	8	0.20	3.11	**0.004**	9893	**0.004**
H x L	2	0.29	1.58	0.244	9961	0.238
H x S(L)	16	0.18	2.87	**0.001**	9916	**0.001**
Residual	120	0.06				
Herbivorous gastropods						
Source	df	MS	Pseudo-F	P	Permutations	MC-P
Habitat	2	4.05	86.71	0.129	30	**0.012**
Location	1	0.17	0.24	0.687	12	0.629
Site (Location)	8	0.69	3.22	**0.002**	9945	**0.002**
H x L	2	0.05	0.08	0.937	9945	0.924
H x S(L)	16	0.62	2.91	**0.001**	9908	**0.001**
Residual	120	0.21				
Predatory gastropods						
Source	df	MS	Pseudo-F	P	Permutations	MC-P
Habitat	2	0.61	0.98	0.692	10	0.511
Location	1	1.50	1.46	0.289	5	0.264
Site (Location)	8	1.03	2.38	**0.004**	9923	**0.018**
H x L	2	0.62	1.12	0.392	9966	0.360
H x S(L)	16	0.56	1.28	0.113	9869	0.222
Residual	120	0.43				

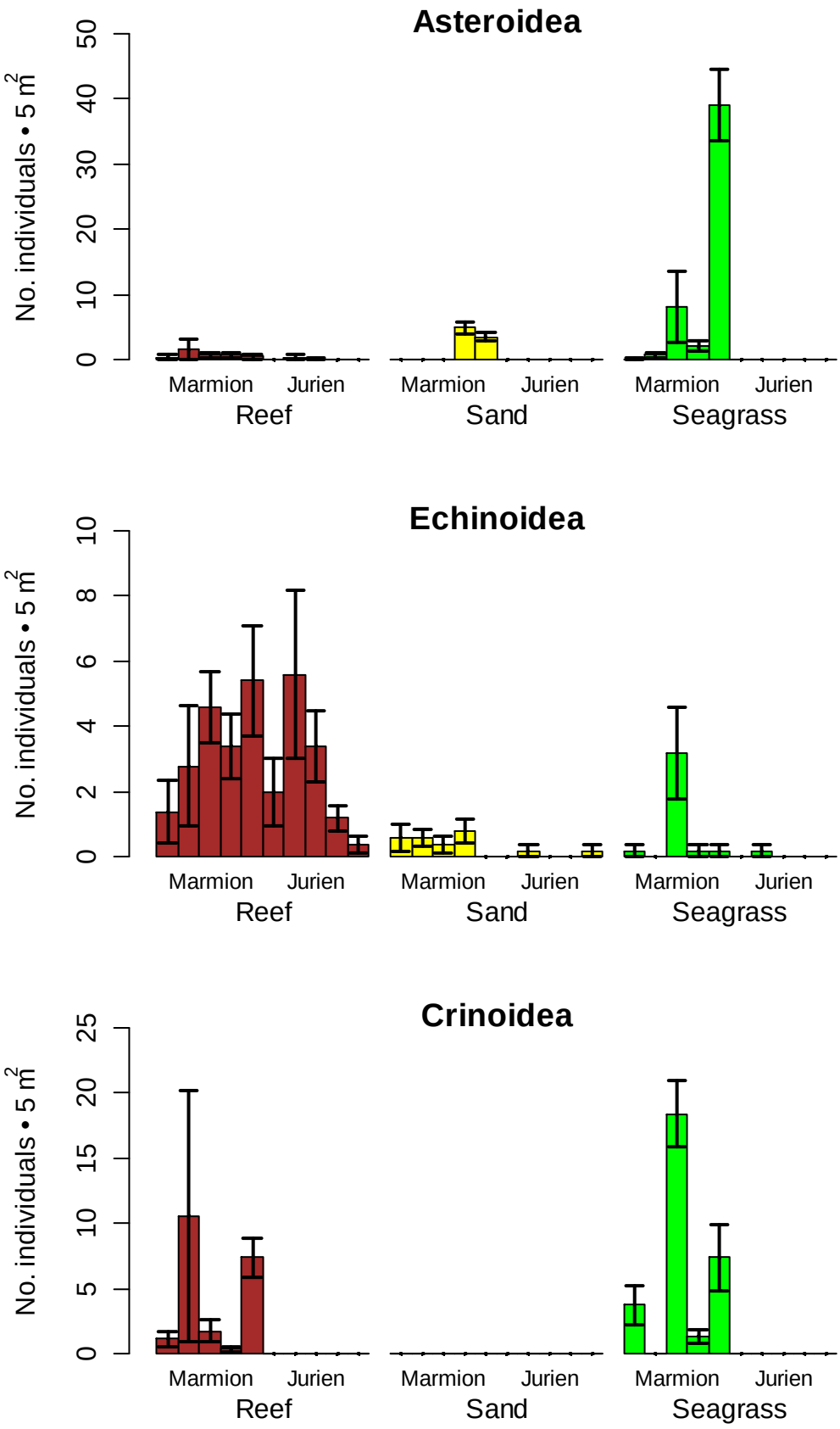

Figure 3.27. Densities of benthic invertebrates (mean ± se, n=5) in each habitat at each of the sites surveyed.

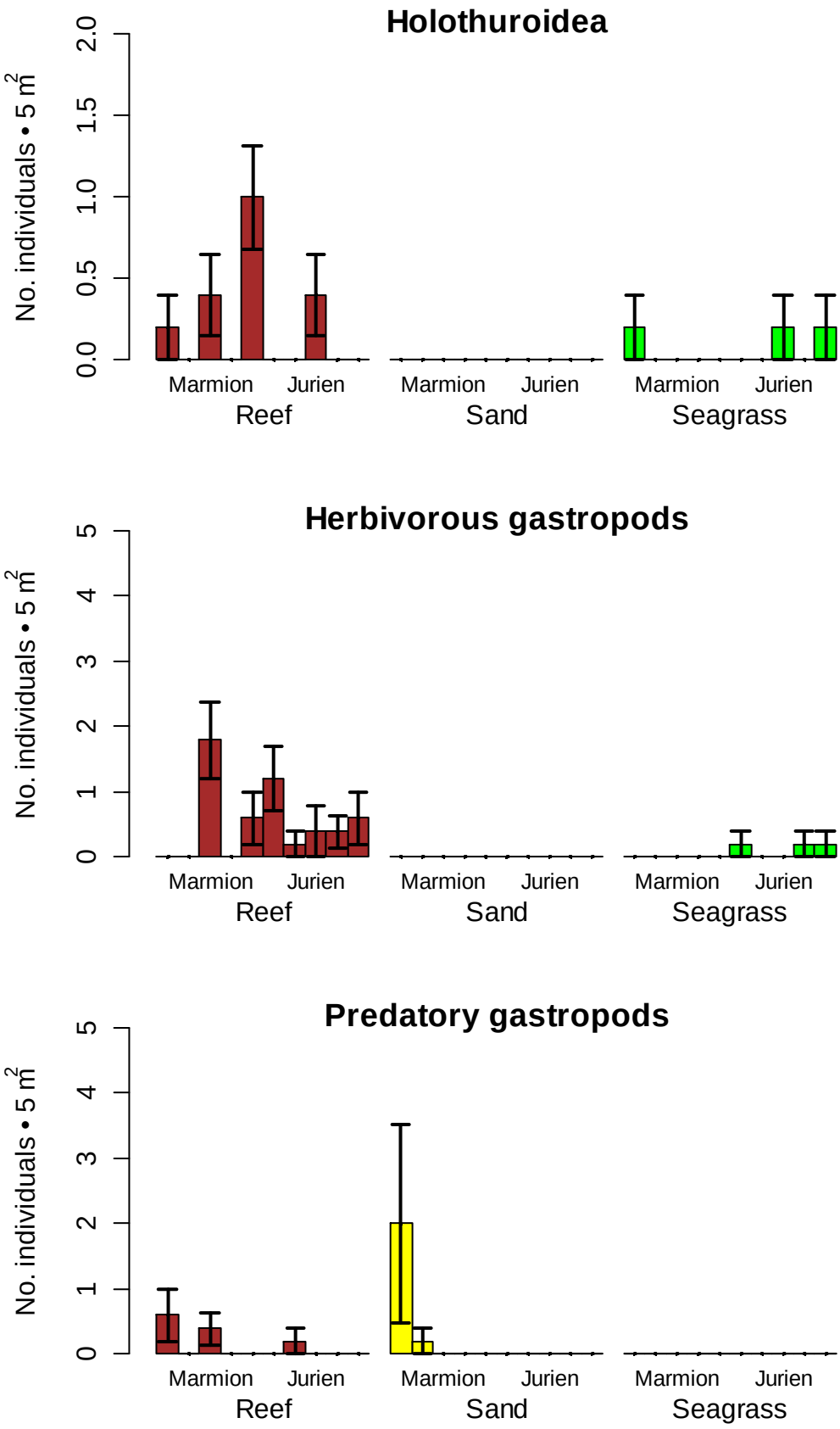

Figure 3.27 continued

Table 3.8. Results of PERMANOVA testing for differences in biomass of each taxonomic or functional group.

Asteroidea						
Source	df	MS	Pseudo-F	P	Permutations	MC-P
Habitat	2	6.27	0.67134	0.6341	30	0.6033
Location	1	290.83	10.743	**0.0086**	56	**0.0105**
Site (Location)	8	27.07	5.896	**0.0001**	9944	**0.0001**
H x L	2	9.34	1.9183	0.1788	9951	0.1791
H x S(L)	16	4.87	1.0604	0.3994	9931	0.4011
Residual	120	4.59				
Echinoidea						
Source	df	MS	Pseudo-F	P	Permutations	MC-P
Habitat	2	275.81	134.67	0.1203	60	**0.0089**
Location	1	23.07	1.9835	0.2097	126	0.1967
Site (Location)	8	11.63	3.1574	**0.0028**	9940	**0.0035**
H x L	2	2.05	0.24274	0.7876	9950	0.7825
H x S(L)	16	8.44	2.2904	**0.0042**	9919	**0.007**
Residual	120	3.68				
Crinoidea						
Source	df	MS	Pseudo-F	P	Permutations	MC-P
Habitat	2	12.82	1	0.5991	10	0.4992
Location	1	50.49	20.154	**0.0072**	16	**0.0023**
Site (Location)	8	2.51	6.0389	**0.0001**	9937	**0.0001**
H x L	2	12.82	6.3866	**0.0083**	9956	**0.0089**
H x S(L)	16	2.01	4.8396	**0.0001**	9914	**0.0001**
Residual	120	0.41				
Holothuroidea						
Source	df	MS	Pseudo-F	P	Permutations	MC-P
Habitat	2	8.31	2.3488	0.3364	30	0.2946
Location	1	1.04	0.30672	0.5276	16	0.6005
Site (Location)	8	3.40	2.9154	**0.0051**	9928	**0.0048**
H x L	2	3.54	1.2909	0.308	9943	0.3048
H x S(L)	16	2.74	2.3533	**0.0054**	9922	**0.0048**
Residual	120	1.16				
Herbivorous gastropods						
Source	df	MS	Pseudo-F	P	Permutations	MC-P
Habitat	2	27.36	7.5675	0.1659	30	0.1185
Location	1	11.65	3.2028	0.08	56	0.1173
Site (Location)	8	3.64	1.6693	0.1045	9938	0.113
H x L	2	3.62	1.2739	0.3073	9952	0.3029
H x S(L)	16	2.84	1.3029	0.2101	9920	0.2036
Residual	120	2.18				
Predatory gastropods						
Source	df	MS	Pseudo-F	P	Permutations	MC-P
Habitat	2	1.30	2.2662	0.3374	30	0.3046
Location	1	2.23	2.0284	0.2834	8	0.191
Site (Location)	8	1.10	2.6106	**0.0097**	9932	**0.0129**
H x L	2	0.58	1.013	0.4001	9958	0.381
H x S(L)	16	0.57	1.3488	0.161	9926	0.1779
Residual	120	0.42				

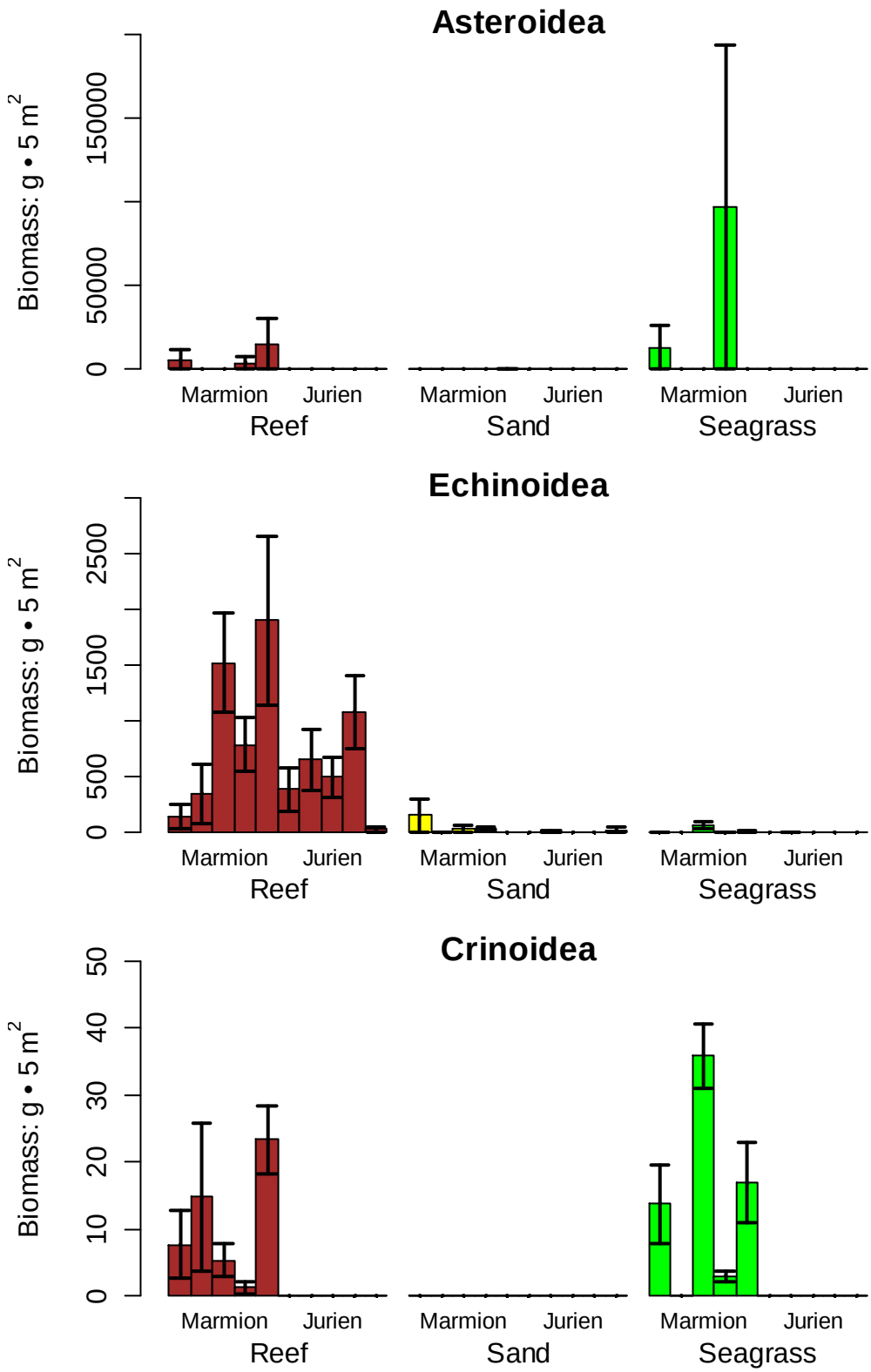

Figure 3.28. Biomasses of benthic invertebrates (mean ± se, n=5) in each habitat at each of the sites surveyed.

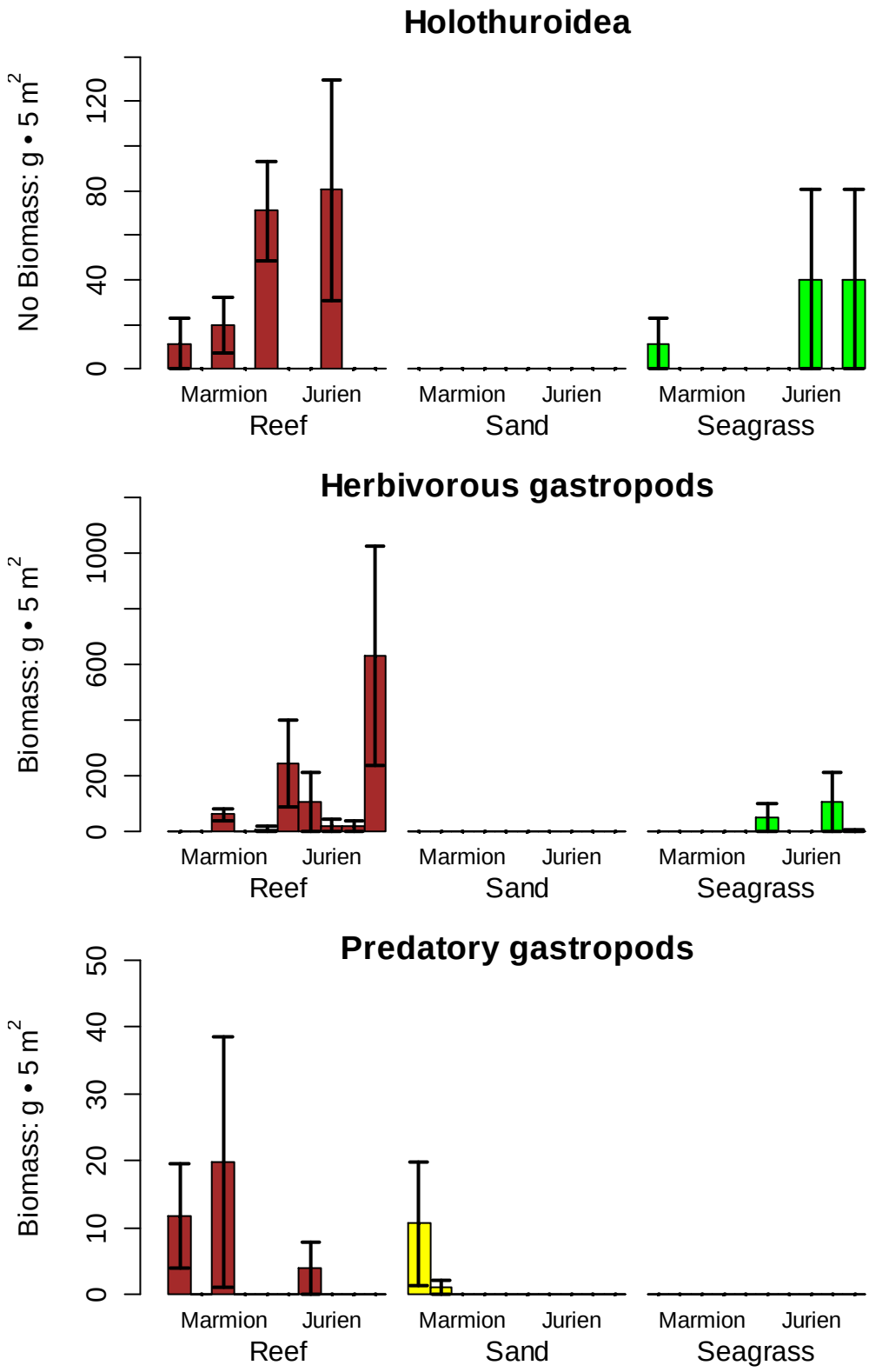

Figure 3.28 continued

3.1.7 Biomass: sessile benthic invertebrates

Methods

Study area

The study focused on locations in Marmion Lagoon in south-western Australia (31º49.4 S, 115º02.5 E). Sandy habitats colonised by seagrass are interspersed between reefs and provide a habitat for a considerable biomass of suspension feeders (Lemmens 1996). This community is composed of organisms such as sponges, solitary and colonial ascidians, corals, bryozoans and gorgonians as well as other animals.

Survey design, field and laboratory methods

The area of study was inshore and offshore reefs and seagrass sites of Marmion Lagoon (Figure 3.29). Within each site, two or three replicate 0.5 m x 0.5 m quadrats were dropped haphazardly onto the substratum on different habitat patches and all sponges, ascidians, bivalves, crinoids, bryozoans, vermetid snails, holothurians and corals within quadrats were collected and placed in plastic bags. The biomass of the various species collected was measured by weighing samples after drying at 60 °C in crucibles for several days and then again after ashing at 550 °C for two hours, and calculating the AFDW as the difference between the two weights. Examples of relationships between dry weight and ash free dry weight are shown in Figure 3.30, Figure 3.31 and Figure 3.32. Organisms were identified to lowest possible taxonomic level. Filter feeder biomass did not include organisms growing in many caverns and crevices which were not sampled. Reef sites were either covered by turfing algae, *Sargassum* sp or *Ecklonia radiata*. Seagrass sites comprised of *Heterozostera tasmanica*, *Halophila* spp., *Posidonia* spp., *Amphibolis antarctica* or *Amphibolis griffithii* (Table 3.9. List of sites surveyed, with habitats present at each site.). All seagrass plants contained within a 0.2 m x 0.2 m quadrat placed at one corner of the larger 0.5 m x 0.5 m quadrat were collected and above and below ground biomass was measured using ash free dry method (AFDW).

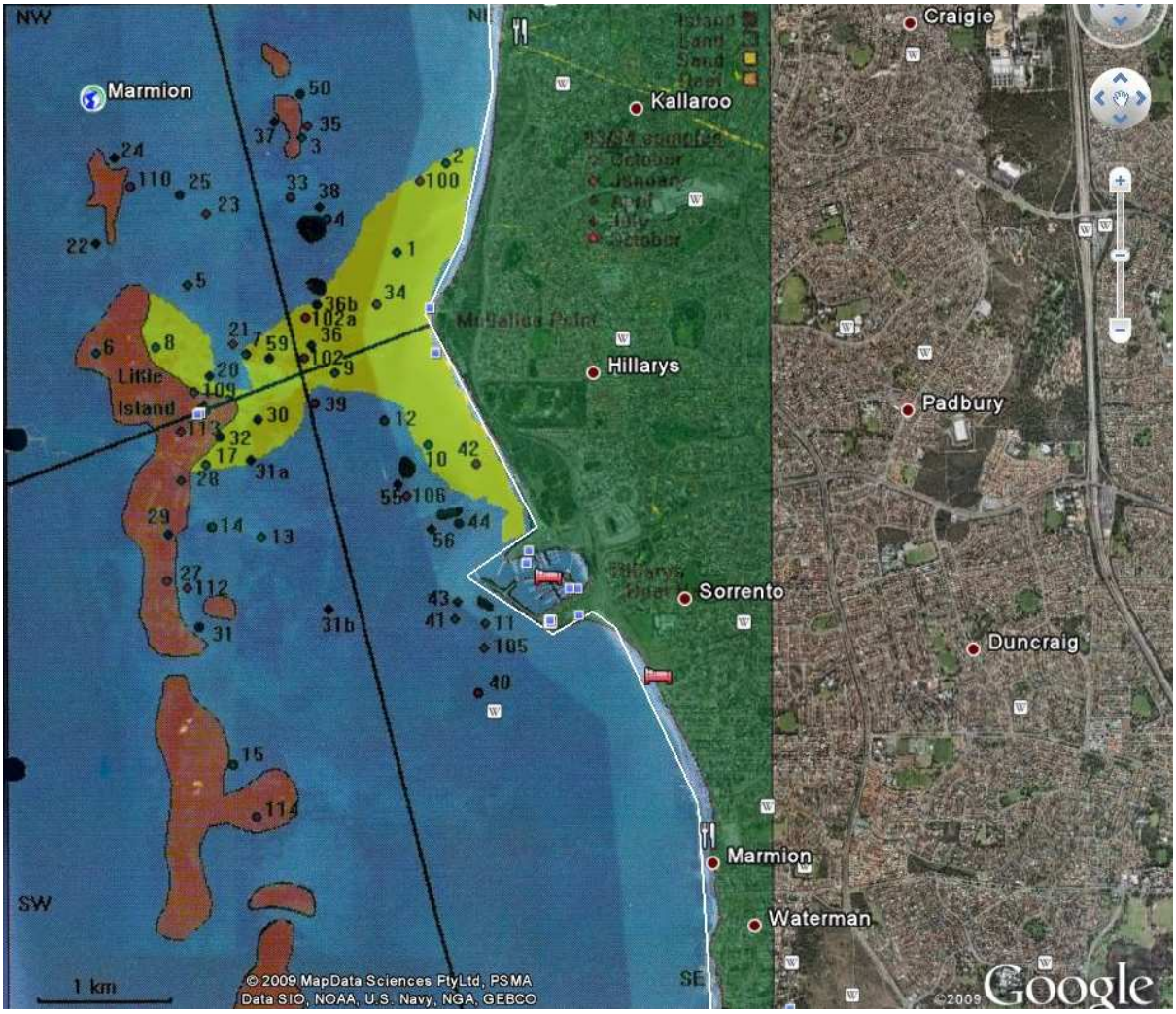

Figure 3.29.Survey sites in Marmion Lagoon. Black lines separate north from south and inshore from offshore.

Table 3.9. List of sites surveyed, with habitats present at each site.

Site	Habitat
1	sand edge, *Amphibolis antarctica*, *A. griffithii*, *Halophila ovalis*, *Halophila sp.*, *Heterozostera tasmanica*, *Posidonia* sp.
2	sand edge, *A. antarctica*, *A. griffithii*, *Halophila australis*, *Posidonia* sp.
3	open reef with turfing algae, *Ecklonia radiata*, *Sargassum* sp., *H. tasmanica*
4	open reef with turfing algae, *E. radiata*, *Sargassum sp.*,
5	open reef with turfing algae, *E. radiata*, *Sargassum* sp., Sand edge, *A. antarctica*, *A. griffithii*, *H. tasmanica*
6	open reef with turfing algae, *E. radiata*, Sand edge
7	*A. antarctica*, *Halophila* sp.
8	sand edge, *H. australis*, *Halophila* sp., *H. tasmanica*, *Posidonia australis*
9	sand edge, *A. antarctica*, *A. griffithii*, *Halophila* sp., *H. tasmanica*, *Posidonia* sp.
10	open reef with turfing algae, *E. radiata*, *Sargassum* sp., *A. griffithii*, *H. tasmanica*, *Posidonia* sp.
11	*E. radiata.*, *Sargassum* sp., sand edge, *A. antarctica*
12	*H. ovalis*
13	*A. griffithii*, *H. tasmanica*, *P. sinuosa*
14	open reef with turfing algae, *E. radiata*, *Sargassum* sp., sand edge, *A. antarctica*, *H. ovalis*, *H. tasmanica*, *P. australis*, *Posidonia* sp.
15	Open reef with turfing algae, *E. radiata*, *Sargassum* sp.
16	*A. griffithii*
17	*A. antarctica*
18	*A. griffithii*
20	open reef with turfing algae, *E. radiata*, *Sargassum* sp., *A. antarctica*, *A. griffithii*, *H. ovalis*, *P. australis*, *P. sinuosa*
21	*Amphibolis* sp., *H. tasmanica*, *Posidonia* sp.
22	open reef with turfing algae, *E. radiata*, *Sargassum* sp.
23	open reef with turfing algae, *E. radiata*, *Sargassum* sp.
24	open reef with turfing algae, *E. radiata*, *Sargassum* sp.
25	open reef with turfing algae, *E. radiata*, *Sargassum* sp.
26	*A. antarctica*, *H. ovalis*, *P. australis*
27	open reef with turfing algae, *E. radiata*, *Sargassum* sp., *Amphibolis* sp., *Halophila sp.*, *Posidonia* sp.
28	open reef with turfing algae, *E. radiata*, *Sargassum* sp.
29	open reef with turfing algae, *E. radiata*, *Sargassum* sp., *A. antarctica*, *H. australis*, *Heterozostera/Halophila*, *P. sinuosa*
30	open reef with turfing algae, *E. radiata*, *Sargassum* sp., *A. antarctica*, *A. griffithii*, *H. ovalis*, *P. augustifolia*, *P. australis*
31	open reef with turfing algae, *E. radiata*, *Sargassum* sp.
32	open reef with turfing algae, *E. radiata*, *Sargassum* sp., *A. antarctica. H. ovalis*, *H. australis*, *P. augustifolia*
33	open reef with turfing algae, *E. radiata*, *Sargassum* sp., *Amphibolis* sp., *H. australis*, *H. tasmanica*, *P. sinuosa*, *Posidonia* sp.
34	*A. antarctica*, *A. griffithii*, *H. tasmanica*, *Posidonia* sp.
35	open reef with turfing algae, *E. radiata*, *Sargassum* sp.
36	*A. griffithii*, *H. australis*, *Heterozostera/Halophila*, *P. australis*, *P. sinuosa*
37	open reef with turfing algae, *E. radiata*, *Sargassum* sp., *A. antarctica*, *A. griffithii*, *H. ovalis*, *H. australis*, *P. sinuosa*
38	open reef with turfing algae, *E. radiata*, *Sargassum* sp., *H. tasmanica*, *P. sinuosa*
39	*Amphibolis* sp., *Halophila* sp., *H. tasmanica*, *Posidonia* sp.
40	*Amphibolis* sp., *Heterozostera/Halophila*, *P. sinuosa*, *Posidonia* sp.

Site	Habitat
41	open reef with turfing algae, *E. radiata, Sargassum* sp.
42	open reef with turfing algae, *E. radiata, Sargassum* sp.
43	open reef with turfing algae, *E. radiata, Sargassum* sp. *A. antarctica, A. griffithii, H. ovalis, H. australis, P. sinuosa*
44	open reef with turfing algae, *E. radiata, Sargassum* sp. *A. griffithii, H. ovalis, P. sinuosa,*
50	open reef with turfing algae, *E. radiata, Sargassum* sp., *A. antarctica, H. ovalis, P. sinuosa*
55	*E. radiata, Sargassum* sp., *A. antarctica, A. griffithii, H. ovalis, P. augustifolia, P. sinuosa*
56	open reef with turfing algae, *E. radiata, Sargassum* sp., *A. griffithii, H. ovalis, P. sinuosa*
59	*A. griffithii, H. ovalis, P. augustifolia, P. australis*
100	*A. griffithii, H. ovalis, H. tasmanica, P sinuosa*
102	*A. antarctica, A. griffithii, H. ovalis, H. australis, P. sinuosa*
104	*E. radiata, Sargassum* sp.
105	open reef with turfing algae, *Ecklonia radiata, Sargassum sp., A. griffithii, H. ovalis, H. tasmanica, P. sinuosa*
106	open reef with turfing algae, *E. radiata, Sargassum* sp., *A. griffithii, H. ovalis, P. augustifolia, P. sinuosa*
109	open reef with turfing algae, *E. radiata, Sargassum* sp., *A. antarctica, H. ovalis, H. australis, H. tasmanica, P. australis, P. sinuosa, Posidonia* sp.
110	open reef with turfing algae, *E. radiata, Sargassum* sp., *A. antarctica, Amphibolis* sp., *H. ovalis, H. australis, P. australis, P. sinuosa*
112	open reef with turfing algae, *E. radiata, Sargassum* sp., *A. griffithii,*
113	open reef with turfing algae, *E. radiata, Sargassum* sp., *A. griffithii, H. ovalis, H. australis, H. tasmanica, P. australis, P. sinuosa*
114	*A. griffithii, H. tasmanica, P. sinuosa*
31A	*H. ovalis*
31B	*A. griffithii, P. sinuosa, Posidonia* sp.
36B	open reef with turfing algae, *E. radiata, Sargassum* sp.
1B	*Sargassum* sp., sand edge
102B	open reef with turfing algae, *Ecklonia radiata, Sargassum* sp.
55A	open reef with turfing algae, *Sargassum* sp.
23B	*Amphibolis* sp., *H. tasmanica, Posidonia* sp.
28B	*Amphibolis* sp., *Heterozostera/Halophila, Posidonia* sp.

Statistical analyses

Multivariate analyses (Primer v.6) were used to explore patterns in biomass among habitats. Data were square-root transformed to enhance the contribution of the intermediately large species to the pattern. The Bray–Curtis similarity matrix was used to obtain multidimensional scaling (MDS) ordinations, and community relationships were examined with two dimensional plots. The MDS was repeated until the same lowest stress was achieved. To determine the species contributing most to dissimilarities among groups, we used the program SIMPER (Warwick 1991). Organisms with a high average contribution and large ratio of average contribution to standard deviation of contribution were considered good discriminating organisms (Clarke 1993). They not only contributed most to dissimilarity but did so consistently. A permutational MANOVA (PERMANOVA) (Anderson 2005) based on the Bray–Curtis distance measure was used to test if there was a statistical multivariate difference between assemblages. SYSTAT v.12 package was used for univariate analysis and data were transformed to satisfy normality and homoscedascity assumptions.

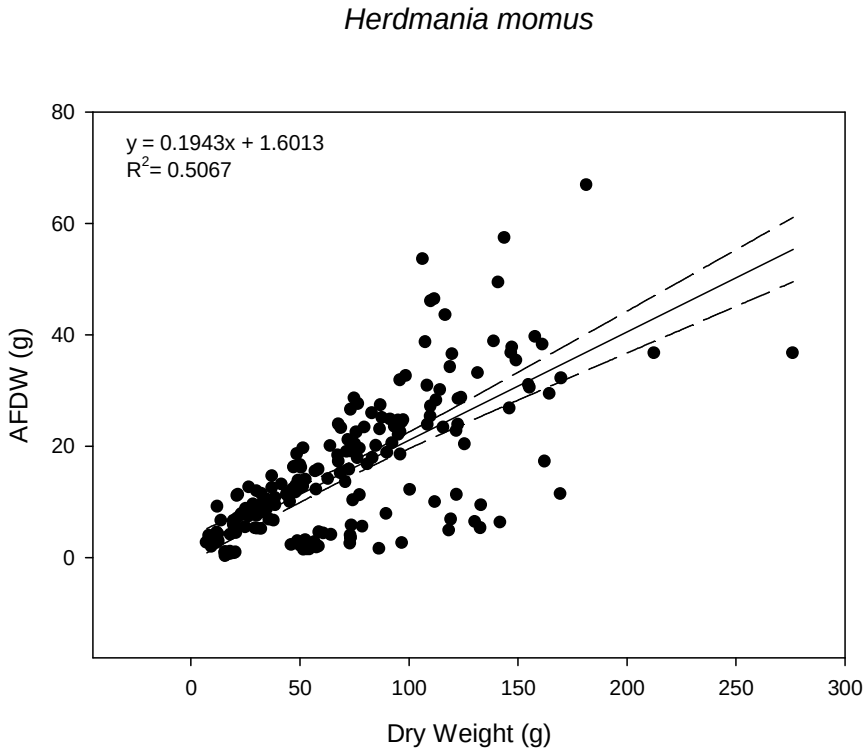

Figure 3.30. Relationship between dry weight and ash free dry weight for ascidian *Herdmania momus.*

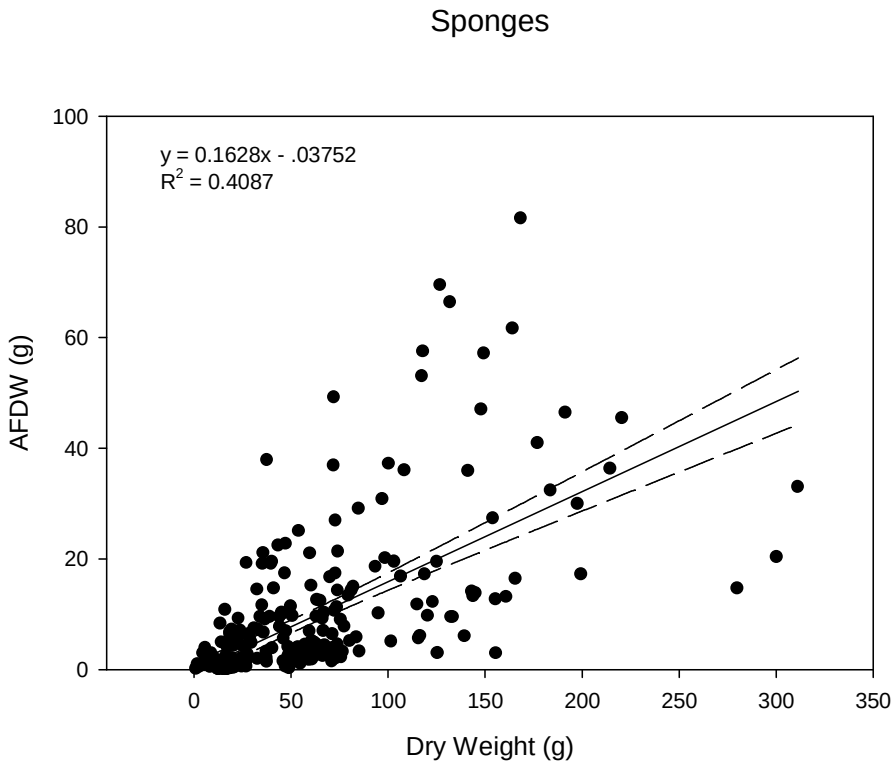

Figure 3.31. Relationship between dry weight and ash free dry weight for sponges.

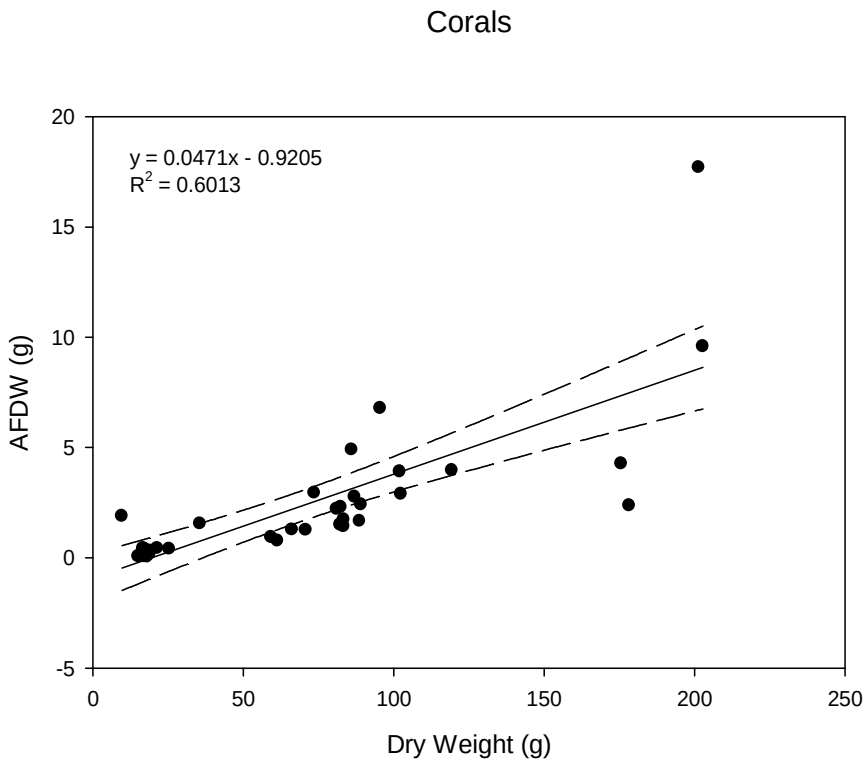

Figure 3.32. Relationship between dry weight and ash free dry weight for corals.

Results

Mean weight of leaves of *Amphibolis* spp ranged from 15 g m^{-2} to close to 500 g m^{-2} and *Amphibolis griffithii* had larger above ground biomass than *A. antarctica* mean 216.9 g m-2 (± 142.7 s.d.) and 87.3 g m^{-2} (± 48.4 s.d) respectively (Figure 3.33). The same pattern followed below ground biomass with 46.1 g m^{-2} (± 57.9) for *A. griffithii* and 18.3 g m^{-2} (±15.7) for A. antarctica (Figure 3.34). Total biomass of *A. griffithii* was twice as high (262.9 g m^{-2} (±168.7 s.d.)) as that of *A. antarctica* (105.6 (±49.4)) (Figure 3.35). There was a greater proportion of living material above ground than below (83% vs 17%) in both species. There was no difference in the biomass of leaves between *H. australis* and *H. ovalis* with mean of 17.2 g m^{-2} ± 8.6 s.d. and 15.9 g m^{-2} ± 10.9 s.d. respectively (Figure 3.36). *H. ovalis* had higher rhizome biomass than *H. australis* 36.4 g m^{-2} ± 40.7 s.d. and 22.3 g m^{-2} ± 16.6 s.d. respectively (Figure 3.37). Total biomass of *H. ovalis* was higher comparing to *H. australis* (52.3 g m^{-2} ± 42.3 s.d versus 39.5 g m^{-2} ± 21.5) (Figure 3.38). Proportion of below ground biomass was higher in both species comparing to above ground 56% and 44% for *H. australis* and 70% and 30% for *H. ovalis*. Average biomass of leaves for *Heterozostera tasmanica* ranged from below 1 g m^{-2} in more inshore sites 38 and 39 to almost 60 g m^{-2} in site 114 further offshore with mean of 26.3 g m-^{2} (± 19.3 s.d.) (Figure 3.39). Mean biomass of rhizomes was 18.7 g m^{-2} (± 15 s.d.) (Figure 3.40). Average total biomass of *Heterozostera tasmanica* was 44.9 g m^{-2} (±24.7 s.d.) and there was proportionately more biomass above ground (58%) comparing to below ground (42%) (Figure 3.41). *Posidonia augustifolia* had twice as high average biomass of leaves than *P. australis* and *P. sinuosa* with mean 141.4 g m^{-2} ±141.1s.d., 61.5 g m^{-2} ± 25.7 and 74.7 g m^{-2} ± 34.9 respectively (Figure 3.42). Above ground biomass was highest for *P. australis* (486.4 g m-2 ± 354.3), followed by *P. augustifolia* (400 g m^{-2} ± 38.8) and *P sinuosa* (251.8 g m^{-2} ± 362) (Figure 3.43). Total biomass was highest for P. augustifolia (541.5 g m^{-2} ± 153.4 s.d.) followed by P. australis

(469.1 g m^{-2} ± 354.3 s.d.) and *P. sinuosa* (326.5 g m^{-2} ± 368.1 s.d.). Over 70 % of biomass was held below ground for all species.

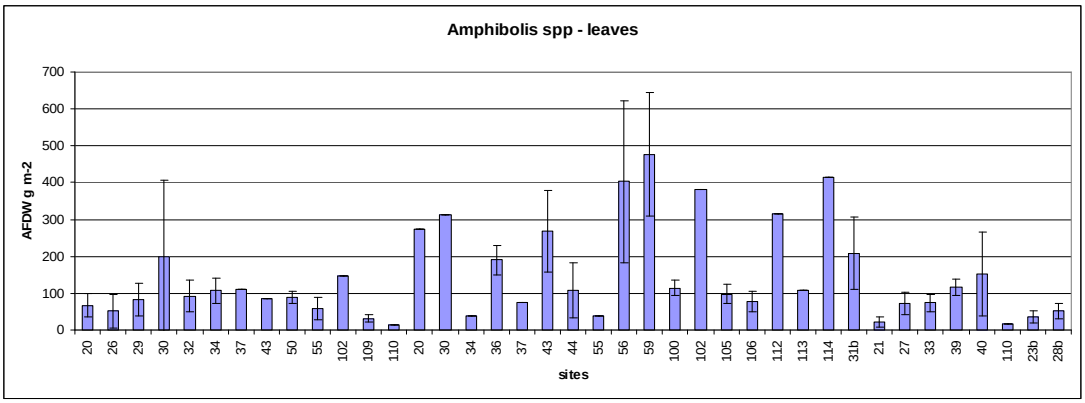

Figure 3.33. Above ground biomass of *Amphibolis* spp.

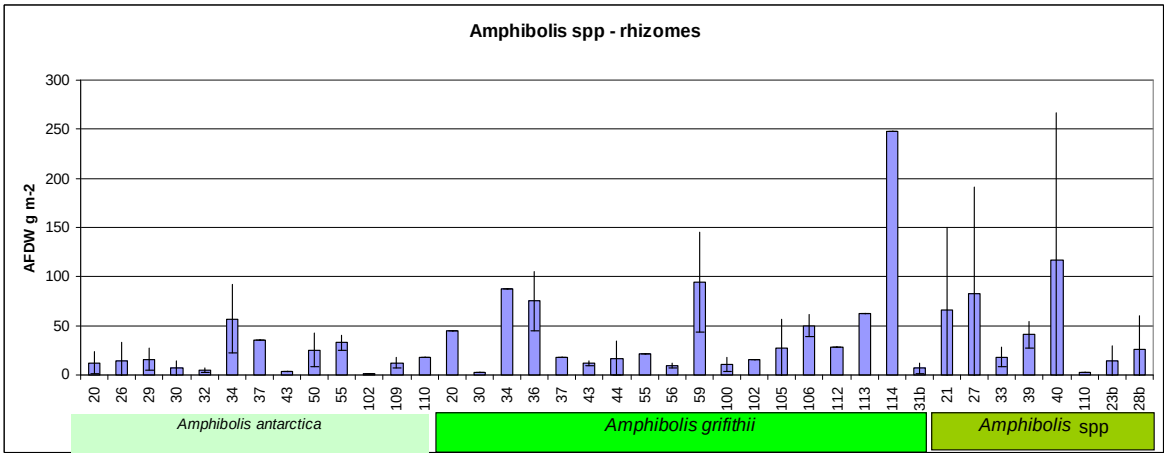

Figure 3.34. Below ground biomass of *Amphibolis* spp.

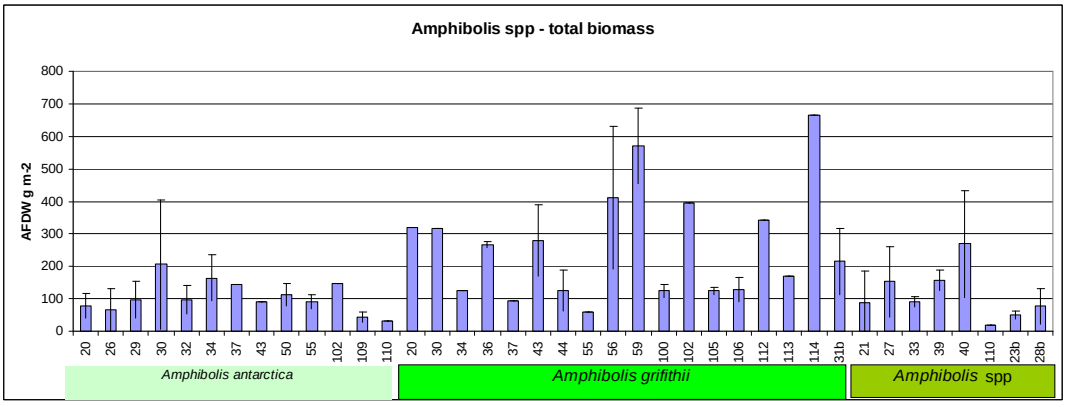

Figure 3.35. Total biomass of *Amphibolis* spp.

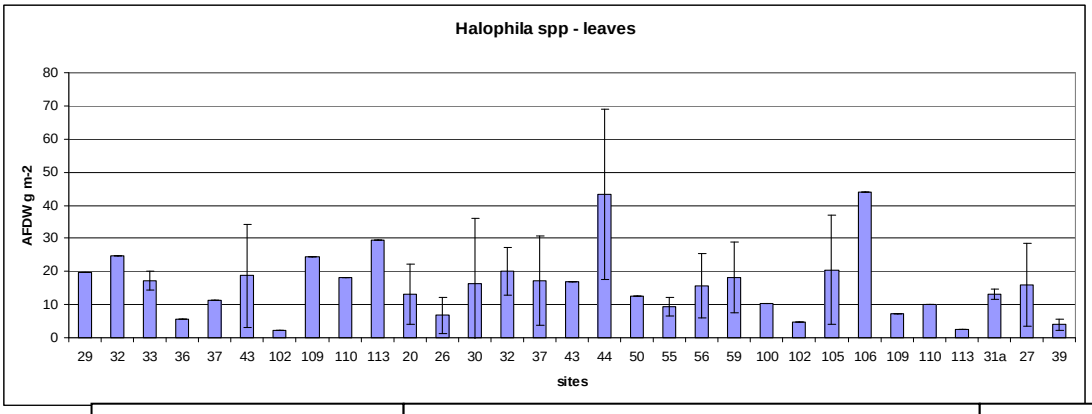

Figure 3.36. Above ground biomass of *Halophila* spp.

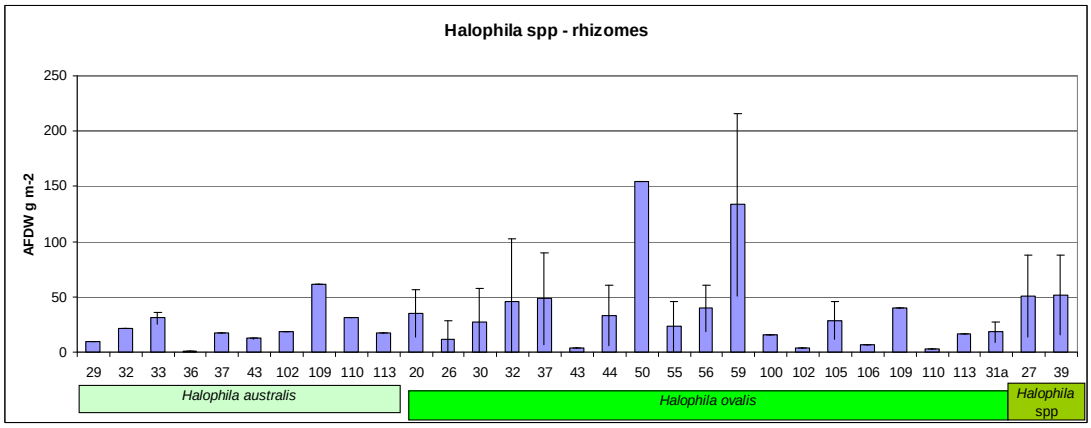

Figure 3.37. Below ground biomass of *Halophila* spp.

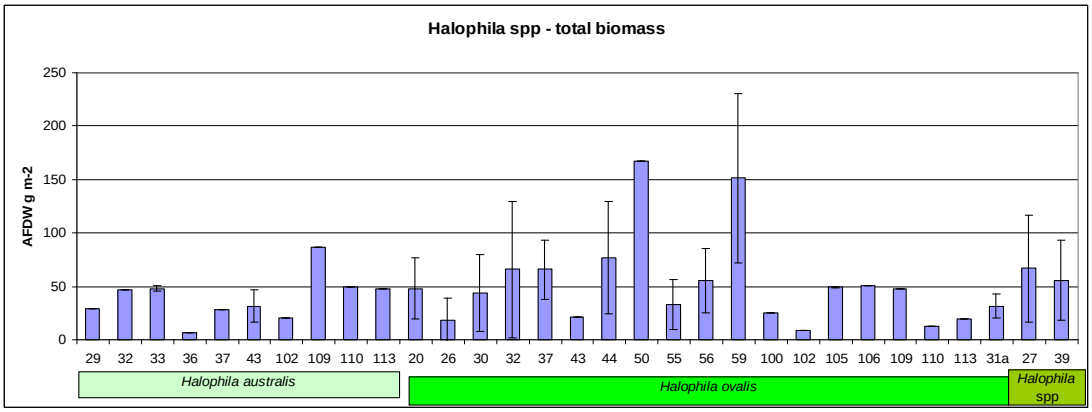

Figure 3.38. Total biomass of *Halophila* spp.

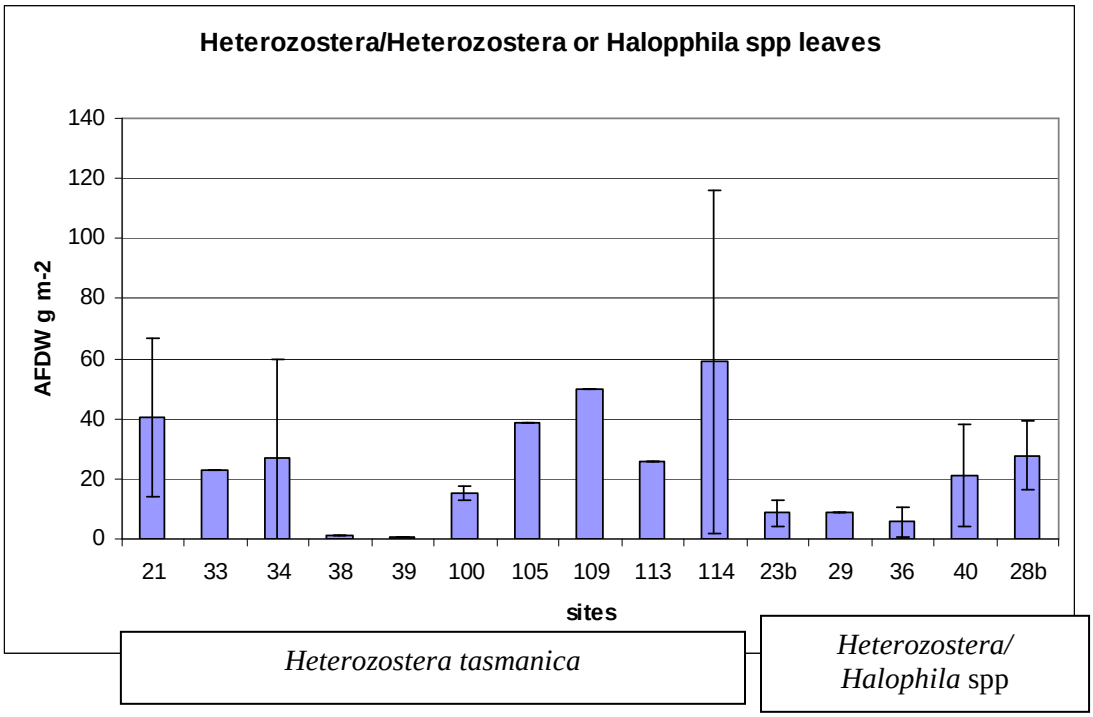

Figure 3.39. Above ground biomass of *Heterozostera tasmanica.*

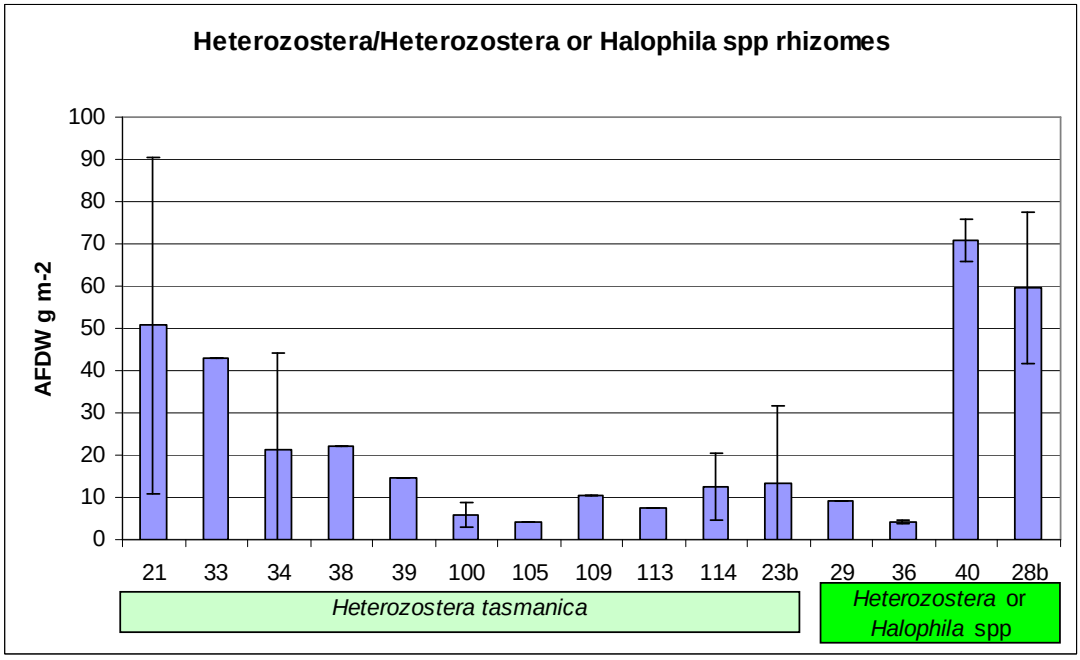

Figure 3.40. Below ground biomass of *Heterozostera tasmanica.*

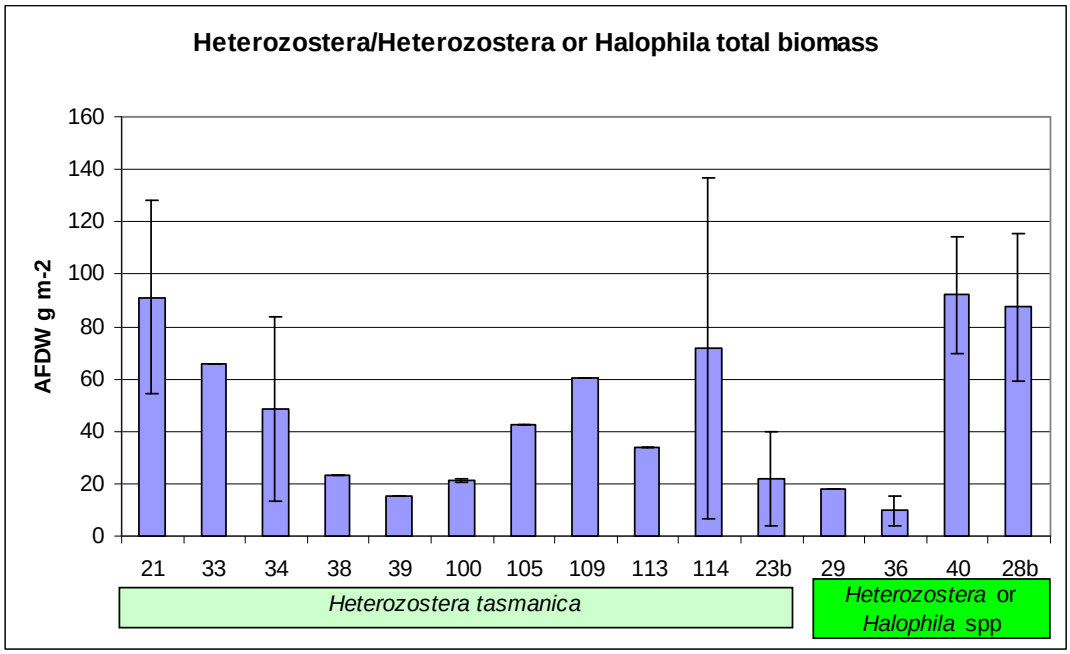

Figure 3.41. Total biomass of *Heterozostera tasmanica.*

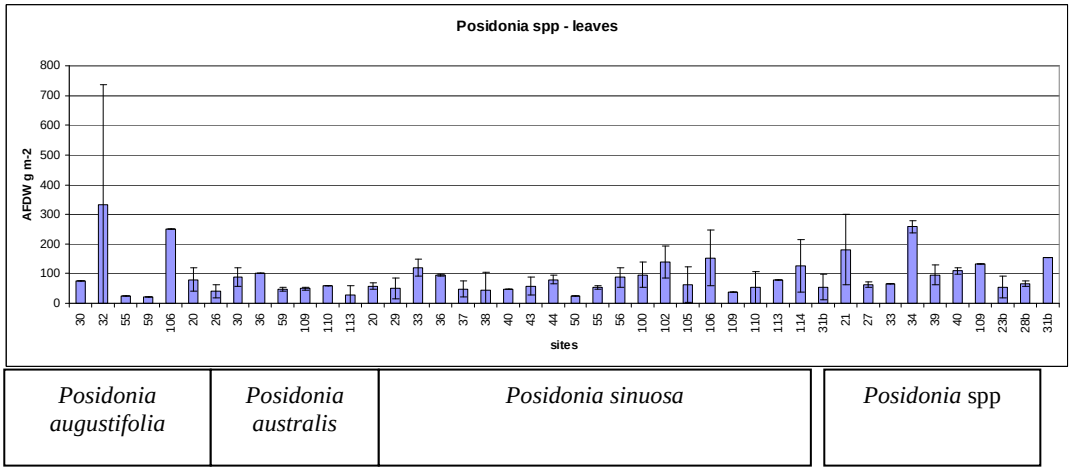

Figure 3.42. Above ground biomass of *Posidonia* spp.

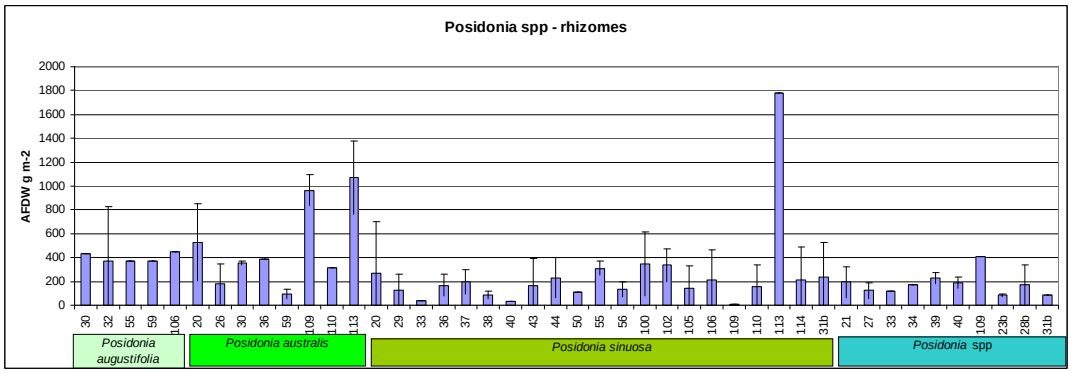

Figure 3.43. Below ground biomass of *Posidonia* spp.

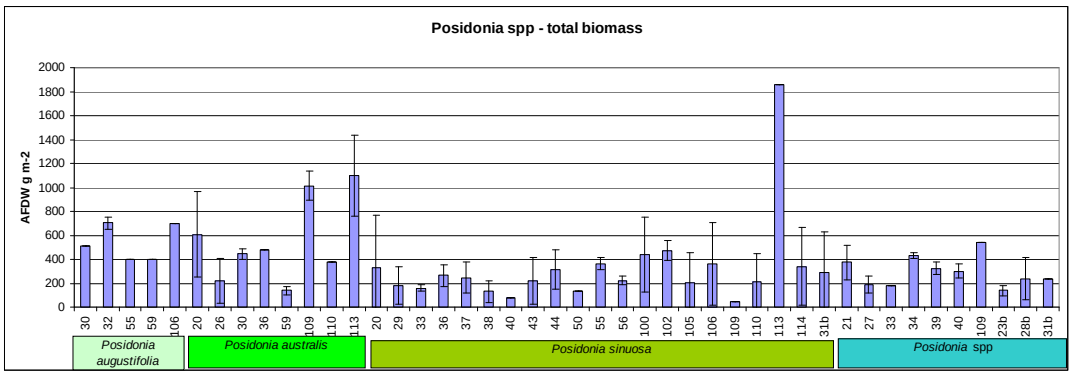

Figure 3.44. Total biomass of *Posidonia* spp.

Reefs harboured more filter feeders than sand habitats (Table 3.10).

Table 3.10. Biomass of main groups of filter feeders in different habitats.

habitat	Ascidiacea	Porifera	Ectoprocta	Crinoidea	Bivalvia	Anthozoa	Actiniaria
seagrass	5.6 (±12.7)	1.0 (±10.7)	0.1 (±0.4)	0.3 (±1.5)	1.5 (±12.1)	0.1 (±0.2)	0.1 (±4.4)
reefs	46.2 (±84.7)	29.9 (±72.4)	0.3 (±1.7)	0.5 (±1.7)	1.2 (±7.7)	5.2 (±25.6)	0.1 (±0.9)
sand edge	3.8 (±5.3)	0.1 (±0.3)	0	0.8 (±1.8)	0	0	1.3 (±4.9)

For the multivariate analyses we grouped two seagrass habitats, *Posidonia* and *Amphibolis* spp and *Heterozostera* and *Halophila* spp and two reef habitats, *Ecklonia radiata* and *Sargassum* spp. Non-metric multi-dimensional scaling (MDS) revealed a clear pattern of change in filter feeders biomass from seagrass to reef habitats (Figure 3.45) despite a rather high 2-d stress arising from the large number of samples and the substantial variability in individual samples reflected in relatively low similarity within habitat with all habitats being just over 30% similar except *Halophila/Heterozostera* spp habitat showing most similarity of 65% (Table 3.11). Two unvegetated habitats, sand and turfing algae, were most dissimilar. Pairwise comparisons showed that biomass of filter feeders in all habitats are significantly different (Table 3.12).

Similarity percentage analysis (SIMPER) indicated that the differences among habitats were due to much higher biomass of dominant taxa like ascidian *Herdmania momus* and sponges on the reefs than in seagrass or sand (Table 3.13). Ascidians A2, crinoids, sea anemones, and *Pyura* sp preferred sand habitat to reef or seagrass. When seagrass or algae habitats were analysed separately MDS plot revealed no natural groupings (Figure 3.46 and Figure 3.47).

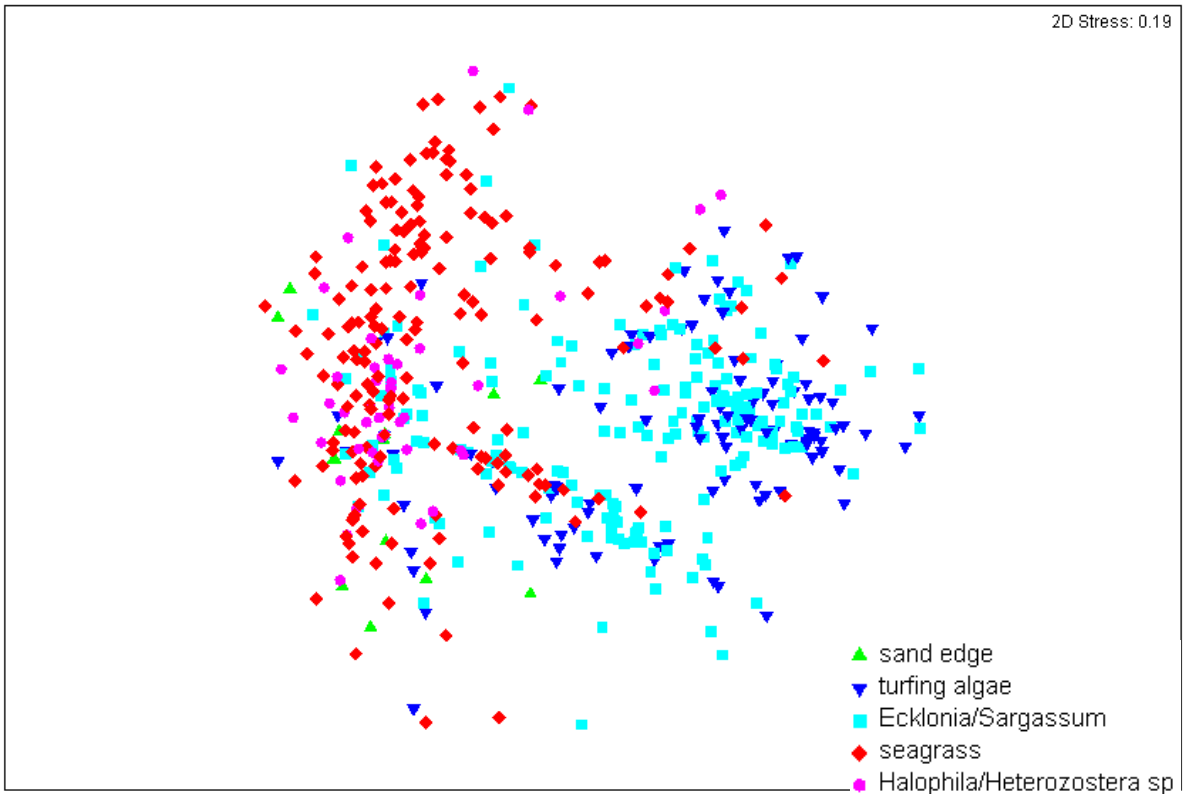

Figure 3.45. MDS plot of biomass of filter feeders in reef, seagrass ad unvegetated habitats.

Table 3.11. Average similarity between/within groups (Permanova test).

	sand edge	turfing algae	*Ecklonia/ Sargassum*	*Posidonia/ Amphibolis* spp	*Halophila/ Hetero zostera* spp
sand edge	34.017				
turfing algae	17.796	34.605			
Ecklonia/ Sargassum spp	24.121	31.38	31.962		
Posidonia/ Amphibolis spp	32.362	19.18	26.037	36.253	
Halophila/ Hetero zostera spp	42.389	20.57	30.97	45.627	65.429

Table 3.12. Pair-wise Permanova results for algae, seagrass and unvegetated habitats.

Groups	t	P(perm)	perms	Den.df
sand edge, turfing algae	3.5922	0.001	998	121
sand edge, *Ecklonia/Sargassum*	2.706	0.001	999	225
sand edge, *Posidonia/Amphibolis*	1.679	0.008	998	251
sand edge, Halophila/Heterozostera	2.5622	0.002	999	143
turfing algae, *Ecklonia/Sargassum*	2.7293	0.001	999	320
turfing algae, *Posidonia/Amphibolis*	8.2922	0.001	998	346
turfing algae, *Halophila/Heterozostera*	10.861	0.001	997	238
Ecklonia/Sargassum, Posidonia/Amphibolis	7.1458	0.001	998	450
Ecklonia/Sargassum, Halophila/Heterozostera	8.8839	0.001	998	342
Posidonia/Amphibolis, Halophila/Heterozostera	4.4666	0.001	999	368

Table 3.13. Species contributing to dissimilarity among habitats (SIMPER analysis).

Species	Group sand edge Av.Abund	Group turfing algae Av.Abund	Av.Diss	Diss/SD	Contrib%	Cum.%
Herdmania momus	0.25	5.52	26.56	1.18	27.33	27.33
sponge	0.08	4.54	23.44	1.13	24.13	51.45
coral	0.00	0.62	6.39	0.42	6.57	58.03
ascidian A2	0.76	0.06	5.84	0.49	6.01	64.04
crinoid	0.44	0.06	3.90	0.44	4.01	68.05
sea anemone	0.40	0.02	3.23	0.30	3.32	71.38
ascidian	0.07	0.52	2.87	0.46	2.96	74.33
Pyura sp	0.31	0.00	2.68	0.31	2.76	77.10
ascidian A3	0.00	0.49	2.45	0.34	2.53	79.62

Species	Group sand edge Av. ab	Group *Ecklonia/Sargassum* Av Abund	Av.Diss	Diss/SD	Contrib%	Cum.%
Herdmania momus	0.25	3.09	20.61	0.88	21.27	21.27
sponge	0.08	2.79	18.89	0.93	19.50	40.78
ascidian A2	0.76	0.14	8.48	0.52	8.76	49.53
crinoid	0.44	0.01	6.01	0.42	6.20	55.73
sea anemone	0.40	0.07	5.28	0.34	5.45	61.18
Pyura sp	0.31	0.01	4.13	0.31	4.26	65.45
ascidian A3	0.00	0.56	3.45	0.41	3.56	69.00
ascidian	0.07	0.43	3.42	0.47	3.53	72.53
Polycarpa nigricans	0.00	0.29	2.66	0.29	2.74	75.28
coral	0.00	0.32	2.38	0.26	2.45	77.73

Species	Group turfing algae Av.Abund	Group *Ecklonia/Sargassum* Av.Abund	Av. Diss	Diss/ SD	Contrib%	Cum. %
Herdmania momus	5.52	3.09	23.53	1.13	29.92	29.92
sponge	4.54	2.79	20.65	1.12	26.26	56.18
coral	0.62	0.32	5.77	0.43	7.34	63.51
ascidian A3	0.49	0.56	3.78	0.49	4.81	68.32
ascidian	0.52	0.43	3.43	0.52	4.36	72.68
Polycarpa nigricans	0.09	0.29	2.09	0.29	2.66	75.34
soft coral	0.37	0.13	1.89	0.26	2.40	77.74
bryozoan	0.21	0.20	1.47	0.44	1.87	79.62

Species	Group sand edge Av Abund	Group *Amphibolis /Posidonia* Av.Abund	Av.Diss	Diss/SD	Contrib%	Cum.%
ascidian A2	0.76	0.15	12.15	0.59	12.45	12.45
sea anemone	0.40	0.23	9.45	0.43	9.69	22.14
crinoid	0.44	0.01	9.36	0.48	9.59	31.73
Herdmania momus	0.25	0.34	8.22	0.42	8.43	40.16
Pyura australis	0.00	0.60	7.27	0.52	7.45	47.61
Pyura sp	0.31	0.01	6.15	0.35	6.31	53.92
sponge	0.08	0.30	4.27	0.38	4.37	58.29
Botrylloides perspicuus	0.09	0.04	3.98	0.25	4.07	62.36
Polycarpa viridis	0.00	0.32	3.96	0.34	4.06	66.42
Polychaete	0.10	0.00	3.54	0.23	3.63	70.05

Species	Group turfing algae Av.Abund	Group seagrass Av.Abund	Av.Diss	Diss/SD	Contrib%	Cum.%
Herdmania momus	5.52	0.34	25.85	1.09	27.00	27.00
sponge	4.54	0.30	23.61	1.10	24.66	51.66
coral	0.62	0.01	6.68	0.40	6.98	58.63
Pyura australis	0.06	0.60	4.78	0.41	4.99	63.63
ascidian	0.52	0.18	3.35	0.46	3.50	67.13
ascidian A3	0.49	0.12	3.04	0.36	3.18	70.31

Species	Group *Ecklonia/Sargassum* Av.Abund	Group seagrass Av.Abund	Av. Diss	Diss/ SD	Contrib%	Cum. %
sponge	2.79	0.30	20.39	0.92	21.39	21.39
Herdmania momus	3.09	0.34	19.30	0.83	20.24	41.63
Pyura australis	0.03	0.60	5.85	0.46	6.14	47.77
Polycarpa nigricans	0.29	0.26	4.79	0.40	5.02	52.79
ascidian A3	0.56	0.12	4.30	0.43	4.51	57.30
ascidian	0.43	0.18	4.23	0.45	4.44	61.74
Polycarpa viridis	0.18	0.32	3.92	0.35	4.12	65.85
sea anemone	0.07	0.23	3.72	0.27	3.91	69.76
Comatula purpurea	0.10	0.19	2.90	0.33	3.04	72.80
coral	0.32	0.01	2.59	0.26	2.71	75.52
bryozoan	0.20	0.13	2.47	0.35	2.60	78.11

Species	Group sand edge Av. Abund	Group *Halophila/ Heterozostera* spp Av.Abund	Av.Diss	Diss/SD	Contrib%	Cum.%
ascidian A2	0.76	0.08	15.46	0.60	15.73	15.73
crinoid	0.44	0.02	14.36	0.55	14.61	30.34
sea anemone	0.40	0.19	12.20	0.46	12.41	42.75
Herdmania momus	0.25	0.18	10.99	0.42	11.18	53.93
Pyura sp	0.31	0.00	9.05	0.38	9.20	63.14
Polychaete	0.10	0.01	5.94	0.27	6.04	69.18
Botrylloides perspicuus	0.09	0.00	5.61	0.26	5.71	74.88

Species	Group turfing algae Av.Abund	Group *Halophila/ Heterozostera* Av.Abund	Av. Diss	Diss/ SD	Contrib%	Cum. %
Herdmania momus	5.52	0.18	29.61	1.10	30.09	30.09
sponge	4.54	0.03	28.01	1.11	28.46	58.55
coral	0.62	0.01	8.96	0.42	9.10	67.65
ascidian A3	0.49	0.06	3.22	0.33	3.27	70.92
ascidian	0.52	0.05	3.10	0.41	3.15	74.07
Polycarpa nigricans	0.09	0.09	2.23	0.23	2.27	76.33
soft coral	0.37	0.00	2.16	0.22	2.20	78.53
sea anemone	0.02	0.19	1.95	0.24	1.98	80.51

Species	Group *Ecklonia/ Sargassum* Av.Abund	Group *Halophila/ Heterozostera* Av.Abund	Av. Diss	Diss/ SD	Contrib%	Cum. %
sponge	2.79	0.03	25.18	0.96	25.70	25.70
Herdmania momus	3.09	0.18	23.15	0.86	23.62	49.31
Polycarpa nigricans	0.29	0.09	5.59	0.34	5.70	55.01
ascidian A3	0.56	0.06	4.76	0.43	4.86	59.87
sea anemone	0.07	0.19	4.72	0.28	4.82	64.69
ascidian	0.43	0.05	4.33	0.39	4.42	69.11
coral	0.32	0.01	3.52	0.27	3.59	72.70
bryozoan	0.20	0.03	2.69	0.26	2.74	75.45
Comatula purpurea	0.10	0.05	2.41	0.24	2.46	77.91
ascidian A1	0.01	0.16	2.27	0.23	2.32	80.22

Species	Group seagrass Av.Abund	Group *Halophila/ Heterozostera* Av.Abund	Av.Diss	Diss/SD	Contrib%	Cum.%
Pyura australis	0.60	0.02	11.79	0.58	12.06	12.06
sea anemone	0.23	0.19	10.94	0.41	11.19	23.25
Polycarpa nigricans	0.26	0.09	7.85	0.43	8.03	31.28
sponge	0.30	0.03	6.96	0.37	7.11	38.39
Polycarpa viridis	0.32	0.00	6.35	0.36	6.49	44.89
Comatula purpurea	0.19	0.05	5.75	0.39	5.88	50.76
ascidian A1	0.12	0.16	4.87	0.34	4.98	55.75
Herdmania momus	0.34	0.18	4.83	0.32	4.94	60.68
ascidian	0.18	0.05	4.60	0.34	4.70	65.38
ascidian A6	0.17	0.02	3.78	0.32	3.87	69.25
bryozoan	0.13	0.03	3.43	0.34	3.51	72.76
ascidian A2	0.15	0.08	2.89	0.29	2.96	75.72

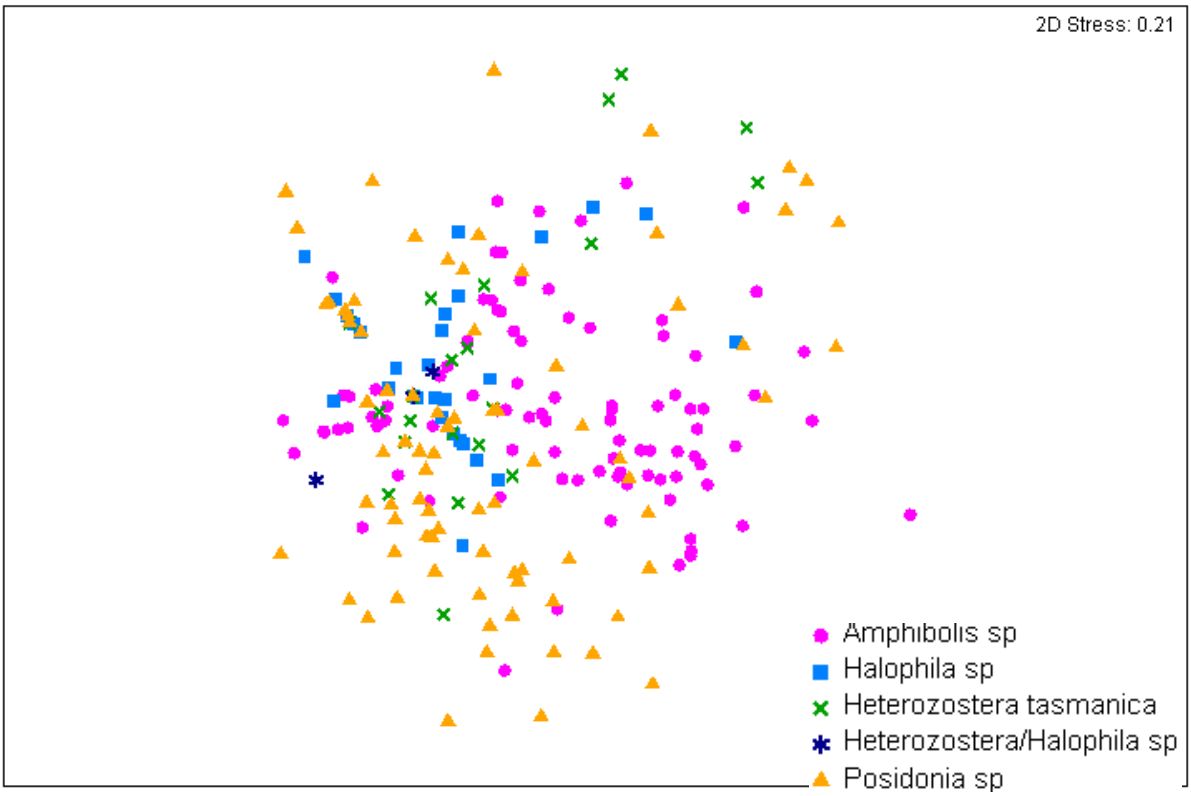

Figure 3.46. MDS plot of filter feeders biomass in seagrass habitats.

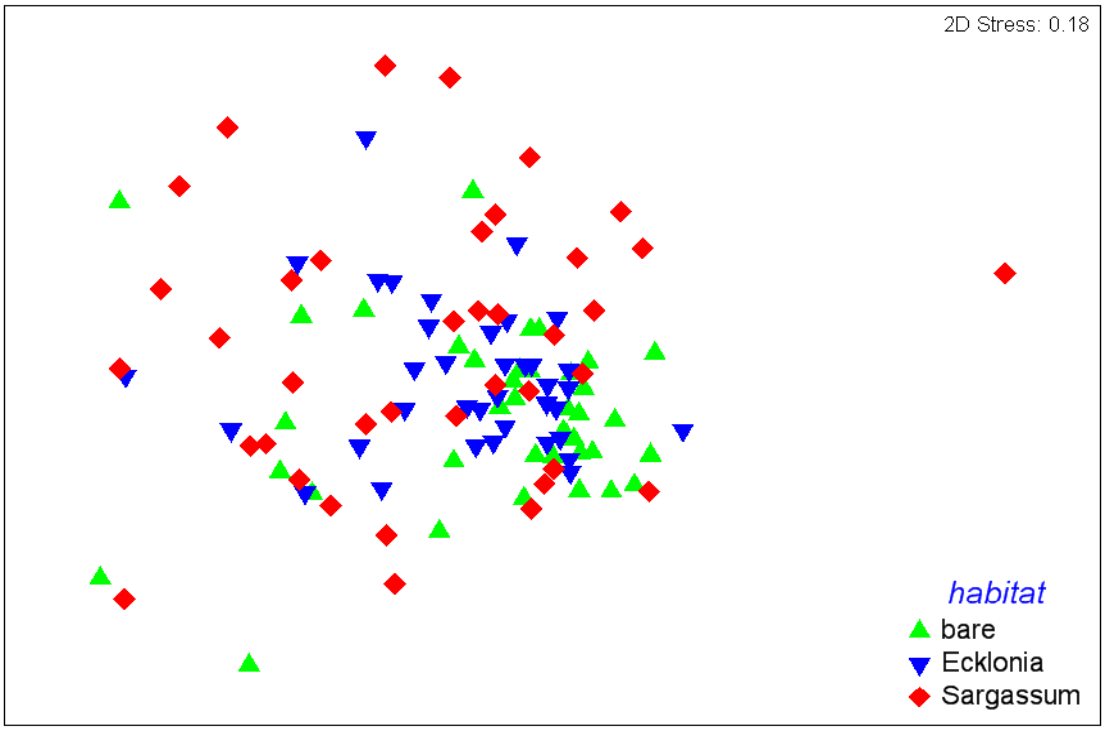

Figure 3.47. MDS plot of filter feeders biomass in reef habitats.

The distribution of biomass of all filter feeders among three reef habitats was analysed using ANOVA. Data was ranked to satisfy normality and homoscedascity assumptions. Inshore turfing algae and *Ecklonia radiata* sites had three time higher biomass than corresponding habitats offshore and *Sargassum* spp inshore sites had one and a half higher biomass than offshore (Figure 3.48). There was no statistically significant interaction between distance from shore and habitat (Table 3.14). Sponges and ascidians were the dominant filter-feeding organisms in reef habitats with mean biomass of 30 (± 46 s.d.) and 43 g m^{-2} (± 63 s.d.) respectively. *Herdmania momus* was a dominant ascidian contributing 37 g m^{-2} (± 58 s.d.) with a small number of other ascidians most notably *Pyura gibbosa*, *Polycarpa viridis* and *Polycarpa nigricans* also present. Similarity percentage analysis (SIMPER) indicated that the differences between inshore and offshore reefs were due not to different species present but to the much higher biomass of dominant taxa inshore (Table 3.15). Total filter feeders in seagrass habitats were highest in *Posidonia* meadows followed by *Amphibolis* spp and *Halophila*/*Heterozostera* spp (Figure 3.49).

Table 3.14. Results of ANOVA using data for the three reef habitats and distance from shore.

Source of variation	DF	SS	MS	F	P
Inshore-Offshore	2	16517.634	8258.817	12.151	<0.001
Habitat	1	26335.758	26335.758	38.749	<0.001
Inshore-Offshore x Habitat	2	1083.732	541.866	0.797	0.453
Residual	105	71364.042	679.658		
Total	110	113960.000	1036.000		
Comparison	Diff of Means	t	Unadjusted P	Critical Level	Significant?
turfing algae vs. *Sargassum* spp	29.915	4.926	<0.001	0.017	Yes
Ecklonia radiata vs. *Sargassum*	15.875	2.614	0.010	0.025	Yes
turfing algae vs. *Ecklonia radiata*	14.040	2.309	0.023	0.050	Yes

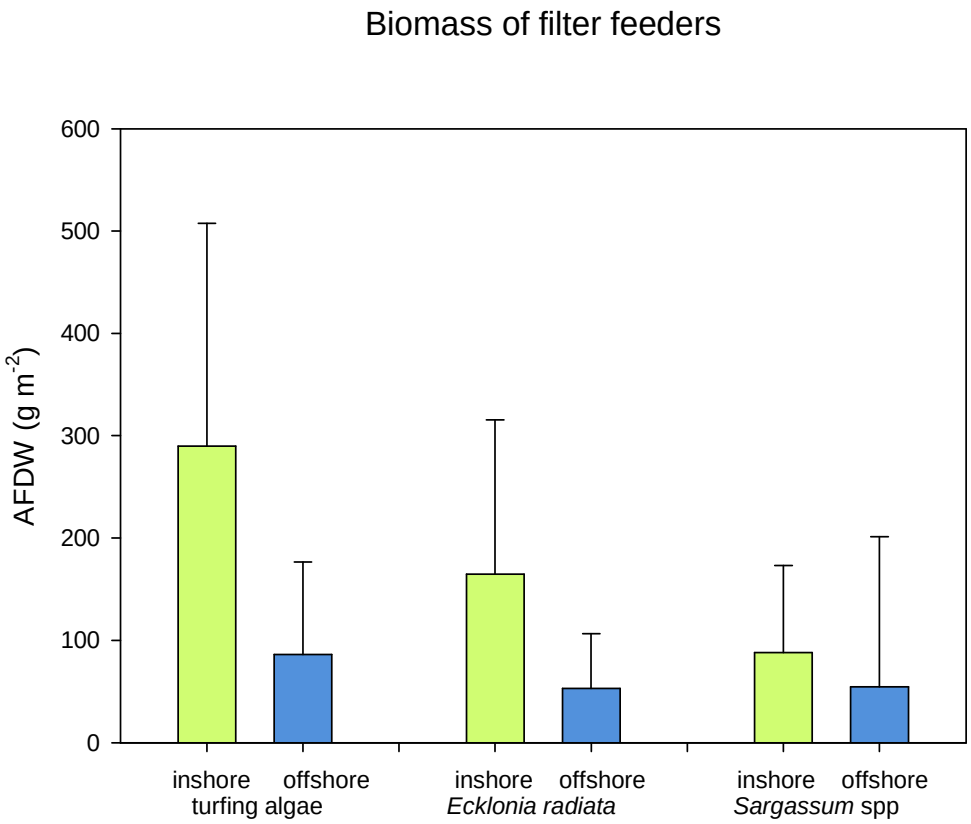

Figure 3.48. Biomass of all filter feeders in inshore and offshore reefs in three reef habitats.

Table 3.15. Species contributing to dissimilarity of inshore and offshore reefs (SIMPER analysis).

turf algae Species	Group inshore Av.Abund	Group offshore Av.Abund	Av.Diss	Diss/SD	Contrib%	Cum.%
Herdmania momus	8.74	3.64	17.64	1.32	28.77	28.77
sponge	8.17	3.42	16.87	1.43	27.51	56.28
ascidian other	1.92	0.98	5.19	1.16	8.47	64.75
coral other	0.82	1.08	4.23	0.97	6.91	71.65
soft coral	0.76	0.38	2.77	0.50	4.51	76.16
mussel	0.50	0.31	2.09	0.39	3.41	79.58
favid coral	0.13	0.57	1.76	0.49	2.88	82.46
Pyura gibbosa	0.38	0.24	1.38	0.60	2.25	84.71
bryozoan	0.35	0.24	1.25	0.88	2.03	86.74
Plesiastrea sp	0.00	0.64	1.17	0.23	1.90	88.65
Polycarpa viridis	0.29	0.06	0.99	0.31	1.61	90.25

Ecklonia radiata Species	Group inshore Av.Abund	Group offshore Av.Abund	Av.Diss	Diss/SD	Contrib%	Cum.%
Herdmania momus	6.25	3.07	14.99	1.41	26.79	26.79
sponge	5.13	3.27	11.10	1.33	19.84	46.63
ascidian other	2.59	1.21	7.23	1.41	12.92	59.55
coral other	0.79	0.36	3.26	0.69	5.83	65.38
Polycarpa nigricans	0.51	0.25	2.32	0.73	4.14	69.52
bryozoan	0.54	0.28	2.13	0.85	3.80	73.32
soft coral	0.17	0.51	2.01	0.45	3.60	76.91
Pyura gibbosa	0.53	0.15	1.91	0.72	3.41	80.32
Cenolia trichoptera	0.35	0.21	1.57	0.73	2.81	83.14
oyster	0.39	0.00	1.40	0.36	2.51	85.65
bivalve other	0.39	0.09	1.04	0.44	1.85	87.50
Polycarpa viridis	0.39	0.09	1.03	0.43	1.85	89.34
Comatula purpurea	0.13	0.09	0.84	0.36	1.51	90.85

Sargassum spp Species	Group inshore Av.Abund	Group offshore Av.Abund	Av.Diss	Diss/SD	Contrib%	Cum.%
Herdmania momus	3.96	2.06	20.46	1.26	28.36	28.36
sponge	3.21	2.62	18.04	1.25	25.01	53.37
ascidian other	1.57	0.70	8.50	1.17	11.78	65.15
coral other	0.61	0.91	6.56	0.69	9.09	74.25
Polycarpa nigricans	0.58	0.31	4.15	0.65	5.76	80.01
Comatula purpurea	0.32	0.00	2.20	0.51	3.05	83.06
Polycarpa viridis	0.43	0.13	2.19	0.53	3.03	86.08
favid coral	0.26	0.20	1.49	0.36	2.07	88.16
Cenolia trichoptera	0.21	0.06	1.48	0.45	2.05	90.21

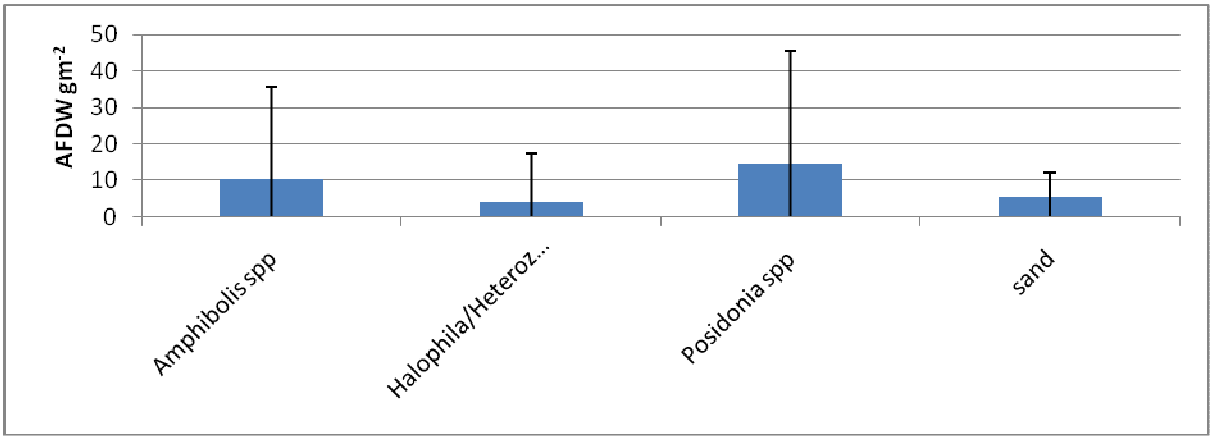

Figure 3.49. Biomass of all filter feeders in seagrass habitats.

3.1.8 Rates of primary production: Benthic Microalgae

Methods

Small scale spatial patterns

We have employed a nested sampling regime to examine the small-scale (up to 1000 m) variability in MPB production to give an indication of patchiness of these processes. These data help us isolate larger scale spatial and temporal trends from random patchiness. Sampling was carried out in Marmion Lagoon and incorporated a nested hierarchical design at five spatial scales: 10cm between replicates, 1m between plots, 10m between sites, 100m between locations and 1000m between stations. At each of the main "stations", two "locations" separated by 100m were randomly selected using GPS to measure the distance between them. Each of these locations was 10 m in diameter. A marker was placed at the centre of the location and two sites separated by 10 m were selected by running a 5m measure out from the marker. Located at each site were two plots 1 m apart. From each plot we also collected three 9.3cm ID sediment cores 10 cm apart which were returned to the laboratory for incubations. We conducted "light" and "dark" incubations on sequential days using the same cores.

Large scale spatial patterns

On a larger scale, primary production by MPB was quantified in winter (August 2008) and in summer (January 2009) at six stations within or near Marmion Lagoon (Cow Rock, AA, BB, MM4, MM1 and M3MRS) (Figure 3.50). We collected twenty four 9.3cm ID sediment cores at each station. The cores were selected from a restricted location to reduce the small scale spatial variability. However, if sand ridges were present cores were evenly distributed between the ridge peaks and troughs to average out this potential source of variability. In this case each experimental aquarium was illuminated by a metal halide lamp. Light exposure was varied using neutral density film sufficient to achieve a range of nominal light intensities up to 1200 μmol quanta m^{-2} s^{-1}. Light readings were taken with a Licor PAR meter equipped with at two pi PAR sensor at the beginning and end of the incubation and the irradiance used in the calculations represents the average of these two measurements. Heavy black plastic was wrapped around the bin containing the cores for the dark treatment. In all, 8 experimental treatments (7 different light intensities and one dark incubation) were conducted for each station by conducting incubations on sequential days using the same cores.

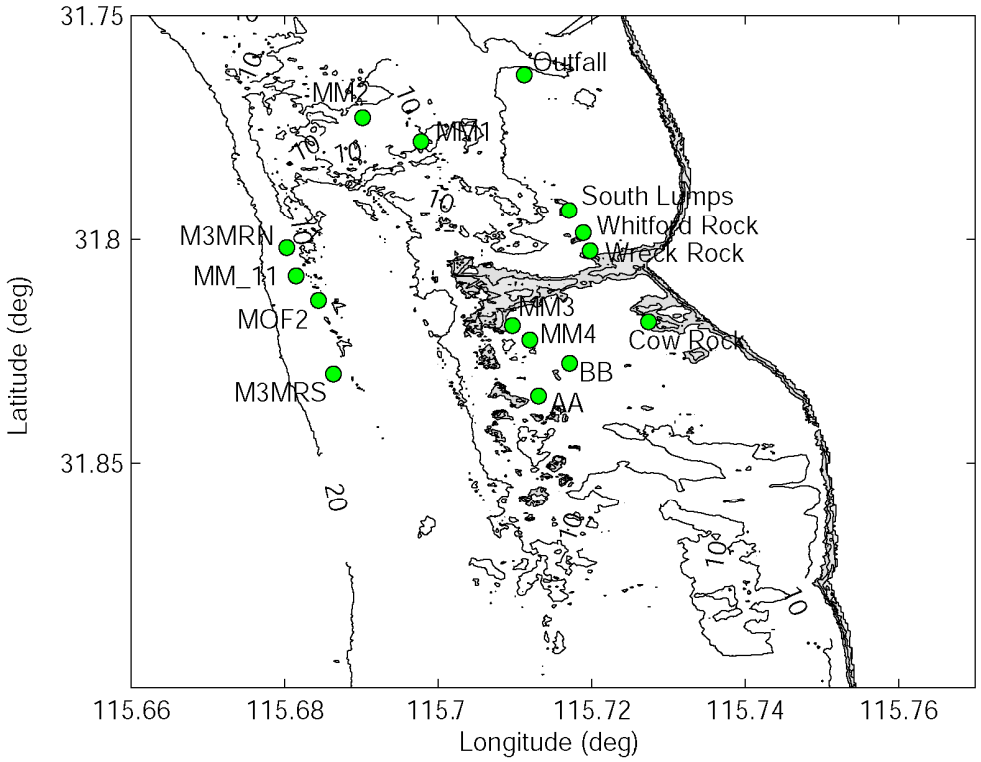

Figure 3.50. Map of Marmion Lagoon sampling stations.

Incubations

Cores were returned to the laboratory and distributed into four tubs (i.e. 6 cores per tub) with a continuous flow of clean ambient seawater (6 litres per minute). The cores in each tub represent replicates of an experimental treatment.

At the beginning of the incubation, each of the cores was sealed with a clear acrylic lid. The lid has two ports, one for sampling and the other to allow the resupply of surrounding water as each sample is collected. The water inside the core is stirred gently by a 4cm Teflon coated magnetic stirrer bar suspended under the lid and driven by a small electric motor. Soon after each core was sealed a 30ml sample of water was collected for dissolved oxygen analysis and a further 35 ml sample of water was collected from each core for dissolved nutrient analyses. This initial sampling serves as a starting reference for the incubation. Two further samples were collected from each core at regular intervals during the incubation. After the incubation was complete the lids were removed and the cores left until the next morning when the same routine was practiced for the remaining light intensity treatments. After the final sampling, the length of the sediment plug and overlying water column were measured and the sediment stored frozen for later geochemical analysis (chlorophyll a, sediment grain size, sediment moisture content, and sediment POC/PON).

Rates of production and nutrient fluxes were calculated as the slope of the solute versus time relationship, normalised by the overlying water volume. Corrections were made for the replacement water from the ambient tank. Gross rates of oxygen production (production independent of concurrent respiration) were calculated by subtracting the rate of oxygen consumption at zero irradiance (dark flux) from the positive rates of oxygen evolution (light

flux). Production by the BMA community was determined by generating production (via oxygen evolution) versus irradiance curves, the currency of our biogeochemical models. A trend line was been fitted to the data using nonlinear curve fitting techniques and the equations of Platt et al. 1980 if photoinhibition was evident or Webb et al., 1974 if it was not.

Results

Small scale spatial patterns

There was no significant variation between the two "stations" located 1000m apart in Marmion Lagoon for either primary production or respiration (Table 3.16). There was however, significant variation in both light and dark treatments among the locations within these stations (the 100m spatial scale, see Table 3.16). Variations at the "location level" potentially obscure differences at the 1000m level, although the components of variance (Table 3.17) at the station level were small relative to the variation amongst locations within each station. Variation was generally not significant at the 10m ("site") and 1m ("plot") spatial scales, although there was significant variation in dark fluxes between the sand ridges and valleys (Table 3.16). In addition, there was high variation in respiration (dark flux) amongst replicate samples within the plots (see the residual term in Table 3.17) indicating patchiness at very smallest spatial scales (<1m). Again this within plot variation may have obscured differences at larger spatial scales.

Table 3.16. Summary of analysis of variance for oxygen flux in light and dark chambers. Data were untransformed. There were 3 replicate cores incubated from the sand ridge an 3 from the valley within each plot, site, location, station combination.

Source	d.f.	Light Flux			Dark Flux		
		m.s.	F	P	m.s.	F	P
Station	1	7690.07	0.96	0.43	1.39	0.01	0.94
Location(S)	2	7999.98	90.98	**<0.001**	180.979	58.45	**0.001**
Site(L(S))	4	87.93	2.15	0.16	3.09	0.28	0.88
Plot(Si(L(S)))	8	40.99	0.58	0.78	10.99	0.35	0.9327
RidgeValley(P(Si(L(S))))	16	71.06	0.92	0.553	31.5	2.09	**0.02**
Residual	64	77.4			15.09		

Table 3.17. Variances estimated from the analysis of variance detailed above.

Source of variation		Light	Dark
Among stations	=S	0	0
Among locations within stations	=L(S)	329.7	7.4
Among sites within locations Site	=(Si(L(S))	3.9	0
Among plots within sites	=P(Si(L(S)))	0	0
Between ridges and valleys within Plots	=RV(P(Si(L(S))))	0	5.5
Among replicates	=Residual	77.4	15.1

At the location within station level, results were temporally confounded (different locations were samples on different days) so we conducted a further set of incubations to test whether these differences were genuinely spatial or actually temporal in nature. In this situation we

investigated only the station and location levels (as well as ridges and troughs which was also significant) but all on the one day to eliminate temporal confounding. In contrast to the original, variation at the location within station level was no longer significant suggesting that those differences were indeed temporal in nature (Table 3.18). The variation in respiration (dark flux) at the largest spatial scale was also now significant (Table 3.18) further suggesting that temporal variations between sampling days may be more important than spatial variations.

Table 3.18. Summary of analysis of variance for oxygen flux in light and dark chambers. Data were untransformed. There were 3 replicate cores incubated from the sand ridge an 3 from the valley within each location, station combination.

Source	d.f.	Light Flux			Dark Flux		
		m.s.	F	P	m.s.	F	P
Station	1	$1.2x10^{-6}$	3.5	0.20	229	14492	**<0.001**
Location(S)	2	$3.2x10^{-7}$	0.05	0.95	0.02	0	1.00
RidgeValley(L(S))	4	$6.5x10^{-6}$	1.58	0.23	61.2	4.4	**0.01**
Residual	16	$4.1x10^{-6}$			13.9		

Large scale spatial patterns

PMax was higher in summer than winter at four of the stations in Marmion Lagoon (BB, MM4, MM1 and M3MRS), suggesting that microphytobenthos communities are capable of fixing carbon more rapidly and efficiently during the summer period. Winter PMax was not different to summer at AA and Cow Rock (Figure 3.51 and Figure 3.52). However, some of the seasonal differences in production rates may be accounted for by variations in biomass. Chlorophyll a concentration was highest at the BB station (6.3 ± 0.4 mg g-1 wet wt during the winter and 5.2 ± 0.2 mg g^{-1} wet wt in summer Figure 3.52). The lowest chlorophyll a concentrations (1.7 ± 0.09 mg g^{-1} wet wt during both the summer and winter sampling) were measured at the deep offshore station (M3MRS) (Figure 3.52). In the absence of the contribution made by differences in biomass (i.e. production data normalised according to chlorophyll content) PMax during the summer remained higher than the winter at three of the stations (BB, MM4 and M3MRS) but the seasonal variation in PMax at the MM1 station was no longer significant.

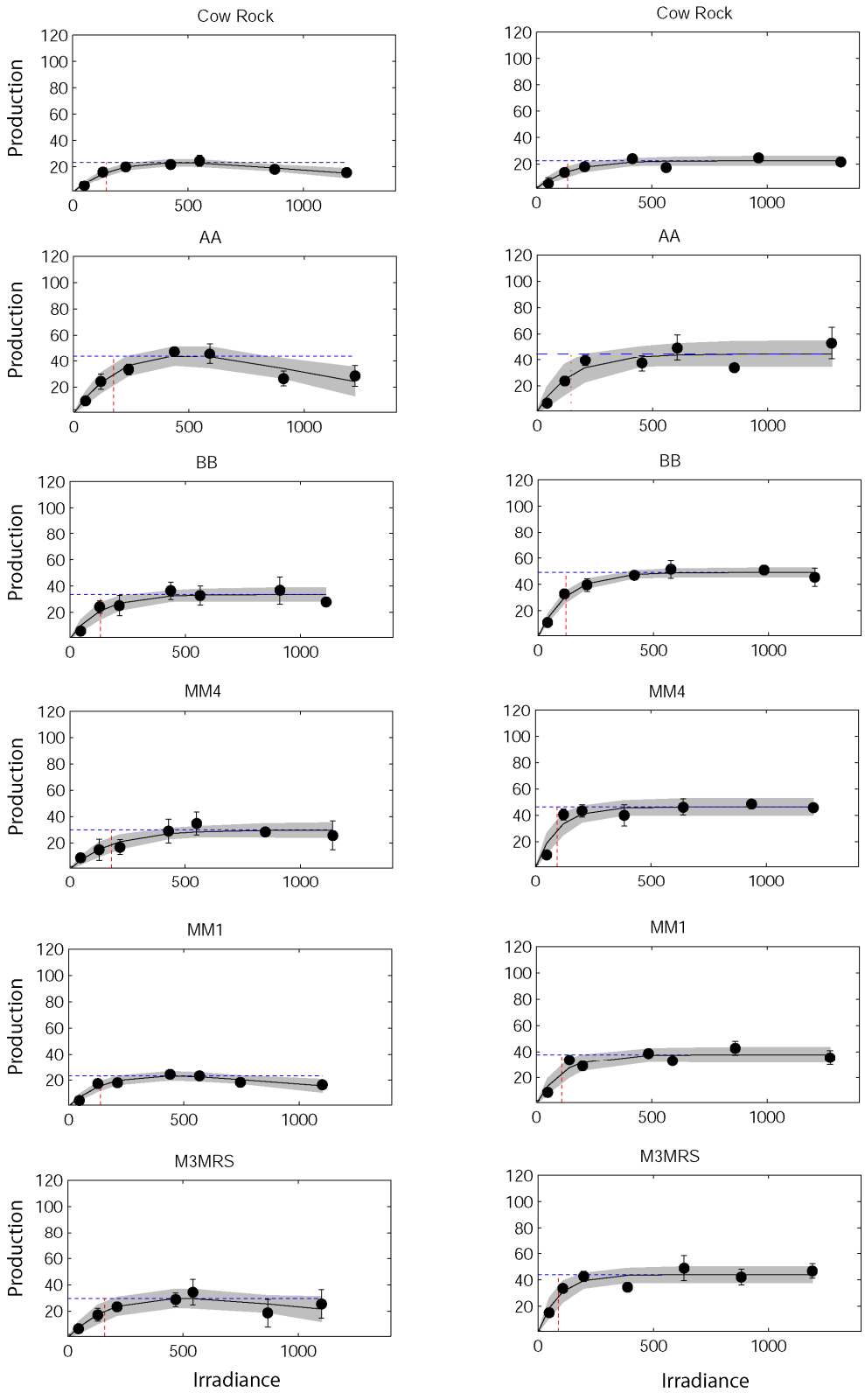

Figure 3.51. Production (mmol O2 m-2 h-1) versus irradiance (µmol m-2 s-2) curves collected during winter (left) and summer (right) from six stations in Marmion Lagoon. The blue dotted line is PMax and the red dotted line is Ik. The shaded area is the 95% confidence interval for the fitted curve.

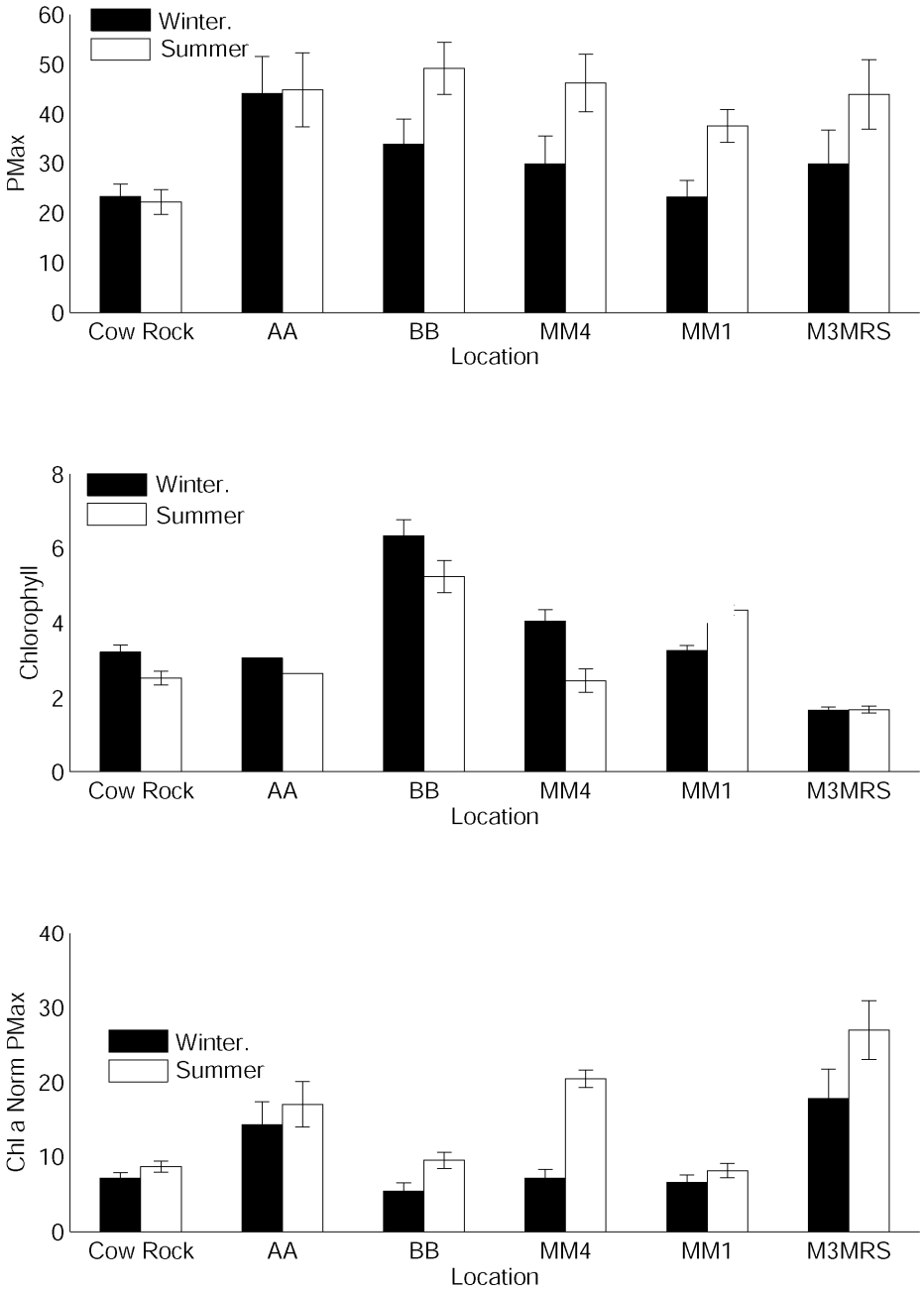

Figure 3.52. Mean (and 95% confidence intervals) of (top) PMax (mmol O_2 m^{-2} h^{-1}), (centre) Chlorophyll a concentration (mg g^{-1} wet weight) and (bottom) PMax calculated from Chlorophyll a normalised oxygen flux data (mmol O_2 m^{-2} h^{-1}/µg g^{-1} wet weight) collected in winter and summer from six stations in marmion Lagoon.

Average respiration rates were universally higher in summer than winter, significantly so at the inner shelf Cow Rock, mid shelf BB and MM1 and outer shelf M3MRS stations presumably as a result of temperature dependant constraints on microbial activity (Figure 3.53). The highest rates of summer time respiration was measured at the deep offshore station and amounted to -12.8 ± 1.3mmol O_2 m^{-2} hr^{-1} (Figure 3.53). These deeper stations are located close to reefs with abundant macroalgal populations and the higher respiration rates may

reflect higher rates of carbon supply from eroding plant material or labile macroalgal exudates.

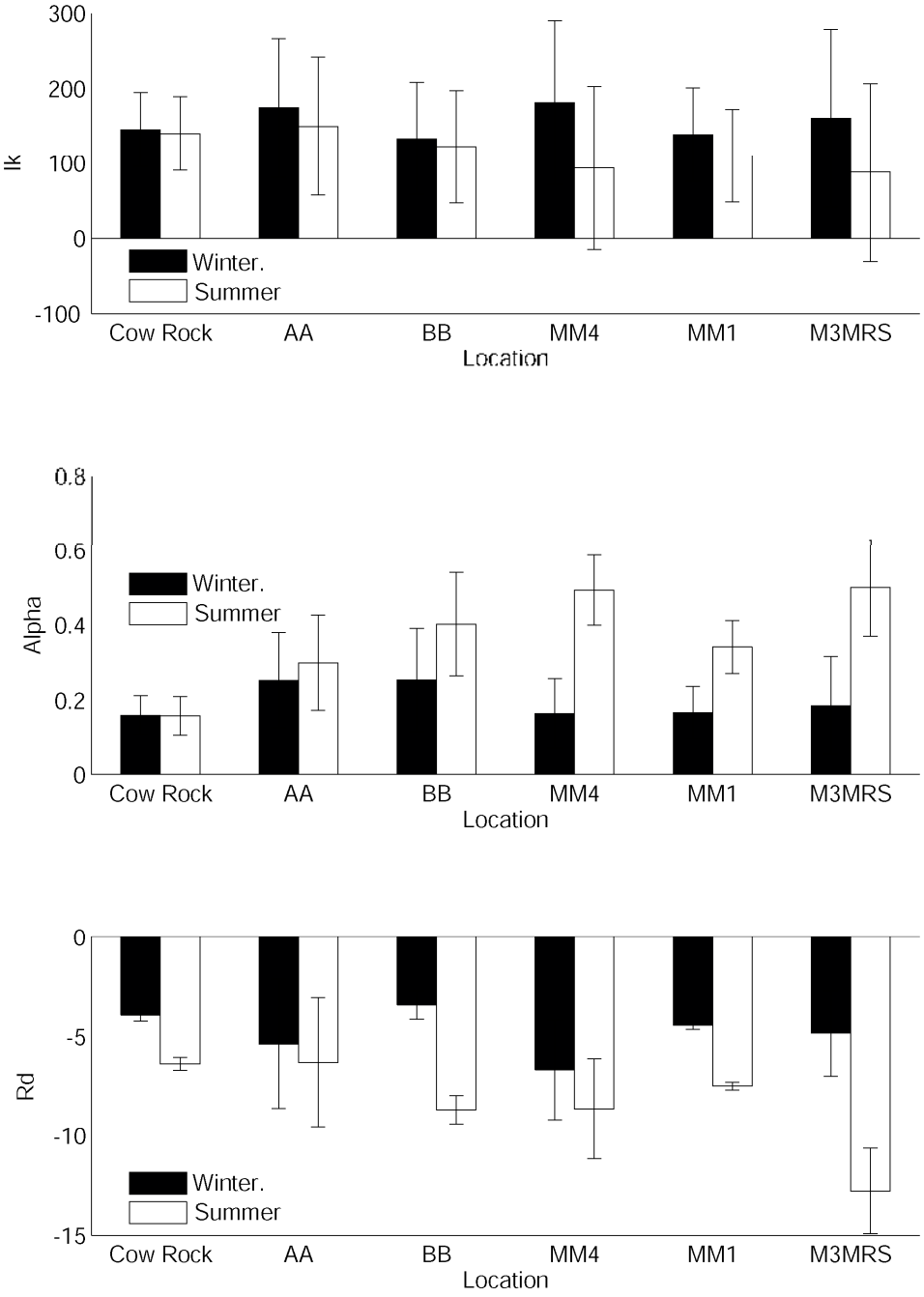

Figure 3.53. Mean (and 95% confidence intervals) of (top) Ik (µmol m−2 s−1), (centre) alpha (mmol O2 µmol photons-1) and (bottom) Rd (mmol O2 m-2 h-1) for data collected in summer and winter from six stations across the disturbance gradient.

Pmax was highest during summer at the three mid shelf stations within Marmion Lagoon (44.8 ± 9.9 at AA, 49.1 ± 3.6 at BB and 46.22 ± 6.5 at MM4) (Figure 3.52). The lowest PMax values were at the inner shelf Cow Rock station (22.1 ± 3.6 mmol O_2 m^{-2} hr^{-1} in Summer and 23.3 ± 2.53 mmol O2 m^{-2} hr^{-1} in winter Figure 3.51 and Figure 3.52). Again variations in chlorophyll a concentration also influence the spatial distribution of PMax. While summer

time Pmax values at the mid and outer shelf stations were similar, biomass at each station was quite different. Of the mid and outer shelf stations, chlorophyll a content was highest at the BB station and lowest at the offshore M3MRS station (Figure 3.52 The highest chlorophyll a normalised Pmax (26.9691 ± 3.9231 mmol O_2 m^{-2} h^{-1}/μg g^{-1} wet weight during summer) was at the deep station M3MRS and suggesting that the cells at the deeper stations may fix carbon more efficiently to account for reduced light intensity (Figure 3.52).

There were no statistically significant seasonal or spatial variations in Ik (Figure 3.53). Average alpha (the relationship between oxygen flux and light intensity at low irradiances) was higher in summer than winter at all stations except the inner shelf Cow Rock station (Figure 3.53). However, this seasonal difference in alpha was only significant at the MM4 (mid shelf in Marmion Lagoon), MM1 (mid shelf outside Marmion Lagoon) and M3MRS (offshore) stations (Figure 3.53).

3.1.9 Rates of primary production: laboratory studies on Macroalgae

Methods

Sampling site

All macroalgae were collected by divers from one small area of limestone reef (North Lumps) located in 10 m water depth in Marmion Lagoon, Western Australia. The relationship between production and irradiance was measured for four species; the brown algae *Ecklonia radiata* and *Sargassum* sp., and the red algae *Pterocladia lucida* and *Hennedya crispa*. Winter experiments were conducted in August – September 2008 while summer experiments were conducted in February – March 2009. 24 replicate plants were divided randomly into four experimental tanks (six per tank. Irradiance was manipulated using neutral density screens. Each plant was transferred into a 10 cm diameter by 30 cm length of plastic tube and sealed with a clear acrylic cap. A sample of the water was collected from each chamber and analysed for dissolved oxygen. Two further dissolved oxygen samples were collected from each of the chambers at one hour intervals to complete the incubation. The system was then left until the next morning when the same routine was followed for four other light intensities.

In April 2008 we conducted analyses on 11 of the most common species encountered at our sampling site. These were *Ecklonia radiata, Sargassum* sp., *Pterocladia lucida*, *Rhodymenia* sp., *Padina* sp., *Lobophora variegata, Dictyomenia sonderi, Echinothamnion hystrix, Caulerpa scalpeliformis, Hennedya crispa,* and *Asparagopsis taxiformis*. In this case, six replicate plants of each species were spread between three tanks (eight per tank) and incubations conducted in the manner described above but at a single light intensity of 190 μmol photons m^{-2} s^{-1} on one day and in the dark the next day. *E. radiata* was incubated twice, as part of the first and last incubations, to test for temporal effects between sampling.

Rates of oxygen consumption/evolution were calculated from the linear regression of the oxygen concentration data as a function of time, the volume of the chamber and the wet weight of the algae. Corrections were made for the replacement water sampled with ambient tank water. Gross rates of oxygen production (production independent of concurrent respiration) were calculated by subtracting the rate of oxygen consumption at zero irradiance (dark flux) from the positive rates of oxygen evolution (light flux). A curve was fitted to the

P vs I data using nonlinear curve fitting techniques and the equations of Platt et al. (1980) if photoinhibition was evident or Webb et al. (1974) if it was not.

Macroalgal biomass data (wet weight) was collected from Marmion Lagoon at 6 stations in summer and 4 stations in winter. Light intensity at 10 m was measured for 40 days in summer (16 Jan 2008 to 25 Feb 2008) and 37 days in winter (6 July 2007 to 12 Aug 2007) by a mooring located in 20 m of water just offshore in Marmion Lagoon (see chapter 1). Summer and winter areal production estimates for reef habitat were made using these estimates of biomass, the P vs I relationship for each species and the underwater light regime. These areal production measurements were then scaled based on the amount of reef habitat in Marmion Lagoon calculated from habitat maps to give an estimate of whole of Lagoon production.

Results

P vs I experiments

The highest P_{max} (94.9 ± 22.0 μmol O_2 g^{-1} wet wt h^{-1} by *Pterocladia lucida* and 70.1 ± 17.7 μmol O_2 g^{-1} wet wt h^{-1} by *Hennedya crispa*) were measured in the smaller species during summer (Figure 3.54 & Figure 3.55). Summer P_{max} (16.3 ± 3.0 μmol O_2 g^{-1} wet wt h^{-1} for *E. radiata* and 31.9 ± 6.4 μmol O_2 g^{-1} wet wt h^{-1} for *Sargassum* sp.) in the larger species were lower (Figure 3.54 and Figure 3.55). On a biomass-specific basis (i.e data presented per gram of plant wet weight), the production efficiency of the macroalgal species studied was strongly correlated to the size of the plant. The P vs I curves suggest that the smaller understorey species (*Pterocladia lucida* and *Hennedya crispa*) fix carbon more efficiently than the larger canopy species (*Ecklonia radiata* and *Sargassum* sp.) (Figure 3.55). Similarly, production by the 11 species investigated at a single light intensity was generally inversely correlated to the size of the plant. Smaller individuals had higher rates of production per gram of biomass (i.e. were more efficient primary producers) than the larger species (Figure 3.56). The highest rate of primary production (42.0 ± 11.4 μmol O_2 g^{-1} wet wt h^{-1}) measured was for *P. lucida*, the second smallest species incubated, while the lowest rate (7.9 ± 3.9 μmol O_2 g^{-1} wet wt h^{-1}) was for *Echinothamnion hystrix*, the largest (Figure 3.56). The size-related variations in production efficiency are likely to be due to differences in the surface area of the plant relative to the volume (SA:V) (Nielsen & Sandjensen 1990). Small plants have a larger relative surface area and more photosynthetic pigment per gram of biomass (because the larger plants require more structural tissue relative to photosynthetic tissue to maintain their integrity) and can collect more light (per unit of volume) than larger plants (Littler 1980, Peckol & Ramus 1988, Agusti et al. 1994, Enriquez et al. 1994, Johansson & Snoeijs 2002). The larger relative surface area in small plants also results in a higher nutrient uptake efficiency (Rosenberg & Ramus 1984, Hein et al. 1995, Taylor et al. 1998). So while the metabolic needs of the plant will increase with its volume (the higher volume plant requiring more nutrients and more light than the lower volume plants), the smaller surface area relative to the volume will result in a lower rate of light harvesting and nutrient delivery to the larger plants.

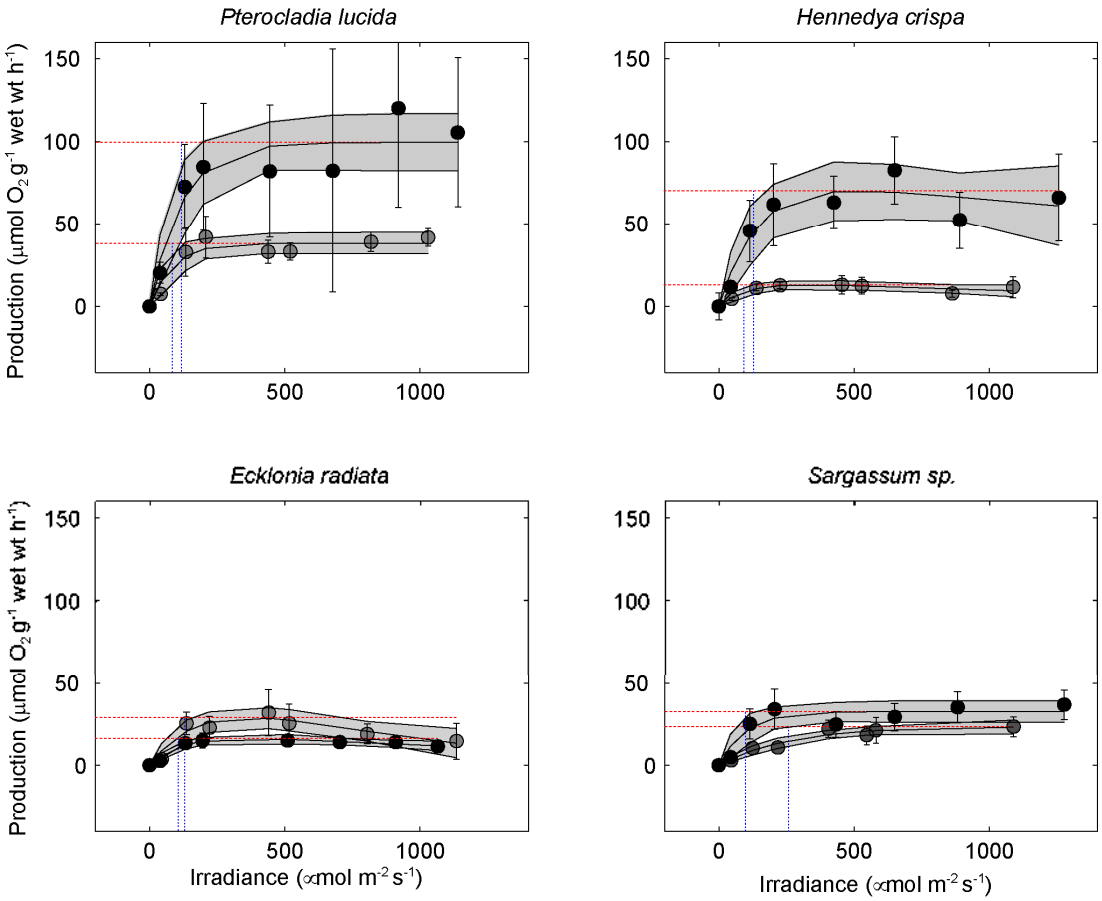

Figure 3.54. The relationship between gross primary production (mean ± 1SD) and irradiance for four species of macroalgae in summer (black) and winter (gray). The trend line has been fitted to the data using nonlinear curve fitting techniques and the equations of Platt et al. 1980 if photoinhibition was evident or Webb et al. 1974 if it was not. The shaded area is the 95% confidence interval for the fitted curve.

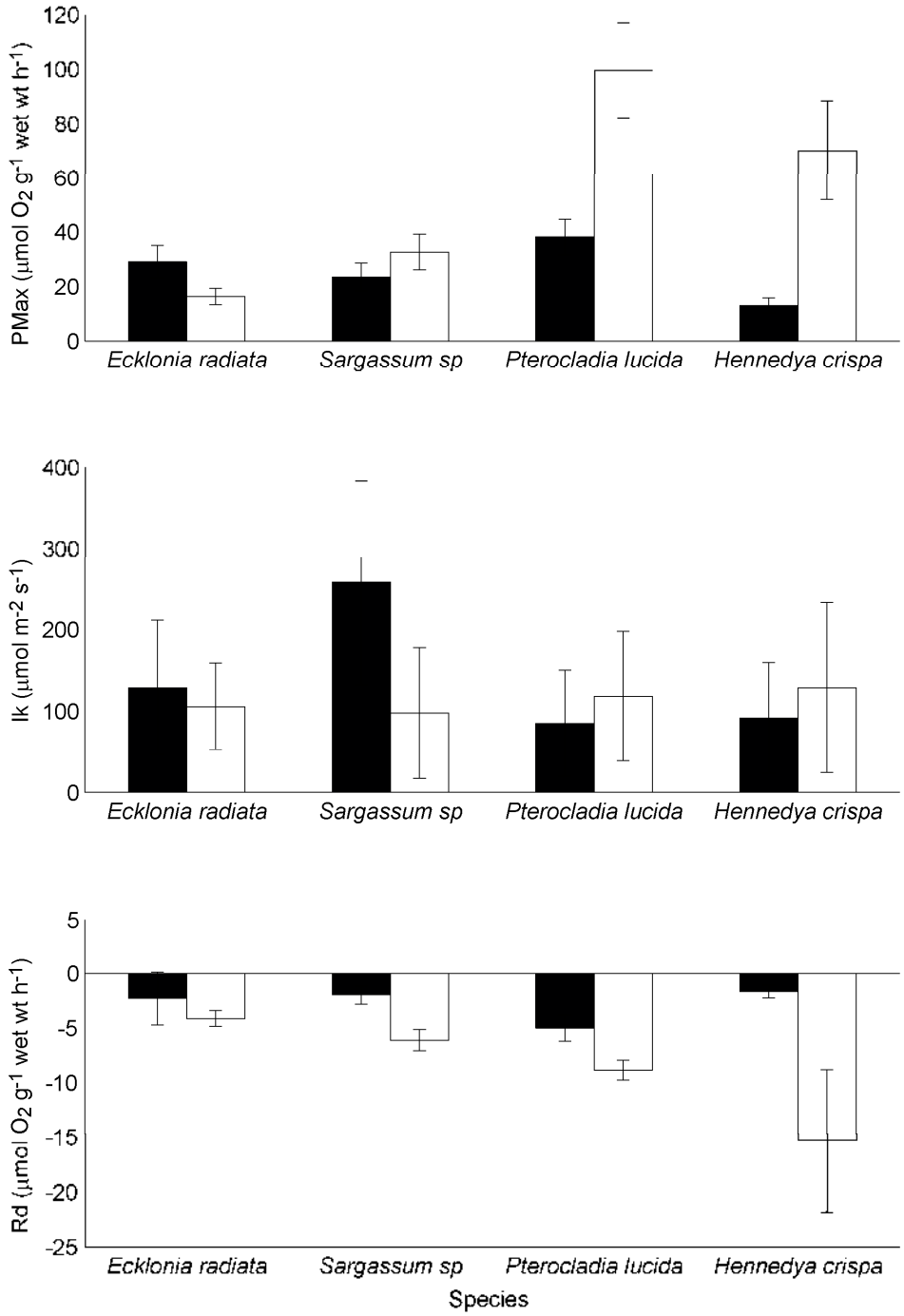

Figure 3.55. Mean (and 95% confidence intervals) of P_{max} (top), I_k (centre) and R_d (bottom) for four species of macroalgae collected in summer (white bars) and winter (black bars) from Marmion Lagoon, Western Australia.

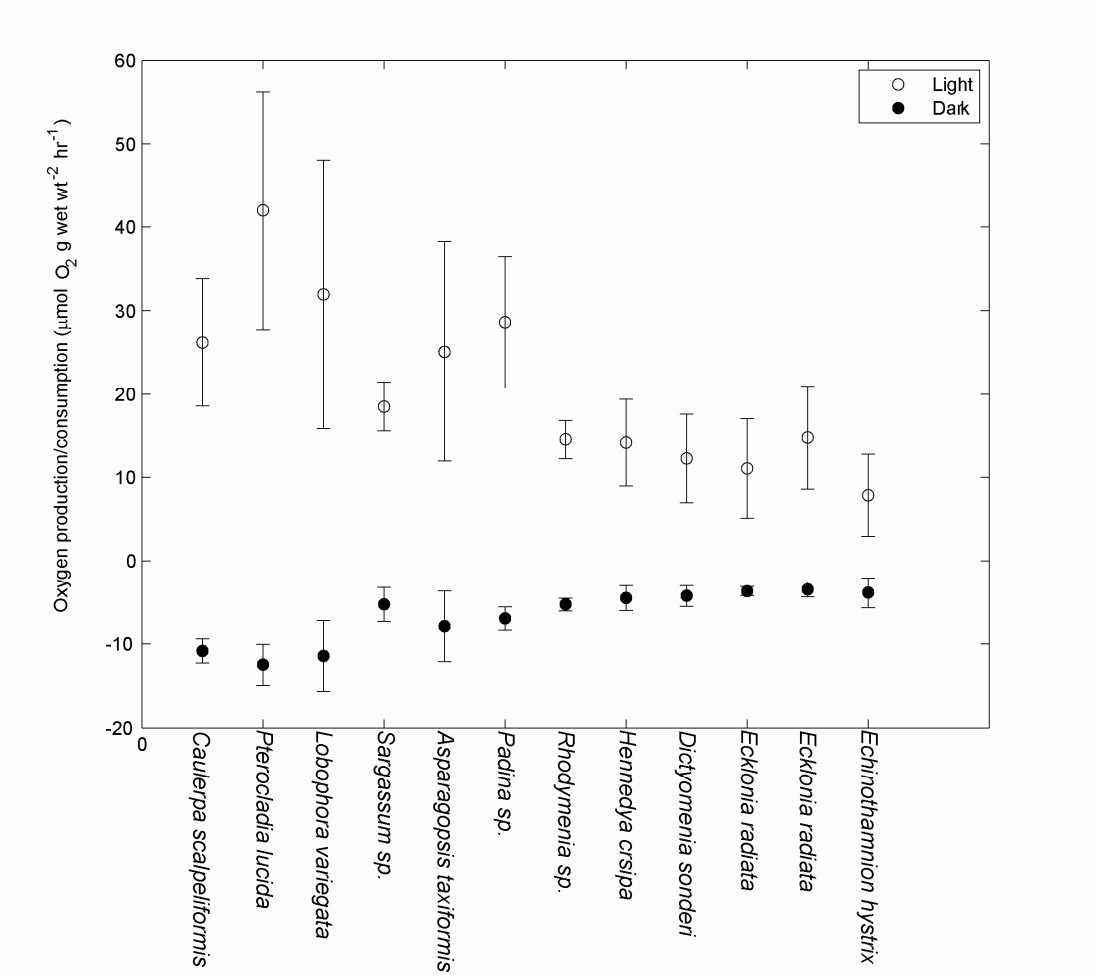

Figure 3.56. Variations in production and respiration (measured by oxygen evolution/consumption) for 11 species of macroalgae collected from Marmion Lagoon, Western Australia. The macroalgae are arranged by the average size of the individual plants used in the incubations, from smallest to largest (L-R). Ecklonia. radiata was incubated in the first and last incubations to test for temporal differences between sampling trips.

Production variations observed here were not solely the result of variations in the efficiency in harvesting and metabolism of light energy and/or nutrients. Rates of respiration (R_d) were also higher (i.e. more negative) in the smaller species (-15.4 ± 6.5 µmol O_2 g^{-1} wet wt h^{-1} by *H. crispa* and -8.9 ± 0.92 µmol O_2 g^{-1} wet wt h^{-1} for *P. lucida*) than the larger ones (-4.14 ± 0.7 µmol O_2 g^{-1} wet wt h^{-1} by *E. radiata* and -6.1 ± 1.0 µmol O_2 g^{-1} wet wt h^{-1} by *Sargassum* sp.) in both the P vs I experiments (Figure 3.55) and 11 species of macroalgae incubated in the dark (-12.5 ± 2.0 µmol O_2 g^{-1} wet wt h^{-1} for *Pterocladia lucida* compared to -3.5 ± 0.7 µmol O_2 g^{-1} wet wt h^{-1} for *Ecklonia radiata*) (Figure 3.56). While the uptake of light and nutrients will no doubt contribute to the SA:V limitation of production in irradiated plants, another SA:V process independent of the capacity of the plant to collect light or nutrients is required to explain the relationship between plant size and respiration. A SA:V-related reduction in diffusion across the boundary layer would reduce gas transfer and cause substrate (i.e. CO_2) limitation and oxygen accumulation, which would limit photosynthesis in larger plants during irradiated periods (Sandjensen et al. 1985, Sandjensen 1989). However, a similar SA:V reduction to the diffusive supply of O_2 and removal of CO_2 during periods of respiration (a rate-limiting process independent of light and nutrient availability) also explains the size-related relationship for respiration as we observed for production.

The functional group or morphology of the species makes a contribution to the plants SA:V ratio that is independent of its mass. Highly-branched species with numerous thin filamentous laterals have a greater SA:V ratio than thicker coarsely-branched species of roughly the same weight (Arnold & Murray 1980, Littler 1980, Littler & Keith 1982, Johansson & Snoeijs 2002). Differences in morphology may explain why the species with the smallest mass (*Caulerpa scalpelliformis*) had only the fourth highest oxygen production per unit of wet weight after species that had a slightly larger mass (*Pterocladia lucida*, *Lobophora variagata* and *Padina* sp.) (Figure 3.56). *C. scalpelliformis* has solid scalpel-like laterals while *P. lucida* is finely branched so, contrary to expectations based on plant weight, *C. scalpelliformis* actually has a smaller surface area.

Despite the higher rates of production per unit mass of the two smaller species (*Pterocladia lucida* and *Hennedya crispa*), the dominance of the kelp *Ecklonia radiata* in terms of biomass causes the gross production of that species to easily eclipse that of the other three. Mean biomass (2,964 g m^{-2} in winter and up to 7,181 g m^{-2} in summer) and production (7.5 x 10^5 µmol O_2 m^{-2} h^{-1} in winter and 2.0 x 10^6 µmol O_2 m^{-2} h^{-1} in summer) of *E. radiata* was typically one order of magnitude higher than in the other species (biomass <275 g m^{-2} for *Sargassum* sp. in winter and production <2.0 x 10^5 µmol O_2 m^{-2} h^{-1} for *P. lucida* in summer) (Figure 3.57).

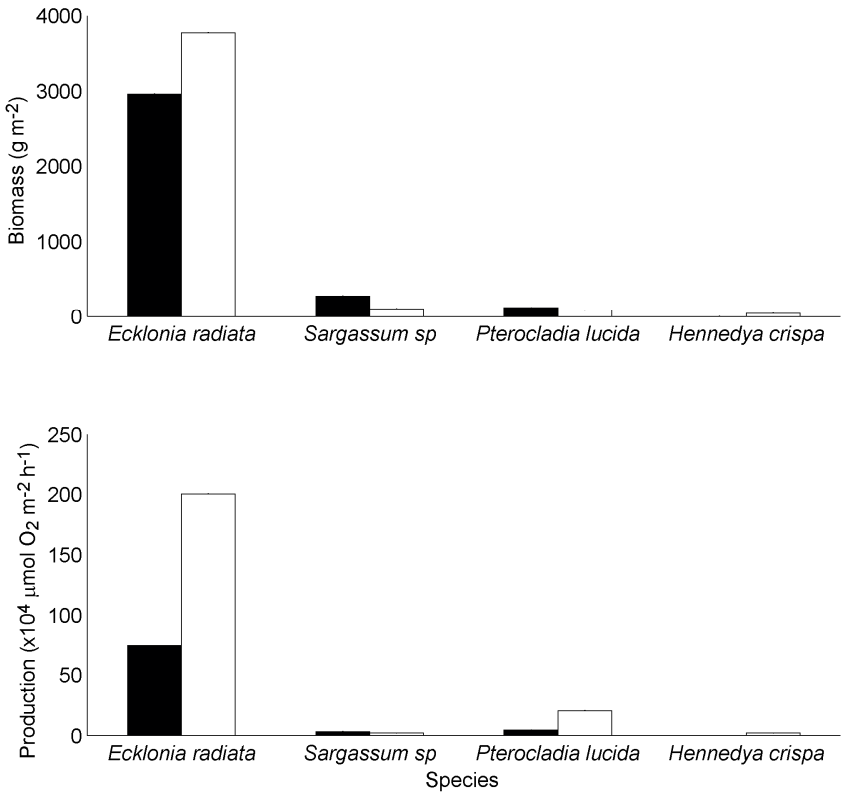

Figure 3.57. Estimates of biomass (top) and areal production (bottom) for four species of macroalgae collected in summer (white bars) and winter (dark bars) from Marmion Lagoon, Western Australia.

For three species studied (Sargassum sp., Hennedya crispa and Pterocladia lucida), Pmax was higher in summer (31.9 ± 6.4, 70.1 ± 17.7 and 95.0 ± 21.0 μmol O2 g-1 wet wt h-1, respectively) than winter (23.4 ± 5.1, 12.9 ± 2.5 and 37.1 ± 6.7 μmol O2 g-1 wet wt h-1, respectively) (Figure 3.55), probably due to temperature-related metabolic differences (Davison 1991), lower winter light levels (Middelboe et al. 2006) and/or natural variations in the plant life cycle (i.e. winter senescence Kilar et al. 1989).

Temperature effects and plant life cycle also explain greater respiration (R_d) in summer than winter for all four species. The largest difference in P_{max} between summer and winter was for the smaller species *P. lucida* (57.9 μmol O_2 g^{-1} wet wt h^{-1}) and *H. crispa* (57.2 μmol O_2 g^{-1} wet wt h^{-1}), while seasonal differences in P_{max} for *E. radiata* and *Sargassum* sp., were small at 12.6 and 8.5 μmol O_2 g^{-1} wet wt h^{-1}, respectively (Figure 3.55). The size related difference is possibly due to higher summer temperatures increasing diffusive gas transfer rates more in the small species (higher SA:V) than the larger ones.

In contrast to the other three species, P_{max} in *Ecklonia radiata* was slightly higher in the winter (29.0 ± 6.0 μmol O_2 g^{-1} wet wt h^{-1}) than summer (16.3 ± 3.0 μmol O_2 g^{-1} wet wt h^{-1}) despite significant seasonal reductions in irradiance (Figure 3.55). Higher *E. radiata* alpha in winter (0.22 ± 0.14 μmol O_2 μmol photons^{-1}) than summer (0.15 ± 0.07 (μmol O_2 μmol photons^{-1}) suggest higher photosynthetic efficiency at lower irradiances during winter (Figure 3.55). It is possible that *E. radiata* is able to alter its photosynthetic capacity/efficiency during winter to compensate for the lower winter irradiances. This may be a photoadaptive response of the photopigments to increase the size of the functional absorption cross section (Fairhead & Cheshire 2004). While our data seem to support the suggestion that *E. radiata* can change its photosynthetic response to maintain optimal performance during winter, the species continued to display variations in P_{max} across a depth gradient (Fairhead & Cheshire 2004) suggesting it has not made the same adjustments to compensate for depth-related variations in irradiance.

Despite the similar seasonal patterns of photosynthetic efficiency (as suggested by P_{max}), a large seasonal biomass accumulation by *Ecklonia radiata* combined with the seasonal variations in light intensity ensured that summer *E. radiata* production (1.1 x 10^6 μmol O_2 m^{-2} h^{-1}) was around 2.7 times higher than in winter (4.8 x 10^6 μmol O_2 m^{-2} h^{-1}). In relative terms, the summer-winter difference in production by *Pterocladia lucida* was higher (4.4 times) but the smaller difference in the magnitude of the biomass difference meant that production differed by an order of magnitude less (1.5 x 10^5 μmol O_2 m^{-2} h^{-1}) (Figure 3.57). These results suggest that variations in *E. radiata* biomass has the largest effect on seasonal production dynamics and are further evidence of the overwhelming contribution that *E. radiata* makes to overall patterns of community production in Marmion Lagoon.

3.1.10 Rates of primary production: field studies on Kelp

Methods

Study area

The small kelp *Ecklonia radiata* (C.Ag.) J. Agardh is the dominant macroalga across most of southern Australia and is the only true kelp found in the warmer seas of Western Australia and southern Queensland. *Ecklonia radiata* forms large, conspicuous beds in subtidal waters on moderate to rough water coasts. *Ecklonia radiata* exhibits a distinct seasonal pattern with a maximum in spring (October to December) with a rapid decline to a minimum during January through March.

We chose nineteen sites to span the widest range in light, temperature and water motion experienced by *Ecklonia radiata* in Marmion Lagoon. The sites encompassed a depth range of 2.5 m to 17.3 m and were all within 3 nm of each other. Measurements were taken in the austral summer (December 2008-January 2009), winter (May-June 2009) and spring (September-October 2009). These periods coincide with periods of change in the growth rates of the kelp (summer and winter) or in maximum growth (spring).

The density of *E. radiata* at each of the sites was calculated by counting all sporophytes >10 cm tall in three 0.25 m^2 quadrats, haphazardly placed within a 10 m radius of a stake marking each site. At all chosen sites, *E. radiata* forms continuous beds.

Measurement of productivity

The productivity (defined here as the rate at which new organic matter is created by photosythesis (Kirkman 1984) of each individual *E. radiata*, was measured following a method described by Mann & Kirkman (1981): adapted by Fairhead & Cheshire (2004). This method takes advantage of the fact that the primary meristem of kelps, including *E. radiata*, is located at the junction of the stipe and blade, so that movement of a hole punched in the basal area of the blade over a certain time period gives a good measure of thallus extension. Individual *E. radiata* were marked by punching two holes into the central lamina, 5 cm and 10 cm from the junction between the stipe and the lamina. The initial 5 cm hole was punched since it was anticipated the majority of growth would be below the 5 cm mark. The second 10 cm hole was to ensure growth was restricted to between the stipe and blade and the initial 5 cm mark. This was indeed the case with 95% of individuals recording all growth in this zone.

Twenty adult individuals were marked at each site during each survey and were collected 31-42 days later. Sampling occurred in the austral summer (December/January 09), winter (May/June 2009) and spring (September/October 2010). Only mature plants greater than 100 g wet weight were used in the study to ensure that all comparisons are made with only the sporophyte life stage. The distance of each hole from the junction between stipe and lamina was then measured in the laboratory (allowing the extension to be calculated by subtraction), and the first 20 cm of the thallus was then cut into 5 cm strips and weighed (wet weight, in grams). The strip with the maximum biomass was then used to calculate biomass accumulation (BA; g ind^{-1} d^{-1}) as $BA = xw/5d$ where x is the thallus extension (cm), w is the weight of the heaviest strip (g), and d is the number of days between punching the hole and collecting the kelp. The rate of BA per plant was then divided by the weight of the entire

thallus to produce an estimate of the relative growth rate. This measure is referred to here as the mass-standardised biomass accumulation (MSBA; mg^{-1} $g.ind^{-1}$ d^{-1}). This growth measure is sometimes referred to as specific growth rate, relative biomass accumulation or productivity (Kirkman 1984, Fairhead & Cheshire 2004).

Environmental characteristics

Light (lux) and temperature (ºC) measurements were measured at each site using a Hobo™ light and temperature logger (Part# UA-002-64 or Part#UA-002-08) set to record these parameters every 10 minutes. Loggers were attached to star pickets 30 cm above the substrate. Two loggers were positioned at four sites to allow assessment of their reliability. All light and temperature values from sites where two loggers were deployed were within 2% of average measurements. Because the loggers measured illuminance, and measures a different spectrum of wavelengths to those used by plants during photosynthesis, a comparison of lux and photosynthetically active radiation (PAR) was also performed. Comparative data were obtained on two occasions (December 2009 and July 2010) by attaching Hobo loggers to a CTD equipped with a PAR sensor. On each occasion average lux light readings from three Hobo loggers were compared to average PAR measurements obtained from the CTD at a series of 5 m depths ranging from 5m to 20m across the lagoon. A simple regression between the average lux values obtained from Hobo loggers and the average PAR values obtained from a CTD indicated a linear relationship (R^2=0.9822) The lux measurements recorded by the Hobo loggers were then converted into a lux $hours^{-1}$ measurement to account for changes in day length. Seven loggers were lost during the winter sampling period. These sites were excluded from the statistical analysis. In addition, one site was inaccessible during winter (site 12) and therefore was also excluded from the analysis. Estimates of wave energy (urms) for each site were obtained using data from the Swan model.

Nutrient samples were obtained by divers before harvesting kelp using 10 ml plastic vials. Samples were obtained from waters below the kelp lamina. 50 ml samples of seawater from the sites were analysed for dissolved silica, phosphate, nitrate and nitrite, as well as ammonia concentrations. Dissolved silica, phosphate and nitrate/nitrite were analysed using a flow injection analysis while ammonia concentration was determined using a flow injection analysis, gas diffusion, derivatisation - fluorescence detection method. For dissolved silica, Si species were reacted with molybdate at 45ºC pH 1.2, and then reduced with stannous chloride to form a heteropoly blue complex which was measured at 820 nm. Phosphate was reacted with molybdate and antimony potassium tartrate in acid medium which was then reduced with ascorbic acid to form a blue complex which was measured at 880 nm. Nitrate was analysed by first undergoing reduction to nitrite by passing it through a copperised cadmium column. Nitrite is then reacted with sulfanilamide under acidic conditions to form a diazonium salt which was then coupled with N-(1-naphthyl) ethylenediamine dihydrogenchloride to form a pink complex which was measured at 520 nm. For ammonia, a Sodium hydroxide solution was added to liberate ammonia which was then diffused across a PTFE membrane to react with ortho-phthaldialdehyde (OPA) - sulfite solution. This solution was then excited at 310nm and the fluorescence measured at 390nm.

Statistical analyses

To assess the relative variations in productivity among sites and among individual kelps, we determined the relative magnitude of effect (ω2: Graham & Edwards 2001);. The relative

magnitude of effects was calculated as the variance component of each factor, divided by the sum of all variance components (Winer et al. 1991). Because different numbers of individuals were retrieved from each site, the analytical model was unbalanced. Consequently, we used a formula for unbalanced models.

The main focus of analyses was determining which of the measured environmental variables (temperature, light, water motion (urms), nutrients (PO_4, DSi, NO_2/NO_3, NH_4) best predicted spatial variation in productivity. To do this we used linear multiple regression searching for the best combination of predictor variables from all possible combinations. The method identifies the best combination of each number of variables (i.e of models of each size). Models of different sizes were compared using three metrics: adjusted R^2, Akaike Information Criterion (AIC) and Schwarz Bayesian Information Criterion (BIC). Analysis was conducted using the leaps package in the R statistical software. Candidate models were then assessed for statistical significance in SPSS 17.0. Regressions were performed separately for each of the summer, winter and spring sample periods. Three metrics of growth and productivity were assessed separately: thallus extension, biomass accumulation and MSBA.

Results

1140 *E. radiata* were tagged during the course of the study and 752 individuals retrieved and processed (Table 3.19). The average number of tagged *E. radiata* retrieved between seasons varied. During the summer sampling the overall average percentage of *E. radiata* retrieved was 68%, in winter 60% and 86% in spring (Table 1). Despite the close proximity of the sites, there was considerable variation in physical characteristics (Table 3.19). Average water temperature of the sites encompassed a range of 1.4ºC (21.6ºC to 23.0 ºC) in summer, 1.2ºC in winter (19.2 ºC to 20.4 ºC), and 0.5 ºC in spring (17.3 ºC to 17.8 ºC) (Table 3.19). Average light intensity varied from 1385 lux h^{-1} to 224959 lux h^{-1} in summer, 4421 lux h^{-1} to 93677 lux h^{-1} in winter and 9940 lux h^{-1} to 112086 lux h^{-1} in spring (Table 3.19). Water movement obtained from the Swann model varied across the lagoon depending on the characteristics of the individual site (Table 3.19). The Swan model predicted water movements between 0.24 and 0.61 ubot (Table 3.19). In general, sites with high water movement were located across the reef in the mid lagoon area and at inshore exposed sites (Table 3.19).

Table 3.19. The number of tagged *Ecklonia radiata* retrieved from each of the Marmion Lagoon sites and the average density of *Ecklonia radiata* from each site. Physical characteristics recorded for each of the sites where kelp growth was recorded in Marmion Lagoon, Western Australia.

			Summer (Dec-Jan 2008/09)				Winter (May-June 2009)				Spring (Sept-Oct 2009)			
Site	Depth (m)	Water Movement (ubot)	Number of retrieved kelp	Density per m^2	Bottom Temp (ºC)	Light intensity (Lux $hours^{-1}$)	Number of retrieved kelp	Density per m^2	Bottom Temp (ºC)	Light intensity (Lux $hours^{-1}$)	Number of retrieved kelp	Density per m^2	Bottom Temp	Light intensity (Lux $hours^{-1}$)
1	11.3	0.37	15	25.3	21.7	71892	4	14.7	20.2	4616	8	16	17.4	13274
2	12.5	0.33	16	18.7	21.6	20475	8	9.3	19.9	4226	14	9.3	17.4	9940
3	17.3	0.26	20	32	21.7	31541	11	2.7	20.4	9987	20	2.7	17.5	16554
4	15.1	0.29	21	30.7	21.7	31541	15	10.7	20.4	4421	18	6.7	17.6	20473
5	14.7	0.27	16	25.3	21.7	1385	20	12.0	20.4	4421	20	1.3	17.6	13099
6	5.3	0.61	12	20	22.5	81667	6	6.7	nd	nd	7	4	17.8	18378
7	10.1	0.31	14	20	22.1	109512	17	9.3	19.4	17743	19	4	17.3	17926
8	2.5	0.50	17	30.7	22.7	158885	5	4.0	nd	nd	15	12	17.3	97389
9	5.4	0.28	17	16	22.7	158885	13	2.7	nd	nd	14	6.7	17.8	112086
10	7.1	0.25	15	20	22.6	109841	12	4.0	nd	nd	20	10.7	17.7	72143
11	9.7	0.38	8	10.7	22.2	158885	12	9.3	19.0	52137	12	8	17.4	19156
12	8.7	0.40	12	16	22.6	2611	0	nd	nd	nd	9	2.7	17.7	74407
13	5.3	0.37	11	22	22.6	187660	18	17.3	nd	nd	20	17.3	17.6	78553
14	3.7	0.24	12	26.7	22.8	48502	18	17.3	19.2	30641	20	8	17.7	58494
15	3.9	0.38	8	26.7	22.9	210025	7	21.0	19.2	30641	19	13.3	17.7	78966
16	4.3	0.35	8	26.7	22.9	129263	13	13.3	19.2	nd	15	8	17. 7	56821
17	4.3	0.30	14	13.3	23.0	215234	17	14.7	19.7	30012	8	6.7	17.6	28754
18	4.6	0.32	12	25.3	22.7	48444	18	12.0	19.6	93677	8	13.3	17.5	63202
19	4.9	0.47	7	14.7	22.9	224959	2	2.0	nd	nd	3	8	17.6	58368

* nd indicates no data. Light and temperature data was unable to be collected at some sites due to loss of loggers during winter. In addition, site 12 was not assessed in winter.

In Summer, magnitude of effects analysis indicated 24.44% of the observed variation was between sites (Table 3.20) for extension rates. When biomass accumulation was used as a growth measure, the between site variation fell to 17.48% (Table 3.20). For MSBA Magnitude of effects analysis suggested that 10.10% of the variation observed was due to between site differences.

Magnitude of effects values for between site variations, were consistently above 20% for winter. Between site variation was 30.69% using extensions as a growth measure (Table 3.20). When biomass accumulation was used as a growth measure the between site variation fell to 20.77% (Table 3.20). 39.26% of the variation observed in our data was between site variation (Table 3.20).

In spring, between sites variations varied widely depending on the growth measure used. For extensions, between sites variation accounted for 26.14% of the variation observed (Table 3.20) while for BA between site variations was higher than individual variation at 60.37% (Table 3.20). Between sites variation was 16.07% of the variation observed for MSBA (Table 3.20).

Table 3.20. Results of analyses of variance testing for differences between and within sites.

Extension	df	MS	F	P	vc	ω^2
Summer	18	18.7	5.37	0.00	1.125	24.44
Residual	239	3.48			3.478	
Winter	17	12.63	6.24	0.00	0.89	30.69
Residual	198	2.03			2.02	
Spring	18	28.48	6.09	0.00	1.65	26.14
Residual	257	4.67			4.67	
BA						
Summer	18	3.32	3.87	0.00	0.182	17.48
Residual	239	0.86			0.859	
Winter	17	0.64	3.38	0.00	0.038	20.77
Residual	198	0.18			0.183	
Spring	18	12.15	9.69	0.00	0.757	60.37
Residual	257	1.25			1.254	
MSBA						
Summer	18	10.13	2.51	0.00	0.452	10.10
Residual	239	4.02			4.025	
Winter	17	22.62	8.66	0.00	1.69	39.26
Residual	198	2.61			2.61	
Spring	18	23.12	3.75	0.00	1.18	16.07
Residual	257	6.16			6.16	

Summer

Analyses of summer growth data yielded statistically significant models in each case. The best model for each measure of growth or productivity depended on the metric used to assess each model. Temperature was the first factor to be added to all candidate models.

For thallus extension, both AIC and BIC suggested temperature alone (Table 3.21). Overall, both metrics found temperature to have the most influence on the average length of extensions in *E. radiata* during summer (Table 3.21; adj R^2=0.60;*p*=0.000).

The best model to predict kelp biomass accumulation depended on the metric used to assess each model. AIC suggested temperature alone (Table 3.21) while BIC suggested a model that included Temperature and Light however this model was not statistically significant. Overall, both models found temperature to have the most influence on the average biomass accumulation of *E. radiata* (Table 3.21; adj R^2=0.22; *p*=0.025) during summer.

When the BA was adjusted for the size of each individual *E. radiata*, then BIC suggested a model consisting of Temperature with the nutrients phosphate, dissolved silica, ammonia and Water Movement. AIC suggested a model containing all of these factors except ammonia. Neither of these models was statistically significant. The only model to yield a statistically significant result contained temperature only (Table 3.21; adj R^2=0.4528; *p*=0.001).

Table 3.21. Candidate models obtained from linear multiple regressions in R comparing summer growth data for *E. radiata* to environmental parameters in Marmion Lagoon Western Australia. Values in bold indicate the best values for adjusted R^2, Mallow's Cp and BIC.

No of predictors	Model	Adj R2	AIC	BIC	Model Significance (p)
Extension					
1	Temperature	0.60	-0.84	-12.45	0.000
2	Temperature+N	0.61	-0.25	-11.50	0.201
3	Temperature+N+PO_4	0.61	1.00	-9.71	0.493
4	Temperature+N+PO_4+Water Movement	0.59	2.65	-7.32	0.725
5	Temperature+N+PO_4+Water Movement +NH_4	0.58	4.24	-5.06	0.753
6	Temperature+N+PO_4+Water Movement +NH_4+Si	0.55	6.00	-2.51	0.768
7	Temperature+N+PO_4+Water Movement +NH_4+Si+ Light	0.52	8	0.41	0.855
Biomass Accumulation					
1	Temperature	0.22	3.12	0.11	0.025
2	Temperature+Light	0.31	1.91	-0.65	0.085
3	Temperature+Light+PO4	0.34	2.32	0.15	0.314
4	Temperature+Light+PO4+ Water Movement	0.36	3.14	1.34	0.384
5	Temperature+Light+PO4+ Water Movement +NH4	0.35	4.52	3.24	0.616
6	Temperature+Light+PO4+ Water Movement +NH4+Si	0.33	6.05	5.43	0.677
7	Temperature+Light+PO4+ Water Movement +NH4+Si +N	0.27	8	8.28	0.703
MSBA					
1	Temperature	0.4528	16.12	-6.65	0.001
2	Temperature+PO4	0.5067	13.40	-6.83	0.095
3	Temperature +PO4+Water Movement	0.6394	7.09	-11.06	0.181
4	Temperature +PO4+Water Movement+Si	0.7206	2.66	-12.746	0.484
5	Temperature +PO4+Water Movement+Si +NH4	0.7446	4.11	-14.449	0.627
6	Temperature +PO4+Water Movement+Si +NH4+Light	0.7379	5.52	-12.533	0.708
7	Temperature +PO4+Water Movement+Si +NH4+Light+N	0.6618	8.000	-5.2663	0.953

Winter

Light was generally less abundant during winter compared to summer and deeper offshore sites received only 10% of the average illuminance they had received during summer (Table 3.19). The temperature gradient that occurred in summer (i.e cooler temperatures at offshore reefs) was reversed in winter with lower temperatures at inshore sites (Table 3.22). All of the offshore sites had considerably lower growth compared to the summer period while those closer to shore had higher growth in winter compared to summer (Figure 3.1).

Analyses of the winter growth data yielded statistically significant results only for smaller models for thallus extension and BA-in each case the full models were not statistically significant. For thallus extension AIC suggested a model containing only light intensity (Table 3.22; AIC=0.52) while BIC suggested a model with light, phosphate and ammonia (Table 3.22; BIC=-6.09). The only statistically significant model contained light intensity only (Table 3.22; adj R^2=0.50; p=0.006).

For BA, BIC suggested a model consisting of temperature and dissolved silica (Table 3.22; BIC=-0.93). AIC suggested a model containing only temperature (Table 3.22;AIC=0.67). This model was also the only statistically significant model (Table 3.22; adj R^2=0.29; p=0.04).

For MSBA, BIC suggested a model consisting of Light, Water Movement and NH_4 (Table 3.22; BIC=-12.60) while AIC suggested a model containing Light and Temperature (Table 3.22; AIC=0.32). The model suggested by AIC was also statistically significant (Table 3.22; adj R^2=0.73; p=0.027).

Table 3.22: Candidate models obtained from linear multiple regressions in R comparing winter growth data for *E. radiata* to environmental parameters in Marmion Lagoon Western Australia. Values in bold indicate the best values for adjusted R^2, Mallow's Cp and BIC.

No of predictors	Extension	Adj R2	AIC	BIC	Model Significance (p)
Extension					
1	Light	0.50	0.52	-4.70	0.006
2	Light+Si	0.56	0.91	-4.74	0.082
3	Light+PO_4+NH_4	0.64	1.02	-6.09	0.534
4	Light+PO_4+NH_4+Si	0.63	2.51	-4.88	0.614
5	Light+PO_4+Si +Temperature+Water Movement	0.58	4.32	-2.90	0.637
6	Light+PO_4+Si +Temperature+Water Movement+ N	0.53	6.05	-1.19	0.806
7	Light+PO_4+Si +Temperature+Water Movement+ N + NH_4	0.42	8	1.13	0.909
Biomass accumulation					
1	Temperature	0.29	0.67	-0.33	0.040
2	Temperature+ Si	0.39	0.71	-0.93	0.221
3	Temperature+ Si+Water Movement	0.39	1.99	0.21	0.233
4	Light+Water Movement +NH4+Si	0.44	2.79	0.01	0.620
5	Light+ Water Movement +NH4+Si+PO4	0.46	4.00	0.32	0.623
6	Light+ Water Movement +NH4+Si+PO4+N	0.34	6.00	2.80	0.685
MSBA					
1	Light	0.68	0.32	-9.97	0.001
2	Light+Temperature	0.73	0.32	-10.80	0.027
3	Light+Water Movement+NH4	0.79	0.42	-12.60	0.201
4	Light+Water Movement+NH4+ Temperature	0.77	2.26	-10.56	0.452
5	Light+Water Movement+NH4+ Temperature +PO4	0.73	4.19	-8.26	0.630
6	Light+Water Movement+NH4+ Temperature +PO4+Si	0.70	6.00	-6.34	0.639
7	Light+Water Movement+NH4+ Temperature +PO4+Si+N	0.62	8	-3.87	0.736

Spring

Average maximum daily light intensity increased in spring compared to winter. There was considerable variation in light intensities between sites in spring with the lowest recording 3414 Lux (Site 5; Table 3.19; Table 3.23) compared to the highest at 38104 Lux (Site 9; Table 3.19). However, temperature varied considerably less in spring compared to summer and winter encompassing a range of only 0.5 ºC (Table 3.19).

Analyses of spring data yielded statistically significant models only for the smallest models for each of the measures of growth. For thallus extension, both BIC and AIC suggested that ammonia was the only parameter to have a significant effect on the rate of extensions during spring (Table 3.23; adj R^2=0.28; p=0.013).

For BA, both BIC and AIC suggested light intensity was the most important characteristic to predict BA in *E. radiata* during spring (Table 3.23). This model was also statistically significant (Table 3.23; adj R^2=0.23; p=0.024)

For MSBA, AIC suggested the most important drivers of kelp growth were water movement, light, and the nutrients dissolved silica, ammonia and phosphate (Table 3.23; AIC=4.87). BIC suggested that ammonia and phosphate should be removed from the model (Table 3.23; BIC= -12.36). Only a model containing water movement and light intensity was statistically significant (Table 3.23; adj R^2=0.6047; p=0.003).

Table 3.23. Candidate models obtained from linear multiple regressions in R comparing spring growth data for *E. radiata* to environmental parameters in Marmion Lagoon Western Australia. Values in bold indicate the best values for adjusted R^2, Mallow's Cp and BIC.

No of predictors	Model-Spring Extension	Adj R2	AIC	BIC	Model Significance (p)
Extension					
1	NH_4	0.28	-0.76	-1.29	0.013
2	NH_4+Si	0.28	0.52	0.59	0.364
3	NH_4+Si+Temperature	0.29	1.45	1.85	0.394
4	NH_4+Si+Temperature+PO4	0.29	2.59	3.34	0.558
5	NH_4+Si+Temperature+PO4+Light	0.25	4.34	5.82	0.767
6	NH_4+Si+Temperature+PO4+Light+N	0.20	6.11	8.31	0.837
7	NH_4+Si+Temperature+PO4+Light+N+Water Movement	0.13	8	10.99	0.939
Biomass accumulation					
1	Light	0.23	-0.91	-0.11	0.024
2	Light+PO4	0.27	-0.32	0.72	0.19
3	Light+PO4+Temperature	0.27	0.88	2.33	0.365
4	Light+PO4+Temperature+Water Movement	0.25	2.42	4.45	0.498
5	Light+PO4+Temperature+Water Movement+N	0.18	4.16	6.87	0.802
6	Light+PO4+Temperature+Water Movement+N +NH4	0.11	6.08	9.63	0.809
7	Light+PO4+Temperature+Water Movement+NH4+ N+Si	0.00	8	12.38	0.951
MSBA					
1	Water Movement	0.3299	28.93	-2.52	0.002
2	Water Movement+Light	0.6047	11.74	-10.29	0.003
3	Water Movement+Light+Si	0.6784	8.02	-12.36	0.115
4	Water Movement+Light+Si+NH4	0.6972	7.76	-11.88	0.257
5	Water Movement+Light+Si+NH4+PO4	0.7736	4.87	-15.67	0.671
6	Water Movement+Light+Si+NH4+PO4+N	0.7709	6.09	-14.13	0.829
7	Water Movement+Light+Si+NH4+PO4+N+Temperature	0.7503	8	-11.40	0.832

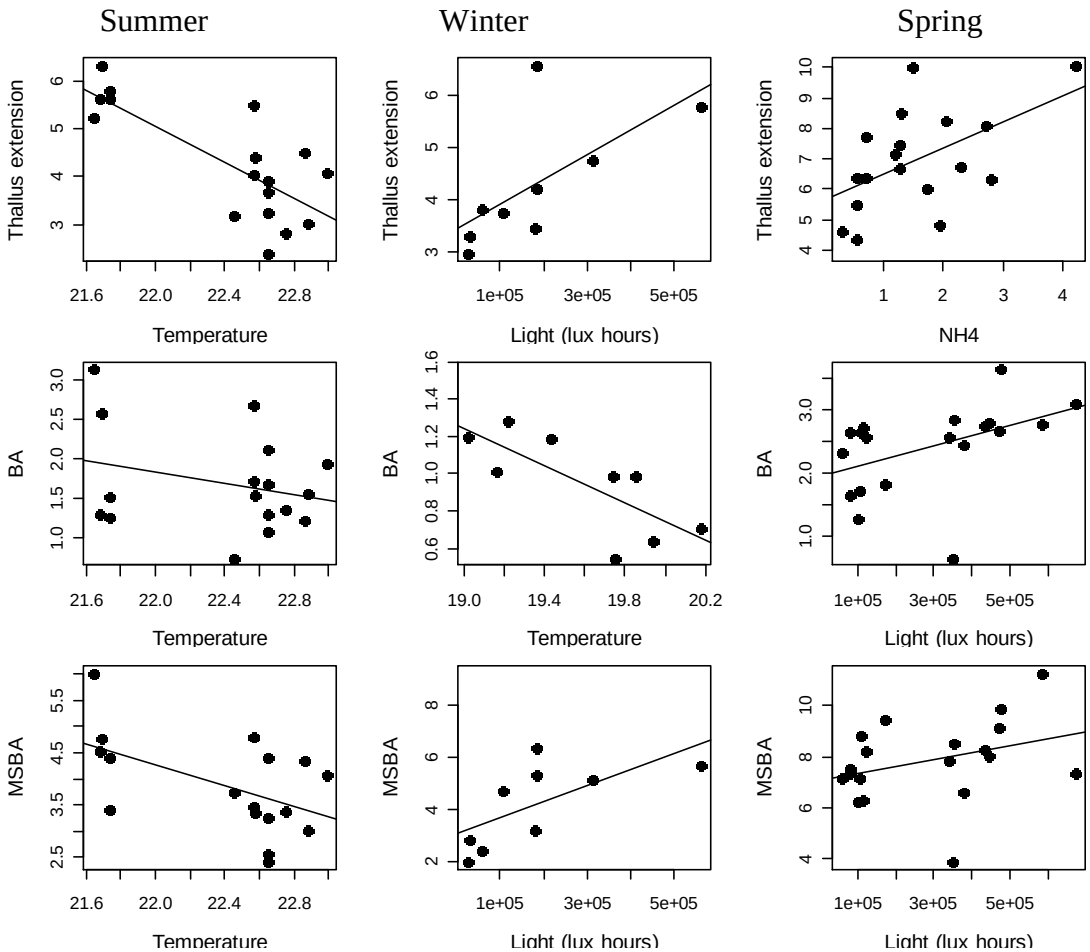

Figure 3.58. Scatterplots comparing the variable identified as the most significant for kelp growth with the growth measure used.

3.1.11 Rates of grazing on macroalgae

Methods

Surveys

Measurements of kelp consumption were taken from five sites in Jurien Bay and six sites in Marmion Lagoon (tethered kelp were deployed at a sixth site in Jurien Bay, but could not be retrieved). Consumption of kelp *Ecklonia radiata* was measured following a method described by Vanderklift & Wernberg (2008). At each site fifteen kelp laterals free of epiphytes were collected, placed between 2 sheets of acrylic glass (the top sheet clear and the bottom sheet white), and photographed. Laterals were secured by a clothes peg and five were assigned to each of 3 treatments: (1) caged, enclosed in a cage of plastic mesh (Nylex GutterGuard: mesh size 3 × 3 mm) to exclude all large herbivores; (2) understorey, clothes peg attached to a length of chain placed on the reef surface; and (3) canopy, clothes peg attached to a float tied to a ~50 cm length of black nylon cord. The understorey treatment was intended to mimic kelp at the level of the understorey and estimate consumption by all large mobile herbivores; the canopy treatment was intended to mimic kelp at the level of the canopy and estimate consumption by herbivorous fish only. After 1 to 3 d, the laterals were collected and rephotographed.

Photographs of each lateral before and after deployment were analysed using image analysis software (ImageJ, rsb.info.nih.gov/ij/) to calculate surface area, and the consumption (% loss d^{-1}) of each lateral was then calculated. The error in area measurements between photographs was up to ±9% (Vanderklift et al. 2009), so any change in area <10% was considered to be 0%.

We used statistical analyses to test for the presence of patterns in consumption among treatments (3 levels, fixed factor), locations (2 levels, random factor), and sites (10 levels, random and nested in location). Because the data contained many zeros, parametric statistics were unsuitable and so data were analysed using permutational multivariate ANOVA (PERMANOVA; Anderson 2001), which uses permutation to test for statistical significance. Euclidean distances were calculated from untransformed data, and the permutation tests used 9,999 permutations of residuals under a reduced model.

Results

Analysis of the rates of kelp consumption indicated that rates varied among treatments, but that the nature of differences was not consistent among sites (significant treatment × site interaction in Table 3.24). Pairwise comparisons among treatments for each site indicated that this effect was influenced by Cow Rocks in Marmion, where rates of consumption of kelps in the ‘canopy’ treatment were significantly higher than kelps in the ‘cage’ or ‘understorey’ treatments. (Figure 3.59). At Cow Rocks, all kelp laterals in the ‘canopy’ treatment were heavily consumed.

Some consumption was also recorded at Booka Rocks, Essex Rocks and JV007 at Jurien Bay, and North Lumps at Marmion Lagoon – most of the recoded instances of consumption were from the 'canopy' treatment. The observation of relatively low rates of consumption at 10 of the 11 sites indicates that direct herbivory is typically low on reefs on the western Australian coast. The observation that wherever consumption occurred, it was typically on the 'canopy' treatment indicates that kelp consumption is typically due to fish.

Table 3.24. Results of PERMANOVA testing for differences in consumption of tethered kelp laterals

Asteroidea						
Source	df	MS	Pseudo-F	P	Permutations	MC-P
Treatment	2	96.92	2.68	0.272	360	0.267
Location	1	2.08	0.02	0.824	8409	0.879
Site (Location)	9	91.15	6.79	**<0.001**	9936	**<0.001**
T x L	2	36.18	0.49	0.656	9941	0.622
T x S(L)	18	74.66	5.56	**<0.001**	9920	**<0.001**
Residual	123	13.43				

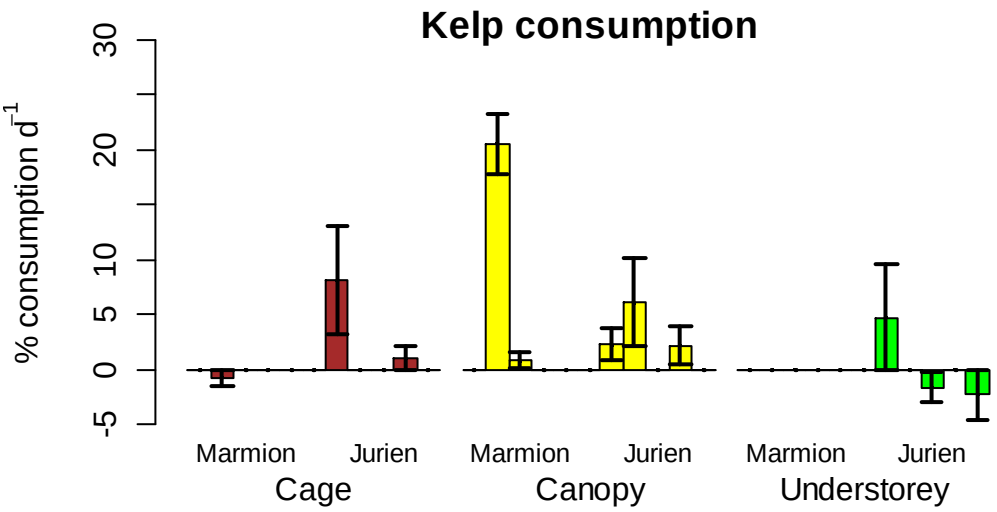

Figure 3.59. Consumption of tethered kelp laterals (mean ± se, n=5) in each treatment (caged, canopy mimic, understorey mimic) at each of the sites surveyed.

3.1.12 Rates of secondary production

Methods

The common blue mussel (*Mytilus edulis*) was selected as a proxy to measure secondary production. Mussels obtained from Blue Lagoon Mussels Pty Ltd and were deployed for three months from December to March in the austral summer of 2008/09 and in 2009/10. The mussels were deployed to nine sites along the -31.850 latitudinal parallel at depths of 3m, 5m, 10m, 15m, 20m, 25m, 30m, 35m, 40m (Table 3.25).

Approximately six hundred mussel spat were attached to lengths of rope with a cotton stocking (Table 3.25). The cotton stockings eroded away after twenty days leaving the mussels by their Byssal threads. Mussels were held in a filtered seawater tank prior to being deployed. Four ropes with mussels attached were then fixed to moorings deployed at each of the sites. Due to a high level of predation or natural mortality in the 2009-2010 summer mussel numbers where relatively low (Table 3.25).

Table 3.25. Site location and total number of mussels sampled in both the 2008/09 and 2009/10 sampling period.

			Total number of mussels retrieved		Total mussels analysed for stable isotopes	
Site	**Lat**	**Long**	**2008/09**	**2009/10**	**2008/09**	**2009/10**
Pre deployment			100	40	15	10
3m	31 48.266	115 43.385	100	40	16	11
5m	31 48.282	115 42.461	100	11	16	
10m	31 50.063	115 42.913	100		16	
15m	31 49.136	115 41.212	100		16	26
20m	31 49.688	115 40.728	100	59		3
25m	31 49.880	115 38.731		3	16	10
30m	31 49.007	115 37.539		10		9
35m	31 48.792	115 35.215	100			
40m	31 44.632	115 30.162		9		

After three months the mussels were processed and morphometric and stable isotope measurements were obtained. Morphometric measurements included shell height, shell width, shell weight, wet meat weight, and dried meat weight. Two types of condition index were derived from these data. The Taleb condition index was calculated by dividing the wet weight of the mussel meat by the total wet weight and then multiplying by 100. The Rayyan condition index was calculated by dividing the mussel's dry weight by the product of the total wet weight minus the shell weight.

Where enough mussels were retrieved measurements were taken for 25 mussels on each rope (Table 3.25). Stable isotope analysis was carried out on 16 mussels per site (4 per rope). Separate stable isotope measurements were obtained for the gill and abductor mussel tissue.

Water Sampling

Monthly water sampling was conducted through-out each deployment. Water samples were collected from less than 2 m above the sea floor by CTD. Water samples were obtained for total suspended solids (TSS), particulate organic matter (POM), particulate inorganic matter (PIM), Chlorophyll-a, stable isotopes (C and N), fatty acids and HPLC (Table 3.26).

Table 3.26. Summary of water samples collected by CTD at depth.

Sample	Filtered seawater volume	Number of samples 2009	Number of samples 2010
TSM/PIM/POM	2l	70	126
Chl-a	1l	50	101
Isotope C and N	2l	47	133
HPLC	4l	48	87 collected 34 processed
Nutrients	50ml	72	96

Two litres of seawater from each sample point was individually filtered through a pre-ashed and weighed GF/F microfibre Whattman filter (diameter 47mm, pore size 0.7µm). The filter was frozen on site and transported to CMAR Floreat. The filter was thawed, dried at 80ºC for 12 hours until a constant weight was reached and filter was weighed with an accuracy of four decimal places. This measurement represented the total suspended solids (TSS) present on the filter. Then the filter was then ashed at 450ºC for 4 hours and re-weighed in order to obtain a measurement of the particulate inorganic matter (PIM) present in the sample. The particulate organic matter (POM) was calculated as the difference between the TSS and PIM. All measurements were then divided by two to give a per litre measurement.

Each water sample collected was also analysed for chlorophyll-a using a Turner 10-AU Fluorometer. This fluorometer was calibrated using primary standards of ultrafiltered seawater samples at 35 ppt and two chlorophyll samples within the expected Chl-a range. As the chlorophyll range in the field samples were near the lower detection limit, the supplied secondary standard could not provide a reading. An ultrafiltered seawater sample at 35 ppt was used to ensure calibration accuracy throughout field sampling. The fluorometer was configured for discrete sampling.

Two litres of seawater from each sample point was individually filtered through a pre-ashed 47 mm GF/F Wattman filter (0.7 µm pore size). The filter was frozen on site and stored at -80C at CMAR Floreat. Isotope analyses were performed by Natural Isotopes Pty Ltd using an elemental analyser (ANCA-GSL, Europa, Crewe, United Kingdom). The samples were combusted to N_2, and purified by gas chromatography. The elemental composition and stable isotope ratios of C and N were determined by continuous flow isotope ratio mass spectrometry (20-20 IRMS, Euroopa, Crewe, United Kingdom). Reference materials of known elemental composition and isotopic ratios were interspaced with samples for calibration.

Four litres of sample water was filtered through a 47 mm glass fibre filter (Whatman GF/F) and then stored in liquid nitrogen until analysis. Samples were extracted over 15-18 hours in an acetone solution before analysis by HPLC using a C_8 column and binary gradient system with an elevated column temperature. Pigments are identified by retention time and

absorption spectrum from a photo-diode array (PDA) detector and concentrations of pigments were determined from commercial and international standards (Sigma; DHI, Denmark). Separation of algal pigments by HPLC provides a method to accurately quantify the presence of various pigment groups in the water column.For example, fucoxanthin is characteristic of the presence of diatoms, zeaxanthin suggests the presence of *Synechococcus*, Divinyl chlorophyll-a is linked to the presence of *Prochlorococcus*, butanoyloxyfucoxanthin suggests pelagophytes (and coccolithophorids) while hexanoyloxyfucoxanthin suggests the presence of coccolithophorids. Fucoxanthin and chlorophyll-c pigments characteristic of kelps and diatoms.

50 ml samples of seawater from the sites were analysed for dissolved silica, phosphate, nitrate and nitrite, as well as ammonia concentrations. Dissolved silica, phosphate and nitrate/nitrite were analysed using a flow injection analysis while ammonia concentration was determined using a flow injection analysis, gas diffusion, derivatisation - fluorescence detection method. For dissolved silica, Si species were reacted with molybdate at 45ºC pH 1.2, then reduced with stannous chloride to form a heteropoly blue complex which was measured at 820nm. Phosphate was reacted with molybdate and antimony potassium tartrate in acid medium which was then reduced with ascorbic acid to form a blue complex which was measured at 880nm. Nitrate was first reduced to nitrite by passing it through a copperised cadmium column. Nitrite is then reacted with sulfanilamide under acidic conditions to form a diazonium salt which was then coupled with N-(1-naphthyl) ethylenediamine dihydrogenchloride to form a pink complex which was measured at 520nm. For ammonia a sodium hydroxide solution was added to liberate ammonia which was then diffused across a PTFE membrane to react with ortho-phthaldialdehyde (OPA) - sulfite solution. This solution was then excited at 310nm and the fluorescence measured at 390nm.

Results

2008-2009

The average mussel Taleb condition index for 2008/09 was 58.59. Taleb condition index was highest at the 5m site and decreased with site depth (Figure 3.60). There was a significant difference between the 5m and 10m sites compared to the 15m, 20m and 35m sites. The average mussel Rayyan condition index for 2008/09 was 6.45. Rayyan condition index increased with depth apart from the 15m site which was lower than the 10m and 20m sites (Figure 3.61). There was a significant difference between the 5m, 10m and 15m sites compared to the 20m and 35m sites.

The average shell height for mussels deployed in 2008/09 was 35mm. Mussels had the largest shell heights at the 5m and 10m sites while mussels from the 15m site were significantly shorter compared to all other sites (Figure 3.62). There was a significant difference between the average shell height of mussels from the 5m and 10m sites compared to the 20m and 35m sites. The average wet weight of mussels was significantly higher at the 5m and 10m sites compared to all other sites (Figure 3.63). Mussels from the 15m site were lighter than all other sites. There was a significant difference between the wet weight of mussels from the 5m and 10m sites compared to the 20m and 35m sites. $\delta^{15}N$ was highest at 5m and decreased from

25m to 40m (Figure 3.64). $\delta^{13}C$ generally decreased with depth especially beyond the 10m site (Figure 3.64).

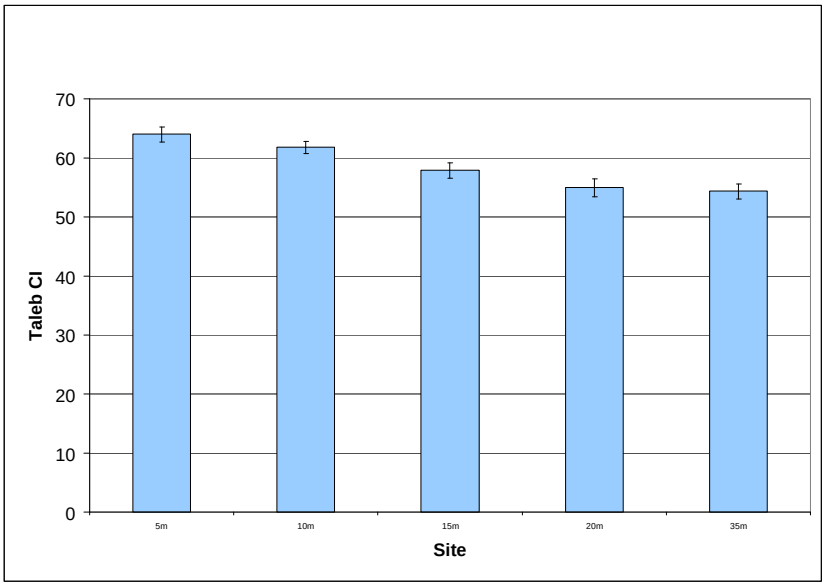

Figure 3.60. The average Taleb condition index for mussels from each of the sample sites. Samples were obtained in March 2009. No mussels were obtained from some sites due to predation. Error bars indicate a 95% confidence interval.

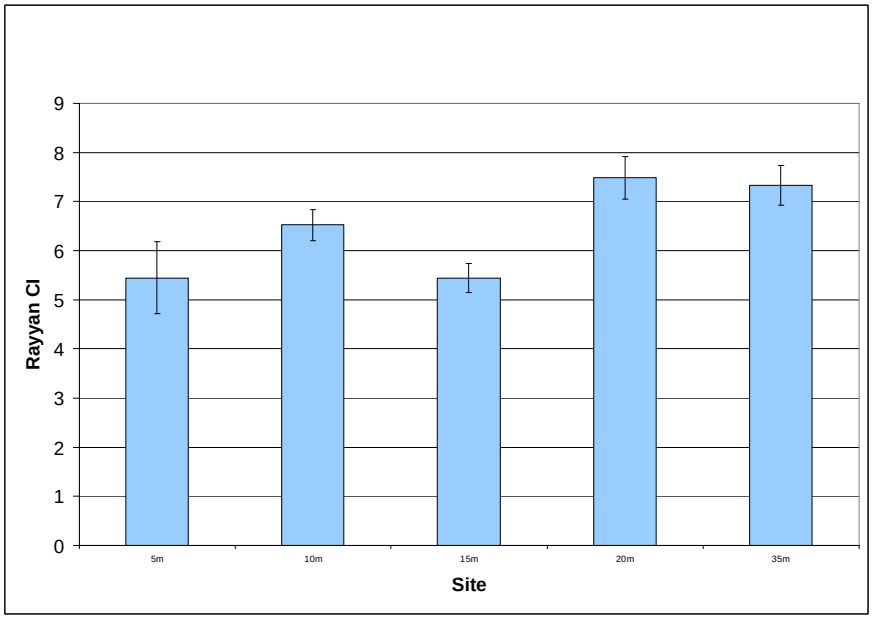

Figure 3.61. The average Rayyan condition index for mussels from each of the sample sites. Samples were obtained in March 2009. No mussels were obtained from some sites due to predation. Error bars indicate a 95% confidence interval.

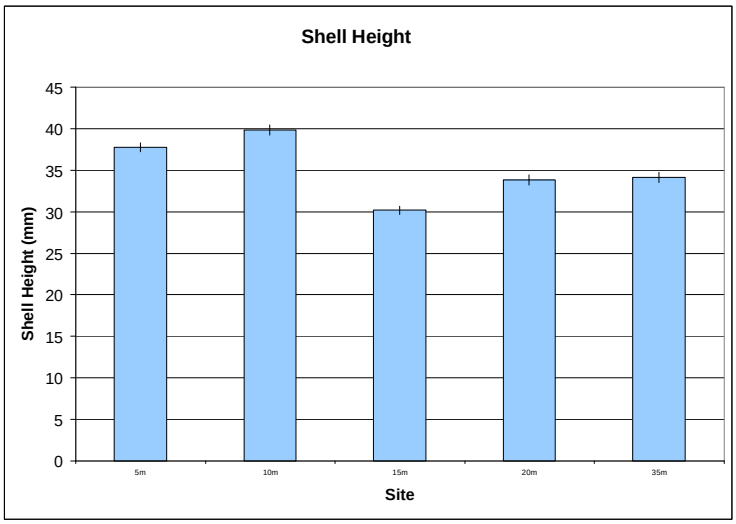

Figure 3.62. The average shell height (mm) for mussels from each of the sample sites. Samples were obtained in March 2009. No mussels were obtained from some sites due to predation. Error bars indicate a 95% confidence interval.

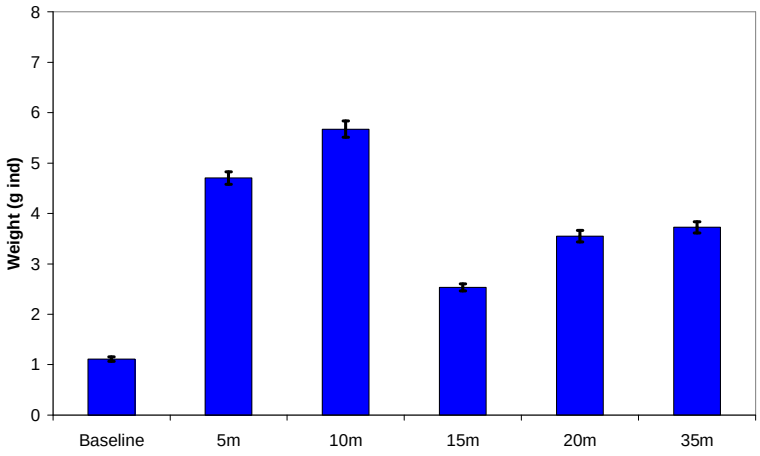

Figure 3.63. The mussel wet weight for mussels from each of the sample sites. Samples were obtained in March 2009. No mussels were obtained from some sites due to predation. Error bars indicate a 95% confidence interval.

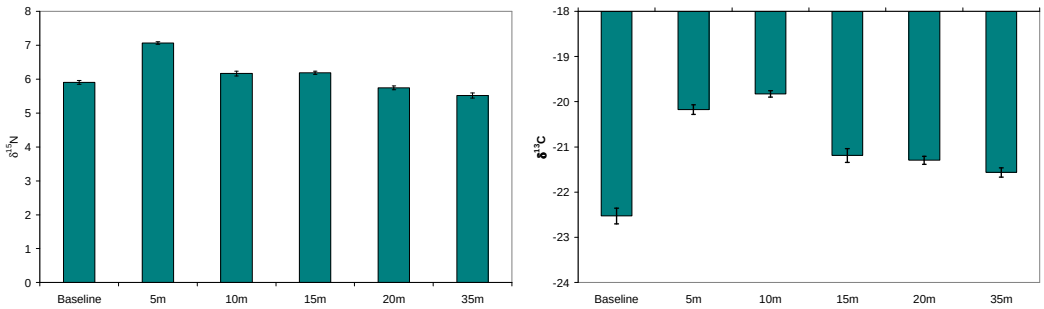

Figure 3.64. Average $\delta^{15}N$ and $\delta^{13}C$ of muscle tissue from *Mytilus edulis* deployed at each of the sites. No mussels were obtained from some sites due to predation. Error bars indicate a 95% confidence interval.

292 water samples were obtained from December 2008 to March 2009. The average total suspended solids was 0.0315 g/L, POM was 0.00751 g/L, average percentage organic matter was 23.68%, chlorophyll-a was 0.349 and average concentrations of pheopigments was 0.3452.

Total suspended solid (TSS) concentrations generally decreased as the study continued (Figure 3.65). The highest concentrations were observed at shallow sites in November and December. The overall average POM concentration for the 2008/09 was 0.0075 g/L. POM concentrations were more variable than TSS concentrations. POM was generally highest in November and December at the sites 15m and shallower depth (Figure 3.66). At sites deeper than 20m a different pattern was observed. These sites generally had high POM concentrations in December falling in January and then rising in February and March. Percentage organic matter was driven by POM. A similar pattern was observed to the POM graph where sites shallower than 15m had a falling trend from November/December to March while sites deeper than 15m had a fall from December to January followed by a rise from February to March (Figure 3.66, Figure 3.67). The overall average %OM concentration for the 2008/09 was 23.69%.

The overall average chlorophyll-a concentration for 2008/09 was 0.349 mg/m^3. Chlorophyll-a concentrations increased significantly over the coarse of the study at sites below 15m (Figure 3.68). This trend was not observed in sites deeper than 15m. However, high chlorophyll-a concentrations were observed in January at the 35m and 40m sites. Pheopigment concentrations indicated a similar pattern as that observed with the chlorophyll-a concentrations. There was an increasing trend from December to March at sites below 15m depth (Figure 3.69). High pheopigment concentrations were also observed in samples from January at the 35m and 40m sites. The overall average pheopigment concentration for 2008/09 was 0.345 mg/m^3.

The overall average dissolved silica concentration for 2008/09 was 1.55 mg/m^3. Dissolved silica concentrations were generally lowest between the 15m and the 30m sites (Figure 3.70). Peaks of dissolved silica occurred at December 10m and at December 40m. The overall average phosphate concentration for 2008/09 was 0.187 mg/m^3. Phosphate concentrations had a similar pattern as the chlorophyll-a concentrations with and increasing trend at shallow sites below 15m (Figure 3.71). Concentrations were low at the 20m to 30m sites. Phosphate concentrations increased at the 35m site over January and February. The overall average combined nitrate and nitrite concentration for 2008/09 was 0.937 mg/m^3. Nitrate and nitrite concentrations were highest between 15m and 25m sites. At these sites there was a falling trend as the study progressed from December to March (Figure 3.72). Sites deeper than 25m often had lower concentrations than the detectable limit. The overall average ammonia concentration for 2008/09 was 0.173 mg/L. Ammonia concentrations were variable but generally had a rising trend at the 3m and the 10m sites while having a falling trend over the 5m and 15m sites (Figure 3.73).

PCA analysis categorised samples according to the month of sampling rather than the depth. December samples appeared to be distinguished from other months on the basis of POM, %OM and nitrate/nitrite concentrations (Figure 3.74). CAP analysis supported this analysis when variation among months was examined, with December samples distinguished by higher POM, TSS and nitrate/nitrite concentrations (left; Figure 3.75). March samples were

distinguished by higher phosphate concentrations and January and February samples were separated by relatively higher Chlorophyll-a and pheopigment concentrations. When CAP was used to examine variation among depths (right; Figure 3.75) 15m and 20m samples were distinguished relatively more nitrate/nitrite and ammonia, 3m samples were distinguished by pheopigment concentrations and dissolved silica, and 5m samples were characterised by higher phosphate concentrations.

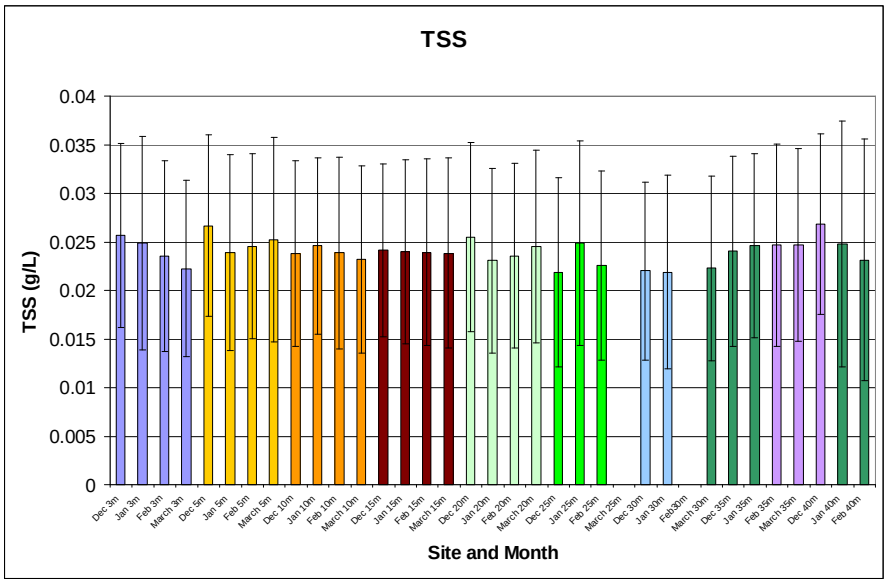

Figure 3.65. Total suspended solids (TSS) concentrations determined from each water sample between December 2008 and March 2009 at each of the sites. Error bars correspond to 95% confidence intervals.

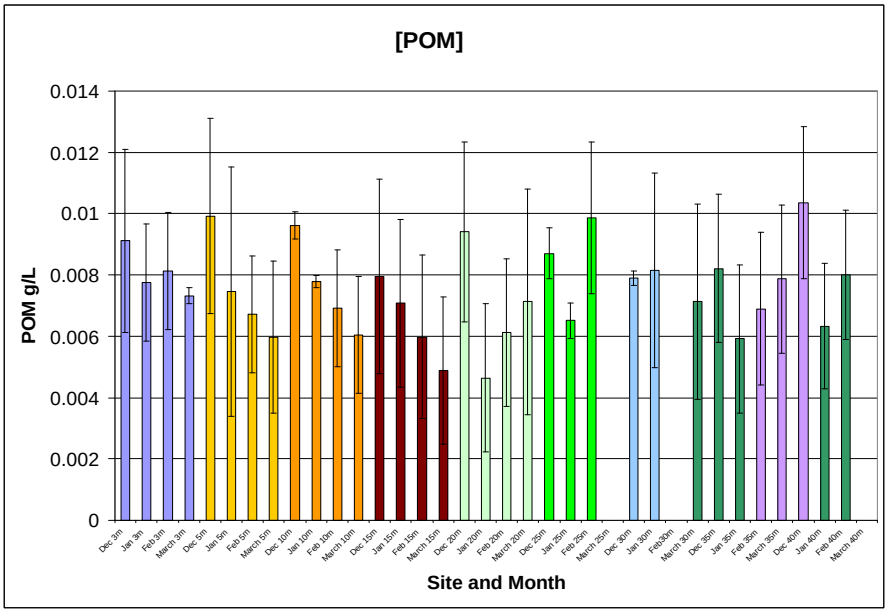

Figure 3.66. Particulate organic matter (POM) concentrations determined from each water sample between December 2008 and March 2009 at each of the sites. Error bars correspond to 95% confidence intervals.

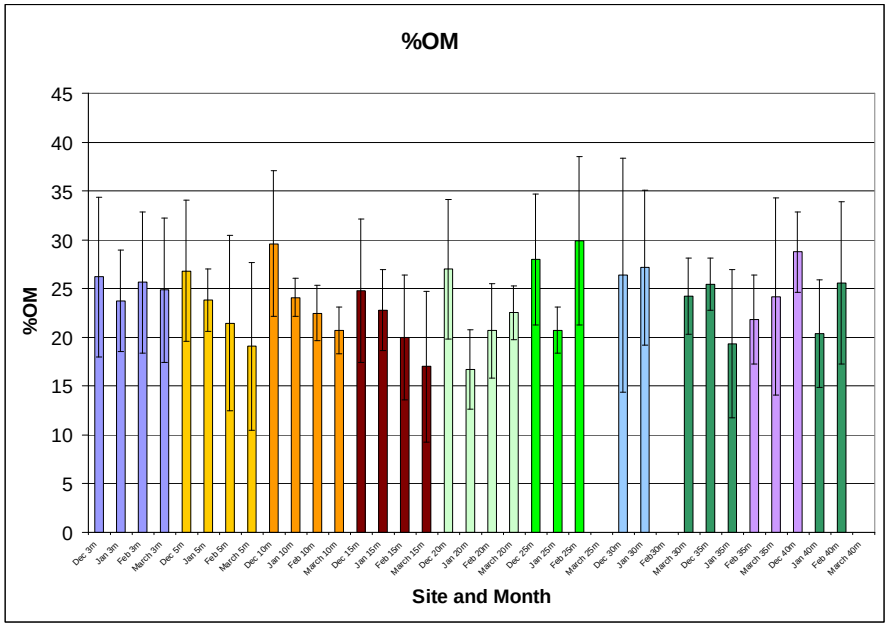

Figure 3.67. Percentage organic matter (%OM) determined from each water sample between December 2008 and March 2009 at each of the sites. Error bars correspond to 95% confidence intervals.

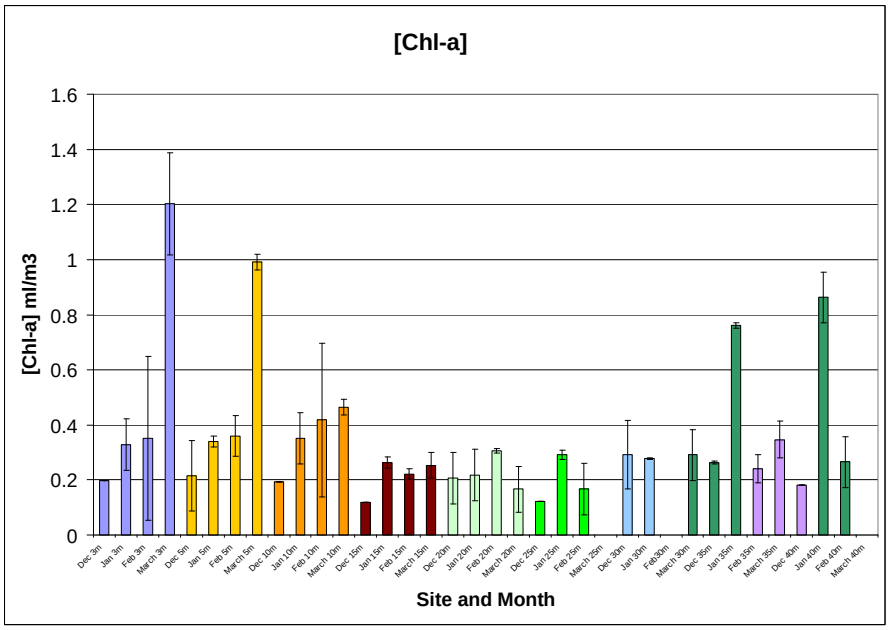

Figure 3.68. Chlorophyll-a concentrations (mg/m^3) determined from each water sample between December 2008 and March 2009 at each of the sites. Error bars correspond to 95% confidence intervals.

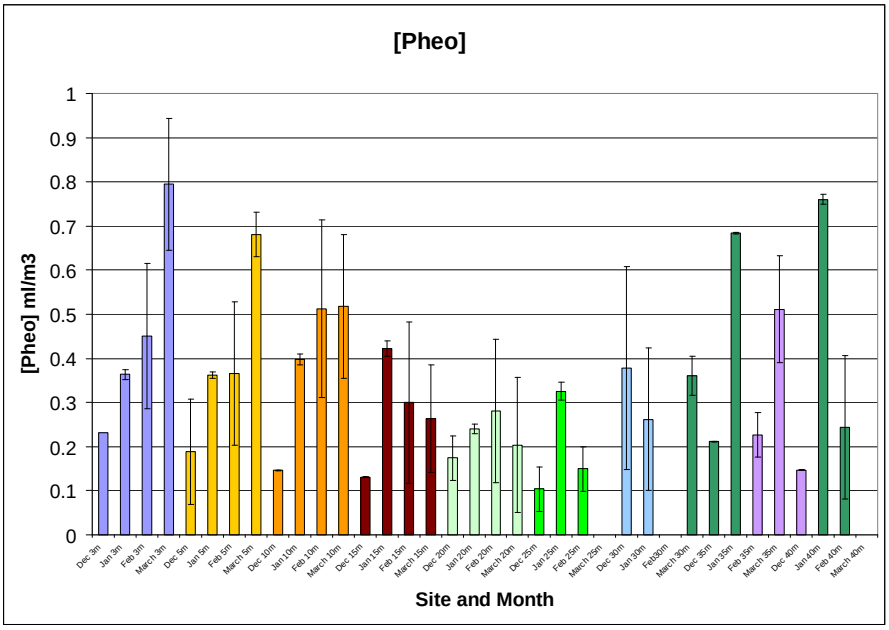

Figure 3.69. Pheopigment concentrations (mg/m^3) determined from each water sample between December 2008 and March 2009 at each of the sites. Error bars correspond to 95% confidence intervals.

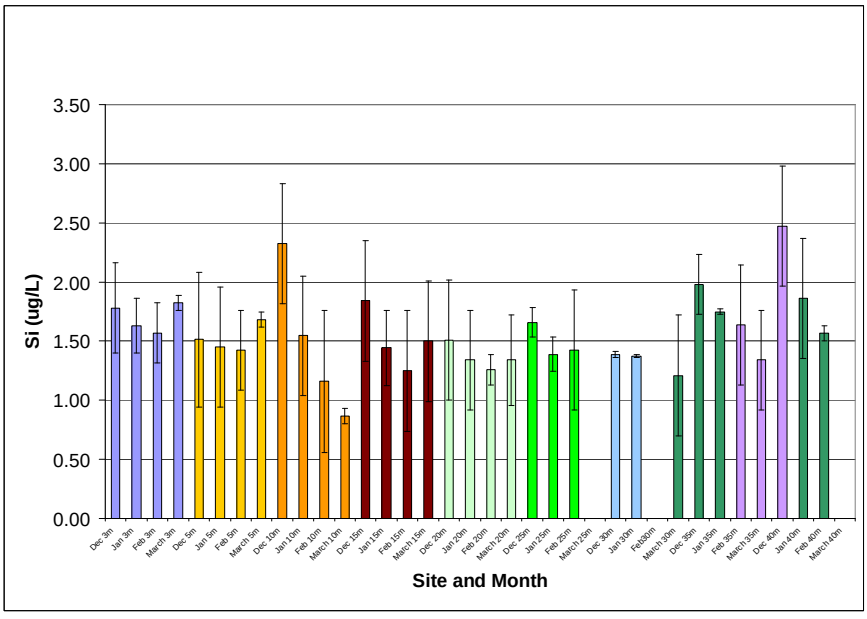

Figure 3.70. Dissolved silica concentrations determined from each water sample between December 2008 and March 2009 at each of the sites. Error bars correspond to 95% confidence intervals.

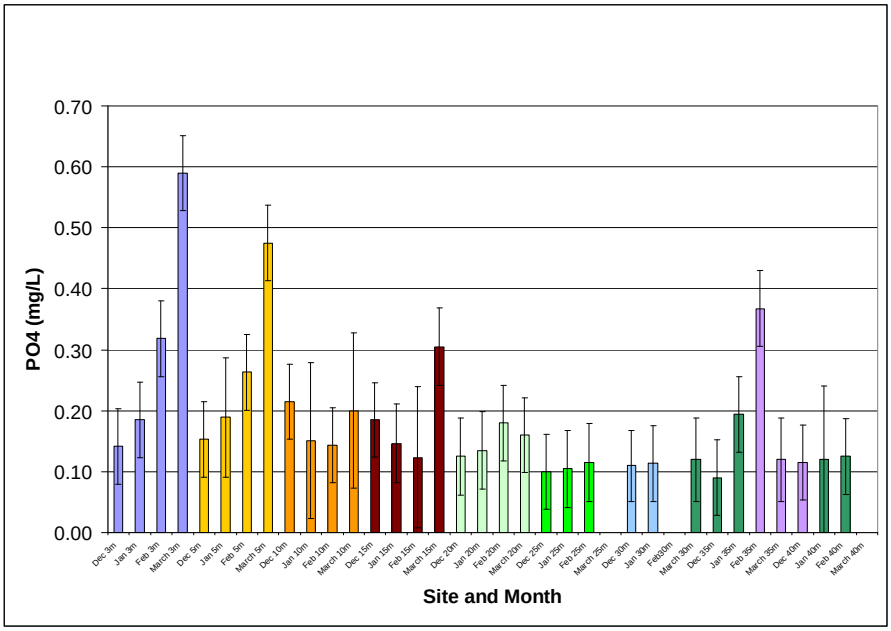

Figure 3.71. Phosphate concentrations determined from each water sample between December 2008 and March 2009 at each of the sites. Error bars correspond to 95% confidence intervals.

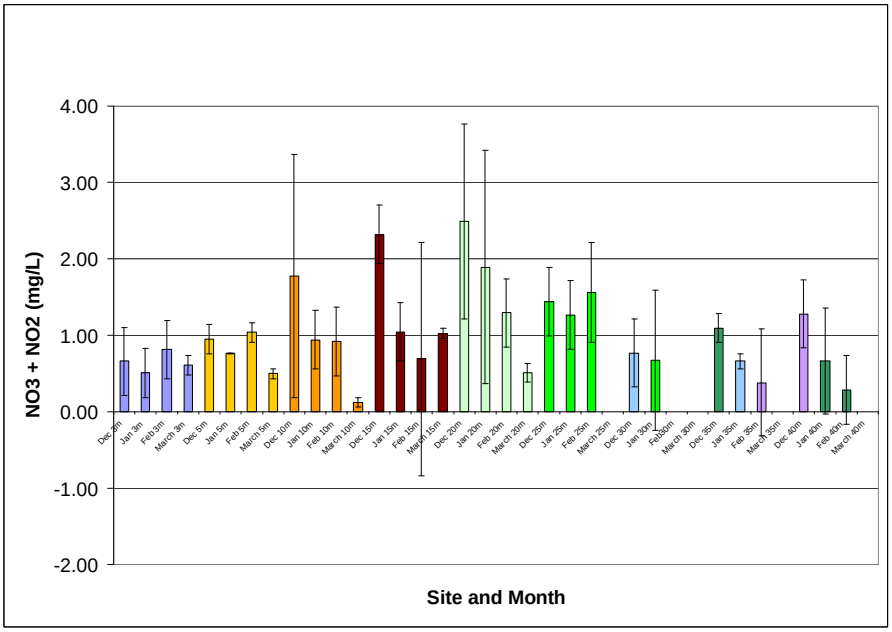

Figure 3.72. Combined nitrate and nitrite concentrations determined from each water sample between December 2008 and March 2009 at each of the sites. Error bars correspond to 95% confidence intervals.

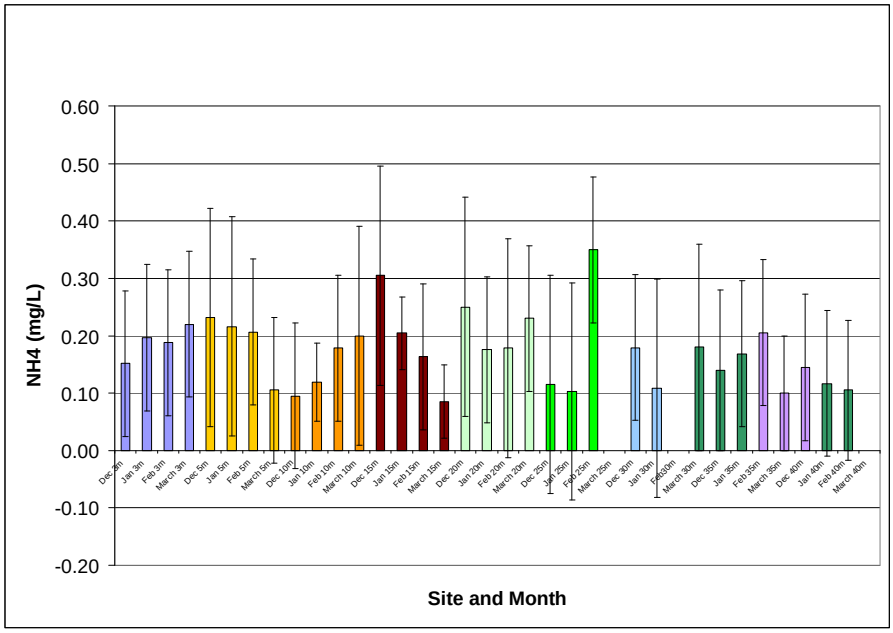

Figure 3.73. Ammonia concentrations determined from each water sample between December 2008 and March 2009 at each of the sites. Error bars correspond to 95% confidence intervals.

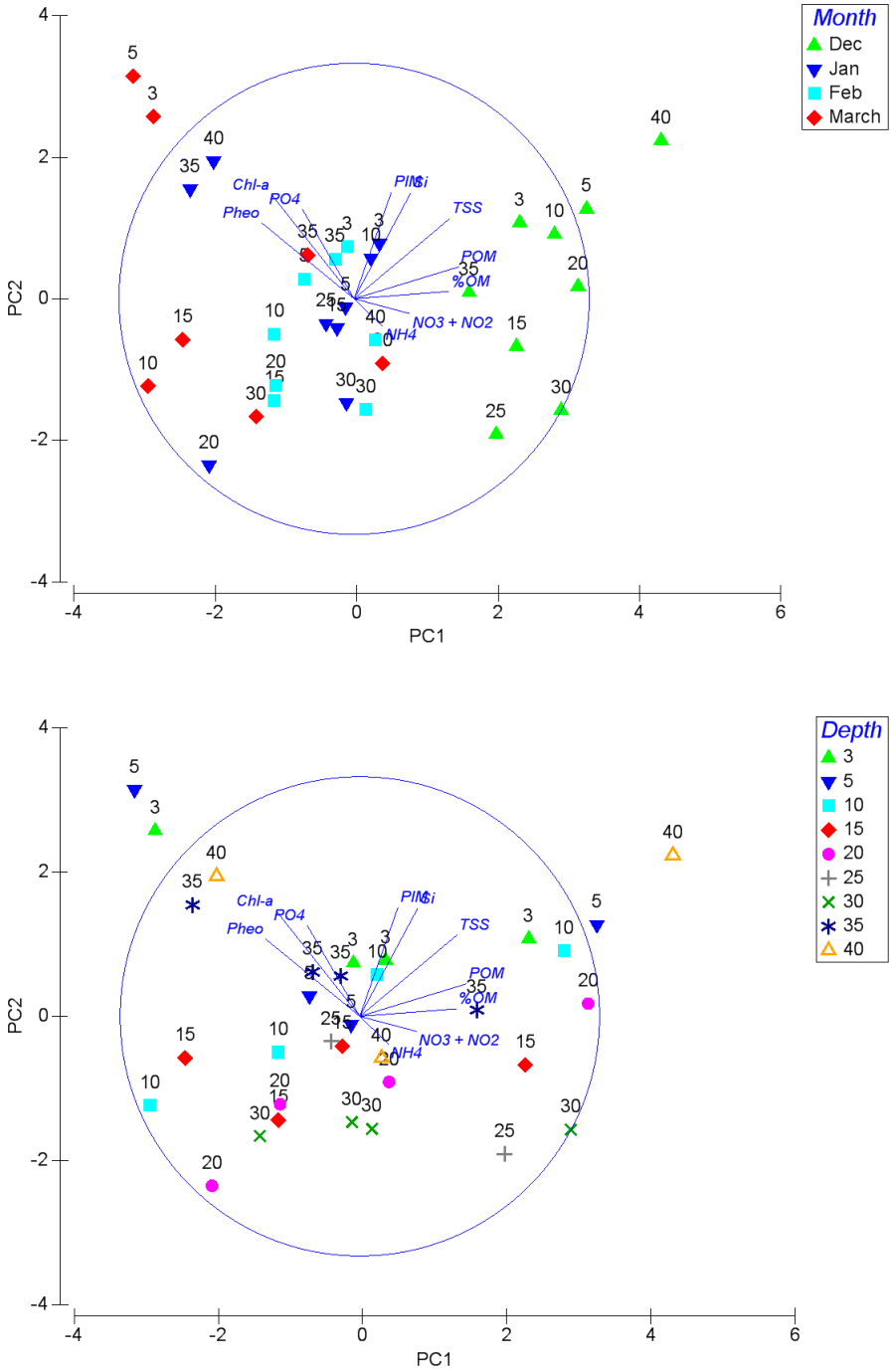

Figure 3.74. PCA analysis of the 2008/2009 water quality data. On analysis to the left symbols represent month of sampling while on the right symbols represent the sample site.

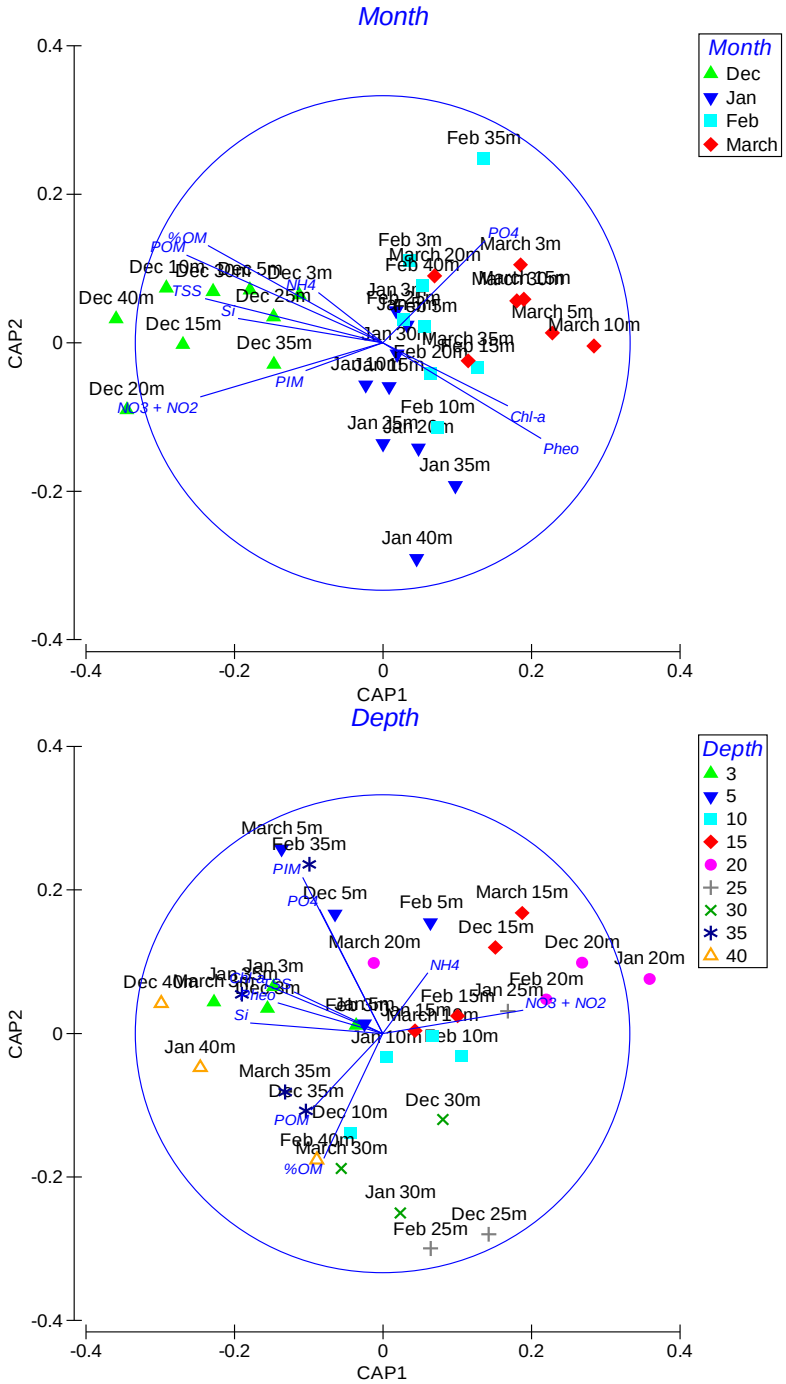

Figure 3.75. CAP analysis of the 2008/2009 water quality data. On analysis to the left symbols represent month of sampling while on the right symbols represent the sample site.

Pigment concentrations increased with depth in all months, and this pattern was especially evident in December. In December fucoxanthin concentrations (characteristic of diatoms) fell with increasing depth while hexanoyloxyfucoxanthin (characteristic of coccolithophorids) increase strongly (Figure 3.76). Chlorophyll-b concentrations also increased with depth. Pigment concentrations in January were lowest at the 10m and 15m sites and highest at the 20m sites and deeper (Figure 3.77). Butanoyloxyfucoxanthin concentrations increased with depth. Fucoxanthin concentrations (characteristic of the presence kelp and diatoms) decreased with depth. Prasinoxanthin and lutein were only present at sites 10m and shallower. hexanoyloxyfucoxanthin (characteristic of coccolithophoridis) increased with depth. Chl-b concentrations were lowest over the reef at the 10m and 15m sites. In February (Figure 3.78) butanoyloxyfucoxanthin was only observed in samples 15m and deeper while peridinin was only observed at the 40m site. Hexanoyloxyfucoxanthin concentrations increased with depth. In March (Figure 3.79), peridinin was only observed in samples deeper than 30m or shallower than 5m while lutein was only observed in samples shallower than 15m. Hexanoyloxyfucoxanthin and butanoyloxyfucoxanthin concentrations increased with depth. Pigment concentrations were highly variable. PCA analysis of the data clustered samples according to the month of sampling rather than the sample depth (Figure 3.80).

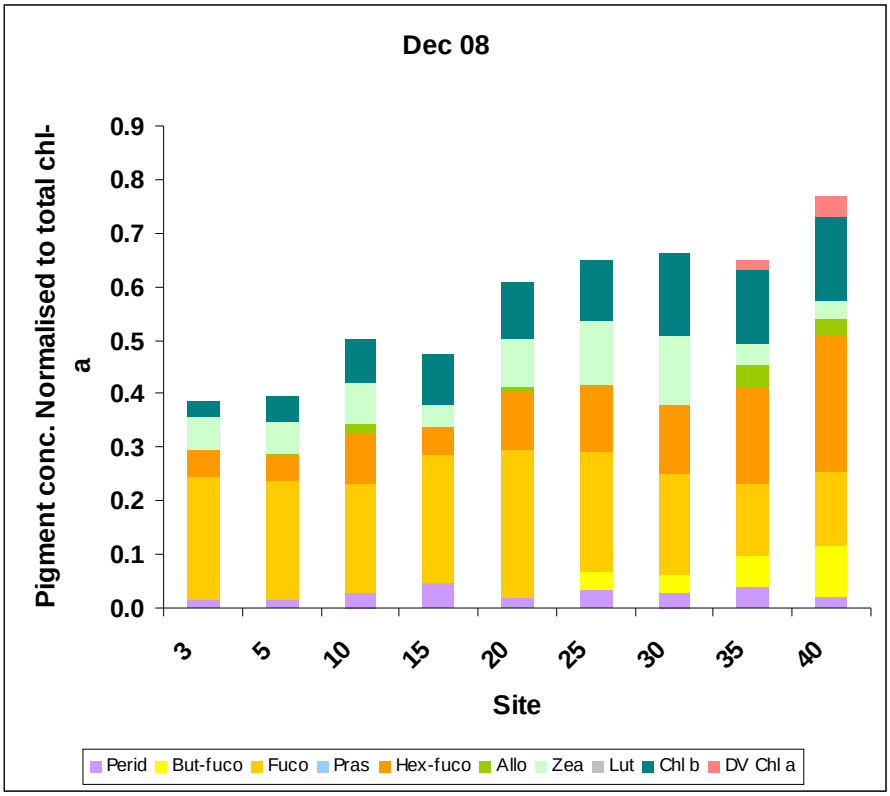

Figure 3.76. Pigment concentrations normalised to chlorophyll-a concentration for the December 2008 water samples.

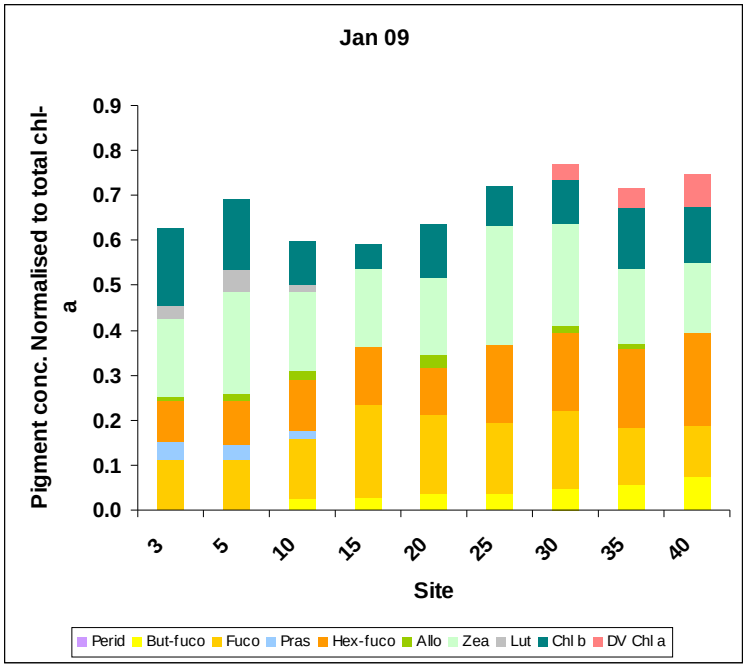

Figure 3.77. Pigment concentrations normalised to chlorophyll-a concentration for the January 2009 water samples.

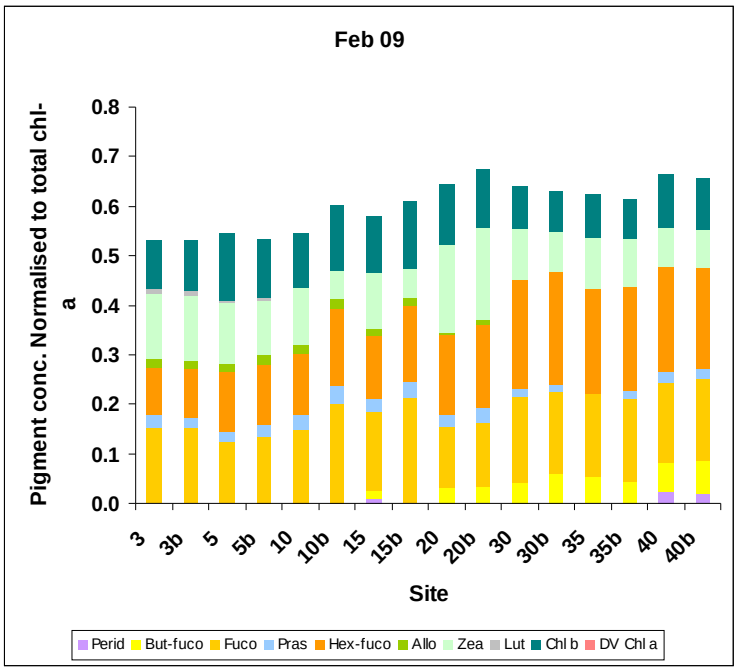

Figure 3.78. Pigment concentrations normalised to chlorophyll-a concentration for the February 2009 water samples. B samples represent replicates from the same site.

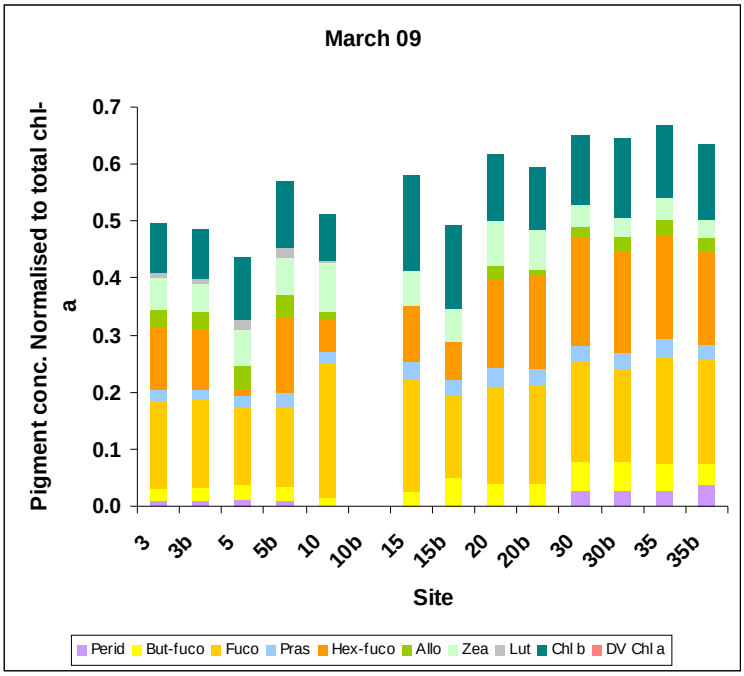

Figure 3.79. Pigment concentrations normalised to chlorophyll-a concentration for the March 2009 water samples. B samples represent replicates from the same site.

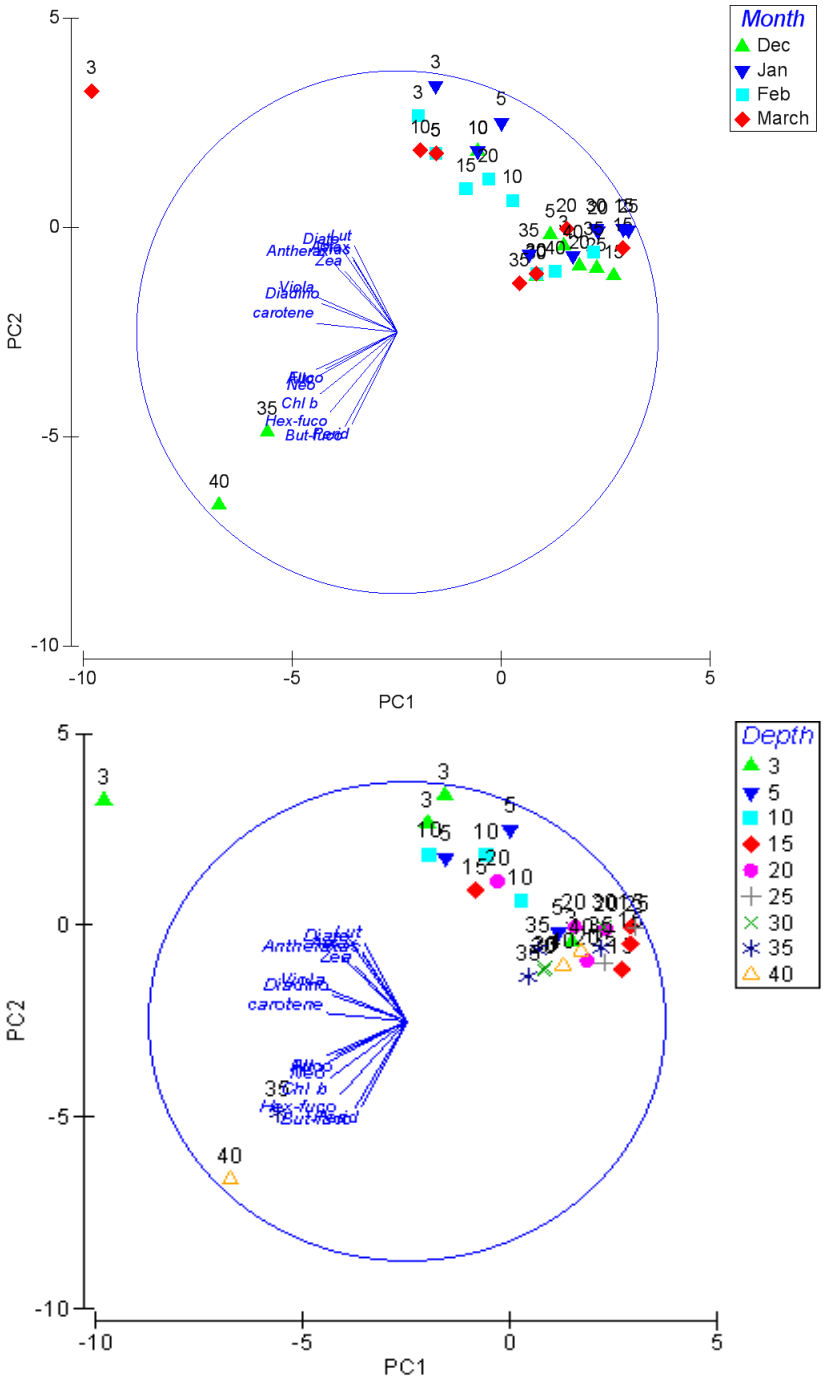

Figure 3.80. PCA analysis of the 2008/2009 water quality data obtained through HPLC analysis. Left: Symbols represent the sampling month. Right: Symbols represent the depth of sampling while the number represents the site depth the sample was obtained.

2009-2010

The overall average Taleb condition index of mussels in 2009/10 was 27.74 compared to58.59 in 2008/09. There was a significant difference observed in the Taleb condition index for mussels obtained from the 5m site compared to mussels obtained from the 20m and 40m sites (Figure 3.81). There was no significant difference observed in mussels from the 20m and deeper sites. The overall average Rayyan condition index of mussels in 2009/10 was 6.43 compared to 6.45 in 2008/09. Rayyan condition index increased with depth (Figure 3.82). The 5m site had the lowest Rayyan condition index and was significantly different to the 20m site. There was also a significant difference between the 20m and 40m sites.

The overall average shell height of mussels in 2009/10 was 26.17mm compared to 35mm in 2008/09. Shell height was highest at the 5m site (Figure 3.83). There was a significant difference observed between the 5m site and the 20m, 30m and 40m sites. Mussel wet weight was highest at the 5m site and generally decreased with depth (Figure 3.84). $\delta^{15}N$ was highest at 5m and decreased sharply from 25m to 40m (Figure 3.85). There was a significant difference between the 3, 5m and 10m sites compared to the 30m, 35m and 40m sites. $\delta^{13}C$ generally decreased with depth especially beyond the 15m site (Figure 3.85).

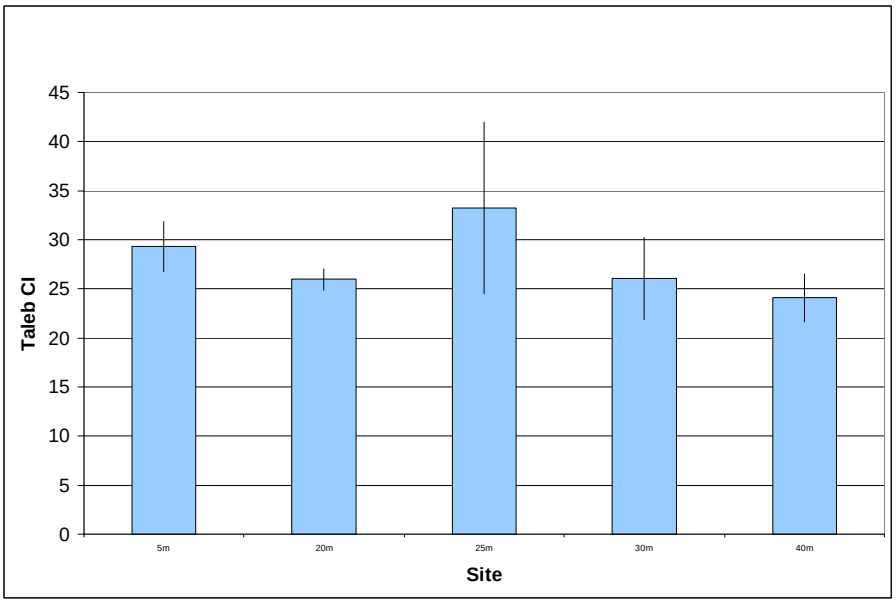

Figure 3.81. The average Taleb condition index for mussels from each of the sample sites. Samples were obtained in March 2010. No mussels were obtained from some sites due to predation. Error bars indicate a 95% confidence interval.

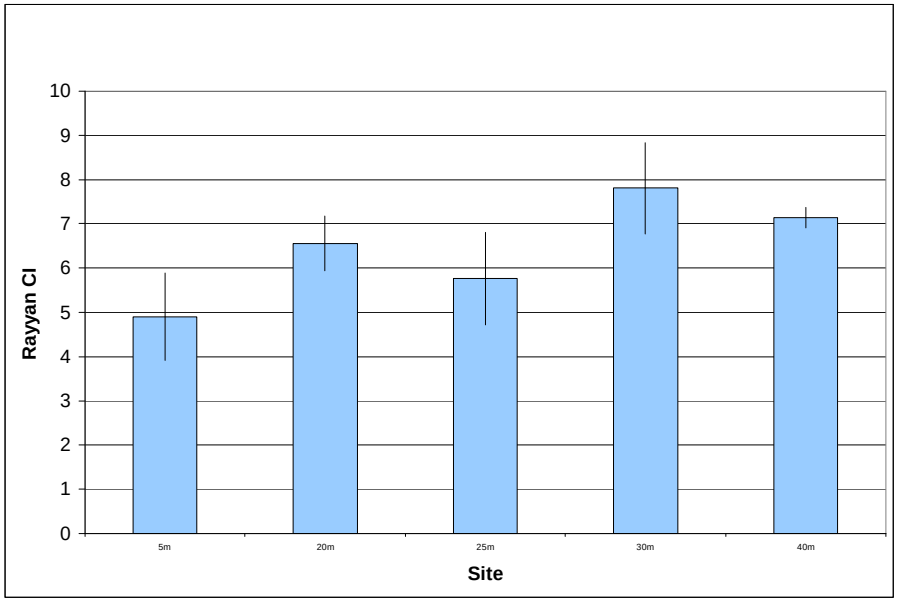

Figure 3.82. The average Rayyan condition index for mussels from each of the sample sites. Samples were obtained in March 2010. No mussels were obtained from some sites due to predation. Error bars indicate a 95% confidence interval.

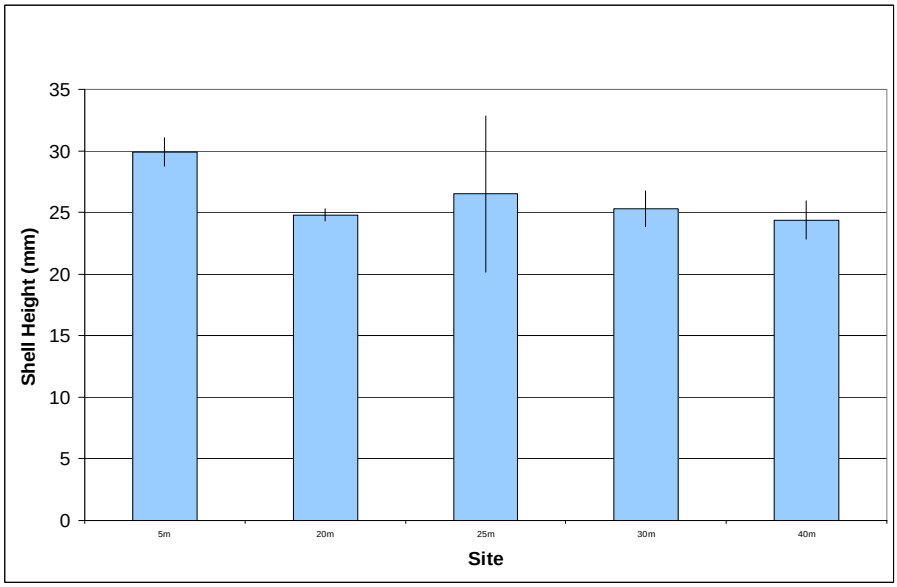

Figure 3.83. The average shell height (mm) for mussels from each of the sample sites.

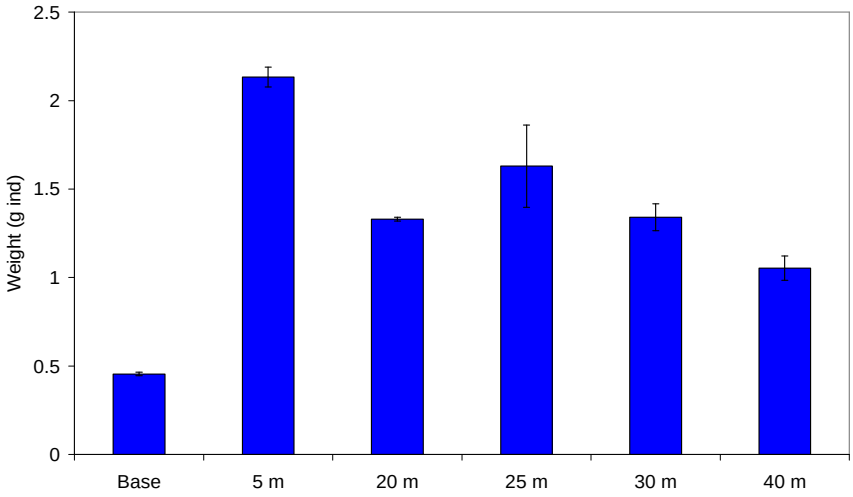

Figure 3.84. The average wet weight (g) for mussels from each of the sample sites. Samples were obtained in March 2010. No mussels were obtained from some sites due to predation. Error bars indicate a 95% confidence interval.

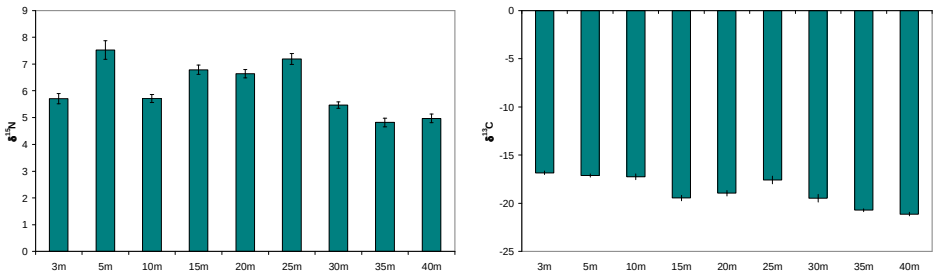

Figure 3.85. The average $\delta^{15}N$ and $\delta^{13}C$ of *Mytilus edulis* deployed at each of the sites. No mussels were obtained from some sites due to predation. Error bars indicate a 95% confidence interval.

The overall average concentration of total suspended solids for 2009/10 was 0.0335 g/L compared to 0.0315 g/l in 2008/09. Total suspended solids were generally highest in November and December (Figure 3.86) and fell to their lowest concentrations in March. Concentrations were similar across the depth gradient. The overall average concentration of POM for 2009/10 was 0.0092 g/L compared to 0.0075 g/l in 2008/09. Considerably more variation was observed in POM concentrations compared to TSS. POM was generally highest in November and December with strong falls in concentration observed at shallower sites (Figure 3.87). Less temporal variation was observed at the deeper sites. Percentage organic matter was driven by variations in POM (rather than PIM). Consequently, %OM was highest in November and December in shallow water stations (Figure 3.88), but less temporal variation was observed in the 35m and 40m stations. The overall average percentage OM for 2009/10 was 27.30% compared to 23.69% in 2008/09.

The overall average concentration of chlorophyll-a for 2009/10 was 0.364 g/L compared to 0.349 g/l in 2008/09, while the overall average pheopigment concentrations for 2009/10 at 0.466ml/m3 were considerably higher than in 2008/09 at 0.345mg/m3. Chlorophyll-a concentrations varied considerably over the course of the 2009/10 surveys (Figure 3.89).

Concentrations were generally low in November and December rising in January and February. Concentrations were highest at the sites deeper than 15m from January to March. Pheopigment concentrations followed a similar pattern to chlorophyll-a concentrations. Low concentrations were observed in samples obtained in November and December (Figure 3.90). Concentrations increased over January to March especially at the sites deeper than 15m.

The overall average concentration of dissolved silica for 2009/10 was 1.23 ug/l compared to 1.55 ug/l in 2008/09. Dissolved silica concentrations varied across the sites. Low concentrations were observed in samples shallower than 15m in January (Figure 3.91), while high concentrations were observed at sites deeper than 15m in January. Concentrations at the deeper sites generally fell over February and March. The overall average concentration of phosphate for 2009/10 was 0.134 mg/l compared to 0.187 mg/l in 2008/09. Phosphate concentrations were generally highest at the sites shallower than 15m, especially in November and December (Figure 3.92). At these sites concentrations fell through to January where they then began to rise over February and March. The overall average combined nitrate and nitrite concentration of the 2009/10 water samples was 0.133 mg/l compared to 0.937 mg/l in 2008/09. Combined nitrate and nitrite concentrations were highest across the 5m to 15m sites especially in November (Figure 3.93). Concentrations above 0.1mg/L were observed at the 15m site at each sampling date. Higher nitrate and nitrite concentrations were also observed in December and January for sites at 30m or deeper. The overall average concentration of ammonia for 2009/10 was 0.121 mg/l compared to 0.173 mg/l in 2008/09. Ammonia concentrations increased over the course of the study at the 15m, 20m and 40m sites (Figure 3.94). The highest Ammonia concentration was observed at the December 30m sample.

In the PCA analysis, samples generally grouped according to the month of sampling rather than the sample depth (Figure 3.95). This grouping appeared to be especially influenced by the February and March samples, and the trend seemed to be driven by chlorophyll-a concentrations. December samples were separated on the basis of difference in TSS and POM. CAP analysis of variation among months indicated that November samples were distinguished by nitrate and nitrite concentrations while December samples were grouped according to POM concentration (Figure 3.96). Analysis of variation among depths indicated that shallower stations were distinguished by higher concentrations of POM and phosphate.

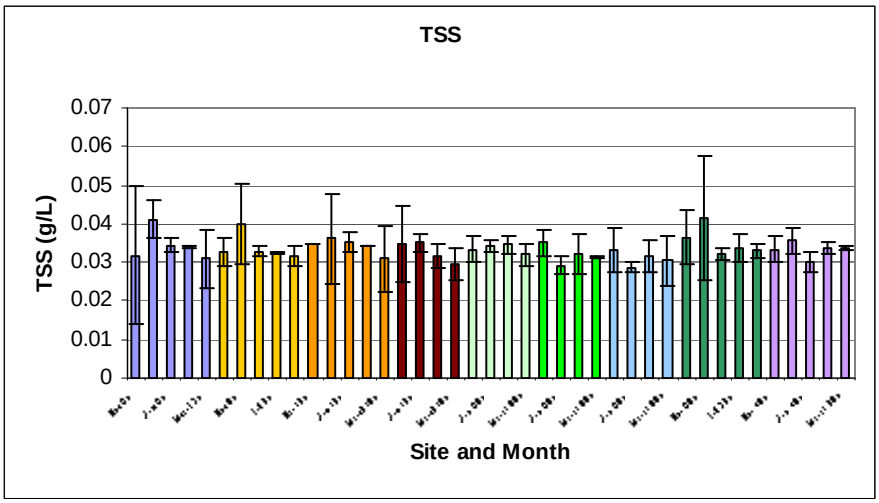

Figure 3.86. Total suspended solids (TSS) concentrations determined from each water sample obtained between November 2009 and March 2010 at each of the sites. Error bars correspond to 95% confidence intervals.

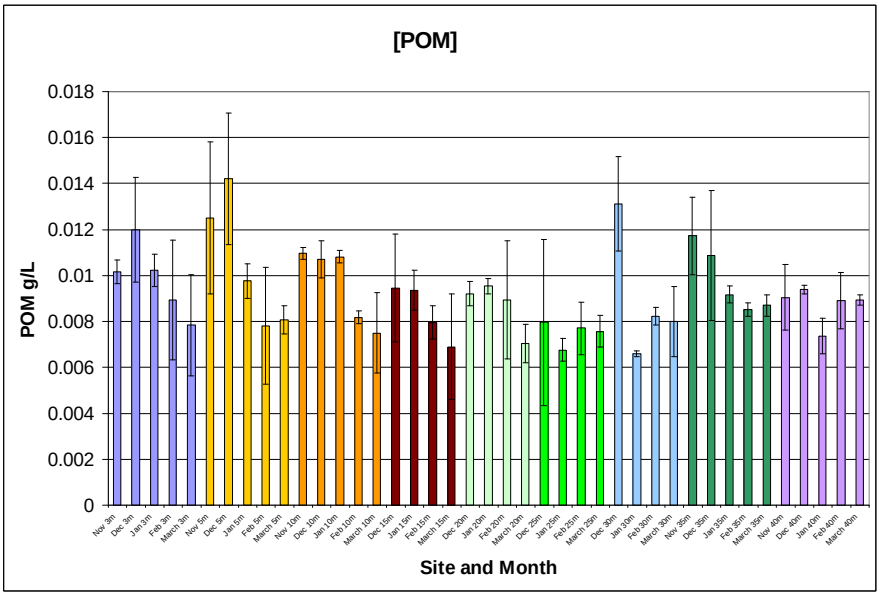

Figure 3.87. Particulate organic matter (POM) concentrations determined from each water sample obtained between November 2009 and March 2010 at each of the sites. Error bars correspond to 95% confidence intervals.

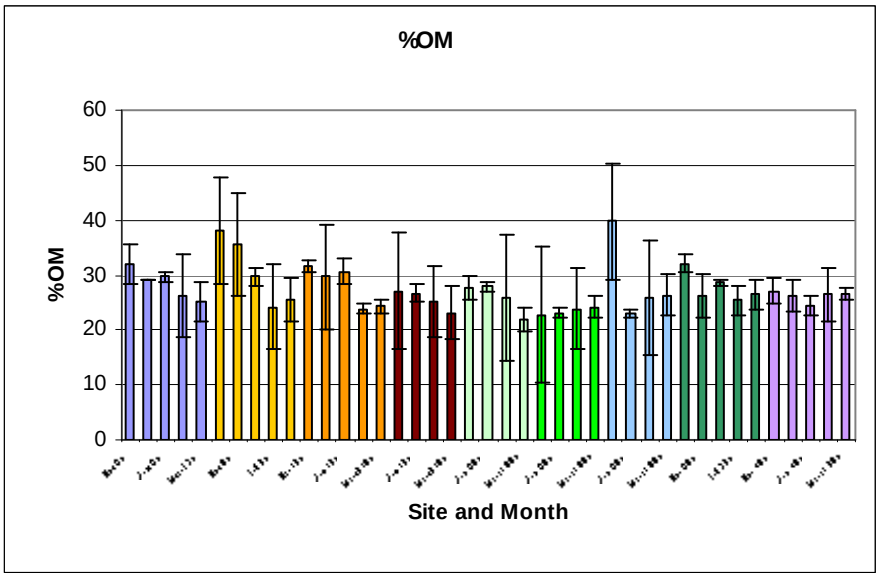

Figure 3.88. Percentage organic matter (%OM) concentrations determined from each water sample obtained between November 2009 and March 2010 at each of the sites. Error bars correspond to 95% confidence intervals.

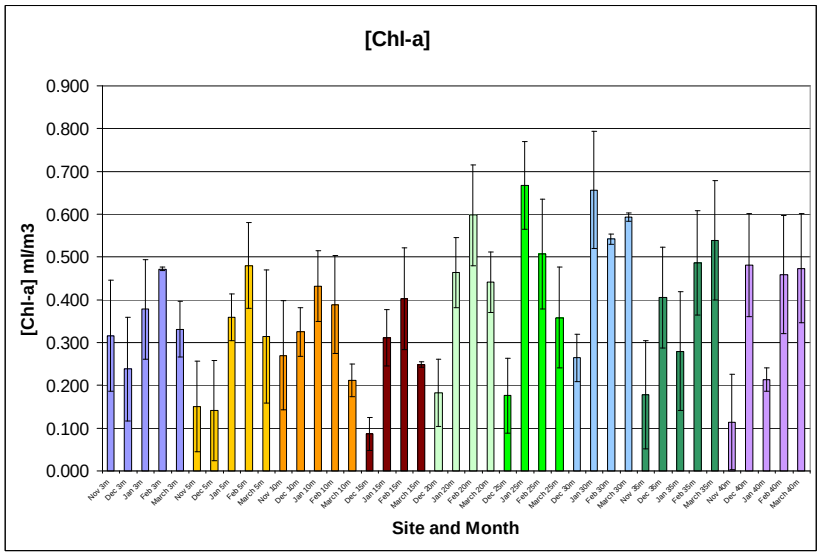

Figure 3.89. Chlorophyll-a concentrations determined from each water sample obtained between November 2009 and March 2010 at each of the sites. Error bars correspond to 95% confidence intervals.

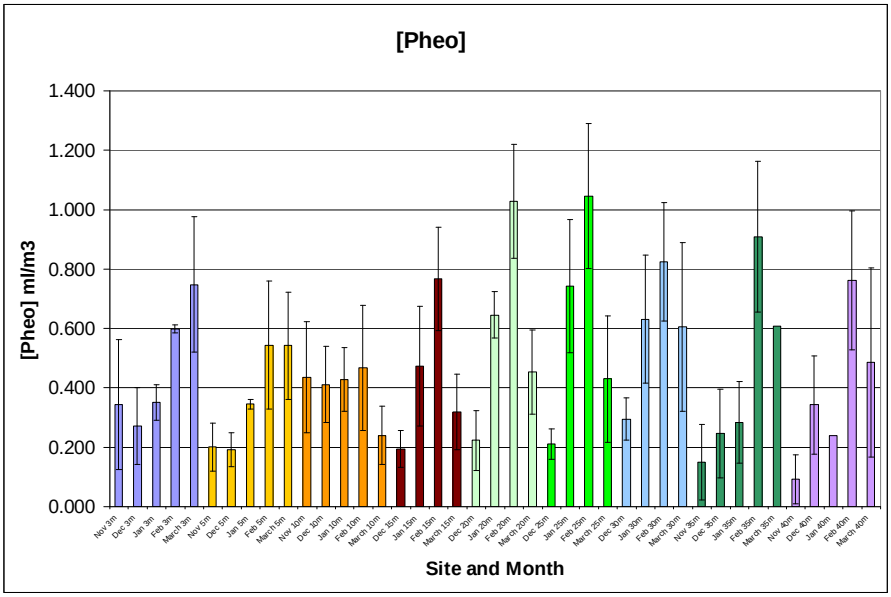

Figure 3.90. Pheopigment concentrations determined from each water sample obtained between November 2009 and March 2010 at each of the sites. Error bars correspond to 95% confidence intervals.

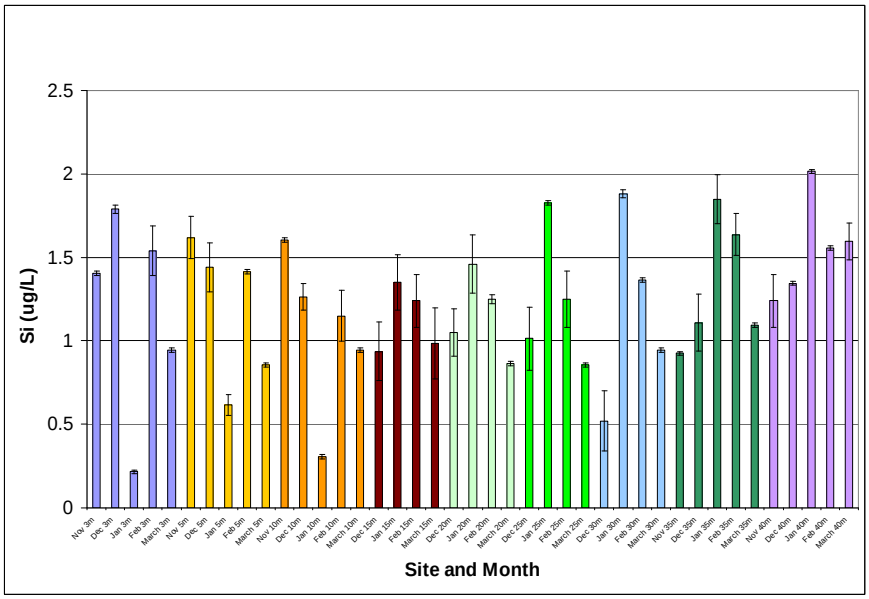

Figure 3.91. Dissolved silica concentrations determined from each water sample obtained between November 2009 and March 2010 at each of the sites. Error bars correspond to 95% confidence intervals.

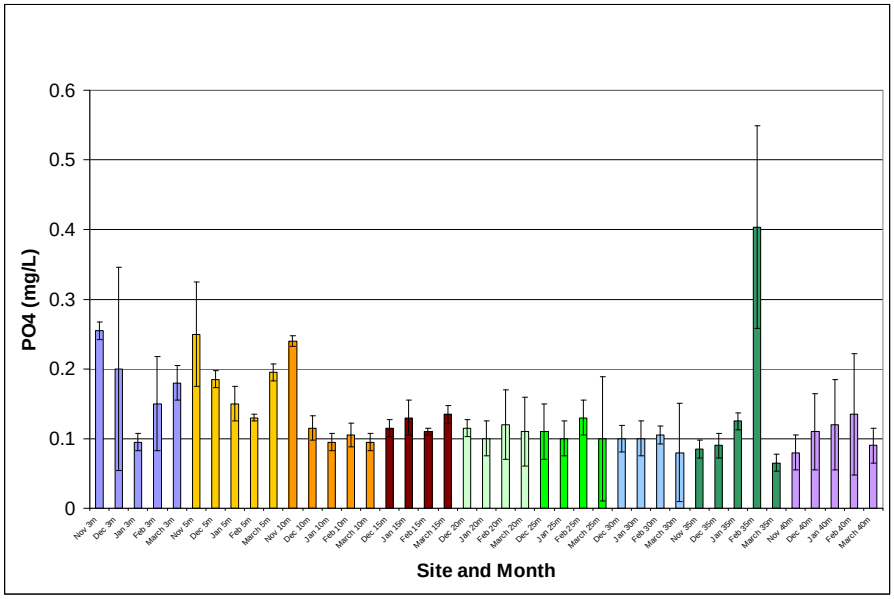

Figure 3.92. Phosphate concentrations determined from each water sample obtained between November 2009 and March 2010 at each of the sites. Error bars correspond to 95% confidence intervals.

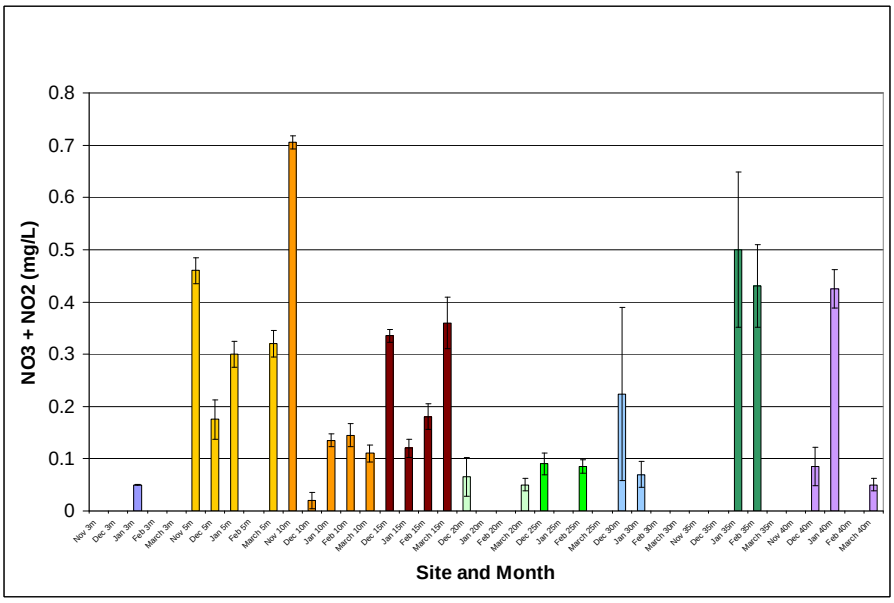

Figure 3.93. Combined Nitrate and Nitrite concentrations determined from each water sample obtained between November 2009 and March 2010 at each of the sites. Sites with concentrations below the detectable limit are indicated with a zero concentration. Error bars correspond to 95% confidence intervals.

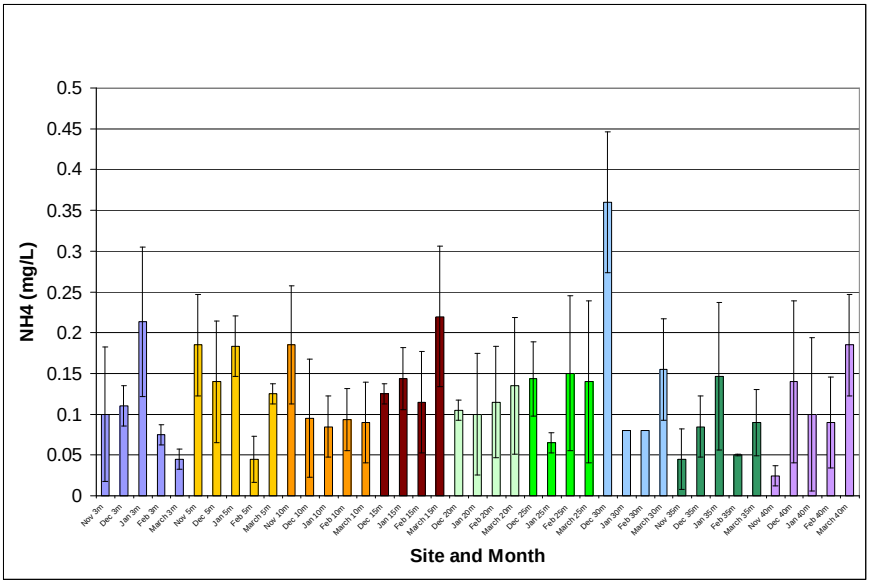

Figure 3.94. Ammonia concentrations determined from each water sample obtained between November 2009 and March 2010 at each of the sites. Error bars correspond to 95% confidence intervals.

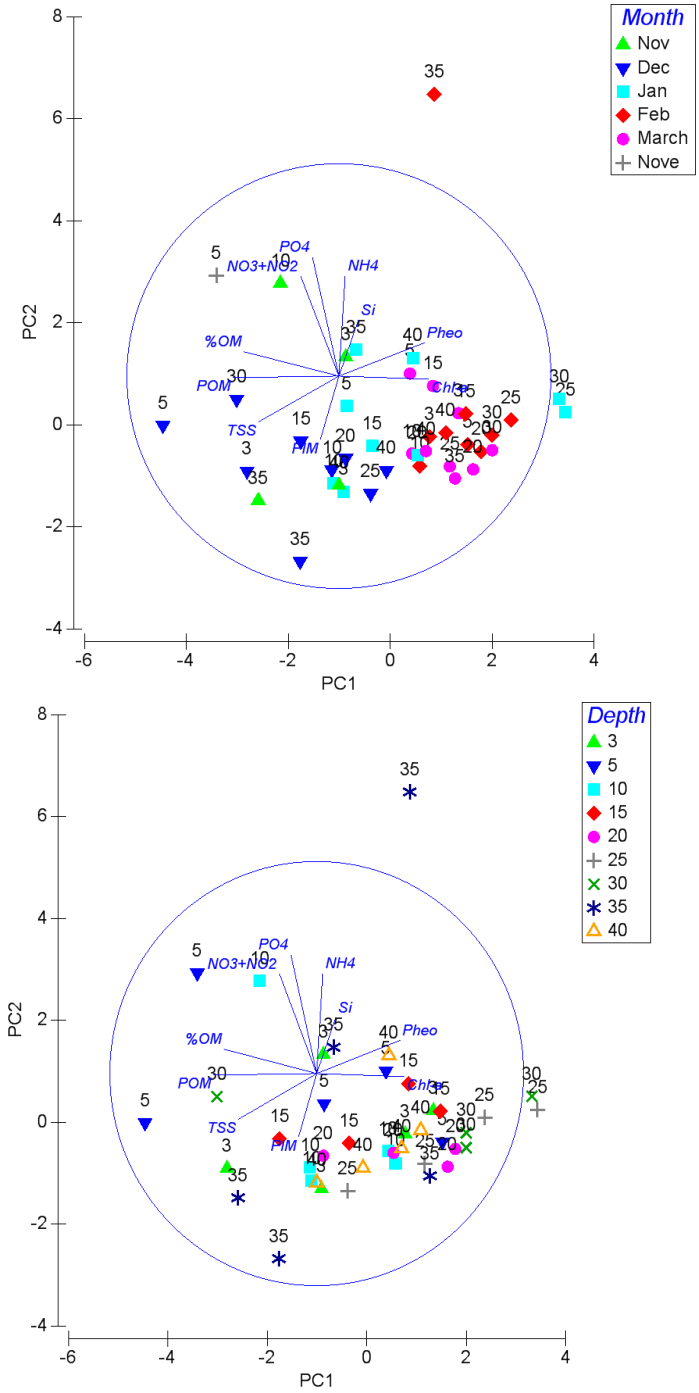

Figure 3.95. PCA analysis of the 2009/2010 water samples. Symbols represent the month of sampling while the number represents the site depth the sample was obtained.

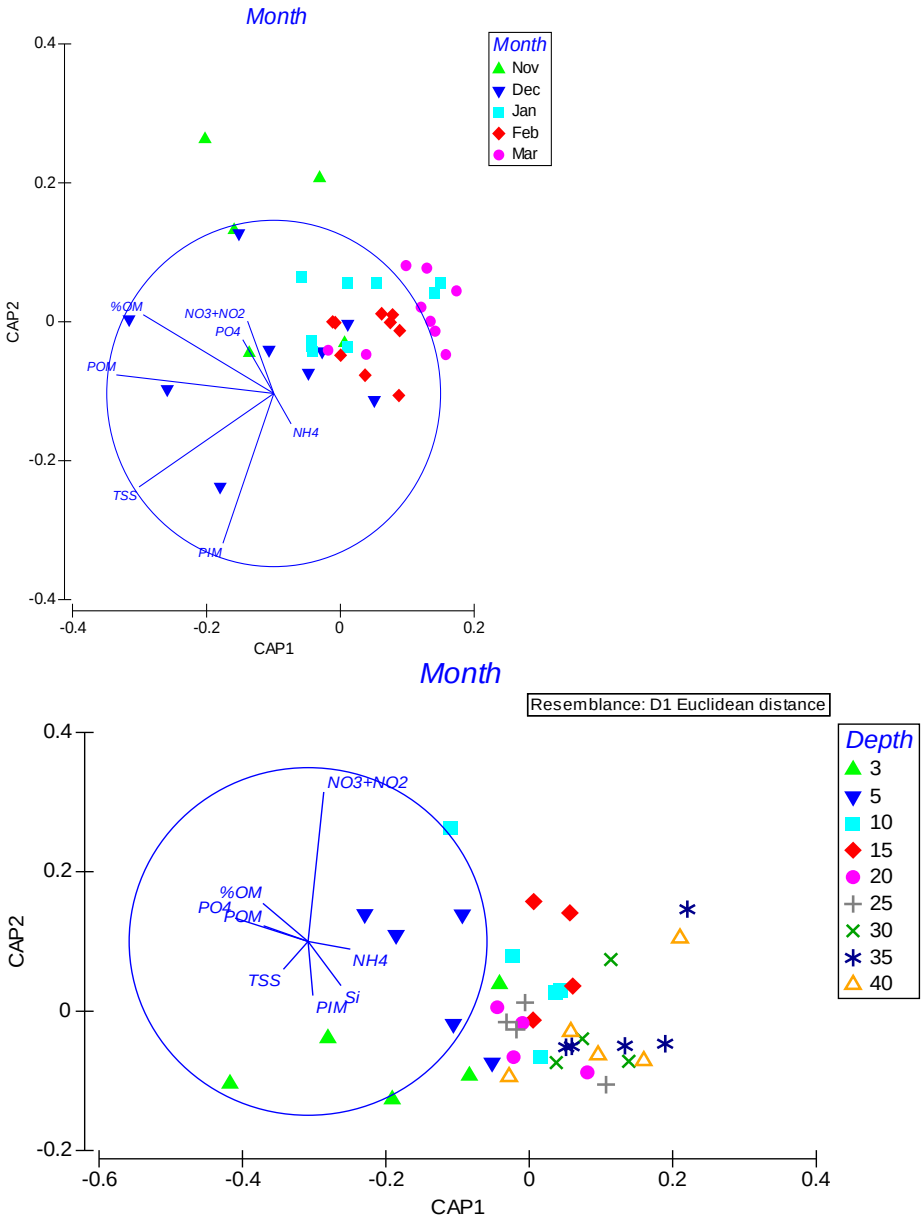

Figure 3.96. CAP analysis of the 2009/2010 water samples. Symbols represent the month of sampling while the number represents the site depth the sample was obtained.

Fucoxanthin concentrations were higher over during (Figure 3.97), suggesting the presence of kelps and/or diatoms. Prasinoxanthin concentrations were highest at the 30m site. No butanoyloxyfucoxanthin was observed at sites less than 20m in depth, while lutein was only observed at the 5m site. High concentrations of hexanoyloxyfucoxanthin was only observed at sites deeper than 20m, possibly indicating the presence of coccolithophorids. PCA analysis suggested that samples from within the same month were more similar than samples from similar depths surveyed in different months (Figure 3.98).

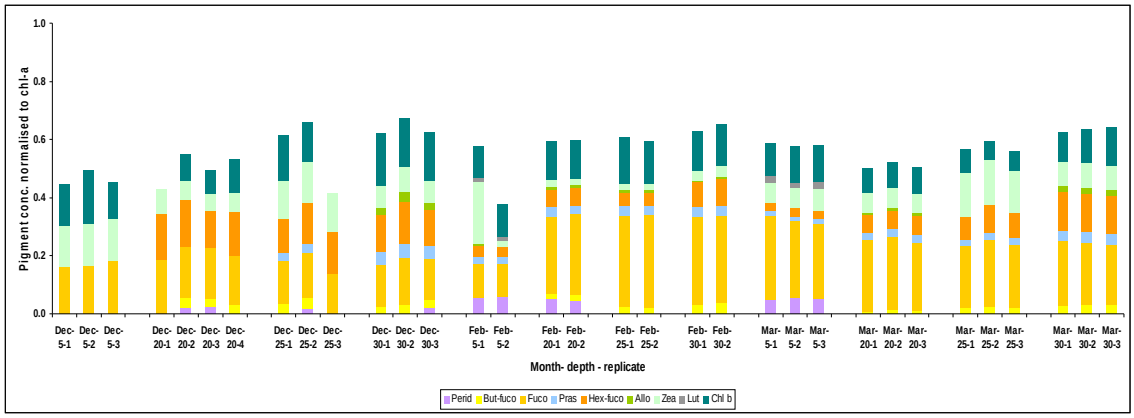

Figure 3.97. Pigment concentrations normalised to chlorophyll-a for the 35 HPLC samples analysed in 2009/2010. Samples are groups by sample replicates and month rather than depth.

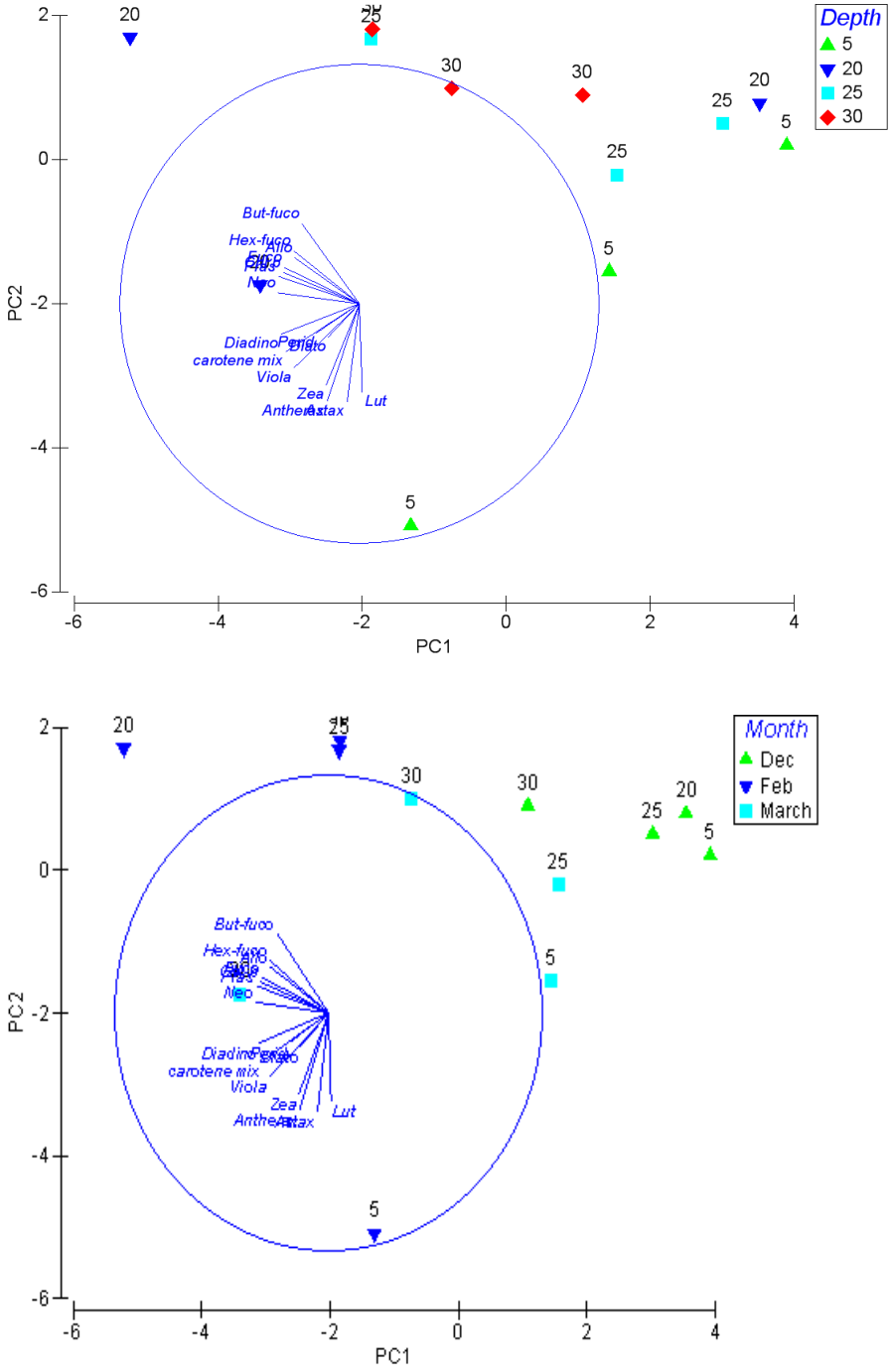

Figure 3.98. PCA analysis of the 2009/2010 water quality data obtained through HPLC. Symbols represent the depth of sampling while the number represents the site depth the sample was obtained.

3.1.13 Rates of filter feeding

Methods

Five nearshore reefs: South Lumps, Whitfords Rock, The Lumps, Cow Rock and Wreck Rock (Table 3.27, Figure 3.99) were sampled. All sites were sampled in summer and autumn (January 2007 to April 2008) during calm conditions. Sponges and ascidians at each site were chosen haphazardly. Organisms on top of the reefs and reef walls were sampled. Filtration rates were measured following InEx method (Yahel G 2005). A small amount of dye (fluorescein, 100 mg L^{-1}) was placed inside polystyrene Sterilin pipette while the other end of the tube was sealed by the sample's thumb. The tube diameter was chosen to correspond closely to the osculum or exhaling syphon to account for filtering rate of the entire aperture or the organism. When the tube was in place the thumb was released to allow the pumped water flow through the tube. The movement of the dye within the tube was videotaped using high definition digital video camera recorder Sony DCR-HC15E. The measurements were replicated 3 to 5 times per organism. The filtering rate was determined with frame-by-frame analysis using scale on the tube for distance. Rate was calculated as the product of aperture diameter and mean dye front speed. Diameter of exhalent siphon, siphon to siphon distance, height (excluding siphon height), and widths were recorded in field for each ascidian. Oscula number and diameter, height and widths were measured for sponges. Organisms were collected for identification and biomass determination. We expressed filtration rates per biomass (g Dry Weight) and per biovolume (L^{-1} sponge or ascidian). Biomass was obtained by washing organisms from sand and removing epiphytes and drying in oven to constant weight at 60°C. Biovolume was obtained by approximating the shape to frustum cone.

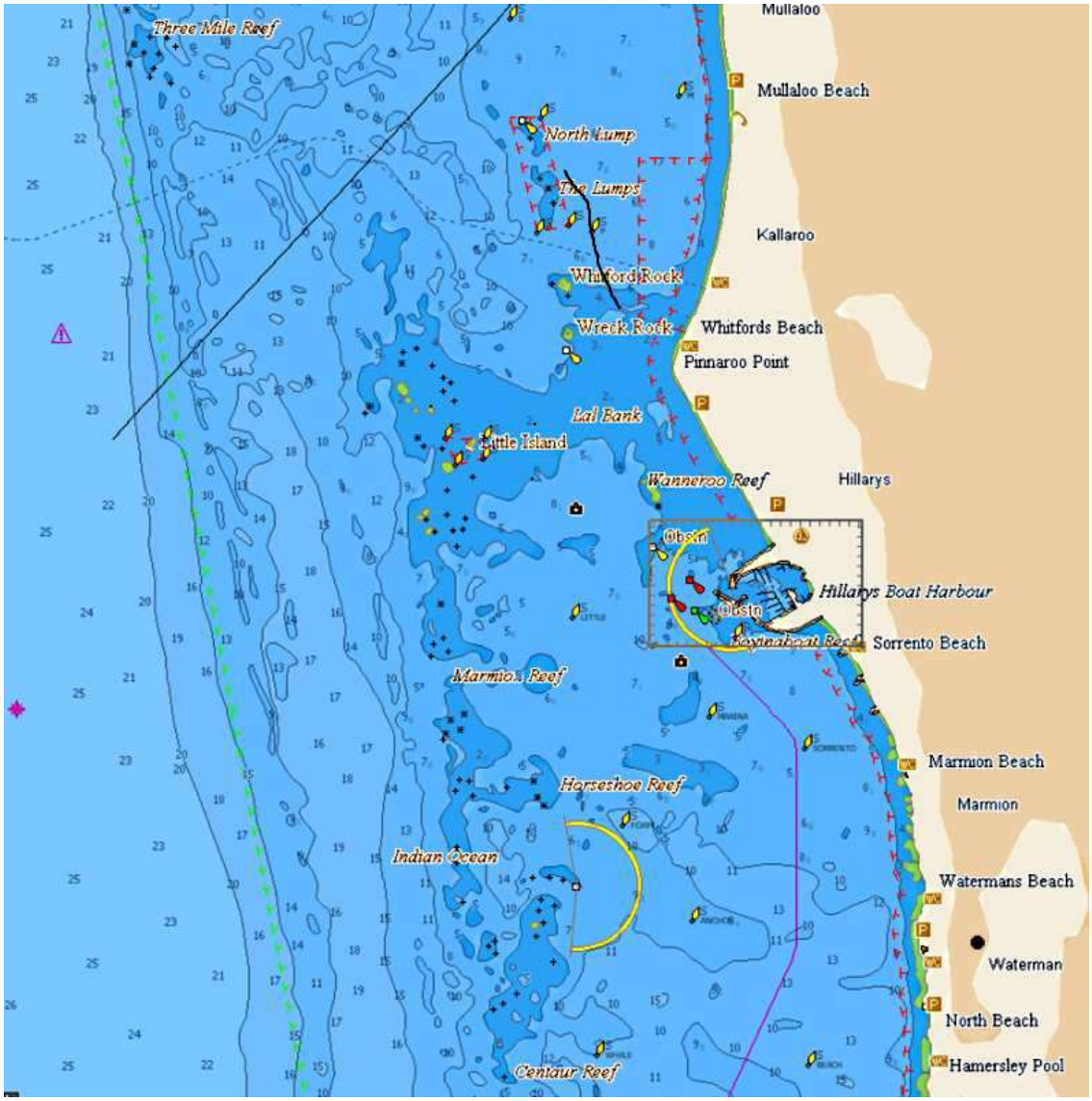

Figure 3.99. Map of shallow reefs in Marmion Lagoon showing locations surveyed.

Table 3.27. Location and depth of study sites.

Location	Reef	Latitude	Longitude	Depth (m) mean (range)
Marmion Lagoon Western Australia	South Lumps	31°47.612S	115°42.990E	5.5 (4.4-7.2)
Marmion Lagoon Western Australia	Whitfords Rock	31°48.318S	115°43.054E	4.4 (2.9-5.6)
Marmion Lagoon Western Australia	Cow Rock	31°49'176S	115°43.647E	4.2 (3-5.1)
Marmion Lagoon Western Australia	The Lumps	31°47'39"S	115°42'54"E	7.3 (7-9)
Marmion Lagoon Western Australia	Wreck Rock	31°47.955S	115°42.955E	8.3 (7.4-9)

To determine feeding on picoplankton In-Ex method of Yahel et al. (2005) was followed. Paired water samples were collected simultaneously and in duplicates from the water inhaled

and exhaled using 3 ml syringes. Pistons were removed from syringes so sampling was passive. Pistons were not used to avoid accidentally drawing bacteria found within sponge or ascidian tissue (Hentschel 2006). One diver was holding syringe next to the animal's inhaling aperture sampling incoming water while the second diver using identical syringe held within few millimetres of exhaling aperture sampled excurrent water. At the end of sampling both ends of syringe were plugged. Samples were kept on ice in dark until brought to shore and placed into sterile 1.8 ml cryovials and preserved with freshly prepared paraformaldehyde (1% final concentration), placed in liquid nitrogen and then transferred to a -80°C freezer for storage. Organisms sampled were collected for identification and biomass determination.

Water samples for nutrient determination were collected at random locations at each reef. 10 samples each were taken next to filter feeders and away from filter feeders. Locations differed only in presence or absence of filter feeders i.e. samples were collected from vertical parts of the reef and from the same depth on each reef. 10 ml nutrient vials were opened under water and allowed to fill within 5 cm from the substrate covered with sponges or ascidians or reef substrate devoid of filter feeders. Tubes were put in boat freezer immediately upon collection and transported to shore and placed in -20°C freezer for storage. Nitrate, nitrite, ammonium, silicate and phosphate analyses were performed using Quick-ChemTM methods on a flow injection LACHATs 8000 Series instrument using the following protocols: for nitrate and nitrite we used Quik-ChemTM Method 31-107-04-1-A; detection limit 0.01 mmol L^{-1}. For silicate analyses, we used Quik-ChemTM Method 31-114-27-1-D; limit of detection 0.05 mmol L^{-1}, and for phosphate: Quik-ChemTM Method 31-115-01-1-G; limit of detection 0.02 mmol L^{-1} (adapted from Armstrong 1951). Ammonium concentrations were determined using a technique developed by Kerouel and Aminot (1997) and adapted for flow injection. For chlorophyll a determination as a measure of phytoplankton biomass we collected 3 L of water about 1 m from filter feeders and about 3 m away from filter feeders. We filtered 2 L of water through 5 µm nitex filter and 1 L through GFF filter to measure contribution of small phytoplankton to total biomass.

Results

A good correlation was obtained between filtration rates and diameter of exhalent siphons in ascidians and oscula in sponges (Figure 3.100). This would allow future estimation of community filtration rates based on measurements of excurrent siphons or oscula in field without the need for destructive sampling to obtain biomass.

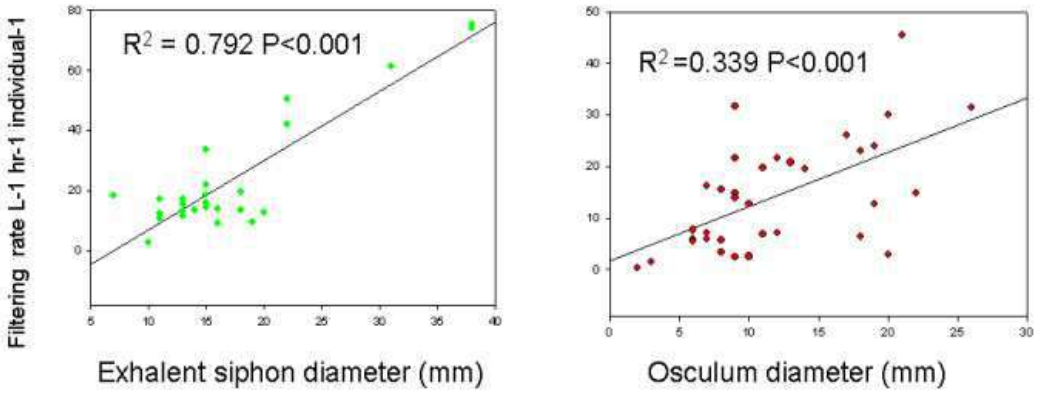

Figure 3.100. Relationship between siphon or osculum diameter and filtration rate.

Nutrient analysis showed an overall increased nitrate/nitrite and ammonia near filter feeders (Table 3.28).Looking at 5 sites separately ammonium was higher in all sites next to filter feeders but Wreck Rock showed no difference in concentration of nitrate/nitrite between filter feeders and away from filter feeders. At the time of sampling this site had a lot of detritus floating on top two meters of the water column. The source of detritus was not immediately obvious. Other nutrients were no different between near filter feeders and away (Figure 3.101). Chlorophyll a concentrations next to and away from filter feeders has not shown significant difference in total, small or large size fraction at 4 locations (Figure 3.102).

Table 3.28. Nitrite/Nitrate and Ammonium measured next and away from filter feeders.

Nutrient	Group	N	Median	Mann-Whitney U Statistic	P
Nitrate/Nitrite	Filter Feeders	50	0.654	791.000	0.002
	Not Filter Feeders	50	0.472		
Ammonium	Filter Feeders	50	0.280	639.500	<0.001
	Not Filter Feeders	50	0.204		

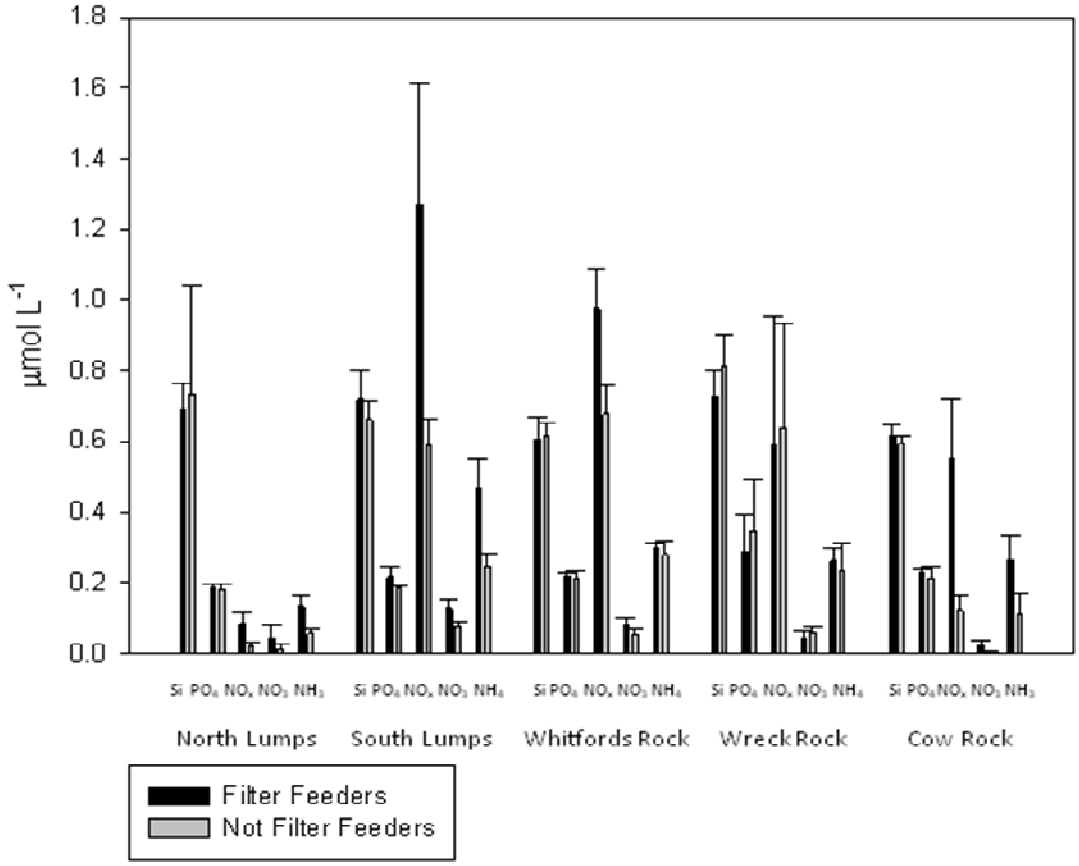

Figure 3.101. Mean concentration of nutrients next to and away from filter feeders in 5 sites (error bars are standard deviations of mean).

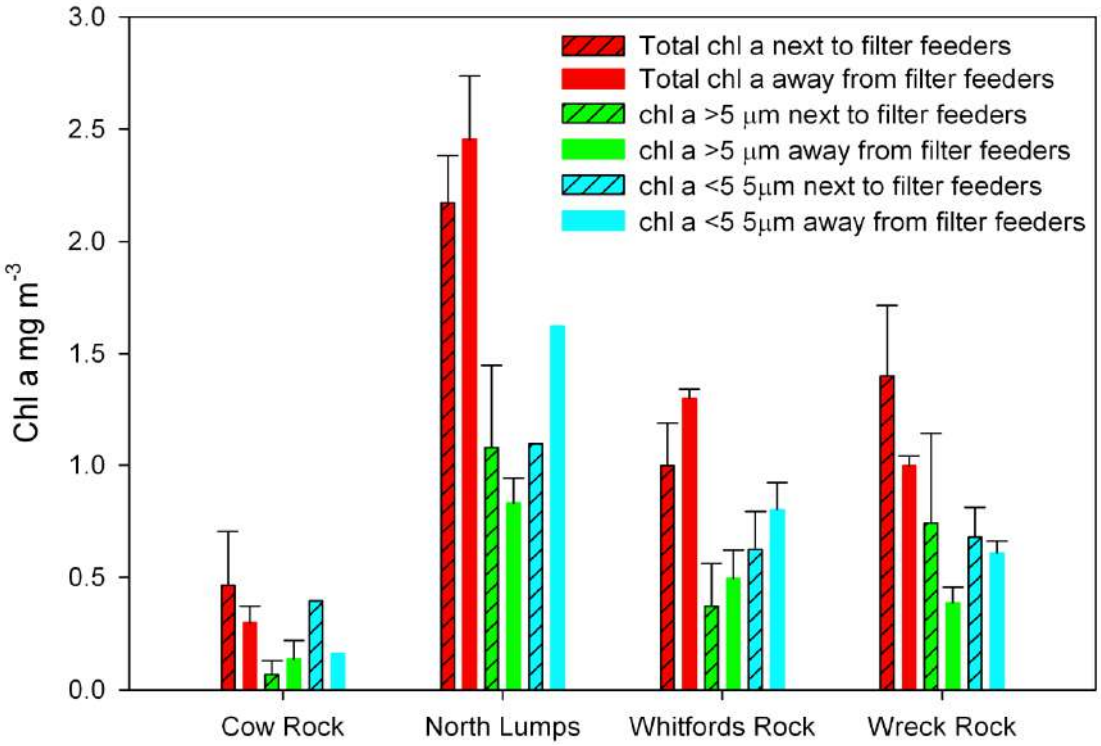

Figure 3.102. Chlorophyll a concentration next to and away from filter feeders.

Sponges filtration rates ranged from 0.0004 for Callyspongiidae A to 0.4 l^{-1} s^{-1} l for Mycalidae (Figure 3.103). This falls within the range reported in other studies (Table 3.29). Variability of pumping was different for different taxa and for individuals within taxa. For example coefficient of variation for Callyspongidae A ranged from 0 to 0.5. Average pumping rate (l s^{-1} kg^{-1} dry weight) was 5 .75 (±9.76 SD) which was comparable to values between 0.5 and 8.5 reported in Weisz et al, (2008). Individual sponge pumped on average almost 2 L of water per minute (±1.82 SD).

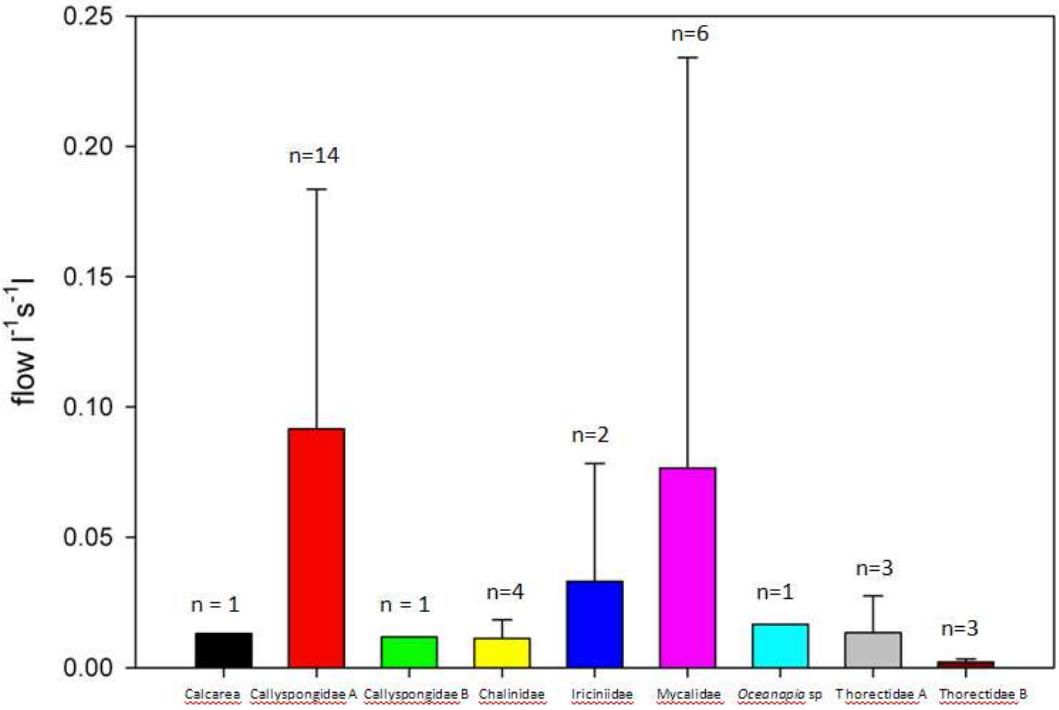

Figure 3.103. Pumping rates of different taxa of sponges. Error bars are standard deviations of mean.

Table 3.29. Previously published sponge pumping rate data. *TT* Tracer in tank, *HT* heated thermistor, *DF* dye in field (Modified from Weisz 2008).

Species	Flow (l^{-1} s^{-1} l)	Method	Reference
Aplysina lacunosa	0.005–0.034	TT	Gerrodette and Flechsig (1979)
Spheciospongia vesparium	0.069	TT	Lynch and Phlips (2000)
Halichondria melanodocia	0.080	TT	Lynch and Phlips (2000)
Biemna sp.	0.221	TT	Lynch and Phlips (2000)
Halichondria panicea	0.045	TT	Riisgard et al. (1993)
Haliclona urceolus	0.042	TT	Riisgard et al. (1993)
Halichondria bowerbanki	0.240	TT	Vogel (1974)
Thenea muricata	0.050	TT	Witte et al. (1997)
Aplysina Wstularis	0.049–0.276	HT	Reiswig (1971b)
Verongula gigantea	0.050–0.100	HT	Reiswig (1974)
Tethya crypta	0.180	HT	Reiswig (1974)
Mycale sp.	0.210–0.270	HT	Reiswig (1974)
Haliclona permollis	0.049–0.116	HT	Reiswig (1975a)
Haliclona permollis	0.131	HT	Reiswig (1975b)
Dysidea avara	0.017	DF	Ribes et al. (1999)
Baikalospongia bacillifera	0.040–0.60	DF	Savarese et al. (1997)
Theonella swinhoei	0.043	DF	Yahel et al. (2003)
Callyspongia plicifera	0.578	DF	Weisz et al (2008)
Callyspongia vaginalis	0.374	DF	Weisz et al (2008)
Niphates digitalis	0.365	DF	Weisz et al (2008)
Agelas conifera	0.073	DF	Weisz et al (2008)
Aplysina archeri	0.102	DF	Weisz et al (2008)
Ircinia strobilina	0.093	DF	Weisz et al (2008)
Spheciospongia vesparium	0.176	DF	Weisz et al (2008)
Xestospongia muta	0.078	DF	Weisz et al (2008)
Calcarea1	0.013	DF	this study
Callyspongiidae1	0.0004- 0.34	DF	this study
Callyspongiidae2	0.01	DF	this study
Chalinidae1	0.001-0.015	DF	this study
Irciniidae1	0.001- 0.065	DF	this study
Mycalidae1	0.004-0.397	DF	this study
Oceanapia sp	0.017	DF	this study
Thorectidae2	0.008-0.029	DF	this study
Thorectidae4	0.001-0.003	DF	this study

Ascidians filtration rates ranged from 0.012 to 0.12 l^{-1} s^{-1} l. Individual ascidian pumped on average almost 1.2 L of water per minute (±1.98 SD). Pumping rates of ascidians were significantly more variable than pumping rates of sponges (Mann Whitney P = 0.002). The variability was high on a scale of individual organisms (Figure 3.104). Comparison with published some data shows that values obtained were within the range published for other species (Table 3.30). The filtration rates were positively and significantly correlated with the mass (Figure 3.105). We estimated grazing impact on picoplankton by sponges. Sponges retained high proportion small particles from 0.2 to 2 µm (Figure 3.106).

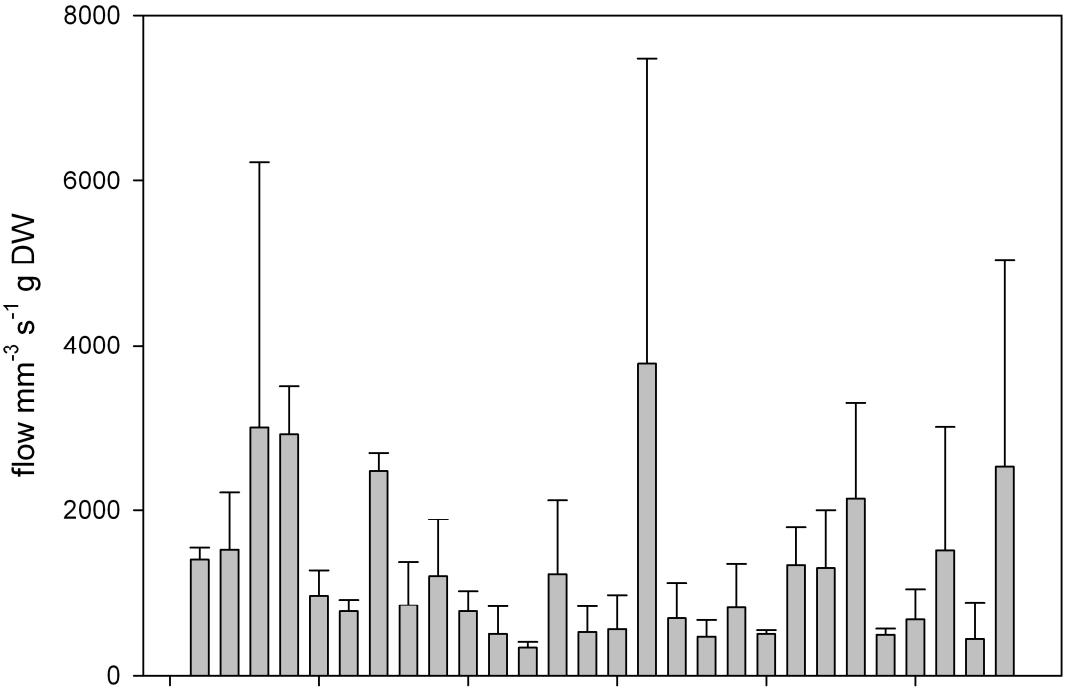

Figure 3.104. Pumping rates of individual ascidians based on at minimum 3 replicates per organism.

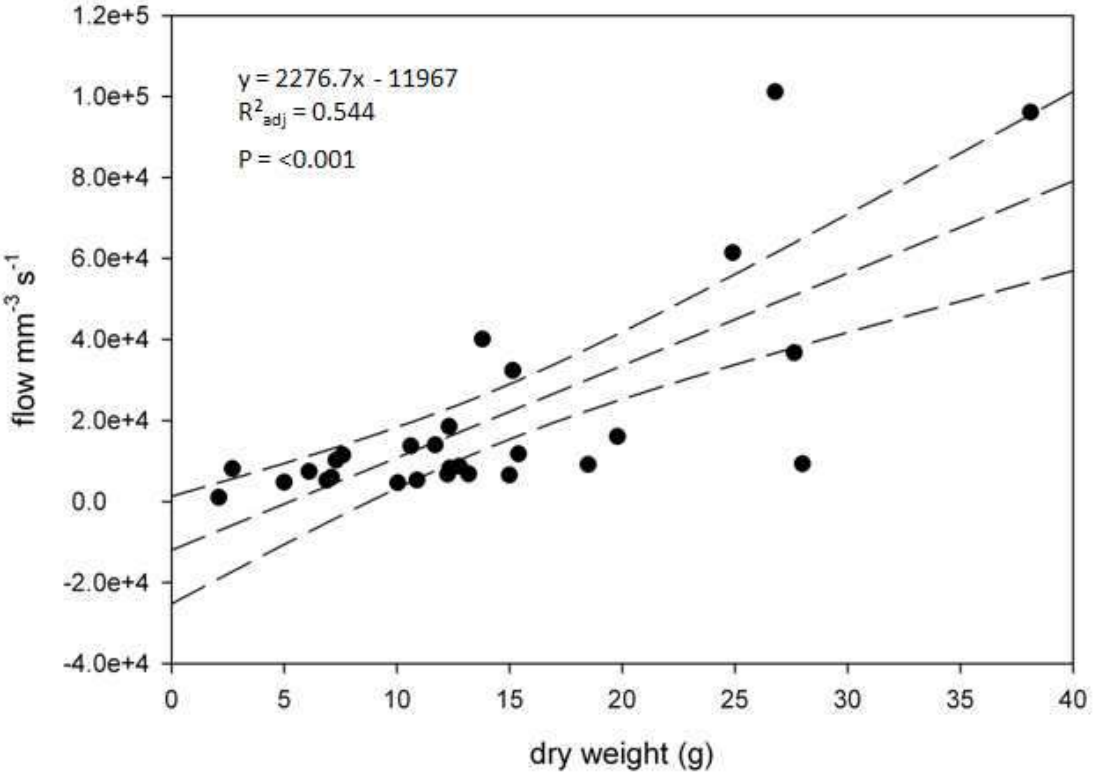

Figure 3.105. Correlation between ascidian biomass and pumping rate.

Table 3.30. Dry weight specific filtration rates of ascidians. *CL* clearance rate of algal cells, *DF* dye in field (mean ±SE).

Species	Flow (ml min^{-1} mg^{-1})	Method	Reference
Clavelina lepadiformis	0.74 ± 0.32	CL	Petersen and Svane, 2002
Ascidia virginea	0.18 ± 0.07	CL	Petersen and Svane, 2002
Ciona intestinalis	0.40 ± 0.15	CL	Petersen and Svane, 2002
Corella parallelogramma	0.34 ± 0.11	CL	Petersen and Svane, 2002
Boltenia echinata	0.15 ± 0.04	CL	Petersen and Svane, 2002
Molgula manhattensis	0.07 ± 0.03	CL	Petersen and Svane, 2002
Pyura tesselata	0.07 ± 0.01	CL	Petersen and Svane, 2002
Styela clava	0.02	CL	Holmes, 1973
Ascidiella aspersa	0.04	CL	Holmes, 1973
Ciona intestinalis	0.142	CL	Robbins, 1983
Clavelina lepadiformis	0.04	CL	Fiala-Medioni, 1974
Halocynthia papillosa	0.11	CL	Fiala-Medioni, 1974
Microcosmus sabatieri	0.11	CL	Fiala-Medioni, 1974
Phallusia mamillata	0.07	CL	Fiala-Medioni, 1974
Styella plicata	0.15	CL	Fiala-Medioni, 1978
Pyura stolonifera	0.02	CL	Klumpp, 1984
Herdmania momus	0.08 ± 0.01	DF	this study
Phallusia obesa	0.05 ± 0.01	DF	this study

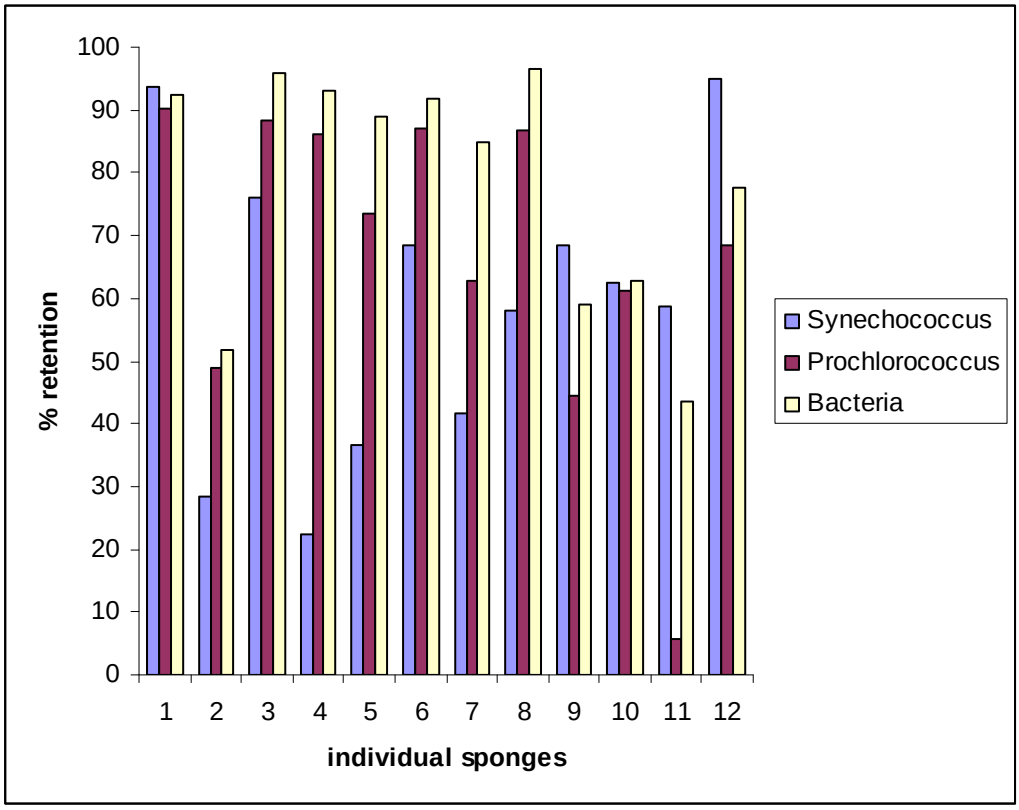

Figure 3.106. Retention rate of picoplankton by sponges.

We partitioned the grazing impact on small phytoplankton by pelagic (microzooplankton) and benthic (sponges and ascidians) grazers. Using data collected in SRFME we estimated that

microzooplankton graze 55% of primary production of small phytoplankton while ascidians and sponges 30% (Figure 3.107).

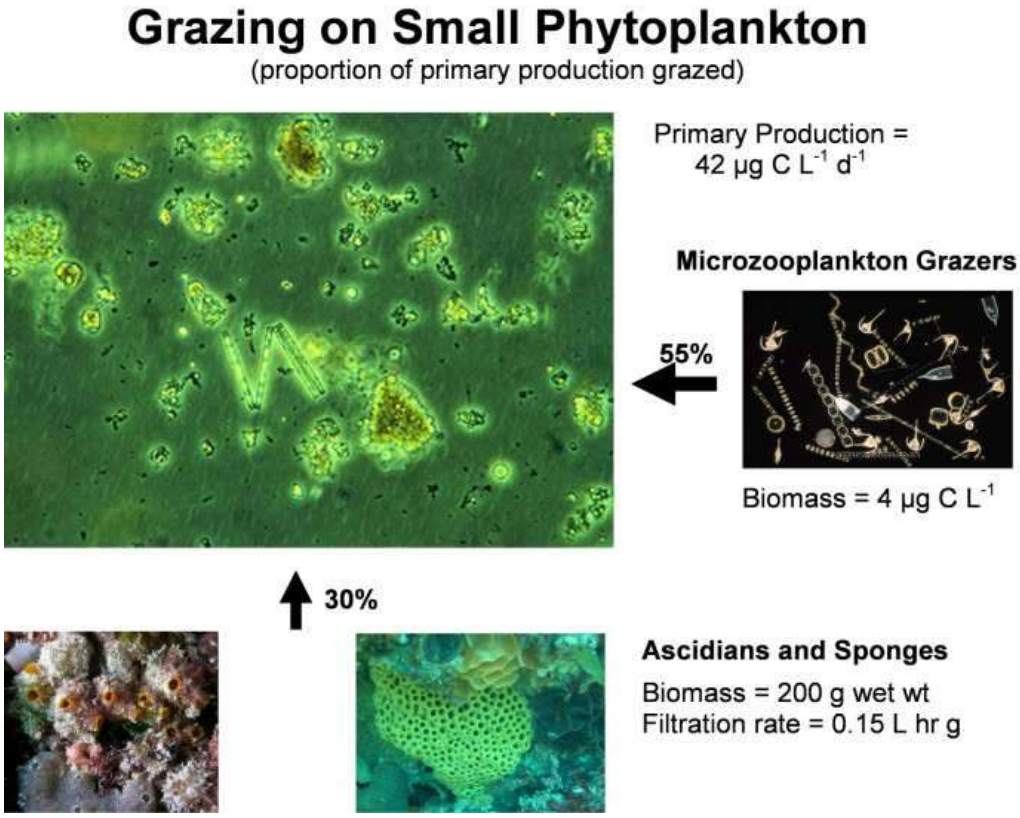

Figure 3.107. Impact of pelagic and benthic grazers on small phytoplankton.

3.1.14 Predation on mussels

Methods

Predation rates on mussels, *M.edulis*, were measured using predator exclusion cages. To test the hypothesis that large predators, including *P.cygnus*, may be influencing abundances of molluscs, caged and uncaged mussels were deployed inside and outside fished reserves at Marmion, Rottnest Island and Jurien Bay. At each location, eight replicate groups of 12 similar sized mussels (70mm total length) were attached to a series of plastic mesh grids, with 4 of the grids being fully enclosed to prevent predator access and 4 of the grids remaining open to allow predator access (Figure 3.108). After a deployment period of seven days all grids were retrieved and the mussels on each plastic grid recorded as alive or dead. Permutational MANOVA (Anderson 2001) was used to test for differences in the survivorship of the mussels deployed by each method (caged versus uncaged) and between reserves and non-reserves (fished versus unfished). Analyses were performed using Euclidian distances calculated from square root transformed data using the PRIMER statistical software.

Figure 3.108. Image showing mussels within four caged (enclosed) and four uncaged (open) grids prior to deployment.

Results

Survivorship of mussels suggested that predation rates were generally high at all three locations, with significantly higher survivorship in mussels deployed in cages than mussels deployed uncaged (P = 0.001) (Table 3.31, Figure 3.109). Overall mean survivorship for each group of caged mussels was 11.19 (95% CI= ±0.4) or 93.25% (± 3.33%) while the overall mean survivorship for each group of uncaged mussels was 3.69 (95% CI= ±1.19) or 30.75% (±9.92%) (Table 3.31).

Table 3.31. Results of PERMANOVA testing for (a) differences in the survivorship of mussels in caged versus uncaged treatments (b) survivorship of uncaged mussels in fished versus unfished reserves.

(a) Source	df	SS	MS	Pseudo-F	P(perm)	Unique perm
Treatment	1	131.78	131.78	110.05	0.001	995
Residual	126	150.88	1.1974			
Total	127	282.66				

(b) Source	df	SS	MS	Pseudo-F	P(perm)	Unique perm
Treatment	1	34.516	34.516	1.5663	0.222	53
Residual	62	1366.2	22.036			
Total	63	1400.7				

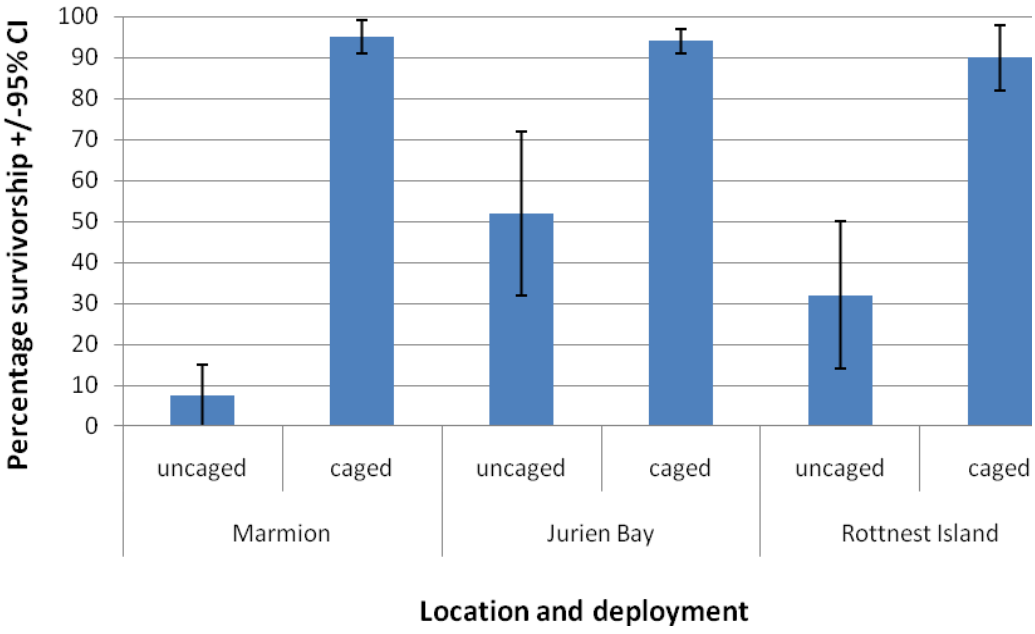

Figure 3.109. Mean percentage survivorship (±SE) of caged and uncaged mussels at Marmion, Jurien Bay and Rottnest Island after seven day deployment.

In contrast, there was no difference in the survivorship of uncaged mussels in fished versus unfished reserves (Table 3.31, Figure 3.110), suggesting fishing status had little or no influence on the rate of mussel predation. Overall mean survivorship for each group of

uncaged mussels in reserves was 4.08 (95% CI= ±1.68) or 34% (± 14.2%) while the overall mean survivorship for each group of uncaged mussels in non-reserves was 3.65 (95% CI= ±1.78) or 30% (±15.2%).

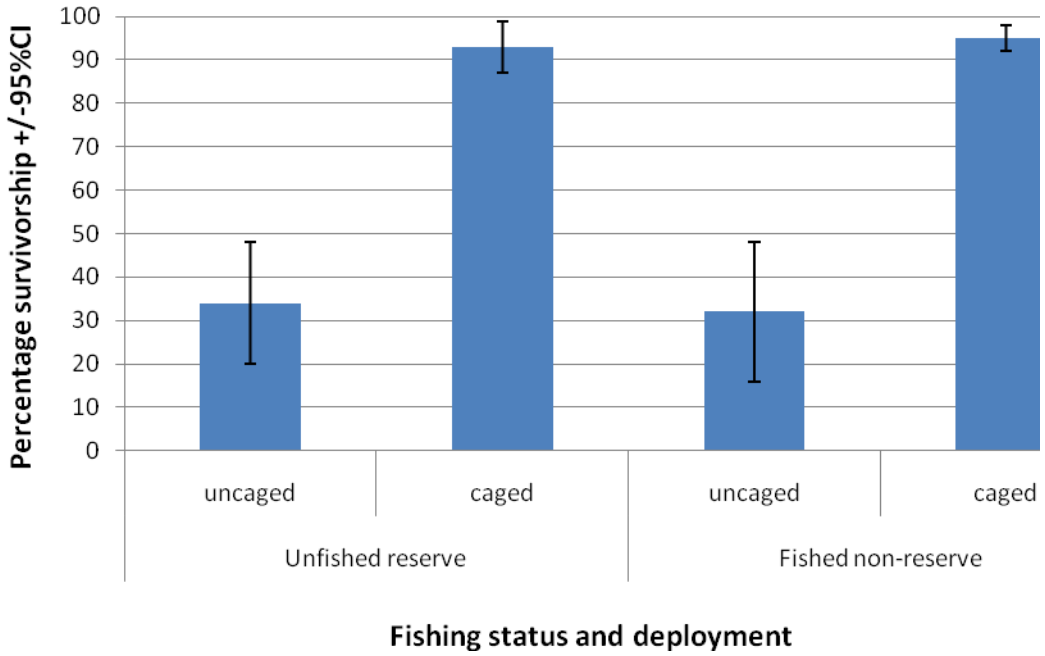

Figure 3.110. Mean percentage survivorship (±95% CI) of caged and uncaged mussels in fished and unfished reserves.

Variability in mussel survivorship was considerably larger in uncaged treatments than in caged treatments (Figure 3.109). For example the variability (95% CI) in survivorship of uncaged mussels at Marmion was ± 6.73% in comparison to ± 3.68% for caged mussels at Marmion. Similarly, the variability in the mean survivorship of uncaged mussels at Jurien Bay and Rottnest Island was ±20.23% and 17.69% respectively, again considerably higher than that for caged mussels at ±3.17% and ±8.39% respectively.

However care must be taken when determining whether observed gradients in predator abundance translated to spatial patterns in predation. This preliminary study suffered from a high amount of variability in mussel survivorship between the reserve and non-reserve sites. It is also acknowledged that whilst it can be reasonably assumed predator abundances are higher in non-fished reserves than in fished areas, this assumption was not tested at the time of deployment. Uncaged mussels outside the reserves had lower survivorship than those inside the reserves but future work requires much better resolution to obtain a statistically significant result. Obtaining this resolution is likely to be particularly difficult given the magnitude of the difference compared to the variability of the data (size of the 95% CI).

3.1.15 Discussion

Nutrients and primary production

Temperature and nutrients, and to a lesser extent salinity, exhibited spatial and temporal trends that highlight the heterogeneity of processes occurring in nearshore ecosystems. Temperature measurements from CTD deployments, as well as by sensors deployed on the seafloor, showed that fluctuations were greatest in the shallowest nearshore sites, which tended to yield the coldest measurements in winter and the warmest measurements in summer.

Spatial patterns in nutrient concentrations – in particular nitrate – were more evident than seasonal patterns, but re-analysis of historical nitrate concentrations revealed that there was a great deal of variation across relatively short time periods (hours to days). Spatial patterns appeared to be related to the distribution of reefs, with the highest concentrations during each survey event being yielded by sites over reef. The source(s) of the high nutrient concentrations, and the mechanisms that produce this pattern remain to be identified, but plausible sources include groundwater and benthic biota.

Importantly, some of the short-term temporal variation in nitrate could be explained by waves($r = 0.21$). Frequently, the periods corresponding with high concentrations of nitrate were also periods where wave heights were highest. There are a number of mechanisms that might lead to this observed correlation, and the data do not allow the alternative mechanisms to be distinguished, but they do suggest that waves very likely play an important role in nitrogen cycling by promoting release of nutrients into the water column. This observation is particularly important in the context of the laboratory studies, which revealed that nutrients were rapidly consumed – likely by sediment biota including benthic microalgae – in both the presence and absence of light. The rapid consumption of nutrients provides a possible explanation for the generally low levels of nutrients present most of the time.

Laboratory studies of production by benthic microalgae and by different species of macroalgae revealed that the highest rates of mass-specific production (i.e. production per unit biomass) were yielded by several species of relatively small red macroalgae. The most plausible general mechanism to explain these results is that these species have a greater surface area relative to volume, but the detailed physiological mechanisms that generate these patterns remain to be identified. Nevertheless, despite the relatively high rates of production by these species, the biomass of benthic autotrophs in Marmion Lagoon is dominated by kelp *Ecklonia radiata*, and this dominance means that benthic production is also very likely dominated by this single species.

The laboratory studies also highlighted that rates of production varied between summer and winter months, but that the nature of this difference was not the same for all species. For example, while the smaller macroalgae were more productive in summer, *E. radiata* was more productive in winter.

In the field-based studies, there was considerable among-individual variation in productivity of kelp *Ecklonia radiata*, but despite this there were among-site differences in rates of thallus extension and productivity that were well-explained by environmental variables. Water

temperature and light intensity in particular were reliable predictors of among-site patterns in growth, but the relative influence of each predictor varied depending on the season. Overall, individual variation was consistently higher than between site variation perhaps due to the variation in microclimates at each site. The only exception was during spring when most of the variation in biomass accumulation was due to among-site differences.

A high variation in bottom temperatures and light intensities derived from in situ loggers were observed during the study. Bottom temperatures varied on an inshore to offshore gradient of up to 1.4ºC during summer. This gradient was reversed in winter. In addition, average maximum light intensities varied by up to 34,690 Lux during the spring sampling period. Some sites had consistently lower light intensities than neighbouring sites due to factors such as localised turbidity or substrate characteristics.

Secondary production and filter feeding

The biomass and the identity of species were quite different among habitats for the benthic invertebrate groups studied. In general, reefs supported much higher biomasses than seagrass beds, which in turn supported higher biomasses than unvegetated sand. This pattern was observed for mobile invertebrates like sea urchins (a group comprising several species of herbivores and omnivores), gastropods (both herbivorous and predatory groups) and sponges and ascidians. However, for feather stars (crinoids: suspension feeders) and sea cucumbers (holothuroids: deposit feeders) biomasses in some seagrass beds were as high as those observed on reefs. Re-analysis of historical data revealed that within the broad among-habitat patterns, other gradients are present: inshore reefs tended to support higher biomasses of sponges and filter feeders than offshore reefs, and specific habitats within reefs and seagrass beds supported higher biomasses than others.

The high rates of primary production by benthic autotrophs, combined with the low rates of direct grazing, suggest that nearshore food webs are perhaps reliant on detritus. The results from deployments of mussels at different depths are consistent with this expectation. Growth rates of mussels were highest for mussels deployed in shallow water in two consecutive years. Analyses of stable isotopes of carbon and nitrogen in mussel tissue supported the conclusion that the different in growth rates was due to different nutrition – stable isotopes of water column particulate matter further suggested that this reflected the availability of different food sources. Stable isotope ratios of carbon from mussels and particulate matter were higher in shallow water, consistent with the pattern expected if particulate matter comprised a proportion of detritus from benthic autotrophs in shallow water.

Patterns in measurements of the amount and composition of particulate matter in the water column were quite variable among depths and months of sampling. However, some trends were apparent. The concentration of particulate organic matter (POM), and the percentage contribution of organic matter, tended to be higher in shallow depths – although this pattern was not always present. The patterns tended to be strongest in late spring to early summer (November-December), when measurements of these two variables tended to be highest, but patterns tended to be weakest later in summer, when measurements were typically low at all depths. The pattern of highest measurements in shallow depths in late spring to early summer is consistent with the pattern expected if a seasonal decrease of benthic autotroph biomass due to erosion leads to an increase in particulate detritus in the water column.

By ingesting and assimilating particles of detritus and plankton, and excreting ammonia filter feeders might be a vital link in nitrogen cycling in nearshore ecosystems. Results of field measurements of nutrients yielded generally higher nitrite/nitrate and ammonium levels near filter feeders than away from them, an observation that supports this idea. In addition, rates of filtrationwere in some cases among the highest recorded anywhere. There was variation in these rates among individuals and among species, but this variation was well-explained by size, with large individuals filtering at a greater rate.

The types of particles (i.e. detritus or plankton) ingested and assimilated by different types of filter feeders remain to be characterised in detail (although some sponges retained a relatively high proportion of picoplankton), however, the high biomasses of filter feeders on reefs and in seagrass beds, the high growth rates we observed inshore, and the high rates of filtration all indicate that they very likely play a key role in detrital food webs and nitrogen cycling in nearshore ecosystems.

Predation and grazing

Observations of direct grazing on kelp *E. radiata* support previous observations that rates of direct grazing are typically low. We did record relatively high rates of grazing at some reefs, and the location of the grazing suggested that it was likely due to herbivorous fish. This direct grazing might be important to some species of herbivores, but most of the biomass produced is not directly grazed, and so nearshore food webs are more likely reliant on detritus. If this were true, then we would expect heavy predation on organisms that rely on detritus for their food. Measurements of rates of predation on one species of suspension feeder (the blue mussel, *Mytilus edulis*) is consistent this inference: mussels that were deployed outside cages had very low survival rates, while mussels that were deployed inside cages had high survival rates, suggesting that potential predation on this group is very high. These measurements were taken using only a single species of potential prey, but they are consistent with those of other studies that have highlighted high rates of predation.

Key findings:

Overall, this study has demonstrated that: although nutrients are generally low there are episodic events where high concentrations are present in the water (probably due to waves), that rates of productivity by benthic autotrophs are high and that production by the most dominant (in terms of biomass) species is heavily influenced by variations in light and temperature, that the identity and biomass of benthic invertebrates varies among habitats and that reefs (and to a lesser extent seagrass beds) support particularly high biomasses, that growth of a model suspension feeder was highest inshore, and that rates of grazing on macroalgae are low but that rates of filtration are predation are high.

Broad inferences to be derived from these key findings are that:

- **high benthic production is enhanced by favourable light and temperature conditions, coupled with occasional pulses of nutrients**
- **this production is not directly grazed but is exported to detritus**
- **this detritus is the main source of nutrition sustaining food webs, and filtration of small particles of detritus is likely a key pathway**
- **these processes do not occur evenly across Marmion Lagoon, but are concentrated in particular areas and habitats.**

3.1.16 References

Agusti S, Enriquez S, Frostchristensen H, Sandjensen K, Duarte CM (1994) Light-harvesting among photosynthetic organisms. Functional Ecology 8:273-279

Anderson MJ (2001) A new method for non-parametric multivariate analysis of variance. Austral Ecology 26:32-46

Anderson MJ (2005) PERMANOVA: a FORTRAN computer program for permutational multivariate analysis of variance.

Armstrong FAJ (1951) The determination of silicate in sea water. . Journal of the Marine Biological Association of the United Kingdom 30:149–160

Arnold KE, Murray SN (1980) Relationships between irradiance and photosynthesis for marine benthic green-algae (chlorophyta) of differing morphologies. Journal of Experimental Marine Biology and Ecology 43:183-192

Clarke KR (1993) Non-parametric multivariate analyses of changes in community structure. . Australian Journal of Ecology 18:117–143

Colijn F, Vanbuurt G (1975) Influence of light and temperature on photosynthetic rate of marine benthic diatoms. Marine Biology 31:209-214

Davison IR (1991) Environmental-effects on algal photosynthesis - temperature. Journal of Phycology 27:2-8

Enriquez S, Agusti S, Duarte CM (1994) Light-absorption by marine macrophytes. Oecologia 98:121-129

Fairhead VA, Cheshire AC (2004) Rates of primary productivity and growth in Ecklonia radiata measured at different depths, over an annual cycle, at West Island, South Australia. Marine Biology 145:41-50

Graham MH, Edwards MS (2001) Statistical significance versus fit: estimating the importance of individual factors in ecological analysis of variance. Oikos 93:505-513

Hatcher A (1989) Variation in the components of benthic community structure in a coastal lagoon as a function of spatial scale. Aust J Mar Freshwater Res 40:79-96

Hein M, Pedersen MF, Sandjensen K (1995) Size-dependent nitrogen uptake in micro- and macroalgae. Marine Ecology-Progress Series 118:247-253

Hentschel U, Usher KM, Taylor MW (2006) Marine sponges as microbial fermenters. . FEMS Microbiology and Ecology 55:167-177

Jiménez E, Ribes M (2007) Sponges as a source of dissolved inorganic nitrogen: Nitrification mediated by temperate sponges. Limnol Oceanogr 52:948-958

Johannes RE (1980) The ecological significance of the submarine discharge of groundwater. Marine Ecology-Progress Series 3:365-373

Johansson G, Snoeijs P (2002) Macroalgal photosynthetic responses to light in relation to thallus morphology and depth zonation. Marine Ecology Progress Series 244:63-72

Kerouel R, Aminot, A. (1997) Fluorometric determination of ammonia in sea and estuarine waters by direct segmented flow analysis. Marine Chemistry 57:265–275

Kilar JA, Littler MM, Littler DS (1989) Functional-morphological relationships in sargassum-polyceratium (phaeophyta) - phenotypic and ontogenetic variability in apparent photosynthesis and dark respiration. Journal of Phycology 25:713-720

Kirkman H (1981) The 1st year in the life-history and the survival of the juvenile marine macrophyte, *Ecklonia-radiata* (C.Ag.) J. Agardh *a*. Journal of Experimental Marine Biology and Ecology 55:243-254

Kirkman H (1984) Standing stock and production of *Ecklonia radiata* (C.Ag.) J. Agardh. Journal of Experimental Marine Biology and Ecology 76:119-130

Koslow JA, Pesant S, Feng M, Pearce AF, Fearns P, Moore T, Matear R, Waite AM (2008) The effect of the Leeuwin Current on phytoplankton biomass and production off Southwestern Australia. Journal of Geophysical Research 113

Lemmens SJ, Kirkpatrick D., Thompson P (1996) The clearance rate of four asidians from Marmion Lagoon, Western Australia. In Seagrass Biology: Proceedings of an International Workshop, Rottnest Island, Western Australia, , Rottnest Island, Western Australia, , p 277-282

Littler MM, Keith EA (1982) Primary productivity of marine macroalgal functional-form groups from southwestern north america¹ Journal of Phycology, p 307-311

Littler MM (1980) Morphological form and photosynthetic performances of marine macroalgae - tests of a functional-form hypothesis. Botanica Marina 23:161-165

Lourey MJ, Dunn JR, Waring J (2006) A mixed-layer nutrient climatology of Leeuwin Current and Western Australian shelf waters: Seasonal nutrient dynamics and biomass. Journal of Marine Systems 59:25-51

Lourey MJ, Kirkman H (2009) Short-lived dissolved nitrate pulses in a shallow Western Australian coastal lagoon. Marine and Freshwater Research 60:1068-1080

Mann EH, Kirkman H (1981) Biomass method for measuring productivity of Ecklonia radiata, with the potential for adaptation to other large brown algae. Australian Journal of Marine and Freshwater Research 32:297-304

Middelboe AL, Sand-Jensen K, Binzer T (2006) Highly predictable photosynthetic production in natural macroalgal communities from incoming and absorbed light. Oecologia 150:464-476

Nielsen SL, Sandjensen K (1990) Allometric scaling of maximal photosynthetic growth-rate to surface volume ratio. Limnology and Oceanography 35:177-181

Peckol P, Ramus J (1988) Abundances and physiological-properties of deep-water seaweeds from carolina outer continental-shelf. Journal of Experimental Marine Biology and Ecology 115:25-39

Platt T, Gallegos CL, Harrison WG (1980) Photoinhibition of photosynthesis in natural assemblages of marine-phytoplankton. J Mar Res 38:687-701

Ribes M, Coma, R.. Atkinson, M. J and Kinzie III., R. A (2005) The role of sponges and ascidians in removal of picoplankton from coral reef water. Limnol Oceanogr 50:1480–1489

Rosenberg G, Ramus J (1984) Uptake of inorganic nitrogen and seaweed surface-area - volume ratios. Aquatic Botany 19:65-72

Sandjensen K (1989) Environmental variables and their effect on photosynthesis of aquatic plant-communities. Aquatic Botany 34:5-25

Sandjensen K, Revsbech NP, Jorgensen BB (1985) Microprofiles of oxygen in epiphyte communities on submerged macrophytes. Marine Biology 89:55-62

Strickland JDH, Parsons TR (1972) A Practical Handbook of Sea-Water Analysis. Fisheries Research Board of Canada, Ottawa

Taylor RB, Peek JTA, Rees TAV (1998) Scaling of ammonium uptake by seaweeds to surface area : volume ratio: geographical variation and the role of uptake by passive diffusion. Marine Ecology-Progress Series 169:143-148

Thompson P, Waite A (2003) Phytoplankton responses to wastewater discharges at two sites in Western Australia. Marine and Freshwater Research 54:721-735

Vanderklift MA, Lavery PS, Waddington KI (2009) Intensity of herbivory on kelp by fish and sea urchins differs between inshore and offshore reefs. Marine Ecology-Progress Series 376:203-211

Vanderklift MA, Wernberg T (2008) Detached kelps from distant sources are a food subsidy for sea urchins. Oecologia

Warwick RM, Clarke KR (1991) A comparison of some methods of analysing changes in benthic community structure. Journal of the Marine Biological Association of the UK 71:225–244

Webb WL, Newton M, Starr D (1974) Carbon-dioxide exchange of alnus-rubra - mathematical-model. Oecologia 17:281-291

Weisz JB, Lindquist N, Martens CS (2008) Do associated microbial abundances impact demosponge pumping rates and tissue densities? Oecologia 155:367-376

Winer BJ, Brown DR, Michels KM (1991) Statistical principles in experimental design. McGraw-Hill Inc.

Yahel G, Marie D, Genin A (2005) InEx—a direct in situ method to measure Filtration rates, nutrition, and metabolism of active suspension feeders. Limnol Oceanogr Methods 3:46–58

3.2 Continental Shelf Pelagic Ecosystem Biology

Peter Thompson, Martin Lourey, Joanna Strzelecki, Karen Wild-Allen and James McLaughlin

CSIRO Marine and Atmospheric Research

3.2.1 General Introduction to the pelagic ecology of Western Australia

Research to understand the physical, chemical and ecological functioning of the Indian Ocean has lagged far behind the other oceans of world. In general this lack of understanding did not constrain early exploitation of our marine resources with unregulated harvesting of many species occurring throughout the southern hemisphere. In the colony of Western Australia targeted species included flat oysters and whales. By the first half of 20th century the Commonwealth Government had established the CSIR which dominated early Australian fisheries research and management with a focus on identifying Australia's fisheries resources (Thompson 1939). Shortly after WWII there was an expanding group of CSIRO scientists in Australia investigating the new field of "fisheries oceanography" and this effort included large scale surveys around the continent. While the focus of this research was still the identification of fisheries resources (e.g. Thompson 1951, Tranter 1957) the range of new disciplines included physical, chemical and biological oceanographers.

During the late 1950s and 1960s CSIRO's research in Western Australia was primarily upon the western rock lobster using the recommission RAN frigate HMAS *Diamantina*. In conjunction with the WA Department of Fisheries (formerly 'and Fauna') this provided the initial understanding and methods to manage Australia's most valuable, single-species, fishery. Western Australia rock lobster are about 20% of the total value of Australia's fisheries (~AUS$400 million) and exported to markets including Taiwan, Japan, Hong Kong, China, USA. Eight species of rock lobster are found off the WA coast, however, virtually the entire commercial catch consists of the western rock lobster *Panulirus cygnus*. Similar to most exploited fisheries globally the landings of western rock lobster appear to have peaked late last century. By the beginning of the 21st century there were management plans for ~ 35 harvested species in Western Australia ranging from, for example, oysters (crustaceans) to sharks (elasmobranches) and Dhufish (teleost fishes) and a total catch of ~ 23,000 tonnes. As in most of the world, most commercially harvested species in WA are now fully exploited. It has become a significant challenge that is undertaken by the Western Australian Government's Department of Fisheries to manage these resources in an ecologically sustainable manner. The challenge has grown as both commercial and recreational fishers use increasingly sophisticated technologies (boats, motors, depth sounders, global positioning systems, fish locators [echo sounders or active sonar]) that have dramatically increased their harvest per unit effort (person or boat).

As our exploitation of marine resources has increased it has become very clear that understanding the underlying processes that allow fish to grow and reproduce is necessary if they are to be managed in an ecologically sustainable manner. For Western Australia the early efforts included a substantial contribution by CSIRO as part of the International Indian Ocean Expedition to sample along the 110°E meridion. These studies provided the first scientific investigations of ecosystem functioning in the eastern Indian Ocean. Pioneering studies by Wyrtki (1962) Rochford (1952, 1962, 1969), Jitts (1969), Tranter (1973) Wood

(1964) put Australia, and the eastern Indian Ocean, on the map providing early benchmarks for Australian's commitment to ecosystem understanding in an oceanographic context. By the 1970s the anomalous nature of Australia's west coast was known: a productive coast with no upwelling or obvious source of nutrients to fuel that productivity (Austin 1973).

Since the 1960s new technologies including satellite oceanography, computers and mathematical modelling have brought profound new insights into oceanography including the description of the Leeuwin Current (Creswell and Golding 1980, Thompson 1984, 1987). While the available fisheries resources may have peaked powerful methodological and technological advances have continued to provide increasing capability to observe our oceans. Combined with greater access to the CSIRO's research vessels SS *Franklin* and *Southern Surveyor* funded by the Marine National Facility and increased support for marine science in Western Australia through SRFME and WAMSI there has been dramatically more oceanographic research undertaken along the west coast of Australia since 2000. Physical oceanography has been extensively studied by Pattiaratchi and students (e.g. Woo and Pattiaratchi, 2008) while sophisticated modelling has revolutionised our understanding of large scale circulation (Schiller et al. 2008). Satellites have made it possible to detect mesocale features such as Leeuwin Current meanders and eddies providing daily updates to oceanographers on ships to hunt them down and study the impacts of these phenomena (e.g. Waite et al. 2007). We now know that a great deal of the inter annual variation in primary production (Thompson et al. 2009) and fisheries harvest (Caputi 2008) is dependent upon our connection with the global phenomenon, the Southern Oscillation (El Nino/La Nina) and its effects on the behaviour of the Leeuwin Current. For example, one Leeuwin Current eddy can drag 60,000 tonnes of phytoplankton offshore (Feng et al. 2007) and eddies are much more abundant during La Nina years. The time series of observations on the west coast at Rottnest Island, reinvigorated under Australia's new Integrate Marine Observing System (IMOS), have provided unique insights into how our marine environment is changing over decades (Thompson et al. 2009). Finally the discovery that the Leeuwin Current carries thin layers of high nitrate water south to fuel the annual bloom along the continental shelf of WA provides the answer to the question first identified 40 years ago by the early pioneers of oceanography on this coast (Thompson et al. 2011). This and other highlights of CSIRO's contributions through WAMSI to our understanding of pelagic ecology of Western Australia are presented in the following chapter.

3.2.2 Introduction to WAMSI Node 1 research on the Continental Shelf Pelagic Ecosystem Biology

Generally the productivity of marine ecosystems is nitrogen limited (Smith 1984) and the central gyre of the Indian Ocean from 5 to 45°S is amongst the world's most nutrient limited or, oligotrophic, regions (Polovina et al. 2008). Based upon extensive sampling it is known that the availability of nitrogen along the west coast of Australia is extremely limited (Condie and Dunn 2006, Lourey et al. 2006) much more nitrogen limited than equivalent latitudes along the east coast of Australia (Thompson et al. 2010). Therefore the processes that supply nitrogen to this ecosystem are fundamentally important to our understanding of the ecosystem and its capacity to reliably supply natural resources that can be harvested. Indeed many of the fishery resources along the west coast of Australia undergo significant inter annual variation in abundance (Caputi 2008, Caputi et al. 2001). These variations often have positive, or negative, associations with climate variability (e.g. Southern Oscillation Index, SOI) or Leeuwin Current strength depending upon location and taxa. In addition the base of the food chain, the phytoplankton, are more abundant during positive SOI, strong Leeuwin Current and La Nina years along the southern half of the west coast from 27 to 31°S (Thompson et al.

2010, Figure 3.111). The links between SOI, Leeuwin Current, the variation in primary production and its impacts on higher trophic levels resulting in changes in the recruitment of rock lobster and other fisheries in West Australia seem clear but understanding the mechanism is pivotal for successful long term management.

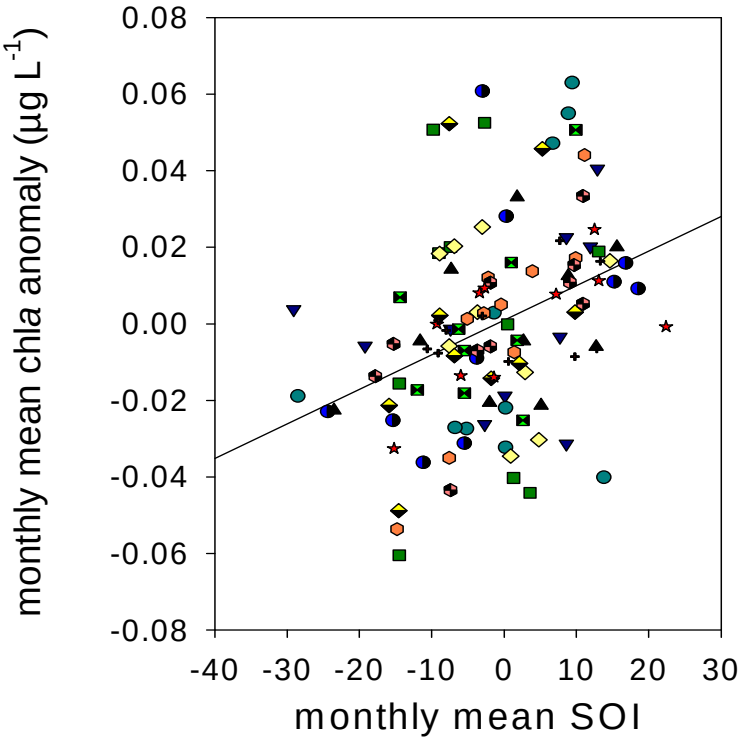

Figure 3.111. Increased phytoplankton measured as the chlorophyll *a* anomaly (= chlorophyll *a* deviations from mean concentration estimated from SeaWiFS NASA GIOVANNI over the period from Sept 1997 to Sept 2007) plotted against the monthly Southern Oscillation Index (SOI).

One of the most distinctive features of the eastern Indian Ocean along the west coast of Australia is the midwinter peak in phytoplankton biomass that spans more than 15° of latitude and extends from the coast to several hundred km offshore (Moore et al. 2007).The source of nutrients to support this primary production has been the subject of considerable investigation resulting in a number of different hypotheses on the source(s) of nitrogen (Feng et al. 2009). These include transport (Koslow et al. 2008) in the Leeuwin Current (LC), a coastal source (Dietz et al. 2009), upwelling (Hanson et al. 2005), deep mixing associated with eddy formation (Waite et al. 2007), or seasonal cooling that results in deepening of the seasonal thermocline and the entrainment of more nitrate into the euphotic zone (Koslow et al. 2008).

In spite of the strong associations between the magnitude of the annual west coast bloom, the strength of the Southern Oscillation Index (Thompson et al. 2009) and the strength of the Leeuwin Current (Feng et al. 2003) the lack of a defined process that links these phenomena makes it impossible to model and predict future variation. The mechanism(s) that supplies nitrogen to the euphotic zone needed to be found (Feng et al. 2010).

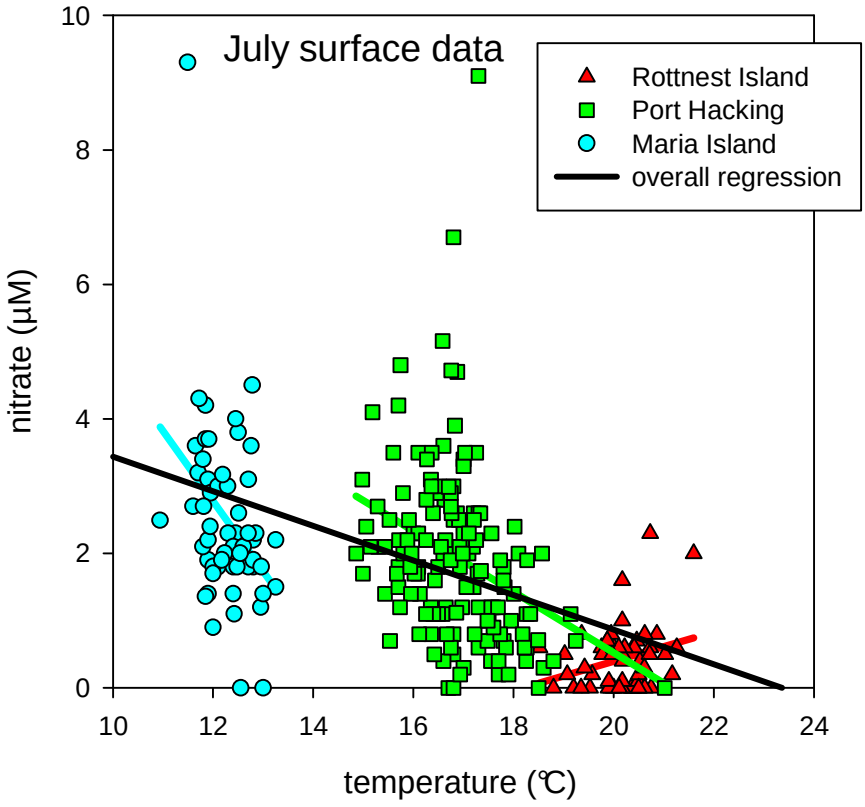

Figure 3.112. The relationship between water temperature and nitrate concentration for three locations around Australia (adapted from Thompson et al. 2009).

Several of the hypothesised mechanisms that could explain the annual resupply of nitrogen to the euphotic zone (as above) involved mixing deep water from below the thermocline towards the surface. As this is the dominant mechanism resupplying nitrogen to the euphotic zone in the global ocean it would not be surprising for it to be important along the west coast of Australia. Because those deep waters are universally colder than the surface this process almost always results in a negative relationship between temperature and winter nitrate (Kamakowski et al. 2002). Indeed such negative relationships are found off Port Hacking (NSW) and Maria Island (Tasmania) but not at Rottnest (Thompson et al. 2009, Figure 3.112). Most unusually the winter maxima in nitrate concentrations measured at Rottnest Island since 1951 showed a positive association with water temperature. Based on this positive relationship between winter water temperature and nitrate the following hypotheses: upwelling (Hanson et al. 2005), deep mixing associated with eddy formation (Waite et al. 2007), or seasonal cooling that results in deepening of the seasonal thermocline and the entrainment of more nitrate into the euphotic zone (Koslow et al. 2008); are not likely to explain the source of nutrients that supports the annual winter bloom.

In 2007 WAMSI, CSIRO. UWA, Murdoch University and the Marine National Facility supported a research cruise along the entire west coast of Australia. One of the goals of this cruise was to investigate possible sources of nitrogen to support the annual winter phytoplankton bloom. The cruise occurred in May and June, during the time when the bloom would normally be reaching its greatest biomass. Using a range of techniques to investigate physical structure including mixing combined with high density of nutrient sampling and a

new spectrophotometric technology for nitrate detection (Johnson and Coletti 2002) the potential sources of nutrients were investigated.

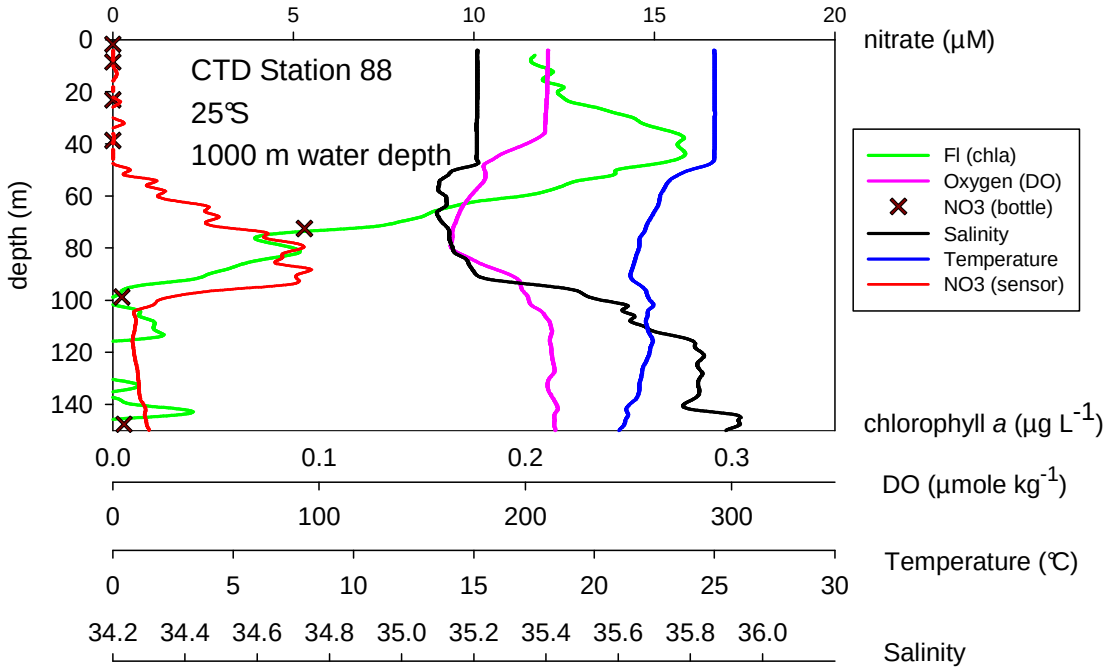

Figure 3.113. CTD profiles at 25°S (stn 88) where a narrow peak in nitrate and low DO from 50 to 100 m depth with warm Leeuwin Current water from 0 to 50 m that was high in fluorescence.

The results from the 2007 cruise showed the presence of thin layers of high nitrate water present at relatively shallow depths offshore at latitudes of 24 and 25°S. An example is shown for the offshore station at 25°S in 1000 m water depth where nitrate was measured conventionally from bottle samples (X) and continuously using a novel spectrophotometer. These thin, shallow layers were also markedly depleted of oxygen and the presence of low DO layers has been reported previously for this region (Woo and Pattiaratchi 2008). At these latitudes the high nitrate, low dissolved oxygen (HNLDO) layers existed immediately under the warm (~25°C) surface layer that is the signature of the Leeuwin Current (Figure 3.113). The surface layer of the Leeuwin Current also contained high chlorophyll *a*. At depths of 60 to 100 nitrate concentrations increased markedly reaching 5 (Figure 3.113) to 8 µM. These concentrations of nitrate represent about 60% of the nitrogen that would be produced by microbial processes consuming sufficient organic matter to produce the observed oxygen deficit. The recycling of organic matter to produce nitrate at these shallow depths is unusual and under further investigation.

As the Leeuwin Current progresses southward it carries this thin layer of low dissolved oxygen (Figure 3.114) and high nitrate at depths ~ 100 m. As the LC flows further south it cools and therefore entrains the thin layers of high nitrate water into the euphotic zone. The LC also forms large (greater than 100km diameter) warm core eddies with a deep mixed layer that also entrains nitrate from these thin layers. In some locations as far south as 32°S the LC was still present with the thin layer of high nitrate intact but now within the euphotic zone.

This formation would nicely explain the 60 year record of high nitrate and warmer water during winter.

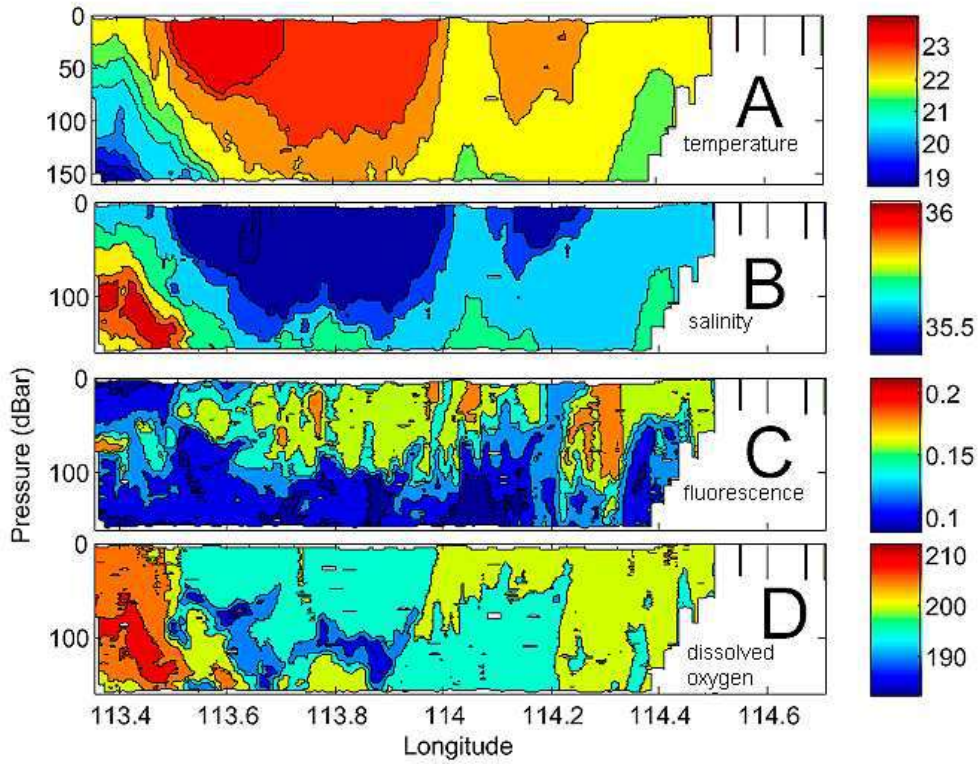

Figure 3.114. A section composed from hundreds of CTD profiles made by the Seasoar towed from inshore at 30°S 114.6°E to offshore at 31°S 113.3 °E during the 2007 SS voyage. Top panel shows vertical profiles of chlorophyll a, dissolved oxygen, nitrate (bottle samples X), nitrate by sensor, temperature and salinity. The salient feature is the high nitrate layer at ~ 80 coinciding with the low in dissolved oxygen. Bottom panels show high resolution sections across the Leeuwin Current for temperature, salinity, fluorescence (chlorophyll a) and dissolved oxygen.

Thus the available evidence suggests the LC arises in a region with widespread and shallow organic matter respiration (oxygen consumption) and nitrogen remineralisation through to nitrification. This nitrification appears to be sufficient to fuel a shelf scale bloom on an otherwise strongly downwelling favourable coast. Given expected rates of nitrification the source of the particular organic matter is probably not recent production but is likely to be produced elsewhere and remineralised while being delivered to the west coast of Australia. Based on reports of a similar thin layer of low DO at about 200m reported in the Indian Ocean from 0 to 25°S at 75°E (Wyrtki 1971, Warren 1981), by Rochford (1969) at 110°W and under the northern region of the LC by Woo and Pattiaratchi (2008) we produced a novel conceptual model for the supply of nitrogen to the west coast of Australia (Figure 3.115). In this conceptual model a subsurface, thin layer of low DO and high nitrate water is entrained into the base of the Leeuwin Current between the equator and 25°S. This layer is mixed into the euphotic zone at latitudes > 28°S. South of 28°S the layer was observed in one of three states: 1) mixed throughout a warm core eddy arising from the Leeuwin Current meander, 2) as a thin layer but within the euphotic zone (< 100 m deep) and 3) mixed to the surface in a portion of the Leeuwin Current.

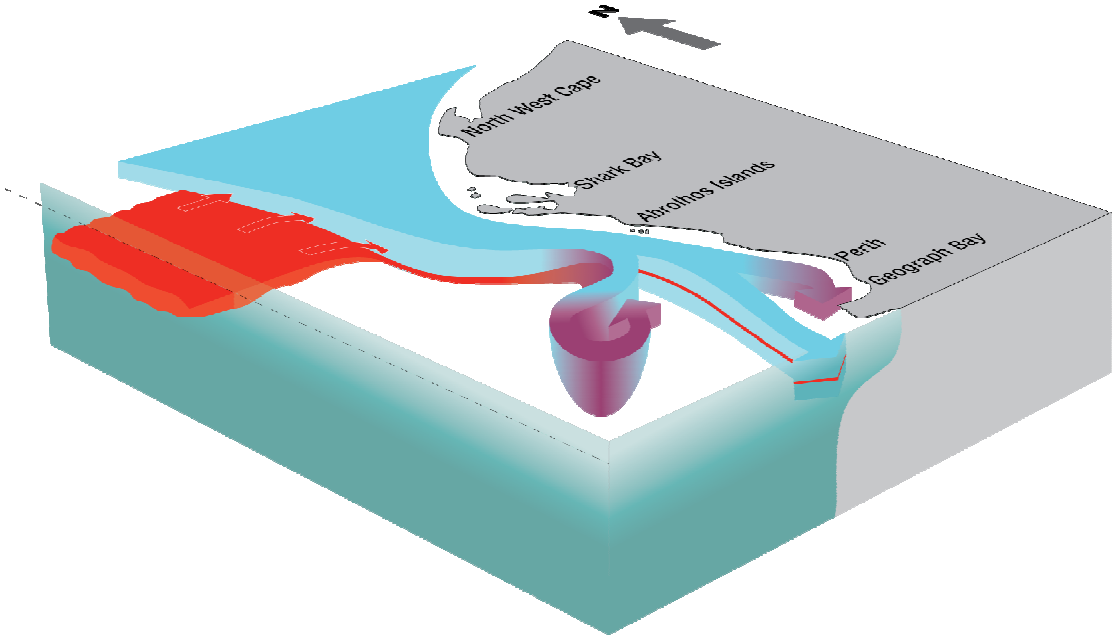

Figure 3.115. A conceptual model for the source of low dissolved oxygen and high nitrate being entrained into the Leeuwin Current during autumn. Red colour = nitrate, light blue = Leeuwin Current.

Key Findings:
The pelagic productivity of the west coast results from the interaction of the Leeuwin Current with shallow and thin layers of high nitrate water that are carried south.

3.2.3 Long term analysis of biological oceanography

In conjunction with colleagues in NSW we have analysed the long term records obtained from 4 coastal stations around Australia. The comparison provides unexpected insights into regional differences in oceanography and long term change. There were significant differences in the magnitude and timing of seasonal dynamics in temperature, salinity, nutrients, chlorophyll *a* and stratification (Figure 3.116A-E). All coastal stations from around the country showed positive long term (> 10 year) trends in temperature, salinity, nitrate, and phosphate concentrations (Table 3.32). All stations showed a long term increase in depth-averaged salinity of ~ 0.003 ± 0.0008 y^{-1}. The fastest warming was observed in the western Tasman Sea; where it averaged 0.0202°C y^{-1} over more than 60 years. Warming trends were not intra-annually uniform with some months showing strong long term trends while there was no evidence of any warming in midwinter (July) at any of the coastal stations.

A pronounced decline in the concentration of silicate was evident at the 3 east coast stations with depth-averaged concentrations falling by as much as 0.058 µM y^{-1} over the last ~ 30 y. A large region of the ocean off the southern west coast had positive chlorophyll *a* anomalies strongly associated with La Nina conditions (Figure 3.111). Although the phytoplankton data sets were much less comprehensive in terms of spatial coverage; diatoms tended to dominate near these coastal stations. This was especially true during periods of low stratification (winter). In conclusion, changes in ocean circulation associated with climate variability appear to have pronounced effects on temperate zone biological oceanography including some effects that were not readily generalised from existing conceptual models.

Rottnest Island

Surface nitrate concentrations at Rottnest Island tended to be variable with near zero values recorded in every month of the year (Figure 3.117A). In spite of the high temporal variability there was a significant seasonal trend and fitting the data to a Gaussian curve showed a significant (r^2 = 0.111, P < 0.0001, n = 462) rise to ~ 0.7 µM in June peaking at day 172 ± 4.8 (P < 0.001). Silicate concentrations showed less seasonal variation than nitrate (data not shown) and no inter annual trend (Table 3.32) or correlation with SOI (data not shown). Over the 31 years between 1971 and 2002, silicate concentrations over all depths from 0 to 50 m averaged 2.28 µM while the mean nitrate concentration (0 – 50 m) was 0.59 µM giving an average NO_3:Si molar ratio of 0.26 or about ¼ the ideal ratio for diatoms. The seasonal peak in surface nitrate was consistent with the minimum in stratification which also occurred in June. The seasonal dynamics of both nitrate concentration and stratification were extremely similar to those for chlorophyll *a* (Figure 3.114A, C) with a June maximum. Thus of the four coastal stations Rottnest Island was the station with the smallest temporal offset between the seasonal minimum in stratification and annual maximum in chlorophyll *a*. This temporal offset between the stratification minimum and the peak chlorophyll *a* concentration was ~ 4 months at Maria Island.

Over the period 1997 to 2007 the seasonal variation in chlorophyll *a* at Rottnest Island was well described by a Gaussian curve (r^2 = 0.743, P < 0.001) with a peak on day 185 ± 1.5. The annual anomalies in chlorophyll *a* were a positive linear function of the annual mean southern oscillation index (SOI) across most of the southern west coast of Australia (28° to 34° by 114°E to shore). For example, in the region from 31° - 33°S by 114°E to 115°E, annual chlorophyll *a* anomalies were correlated with SOI (P < 0.027). Mean monthly chlorophyll *a* anomalies were also significantly (P < 0.001) correlated with mean monthly SOI values. Positive SOI years (1999, 2000) showed greater than normal chlorophyll *a* during late summer and early autumn across 2 large areas 29 31°S [=S] and 31 to 33°S [=N] between 115 to 114°E (Figure 3.114C). Early 2001 was also SOI positive and showed greater than average chlorophyll *a* in the first half of the year. There are no long term records of phytoplankton at Rottnest Island but sampling has occurred ~ 25 km away at the mouth of the Swan River Estuary. This estuary is fully marine during late summer. Depth integrated, monthly mean $\log_{10}$ diatom abundance in February (weekly samples) showed a strong relationship (P = 0.034) with annual mean SOI (Figure 3.114D). Similarly weekly samples from January to April (n = 224) also showed a significant (P = 0.012) relationship between $\log_{10}$ diatom abundance and monthly mean SOI.

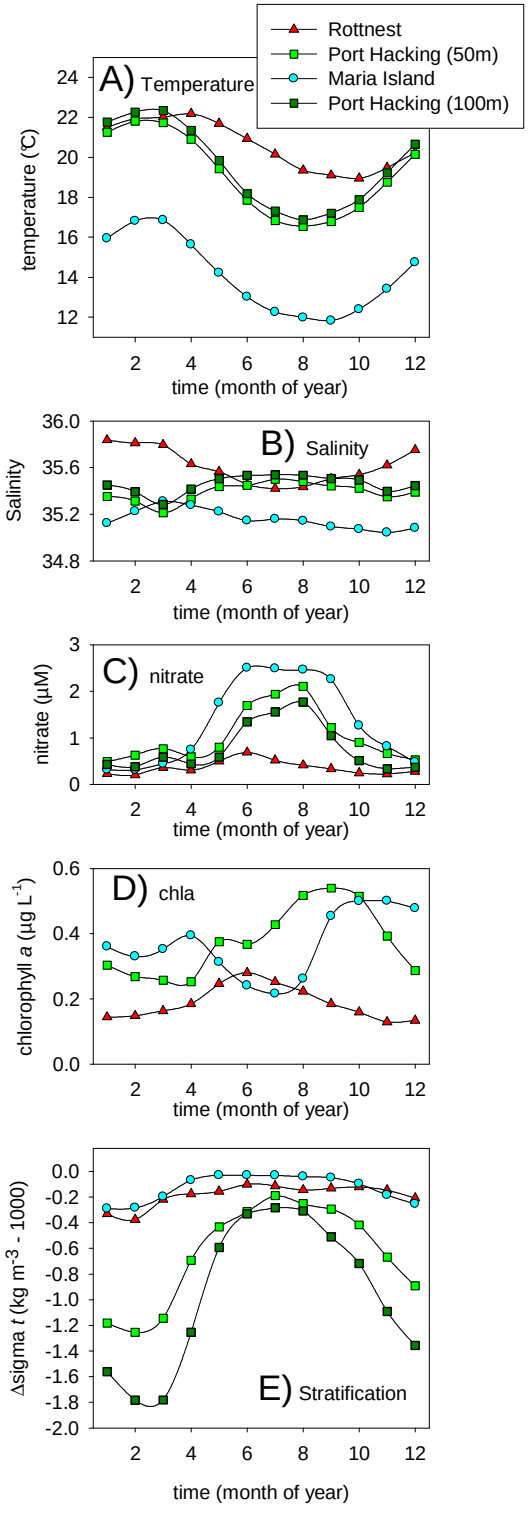

Figure 3.116. Monthly mean surface (A) temperature; (B) salinity; (C) dissolved nitrate, (D) chlorophyll *a* (E) stratification; from the Coastal Monitoring Stations around temperate Australia from ~1942 to 2007 (see Table 3.32 for sample details). Satellite-derived mean monthly chlorophyll *a* (F) between 1997 and 2007 from areas near each coastal station (adapted from Thompson et al. 2009).

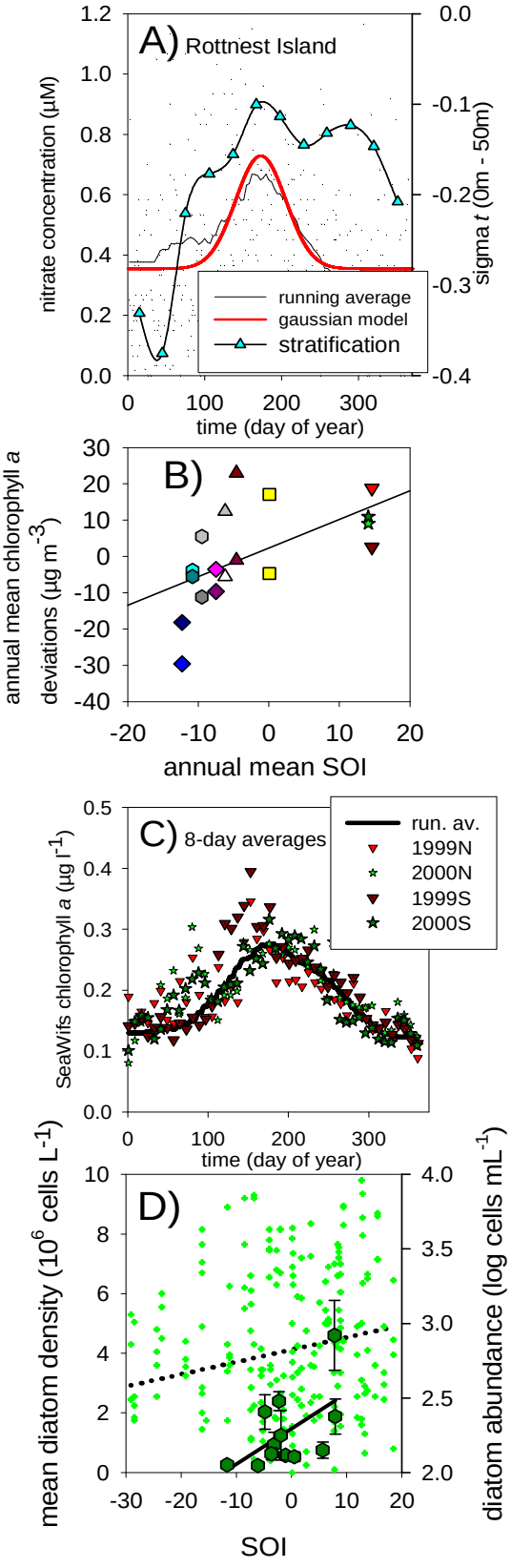

Figure 3.117. Rottnest Island sampled at 0, 10, 20, 30, 40, 50 m approximately monthly from 1951-2001 (see Table 3.32 for details). A) Nitrate concentrations (small symbols), running mean (solid black line), Gaussian model fit to data (thin red line). (▲) Mean monthly stratification (=density at the surface minus density at 50m (Δσt50 = sigma t @0 – sigma t @50 m). B) Chlorophyll *a* deviations from mean concentration estimated from SeaWiFS NASA GIOVANNI over the period from Sept 1997 to Sept 2007 plotted against the Southern Oscillation Index (SOI). Solid line is regression (P = 0.027), C) SeaWiFS chlorophyll *a* data for La Niña years; solid line = 1997 to 2007 long term running mean; D) diatom abundance at nearby site versus SOI. Large symbols are monthly mean diatom cell density (left X axis) for weekly observations from February in each year (1994 to 2007), error bars are standard deviations, solid line is regression (P = 0.034). Small symbols are weekly samples (right X axis) for January to April from 1994 to 2007, dotted line is regression (P = 0.012). Modfied from Thompson et al. 2009.

Table 3.32. Long term (> 10 y) linear trends in surface parameters after seasonally detrending by removing monthly means. (Probabilities for all trends < 0.001 except nitrate where P < 0.008). Blank cells indicate non-significant result. Modifed from Thompson et al. 2009.

	Maria Island	Port Hacking (100 m)	Port Hacking (50 m)	Rottnest Island
Location	43.3°S 147.1°E	34.1°E 151.3°S	34.1°E 151.2°S	32.1°S 115.8°E
Span (years analysed)	1944-2005	1953-2005	1944-2004	1969-2001
Maximum total # observations*	3273	9263	9882	2736
Temperature (°C/century)	2.02		0.744	1.23
Salinity (psu/century)	0.346	0.232	0.269	0.407
Nitrate (μM/century)		0.556		0.400
Phosphate (μM/century)	0.530		0.611	0.313
Silicate (μM/century)	-5.84	-1.97	-2.30	
dissolved oxygen (μM/century)			-12.9	-49.1

* for any parameter

More details of this research including a full comparison with other locations around Australia can be found in Thompson, PA , Baird, ME, Ingleton, T, Doblin, MA. 2009 Long-term changes in temperate Australian coastal waters and implications for phytoplankton. Marine Ecology Progress Series 384: 1-19.)

Key findings:
Significant seasonal, interannual and long term changes in the marine environment have been observed near Rottnest Island over the last ~ 40 years including a warming trend of 1.23°C century^{-1} and a rise in salinity of ~ 0.41 parts per thousand century^{-1}.

3.2.4 Shelf scale observations

The WAMSI Program, CSIRO, the Marine National Facility, UWA, WA Museum and Murdoch University supported the 2007 cruise along the west coast of Australia. The cruise was hugely successful and we were fortunate enough to complete all the cruise objectives. The timing of the cruise was perfect, the Leeuwin Current was running very strongly and the entire continental shelf was experiencing a very large phytoplankton bloom. A brief summary of the voyage and several more detailed examples of the research undertaken are provided through out this chapter.

The first leg of the voyage included a sampling regime designed to characterise benthic habitats and measure benthic biomass and primary productivity and sediment nutrient fluxes across the shelf between 30 and 150 m depths. Sampling across the domain shown in Figure 3.118 below included swath mapping, towed video, benthic sleds, sediment grabs and cores and CTD

profiles. Detail from the first leg of the voyage relating to benthic work is included in Chapter 2.

The Scientific Objectives for the 2nd and 3rd legs of the voyage relate to factors regulating the seasonal plankton cycle and it's inter annual variability, which remain poorly understood in this region. One of its most interesting features is the ~ ten-fold increase in chlorophyll, which coincides with the seasonal intensification of Leeuwin Current flow. Research conducted during the voyage was designed to examine:

1. the regional extent of this bloom;
2. the key drivers for primary production including:
    a. stratification;
    b. depth of the mixed layer;
    c. the influence of Leeuwin eddy dynamics;
    d. local wind-driven upwelling;
    e. alongshore and cross-shelf advection;
3. the plankton food web structure during the bloom including;
    a. the relative importance of picoplankton and larger phytoplankton;
    b. micro- and meso-zooplankton; and
    c. links with larval and juvenile fish in relation to onshore-offshore and north-south oceanographic features.

If a suitable eddy had formed off the west coast between May 15th and May 20th we proposed to spend 1-3 days mapping the features of the eddy and sampling it. We were fortunate to encounter a large eddy forming at ~ 31°S. We took the opportunity to sample across the eddy providing additional data for comparison with eddies studied in 2003 and 2006. The data collected will be extensively used in David Holliday's PhD thesis.

The voyage plan was based on 13 CTD onshore-offshore transects undertaken every degree of latitude from Northwest Cape (22º S) to Capes Naturaliste and Leeuwin (34º S). Each transect extended from as near shore as is practicable (25 – 30 m depth) to 2000 m depth (Figure 3.118). Stations were undertaken at 25 (inshore), 50, 75, 100 (mid-shelf), 200 (shelf-break), 300, ~500 (Leeuwin core), 750, 1000, and 2000 (offshore) m water depths.

Each transect leg had a complimentary seasoar return leg to giving very high resolution vertical and horizontal X-sections of temperature, salinity and fluorescence. These have provided the best physical description of the Leeuwin Current ever obtained. They were also used to locate a station in the middle of the Leeuwin Current on each subsequent CTD transect. The SeaSoar mapping combined with current satellite images enabled us to place the 'Leeuwin' station within the core of the Leeuwin Current on each transect. CTD profiles were carried out at all stations to measure temperature, salinity, dissolved oxygen, PAR, and chlorophyll fluorescence. Water samples were taken at standard depths to measure salinity and nutrients (nitrate/nitrite, ammonia, dissolved organic nitrogen, particulate nitrogen, phosphate, silicate). Full biological sampling was carried out at the inshore (25 m), Leeuwin Current (200 - 500 m) stations, and offshore (2000 m), incorporating: replicate oblique bongo tows to 150 m maximum; the light profile to 50 m using a hyperspectral radiometer; water samples for phytoplankton pigment (HPLC) analysis and species composition from near-surface and chlorophyll maximum depths; measurement of size-fractionated primary productivity (^{14}C incubation method and PAM measurements from standard sampling depths); nitrogen uptake from labelled nitrate, ammonia, and N_2; sampling of stable C and N isotopes in the size-fractionated phytoplankton and in selected zooplankton and ichthyoplankton species to examine food web pathways;

microzooplankton grazing based on the dilution method total alkalinity & DIC (to assess pH); and secondary production estimates based on egg production and a biochemical (aminoacyl-tRNA synthetase (Yebra and Hernandez-Leon, 2004)) assay. Zooplankton acoustic backscatter (using the 6-frequency Trachor Acoustic Profiling System, TAPS) was measured through the water column to a depth of 200 m. Net tows for zooplankton were split, with part retained in ethyl alcohol to examine selected larval fish otoliths for growth to be related to oceanographic conditions. Neuston sampling was also carried out at each production station. The voyage track is shown in Figure 3.118.

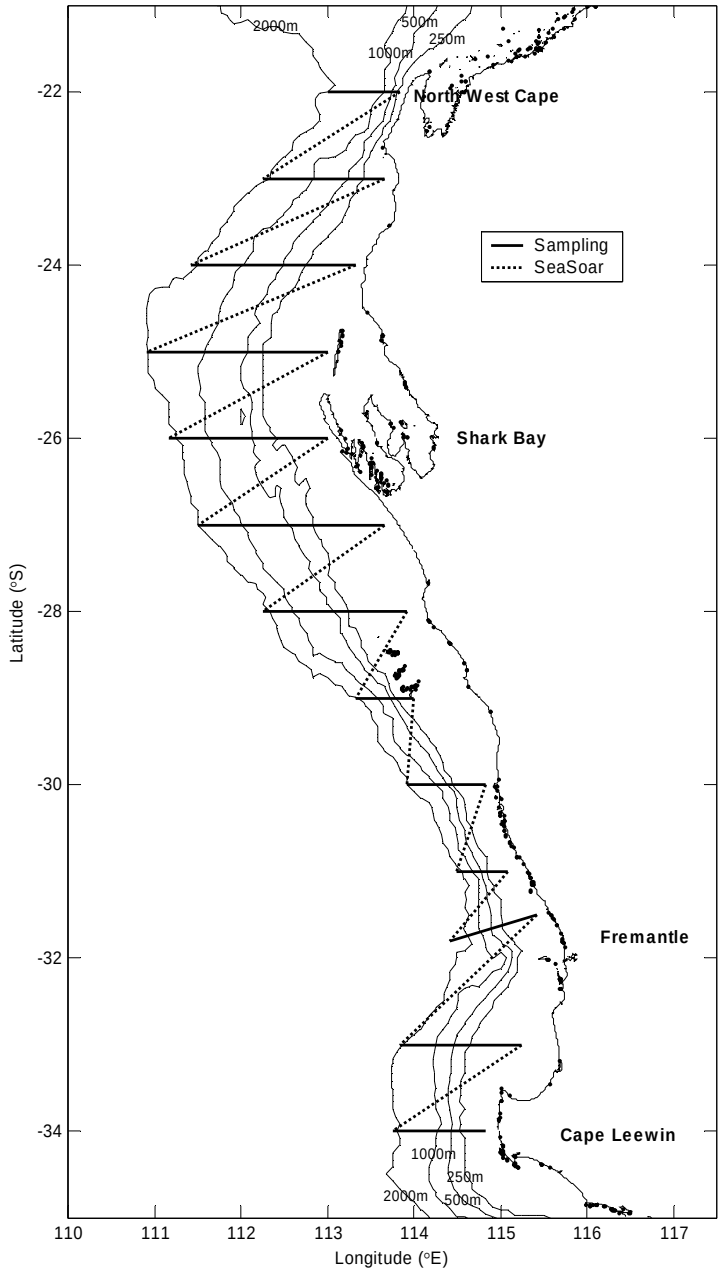

Figure 3.118. Southern Surveyor voyage track from the May/June "autumn bloom" SS04/2007 cruise.

Mesozooplankton sampling during the Southern Surveyor cruise included collecting replicate Bongo tows using 355 and 100 μm mesh nets at 25, 50, 100, 300 and 100 m stations to 150 m

depth for species composition and biomass on the 13 transects. Sampling was conducted during both the day and night. Grazing experiments to quantify mesozooplankton grazing on microzooplankton and phytoplankton were conducted at 4 transects (once at every geographic region) at 3 stations situated nearshore of Leeuwin Current, in Leeuwin Current and offshore of Leeuwin Current. Secondary production samples for Aminoacyl-tRNA synthetases (AARS) activity were collected. Female copepods were collected to measure the DNA/RNA ratio. The mesozooplankton portion of the project involves collaboration with AIMS where Felipe Gusmao is testing new techniques of estimating secondary production of zooplankton. In addition standard techniques of estimating secondary production: egg production and artificial cohort incubation will be run at 3 stations on all transects. A total of 23 CSIRO scientists and support staff were involved in the cruise plus others from a range of institutions.

Much of the data collected during the research voyage has been fully processed since the voyage was completed and is currently undergoing interpretation. Examples include CTD data (available in August 2007) and ADCP data (available in December 2007). In some cases samples are still undergoing analysis (e.g. stable isotopes). Some samples have been analyzed but are still undergoing quality control checks (e.g. nutrients). As a consequence of the variable status of the data from this cruise different components of the interpretation are at different stages. Several examples of the cruise outputs are presented below. These are only representative, sometimes only partly completed and are meant to be indicative. A symposium based on the early results from the cruise was conducted in February 2008.

3.2.5 Nutrients

New in-situ observations of nitrate with very high vertical resolution have been obtained during the SS04/2007 cruise. For the first time in Australia an in-situ profiling underwater spectrophotometer was deployed with the capability to resolve nitrate concentrations at 2 m depth resolution. The preliminary calibration shows significant sub-bottle scale structure in nitrate profiles consistent with temperature and salinity structure, particularly in the vicinity of the Leeuwin Current fronts and mesoscale eddies (e.g. Figure 3.119 shows examples of this nitrate data).

Full calibration of the instrument has been completed.

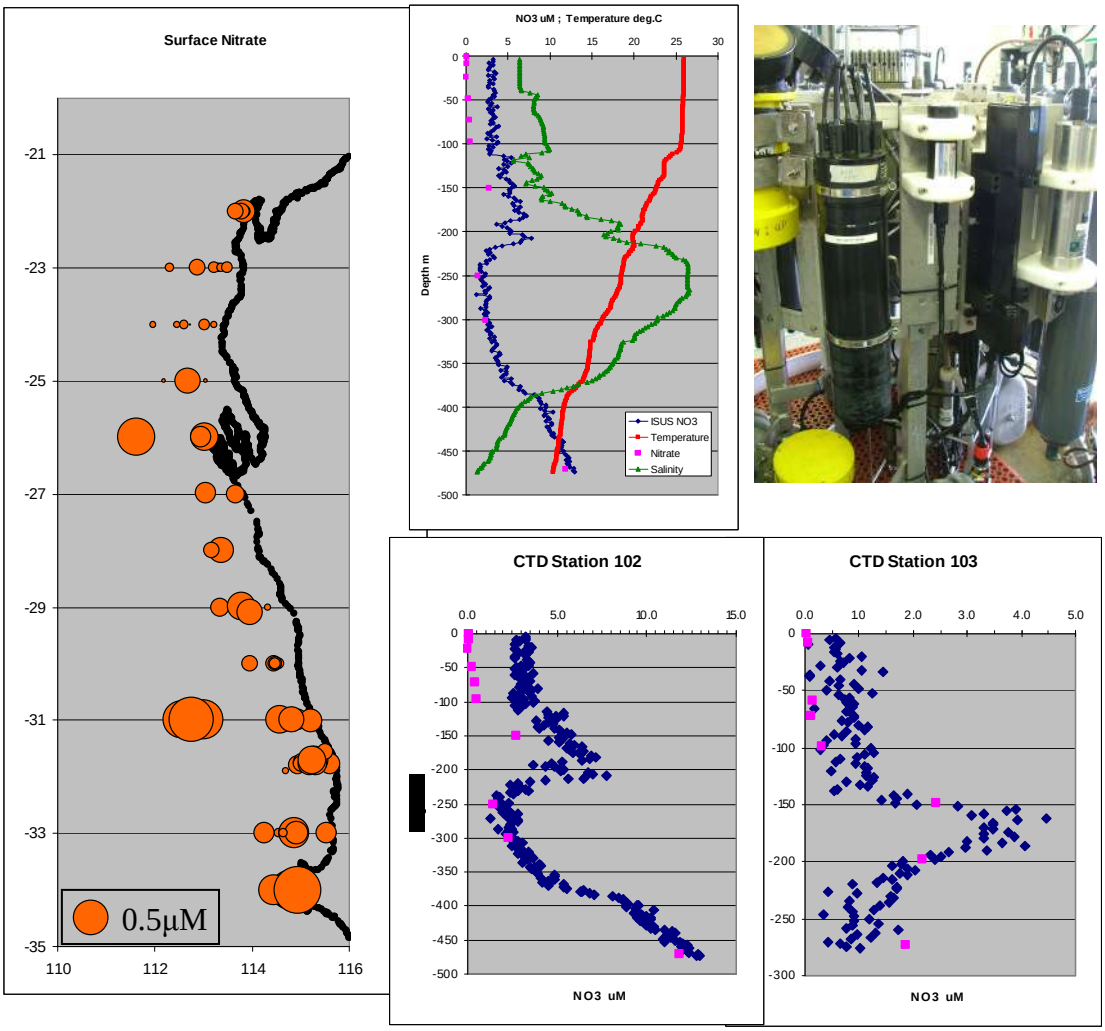

Figure 3.119. Example nitrate data from the SS042007 cruise. Preliminary in-situ nitrate sensor (SAtlantic ISUS) calibration suggests significant spatial and sub-bottle scale variation in nitrate concentration.

The analysis of nutrients from the 2007 cruise has revealed some very important aspects of the nutrient supply to the west coast of Australia. Nitrate was the most abundant dissolved inorganic N species with an average concentration over all depths (0 to 2000m) of 3.0 µM followed by 0.15 µM for ammonium and 0.08 µM for nitrite. Over the entire cruise, but restricted to the euphotic zone (defined here as 0 to 100m), the average ± SD nitrate (NO_3), silicate ($Si(OH)_4$) and phosphate (PO_4) concentrations were 0.26 ± 0.46 (n = 550), 2.42 ± 0.71 (n = 531) and 0.076 ± 0.046 µM (n = 536), respectively.

Nutrient concentrations tended to covary with depth and with each other; NO_3, $Si(OH)_4$ and PO_4 reaching greater than 30, 100 and 2 µM, respectively, at 1000 m (Figure 3.120). The relative availability of dissolved macronutrients deviated significantly from the Redfield (1963) ratios of 16:16:1 (N:Si:P) required by phytoplankton. The excess of $Si(OH)_4$ over NO_3 was considerable, and over all depths, only 11% of samples had N:Si ratios greater than Redfield (greater than 1) while 63% of all measurements were < 0.1 or less than Redfield by a factor of 10. In the case of PO_4 the excess relative to NO_3 was still extreme, albeit differently distributed. Only 0.6% of all measurements exceeded Redfield (N:P greater than 16) while 34% of all measurements were 10 times less than Redfield.

The average euphotic zone nitrate concentration (0.26 µM) and ratios for dissolved inorganic NO_3:$Si(OH)_4$:PO_4 of ~ 3:30:1 suggest the likelihood of extreme N limitation with both Si and P available to phytoplankton in relative excess. This conclusion is in keeping with previous analyses the west coast of Australia (e.g. Condie and Dunn 2006, Lourey et al. 2006).

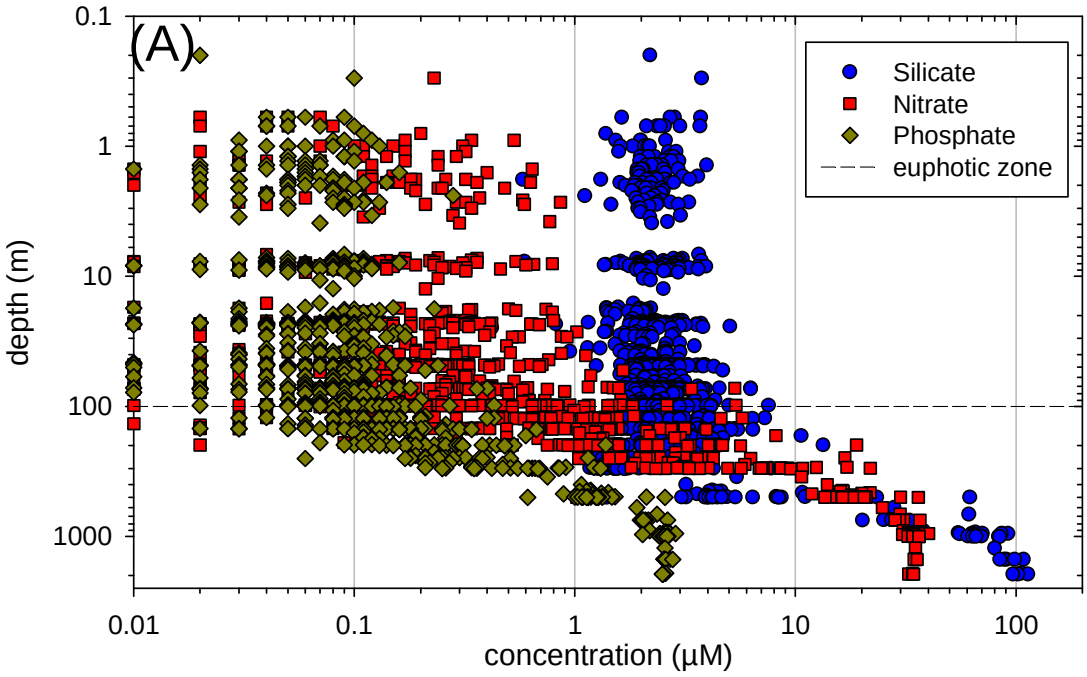

Figure 3.120. All nutrient concentrations from the entire SS03/2007 cruise over all depths from the surface to 2000 m with just 20 nitrate concentrations above 100m ≥1 µM (modified from Thompson et al. 2011).

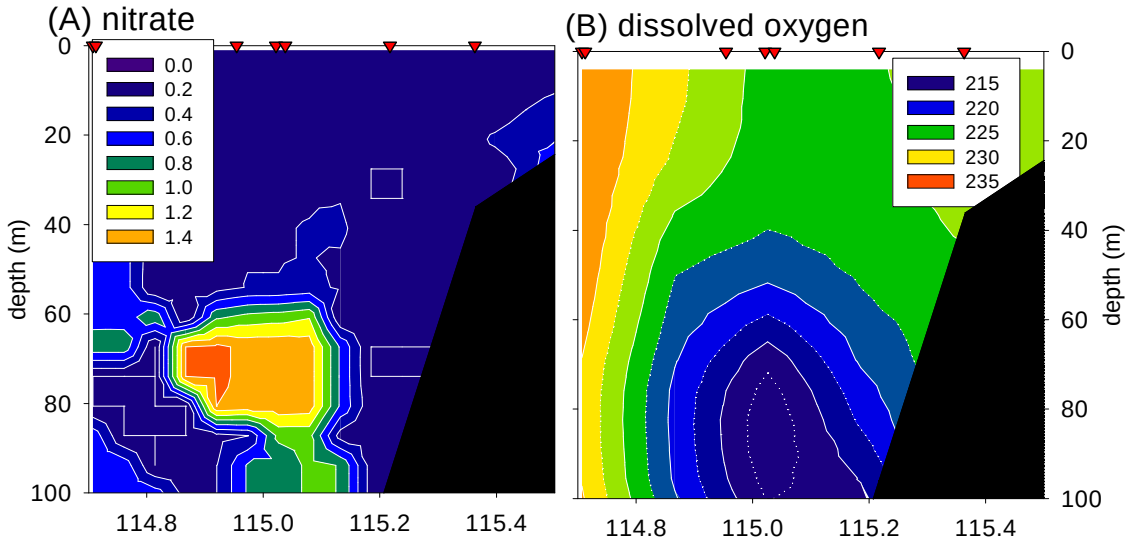

Figure 3.121. Sections of the Leeuwin Current and associate region at 32°S from near shore to 1000m water depth. (A) Nitrate section from sensor showing thin layer of high nitrate under core of Leeuwin Current. (B) Dissolved oxygen section with low dissolved oxygen at base of LC. Red triangles indicate locations of CTD profiles.

High concentrations of nitrate were found in thin layers at the base of the Leeuwin Current from 22 to 34°S (e.g.Figure 3.114 and Figure 3.115).At latitudes of 22 to 25° these thin layers were found further offshore over a wide area. The thin layers of high nitrate water found at these unusually shallow depths were always associated with areas of low dissolved oxygen (Figure 3.121).

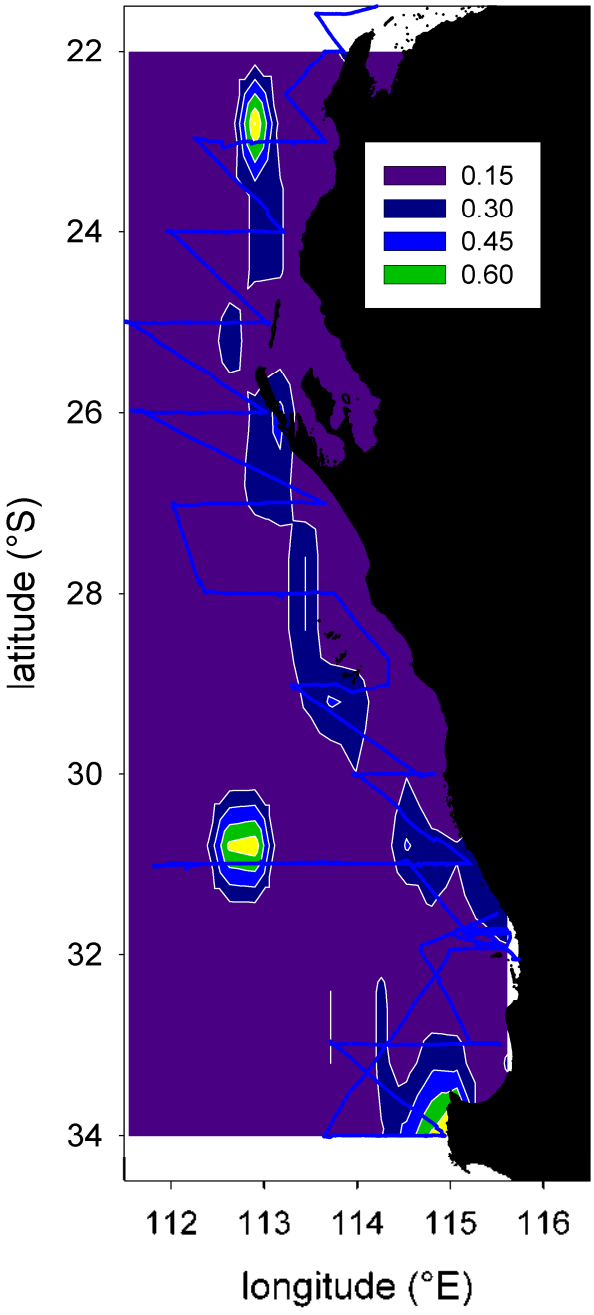

Depth-averaged, euphotic zone nitrate concentrations showed a strong pattern of greatest concentrations along the shelf break with lower concentrations found closer to shore or further offshore (Figure 3.122). These shelf break stations were selected to coincide with the centre of the Leeuwin Current (LC). The shelf break stations had depth-averaged euphotic zone (0 to 100m) nitrate concentrations consistently in the range of 0.15 to 0.30 µM NO_3 in the vicinity of the LC. Based on the salinity and temperature derived estimates of mixed layer depth these shelf break stations with greater depth-averaged nitrate concentrations (Figure 3.115) were generally not areas of particularly deep vertical mixing. Due to the presence of the LC along the shelf break between 23 and 33°S the mixed layer depths were mostly quite shallow averaging ~ 40 to 60m. In general a surface mixed layer depth of 60m is not sufficient to entrain nutrients from below the seasonal thermocline in these locations.

Figure 3.122. Depth averaged (0 to 100 m) and contoured nitrate concentrations from all 111 CTD stations on SS03/2007 (bottle samples, n = 6 per station); cruise track (blue line).

We propose that the dissolved inorganic nitrogen (DIN) in these layers enters the LC at depths between 50 and 200m at latitudes from 22 to 25°S.

There appeared to be three mechanisms whereby the nitrate could enter the euphotic zone: instability that results in a warm core eddy, cooling that deepens the surface mixed layer and shallowing of the thin layer.

Between 24 and 26°S the core of the LC was present as a 50 to 100 m deep layer over one or more thin layers, 15 to 50m thick, with high nitrate and low dissolved oxygen (DO). These layers were of lower salinity, cooler water with markedly reduced DO, high nitrate concentrations and distinct nitrate:silicate (NO_3:$Si(OH)_4$) nutrient ratios (Figure 3.120).

As the LC flowed south it cooled and deepened thereby entraining the thin layers of high nitrate water into the euphotic zone. The LC also formed large (greater than 100km diameter) warm core eddies with a deep surface mixed layer that also entrained nitrate from these thin layers (Figure 3.115).

In some locations as far south as 32°S the LC was still present with the thin layer of high nitrate intact but now within the euphotic zone. Thus, the available evidence suggests the LC arises under conditions that favour rapid and shallow nitrification. This nitrification fuels a shelf scale bloom on a downwelling favourable coast. Depending upon the rate of nitrification the source of the particular organic matter may be local or delivered from the tropics via horizontal advection in a subsurface layer of the LC. The use of the new methodology (in situ spectrophotometric nitrate detection) and new instrumentation (SAtlantic ISUS sensor) were pivotal in resolving the source of the nitrate to the west coast phytoplankton bloom.

Key Findings:
Novel technology made it possible to discover the source of the key nutrient fueling primary production along the west coast of Australia.

More details on this section can be found in Thompson, P.A., Wild-Allen, K., Lourey, M., Rousseaux, C., Waite A.M., Feng, M., Beckley L.E. Nutrients in an oligotrophic boundary current: Evidence of a new role for the Leeuwin Current. Progress in Oceanography. (in press, preprint available on line, accepted 21/02/2011).

3.2.6 Phytoplankton

Using samples from the cruise (SS04/2007) a new analysis of the phytoplankton community composition, its temporal and spatial patterns has been undertaken. While the SS04/2007 cruise gives an unparalleled semi-synoptic data set, previous cruises expand the geographic range and pooling the data provides more opportunity for the analyses of seasonal and inter annual variability. Much of these data had not been published prior to WAMSI and there had not been a review of WA phytoplankton since the 1960s. In addition, since the early research relied exclusively on net samples, the vast majority of the phytoplankton biomass was not examined or quantified by earlier phytoplankton ecologists.

Samples for this analysis are drawn from a range of cruises along the west and south west coasts of Australia (Table 3.33).

Table 3.33. A description of the pigment samples from the west and southwest coasts of Australia used in this study sorted by season, month or cruise. FR = Franklin, SS = Southern Surveyor, LB = Lady Basten, MD = Marion Dufresne.

season	Cruise or vessel	Number of pigment samples	Taxonomic samples
Autumn	SS04/2007	83	Yes
Autumn	SS05/2006	120	
Autumn	SS04/2006	80	Yes
Winter	SS07/2005	125	Yes
Summer	Beagle	3	
Spring	SS09/2003	73	
Spring	SS08/2003	80	
Spring	FR10/2000	102	Yes
Various	7 Ships of opportunity	57	
Spring	MD TIP	54	
Winter	LB21	32	
	SS07/2006		Yes
	SS05/2005		Yes
	FR5/1995		Yes

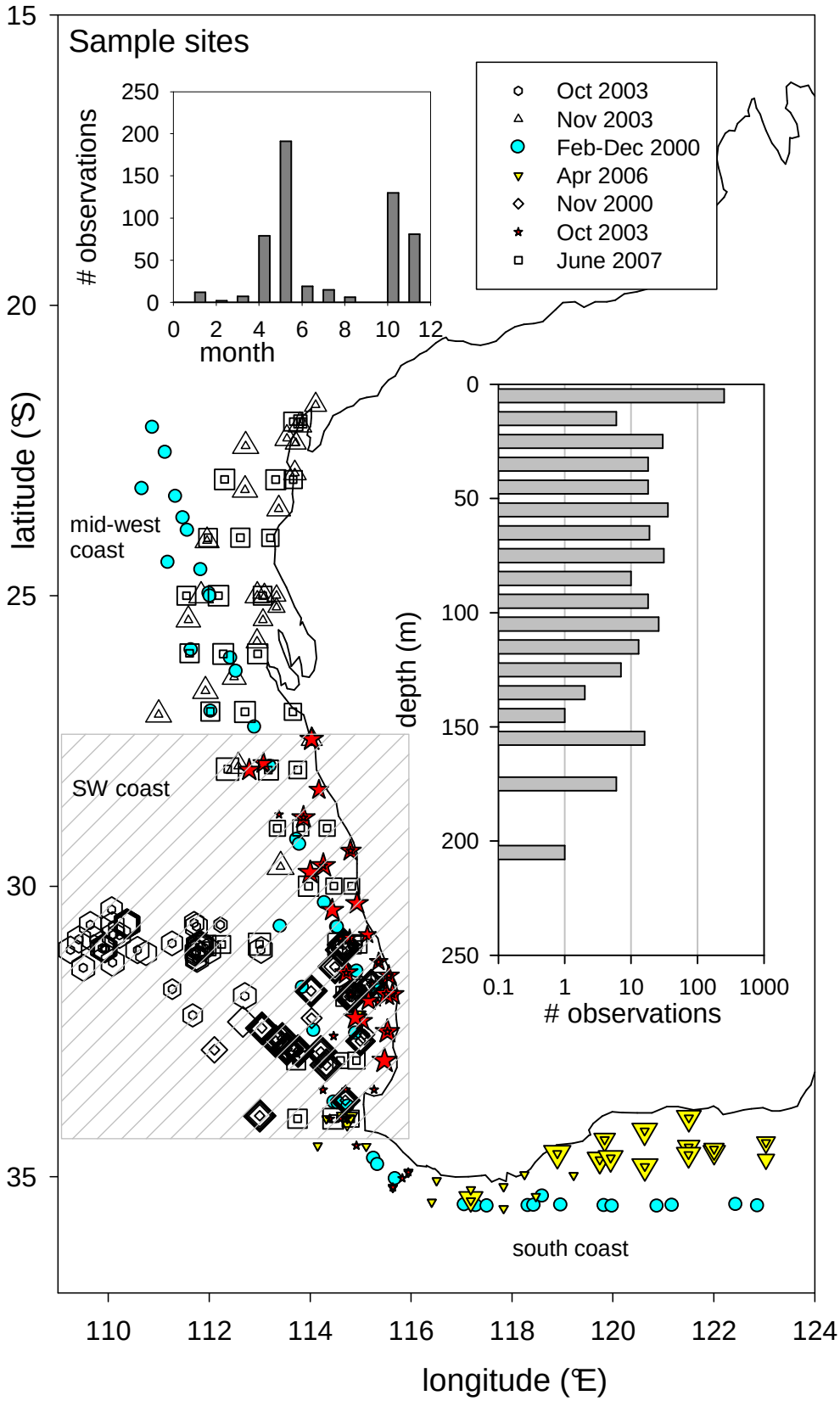

Figure 3.123. Map of sites with samples analysed by HPLC allowing chemotaxonomic phytoplankton assessment. Larger symbols are from greater depths.

Methods

From the voyage SS04/2007 samples for phytoplankton taxonomy were collected from stations inshore (~ 50m deep), at the shelf break (~ 200 to 300m deep) and offshore (1000 or 2000m deep). They were preserved using acid Lugol's solution (Parsons et al. 1984). The preserved samples were transferred to 1-litre measuring cylinders, measured and allowed to settle for at least 24 hours. After this time, approximately 90% of the volume was siphoned off and the remaining sample was transferred to a 100 ml measuring cylinder, measured and again allowed to settle. After at least 24 hours approximately 90% of the volume was siphoned off and the final volume recorded before the remaining sample was thoroughly mixed and an aliquot was taken for counting. The aliquot was put into a 1 mL Sedgwick Rafter counting chamber and examined using an inverted Olympus IX 71 microscope. For most microplankton (cells generally larger than 20 µm diameter) at least 10% of a single slide was enumerated at 100 x magnification (except when there were dense blooms of one or more microplankton species, when at least 20% was scanned). For nanoplankton, (2 to 20 µm in diameter) the chamber was examined at 400 x magnification until at least 200 cells of the dominant nanoplankton "taxon" had been counted. Small flagellates (< 10 µm in diameter) in the nanoplankton were assigned to a two groups (reported as "round or fusiform flagellates") unless they could be readily identified as either dinoflagellates, chrysophytes, cryptophytes, prasinophytes or haptopytes.

Phytoplankton pigments also provide a very useful method of quantifying the abundance particularly for small cells which often lack taxonomically useful morphological features for identification when observed by epifluorescence microscopy or conventional light microscopy. We define 4 types of associations between pigments and taxa relevant to Australian waters (Table 3.34):

1. pigments found within a narrow range of taxa and a limited range per cell, such as divinyl chlorophyll *a* in *Prochlorococcus,* where the conversion to cell density can be relatively precise
2. pigments, such as zeaxanthin, that are found in more than one taxon but within some taxa the content per cell may be relatively constrained (e.g. *Synechococcus*).
3. pigments that are highly constrained to a recognised taxon such as peridinin (dinoflagellates), alloxanthin (Cryptophytes), prasinoxanthin (Prasinophytes), 19'-hexanoyloxyfucoxanthin (Haptophytes) but with a wider range per cell.
4. pigments that are found in a range of taxa, such as diadinoxanthin.

Where pigments are found across a range of taxa the conversion to taxonomic affiliation can be achieved using a various methods such as CHEMTAX which uses a steepest-descent algorithm to fit a matrix of expected pigment ratios from those taxa to the observations (Mackey et al.1996).

Microplankton

Microplankton are often defined as 20 to 200 µm in size. This is a cell size that is relatively easy to identify and simultaneously enumerate using a light microscope. Of the cells smaller than ~ 10µm the most abundant were round flagellates > fusiform flagellates > cryptophytes > prymnesiophytes > prasinophytes & chlorophytes, > small dinoflagellates.

Of the taxa that were identified to species or genera using light microscopy dinoflagellates in the genera, *Ceratium,* were the most abundant. These were followed by a range of coastal and

oceanic diatom genera, *Pseudonitzschia*, *Chaetoceros*, *Nitzschia*. Trichodesmium, the N_2 fixing, filiament and bundle forming cyanobaterium was 6th most abundant.

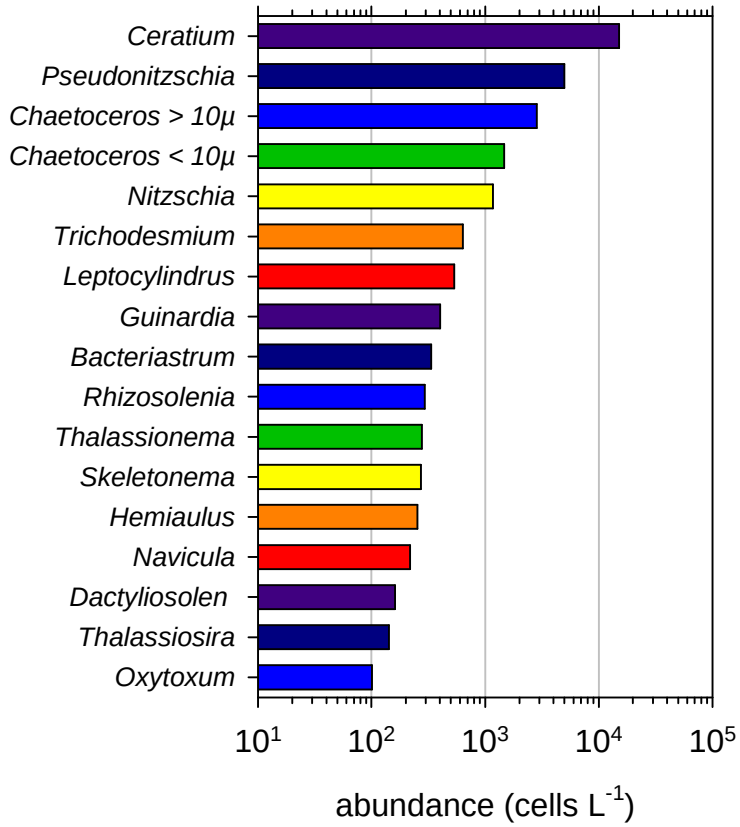

Figure 3.124. Average phytoplankton cell densities for the most abundant genera as observed at 84 stations between 22 and 34°S and near shore (~ 50m water depth) to offshore (> 1000m water depth) during SS04/2007.

Phytoplankton distribution and abundance as assessed by pigments.

A range of taxa are too small to be identified using a light microsrope, especially those smaller than 1 µm such as *Synechococcus* and *Prochlorococcus*. Fortunately many phytoplankton have unique pigments or pigment combinations that can be used to identify their presence, absolute and relative abundances (Table 3.34, Mackay et al. 1996). This approach has been applied to the samples collected during SS04/2007 and other research cruises off the west coast of Australia.

Table 3.34. Phytoplankton pigment abbreviations and classification into 4 categories: 1) pigments found within only a few taxa and a limited range per cell 2) pigments that are found in more than one taxon but within some taxa the content per cell may be tightly constrained 3) pigments mostly constrained to one taxon but with a wide range per cell, 4) pigments found in a range of taxa.

abbreviation	Pigment	category	Taxa
caro	β,ε carotenoids	4	
peri	Peridinin	3	Most autotrophic dinoflagellates
19but	19'-butanoyloxyfucoxanthin	3	Pelagophytes
fuco	Fucoxanthin	4	often used as a marker for diatoms but found in other taxa
neo	neoxanthin	4	Chlorophytes, Prasinophytes
pras	prasinoxanthin	3	Prasinophytes
viol	violaxanthin	4	
19hex	19'-hexanoyloxyfucoxanthin	3	Haptophytes
DD	diadinoxanthin	4	
DT	diatoxanthin	4	
allo	alloxanthin	3	Cryptophytes
zea	zeaxanthin	2	cyanobacteria, Prochlorophytes
DVchlb	divinyl chlorophyll *b*	1	Prochlorophytes
chlb	chlorophyll *b*	4	All greens, e.g. Chlorophytes, Prasinophytes, Euglenophytes
DVchla	divinyl chlorophyll *a*	1	Prochlorophytes
chla	monovinyl chlorophyll *a*	4	all photosynthetic phytoplankton except Prochlorophytes

The fucoxanthin, or diatom concentrations, along the west coast showed a distribution with significantly more inshore biomass and more diatoms in the southern regionof this domain (Figure 3.125). Patches of high diatoms were found near Shark Bay, Cape Leeuwin, along the south coast and in a few offshore eddies. Considering only the latitudinal band from 27.5 to 34.5°S (Figure 3.125) the average concentration of fucoxanthin in the SW was 0.028± 0.028 µg l^{-1}.

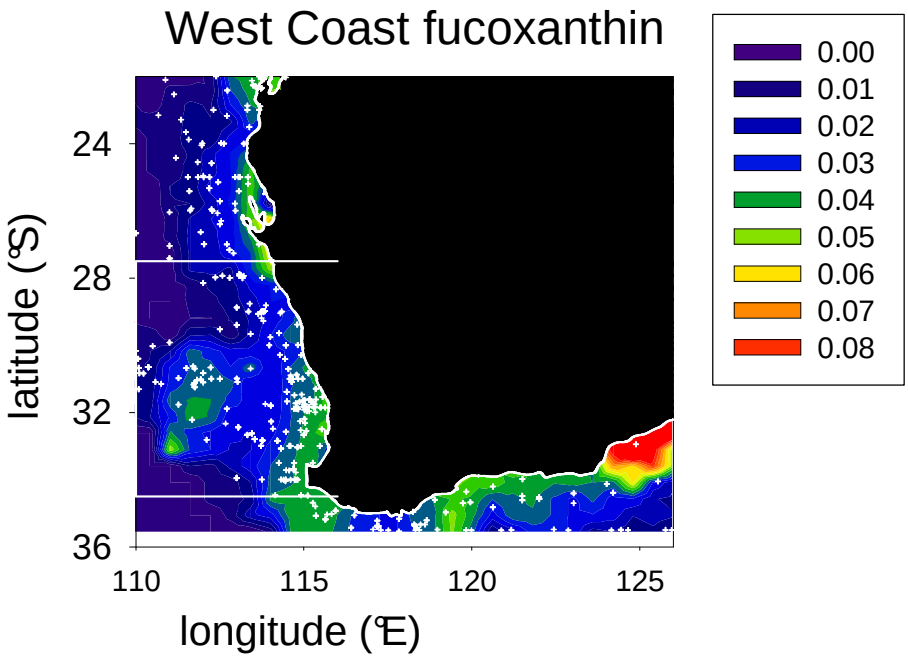

Figure 3.125. The depth averaged concentrations (µg l-1) of fucoxanthin (diatoms) on the west coasts of Australia. White symbols represent sample locations. Concentrations estimated away from these locations cannot be considered reliable. White lines demark 27.5 to 34.5°S and are referred to as the southwest (SW) region.

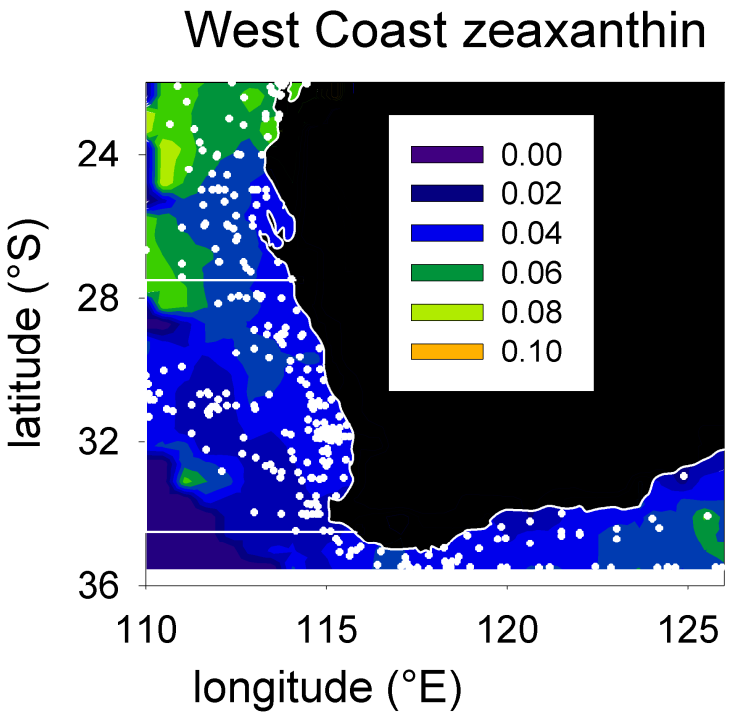

Figure 3.126. The depth averaged concentrations (µg l-1) of zeaxanthin (Synechococcus) on the west coast of Australia. White symbols represent sample locations. Concentrations estimated away from these locations cannot be considered reliable. White lines demark 27.5 to 34.5°S and are referred to as the southwest SW regions.

The distribution of zeaxanthin (*Synechococcus*) showed a strong latitudinal gradient with the mean concentration increasing by a factor of 3 along the west coast from ~ 34 to 22°S. The greater zeaxanthin concentrations tended to be further offshore relative to those for diatoms (fucoxanthin concentrations).

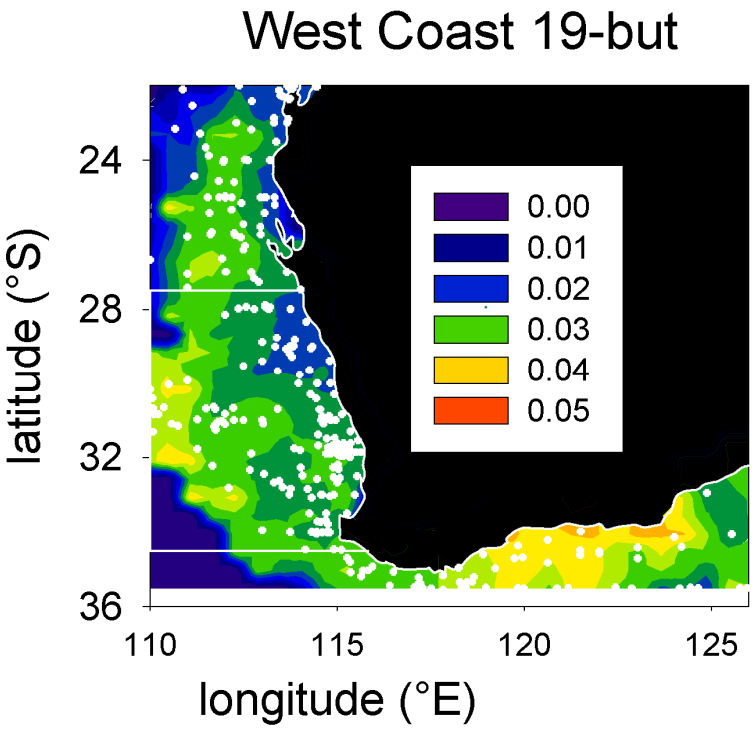

Figure 3.127. The depth averaged concentrations (µg l-1) of 19'-butanoyloxyfucoxanthin (Pelagophytes) on the west coast of Australia. White symbols represent sample locations. Concentrations estimated away from these locations cannot be considered reliable.

The pigment 19'-butanoyloxyfucoxanthin (Pelagophytes) was widely distributed along the entire west coast (Figure 3.127). There are indications that Pelagophytes abundance was greater offshore and in the Great Australian Bight than in the north of this region. Pelagophytes also tended to be deep in the water column relative to other phytoplankton.

To examine the size structure of the phytoplankton community the HPLC pigment data was used to estimate three size classes: micro (>20 µm), nano (2 to 20 µm) and pico (< 2 µm) using the approach of Vidussi et al. (2001) and Uitz et al. (2008). The fractions of these three pigment-based size classes (pigment abbreviations are listed in Table 3.34) relative to the total algal biomass were calculated as:

micro = (1.41*fuco + 1.41*peridinin)/wDP
nano = (0.60*allo + 0.35*19but + 1.27*19hex)/wDP
pico = (0.86*zea + 1.01*[Chlb – DVChlb])/wDP
where wDP is the weighted sum of the concentrations of the seven diagnostic pigments:
wDP = 1.41*fuco + 1.41*peridinin + 0.60*allo + 0.35*19but + 1.27*19hex + 0.86*zea +
1.01*[Chlb – DVChlb]

All size classes of phytoplankton on both the east and west coasts of Australia showed significant (spearman rank order) correlations with latitude. Thus the abundance of pico-phytoplankton was significantly greater in the northern portion of the study region than in the south (Figure 3.128). Nano and microplankton were significantly more abundant in the south, although there was a marked increase in microplankton at 22 to 23°S (offshore of Ningaloo Reef) on the west coast.

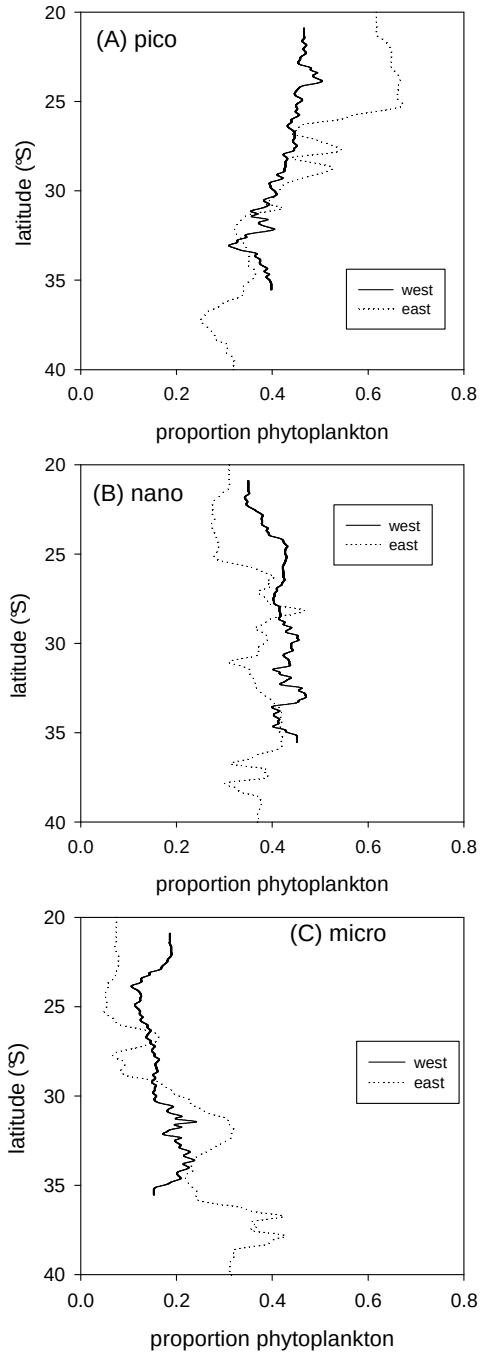

Figure 3.128. The east and west coast latitudinal distributions of phytoplankton in 3 size classes as estimated from pigments apportioned as in Uitz et al. (2008). Lines are running averages. (A) picoplankton < 2 µm, (B) nanoplankton >2 and < 20, (C) microplankton > 20 µm.

The average proportion of picoplankton was similar on both coasts at 42% on the east coast and 40% on the west coast (Figure 3.128A). Picoplankton reached its greatest proportion of biomass, ~ 60%, north of 27°S on the east coast and declined further south to a low of ~ 30% at 40°S. On the west coast the proportion of picoplankton increased by 0.88±0.13% per degree of latitude ($P < 0.001$). On the east coast the rate of increase was faster ($P = 0.018$) at 1.3±0.1% per degree of latitude ($P < 0.0001$). On both coasts the observed latitudinal variation, measured as coefficient of variation over all data, tended to be lower for nanoplankton than pico or micro plankton (Figure 3.128A, B, C). Microplankton were the least abundant group overall, with less than 10% of total biomass north of 20°S rising to nearly 40% at ~ 40°S. Overall microplankton were 18% of the phytoplankton on the west coast and a significantly ($P < 0.001$) greater proportion, averaging 27% of the phytoplankton, on the east coast.

An overview of Phytoplankton community composition.

The average total chlorophyll *a* concentration (via HPLC) over the period from 1996 to 2010, 9 research voyages and > 600 samples (Table 3.33) from the west coast was 0.28± 0.16 µg L^{-1}. The pigments with taxonomic associations were normalised to chlorophyll *a* to removed effects of biomass (Table 3.35) and then analysed by CHEMTAX (Mackay et al. 1996) to determine the relative abundance of the major taxa off the west coast (Figure 3.129). *Synechococcus* was the dominant taxon with 43% of the total biomass, Pelagophytes ~ 24%, Haptophytes ~ 14%, Prochorophytes 12%, Prasinophytes 12% and decreasing proportions of: Cryptophytes, Chlorophytes, Bacillariophytes and Dinophytes (Figure 3.129, Table 3.35).

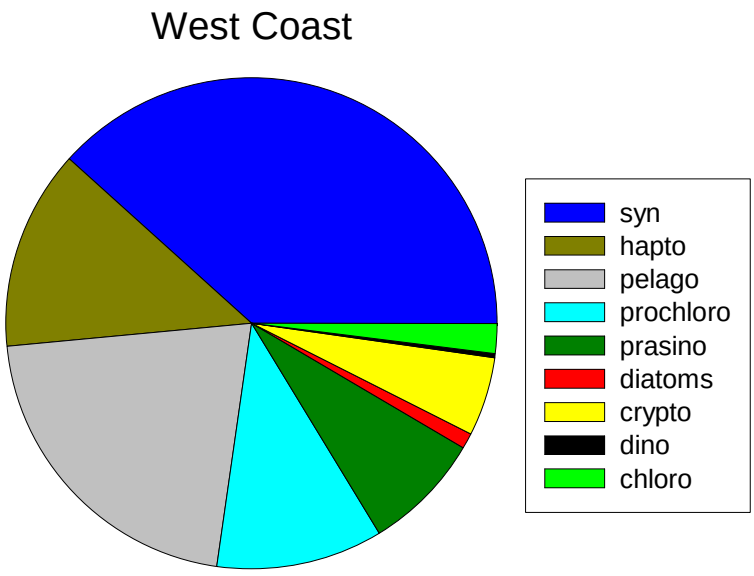

Figure 3.129. Taxonomic composition based on pigment data followed by CHEMTAX (Mackay et al. 1996) using data from within the latitudinal range 27.5 to 34.5°S, n = 472 with mean depth = 42 ± 46m, average month was July (7.2 ± 2.6). Synechococcus (syn), Pelagophytes (pelago), Prochlorophytes (prochlor), Prymnesiophytes = Haptophytes (hapto), Chlorophytes (chloro), Bacillariophytes (diatoms), Prasinophytes (prasino), Dinophytes (dino).

Table 3.35. Summary of normalised pigments to chlorophyll *a* from the SW region of coastal Western Australia.

Pigment	SW coast (n=477)* (pigment:chl*a*)x10^3	
	Mean	SE
Peridinin	2.3	0.4
19'-butanoyloxyfucoxanthin	123	3.3
Fucoxanthin	98	3.2
Neoxanthin	8.0	0.4
Prasinoxanthin	18.8	0.9
Violaxanthin	6.4	0.4
19'-hexanoyloxyfucoxanthin	191	3.4
Alloxanthin	12.9	0.6
Zeaxanthin	155	6.6
Lutein	0.2	0.1
Divinyl chl*a*	123	6.3
chlorophyll *b*	146	4.0
Taxonomic composition	%	
Synechoccocus	43.0	
Haptophytes	14.8	
Pelagophytes	23.9	
Prochlorophytes	12.3	
Prasinophytes	8.8	
Bacillariophytes	1.4	
Cryptophytes	5.8	
Dinophytes	0.03	
Chlorophytes	2.2	
N:P molar ratio, 0 to 100m (# samples)	3.93 (2601)	0.12
N:Si molar ratio, 0 to 100m (# samples)	0.179 (2735)	0.004

*maximum number, some pigments have fewer observations.

More details on this section including full methods and the contrast with the east coast of Australia can be found in Thompson PA, Bonham P, Waite AM, Clementson LA, Cherukuru N, Doblin MA. Contrasting oceanographic conditions and phytoplankton communities on the east and west coasts of Australia. Deep Sea Research II 58: 645-663.

Key findings:
The phytoplankton are dominated by < 2 µm cells, primarily *Synechococcus* and *Prochlorococcus*, with their dominance decreasing with latitude and proximity to shore.

Pelagic Production

Previousy there had never been a shelf scale survey allowing a quasi-synpotic view of primary production along the west coast of Australia. The pelagic primary production was measured by ^{14}C uptake. Water samples were gently mixed and poured into replicate clear, 140ml polycarbonate bottles and 20 μCi of $NaH^{14}CO_3$ added to each. At each station (Figure 3.130) and 6 depths per station, one bottle was incubated at approximately *in situ* irradiance and temperature for 24 hours (dawn to dawn) and the second in darkness. After 24 hours, the incubations were terminated by filtration into two size classes (> and < 5 μm). Filters were acidified and left to stand to drive off the residual labelled ^{14}C. The next day, 10ml of scintillation cocktail was added to each vial and the activity measured.

Primary production was highest in or near unstable features of the Leeuwin Current (Figure 3.131) and it appears that variations are strongly driven by these underlying oceanographic features. The most significant feature is the mesoscale meander at 31°S (Figure 3.130). In the very centre of the meander/forming eddy depth integrated primary production (416 mg C m^{-2} d^{-1}) and Chl *a* normalised primary production (24.4 mg C mg Chl a^{-1} m^{-2} d^{-1}) were elevated (Figure 3.131). Enhanced production in the centre of this feature is further evidence that LC warm core eddies behave differently to similar eddies in other southern hemisphere regions where warm core eddies are generally regarded as production "deserts". It has been hypothesised that nutrient injection or seeding into warm core eddies at formation is necessary to stimulate the enhanced primary production found in older eddies (Greenwood et al., 2007). In contrast to older warm core eddies where nitrate concentrations were undetectable (Waite et al., 2007), the depth integrated nitrate concentration at the centre of the forming eddy studied here was elevated (65 μM m^{-2}) suggesting that new nitrogen is drawn into the centre warm core eddy during formation and through efficient retention and recycling goes on to stimulate biomass and support ongoing primary production in warm core eddies. The activity of the warm core eddy appears to cause the mixed layer to deepen (to 164m) which may mix deep water nutrients towards the surface (Lourey et al., 2006). Early in the formation production is high relative to the biomass (high chlorophyll a normalised primary production) suggesting there has been a recent addition of nutrients and biomass has not yet responded. The mixed layer continues to deepen as the eddy matures (compare the MLD of 164m here and 275m in Waite et al., 2007; and simulations by Greenwood et al., 2007) although it is not clear that there is further exchange. In the older eddies the normalised production does not appear to be elevated (Waite et al., 2007) and it is possible that the deep water may is actually displaced by the depression of the mixed layer during evolution and ongoing exchange across the base of the mixed layer is minimal (Waite et al., 2007).

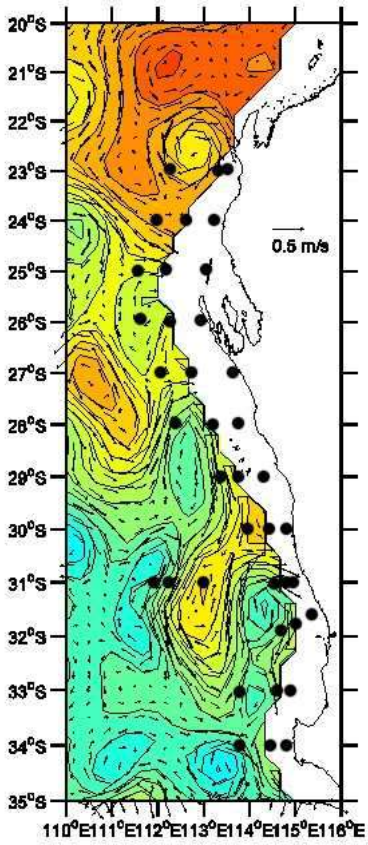

Figure 3.130. Satellite altimetry and current vectors during Southern Surveyor voyage SS0407.

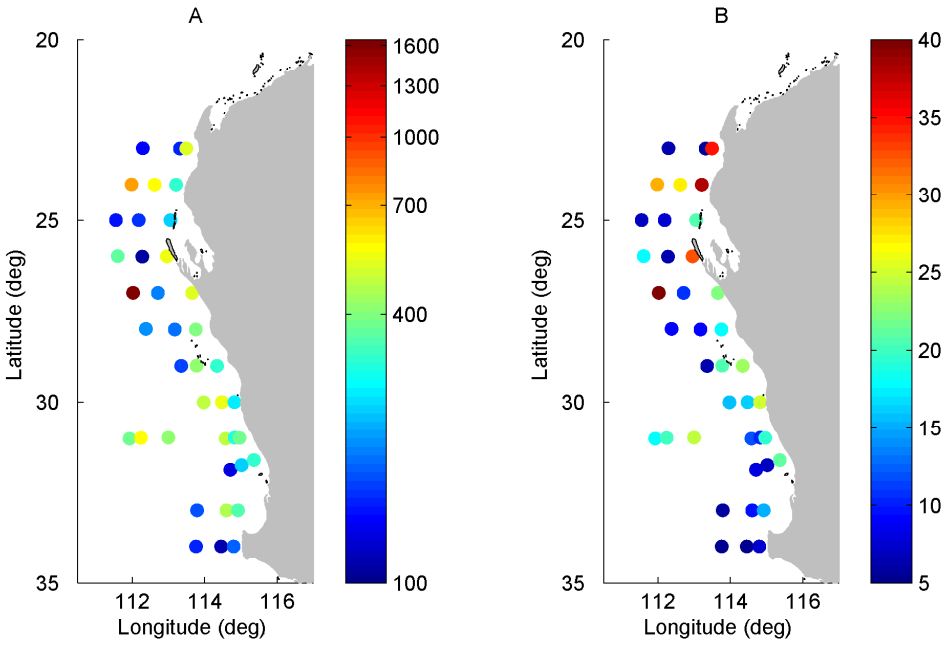

Figure 3.131. Total depth integrated primary production (A, in mg carbon m^{-2} d^{-1}) and chlorophyll *a* normalised primary production (B, grams carbon gram chlorophyll *a* m^{-2} d^{-1}) measured during SS04/2007.

There is a sizable difference between this and a discrete fully formed eddy. Here, the feature is effectively open. There is a connection between the eddy and the Leeuwin current and while there is clearly a substantial flow of Leeuwin Current water through the meander it is likely that a proportion of the flow makes the junction directly across the top of the feature. Despite this, the feature appears to have a strong influence on primary production downstream of the meander. Upstream of the meander, primary production in the current was uniformly low (mean 152 ± standard deviation 33 mg C m^{-2} d^{-1}) while downstream it was considerably higher (370 ± 112 mg C m^{-2} d^{-1}) and similar to the levels observed in the main flow of the feature (385 and 573 mg C m^{-2} d^{-1} , see Figure 3.131). This contribution has important implications for primary production in the southwest and beyond as the current makes its way south and then east as it rounds the southern extend of the Australian mainland (Ridgeway and Condie 2004).

A smaller feature emanated from the Leeuwin current in the vicinity of 27°S and its action generates the highest rates of primary production measured (1650 mg C m^{-2} d^{-1} at the outer station of the 27°S transect, see Figure 3.131). There is a well defined warm core eddy lying to the west of and well removed from this sampling station but it appears that this feature (possibly with the combined effect of the cold core feature located to the south east) may draw water off the shelf and direct it firstly off shore and than towards the northwest. This generates a clockwise flowing feature and although the velocities associated with this feature do not appear significant compared to the mesoscale meander, it has a significant influence on primary production. In addition to the greatest rate of over all primary production measured (double the next highest) the outer 27°S station also had high chlorophyll a normalised primary production (39.8 mg C mg Chl a^{-1} d^{-1} was the highest measured, see Figure 3.131) despite the second highest depth integrated biomass (41.5 mg Chl a m^{-2}). Despite the exceptional biomass and relative rates primary production neither the depth integrated nitrate concentration nor mixed layer depth are elevated at this point. While it is not necessarily surprising that the nitrate concentrations at this point are low. These surface waters are uniformly nitrogen limited and it is probable that the nitrate that generated the high production/biomass observed here has been rapidly consumed (Lourey et al., 2006). The relatively shallow mixed layer suggests that the mechanism for supply here does not include vertical exchange associated with variations to the mixed layer depth.

A region of high production (727 mg C m^{-2} d^{-1}, see Figure 3.131) and chlorophyll *a* normalised primary production rate of (29.4 mg C mg Chl a^{-1} d^{-1}, see Figure 3.131) in the north of our domain (outer station at 24°S) appears to have a different structure and water mass composition to the other features (Figure 3.132). Most of the stations sampled here were evenly distributed between two temperature-salinity end members. In the north, Leeuwin Current water has a low salinity and high temperature that gradually becomes colder and more saline as it travels southwards due to a loss of surface heat and evaporation as well as mixing with subtropical surface waters (Feng et al., 2007). The T-S relationship at the high production station at 24°S was considerably different to the general relationship (Figure 3.132) and the depth integrated nitrate concentration was the highest measured (136 μM m^{-2}), indicative of significant variation in the composition of the water mass at this station. This variation in T-S characteristics and depth integrated nitrate concentration stems from the euphotic zone extending below a very shallow mixed layer. As a consequence, deeper samples were effectively collected from a different water mass to the surface samples. The high nitrate concentration at relatively shallow depth generates considerable deep primary production. The production at 100m was similar to shallower depths and as a result 46% of the depth integrated primary production is occurring below 50m. Low biomass and light conditions that normally limit production at these depths suggests that the deep photosynthesis here must be highly efficient to generate rates of carbon uptake equivalent to those closer to the surface.

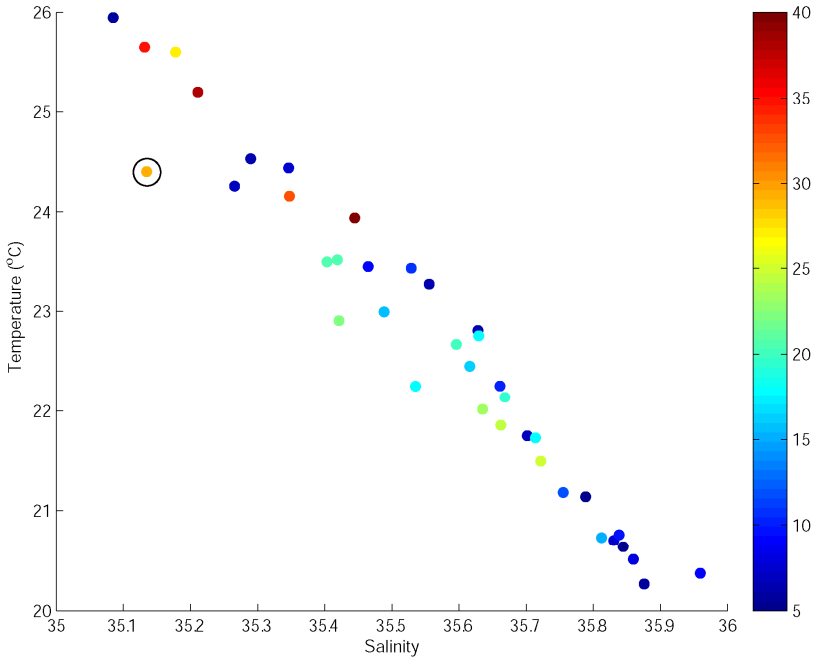

Figure 3.132. Depth averaged temperature (ºC) versus salinity. The circled point is the outer station at 24ºS.

The water mass below the mixed layer at 27°S has an extremely high nitrate concentration (5.4 µM) and makes a considerable contribution to depth integrated rates of primary production at that station. The proximity of this high nutrient water close to the surface (strong nitracline between the 50 and 100m samples) in the region of the Leeuwin Current's source introduces the possibility of entrainment of nutrients into the core of the Leeuwin current as a mechanism for the transport of nutrients to the south (Koslow et al., 2008). However, there is scant evidence of a broader influence of this feature. Firstly, the unique TS profile of the nutrient rich deeper water does not appear in the surrounding stations or the core of the Leeuwin current which suggests that any exchange has not been sufficient to noticeably modify the TS signature. Secondly, primary production in the Leeuwin Current is very low (down stream of feature A notwithstanding) and we would probably have expected any such exchange to have an immediate and significant influence on rates of primary production in the Leeuwin Current.

Key findings:
Regions of high primary production along the west coast of Australia were associated with features of the Leeuwin Current such as a productive eddy-forming meanders, thin and shallow layers of high nitrate offshore at ~ 22 to 24°S and the LC transport and entrainment of this thin layer into the photic zone at latitudes > 28°S.

Zooplankton Biomass

Introduction

We measured zooplankton biomass to provide information on inshore-offshore and north-south abundance of these important organisms. The spatial pattern in zooplankton is important for understanding the functioning of marine ecosystems since these organisms are abundant and form a trophic link between primary producers and fish. All larval fish and many adult feed directly on zooplankton. Also, zooplankton biomass cycles with nutrients and pollution levels. Zooplankton play important role in carbon sequestration, are water mass and climate change indicators. The spatial heterogeneity in plankton biomass is important for various processes like species reproduction, population dynamics and prey-predator interactions. In our study we examined the spatial variability in biomass with respect to environmental variables measured. We considered several size classes: 3000+, 3000-1000, 1000-355,355-250, 250-150 and 150 to 100 µm.

Methods

Zooplankton was collected using oblique Bongo tows with 355 and 100 µm mesh inshore of the Leeuwin Current, in the Leeuwin Current and offshore of the Leeuwin Current (Figure 3.133) Biomass of zooplankton was determined using Ash-Free Dry Weight which is a measurement of the weight of organic material. Samples were collected by oblique tows of Bongo nets with 50 cm diameter opening and 100 and 355 µm mesh nets. Samples were immediately preserved in 5 % borax buffered formalin (2 g of borax to 98 ml of 40% formaldehyde, Griffiths et al, 1976). Samples were processed for biomass between September 2007 and February 2008. In the lab samples from 100 µm mesh net were size fractionated on precombusted and pre-weighted Whatman GFC filters. Filters were pre-combusted at 500 C for 2 hours (Nagao et al, 2001). Samples were dried at 60º C for 48 h in Qualtex Solidstat oven. Samples were transferred to desiccator and allowed to cool to room temperature. Next the dry weights were weighted on balance Sartorius MC1. The resulting dry weight was the weight of both the organic and inorganic contents of the sample. The weighted samples on glass fiber filters were combusted in a muffle furnace (Heraeus Electronic) starting at room temperature and reaching 500 ºC for 12 hours to determine ash weight (Postel et al, 2000). The AFDW (the organic content of the sample) was obtained by dry weight (inorganic and organic contents) minus the weight of the ash (inorganic contents only). We used multivariate package PRIMER + PERMANOVA to analyse data.

Results

Net plankton samples especially from shallower waters contained considerable amount of ash (from 35% ±20% of dry weight inshore to 18% ± 7 % and 23% ± 4 % in LC and offshore respectively) caused by contamination of inorganic materials from re-suspension of sediments and phytoplankton originated detritus.

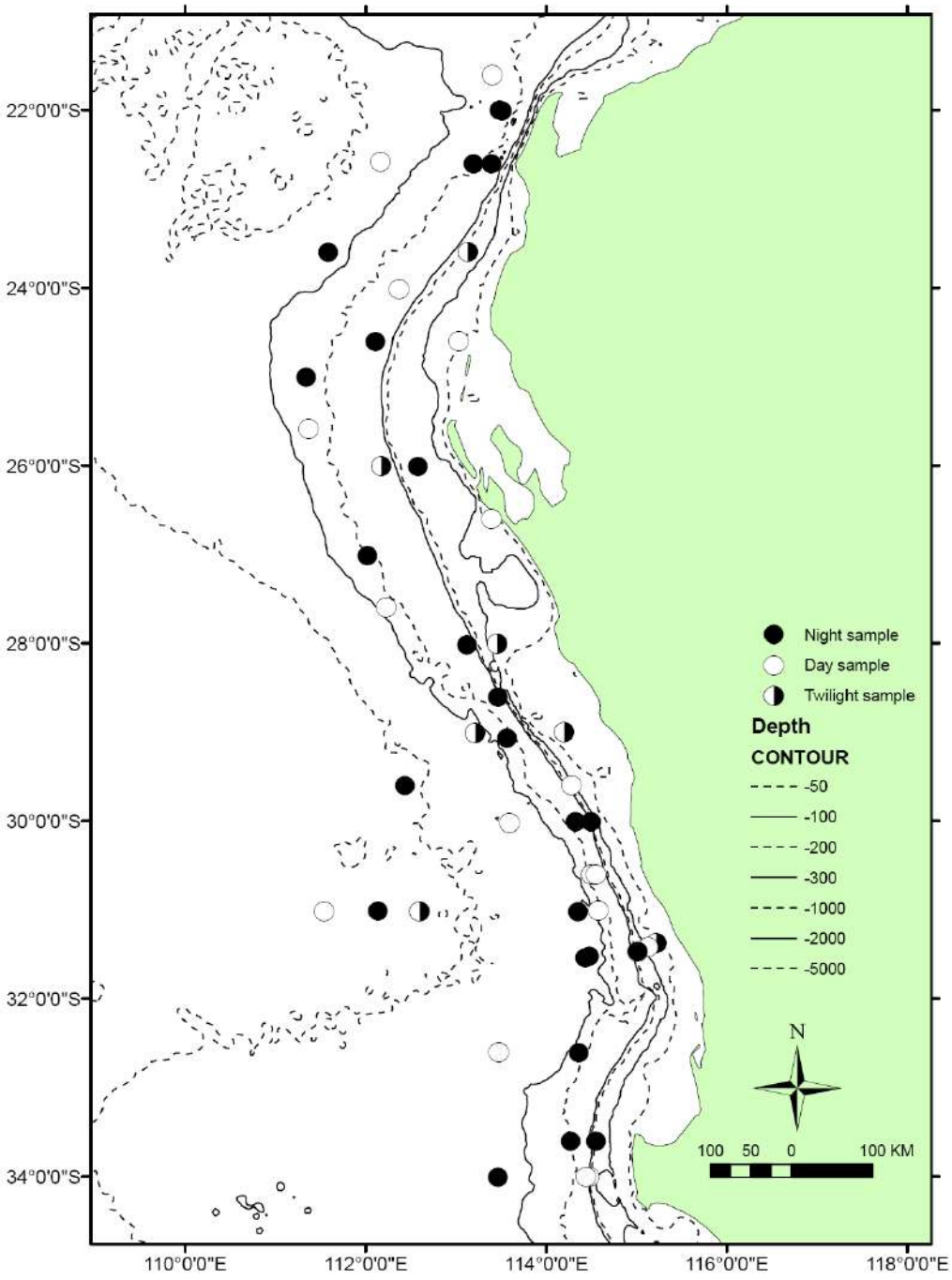

Figure 3.133. Zooplankton stations showing time of sampling.

Total and size fractionated biomass showed strong pattern following water masses. Biomass was higher inshore than in Leeuwin Current (LC) and offshore waters (Figure 3.134). From 34 to 29ºS biomass offshore was lower than in LC waters but the difference disappeared north of 29 parallel. There was a clear South-North pattern in LC and offshore waters showing bimodal distribution with higher values between 33 and 29 ºS and again between 24 and 22 ºS and low of around .005 g AFDW m^{-3} between 28 and 27 ºS. Inshore samples showed no geographic

trend on the scale of sampling (every degree) implying possible smaller scale pattern or spatial autocorrelation.

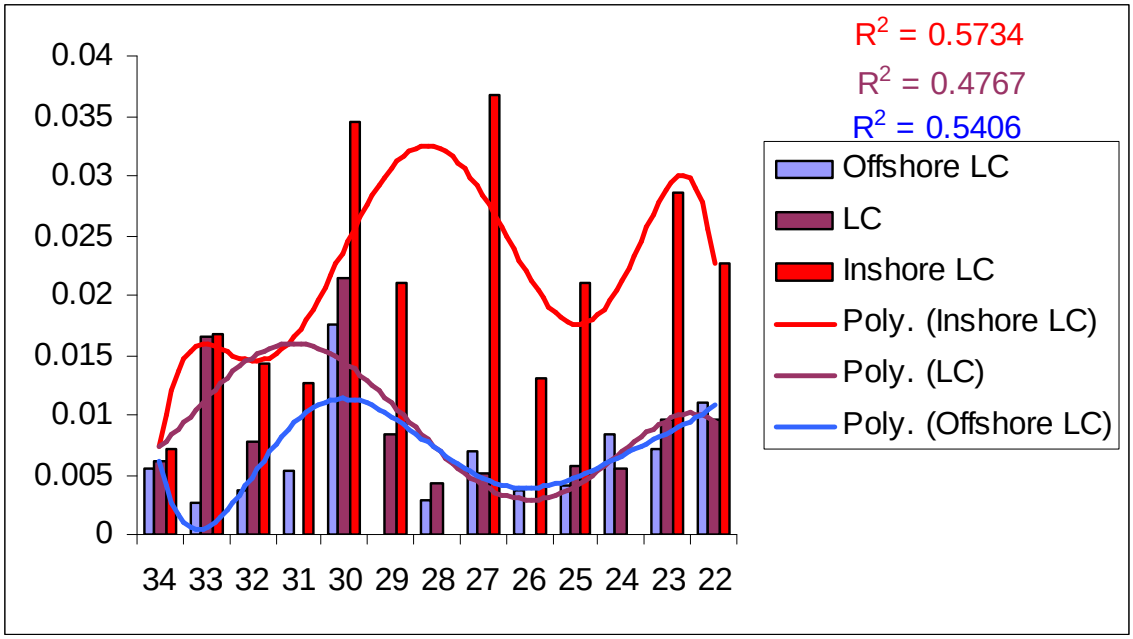

Figure 3.134. Biomass of zooplankton (g AFDW m^{-3}) inshore, in Leeuwin current (LC) and offshore from 34 to 22 ºS.

Larger size fraction (355 to 1000 µm) was a major contributor to total biomass in most stations (Figure 3.135). This size fraction consists mainly of larger copepods, smaller chaetognaths and siphonophores. In general inshore largest organisms (1000 µm +) were more important than offshore and in LC.

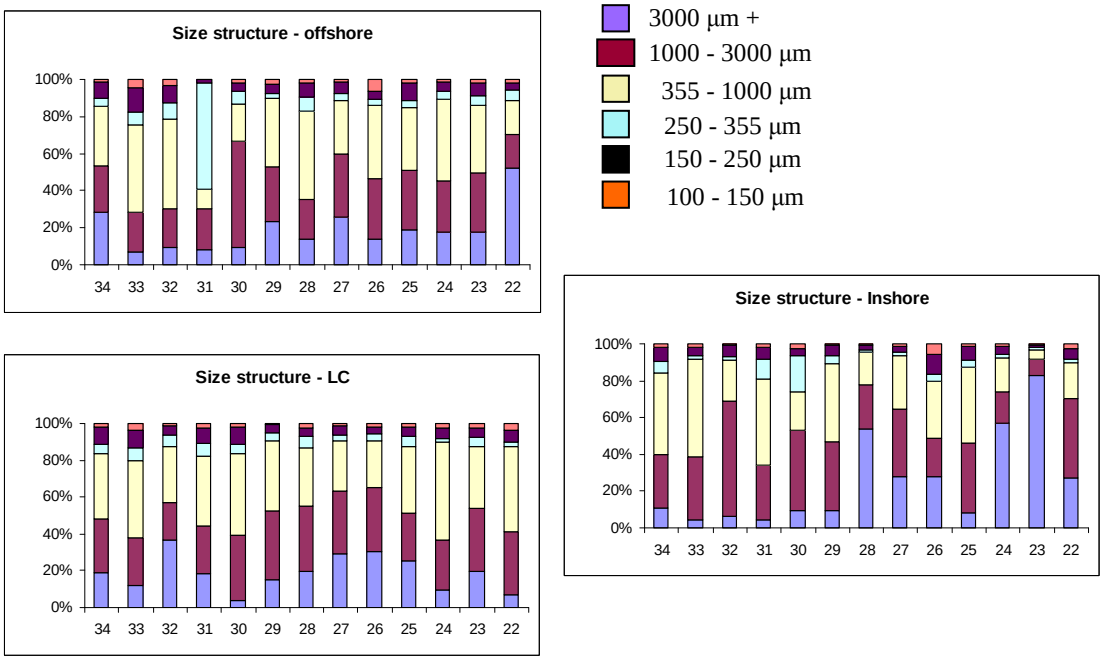

Figure 3.135. Size fractionated biomass of zooplankton (g AFDW m^{-3}).

Size fractionated zooplankton biomass followed total biomass pattern. LC and offshore samples clearly separated from inshore ones (Figure 3.136).

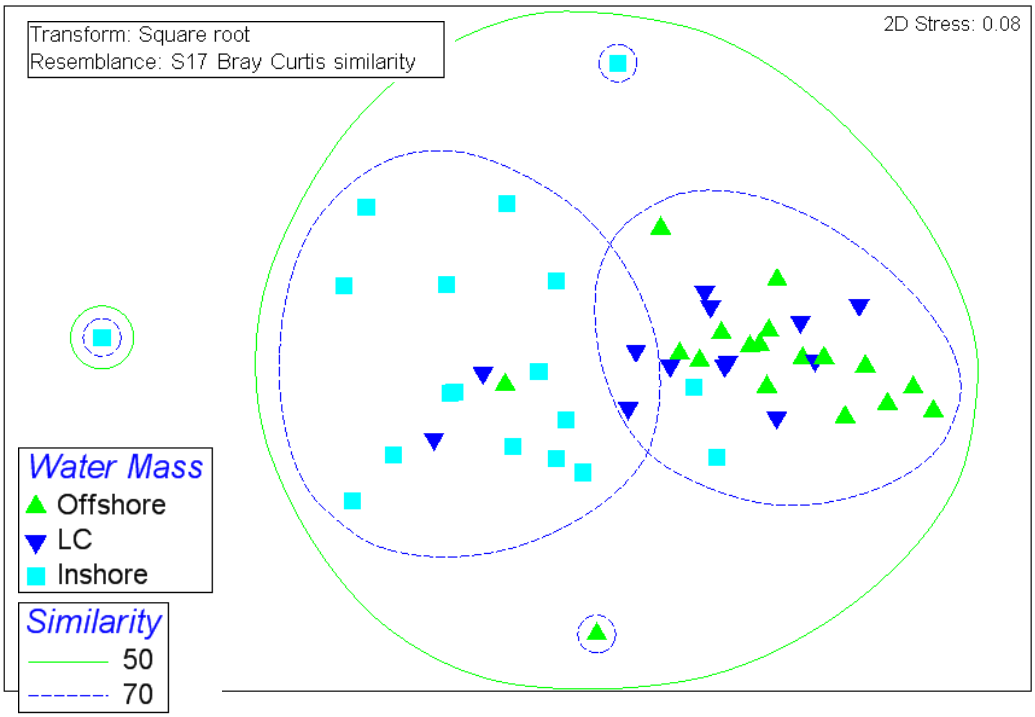

Figure 3.136. Size fractionated biomass: offshore-inshore gradient.

Investigations of process behind the pattern indicated that fluorescence was an important environmental variable best explaining the biomass pattern with Spearman rank correlation Rho = 0.479 (Figure 3.137).

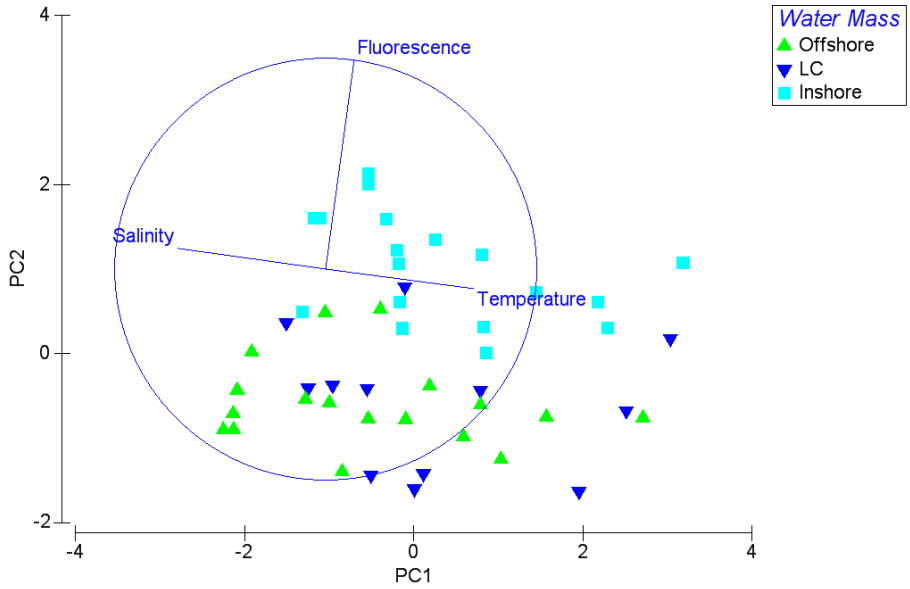

Figure 3.137. Linking biomass to environmental patterns.

We compared zooplankton biomass after conversion to wet weight (using factor of 0.2) with data from Tranter (1962) (Figure 3.138 and Figure 3.139).

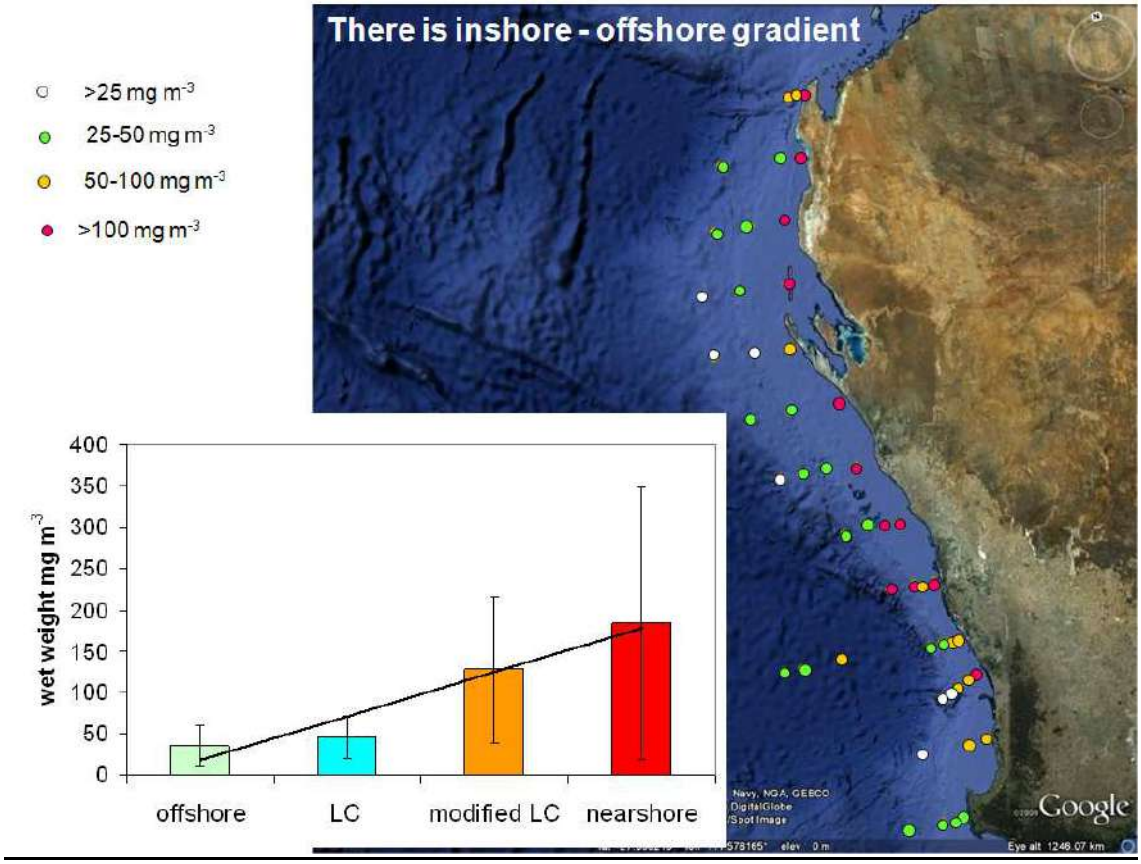

Figure 3.138. Zooplankton biomass (wet weight).

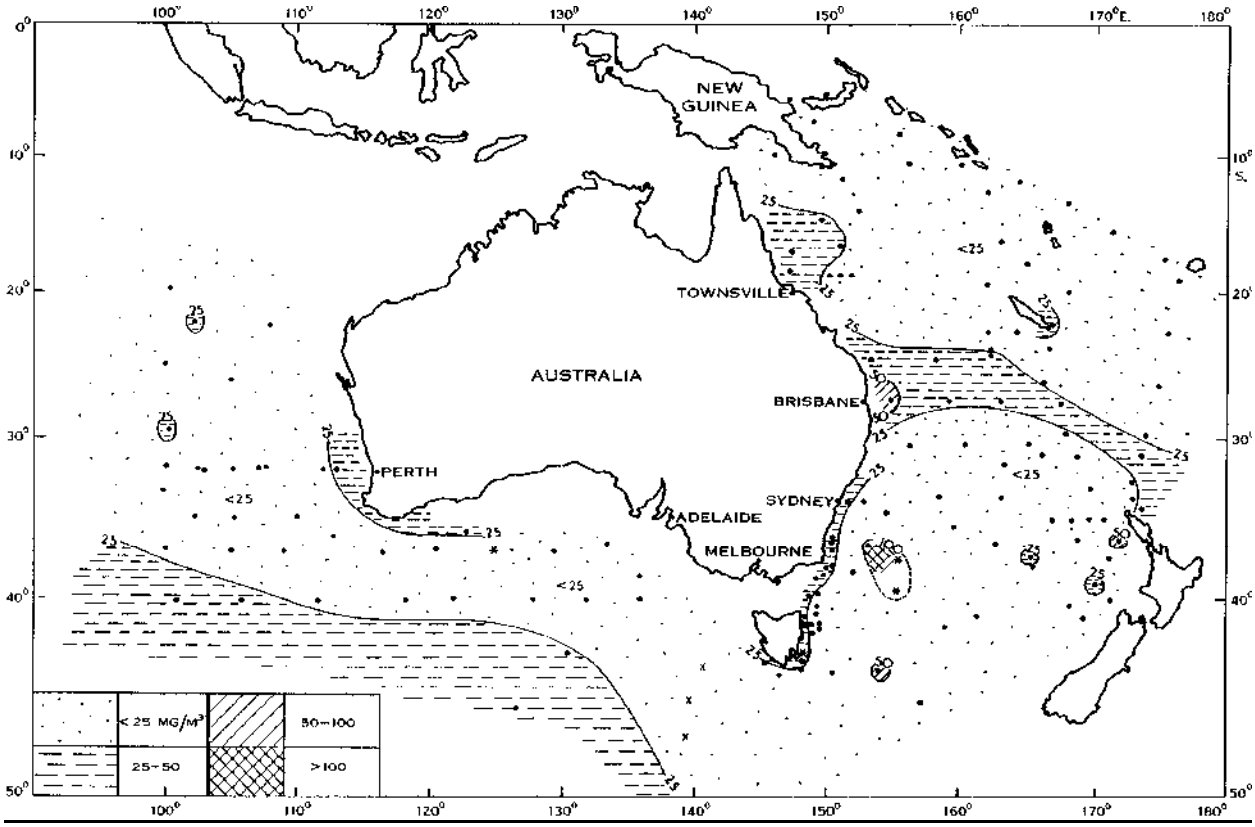

Figure 3.139. Biomass of zooplankton around Australia (from Tranter, 1962).

The comparison with Tranter data shows that biomass was comparable and low offshore but higher in shelf waters during Tranter's survey than during our sampling in the Leeuwin Current. On the global scale zooplankton biomass along our west coast is low (Figure 3.140).

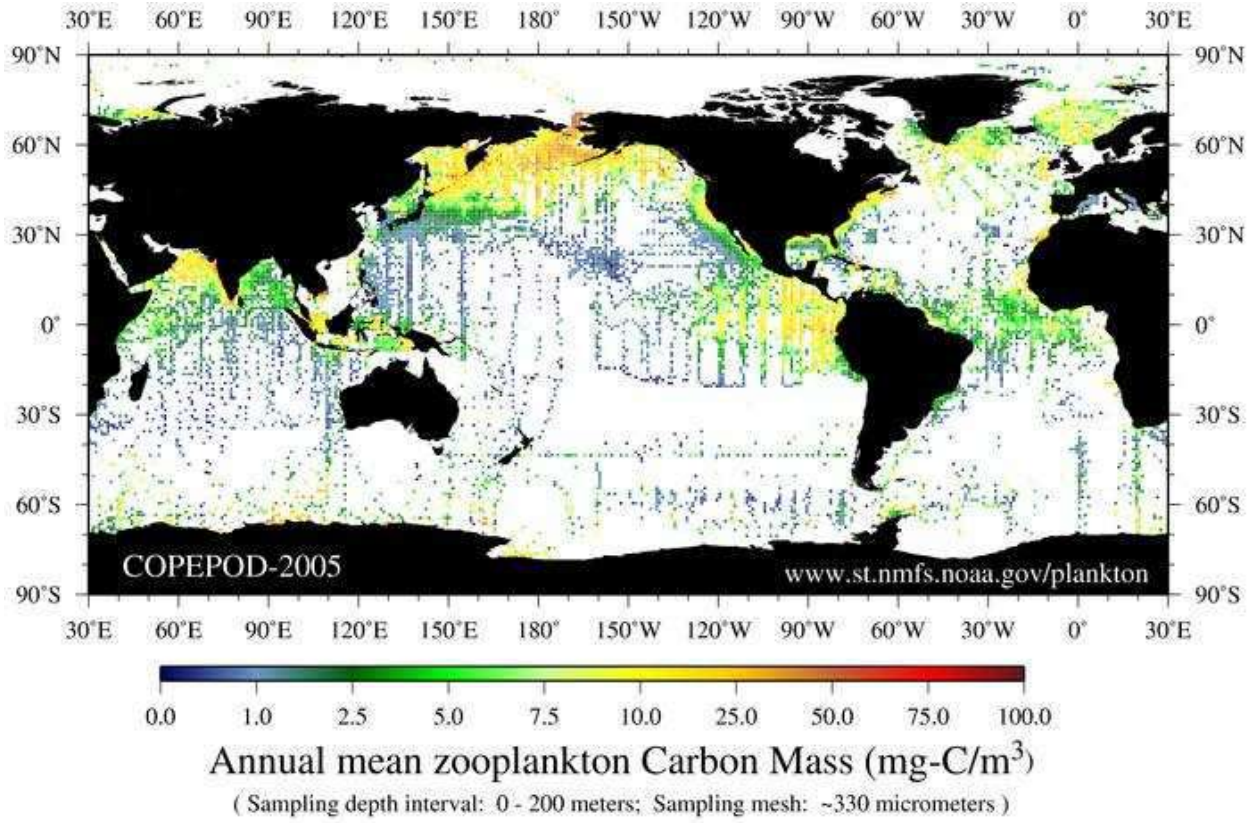

Figure 3.140. Zooplankton biomass around the world.

Discussion

Zooplankton biomass off the west coast showed a strong offshore-inshore trend. North- South pattern was more complicated and asynchronous among the water masses. Large size fractions contributed strongly to biomass however small zooplankton was very important with copepods <355 µm contributing on average about 30% to total biomass. We have no long time series on zooplankton around Australia and only comparison we were able to make was with Tranter, 1962. This gap in reseach is partially being addressed through IMOS reference stations.

Key findings:
In the first large scale survey of zooplankton along the west coast of Australia they were found to be > 5 times more abundant neashore providing a relatively rich coastal environment for the growth of planktonic carnivores such as larval fish.

Zooplankton Nutrition

Introduction

Mesozooplankton from SS04/2007 cruise was analysed for fatty acid composition. Mesozooplankton forms a key trophic link in marine ecosystem and an important mediator of carbon flux. Mesozooplankton uses a wide range of prey including phytoplankton, microzooplankton, bacteria and marine snow. The analysis of fatty acid composition has been applied to reveal dietary components of marine organisms. The use of fatty acid trophic markers is based on the premise that phytoplankton, microzooplankton and bacteria all produce

taxon-specific fatty acids which are retained by their predators and which can be used to quantitatively assess the relative trophic position and dietary quality. The time it takes for copepods (which usually form the bulk of mesozooplankton) to display changes in the fatty acid signatures of their diets varies considerably across genera and also depends on physiological condition but biomarkers integrate the trophic information over a longer time scale of several weeks while traditional approaches like gut content analysis provide information only on recent feeding. Fatty acids can be used to infer trophic relations in copepods because copepods acquire many of the fatty acids required for their growth and reproduction from their diets. Experimental studies have confirmed the trophic biomarker approach. Clear changes in fatty acid compositions could be induced by different phytoplankton diets. However, there are limitations in using fatty acids: no single fatty acid can be assigned uniquely to any one species. Fatty acids are not necessarily metabolically stable and turnover rate can be species specific and depends on metabolic condition of the organisms. Consequently fatty acids have been so far used as quantitative food web markers.

The aim of the project was to examine the variability in mesozooplankton feeding from south to north off Western Australia in three water masses: inshore of Leeuwin Current, in Leeuwin Current and offshore of Leeuwin Current. We hypothesised that mesozooplankton from coastal waters that tend to be more productive would have higher proportion of fatty acids associated with diatoms e.g. 16:1 n-7 and 20:5 n-3 and mesozooplankton from oceanic waters would have more fatty acids associated with small phytoplankton e. g. 18:3 n-3 and 18:4 n-3 and more omnivory or carnivory markers e.g. 18:1(n-9)/18:1(n-7), the proportion of PUFA to saturated fatty acids or ratio of DHA/EPA from microzooplankton prey. The inclusion of biochemical indices of zooplankton can add valuable information about the potential of food quality to higher trophic levels like fish.

Pelagic food webs can be microbial, when small phytoplankton dominates or herbivorous when large phytoplankton dominates. Protozoea (i.e. flagellates and ciliates) feeds on small algae and bacteria. Metazoans graze phytoplankton, flagellates and ciliates ≥ 5 µm. In oligotrophic waters main trophic links to the metazoan is via protozoa. Herbivorous food web is usually dominated by large diatoms and is characterised by efficient transfer of energy to higher trophic levels. Microbial food wed is based in flagellates. Diatoms vs dinoflagellates food web can be differentiated by 16:1 n-7/16:0 ≥ 1, high proportion of 20:5 n-3, high ratio of $\sum$C16 to $\sum$C18 and high ratio of EPA (20:5 n-3) to DHA (22:6 n-3).

The fatty acids were examined to reveal main food web patterns in mesozooplankton from different water masses. 16:1 n-7/16:0 and EPA/DHA ratios exemplify a high degree of correlation of diatom vs dianoflagellate markers (Mayzaud et al. 1976).

Methods

We collected zooplankton using Bongo nets (355 and 100 µm mesh) towed obliquely to depth of the station (nearshore) or 150 m in the Leeuwin Current and offshore waters every parallel from 22 to 34 °S. Mesozooplankton for fatty acid analysis was size fractionated on board and frozen immediately after collection. Therefore fatty acids are a mixture of fatty acids from the food in the guts and fatty acids assimilated into the mesozooplankton body tissues. Lipids were quantitatively extracted from the samples by a single-phase chloroform/methanol method (Bligh and Dyer, 1959), which was modified by substituting dichloromethane for the chloroform. Each sample was added to 20 ml of a 3:6:1 v/v/v dichloromethane/methanol/water solution and held at room temperature overnight. Samples were then centrifuged at 10,000rpm (Orbital 420). After centrifugation, 10 ml of the solution was taken, with 10 ml of dichloromethane, followed by 10 ml of water, added and the mixture centrifuged again. The

bottom dichloromethane solution was then concentrated using a rotatory evaporator under vacuum. The resulting sample was mixed with 2% sodium hydroxyl in methanol refluxing for 10 minutes. Borontrifluoride-methanol complex was then added into the samples and mixed for 2 minutes. Finally, hexane was added. The upper hexane solution was transferred to a gas chromatography (GC) vial for fatty acid analysis by GC analysis.

Gas chromatography (GC) was initially performed using a HP 5890 GC system equipped with FID detector and Agilent 6890 Series injector. The gas chromatograph was equipped with a 60 m x 0.25 mm i.d. and 0.25 um BPX 70 (SGE) with hydrogen (ultra pure) as the carrier gas. The initial oven temperature was set for 100°C, increasing at a rate of 2.5°C/minute to 150°C (held for 2 minutes). Temperature was then increased at 1.5°C/minute to 220°C (held for 1 minute). Finally, the temperature increased at 12°C/minute to 250°C (held for 8 minutes). The peak areas were determined with an integrator (Hewlett-Packard 5890). Peak identifications were based on comparison of retention times with authentic and laboratory standards and subsequent gas chromatographic-mass spectrometric (GC-MS) analysis using an Agilent Technologies 6890N network GC System and 5973 Network Selective Detector. Data were acquired and peak area quantified using ChemStation chromatography software. The abbreviated fatty acid nomenclature used within this paper is A:Bn-X, where A designates the total number of carbon atoms, B the number of double bonds, and X the position of the double bond closest to the terminal methyl group. Since the analysis are derived only from zooplankton fatty acid profiles and there is no information on prey fatty acids it can only provide comparative information.

Size dependent patterns are important in marine ecosystems because invertebrates and planktivorous fish are size selective predators. Remotely sensed ocean colour (SeaWiFS chlorophyll a concentration as indication of phytoplankton biomass) generated by NASA (Giovanni.gsfc.nasa.gov) from April to May 2007 was used to correlate phytoplankton with zooplankton biomass from June-May 2007 cruise. Historical data was used in preference to phytoplankton data collected during the cruise because there is an observed time lag of about 10 weeks between phytoplankton and zooplankton biomass.

Results

There was a significant correlation ($P < 0.01$) between zooplankton and phytoplankton biomass (Figure 3.141) indicating that zooplankton was feeding directly or indirectly (by consuming protozoa that were feeding on phytoplankton) on phytoplankton (Figure 3.141). Note that 4 data points with high biomass were removed from the second (b) analyses. It is not possible to estimate contribution of large zooplankton to total biomass from satellite data however all the samples collected from waters off Western Australia coast indicate that small ($< 5\mu m$) phytoplankton dominates. Since there is a general relationship between chlorophyll and particulate organic carbon (POC) in the euphotic zone of the oceans POC can be estimated from chlorophyll a (Legendre and Michaud, 1999). In turn the concentration of suspended POC provides estimates of biogenic carbon that is a potential food by zooplankton. This correlation indicated that sampled zooplankton was feeding on phytoplankton indirectly by consuming protozoa.

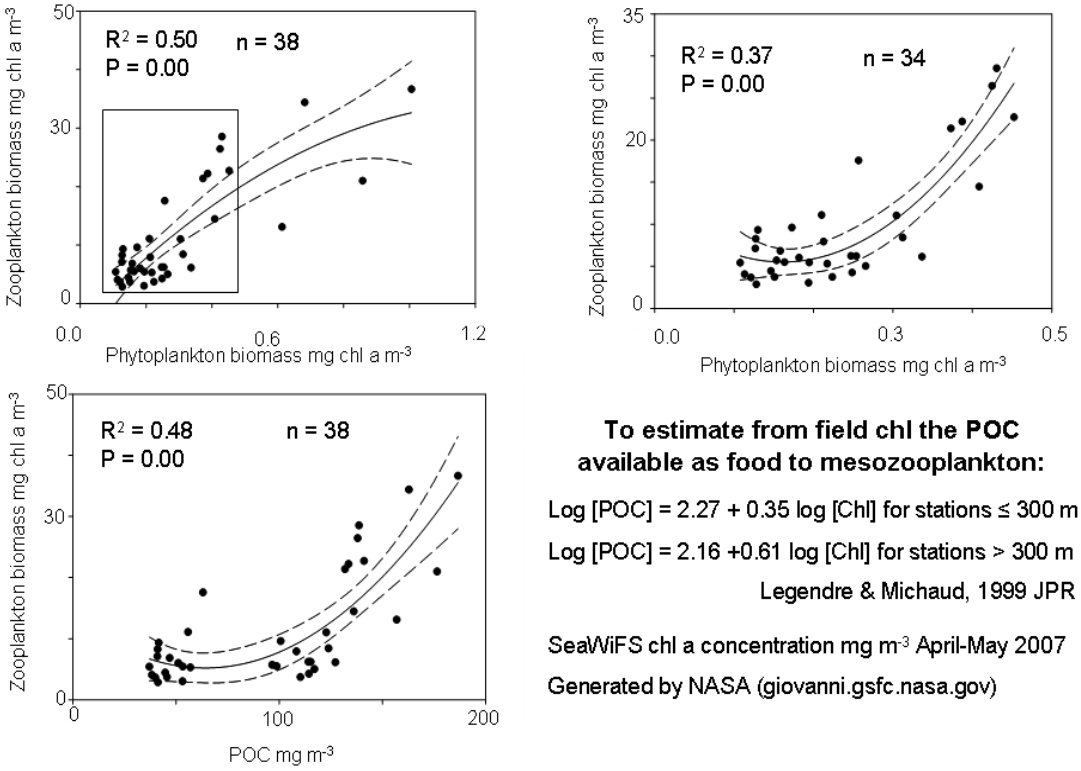

Figure 3.141. Correlation of mesozooplankton biomass with biomass of potential food sources.

We analysed physical and chemical properties of water masses sampled for zooplankton during Southern Surveyor cruise. We averaged temperature, salinity and nutrient values over the depth of zooplankton sampling i.e. from 0 to 150 m or depth of the station. We named water masses based on the stations depths: Oceanic, Leeuwin Current (LC), Modified LC and Coastal corresponding to 1000 to 2000 m, 250-300 m, 70 – 100 m and ≤ 50 m depth respectively.

Water became progressively warmer and less saline from south to north Temperature-salinity diagrams obtained from the measurements from 0 to 150 m (or depth of the stations) show that only oceanic waters clearly separated from the rest in 4 southerly transects. North of 30 ºS all water masses were pretty mixed (Figure 3.142). Physical and chemical properties of the water masses in the upper 150 m were not very different except for offshore waters in most southern parallels.

Nitrate and phosphate were low across the study area and the values decreased from offshore to inshore (Figure 3.143). Redfield ratio of nitrate to phosphate was highest (11 and 12 respectively) in oceanic stations on parallel 33 ºS and 24 ºS and lowest in coastal waters on parallel 32, 29 and 28 ºS and in Modified LC on parallel 23 ºS (<1). At the time of the cruise nutrients in upper 150 m depth in all water masses were too low for large phytoplankton growth. Diatoms would require silicate, phosphate and nitrate concentrations of 3.9, 0.24 and 1.6 µM respectively for growth (Sarthou et al., 2005). In addition Redfield ratio was lower than 16:1 that is optimal for phytoplankton.

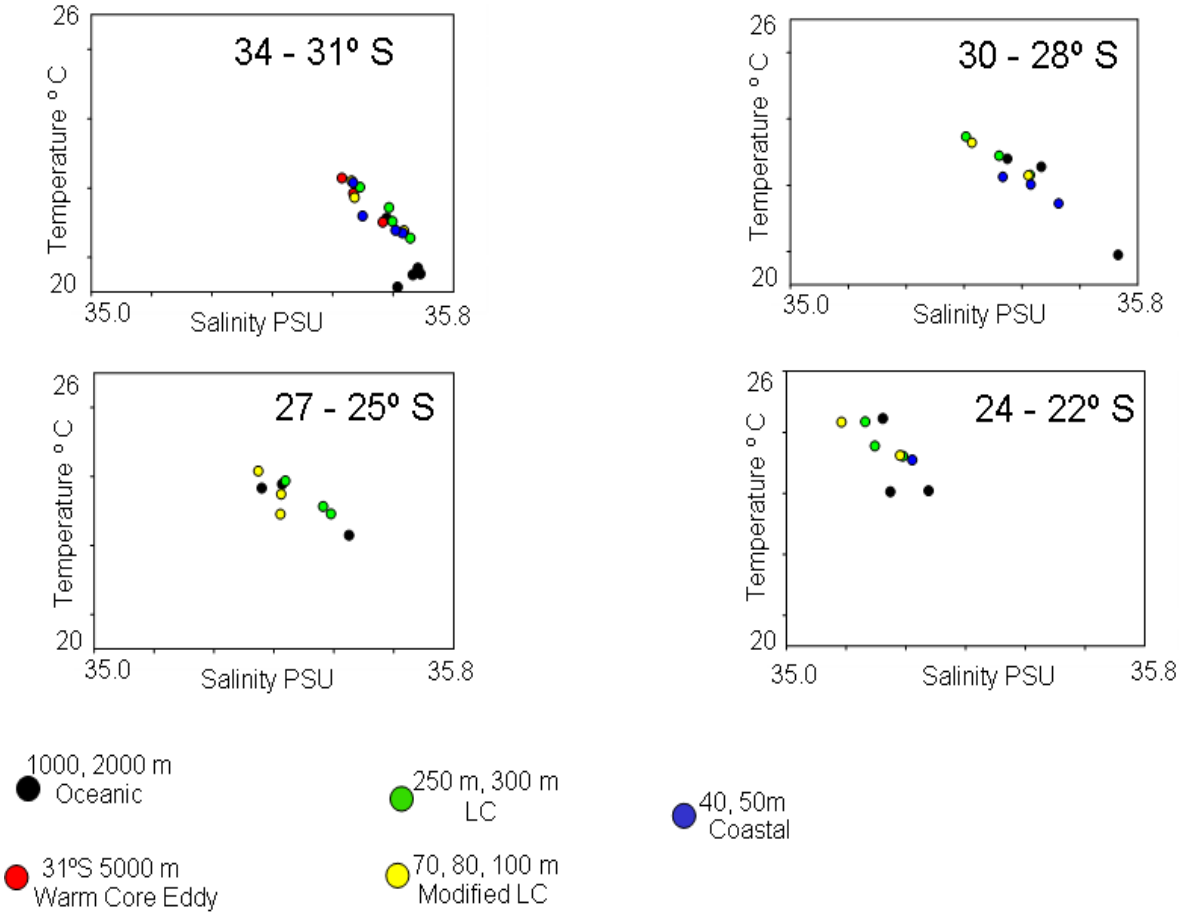

Figure 3.142. Temperature and salinity plots for the study area. Values are an average from 0 to 150 m depth or the depth of the station.

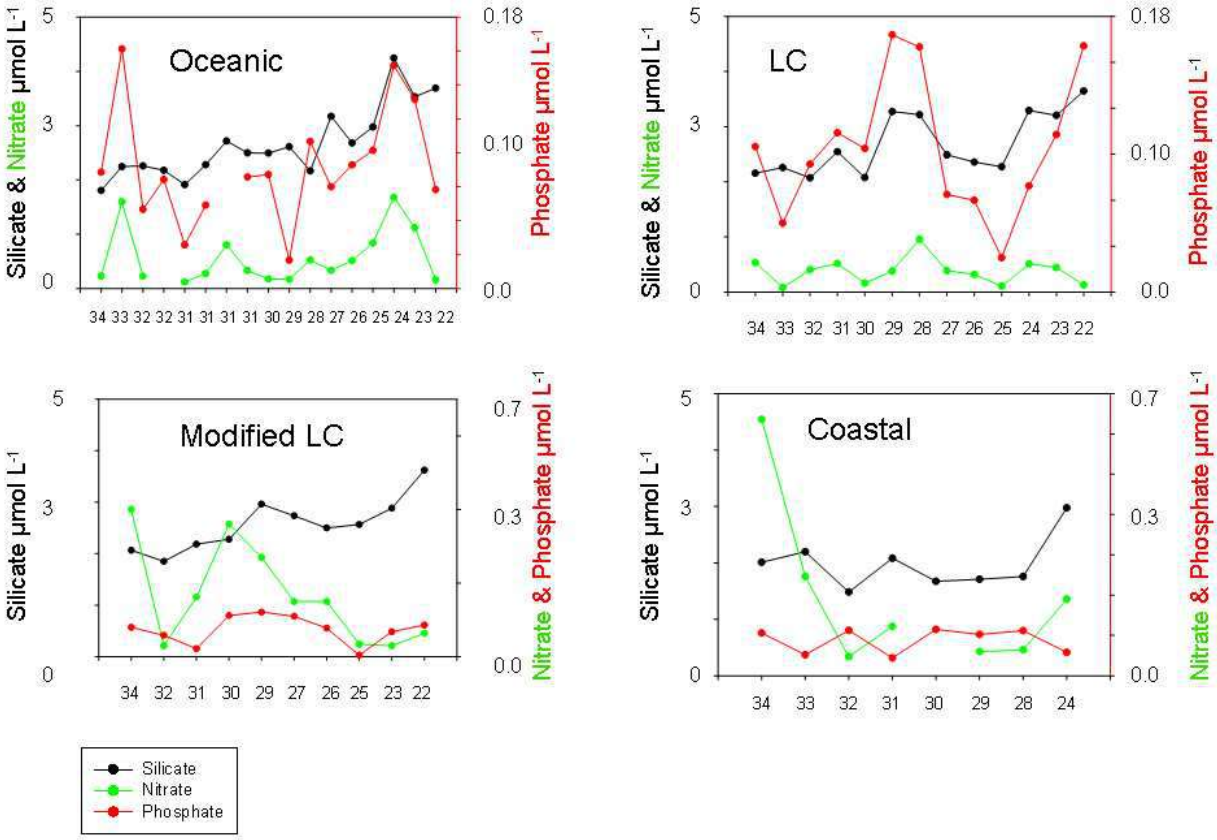

Figure 3.143. Nutrients (mean from 0 to 150 m or station depth) for each parallel. Water masses correspond to same depths as in Figure 3.142.

We extracted SeaWiFS ocean colour data produced from global area coverage with a spatial resolution of 9 km[1] to compare the annual cycle of chlorophyll *a* from 34 to 22 ° S at the stations visited during our cruise to the pattern described by Koslow et al. (2008). Chlorophyll *a* dynamics in 2007 offshore and in the LC waters conformed to observations of Koslow et al. (2008) with autumn/winter peaks throughout the cruise area. Shallower waters between 100 and 50 m deep showed two types of pattern: autumn/winter peak in southern half off WA coast from 34 to 28 ºS and summer peak from 27 to 22 ºS (Figure 3.144).

[1] http://reason.gsfc.nasa.gov/OPS/Giovanni/ocean.seawifs.2.shtml, last visited June 2009.

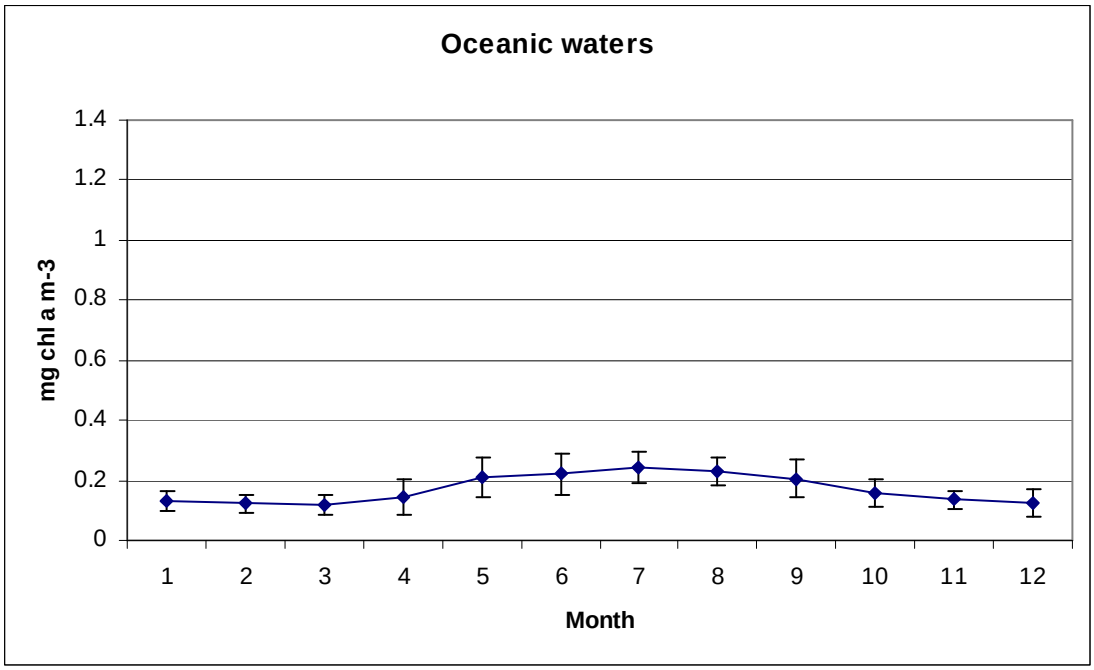
Oceanic waters
mg chl a m-3
1.4
1.2
1
0.8
0.6
0.4
0.2
0
1
2
3
4
5
6
7
8
9
10
11
12
Month

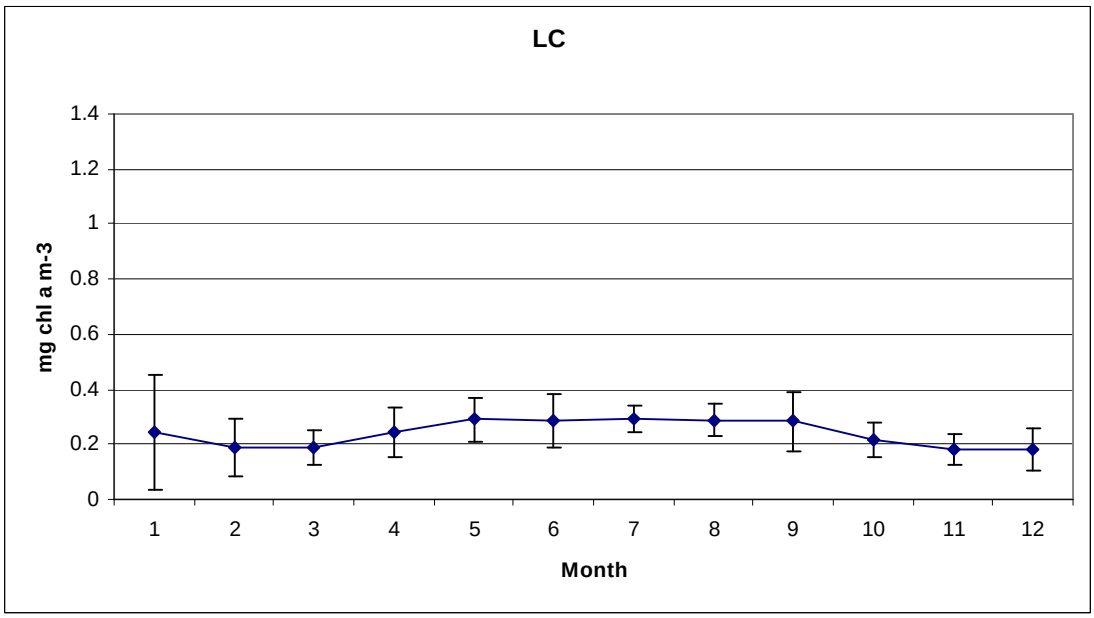
LC
mg chl a m-3
1.4
1.2
1
0.8
0.6
0.4
0.2
0
1
2
3
4
5
6
7
8
9
10
11
12
Month

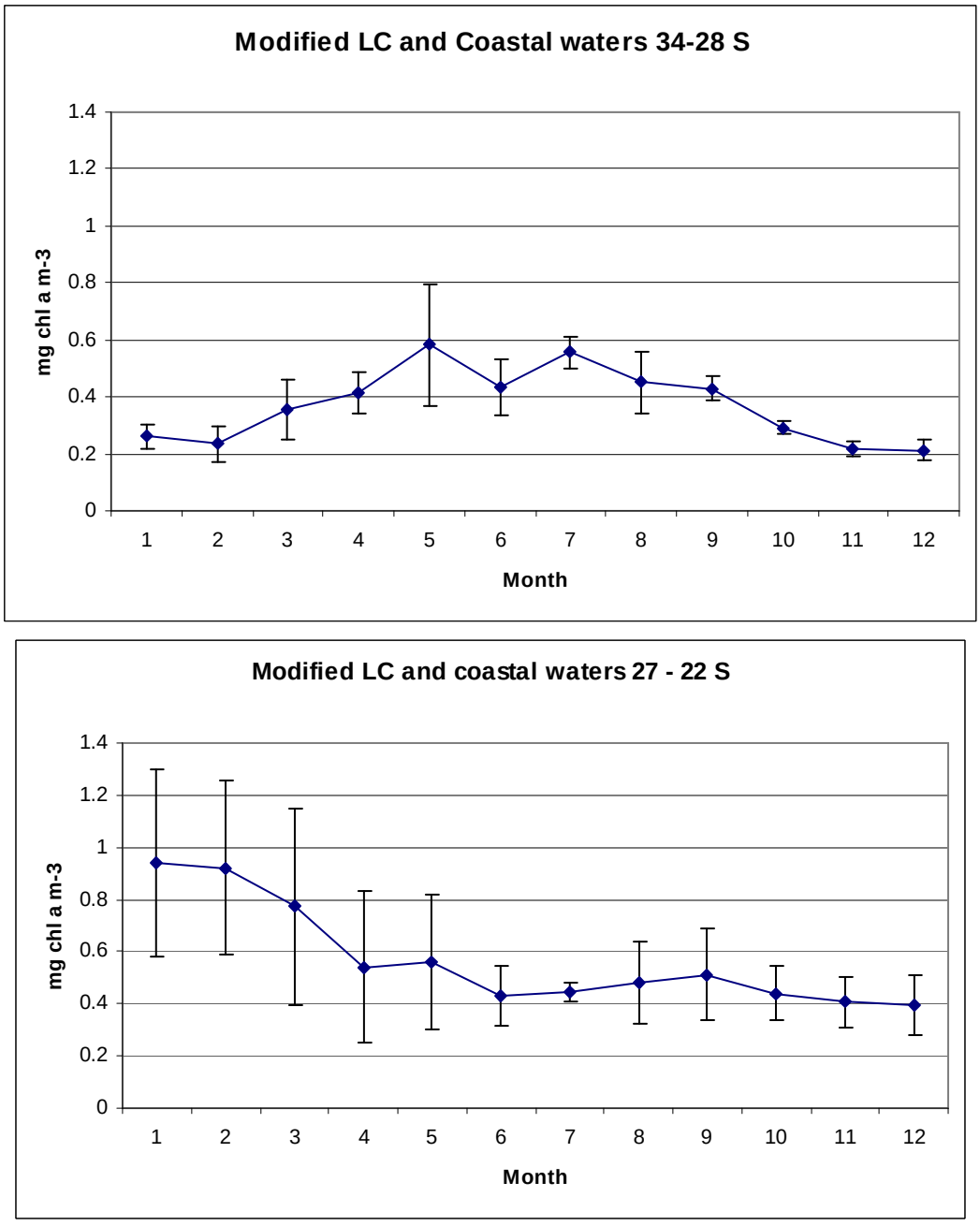

Figure 3.144. Annual pattern of chlorophyll from January to December 2007 in study area.

These environmental data will be used to discuss the pattern of feeding of mesozooplankton revealed by fatty acid analysis.

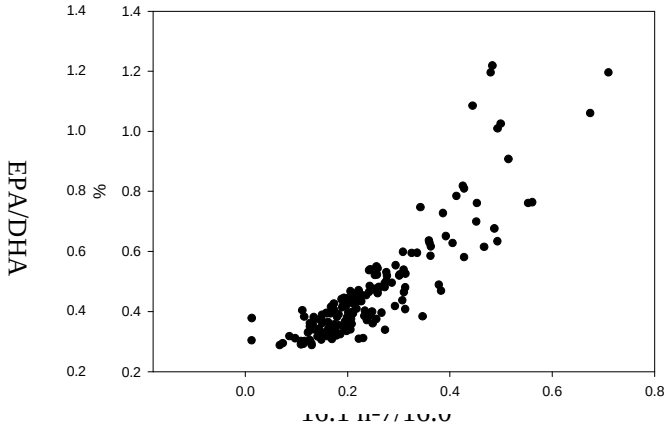

Figure 3.145. Degree correlation r = Pearson's product movement correlation coefficient between diatoms and dinoflagellates markers.

Diatoms vs dinoflagellates food web can be differentiated by 16:1 n-7/16:0 ≥ 1, high proportion of 20:5 n-3, high ratio of ∑C16 to ∑C18 and high ratio of EPA (20:5 n-3) to DHA (22:6 n-3). The fatty acids were examined to reveal main food web patterns in mesozooplankton from different water masses. 16:1 n-7/16:0 and EPA/DHA ratios exemplify a high degree of correlation of diatom vs dinoflagellate markers (Figure 3.145).

There was no difference between inshore and offshore or Leeuwin current water masses in diatom food web markers in zooplankton (Mann Whitney P = 0.9). Dinoflagellate food web dominated of the coast of Western Australia in May/June 2007. Eddy Edge bordering Leeuwin Current had the highest diatom to flagellate ratio however it was still below 1 (a cut off point for diatom dominance) (Figure 3.146).

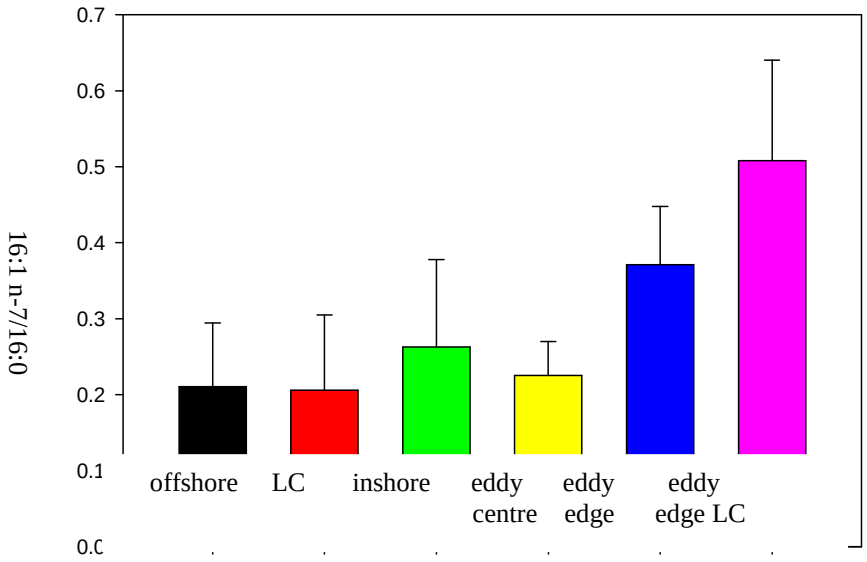

Figure 3.146. Herbivorous (Diatom) vs microbial dinoflagellate food web.

Microbial food web often leads to increase in omnivory where zooplankton selects microzooplankton over phytoplankton. Omnivorous diet is characterised by high 18:1 n-9/18:1 n-7 and high DHA to EPA ratios (Stevens et al. 2004). There was a high degree of correlation between omnivory markers (Figure 3.147).

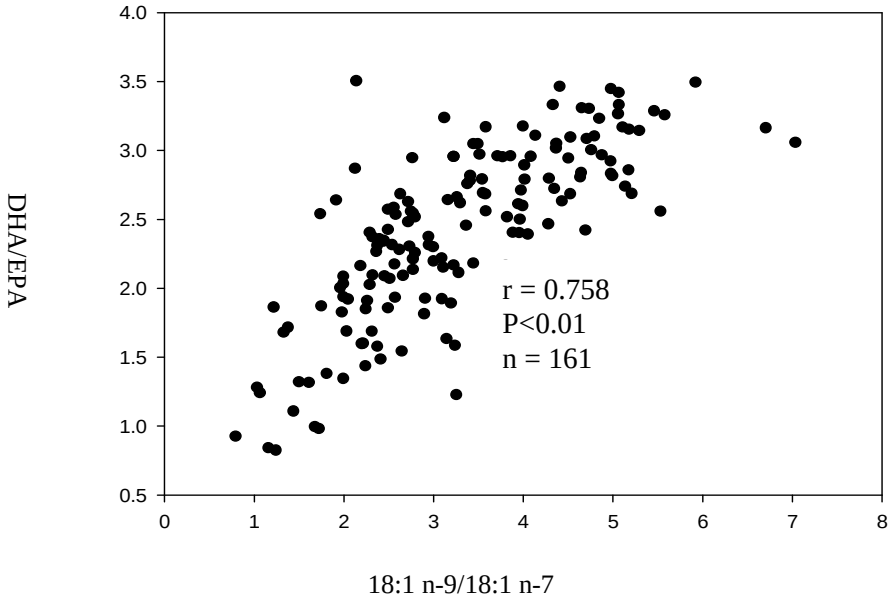

Figure 3.147. Degree of correlation r = Pearson's product movement correlation coefficient between omnivory markers.

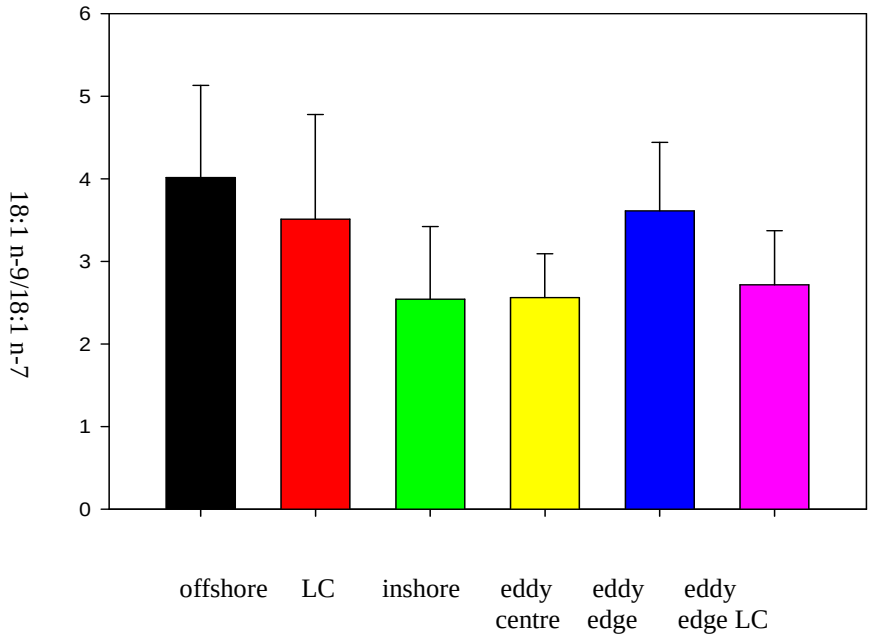

Figure 3.148. Estimated relative degree of omnivory was greatest offshore.

We examined the quality of food for planktivorous fish and fish larvae. Long chain n-3 PUFA are important for fish since they can not convert short chain fatty acids into EPA or DHA. Lack of these essential fatty acids results in low growth and failed recruitment. Fish have higher demand for DHA than EPA. High dietary DHA to EPA ratios are correlated to enhanced growth and survival. High DHA to EPA is critical for growth and neural and eye development of larval and juvenile fish. All water masses had similar levels of EPA and DHA and EPA to AA and there were no significant differences in ratios from offshore to inshore (Kruskal-Wallis, p = 0.8) (Figure 3.149 and Figure 3.150).

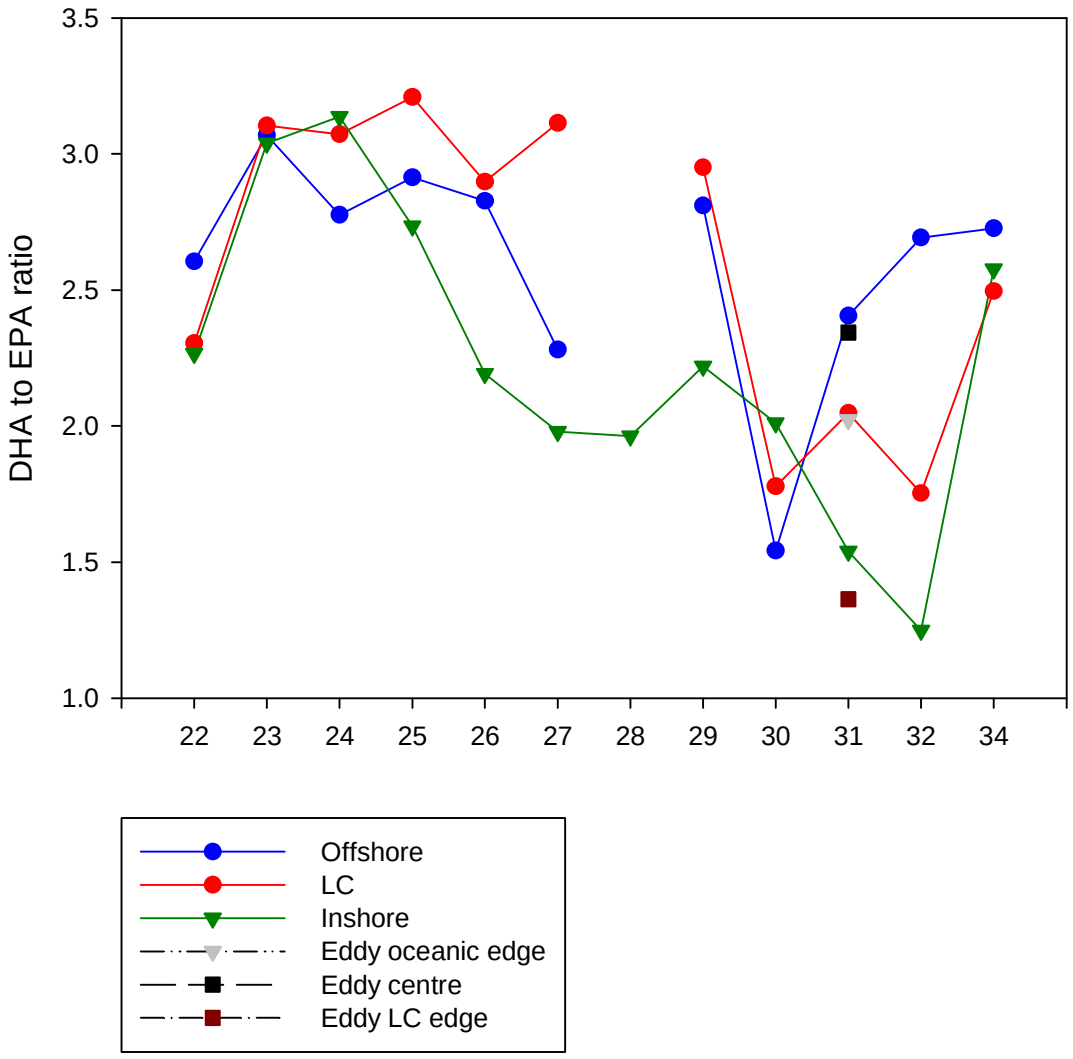

Figure 3.149. Ratio of docosahexaenoic acid (DHA) to eicosapentoic acid (EPA).

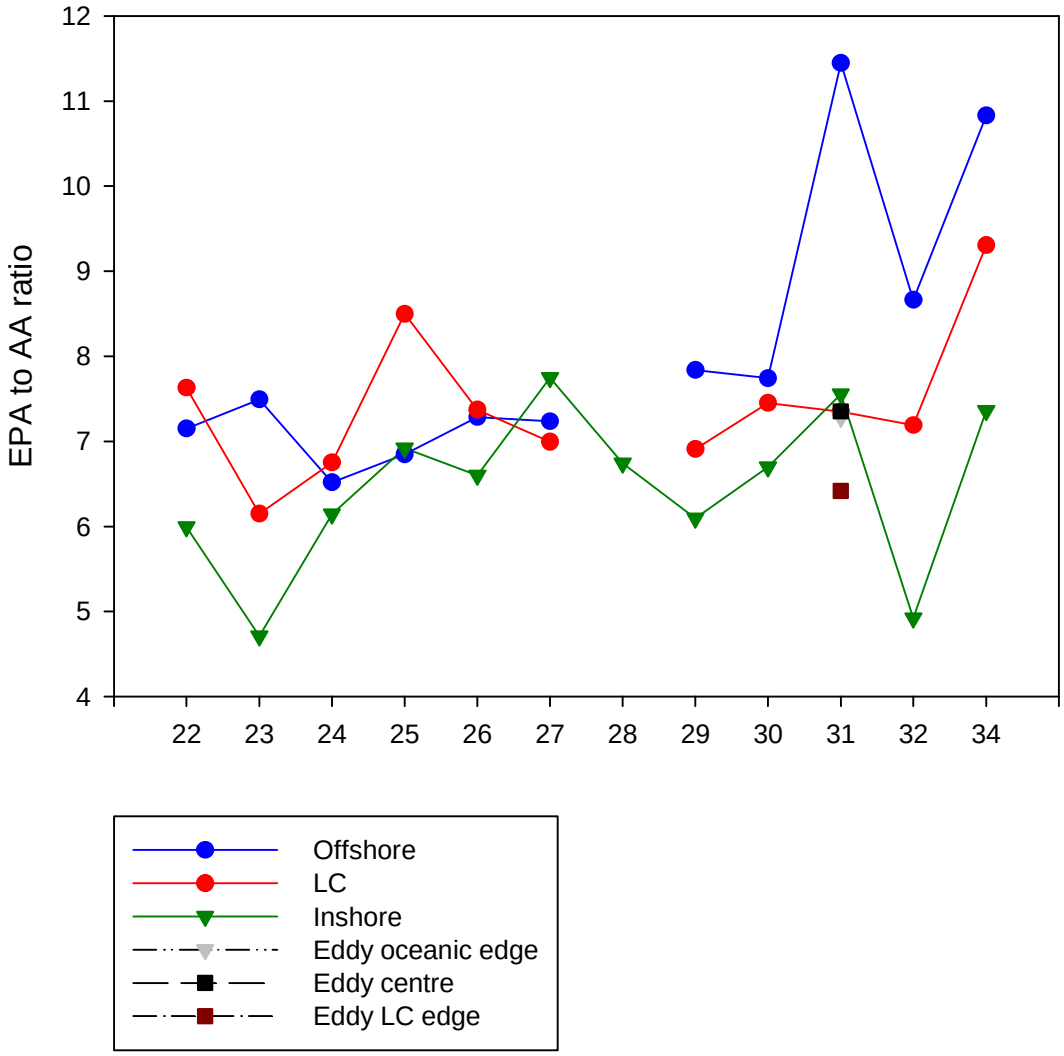

Figure 3.150. Ratio of eicosapentaenoic acid (EPA to arachidonic acid (AA).

Discussion

This is the first study to examine fatty acids in the size fractionated zooplankton samples from the west coast of Western Australia (WA). The fatty acid distribution of zooplankton indicated the dominance of the heterotrophic dinoflagellate food web present off the coast of WA in March - May 2007 based on the diatom to dinoflagellate ratio < 1. Indeed cell counts showed that the dinoflagellate, *Ceratium*, was the dominant microplanktor on the west coast (Figure 3.124) while the pigment biomarker for photosynthetic dinoflagellates was extremely low along the west coast. A largely microbial food web is expected in the oligotrophic waters dominated by small phytoplankton. Copepods fed on a mixed assemblage of small flagellates including cryptophytes, haptophytes and prymnesiophytes. The observed lack of 18:5 n-3 which is a marker for photosynthetic dinoflagellates suggested that zooplankton were feeding on heterotrophic dinoflagellates (i.e. lacking photosynthetic pigment) since only photosynthetic

dinoflagellates contain this fatty acid (Henderson et al, 1988, Okuyama et al., 1993). This result is also consistent with the very low concentrations of peridinin, the pigment marker found in photosynthetic dinoflagellates (Table 3.34) indicating photosynthetic dinoflagellates were about 100 times less abundant than *Synechococcus*, Pelagophytes, Coccolithophorids (haptophytes) and *Prochlorococcus* along most of the west coast. Photosynthetic dinoflagellates were found only infrequently in coastal waters and not found at all at stations further offshore during monthly surveys from 2002 to 2004 along the Two Rocks transect north of Perth, Western Australia yet high proportion of heterotrophic dinoflagellates especially in offshore waters were identified in cell counts from that region throughout the study (Keesing and Heine, 2006). The straight chain 15:0 and iso branched 15:0 and 17:0 suggest some zooplankton feeding on protozoa. Another characteristic that can indicate carnivorous feeding was presence of 18:1 n-9 fatty acids and west coast zoopankton had a mean of 6% ± 1.8 standard deviation (range between 2.7 and 11.3%) compared to over 20% in Arctic copepods and 4.6 and 5 % reported for *Mesocalanus tenuicornis and Nannocalanus minor* respectively from the tropics. Carnivory increased from inshore to offshore while diatom markers were higher in copepods caught inshore (Kattner and Hagen 2009). Fish require three long chain polyunsaturated fatty acids: docosahexaenoic acid DHA, 22:6n-*3*, eicosapentaenoic acid EPA, 20:5n-3 and arachidonic acid AA, 20:4n-6 (Sargent et al, 1999). Ratio of DHA to EPA was above 2 in most west coast stations, sufficient for the dietary requirement of marine fish larvae for normal growth and development. The optimal ratio of AA:EPA is more likely species specific and related to environment ranging from 1:1 in stressful, turbulent environment to 10:1 or greater in stable environment. Zooplankton from offshore and LC contained higher ratio of this PUFA than zooplankton from inshore and the warm core eddy at 31°S sampled in autumn 2007.

Zooplankton Secondary Production

Methods

Using samples from the cruise (SS04/2007) we analysed the size fractionated zooplankton secondary production and its spatial pattern. We assessed the use of the enzymes aminoacyl-tRNA synthetases (AARS) as a proxy of growth of zooplankton. Samples were collected from 22°S to 34°S in the coastal zone, the Leeuwin current (LC) and oceanic environments (station depths of 50m, 300m and 1000-2000m respectively), and in an offshore anticyclonic eddy (Figure 3.151). Mesozooplankton was sampled with a 100µm mesh net from the bottom (coast) or from 150m depth (LC and oceanic stations) to the surface. The samples were size fractioned through 150µm, 250µm and 355µm meshes and frozen inliquid nitrogen for later enzymatic analysis. The biomass (protein), growth (specific Aars activity) and production (community Aars activity) were estimated in four zooplankton size fractions (100-150 µm, 150-250 µm, 250-355 µm and > 355 µm). Aminoacyl t-RNA synthetæses (AARS) are a group of enzymes that catalyse amino acid (αα) activation and the transfer of activated amino acid to their tRNAs It is a first step in protein synthesis, and AARS activity is therefore directly related to protein synthesis. A significant relationship between protein synthesis and growth was observed in cephalopods and fishes. Chang *et al*. (1984) developed a continuous assay for AARS activity. They measured activity based on the release of pyrophosphate (PPi) during aminoacylation (incorporation of PPi into ATP) of tRNA assessed as oxidation of NADH by PPi.

Results

Total zooplankton production was 0.39 mg C m^{-3} day^{-1} nearshore and 0.11 mg C m^{-3} day^{-1} in the Leeuwin Current and offshore. In the eddy centre zooplankton production was 0.07 and 0.07 and 1.18 mg C m^{-3} day^{-1}in the eddy edges. Zooplankton biomass (Figure 3.152), growth

(Figure 3.153) and production (Figure 3.154) were higher inshore than offshore. We observed high production of zooplankton at 29-30°S. The range of growth rates estimated by Aars activity was comparable to rates estimated by more traditional methods (Figure 3.155).

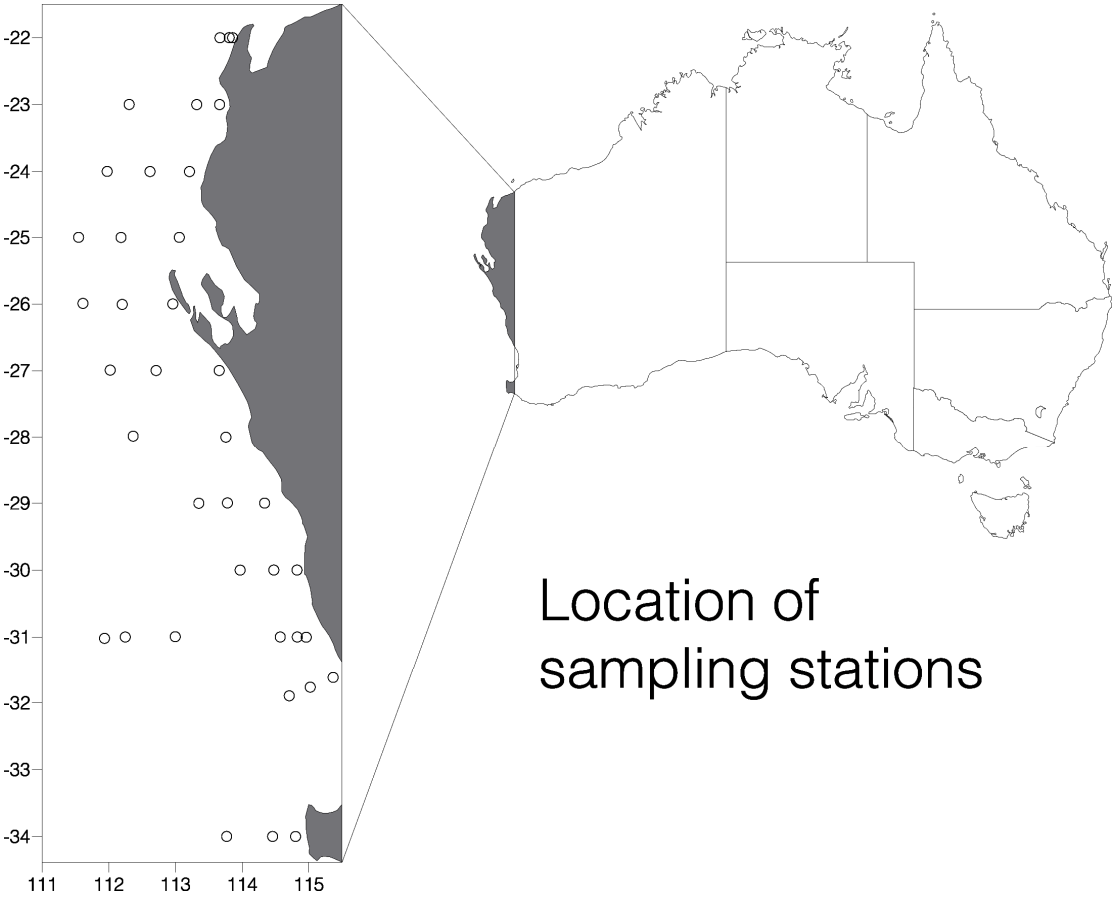

Figure 3.151. Locaton of sampling stations.

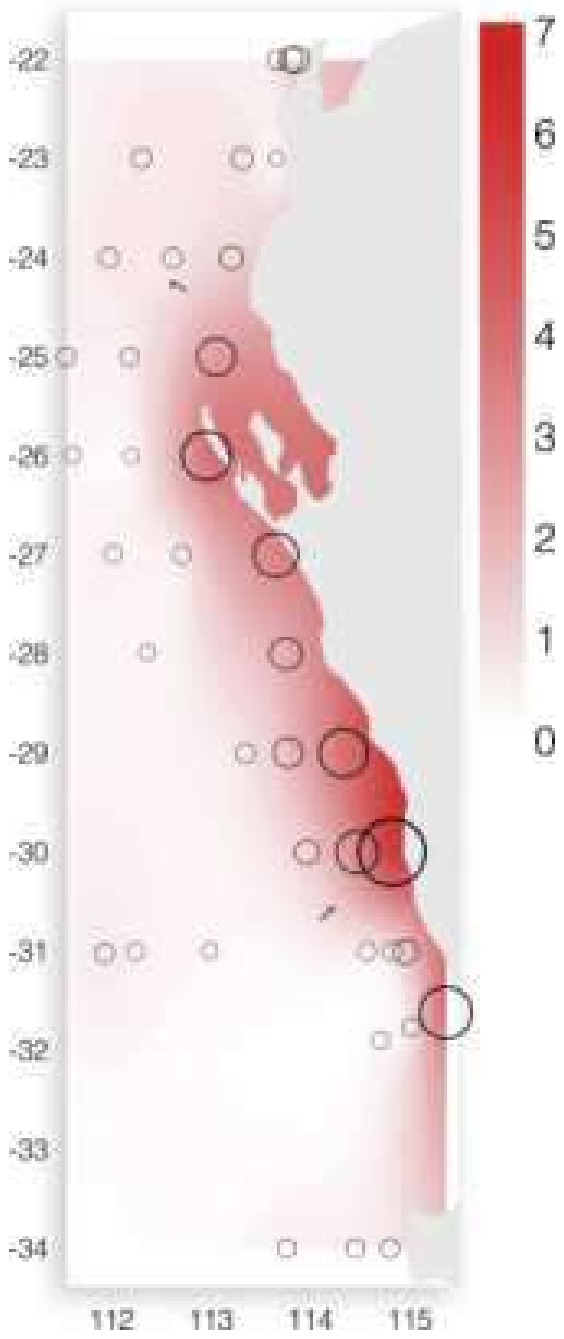

Figure 3.152. Zooplankton biomass (mg Protein m^{-3}).

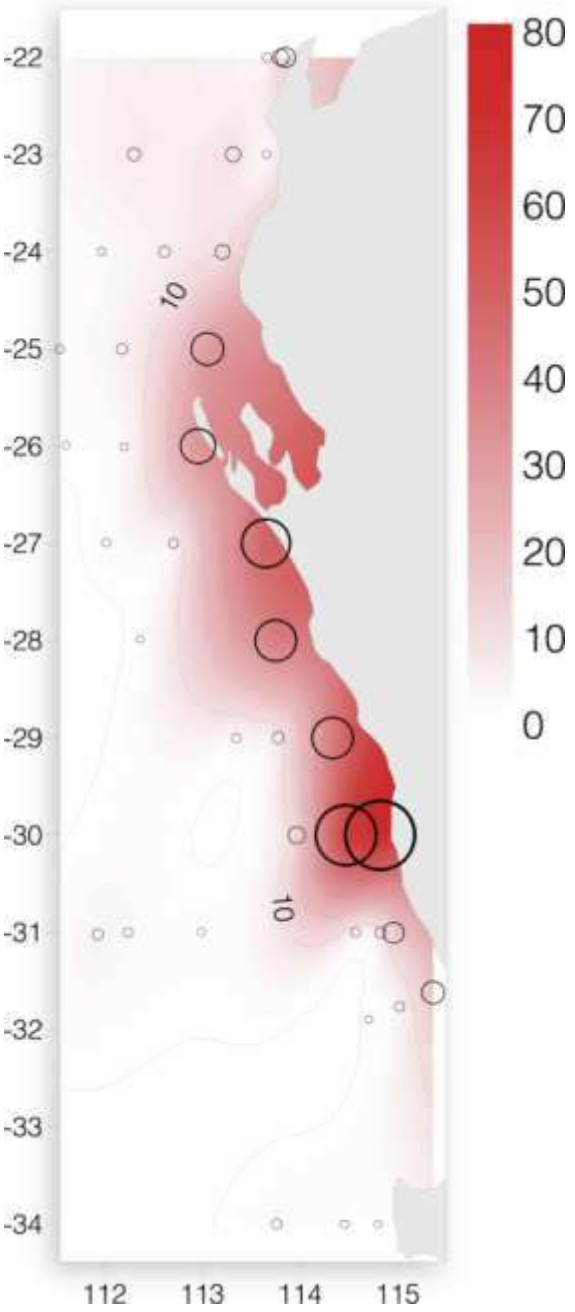

Figure 3.153. Zooplankton growth - specific Aars activity (nm PPi mgProtein^{-1} h^{-1}).

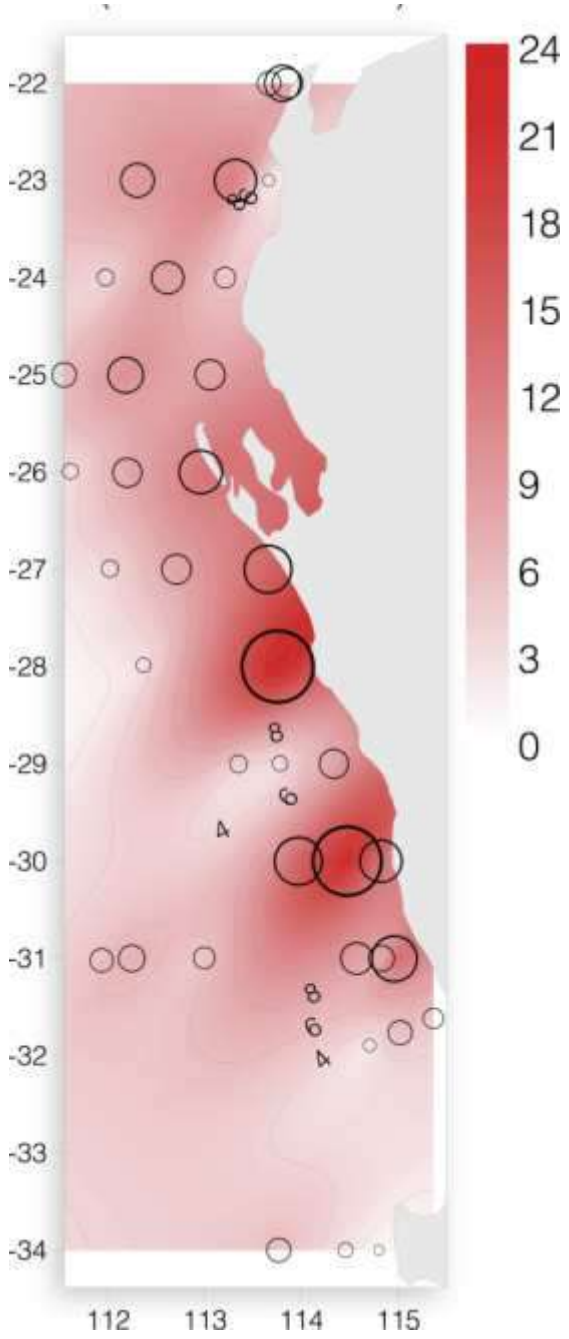

Figure 3.154. Zooplankton Production - community Aars activity (nm PPi m^{-2} h^{-1})

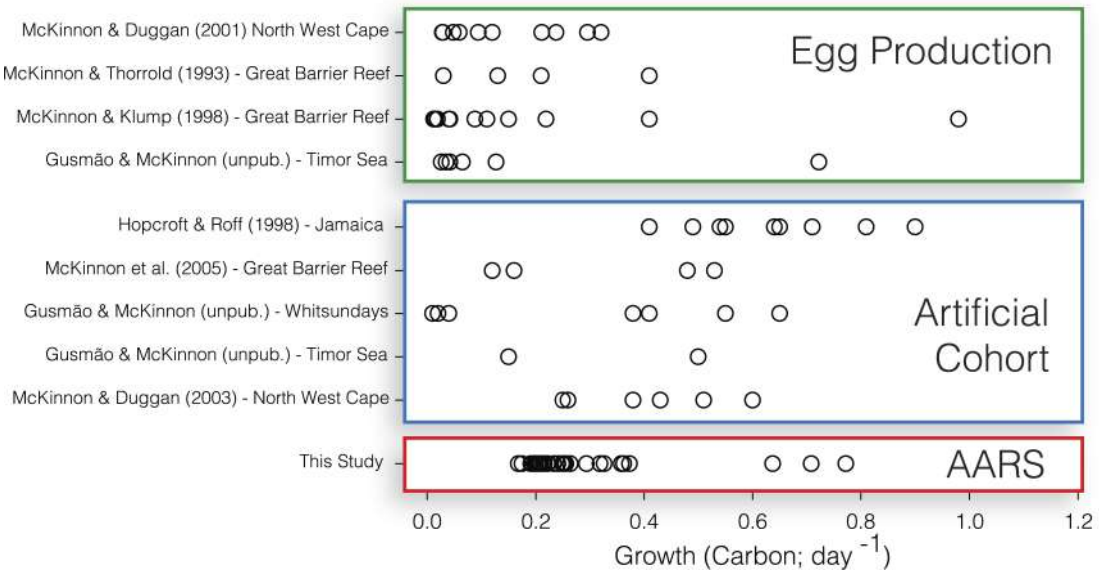

Figure 3.155. Comparison of egg production, artificial cohort and Aars method for estimating growth.

Discussion

There are routine methods in estimating primary production, but no commonly accepted and routine method for measuring secondary production. The 'egg production method' is the most commonly employed, but it is tedious and time consuming. New approaches related to studies of specific enzyme activity are being developed. Our project examined the use of enzyme assay Aars to estimate secondary productioin. The comparison of the growth rates estimated by more traditional methods was comparable to rates from Aars. The use of enzymatic method allows making estimates of zooplankton production on much larger spatial and temporal scale. Samples can be collects during oceanic cruises and frozen for further processing in the laboratory.

The growth rates of zooplankton along WA coast vary spatially but in general coastal areas are more productive than Leeuwin Current or offshore. The enhanced productivity zone at 20-30° S correlated with the deepening of the mixed layer and the production of eddies from the Leeuwin Current. Enhanced production in 5000 m waters in the eddy edge was correlated with advection of more productive nearshore and shelf water masses offshore.

Key findings:
The growth of zooplankton was measured for the first time and found to be associated with mesoscale features of the Leeuwin Current such as eddies and edges.
The microbial food web dominated in all water masses with zooplankton fatty acids profiles suggesting heterotrophic dinoflagellates are a keystone species. Carnivory increased from inshore to offshore while fatty acids originating from diatom were greater in zooplankton caught inshore.

Larval fish

As shown for other boundary current systems (e.g. Hare et el. 2001, Kasai et al. 2002), it is probable that the LC exerts strong influence upon dispersal of pelagic larvae which in turn influences recruitment variability. The LC differs from other eastern boundary currents by transporting low-salinity, warm tropical waters poleward off the WA coast in the south-eastern Indian Ocean (Pearce 1991, Feng et al. 2003, Ridgway and Condie 2004). A recent modelling study of retention and dispersal of shelf waters off WA by Feng et al. (2010) identified several geographical regions of low and high retention based on the physical oceanography. Areas of the continental shelf that experienced low retention were those which were exposed to high alongshore currents, particularly where the LC made considerable incursion over the shelf, and the formation of meso-scale eddies both of which induce vigorous horizontal advection and vertical mixing.

During SS04/2007 13,944 larval fishes from 114 families were sampled and they comprised tropical and temperate as well as oceanic and neritic taxa. In general, the mean abundance of larval fishes was highest at the shelf break (97 larvae m^{-2}) compared to mean abundances on the inner shelf (50 m, 64 larvae m^{-2}) and in oceanic waters (> 1000 m, 70 larvae m^{-2} (Figure 3.156). High abundances at oceanic stations were associated with meso-scale features, for example the very high abundance (mean: 175 larvae m^{-2}) at an oceanic station at 24°S was in association with a cyclonic feature, an eddy situated at 27°S had a mean abundance of 146 larvae m^{-2} but, comparatively, the mean abundance of larval fishes in a developing anti-cyclonic eddy situated offshore at ~31°S was only 34.7 larvae m^{-2}.

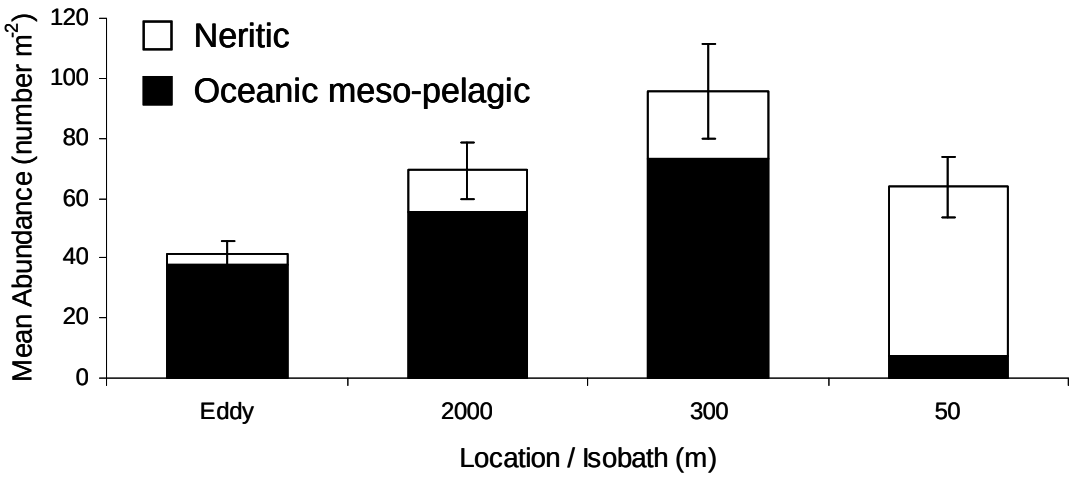

Figure 3.156. Mean abundances of larval fish sampled at every degree of latitude from 34 to 22°S at various depths (isobaths) during May-June 20 07 on SS04/2007.

The shelf break assemblage was dominated by larvae of Myctophidae (particularly *Diaphus* spp.) (>48%) and Phosichthyidae (mostly *Vinciguerria* spp.) (>18%) (Table 3.36). Overall, the larvae of oceanic meso-pelagic taxa accounted for 75% of the total shelf break assemblage. The larvae of neritic families comprised 23% of the total assemblage, the most abundant of which were Bregmacerotidae (4%) and Clupeidae (3%). The diversity of neritic taxa decreased southwards (27 families at 22°S and 9 families at 34°S). In general, the abundances of neritic

larvae at the shelf break at latitudes north of 28°S (mean: 13.9 larvae m^{-2}) were considerably less than those on the inner shelf (mean: 84.3 larvae m^{-2}).

Table 3.36. Percent composition of larval fish assemblages showing the 10 most abundant families by mean abundance (number of larvae / m^{-2}) for each isobath, i.e. 50 m (inner shelf), 300 m (shelf break) and 2000 m (oceanic), which are averaged across latitudes. Spaces with no numbers do not indicate absence. Results are shown for all samples collected off the coast of Western Australia between 22°S and 34°S, May-June 2007.

	Sampling Location			
Family	Inner shelf	Shelf Break	Oceanic	Eddy
	%	%	%	%
Apogonidae	4.3			
Bregmacerotidae	7.2	4.4	3.4	4.9
Callionymidae	1.5			
Champsodontidae	2.8			
Chauliodontidae				1.4
Clupeidae	11.7	3.1		
Engraulidae	37.0	1.4	7.0	
Gobiidae	2.8			
Gonostomatidae		2.0	2.8	0.5
Labridae	1.2	1.7		0.4
Myctophidae	7.2	48.7	45.8	38.5
Notosudidae		2.1	2.0	7.1
Paralepididae			1.1	
Phosicthydae	3.2	18.5	20.5	36.0
Pomacentridae		1.1		
Scombridae		1.5		
Scopelarchidae			1.8	1.2
Serranidae				0.2
Sternoptychidae			2.7	0.8
Triglidae			1.4	
Other neritic taxa	20.2	10.0	8.2	1.8
Other meso-pelagic taxa	0.6	3.6	1.6	2.0

In oceanic waters, the assemblage was dominated by myctophid (46%) and phosychthyid (20%) larvae (Table 3.36). Engraulidae was the most abundant neritic family (7%) but the distribution of these larvae in oceanic waters was spatially restricted and only occurred in high numbers at 27°S (58 larvae m^{-2}). The larvae of coastal and reef-dwelling taxa were also recorded offshore at 27°S and included the acanthurid (*Naso* sp.), Ptereleotrine microdesmids (*Ptereleotris* sp.) and an epinepheline serranid although these tropical larvae were in very low abundances (<1 larva m^{-2}).

Larval fishes were most abundant at the shelf break and high abundances were also recorded in oceanic waters and were in often in association with meso-scale features, for example the cyclonic eddy at 27°S. This eddy assemblage was dominated by larvae of the anchovy *Engraulis* spp. but also comprised the larvae of coastal and reef-dwelling taxa such as the

Acanthurid *Naso* sp., ptereleotrine microdesmids (*Ptereleotris* sp.) and an epinephelin serranid, albeit in concentrations <1 larva m^{-2}. The distribution of these larvae up to 200 nm offshore demonstrates the susceptibility of larvae of coastal neritic fishes to large-scale cross-shelf dispersal off the WA coast in autumn-winter which is, to an extent, in response to circulation of the LC.

Key findings:
During the autumn of 2007 the greatest abundance of larval fishes was found at the continental shelf break where the fast moving surface layer of the Leeuwin Current delivers a flow of phytoplankton and zooplankton. Successful recruitment of neritic larvae to the location of origin probably requires behaviours such as vertical migration out of the surface current.

3.2.7 References

Austin R. H., 1973. CSIRO's role in fisheries and oceanography. Australian Fisheries 32: 8-21.

Bligh, E.G., Dyer W.J., 1959. A rapid method of lipid extraction and purification. Can. J. Biochem. Physiol. 37 (8) 911-917.

Caputi, N., 2008. Impact of the Leeuwin Current on the spatial distribution of puerulus settlement of the western rock lobster (*Panulirus cygnus*) and implications for the fishery of Western Australia. Fish. Oceanogr. 17 (2), 147–152.

Caputi, N., 2008. Impact of the Leeuwin Current on the spatial distribution of puerulus settlement of the western rock lobster (*Panulirus cygnus*) and implications for the fishery of Western Australia. Fish. Oceanogr. 17 (2), 147–152.

Caputi, N., Chubb, C., Pearce, A., 2001. Environmental effects on recruitment of the western rock lobster, *Panulirus cygnus*. Mar. Freshw. Res. 52 1167–1174. doi:10.1071/MF01180

Condie, S.A., Dunn, J.R., 2006. Seasonal characteristics of the surface mixed layer in the Australasian region: implications for primary production regimes and biogeography. Mar. Freshw. Research 57 (6) 569-590.

Cresswell, G. R., and Golding, T. J., 1980. Observations of a south flowing current in the south-eastern Indian Ocean. Deep-sea Res. 27A**,** 449-66.

Dietz, H., Matear, R., Moore, T., 2009. Nutrient supply to anticyclonic meso-scale eddies off western Australia estimated with artificial tracers released in a circulation model. Deep-Sea Research I 56 (9), 1440-1448.

Feng, M., Meyers, G., Pearce, A., Wijfels, S., 2003. Annual and interannual variations of the Leeuwin Current at 32°S. *J Geophys Res* 108: (C11), 3355 doi:10.1029/2002JC001763.

Feng, M., Slawinski, D., Beckley, L.E., Keesing ,J.K., 2010. Retention and dispersal of shelf waters influenced by interactions of ocean boundary current and coastal geography. *Mar Fresh Res* 61(11): 1259-1267.

Feng, M., Majewski, L., Fandry, C. and Waite, A., 2007. Characteristics of two counter-rotating eddies in the Leeuwin Current system off the Western Australian coast. Deep-Sea Research II 54: 961-980.

Feng, M., Waite, A., Thompson, P.A., 2009. Climate variability and ocean production in the Leeuwin Current system off the west coast of Western Australia. Journal of the Royal Society of Western Australia. 92, 67-81.

Greenwood, J.E., Feng, M., Waite, A.M., 2007. A one-dimensional simulation of biological production in two contrasting mesoscale eddies in the south eastern Indian Ocean. Deep Sea Research 54 (8-10) 1029-1044.

Griffiths, F.P., Fleminger, A., Kimor, B. and Vannucci, M., 1976. Shipboard and curating techniques in: Part I Zooplankton fixation and preservation ed Steedman, H.F. pp 17-33. The Unesco Press, Paris,

Hanson, C.E., Pattiaratchi, C.B., Waite, A.M., 2005. Seasonal production regimes off south-western Australia: influence of the Capes and Leeuwin Currents on phytoplankton dynamics. Marine and Freshwater Research 56 (8), 1011-1026.

Hare, J.A., Fahay, M.P., Cowen, R., 2001. Springtime ichthyoplankton of the slope region off the north-eastern United States of America: larval assemblages, relation to hydrography and implications for larval transport. Fish Oceanogr 10:164-192.

Henderson, R.J., Leftley, J.W., Sargent, J.R., 1988. Lipid composition and biosynthesis in the marine dinoflagellate *Crypthecodinium cohnii*. Phytochemistry, 27, 1679-1683

Jitts, H.R., 1969. Seasonal variations in the Indian Ocean along 110°E IV. Primary production. Aust. J. mar. Freshwat. Res., 20, 65-75

Johnson, K.S., Coletti, L.J., 2002. In situ ultraviolet spectrophotometry for high resolution and long-term monitoring of nitrate, bromide, and bisulfide in the ocean. Deep Sea Research I, 53 (3), 561-573.

Kamykowski, D., Zentaram S-J., Morrison, J.M., Switzer, A.C., 2002. Dynamic global patterns of nitrate, phosphate, silicate, and iron availability and phytoplankton community composition from remote sensing data. Global Biogeochemical Cycles 16:1077, doi:10.1029/2001GB001640

Kasai A, Kimura S, Nakata H & Okazaki Y. 2002. Entrainment of coastal water into a frontal eddy of the Kuroshio, and its biological significance. J Mar Syst 37:185-198

Kattner, G. and Hagen, W. 2009 Lipids in marine copepods: latitudinal characteristics and perspective to global warming, In Lipids in Aquatic Ecosystems, Arts, M.T., Brett, M.T., Kainz, M.J. eds.Springer Dordrech Heidelberg London, New York. P 265 table 11.3.

Kattner, G., Albers, C., Graeve, M., Schnack-Schiel S. B., 2003. Fatty acid and alcohol composition of the small polar copepods, Oithona and Oncaea : indication on feeding modes. Polar Biology, 26, 666-671

Keesing, J.K. and Heine, J.N. (Eds.), 2006. Strategic Research Fund for the Marine Environment (SRFME): Final Report, volume two. CSIRO, 274 pp.

Koslow, J.A, Pesant, S., Feng, M., Pearce, A., Fearns, P., Moore, T., Matear, R., Waite, A., 2008. The effect of the Leeuwin current on phytoplankton biomass and production off Southwestern Australia. Journal of Geophysical Research, 113, 1-19.

Legeckis, R., and Cresswell, G. R., 1981. Satellite observations of sea-surface temperature fronts off the coast of western and southern Australia. Deep-sea Res. 28A**,** 297-306.

Lourey, M.J., Dunn, J.R., Waring, J., 2006. A mixed-layer nutrient climatology of Leeuwin Current and Western Australian shelf waters: seasonal nutrient dynamics and biomass, Journal of Marine Systems 59 (1-2), 25–51.

Maxwell, G.J.H., and Cresswell, G.R., 1981. Dispersal of tropical marine fauna to the Great Australian Bight by the Leeuwin Current. Aust. J. Mar. Freshw. Res. 32**,** 493-500.

Mayzaud, P., Eaton, C.A., Ackman, R.G., 1976. The occurrence and distribution of octadecapentaenoic acid in a natural plankton population: a possible food chain index. Lipids 11(12): 858-862

Moore, T.S., Matear, R.J., Marra, J., Clementson, L., 2007. Phytoplankton variability off the Western Australian Coast: mesoscale eddies and their role in cross-shelf exchange. Deep-Sea Research II, 54 (8-10): 943-960.

Nagao, N., Toda, T., Takahashi, K., Hsmasaki, K., Kikuchi, T, and Taguchi, S., 2001. High ash content in net plankton samples from shallow coastal waters: possible source of error in dry weights measurements of zooplankton biomass. Journal of Oceanography, 57, 105-107

Okuyama, H., Kogame, K., Takeda, S., 1993. Phylogenetic significance of the limited distribution of octadecapentaenoic acid in prymnesiophytes and photosynthetic dinoflagellates. Proc. NIPR Symp. Polar Biol., 6 21-26

Pearce, A.F., 1991. Eastern Boundary Currents of the Southern Hemisphere. J R Soc W A 74:35-45.

Polovina, J. J., Howell, E.A., Abecassis, M., 2008. Ocean's least productive waters are expanding, Geophys. Res. Lett., 35, L03618, doi:10.1029/2007GL031745.

Postel, L., Fock, H., and Hagen, W., 2000. Biomass and Abundance in: Chapter 4 Biovolume and Biomass Determination, ICES Zooplankton Methodology Manual eds Harris, R., Wiebe, P., Lenz. J., Skjoldal, H.R. and Huntley, M. pp 83-192 Academic Press, San Diego.

Ridgway, K.R., Condie, S.A., 2004. The 5500-km-long boundary flow off western and southern Australia. J. Geophys. Res. 109, C04017

Rochford, D.J., 1952. A comparison of the hydrological conditions off the eastern and western coasts of Australia. Proc. Indo-Pacific Fish. Coun. 3**,** 61-8.

Rochford, D.J., 1962. Hydrology of the Indian Ocean. 11. The surface waters of the south-east Indian Ocean and Arafura Sea in the spring and summer. Aust. J. Mar. Freshw. Res. 13, 226-51.

Rochford, D.J., 1969. Seasonal variations in the Indian Ocean along 110°E. I. Hydrological structure of the upper 500 m. Aust. J. Mar. Freshw. Res. 20, 1-50.

Rochford, D.J., 1984. Effect of the Leeuwin Current upon sea surface temperatures off south-western Australia. Aust. J. Mar. Freshw. Res. 35, 487-9.

Rochford, D.J., 1969. Seasonal variations in the Indian Ocean along 110°E. I. Hydrological structure of the upper 500m. Australian Journal of Marine and Freshwater Research. 20 (1), 1-50.

Sargent, J.R., Bell, G., Mc Envoy, L., Tocher, D., Estevez, A., 1999. Recent developments in the essential fatty acid nutrition of fish. Aquaculture, 177, 191-199

Sarthou, G., Timmermans, K. R., Blain, S. et al., 2005. Growth physiology and fate of diatoms in the ocean: a review. Journal of Sea Research, 53, 25–42.

Schiller, A., Oke, P.R., Brassington, G.B., Entel, M., Fiedler, R., Griffin, D.A. and Mansbridge, J., 2008. Eddy-resolving ocean circulation in the Asian-Australian region inferred from an ocean reanalysis effort. Progress in Oceanography, doi:10.1016/j.pocean.2008.01.003.

Smith, S.V., 1984. Phosphorus versus nitrogen limitation in the marine environment. Limnology and Oceanography 29: 1149-1160.

Stevens, C.J., Deibel, D., Parrish, C.C., 2004. Incorporation of bacterial fatty acids and changes in a wax ester-based omnivory index during a long-term incubation experiment with Calanus glacialis Jaschnov. J Exp Mar Biol Ecol 303:135–156

Thompson, H., 1939. The investigation of the fishery resources of the Australian Commonwealth. . Aust. J. Sci., 1: 137-142.

Thompson, P.A. , Baird, M.E., Ingleton, T., Doblin, M.A., 2009. Long-term changes in temperate Australian coastal waters and implications for phytoplankton. Marine Ecology Progress Series 384: 1-19.

Thompson, P.A., Bonham, P., Waite, A.M., Clementson, L.A., Cherukuru, N., Doblin, M.A., 2010. Contrasting oceanographic conditions and phytoplankton communities on the east and west coasts of Australia. Deep Sea Research II 58: 645-663.

Thompson, P.A., Wild-Allen, K., Lourey, M., Rousseaux, C., Waite A.M., Feng, M., Beckley L.E. (in press). Nutrients in an oligotrophic boundary current: Evidence of a new role for the Leeuwin Current. Progress in Oceanography.

Thompson, R.O.R.Y., 1984. Observations of the Leeuwin Current off Western Australia. Journal of Physical Oceanography, 14(3): 623-628.

Thompson, R.O.R.Y., 1987. Continental shelf scale model of the Leeuwin Current. Journal of Marine Research, 45(4): 813-827.

Thomson, J.M., 1951. Growth and habits of the sea mullet, *Mugil dobula* Gunther, in Western Australia. Aust. J. Mar. Freshwat. Res., 2: 193-225.

Tranter, D.J., 1957. Pearl culture in Australia. Aust. J. Sci., 19: 230-232.

Tranter, D.J., 1962. Zooplankton abundance in Australasian waters. Aust. J. A4ar. Freshwater Res. 13, 106-42.

Tranter, D.J., 1973. Seasonal studies of a pelagic ecosystem (meridion 110 degree). Ecological Studies of Analytical Synthesis, 3:487-544.

Tranter, D.J., 1977a. Further studies of plankton ecosystems in the eastern Indian Ocean. 1. Introduction - the study and the study area. Australian Journal of Marine and Freshwater Research, 28(5):529-39.

Tranter, D.J., 1977b. Further studies of plankton ecosystems in the eastern Indian Ocean. 5. Ecology of the Copepoda. Australian Journal of Marine and Freshwater Research, 28(5):593-625, 75

Uitz, J., Huot, Y., Bruyant, F., Babin, M., Claustre, H., 2008. Relating phytoplankton photophysiological properties to community structure on large scales, Limnol. Oceanogr. 53 (2) 614–630.

Waite, A.M., Thompson, P.A., Pesant, S., Feng, M., Beckley, L.E., Domingues, C.M., Gaughan, D., Hanson, C.E., Holl, C.M., Koslow, T., Meuleners, M., Montoya, J.P., Moore, T., Muhling, B.A., Paterson, H., Rennie, S., Strzelecki, J. and Twomey, L., 2007. The Leeuwin Current and its eddies: An introductory overview. Deep Sea Research II 54(8-10), 789-796.

Warren, B.A., 1971. The shallow oxygen minimum of the South Indian Ocean. Deep Sea Research I 28 (8) 859-864

Woo, L.M., Pattiaratchi, C.B., 2008. Hydrography and water masses off the western Australian coast. Deep-Sea Research I 55 (9), 1090-1104.

Wood, E.J.F., 1964. Studies in the microbial ecology of the Australasian region. I. Relation of oceanic species of diatoms and dinoflagellates to hydrology. Nova Hedwigia 8 (1-2), 5-20.

Wyrtki, K. 1962. Geopotential topographies and associated circulation in the south-eastern Ocean. Aust. J. Mar. Freshw. Res., 13 (3), 89-105.

Wyrtki, K., 1971: Oceanographic Atlas of the International Indian Ocean Expedition. National Science Foundation Publication, OCE/NSF 86-00-001Washington, DC, 531 pp.

3.3 Continental Shelf Benthic Habitats

John Keesing, Peter Thompson, Jim Greenwood, Tennille Irvine, Joanna Strzelecki, Martin Lourey, Julia Phillips, Mat Vanderklift, Ryan Downie and Gordon Keith

CSIRO Marine and Atmospheric Research

Norm Campbell, CSIRO Mathematics and Information Sciences

Kayley Usher, CSIRO Land and Water

Jane Fromont, Western Australian Museum

Paul Kennedy, Fugro Technical Services

3.3.1 Introduction

The continental shelf break off the Perth region of Western Australia and north for at least 100km occurs at about 200 and between about 57 and 79 km offshore and the photic zone extends to about 90 m.

A nutrient budget developed for this region (see chapter 2, Feng and Wild Allen 2007) suggested that in the absence of significant new nitrogen from wind driven upwelling that about 84% of primary production occurring on the shelf was dependant on recycled sources of nitrogen and that benthic habitats were an important source of this recycling.

In order to more clearly define the importance of benthic habitats in this region to productivity and the extent of benthic pelagic coupling, it was necessary to obtain an improved characterisation of benthic habitats across the shelf.

Our approach was to determine the distribution of habitat types across the depth gradient and in doing so to explore ways of improving the ability to characterise the distribution and area of these habitats using multibeam acoustic profiling.

We also needed to determine the importance of each of these habitat types to primary and secondary production, consumption and nutrient storage and recycling.

We also characterised the patterns of productivity of benthic micro and macroalgae and measured the filtration rates of sponges and ascidians in order to help resolve the importance and contribution of these taxa to bentho-pelagic coupling. This study was also the first to find photosynthetic cyanobacteria in deepwater sponges and we explored the patterns of this occurrence with depth and documented which species were involved and considered the ecological importance of this finding.

Lastly we used the findings of the study to scale up for a shelf scale representation of habitats, biomass distribution and productivity estimates and a revised nutrient budget taking into account improved estimates of benthic primary production and we discuss the importance of benthic – pelagic coupling for recycling nitrogen on the continental shelf .

3.3.2 Methods

The study was focused on a sample belt transect of the continental shelf to 200 m encompassing a section of the Marmion Marine Park between Burns Beach and Hillarys and seaward for 70 km to 200 m (see Figure 3.157). Actual sampling only took place out to 150m and assumed that the benthos from 150m to 200m did not differ. Detailed descriptions of methods are given in each of the sections below.

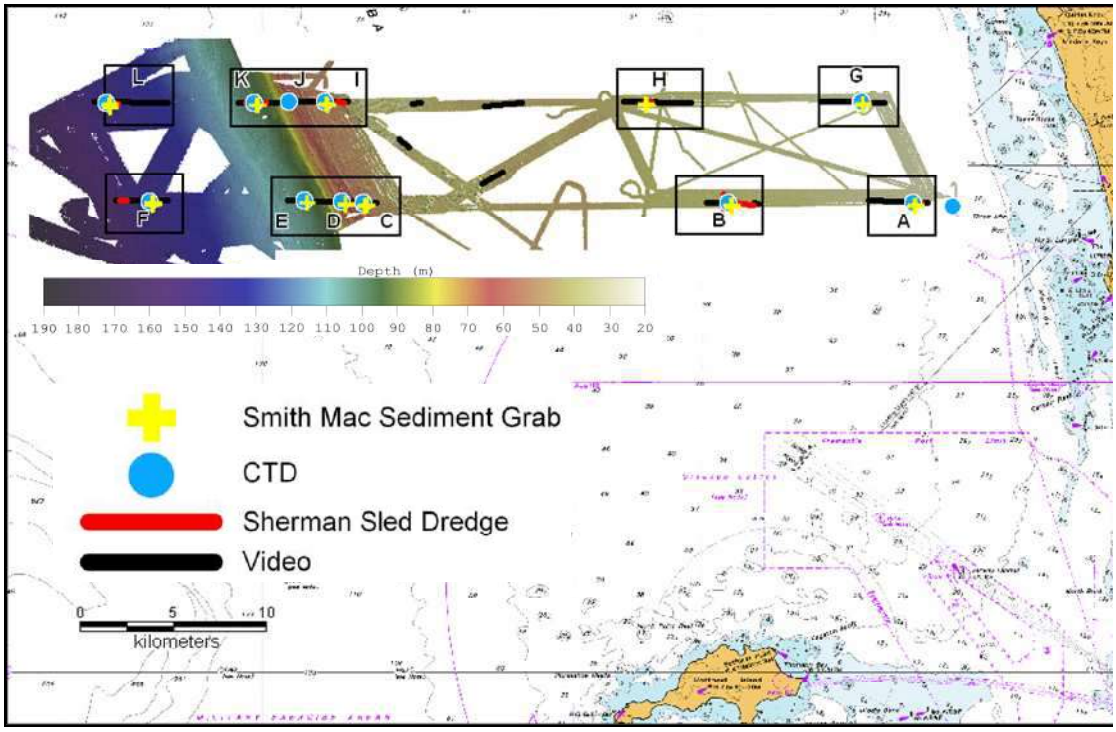

Figure 3.157. Sampling domain for the 1st leg of the May/June 2007 Southern Surveyor voyage.

3.3.3 Habitat characterisation and benthic biomass on the continental shelf

Benthic Habitats inshore of 30 m depth

These habitats have been well mapped (Figure 3.158) and we used this information, data collected in SRFME (Keesing et al. 2006) and new data (see Section 1 of this chapter) to characterise those habitats.

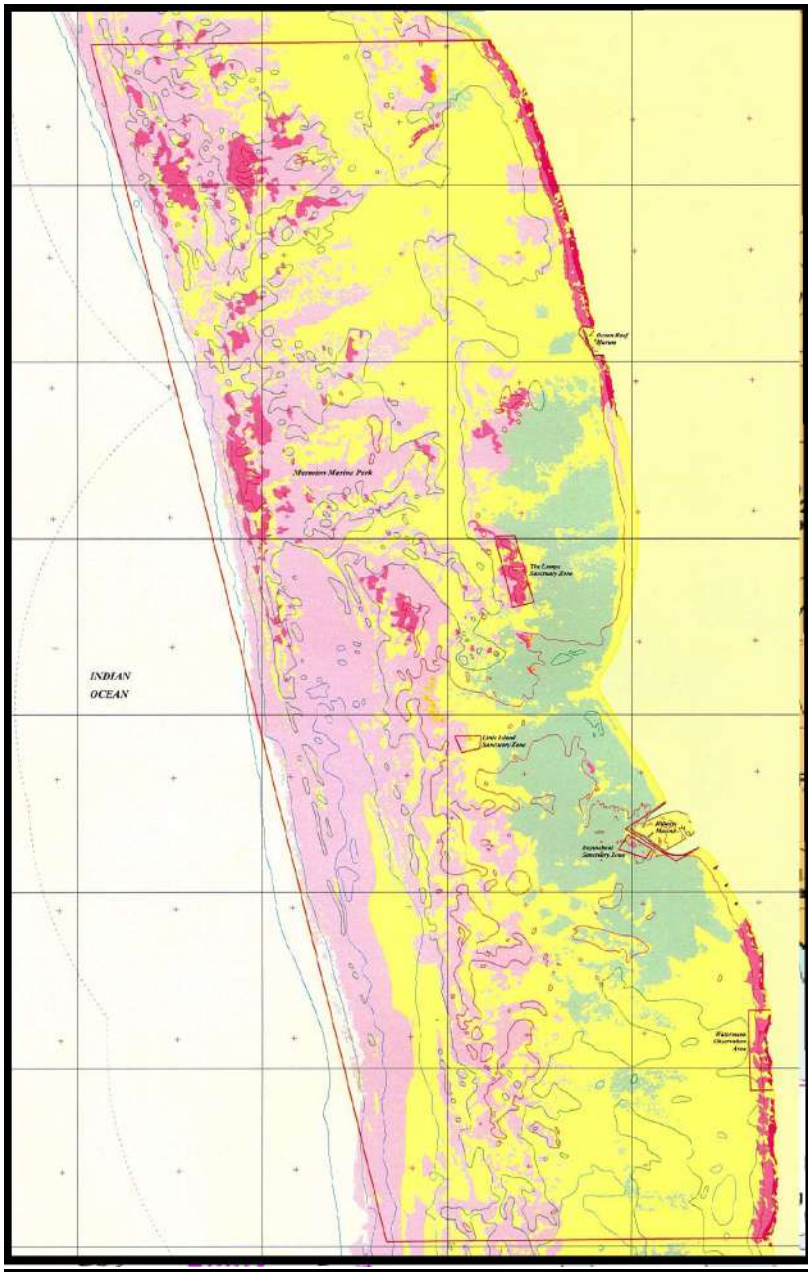

Figure 3.158. Habitat map courtesy of WA Dept of Environment and Conservation. Green is seagrass, Yellow is sand habitat, Light pink is algal dominated low relief reef, Dark Pink is high relief algal dominated reef, Red is intertidal or supratidal reef.

Benthic Habitats from 30 – 150 m

Benthic surveys were performed over two transects near Perth at 31.71ºS and 31.76ºS from 115.63ºE to 115.15ºE with stations at depths of 30, 40, 50, 75, 100 and 150m (Figure 3.157) from aboard the RV Southern Surveyor in May 2007. Acoustic swath mapping (SIMRAD EM300) of the sea-bed was conducted during the entire voyage; at each of the 12 study sites, benthic sled dredges, sediment grabs, benthic video and CTD casts were completed. Thirteen sleds comprised 6 over hard sediment (from 30-75m depth) and 7 over soft sediment (from 40-150m depth); 40 sediment grabs and thirteen CTD casts were executed. Thirteen videos were captured- 1 at each station of 30, 40 and 150m depth and 2 continuous tows from 50-100m

depth. Extra videos were also performed between 35-50m depth to target a range of habitat heterogeneity identified from the swath imagery.

3.3.4 Determination of benthic habitat type using analysis of acoustic backscatter data

During this entire voyage, acoustic swath mapping of the sea-bed was collected as 89 tracks by a Simrad EM 300 135-beam echo sounder, with swath coverage of 150º, covering a depth range of 30 to 180 m. Results of the technique were used to aid the positioning of operations during the voyage and have been useful in GIS mapping of these operations, as seen in Figure 3.159.

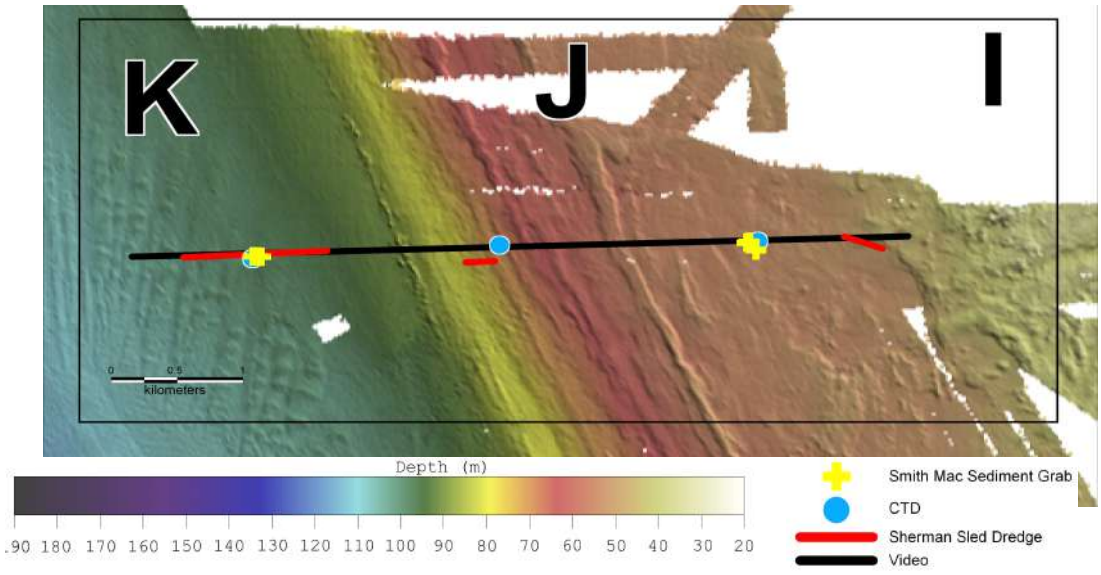

Figure 3.159. Example of GIS mapping of voyage operations over acoustic swath map image.

Multibeam backscatter collected during the voyage is being used to separate and identify benthic habitat types. Work has focused on backscatter tracks with corresponding video of the benthos to determine a relationship between backscatter data and sea-bed type as seen on the video (Figure 3.160).

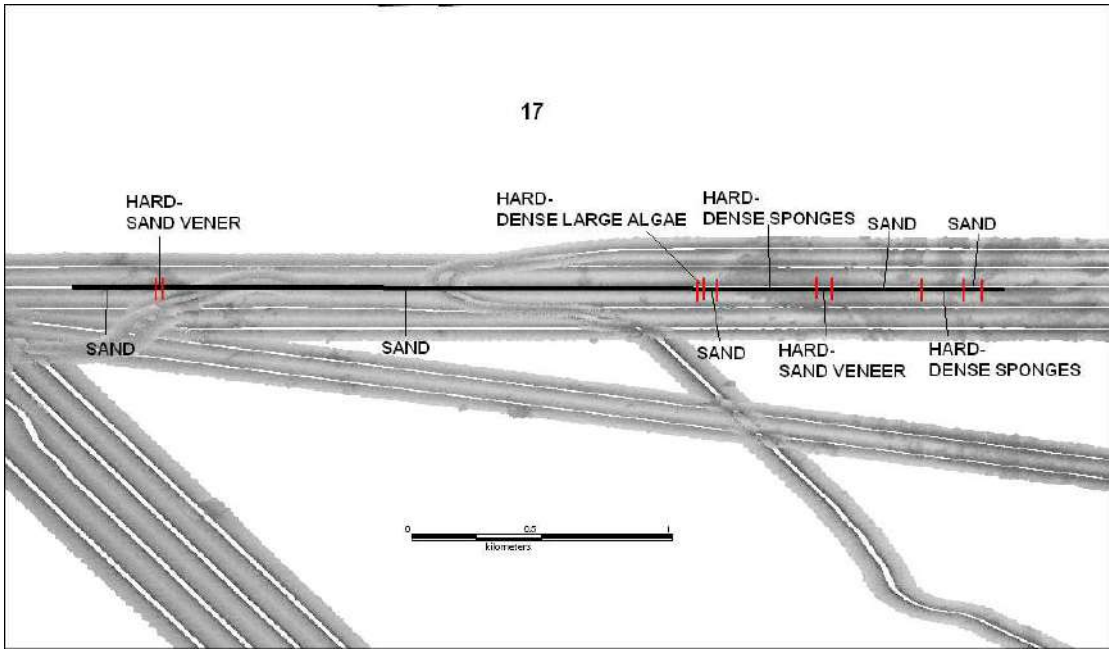

Figure 3.160. Descriptions applied to a video track (black line) overlaid on backscatter information.

Backscatter Image

The resulting multibeam backscatter data can be displayed as an image which shows contrasting light and dark segments (see Figure 3.161).

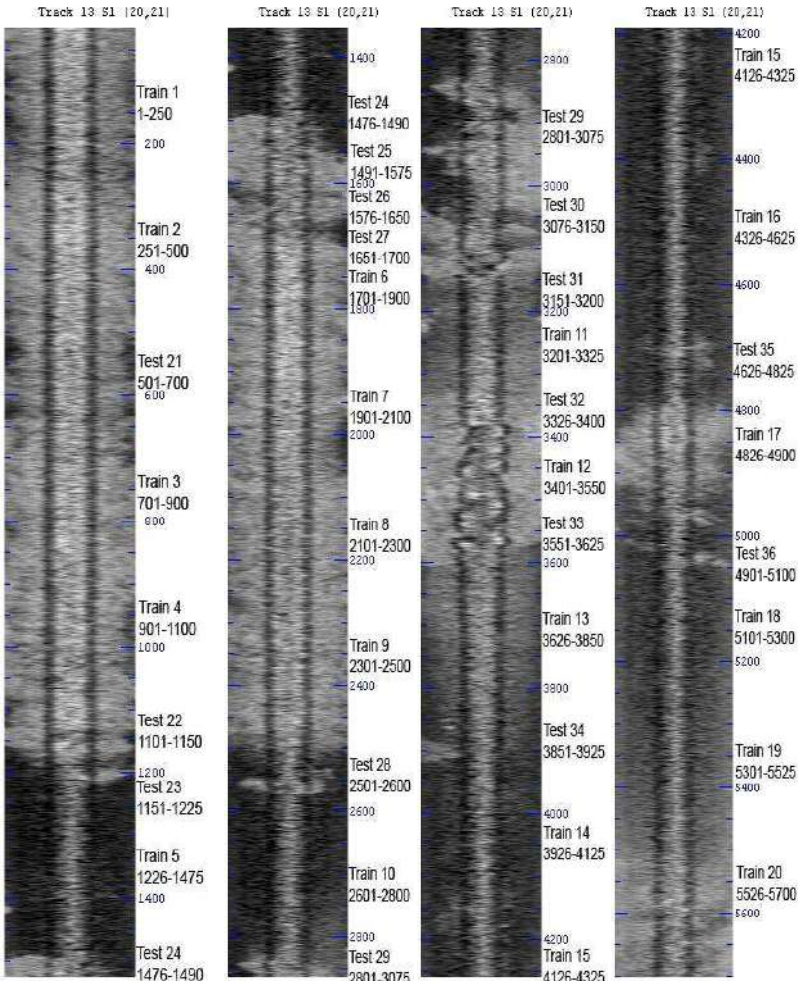

Figure 3.161. Backscatter image of a multibeam track showing contrasting light and dark sections.

Canonical variate analysis (CVA) of contiguous segments

For the analyses reported here, the backscatter data have been interpolated to a constant set of incidence angles using linear interpolation. In order to examine the similarities and differences between the backscatter responses, and their corresponding benthic types, the multibeam tracks were divided into contiguous segments of 100 pings. At this size, the majority of segments will be homogeneous in grey level and texture. Canonical variate analysis is used to find linear combinations of the backscatter data at each angle which best separate the segments, relative to the variation within each segment, providing a clustering of the data. The linear combination providing maximum separation is referred to as CV1, and the next best as CV2.

Figure 3.162 (left) shows the results of the analysis for all pings in the backscatter image in Figure 3.161 and the resulting mean CV scores for each of the 100-ping segments (as defined in Figure 3.161 are plotted in Figure 3.162 (right). There is clear separation along the CV1 axis, with segments on the left of the plot (i.e. lower CV1 scores) corresponding to lighter-coloured responses in the backscatter image of Figure 3.161 and segments on the right (i.e. higher CV1 scores) being the darker-coloured areas.

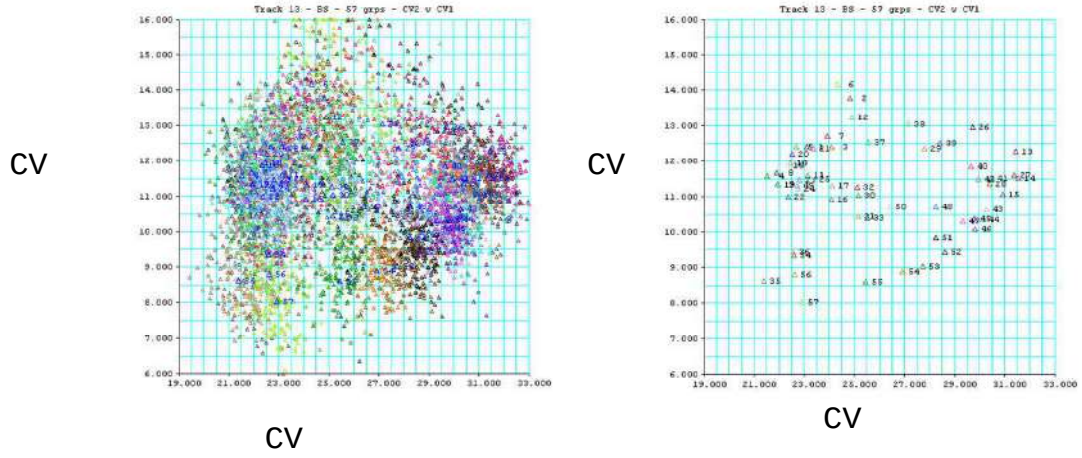

Figure 3.162. Plot of canonical variate scores for each ping (left) and plot of canonical variate segment means (right).

Identifying the CV classes

These plots can be examined further using benthic video footage of the corresponding location of the multibeam data. For the data shown in the backscatter image in Figure 3.161, there is video coverage from ping 3020 to ping 5140; the CV scores for this portion of the multibeam track are shown in Figure 3.163. We focused on the video for portions of the plots in which the CV scores remain “flat” for a reasonable period, as these are likely to indicate habitats which are homogenous within the limits of the multibeam differentiation. Regions of the plot which are “sloping” may indicate transitions between habitat types.

The video shows that the light grey ping segments in Figure 3.161 which plot with low CV1 scores of 21-23 in Figure 3.163 are hard-substrate habitats ranging from bare rock to dense filter-feeder or algal communities covering a hard substrate. Segments which are dark-coloured and plot with high CV1 scores of 32-34 in Figure 3.162 are shown to be sandy habitats (Figure 3.163).

The CV2 scores further define the benthos type. Video from hard benthos sites with low CV2 scores of 8-10 (Figure 3.163) shows areas of dense filter-feeder or algal populations, while higher CV2 scores of 12-14 correspond to habitats of sparse vegetation or animals. Additionally, the video shows that sandy sites with long dominant ripples correspond to ping segments with low CV2 scores of 11-13, and sandy sites with fine diffuse ripples relate to multibeam data with high CV2 scores of 14-16. This interpretation has been shown to hold over a number of tracks examined thus far.

In summary, the CV plots showed patterns relating to the two axes: separation of sand and hard-substrate habitats along the first canonical variate; and for the hard benthos, decreasing CV2 scores are associated with increasing vegetative or faunal cover, while for the sandy areas decreasing CV2 scores are associated with increasing ripple definition.

Areas that appeared to be sand on the video but had mid-range CV scores occurred on a number of tracks, initially causing some confusion in extrapolating the exploratory CV plots to other tracks. It seems likely that these areas have only a thin layer of sand covering a hard benthos.

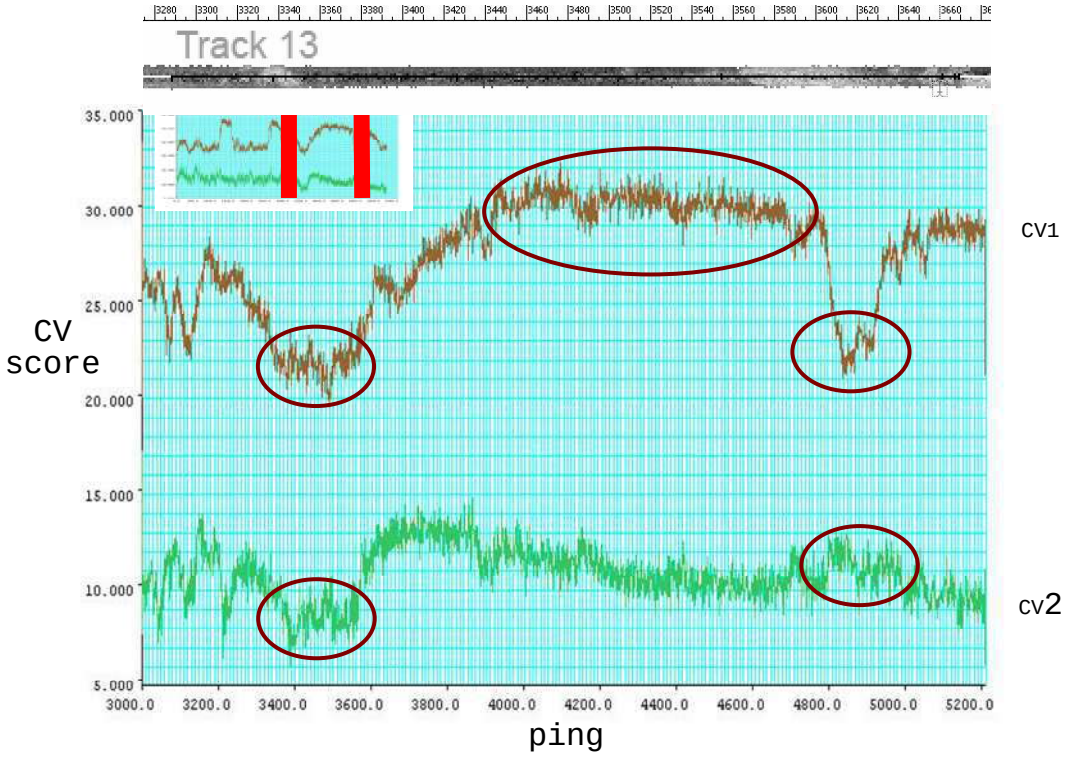

Figure 3.163. Backscatter image of the track portion (upper panel) and CV1 and CV2 scores for individual pings in the multibeam track for the portion with corresponding video footage (inset – CV scores for the entire multibeam track).

These analyses resulted in a mapping of five main seabed cover types as set out in Figure 3.164.

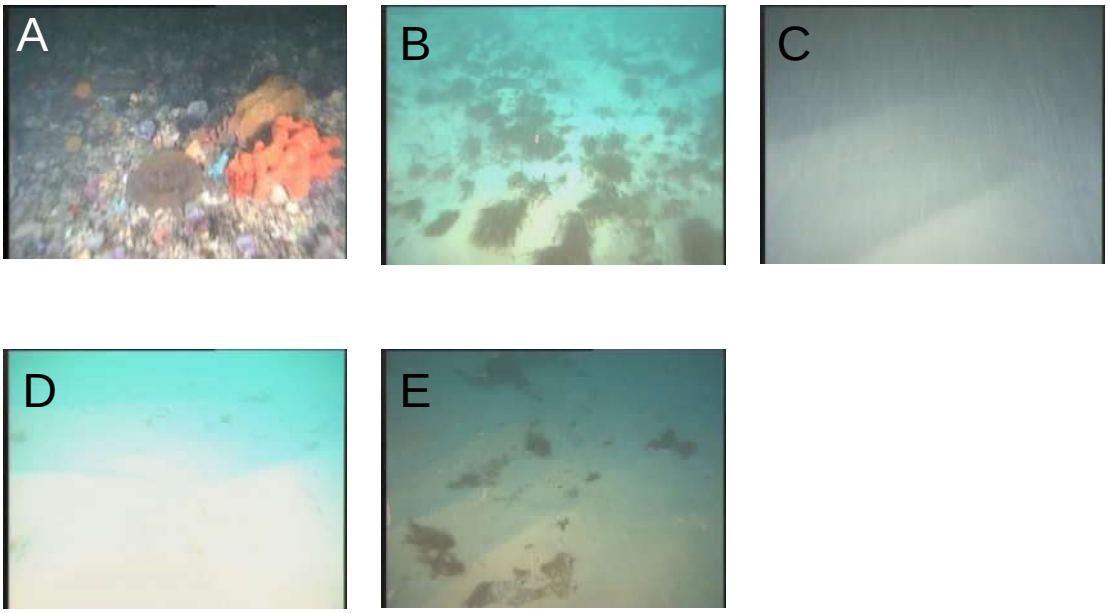

Figure 3.164. Seabed cover types identified.

A. hard-bottomed areas (CV1 scores 21 – 23) with dense vegetative or faunal cover (CV2 scores 8 – 10) such as sponge-covered rock

B. hard-bottomed areas (CV1 scores 21 – 23) with sparser vegetative or faunal cover (CV2 scores 12 – 14)

C. sandy areas (CV1 scores 32 – 34) with strong ripples (CV2 scores 11 – 13)

D. sandy areas (CV1 scores 32 – 34) with more diffuse ripples (CV2 scores 14 – 16)

E. areas which appear to be sandy on the video, with obvious ripples and some sparse cover, but with CV1 scores around 24 – 26

Extrapolating beyond the video coverage

We can then analyse the multibeam tracks which do not have corresponding video to indicate the likely habitat type. For example, in Figure 3.165 we can reasonably infer that the circled area to the left is hard benthos with sparse vegetation or fauna while that to the right is a sand habitat with well-defined ripples. Application of the approach will allow for large-scale analysis of benthic habitats, aiding in site selection, calculation of the size and proportions of particular habitats types within a region, and accurate habitat mapping.

In this chapter we have used this method to determine the proportion of coverage of different habitat types across the area surveyed using acoustic multibeam (Figure 3.157). The results of this habitat characterisation have been used to enable an estimation of biomass in each habitat type across the depth range surveyed (see later in this chapter).

Key Findings:

Habitat assessment using canonical variate analysis of backscatter data, ground truthed with tow video confirmed the ability to discriminate between five habitat classes on the basis of acoustic backscatter surveys:

- **hard-bottomed areas with dense vegetative or faunal cover such as sponge-covered rock**
- **hard-bottomed areas with sparser vegetative or faunal cover**
- **sandy areas with strong ripples**
- **sandy areas with more diffuse ripples**
- **sandy areas overlaying hard bottom (areas which appear to be sandy on the video, with obvious ripples and some sparse cover)**

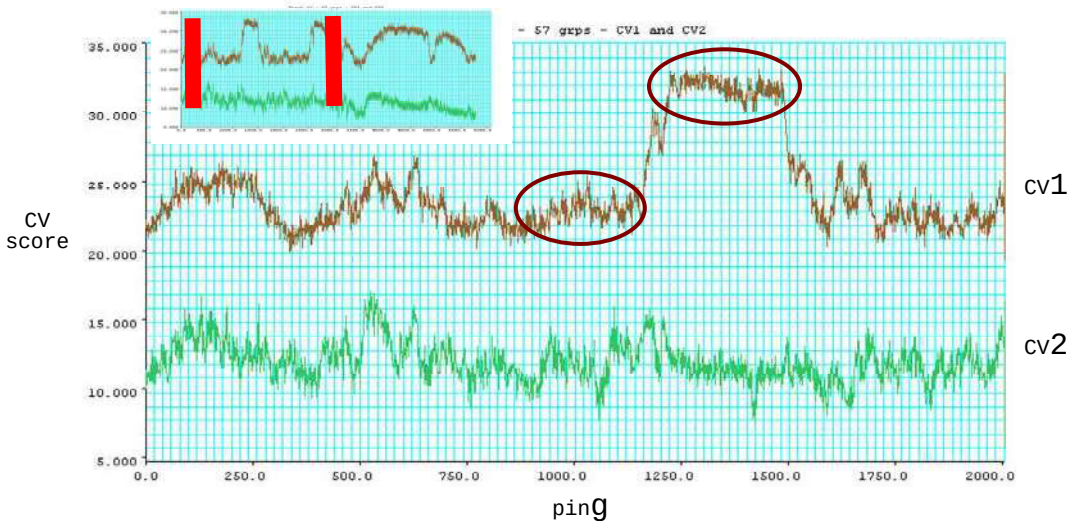

Figure 3.165. Scores for CV1 and CV2 for individual pings in the beginning of the multibeam track (inset – CV scores for the entire multibeam track).

Further advancement in backscatter analysis for habitat characterisation

Backscatter analysis offers significantly greater potential for benthic habitat characterisation and mapping than realised here. Further examples of the development of this work undertaken in this project are summarised here but warrant publication elsewhere.

Canonical Variate Analysis using Contiguous Segments of Multibeam Data

A desirable feature of the CVA approach is that it produces linear combinations of the input variables which can then be displayed and analysed in a lower number of dimensions, for example by plotting the CV scores against ping number and/or eastings and northings.

Since the usual CVA approach can be somewhat time-consuming, a simpler approach is proposed here: the training classes are taken as contiguous segments of pings.

The multibeam backscatter data used to develop this method were collected over the Recherché Archipelago region, off the coast of Esperance, Western Australia, By Fugro Survey using a Reson Seabat 8125 240-beam echo sounder. The track analysed here is characterised by a mixture of sand and rhodolith.

For these analyses, the backscatter data have been interpolated to a constant set of incidence angles using linear interpolation. The resulting multibeam backscatter data are displayed in Figure 3.166.

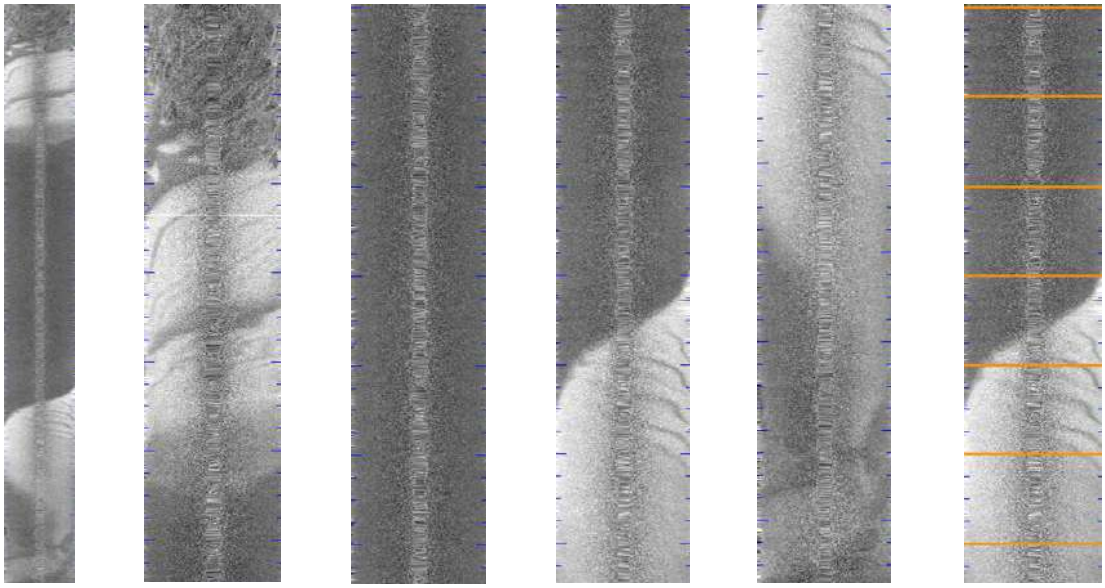

Figure 3.166. Grey-level image of backscatter data showing the total line (left), and four parts -- the right-most image shows 100-ping segments for the 3rd part.

Canonical variate analysis (CVA) on contiguous segments

Canonical variate analysis is used to find linear combinations of the backscatter data at each angle which best separate the segments, relative to the variation within each segment. The linear combination providing maximum separation is referred to as CV1, and the next best as CV2.

Figure 3.167 shows plots of the canonical variate scores for CVAs based on training classes of different numbers of contiguous pings.

The main clusters and patterns are very similar in all four plots in Figure 3.167. Analyses of a number of data sets have shown similar results: the patterns of the between-group differences are consistent for training classes ranging in size from 10 contiguous pings to 100 contiguous pings.

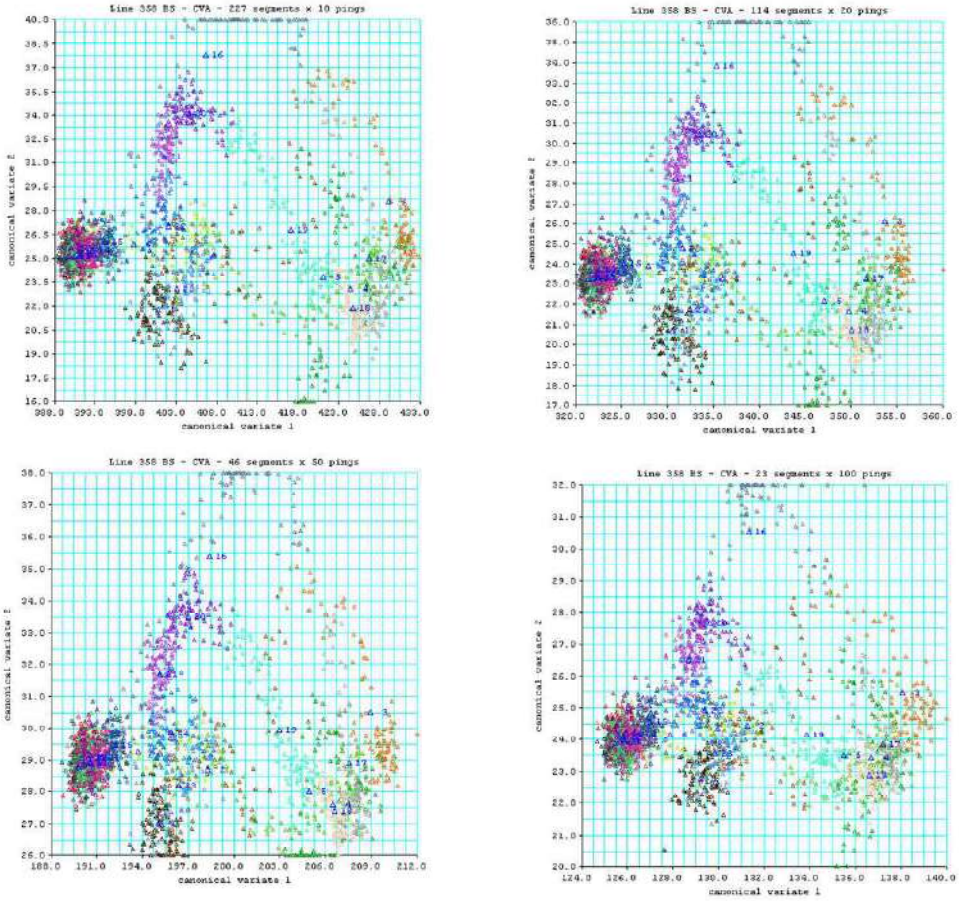

Figure 3.167. Plots of canonical variate scores for a CVA based on training classes of groups of (a) 10 contiguous pings; (b) 20 contiguous pings; (c) 50 contiguous pings; and (d) 100 contiguous pings -- the canonical variate scores in all four plots are colour-coded for the same contiguous segments of 100 pings.

Identifying homogeneous segments

A graphical approach can be adopted to identify those sequences of pings which are homogeneous.

The main steps are as follows:

- calculate the standard deviations for each angle for each of the contiguous ping segments
- for each angle in turn, make a quantile - quantile (Q-Q) plot of the ordered logs of the standard deviations against Gaussian quantiles – the plots will be approximately linear for the homogeneous segments, and will have similar slope, while the more heterogeneous segments will show a distinct departure from the linear trend (see Figure 3.168(b))
- determine a homogeneous-level threshold from the upper limit of the linear segment of the plots

The plots in Figure 3.168 are clearly linear for much of the data; there are also obvious departures from linearity, especially in Figure 3.168(b).

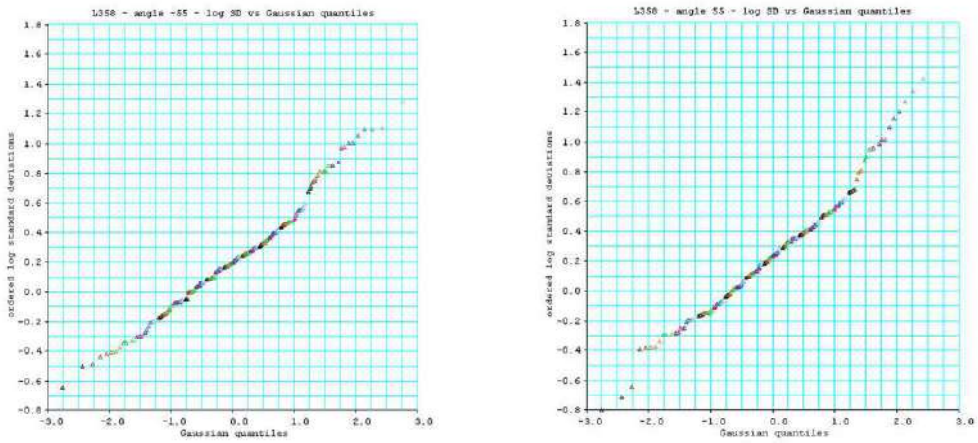

Figure 3.168. Gaussian Q-Q plots of ordered log standard deviations for segments of 10 contiguous pings against Gaussian quantiles for (a) angle -55o and (b) angle 55o.

CVA on homogeneous contiguous segments

The Q-Q plots can be used to eliminate those segments that are heterogeneous, and a CVA re-run on only those contiguous segments of pings which are homogeneous according to some threshold value of the standard deviations.

Figure 3.169 shows plots of the canonical variate scores for all pings for CVAs based on different numbers of training classes (all of 10 contiguous pings), selected according to different thresholds for the standard deviations.

The main clusters and patterns are similar in all four plots in Figure 3.169, and are very similar to the plots in Figure 3.167.

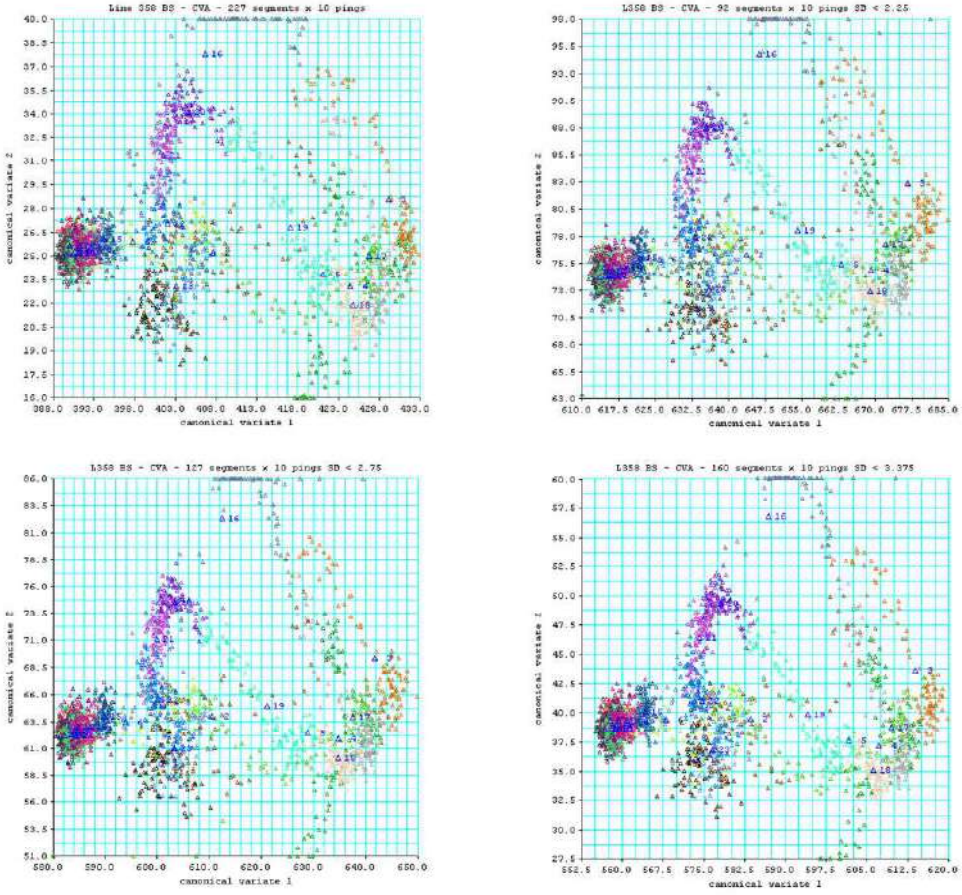

Figure 3.169. Plots of canonical variate scores for a CVA based on training classes of groups of 10 contiguous pings (a) using all pings; (b) which have homogeneous standard deviations (SDs) < 2.25; (c) which have homogeneous SDs < 2.75; and (d) which have homogeneous SDs < 3.375 -- the canonical variate scores are colour-coded for contiguous segments of 100 pings.

Extensive experience with the approach suggests that basing a CVA on training classes defined by contiguous segments of pings gives similar ordinations to those based on a more careful selection of training classes. For the data sets examined to date, where a fair proportion of the image consists of visually uniform areas, the resulting ordinations are relatively insensitive to the number of contiguous pings in the segments defining the training classes, and also to the number of homogeneous segments retained in the analysis.

Ideally, the training classes should all be reasonably homogeneous. However, the results shown here, and considerable experience with the approach, suggests that when some of the training classes are more heterogeneous than is desirable statistically, the relative positions of the homogeneous classes in the ordinations are still consistent, while the individual ping scores for the more heterogeneous classes plot with those clusters of scores representing their respective homogeneous classes.

Distinguishing between Benthic Classes – Full-Ping vs Moving-Window Separation

This analysis focuses on the degree of separation between sand and hard-bottom sites, and within the latter, between hard bare sites and sponge-covered sites. The multibeam backscatter data were collected off the coast of Perth, Western Australia, using a Simrad EM300 135-beam echo sounder. The tracks analysed here are characterised by a mixture of sand and hard benthos. For these analyses, the backscatter data have been interpolated to a constant set of incidence angles using linear interpolation.

Canonical variate analysis (CVA) on contiguous segments

As before the plots of CV scores (see, e.g., Figure 3.170) were examined in conjunction with benthic video footage of the corresponding location of the multibeam data.

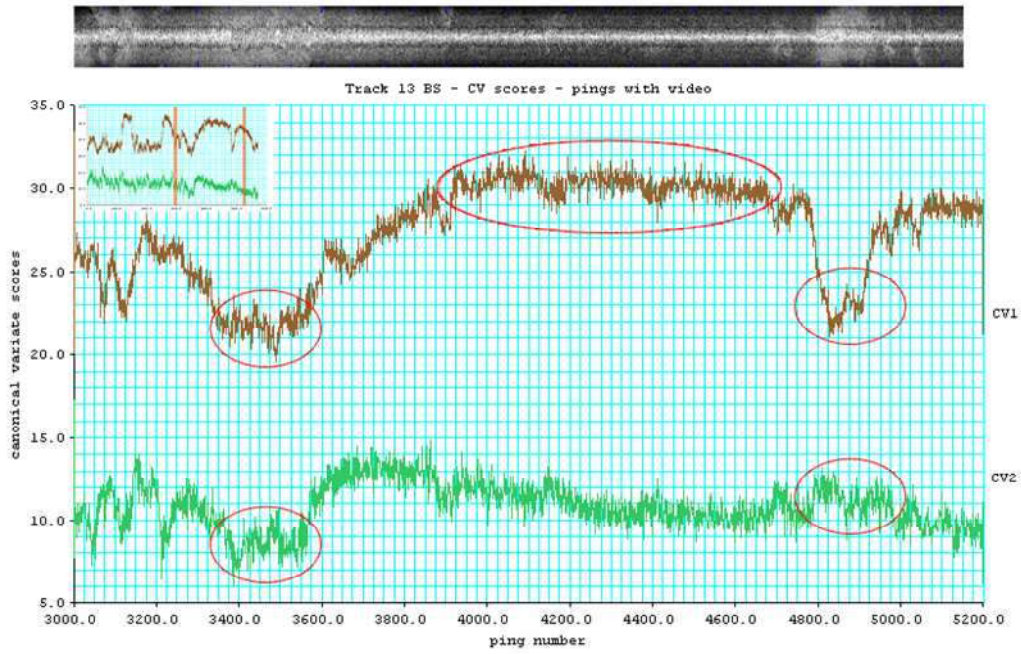

Figure 3.170. Above: backscatter image of the track portion; Below: CV1 and CV2 scores for individual pings in the multibeam track for a portion with corresponding video footage; inset – CV scores for the entire multibeam track with lines indicating the zoomed areas

Interpreting the CV plots

Parts of the CV index plots in which the CV scores remain "flat" for a reasonable period are likely to indicate habitats which are homogeneous within the limits of the multibeam differentiation.

Segments which plot with low CV1 scores of 21-23 in Figure 3.170 were found to be habitats ranging from bare rock to dense filter-feeder or algal communities covering a hard substrate. Segments which plot with high CV1 scores of 32 - 34 in Figure 3.170 were found to be sandy habitats.

Video from hard-benthos sites with low CV2 scores of 8 - 10 (Figure 3.170) showed areas of dense filter-feeder or algal populations, while higher CV2 scores of 12-14 corresponded to habitats of sparse vegetation or animals.

Backscatter – incidence angle mean profiles

Figure 3.171 shows typical profile plots of backscatter – incidence angle (BS – IA) mean curves for five seabed cover types.

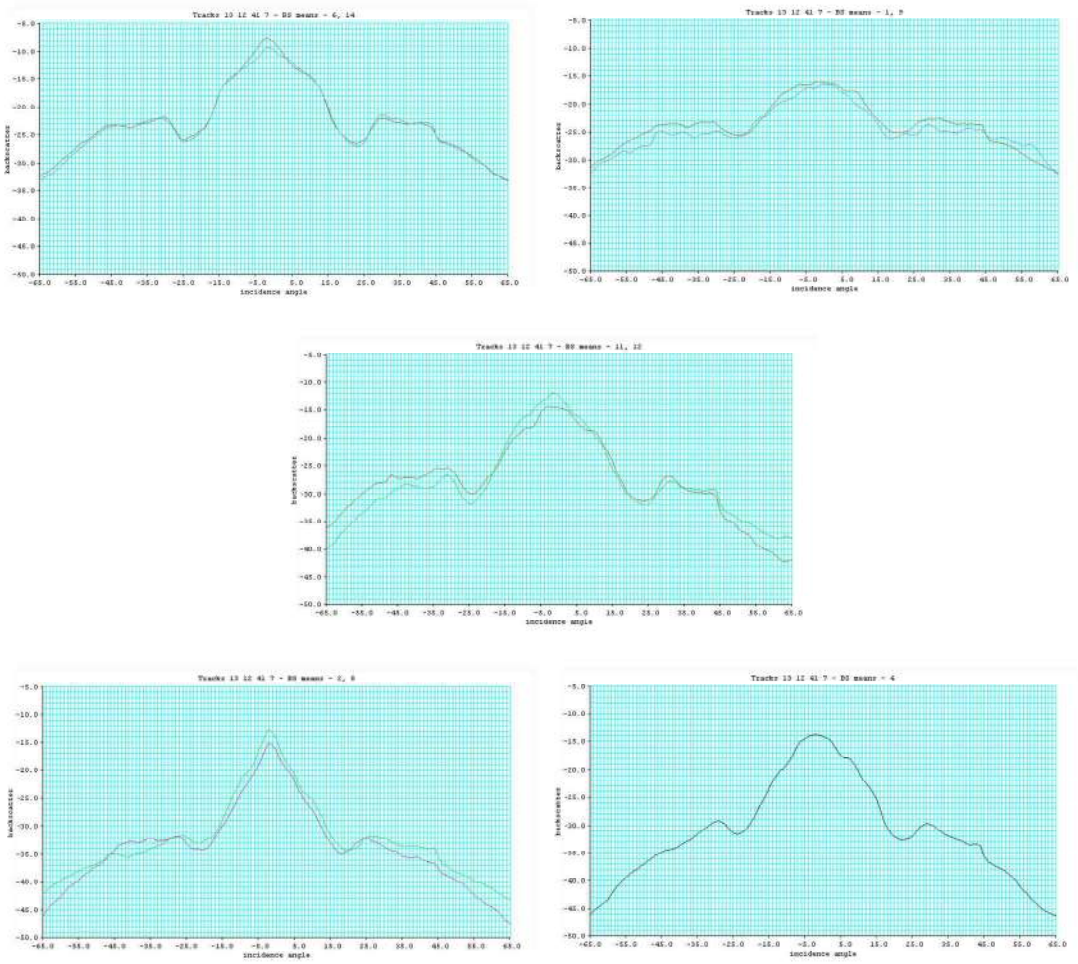

Figure 3.171. Plots of BS – IA means for (a) hard, "rubble" and small rocks; (b) sponges; (c) rippled "hard" sand; (d) soft sand – large ripples; and (e) soft sand – diffuse ripples.

Figure 3.168(a) and (b) show that there are only subtle differences in the BS – IA curves for hard bare areas and dense sponge-covered areas.

Analyses of a number of multibeam data sets collected by CSIRO, Fugro and Curtin University, and plots in published papers (such as Figure 3.168 in Y. Le Gonidec, G. Lamarche and I. C. Wright, 2003, "Inhomogeneous substrate analysis using EM300 backscatter imagery", in Marine Geophysical Researches, v24, pp 311 – 327) suggest that a typical band of variability for a homogeneous area is 3 – 4.5 dB.

The backscatter values for the sponge-covered sites overlap considerably with the backscatter values for the barer hard-bottom sites at any one incidence angle.

The subtle separation between the sponge-covered sites and the barer hard-bottom sites is due to the overall differences in the shapes of the BS – IA curves over part or all of the range from 30° to 65°, as reflected in the obvious differences in "slopes" (see Figure 3.172).

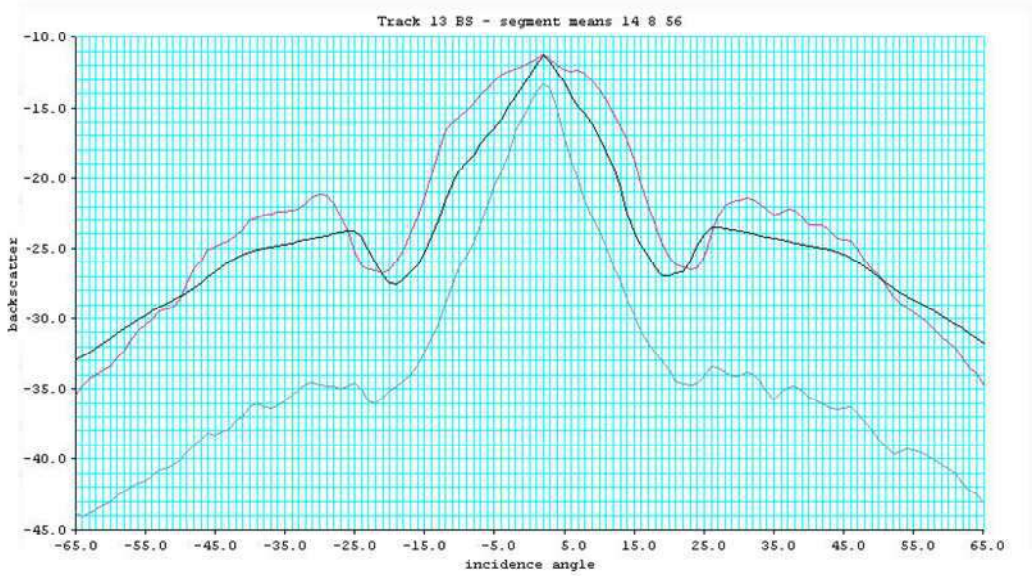

Figure 3.172. Profile plots of BS – IA means for hard-bottom sites with "rubble" and small rocks (top curve at 60°); sponges (middle curve at 60°); and soft sand with large ripples (bottom curve at 60°)

Separation provided by subsets of angles

The canonical roots for the second CV, f2, in Table 3.37 indicate that there is some separation along CV2 (which effects separation between the bare hard-bottom and the sponge-covered areas) for a 30o and 40o range spanning the cross-over at 50o, but little or no separation for a 10o or 20o range spanning the cross-over.

Table 3.37.Separation provided by subsets of angles.

range of incidence angles	f1	f2
-65° to 65°	10.37	1.77
-65° to 0°	6.18	1.18
-65° to -25°	5.91	0.98
-65° to -35°	5.53	0.89
-65° to -40°	4.91	0.56
-55° to -35°	5.38	0.29
-65° to -55°	3.06	0.21
-55° to -45°	4.09	0.16
-45° to -35°	4.26	0.05
-35° to -25°	2.96	0.04

The plots of CV2 scores in Figure 3.173 show that while the dip in CV2 scores is clearly evident at ping 3500 for the CV analyses which include all angles from 0° to 65°, it becomes less apparent as the number of angles is reduced.

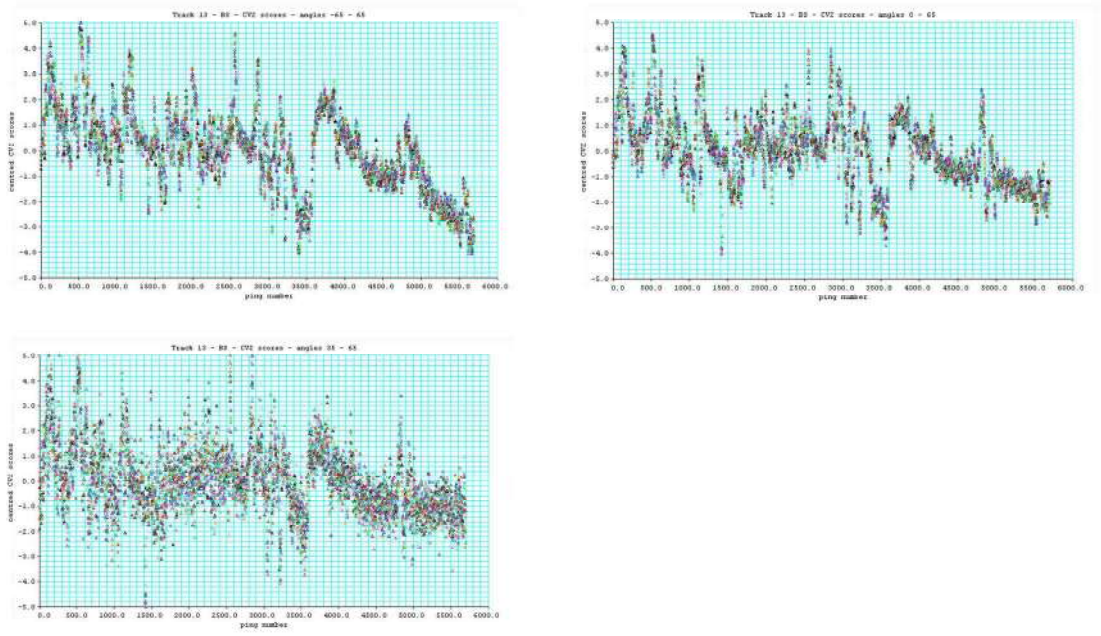

Figure 3.173. CV2 scores for an entire multibeam track for a CVA based on angles from (a) -65° to 65°; (b) 0 ° to 65 °; and (c) 35 ° to 65°

Key Findings:

There are clear differences in both position and shape for the BS – IA curves from hard-bottom and sandy areas – separation can be affected by the backscatter response at one or a few angles. The backscatter values for the sponge-covered sites overlap considerably with the backscatter values for the barer hard-bottom sites at any one incidence angle. There are only subtle differences in the BS – IA plots for hard bare and dense sponge-covered areas. The overall differences in the shapes of the BS – IA curves over much of the range from 25 º to 65 º effect the class separation (in particular, the curves cross over at around 50º). Distinguishing classes within the hard-bottom areas will not be successful if only one or a few angles are used. Such differences as do exist may well be overlooked, unless the analyses are based on homogeneous patches that cover most or all of the backscatter – incidence angle curve.

3.3.5 Towed Benthic Videos and Habitat Structure

The series of towed videos ranged from a distance of 470m to 5.9km, with a total distance of 32.5km of benthic footage, Figure 3.174 demonstrates the depths of video captured. The footage was manually described into 15 categories based on sea-bed type and associated plants and animals and their densities. Analysis revealed a great variety of habitat types between the depths of 30-110m while the benthos at 150m was constant and remained as its own sea-bed category due to different features to shallower depths. For simplicity these 15 categories were pooled into 9 broad categories (Table 3.38):

1. Bare Sand ± Sparse Algae
2. Seagrass
3. Flat Fine Sediment, Sparse Filter Feeders
4. Bare Hard Substrate ± Sparse Algae
5. Patchy Sand & Hard Substrate (Varying Size Algae ± Filter Feeders)
6. Hard Substrate, Low-Med Density Low Algae, Low-Med Density Filter Feeders
7. Hard Substrate, High Density Low Algae
8. Hard Substrate, Med- High Density Large Algae (primarily *Ecklonia*)
9. Hard Substrate, Dense Sponges

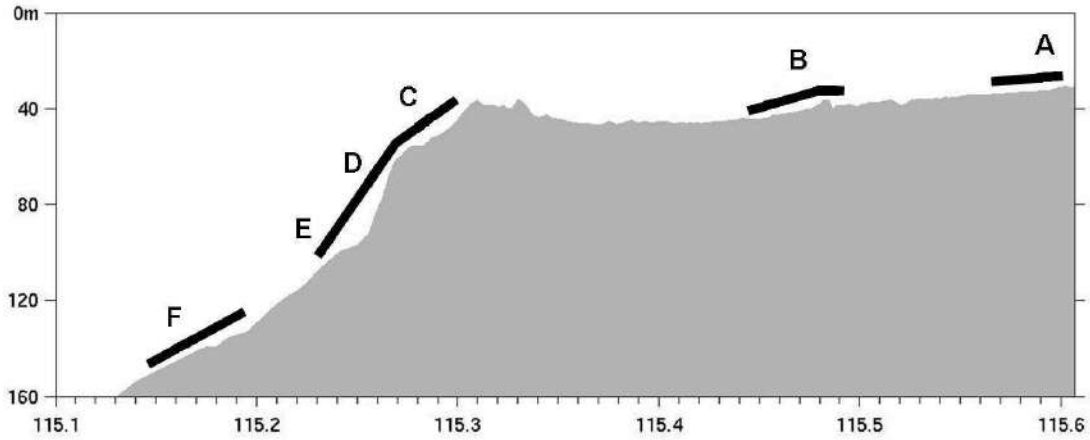

Figure 3.174. Bathymetry cross section of voyage transect and approximate depths of towed benthic videos.

Table 3.38 displays the broad habitat categories observed on videos. These broad categories can be further pooled into sand, reef and patchy habitat types, with the latter referring to areas where both sand and hard substrate are present in very small alternating areas. Analysis has revealed an overall estimate of 51% sand, 31% reef and 18% patchy substrate between 30-110m depth. Perhaps if we make the large assumption that these highly patchy areas are 50% sand and 50% reef then we have overall estimates of 60% sand and 40% reef over this depth range.

Table 3.38 . Percentage of Habitat Types Present on Towed Videos (averaged across depth ranges).

Depth (m)	Bare Sand ± Sparse Algae	Seagrass	Flat Fine Sediment, Sparse Filter Feeders	Bare Hard Substrate ± Sparse Algae	Patchy Sand & Hard Substrate (Varying Size Algae ± Filter Feeders)	Hard Substrate, Low-Med Density Low Algae, Low-Med Density Filter Feeders	Hard Substrate, High Density Low Algae	Hard Substrate, Med- High Density Large Algae (primarily *Ecklonia*)	Hard Substrate, Dense Sponges
30-39	47.9	1.6	-	-	48.7	1.4	-	-	0.4
40-49	57.0	-	-	3.1	9.6	0.5	3.6	9.6	16.6
50-74	13.9	-	-	36.8	3.1	6.3	-	30.2	9.8
75-99	20.6	-	-	14.9	10.1	7.7	9.8	5.7	31.2
100-110	93.4	-	-	-	4.7	-	-	-	1.9
140-150	-	-	100.0	-	-	-	-	-	-

Figure 3.175 illustrates the importance of determining the benthos of the area covered by the Southern Surveyor voyage. While we know the habitat from the coast to 20m depth which falls within Marmion Marine Park, this is only about 10% of the area of the photic zone (to about 90 m). The towed video work has allowed us to fill in habitat composition of the deeper areas. Combination of this habitat characterisation with biomass estimates and the functional role of animals and plants in these deepwater or "mesotrophic" regions (see later) emphasise the importance of characterising areas for which little is known.

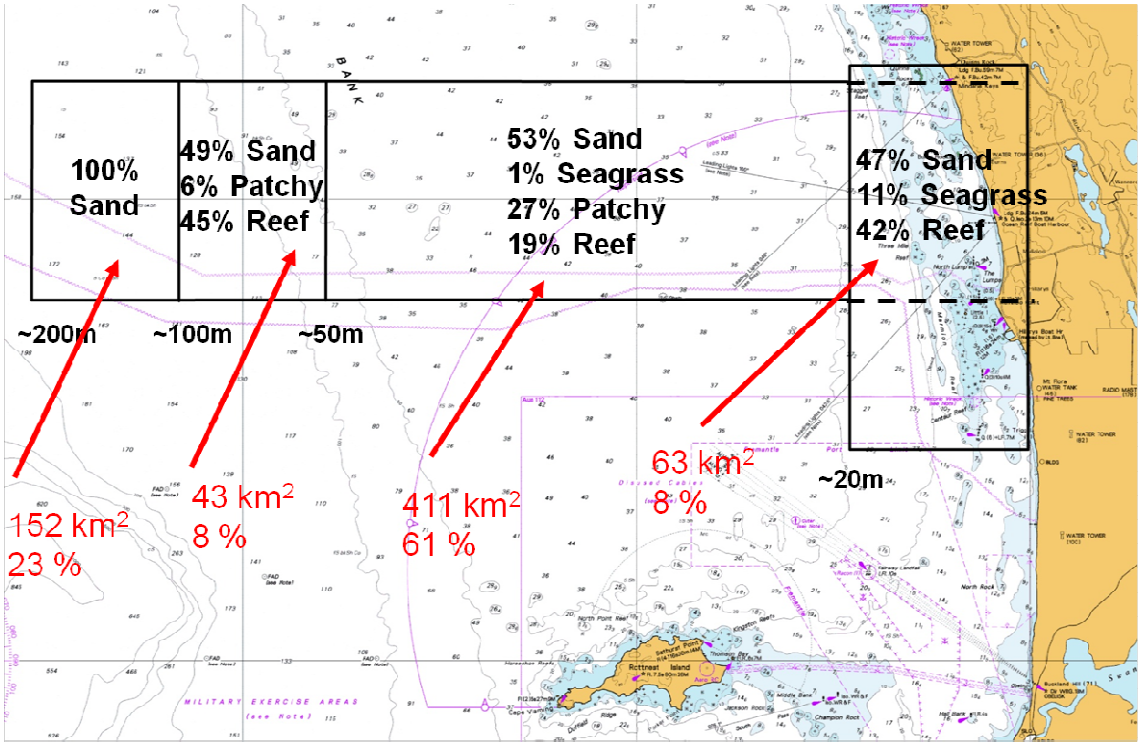

Figure 3.175. Marmion shelf scale domain illustrating proportions of shelf area (in red) and proportions of benthic type in each depth range (in black). Benthic type to 30m depth calculated from Marmion Marine Park Habitat Map, CALM (2002) Map base is AUS754 Navigation Chart (Commonwealth of Australia 2002).

In summary, the continental shelf scale habitat of south-western Australia can be described as having four key zones:

1. a narrow nearshore section (ca. 6 km wide) to about 20m characterised by limestone algal dominated reefs (ca. 42% coverage), seagrass habitats, patchy in places, more extensive in others (ca. 11%) and sandy soft sediment habitats, interspersed patchily between the other habitats and as extensive homogenous habitats (ca. 47%)

2. an extensive gently sloping section 20-50m deep (ca. 40 km wide) characterised by large sections of sandy habitat (53%) and patchy reef (27%), some large areas reef (19%) and small patches of seagrass (1%)

3. a steeply sloping section between 50 and 100m (ca. 4km wide) of predominantly hard reef (45%) and patchy reef (6%) and sandy substrate (49%)

4. a deep and gently sloping section beyond 100m out to about 200m (averaging 15km wide) comprising sand and silt habitat

Key Findings:
The continental shelf scale habitat of south-western Australia can be described as having four key zones:
1. a narrow nearshore section to about 20m characterised by limestone algal dominated reefs, seagrass and habitats.
2. an extensive gently sloping section 20-50m deep characterised by large sections of sandy habitat and patchy reef
3. a steeply sloping section from 50 -100 m dominated by reef
4. a gently sloping fine sand/silty habitat beyond 100m

Among these four zones, 9 key benthic habitat types characterise the patchiness and/or dominance of the habitats and the benthic flora and fauna they support.

The well described shallow water areas of this coastline comprise less than 10% of the area of benthos in the photic zone.

3.3.6 Benthic Biomass Estimates 30-150 m

In order to characterise the plant and animal communities of shelf-scale benthic habitats, a large heavy epibenthic sled, 1.2m wide, was used to dredge the sea-bed at each of the stations; retrieved samples were photographed, identified, catalogued, counted and weighed.

Animals

The average densities of animals at each depth recovered by sled dredge are given in Figure 3.176. The overall average animal density for hard bottom habitats was $0.55.m^{-2}$ and for soft substrata was $1.02.m^{-2}$. The density at 150m is attributed to one sled with large numbers of very small sponges. This sled is also responsible for the increased density of sponges average for all sled dredges (Figure 3.177). Excluding this sample, the average density of sponges for the other 6 sleds on soft sediment was $0.041.m^{-2}$. The densities of all animals captured by the sled dredge remain low (Figure 3.177). Those animals grouped as “other”, consisted largely of echinoderms, molluscs, polycheaetes and crustaceans.

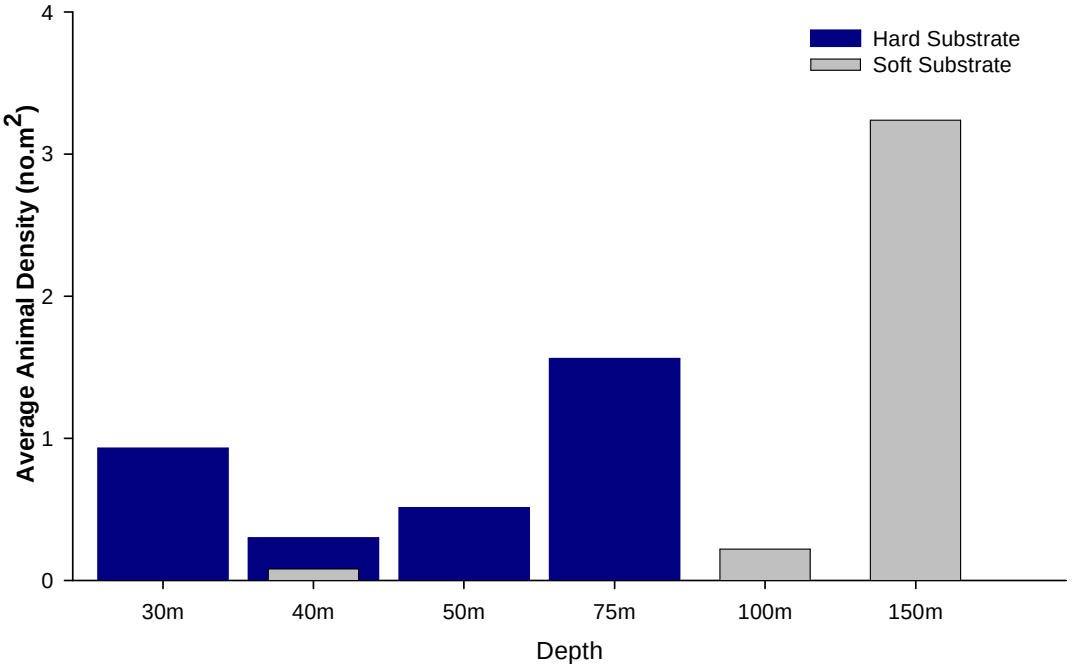

Figure 3.176. Average total animal densities for sled dredges from leg 1 of Southern Surveyor 2007-04.

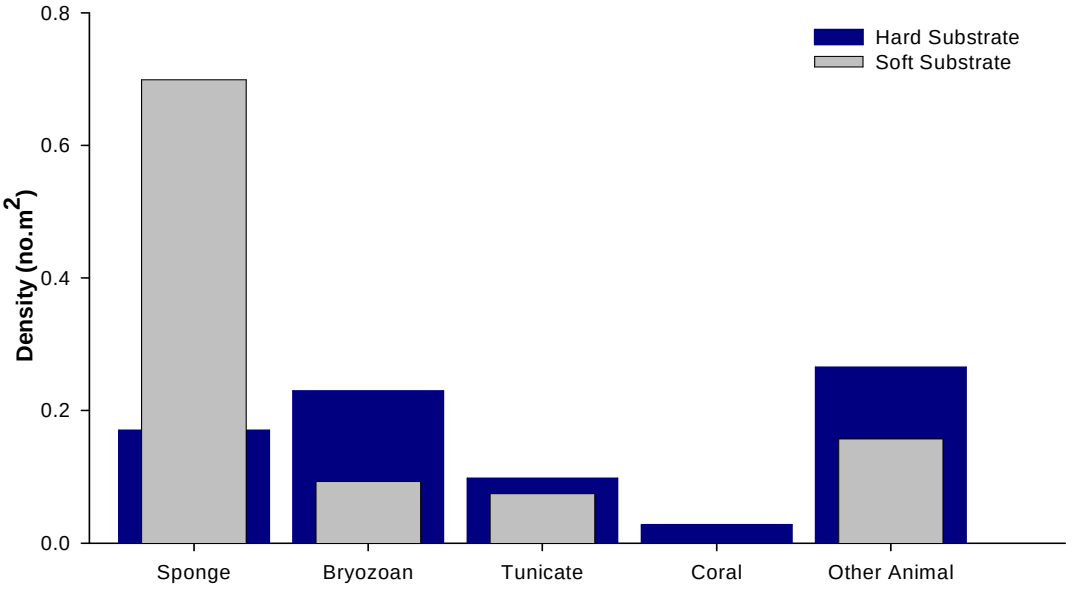

Figure 3.177. Average density of animal types recovered by sled dredge.

Average total animal biomass is shown in Figure 3.178 for sled dredges over hard and soft sediment at specific depths. The overall average for hard sea-bed areas from 30-75m was 121.0g.m^{-2}, for soft sediment at 40 and 100m was 0.8 g.m^{-2} and for the deeper 150m sites was 43.9 g.m^{-2}.

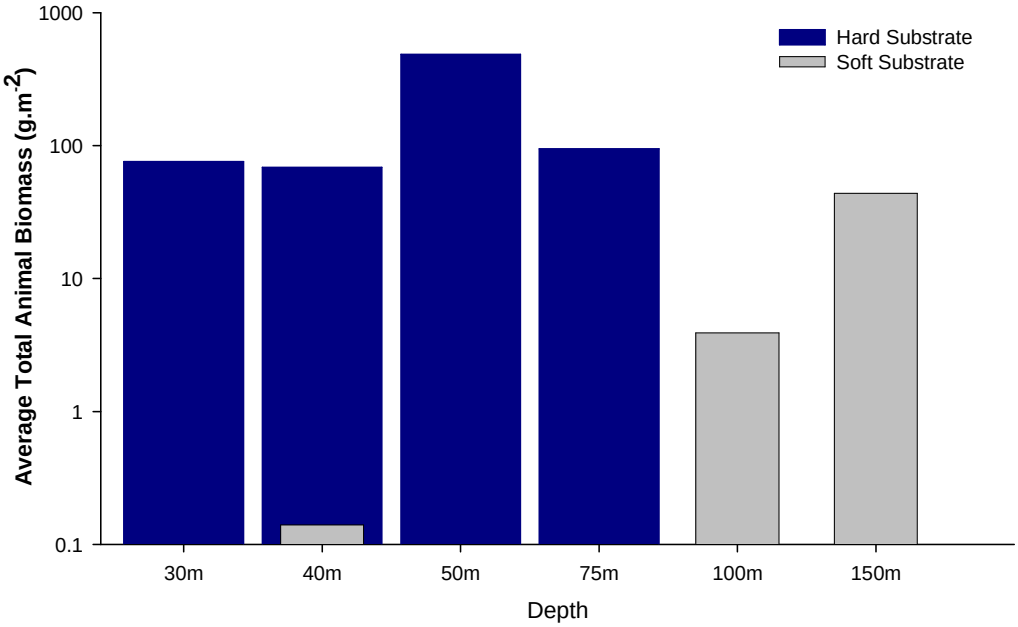

Figure 3.178. Average total animal biomass for sled dredges from leg 1 of Southern Surveyor 2007-04.

Sponges were the dominant biomass of sled samples over both hard and soft sediment, and the biomass of all animal types was greater for hard sea-bed habitats (Figure 3.179).

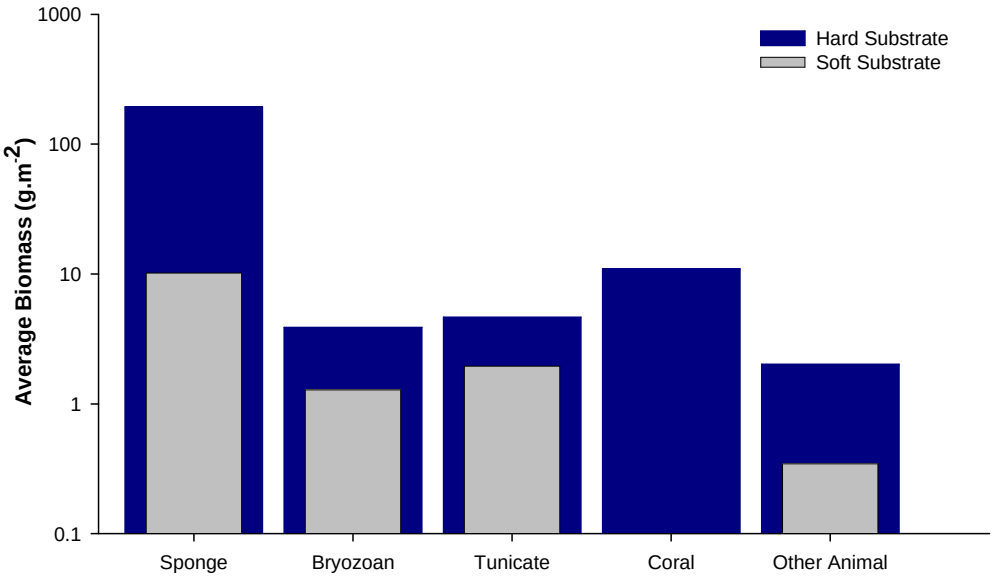

Figure 3.179. Average biomass of animal types recovered by sled dredge.

Plants

Average total plant biomass is given in Figure 3.180 for sled dredges over hard and soft sediment at specific depths, not shown on the figure are the sled over hard substrate at 75m and two over soft sediment at 150m, all of which had no plant material. The overall average for

hard sea-bed areas from 30-75m was 152.1g.m^{-2}, for soft sediment at 40 and 100m was 0.03g.m^{-2} and for the deep 150m sites was 0g.m^{-2}.

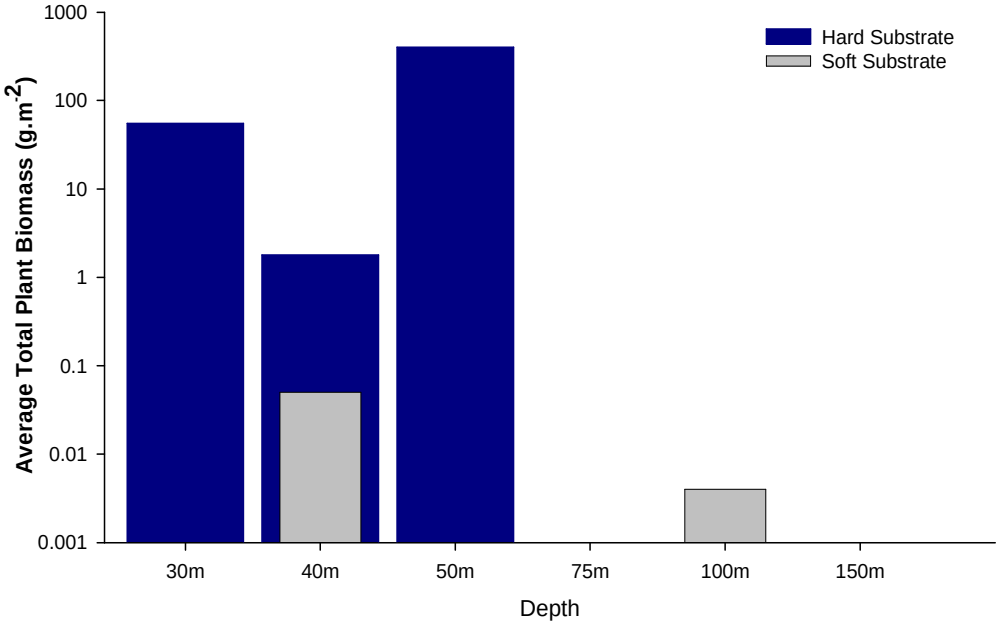

Figure 3.180. Average total plant biomass for sled dredges from leg 1 of Southern Surveyor 2007-04.

The kelp *Ecklonia* dominated hard substrate sled samples by an order of magnitude, this was due to the large biomass retrieved on both sleds at 50m (Figure 3.181).

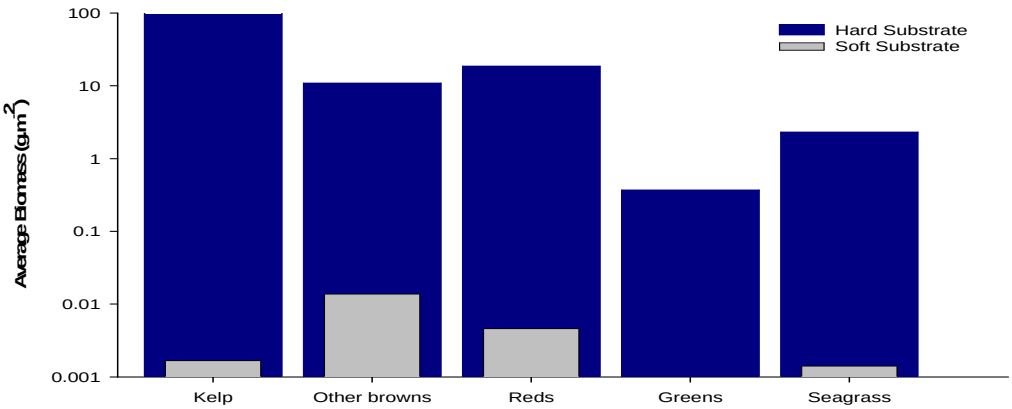

Figure 3.181. Average biomass of plant categories recovered by sled dredge.

Key Findings:

- **Kelp (Ecklonia radiata) dominates the deep water benthic plant biomass**
- **Hard bottom habitats around 50m depth have very high algal biomass**
- **Sponges have the highest biomass on deepwater hard bottom substrates exceeding the biomass of other taxa by almost an order of magnitude**
- **Soft bottom habitats beyond 100m also have a high filter feeder biomass predominantly sponges and bryozoa.**

3.3.7 Role of Key Functional Groups 30-150 m

Benthic Microalgae

One outcome from SRFME has been an increased emphasis upon shelf processes on the cycling of nutrients. Portions of the WA coast have a relatively wide continental shelf with a large area of soft bottom sediments capable of supporting communities of benthic microalgae (BMA). The BMA in these sediments contribute to food webs, and play an important role in the nutrient cycling of coastal ecosystems worldwide but the role of BMA in nutrient cycling and primary production for the west coast of Australia is largely unknown. Worldwide there have only been ~ 85 studies of BMA and none of these have ever determined the depth at which BMA primary production reaches zero (Cahoon 1999). In fact only a handful of measurements exist at depths > 60 m.

The research voyage (SS04/2007) departed Fremantle, WA at 1600hrs, Thursday, 10 May 2007. The first 5 days of scientific investigation were a benthic survey of the shallow (30 – 150 m) bottom habitats off Perth (Figure 3.157). The benthic survey included high resolution 'swath' mapping, underwater video surveys of the bottom, benthic sampling by sledges and grabs with 12 ctd casts and associated water column sampling. The remaining 23 days of the research voyage involved mostly water column sampling from 34°S to 22°S with benthic grabs on the inshore legs of most transects (Figure 3.182).

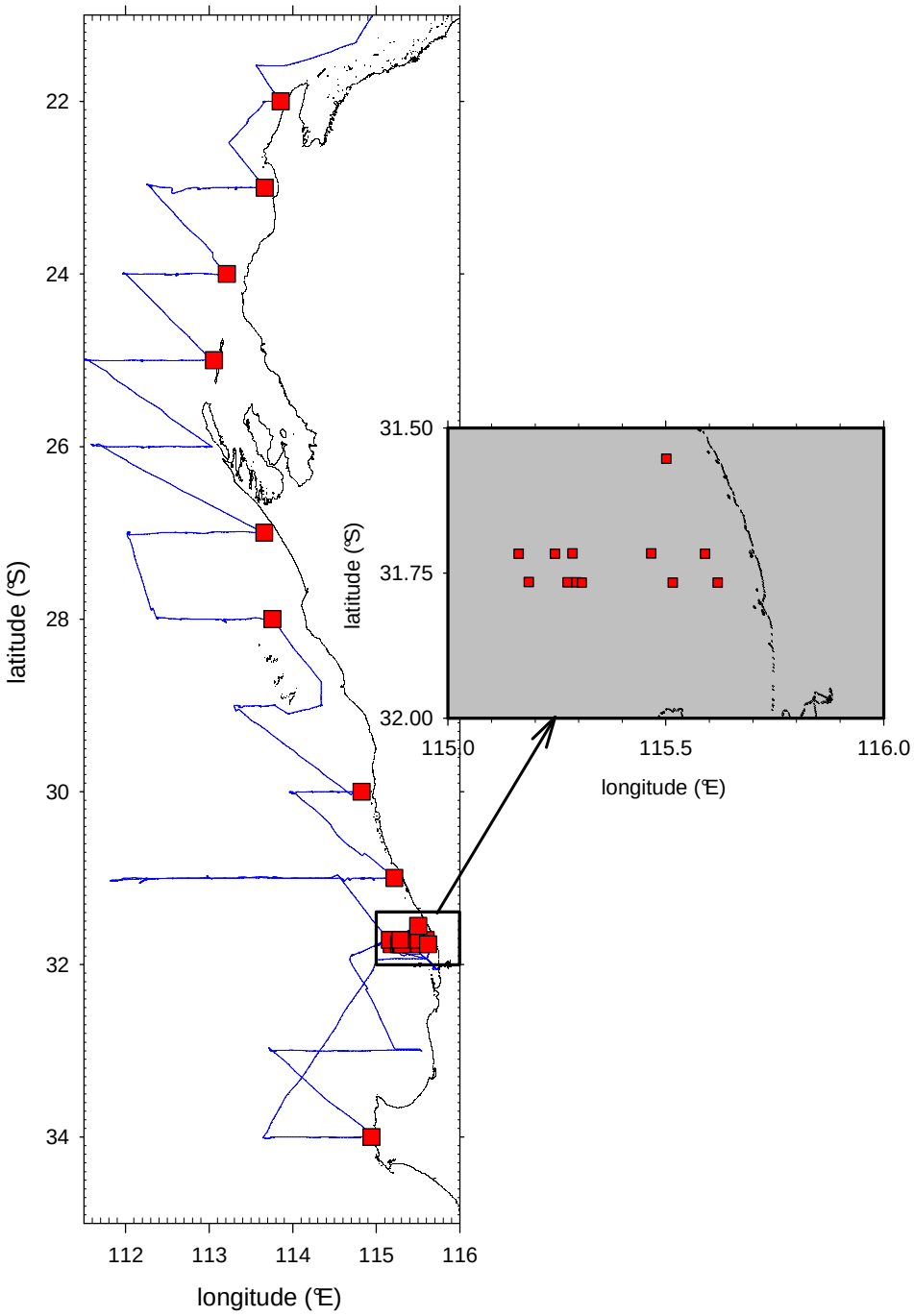

Figure 3.182. Map showing cruise track and sample locations (■) for benthic microalgae.

BMA samples were collected using a Smith MacIntyre grab at depths from 28 to 140 m. Samples were only used if a visual inspection indicated a largely intact sample had been collected. The grab allowed some of the overlying water to escape during recovery and may have dislodged any unattached cells on the surface (e.g. sedimented phytoplankton). Once on deck the grab sample was cored by hand. Cores for flux incubations were sealed at the bottom with overlying water retained on top. At each site a conductivity, temperature and depth (CTD) cast using a Seabird SBE 911 dual conductivity (practical salinity units = PSU), temperature (°C), fluorescence was measured with a Chelsea Aquatracka™ fluorometer and a Licor LI-192SA sensor was used for photosynthetically active radiation (PAR) while multiple depths sampled for nutrients. Continuous underway data included PAR collected by a Licor LI-192SA

sensor attached to the mast head. Samples were analysed for nitrate, nitrite, silicate and phosphate concentrations using Quick-Chem™ methods on a flow injection LACHAT® instrument as per the following protocols for nitrate and/or nitrite (Quik-Chem™ Method 31-107-04-1-A; detection limit ~0.03 µM; adapted from Wood et al. 1967), silicon (Quik-Chem™ Method 31-114-27-1-D; detection limit ~0.05 µM; adapted from Murphy and Riley 1962) and phosphate (Quik-Chem™ Method 31-115-01-1-G; detection limit ~0.02 µM; adapted from Armstrong 1951). Samples were analysed for ammonium on the LACHAT® instrument using the technique of Kerouel and Aminot (1997) adapted for flow injection by Watson et al. (2004), detect limit ~ 0.05 µM.

Material for pigment analysis was taken from the same grab samples used for nutrient, oxygen fluxes and PAM measurements. The top 4mm of the sediment surface was removed for pigment analysis by HPLC analysis. These were immediately preserved in liquid nitrogen. The top 20 mm was removed for pigment analysis by fluorometry. These samples were immediately extracted in 100% acetone in the dark at 4°C ~ 24 h before analysis on the calibrated Turner Designs model 10AU™ fluorometer. For HPLC analysis sediments were extracted twice in 100% acetone at 4°C, firstly for 18 hours and then for 4 hours. Following extraction, water was added to give a ratio of 9:1 acetone:water by volume, and filtered (0.2µm membrane filter; Whatman Anatop, Whatman plc, Brentford, UK) before analysis by HPLC. The analysis was by a Waters high performance liquid chromatography (Waters Corporation, Milford MA, USA), comprising a model 600 controller, 717 plus refrigerated auto-sampler, and a 996 photodiode array detector. Pigments were separated as described by (Wright, Jeffrey et al. 1991), detected at 436 nm, and identified against standard spectra. Concentrations of chlorophyll *a* (chl*a*), chlorophyll *b* (chl*b*), β,β carotene, and β,ε carotene in sample chromatograms were determined from standards, and all other pigment concentrations were determined from standards of purified pigments isolated from algal cultures. Information for the assignment of microalgal marker pigments was drawn from Jeffrey et al. (1997).

Fluorescence parameters of BMA communities were measured in cores with a Phyto PAM multi-channel fluorometer (Heinz Walz GmbH, Effeltrich, Germany) fitted with a Phyto-EDF fibre-optic attachment, designed for use on biofilms. After collection cores were allowed to re-equilibrate for several hours at in situ temperatures and in the dark prior to measuring photosynthetic parameters using the PAM. Microalgal cultures from the CSIRO Collection of Living Microalgae were used to calibrate the taxonomic discrimination of the measuring software (Phyto Win v1.46, Heinz Walz GmbH, J. Kolbowski). The cultures used were- brown: *Navicula jeffreyi* (CS-46), green: *Dunaliella* sp. (CS-353), blue-green: *Oscillatoria* sp. (CS-52). Given the reference spectra used in the Phyto PAM, "browns" are approximately equivalent to any species with chlorophyll c (referred to hereafter as browns) greens would contain chlorophyll b (= "greens") and cyanobacteria would contain zeaxanthin ("blue-greens"). F_o (the initial minimal fluorescence yield) was measured at 25 Hz; all fluorescence terminology is consistent with Buchel and Wilhelm (1993). Saturating irradiance pulses were applied and then a series of pulsed illuminations provided estimates of relative electron transport rates which were used to construct rapid light curves and fit to the model of Eilers and Peeters (1988) to estimate photosynthetic parameters I_k, ETR_{max} (maximum electron transport rate) and alpha (α = initial slope of irradiance vs ETR curve). The parameter ΔF is defined as the difference between the fluorescence yield from a saturating pulse (maximum yield, F_m) and the yield (F) from the measuring level of irradiance i.e.:

$$\Delta F = (F_m - F)$$

Visual inspection suggested the sampled cores ranged from undisturbed to moderately mixed. We therefore suggest that greater than normal variability may be present in the data with a possible negative bias in the results for BMA biomass and production. Pigment biomass (0 –

20mm) was a negative exponential function of depth (Figure 3.183) but with considerable scatter. Work is underway to include a greater range of near shore data from SRFME into these analyses with the hope reducing the variability. Small scale variability, however, is a well know feature of BMA and a well estimated mean value is likely to be the most useful parameter for biogeochemical modelling.

Estimated concentrations of chlorophyll *a* at zero depth (shore) were ~ 54 mg m^{-2}, somewhat below those values observed in Cockburn Sound (Forehead 2006). BMA samples over 0 – 4 mm and analysed by HPLC tended to have less pigment than those from 0 – 20 mm (Figure 3.183). Both 0 – 20 and 0 – 4 mm samples declined exponentially with depth reaching very low concentrations ~ 95m. The irradiance also declined exponentially with depth reaching ~ 0.9 µmoles photons m^{-2} s^{-1} at 95 meters (Figure 3.183). We suggest 95 meters and ~ 0.9 µmoles photons m^{-2} s^{-1} represent the maximum depth of net positive growth for BMA if using light as the sole energy source.

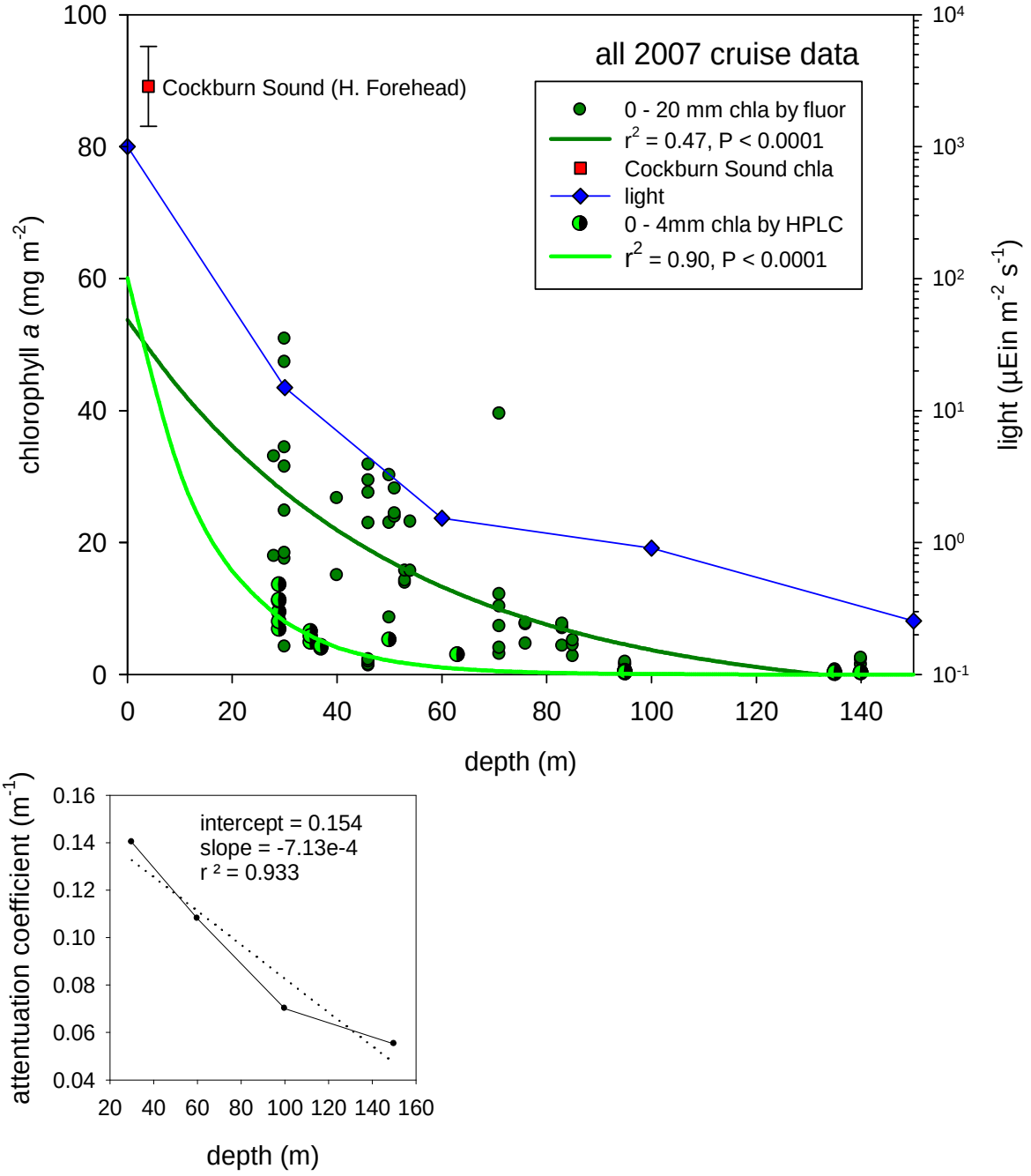

Figure 3.183. Upper panel shows benthic microalgal (BMA) biomass (y-axis, left side) as a function of water depth for 0 – 20 mm cores measured by fluorometry and 0 – 4mm cores measured by HPLC. Both data sets are fit to exponential decay curves: $y_d = y_0 e^{-bd}$ where y_d = BMA biomass at depth (d), y_0 = BMA biomass at zero depth, *b* is a constant and *d* is depth. From the light versus depth data collected during CTD casts in this region the attenuation coefficients were calculated: $E_d = E_0 e^{-kd}$ where E_d = light at depth (d), E_0 = light just below the surface, *k* = the attenuation coefficient and *d* = depth. Attenuation coefficients ranged from 0.14 to 0.055 m^{-1}.

In the middle portion of the continental shelf (30 – 60m) diatoms comprised about 80% of the BMA biomass (Figure 3.184). This result is consistent with many other studies on the community composition of BMA, albeit most published studies have sampled at much shallower depths. Only at depths > 60m did other pigments increase their proportional contribution in a major way. At ~ 90m chlorophyll *b* increased as a proportion of chlorophyll *a* suggesting relatively more chlorophytes (possibly macrophyte debris or seagrass debris,Figure

3.184). At 138m alloxanthin and zeaxanthin were relatively high. The increase in alloxanthin may represent more cryptophytes or longer retention of this pigment by zooplankton. Even though alloxanthin and zeaxanthin both increased at 138 m they remained minor pigments found primarily in relatively deep waters where the BMA biomass was very low and BMA are unlikely to play a significant role in the active nutrient cycling. They may represent the accumulation of phytoplankton cells sinking out of the water column above and thus represent a vertically important flux but their role as active primary producers is likely to be insignificant (see later). They may also have a role in seeding phytoplankton back into the water column during times of strong vertical mixing. In particular the cryptophytes are known to produce a range of cysts for this purpose. They are also notoriously difficult to detect in samples preserved for microscopic examination due to their tendency to decompose.

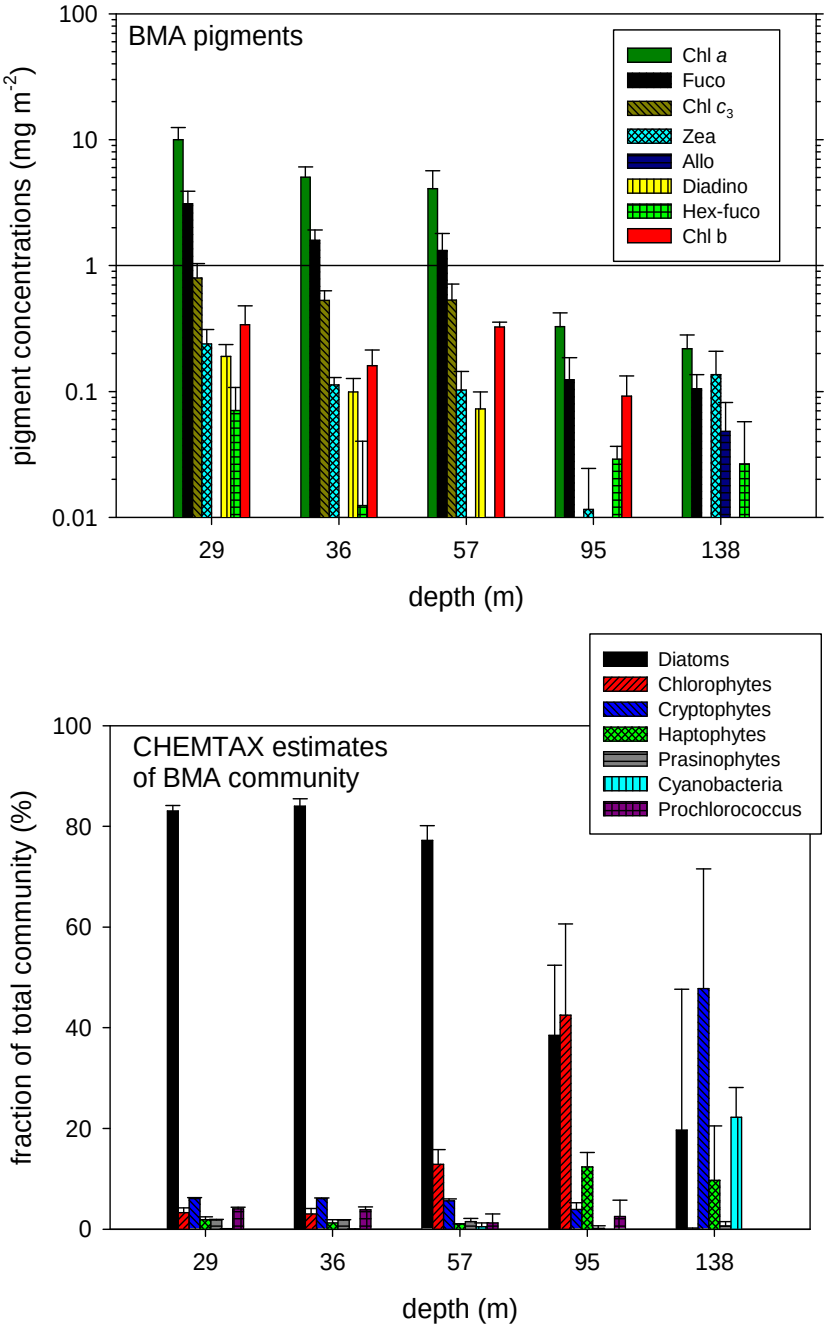

Figure 3.184. Pigment data for 0 – 4 mm cores obtained from benthic grabs at different depths at sites off Perth (see inset Figure 3.182). Samples were analysed by HPLC and data processed through CHEMTAX (Mackay et al. 1996) to estimate community composition of the BMA.

A range of photosynthetic parameters were measured using pulse amplitude modulated (PAM) fluorometry. The data all suggest that at depths > 100m the BMA are not photosynthetically active as both ΔF and active chlorophyll *a* declined to near zero as depths exceed 100 m (Figure 3.185). At shallow depths fluorescence parameters suggest primary production was an exponential function of irradiance. The rate of primary production is proportional to the electron transport rate (ETR) and can be modelled as:

$$ETR = ETR_{max} (1\text{-}e^{aE})$$

where ETR = electron transport rate, ETR_{max} is the maximum rate, *a* is a constant and E is irradiance. The observed data fit the model well as shown in the example (Figure 3.185) where $r^2 = 0.98$. The model output gives estimates of:

1. alpha (α) the initial slope of the primary production versus irradiance slope,
2. ETR_{max}, the maximum rate of electron transport
3. I_k the irradiance which half saturates primary production.

All three of these parameters varied with depth (Figure 3.185), all declining with increasing depth. In particular ETR_{max} was a negative exponential function of depth with a very high correlation ($r^2 = 0.94$) indicating that BMA primary production can be modelled from depth or an estimate of irradiance on the bottom.

Simple model of benthic microalgal primary production

A simple model to calculate benthic microalgal primary production can be represented as follows:

ETR = 58.441 * exp(-0.035*depth)

Substituting our measured primary production (PP) rate of 197.1 gC per m^2 per year at 5m depth and corresponding ETR of 49.05871 we obtain:

PP = ETR * 197.1/49.0587 or more usefully:

*PP = 234.79 * exp (-0.035*depth)*

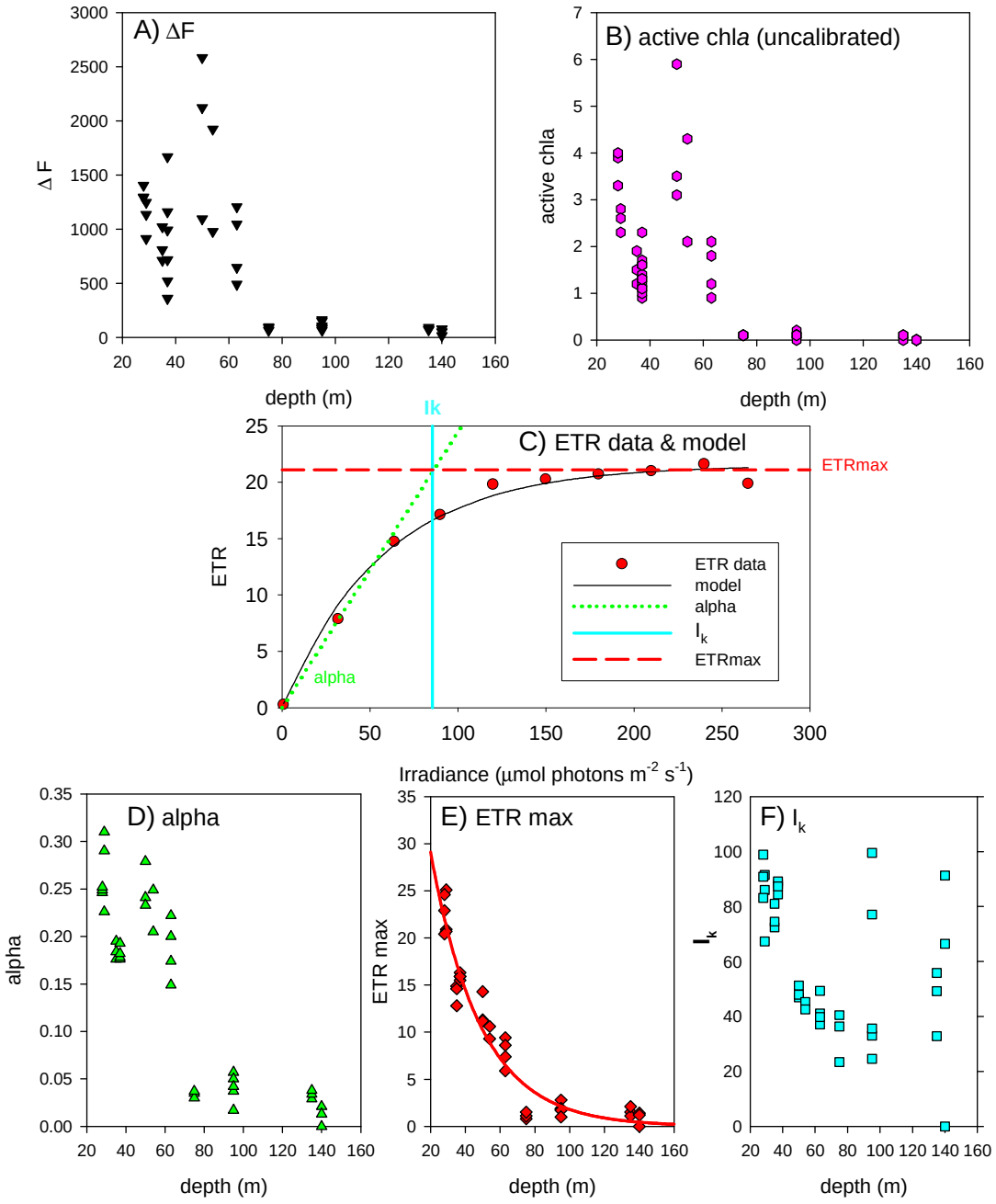

Figure 3.185. Results from PAM fluorometry for cores collected at different depths (see Figure 3.182 for locations).

Key Findings:
Diatoms dominate the benthic microalgal (MBA) community

The results suggest that BMA biomass may be modelled as a simple exponential decay function of depth or as a linear function of bottom irradiance.

BMA primary production can be modelled from depth or an estimate of bottom irradiance according to:

PP = 234.79 * exp (-0.035*depth)

Macroalgae

Productivity measurements were conducted on a number of abundant macroalgal species collected from 40 – 60 m depths during the cruise. Additionally, the diversity and biomass of all species collected was recorded, to allow for estimation of benthic plant biomass and productivity in depths >40 m. Samples were also collected for a number of algal bioassays (e.g. isotopic composition, nutrient status, pigment concentration) that will allow comparison between deep- and shallow-water benthic plants of Marmion Lagoon.

Measurements of the photosynthetic performance of a number of abundant macroalgal species, collected from 33 – 55 m depths, were conducted during the cruise. Additionally, the diversity and biomass of all species collected was recorded, to allow for estimation of benthic plant biomass and productivity in depths >40 m. Samples were also collected for a number of algal bioassays (e.g. isotopic composition, nutrient status, pigment concentration) that will allow comparison between deep- and shallow-water benthic plants of Marmion Lagoon.

The photosynthetic performance of 4 brown and 3 red algal deep-water species was measured in terms of potential quantum yield (Fv/Fm, which indicates 'health' status of photosystem II) and electron transport rates (ETR). Brown algae (Phaeophyta) had significantly higher yield values compared to red algae (Rhodophyta) (see Table 3.39 below). The kelp, *Ecklonia radiata*, had the highest F_v/F_m of 0.80 ± 0.00 (mean ± SE) and highest ETR_{max} of 12.6 μmol electron m^{-2} s^{-1}. ETR_{max} and F_v/F_m related to depth (r^2 = 0.03 and r^2 = 0.01 respectively).

Table 3.39. Algal species, functional form and depth collected, F_v/F_m (mean ± SE), ETRmax (µmol electron m^{-2} s^{-1}), I_k (µmol quanta m^{-2} s^{-1}), absorptance factor (AF), maximum noon irradiance at depth (µmol quanta m^{-2} s^{-1}) and percent surface irradiance.

Species	Functional form	Depth (m)	AF*	F_v/F_m	ETR_{max}	I_k	maximum irradiance at depth	% surface irradiance
Phaeophyta								
Sargassum peronii	corticated foliose	33	0.78	0.76 ± 0.00 ^{A}	8.9 ± 0.6 ^{a}	29.9 ± 1.8 $_{A}$	92	4.6
Dictyopteris muelleri	foliose	33	-	0.74 ± 0.01 ^{A}	-	-	92	4.6
Myriodesma quercifolium	corticated foliose	40	0.78	0.74 ± 0.01 ^{A}	5.3 ± 0.1 ^{b}	16.9 ± 0.3 $_{AB}$	48	2.4
Scytothalia dorycarpa	leathery	50	0.84	0.74 ± 0.01 ^{A}	6.7 ± 0.3 ^{c}	22.1 ± 1.3 $_{AB}$	19	1.0
Ecklonia radiata	leathery	50	0.84	0.80 ± 0.00 ^{B}	12.6 ± 0.2 ^{d}	37.0 ± 1.2 $_{AB}$	19	1.0
Rhodophyta								
Osmundaria prolifera	leathery	33	0.84	0.46 ± 0.02 ^{C}	3.0 ± 0.2 ^{e}	38.0 ± 6.2 $_{AB}$	92	4.6
Hennedya crispa	corticated foliose	55	0.57	0.56 ± 0.01 ^{D}	1.7 ± 0.1 ^{f}	45.5 ± 9.6 $_{B}$	12	0.6
Callophycus costatus	corticated foliose	55	0.57	0.56 ± 0.02 ^{D}	1.2 ± 0.1 ^{f}	35.5 ± 6.8 $_{B}$	12	0.6

** estimated from Markager (1993), Franklin and Badger (2001), Figueroa et al (2003), Beer and Axelsson (2004)*
Letters indicate significant differences among species

Although it is commonly thought that red algal species fare better under low light conditions and are more productive than brown or green species (Gail 1922, Larkum et al. 1967, Dring 1981), the higher F_v/F_m and ETR_{max} of the brown species in this study suggests that in well-mixed oligotrophic waters of Western Australia this is not the case. The biomass of reds and browns was, on average, similar across depths 33 to 55 m, while greens had significantly lower biomass than both reds and browns (Figure 3.181). High F_v/F_m, prolific standing stock and high biomass at low light intensities (<5% of surface irradiance) indicate an efficient utilisation of available light energy (Littler et al. 1986). The high photosynthetic rates of the brown algae may also be due to greater availability of nutrients in the well-mixed waters, or reduced levels of herbivory and grazing, which allowed greater standing stocks to develop.

Nutrient status of macroalgae

The nutrient status of 7 red and brown macroalgal species was determined by extraction of soluble tissue nitrogen (N) pools from the algal tissue. Samples were collected from deep waters (40 – 55 m) during the cruise, and additional shallow water (4 – 15 m) samples were collected immediately after the cruise. Soluble tissue N pools are a useful bioindicator of a plant's recent, short-term exposure to N availability, and as such can be used to supplement data on ambient seawater N levels that were collected during the cruise (Figure 3.186).

Some species examined, such as the brown alga *Sctyothalia dorycarpa* and the red alga *Hennedya crispa*, exhibited increased soluble tissue N pools with increasing water depth, while others such as the brown algae *Ecklonia radiata* and *Dictyopteris muelleri* showed no trend with depth. These differences may be due to localised nutrient availability or to physiological differences in the N requirements among species.

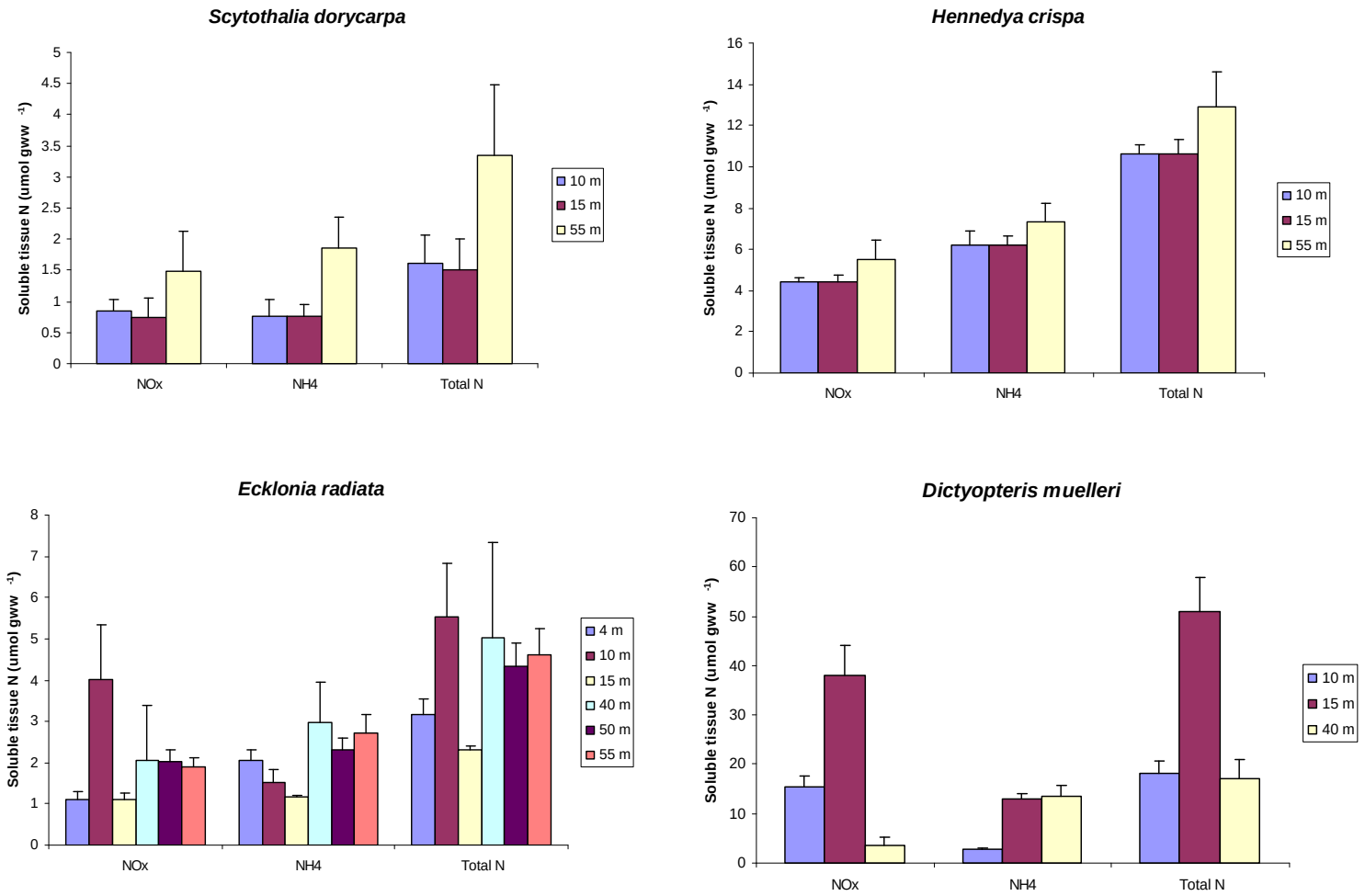

Figure 3.186. Soluble tissue nitrogen pools extracted from macroalgae growing at different depths.

Pigment composition and concentration

Samples for pigment composition and concentration were collected from 9 algal and 1 seagrass species, from 33 – 55 m depths. As with the isotopic analyses, where possible, matching samples were collected from shallow water plants.

Results from pigment analyses varied among species. Some species showed increased pigment concentration with depth, as would be expected in algae that are compensating for lower light availability. Conversely, other species showed either no change, or decreased pigment concentrations with increasing depth. This may result from light levels not falling below critical levels, or from the acclimation of individual species to reduced light availability.

Key Findings:

- **This work represents the first measurements of photosynthetic performance of deep-water algae from Western Australia**
- **Important high biomass communities of deep water kelp were found to at least 50m**
- **The photosynthetic measurements of deepwater brown algae including the kelp *Ecklonia* at 50m water depth suggest high productivity for these species and their high biomass on deep reefs warrant further investigation of their importance.**

Role of benthic filter feeders (30-150 m)

Sponges are ubiquitous marine organisms occurring from the extreme high latitudes to the tropics (Bergquist, 1978). Sponges are common in shallow water habitats where, depending on geography, they share the benthos with primary producers such as algae, seagrass and corals. However, sponges dominate the diversity and biomass of marine benthic environments in deeper waters (e.g. McEnnulty et al. in press; Heyward et al. 2010) at the lower levels of the photic zone, sometimes referred to as the mesophotic zone (Olsen and Kellogg 2010). Their dominance diminishes again at greater depths beyond the photic zone when consolidated bottom gives way to predominantly sedimentary habitats.

In addition to being the dominant features of the benthic biostructure in the mesophotic zone where hard reef substrates occur, sponges are believed to play an important role in the ecology of the habitats they occupy. Sponges are important agents in bentho-pelagic coupling, filtering the products of primary and secondary production from the water column and shifting them into a sedentary form on the seabed. Thus where sponge biomass is high they comprise a significant standing stock of carbon and nitrogen at the seabed.

Filtration rates measured *in situ* in shallow reefs were applied to biomass obtained from sled material to estimate the clearance rates of sponges and ascidians. We used conversion of 16.2 (sponges) and 6.2 % (ascidians) (Ricciardi and Bourget, 1998) for conversion from wet weight to dry weight.

Deeper areas offshore of Marmion lagoon provide a habitat for a considerable biomass of filter feeders. Biomass of sponges and ascidians in sled samples varied from less that 1 g of wet weight to a high of 850 $g.m^2$ (Figure 3.187).

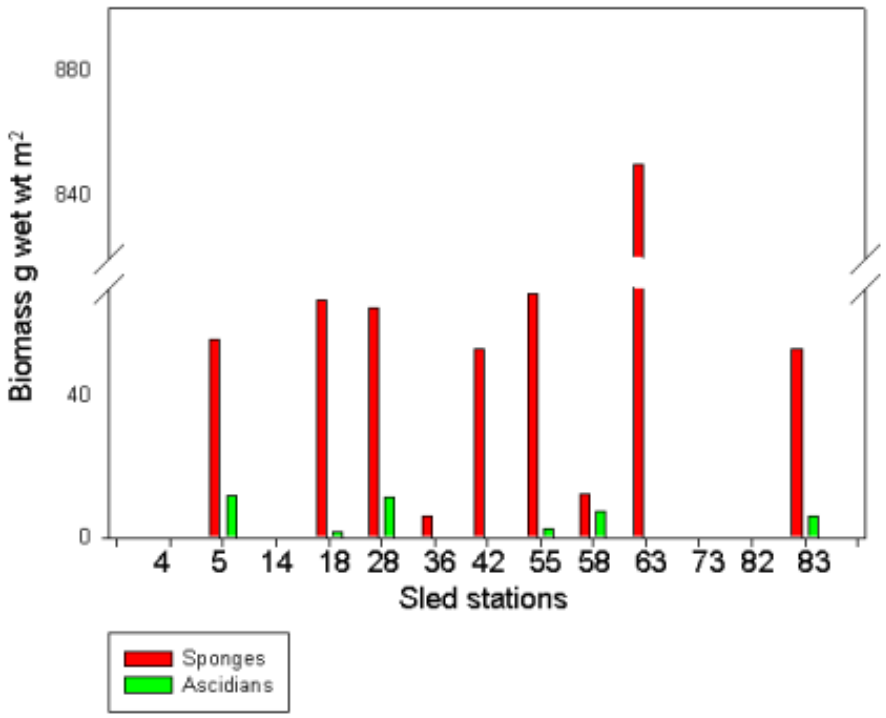

Figure 3.187. Biomass of sponges and ascidians in Marmion Lagoon 30 to 150 m stations.

Comparison of biomass of all invertebrate phyla dredged revealed that sponges and ascidians were present in all stations that were located on hard substrate and sponges dominated in terms of biomass in most of them (Figure 3.188). Ascidians were important in stations 5, 28, 58 and 83.

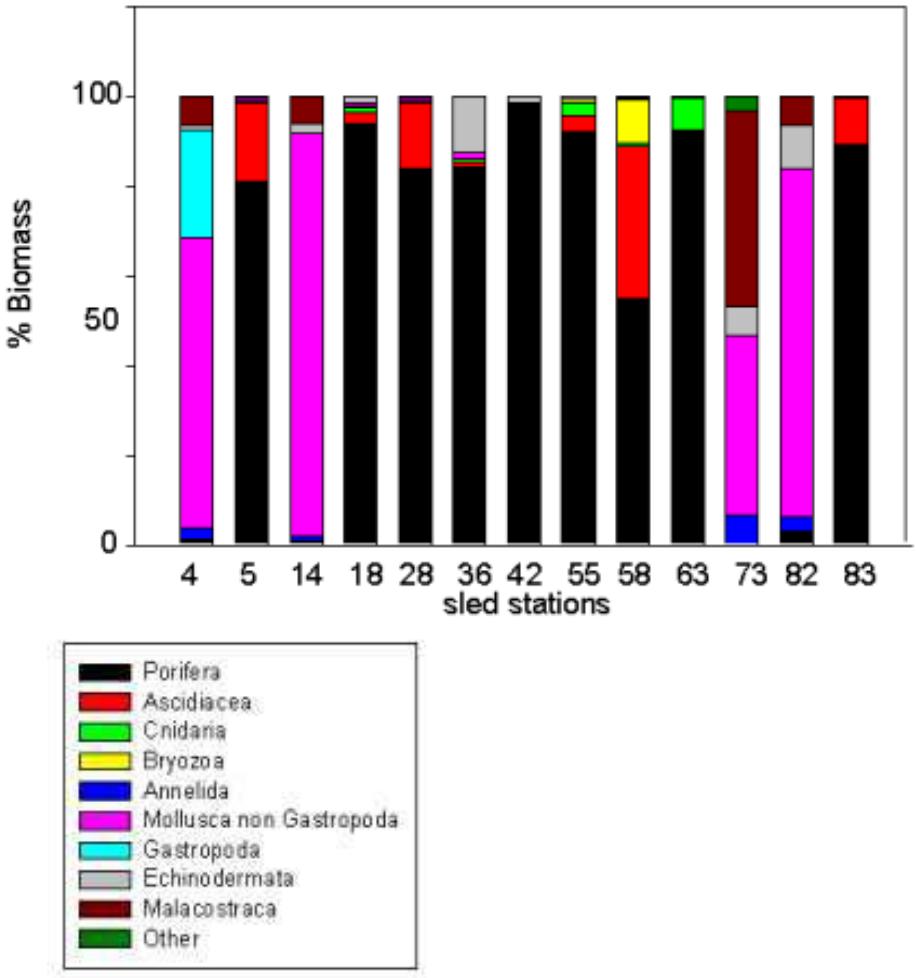

Figure 3.188. Proportion of biomass of invertebrates in 30 to 150 m stations.

Figure 3.189 and Figure 3.190 below show filtration by sponges and ascidians per day based on 12 hours activity.

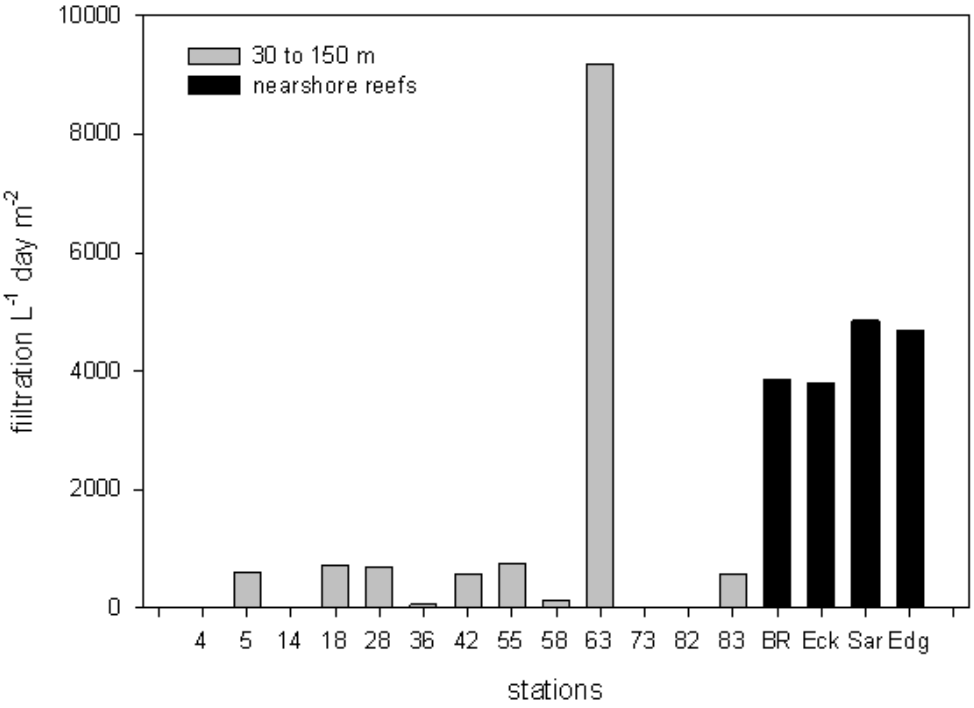

Figure 3.189. Daily filtration rates by sponges nearshore (BR – turfing algae, Eck – *Ecklonia radiata*, Sarg - *Sargassum* spp Edg – sand edge) and in 30 to 150 m depth.

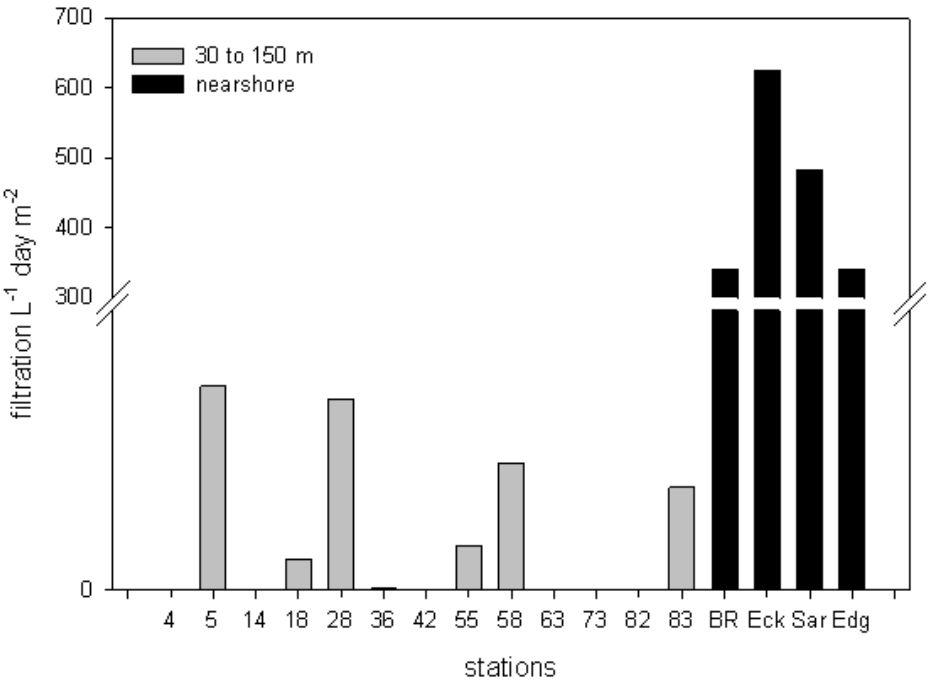

Figure 3.190. Daily filtration rates by ascidians nearshore (BR – turfing algae, Eck – *Ecklonia radiata*, Sarg - *Sargassum* spp Edg – sand edge) and in 30 to 150 m depth.

There is lack of published information on distribution of sponges and ascidians from deeper waters off the south west of Australia. Sponges and ascidians were a major element of benthic marine fauna in 30 to 150 m of water and sponges dominated the biomass in most stations. Considerable spatial variation among stations could be due to the short range dispersal, substrate availability, biological interactions or physical disturbance (Underwood et al, 1991). The filtration of both ascidians and sponges were higher nearshore than offshore. This stems purely from the difference in biomass since the same filtrations per gram of

weight were applied. The variability in filtration was also much higher offshore than inshore. This was due to fewer sites sampled offshore than inshore where 38 sites were sampled in each habitat: turfing algae, *Ecklonia radiata* and *Sargassum* and 9 on the sand edge. Equally, it is important to note that the individual filtration rates measured inshore were highly variable (see chapter 3 of this report) and we used a median rate in our estimates. Sponges were extremely important in some deeper stations e.g. in no 63. Since sponges retain prokaryotic picoplankton and pelagic productivity in our system is dominated by these organisms therefore sponges would have important role in controlling the biomass of this size plankton. The importance of filter feeders in controlling phytoplankton in shallow waters off Western Australia has been evaluated in some places however there has been no estimation of filtering capacity in deeper waters.

Key Findings:

- **Sponges form a high biomass on deep reefs and estimates of filtration rates using data collected on shallow water sponges emphasise their important role in bentho-pelagic coupling and should enable estimates of the incorporation of pelagic primary production into benthic biomass**

.

Photosynthetic cyanobacterial symbionts in sponges

A significant feature of sponges is the bacterial and algal symbioses they support (Taylor et al. 2007, Usher 2008). Sponges also commonly contain photosynthetic algal and bacterial symbionts of which the most common are photosynthetic cyanobacteria (Hentschel et al. 2006, Usher 2008, Lemloh et al. 2009). These bacteria provide the sponge with energy and carbon in the form of photosynthates (Wilkinson 1983, Wilkinson 1987, Arillo et al. 1993) and secondary metabolites which are thought to prevent biofouling and deter predators (Unson and Falkner 1993) and Schmidt et al. (2000). Some of these bacteria are symbiotic nitrifying bacteria and are thought to play an important role in the biogeochemical cycle in coastal and shelf environments as producers of new nitrogen in the form of dissolved inorganic nitrogen (DIN - nitrite and nitrate) (Diaz and Ward 1997, Bayer et al. 2007, Mohamed et al. 2010).

Until recently photosynthetic cyanobacterial symbionts were thought to be confined to oligotrophic tropical waters having evolved similar responses to this environment as hermatypic corals (e.g. Wilkinson 1983). Recent reports by Roberts et al. (1999) and Lemloh et al. (2009) have shown that significant proportions of shallow water sponges in temperate regions host photosynthetic cyanobacteria in symbiotic relationships and the types and species of cyanobacteria associated with photosynthetic sponges were recently reviewed by Usher (2008). The depth profile of sponges with photosynthetic symbionts has not been investigated, however, Wilkinson and Vacelet (1979) report the cyanosponge *Chondrilla nucula* Schmidt, 1862 at 55 m, and we have observed filamentous cyanobacteria in a *Geodia* sp. collected at 82 m at Ningaloo, in tropical Western Australia. This study sought to determine whether this form of symbiosis in temperate sponges extended beyond the shallows into deeper reefs and the mesophotic zone where sponges are the dominant epibenthos.

Sampling of sponges

Sponges were sampled between 10 and 15 May 2007 from the RV Southern Surveyor. A large very heavy epibenthic sled with a 1.2 m wide mouth was deployed at 13 stations at depths of 40 m, 50 m, 75 m, 100m and 150m (lat, long) off the Marmion region of south

Western Australia. All sampling sites were between about 10 and 50 km off shore within a rectangular area bounded by longitudes 115.16556° and 115.62395° East and latitudes 31.71615 ° and 31.76802 ° South. The sled was towed along the seabed at slow speed for distances of between 181 m and 1080 m depending on the site. Sandy soft bottom sites were towed for longer distances, hard bottom expected to have higher biomass was towed for shorter distances. The distance covered by the sled was multiplied by 1.2 to obtain the area sampled by the sled in m^2. Sponges were sorted from the biota sampled by the sled and weighed. Biomass of sponges was determined by dividing the weight of the sponges sampled by the area sampled by the sled. A random selection of sponges from each depth range was assessed for photosynthetic cyanobacteria. Sponges were photographed and small sections of sponge containing surface and internal tissues were dissected and fixed in Dimethylsulfoxide (DMSO) solution pH 7.5 (20% DMSO, 0.25 M Na2EDTA pH 8, NaCl to saturation) and frozen at -20°C. A larger sample of each sponge was fixed in 75% ethanol and retained for identification.

Frozen samples were analysed via fluorescence microscopy to determine the presence, distribution and density of photosynthetic symbionts. Frozen sponge samples were washed with autoclaved sea water and cross sections were cut thinly using a double-sided razor. The sections were examined by fluorescence microscopy using a Leitz Diaplan microscope (Leica Microsystems, Germany). Blue light, using a I3 filter block (450–490 nm excitation filter and 515 barrier filter), and green light, using a N2.1 filter block (515–560 nm excitation filter and 590 barrier filter), were used to detect the distribution and concentration of autofluorescent cyanobacterial or algal pigments. Cyanobacterial and rhodophyte autofluorescence appeared orange-yellow using blue light due to the presence of phycobiliproteins, and were red in colour using green light, while algae (other than rhodophytes) appeared red in blue light. All samples were categorised according to a subjective analysis of the levels of autofluorescence from photosynthetic pigments and the categories 'low', 'medium' and 'high' were given to describe the densities of symbionts. Samples with no autofluorescence and ambiguous samples (very low autofluorescence or potential surface contamination) were deemed 'negative'.

Molecular analysis

Sponges which exhibited epifluorescence were identified by classical methods and their symbionts sequenced where possible. To avoid surface contamination the sponge samples were brushed with a toothbrush and rinsed with distilled water. DNA from approximately 0.3 g of sponge tissue preserved in DMSO was extracted using a PowerSiol DNA isolation kit (MoBio, Australia) as per instructions. Cyanobacterial-specific primers were used for PCR. The forward primer cya359F (5'-GGGGAATYTTCCGCAATGGG) and the reverse primer cya1459R (5'-GGTAAYGACTTCGGGCRT) were used to amplify a 1100 base pair section of the small subunit of ribosomal RNA (16S rDNA). PCR and Denaturing Gradient Gel Electrophoresis were carried out as per Lemloh et al. (2009), but PCR was performed using a KAPA2G Fast PCR kit (KAPA Biosystems, Australia) as per instructions. Sequencing reactions were performed as per Lemloh et al. (2009). Sequence similarities were found using Blast search tool available on the National Centre for Biotechnology Information (NCBI) website (http://www.ncbi.nlm.nih.gov/BLAST/), and sequence identities were analysed using the EMBL-EBI Emboss Water tool for DNA, website (http://www.ebi.ac.uk/Tools/emboss/align/index.html).

Voucher sponge specimens preserved in 75% ethanol were identified by examining classical taxonomic characters including morphological, skeletal and spicule features. The sponge specimens have been lodged in the collections of the Western Australian Museum.

Sponge biomass

Sponges were present in all but two of the epibenthic sleds in the 40 m and 100 m soft sediment habitats. In other sleds targeting soft bottom habitats at both those depths small amounts of sponges < 6 g per m^2 were collected. The two sleds which targeted soft bottom habitat in 150 m recovered 12 – 53 g of sponges per m^2. On hard bottom habitats between 30 and 75 m, sponge biomass was high but variable (53 – 850 g per m^2) and comprised 80 – 97 % of all faunal biomass sampled (Table 3.40).

Photosynthetic cyanobacteria epifluorescence

Of the 48 sponges examined, 25 or 52.1 % showed evidence of symbiotic cyanobacteria (Table 3.41).

Levels of symbiotic cyanobacteria were found to vary with depth. Those sponges that showed high levels of epifluorescence occurred only in 40 and 50 m depths. More than half the sponges at 75 m depth had medium levels of epifluorescence and only 2 or 22% showed no epifluorescence. At 150 m only 4 or 23% of sponges showed epifluorescence and these were at low levels (Table 3.41).

All cyanobacterial symbionts were coccoid, and varied in size. The symbionts of *Clathria* (*Thalysias)* cf *styloprothesis* were less than 1 μm and appeared to be wrapped around the sponge fibres (Figure 3.191). The symbionts of *Sarcotragus* and *Spongia* sp. (Figure 3.192) were relatively large (around 3 μm) coccoid cells typical of *Prochloron* and *Synechocystis*.

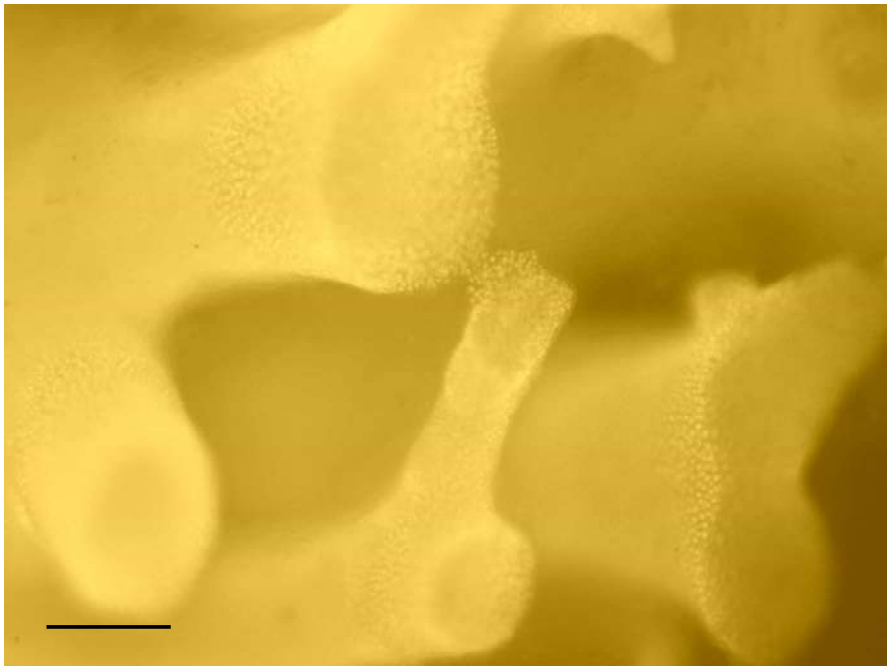

Figure 3.191. Cyanobacterial symbiont in *Clathria (Thalysias)* cf *styloprothesis* from 50 m. Scale bar = 10 μm.

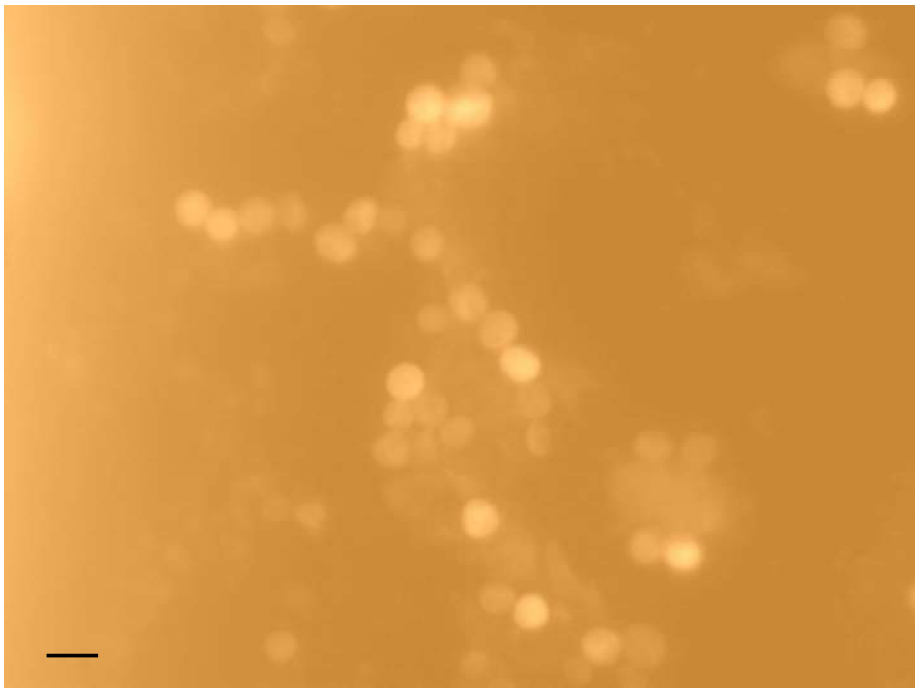

Figure 3.192. Cyanobacterial symbiont in *Spongia* sp. from 50 m, 97.8 % identical 16S rDNA sequence to a *Synechocystis* from an ascidian. Scale bar = 5 µm.

Sequencing of cyanobacterial symbionts

Multiple bands were observed in the DGGE of cyanobacterial PCR product from three sponges, *Tedania* (*Trachytedania*) sp., *Clathria* (*Thalysias*) cf *styloprothesis*, and *Spongia* sp. One band in each sample had much higher staining intensity and was selected for sequencing. High quality cyanobacterial sequences could only be obtained for four sponge specimens, one at 40 m and three from 50 m, which contained high levels of cyanobacterial autofluorescence. These sponges were *Tedania* (*Trachytedania*) sp. which hosted *Synechococcus* sp., *Sarcotragus* which hosted *Synechocystis* sp., *Clathria* (*Thalysias*) cf *styloprothesis* which hosted *Synechococcus* sp., and *Spongia* sp., which hosted *Synechocystis* sp. (Table 3.42).

The closest similarities were 98.7 % between the symbionts of *Clathria* (*Thalysias*) cf *styloprothesis* and *Tedania* (*Trachytedania*) sp. A Blast search and EMBL-EBI alignment shows that the symbionts of *Sarcotragus* and *Spongia* sp. were 96.6 % identical to a *Synechocystis* symbiont sequenced from *Lendenfeldia chondrodes* in Palau (Genbank accession number AY845229, Ridley et al. 2005) and 97.8 % identical to a *Synechocystis* sequenced from an ascidian from Japan (Genbank accession number DQ357958, Muenchhoff et al. 2007). The symbionts of *Clathria* (*Thalysias*) cf *styloprothesis* (collected at 50 m) and *Tedania* (*Trachytedania*) sp (collected at 40 m) had sequence identities up to 99.9 % with free living *Synechococcus* species.

Genbank accession numbers are HQ540322 (*Spongia* sp.), HQ540323 (*Clathria* (*Thalysias*) cf *styloprothesis*), HQ540324 (*Tedania* (*Trachytedania*) sp.) and HQ540325 (*Sarcotragus*).

Table 3.40. Biomass of sponges in g wet weight per m^2 and as a percentage of the total animal biomass sampled at different depth stations targeting both hard and soft bottom habitats.

	30m (hard)	40m (hard)	40m (soft)	50m (hard)	75m (hard)	100m (soft)	150m (soft)
replicate 1	66.6 (93.4%)	55.4 (80.5%)	0.003 (3.3%)	53.0 (96.9%)	70.9 (74.8%)	0.0 (0%)	52.9 (81.5%)
replicate 2	64.3 (80.3%)	-	0.0 (0%)	850.0 (92.5%)	-	6.2 (80.9%)	12.2 (52.7%)
replicate 3	-	-	0.001 (0.9%)	-	-	-	-

Table 3.41. Levels of photosynthetic symbionts in sponges from different depth zones based on epifluorescent microscopy.

Photosynthetic symbionts	40-50m sled	75m sled	150m sled
High Levels	4	0	0
Medium Levels	6	5	0
Low Levels	4	2	4
None	8	2	13
Total Sponges	22	9	17

Table 3.42. Sponge species, depth sampled, associated level of epifluorescence and results of sequencing.

Sponge Identification	WA Museum No.	Depth (m)	Relative Fluorescence	Sequencing result	Comments	GenBank number
Sarcotragus ML1	Z36311	50	High	*Synechocystis sp.*	Prochloron like	HQ540325
Spongia (Spongia) J1	Z36312	50?	High	*Synechocystis sp.*	Prochloron like	HQ540322
Clathria (Thalysias) cf *styloprothesis*	Z36315	50	High	*Synechococcus sp.*	Large single cells	HQ540323
Tedania (Trachytedania) ML1	Z36302	40	Medium/High	*Synechococcus sp.*	Coccoid	HQ540324
Clathria (Thalysias) ML1	Z36303	50	High	*Synechococcus sp.*	Coccoid	
Callyspongia (Callyspongia) bilamellata	Z36306	75	Medium/High	unsuccessful		
Monanchora SS1	Z36307	40	Medium/High	unsuccessful		
Amphimedon SS1	Z36308	75	Medium	unsuccessful		
Axinella SS10	Z36305	75	Medium	unsuccessful		
Crella (Pytheas) ML1	Z36316	40	Medium	unsuccessful		
Fibulia SS1	Z36304	40	Medium	unsuccessful		
Geodia Ng1	Z36310	75	Medium	unsuccessful		
Jaspis SS1	Z36313	50	Medium	unsuccessful		
Asteropus SS2	Z36309	75	Medium/Low	unsuccessful		
Spheciospongia cf. *papillose*	Z36314	50	Medium/Low	unsuccessful		

We found a high proportion of photosynthetic sponges at depths of up to 75m and low levels at 150m depth. These data are the first record of photosynthetic cyanobacteria in temperate sponges beyond the shallow depths sampled by Roberts et al. (1999) (10-20 m) and Lemloh et al. (2009) (8 m). As expected, there are very few, perhaps no, photosynthetic symbioses at 150 m. However, above this depth it appears that these symbioses are viable and relatively common. These results verify that the domain of photosynthetic sponges is not just tropical or hyperphotic shallow water temperate environments where they compete for space with other plant and animal autotrophs. Photosynthetic sponges are important where sponges are the dominant epibenthic organisms by biomass and seabed coverage; that is, hard substrate mesophotic environments.

We found sponges dominated the biomass of both soft and hard bottom habitats between depths of 30 and 150 m. The highest biomass recorded was 850 g wet weight per m^2. Other more comprehensive surveys of marine benthos in this region have made the same findings about dominance of sponges in these depths. In a recent survey in south -western Australia where 172 stations were sampled by epibenthic sled along 2050 kilometres of the western continental margin at depths of 85 to 1584 m, sponges dominated the collection by biomass, comprising 86% of the total catch (wet weight) (McEnnulty et al. in press). In north-western Australia Heyward et al. (2010) found high species diversity and biomass of sponges in depths of 18 to 102 m. In eastern Australia, Roberts and Davis (1996) surveyed depths of 20, 30 and 50 m and found sponge cover typically of 32, 10 and 12 % respectively at these depths, but diversity was highest at 50m. However, high biomass deepwater sponge beds are not confined to Australia. Reed and Pomponi (1997) and Maldonado and Young (1996) found significant sponge species richness and abundance at 150 to 200 m depth off the Bahamas. Deep water sponges are well known to occur in parts of the Mediterranean (e.g. Ilan et al. 1994) and van Soest (1993) found diverse sponge populations to depths of 100 m off Mauritania in northern Africa. Despite the importance of sponges to the benthic biota of mesophotic shelf assemblages world wide (e.g. Olsen and Kellog, 2010) there have been no other studies to determine the presence or importance of photosynthetic sponges in these habitats.

We found that many sponges contained symbionts at low or medium levels. This observation was reported previously by Lemloh et al. (2009), but we do not know the nature of these symbioses, which could be mutualistic, commensal or food items. Denaturing Gradient Gel Electrophoresis in this study indicates that some of the sponges harboured multiple cyanobacterial species, and although efforts were made to reduce contamination, some of these may have been food items. Fluorescence microscopy observations support the presence of one symbiotic genus in each sponge. Sponges containing cyanobacterial symbionts typically have only one species, however, occasionally two or more species are observed (Usher 2008).

It is interesting that sequence similarities were found for the symbionts of *Sarcotragus* and *Spongia* sp., both collected at 50 m, with the *Synechocystis* symbionts of *Lendenfeldia chondrodes* in Palau (Ridley et al. 2005) (96.6 % identity) and to a *Synechocystis* sequenced from an ascidian (Muenchhoff et al. 2007) (97.8 % identical). Ridley et al. (2005) reported that the symbionts were found throughout the matrix of *Lendenfeldia chondrodes*, suggesting that they are capable of photosynthesising in low light, or are providing other benefits to the sponge host. The *Sarcotragus* and *Spongia* sp. symbionts from our study were 97.4 % identical to each other. Cyanobacteria have an extremely flexible system of photosynthetic enzymes consisting of phycobiliproteins and chlorophyll, which are more efficient at harvesting light at depth than are plant and algal photosystems (Usher 2008). Cyanobacteria are able to survive at depths receiving only 1 % of surface irradiance (Furnas and Crosbie 1999), so it is perhaps not surprising that cyanobacterial symbionts are common in sponges at 50 m. Lemloh et al. (2009) also reported *Synechocystis* symbionts in sponges, suggesting that they are relatively common sponge symbionts, at least in temperate Australia.

Although the genus *Oscillatoria* represents one of the major lineages of cyanobacterial symbionts of sponges (Usher 2008), these were not observed by fluorescence microscopy or sequenced in this

study. Some species of *Oscillatoria* are known to fix nitrogen, and so might be expected to dominate sponge symbioses at depths where the rates of photosynthesis, and therefore oxygen levels, are lower. Olsen and Kellog (2010) suggested that in mesophotic environments nitrogen fixation by cyanobacterial symbionts may be a more important contribution to sponges than the benefits of photosynthesis, that is, carbon fixation and energy donation.

The symbionts of *Clathria* (*Thalysias*) cf *styloprothesis* (collected at 50 m) and *Tedania* (*Trachytedania*) sp (collected at 40 m) were 98.7 % identical to each other, and had sequence identities up to 99.9 % with free living *Synechococcus* species. The symbionts of *Clathria* (*Thalysias)* cf *styloprothesis* appeared to be wrapped around the sponge fibres in a similar way to the rhodophyte symbionts of sponges reported by Lemloh et al. (2009).

Early research on photosynthetic cyanosponges occurred in tropical oligotrophic environments and conclusions were drawn about their potential importance, based on the comparatively better studied associations between scleractinian corals and zooxanthellae. For example, in north-eastern Australia, Wilkinson (1987) found a gradient of photosynthetic sponges which decreased from high rates (ca. 60 %) far off shore in the oligotrophic waters of the Coral Sea to lower levels (ca. 10 %) in the nearshore turbid, nutrient rich waters where sponges are an important component of the fauna of the fringing reefs of continental islands. Wilkinson (1987) contrasted these patterns to the predominantly heterotrophic sponges in the higher nutrient waters of the Caribbean. More recent research suggests cyanosponges make up a considerable proportion of sponges in temperate areas where they have been studied such as south eastern (Roberts et al. 1999) and south-western Australia (Lemloh et al. 2009). Nevertheless, the conclusion that these associations are likely to be important in oligotrophic water remains a sound hypothesis and one that can apply equally to temperate regions.

The western continental margin of Australia is subject to the dominant influence of the Leeuwin Current, the only poleward flowing eastern boundary current in the world. The Leeuwin Current brings warm low nutrient, low salinity tropical water along the continental shelf. The region has very low levels of nutrients and pelagic production (Lourey et al. 2006). Despite this, productive benthic ecosystems thrive and a nutrient budget developed for the south-western Australian continental shelf (Feng and Wild-Allen 2010) found that more than 80% of primary production on the shelf relied on recycled nitrogen, with less than 10% provided from new nitrogen as a result of wind driven upwelling or vertical mixing from eddies. These authors concluded that a recycled flux of 6.2 g N m^{-2} $year^{-1}$ was required to balance the nitrogen budget. Hitherto, the main source of recycled nitrogen on the shelf in this region has been thought to be sediments (e.g. Lourey and Kirkman 2009; Greenwood 2010), however, nitrogen excretion by sponges including remineralisation and nitrification by symbiotic cyanobacteria in sponges may be another important source of recycled nitrogen. The high abundance and biomass of sponges in south-western Australia (McEnnulty et al., in press, this study) may provide an important source of recycled nitrogen on the continental shelf. Nitrogen (as DIN) excretion rates in tropical sponges are high but variable. Diaz and Ward (1997) measured rates of 30 – 2 666 nmol N g^{-1} (dry wt) $hour^{-1}$ in four species of sponges in the Caribbean. Also in the Caribbean, Corredor et al. (1988) found rates of nitrogen excretion of (600 nmol N g^{-1} (dry wt) $hour^{-1}$) in *Chondrilla nucula*. For temperate sponges there are fewer data, however, Jimenez and Ribes (2007) found similar rates (180–780 nmol N g^{-1} (dry wt) $hour^{-1}$) in several species in the Mediterranean. Jimenez and Ribes (2007) estimated from their data that sponges which covered 7 to 22 % of the bottom were responsible for nitrogen fluxes of 2.5 to 7.9 μmol N m^{-2} d^{-1} or just 0.01 to 0.04 gN m^{-2} $year^{-1}$. However nitrogen excretion rates (of ammonium) measured in two species of sponges (*Aplysina* sp, and *Iotrochota baculifera*) in our study region of south-western Australia by Hatcher (1994) are higher, between 0.52 and 0.69 μmol g^{-1} (dry wt) $hour^{-1}$. When converted to wet weight based on the data shown in Hatcher (1994) and applied to our survey results of between 53 and 850g wet weight of sponges per m^2, this gives a possible nitrogen flux for sponges of 0.7 and 69.9 gN m^2 $year^{-1}$. At the upper ranges of these figures this would contribute significantly to the recycled nitrogen flux of 6.2 gN m^2 $year^{-1}$ required to balance the nutrient budget calculated for the shelf in this region (Feng and Wild-Allen 2010). This range of potential rates of nitrogen excretion needs to be

confirmed and refined by a dedicated study but is also supported by Lourey and Kirkman (2009) who calculated a nitrogen flux rate of 10.9 gN m^2 $year^{-1}$ attributable to remineralisation of organic carbon and nitrification within the marine benthos (including sediments) in south-western Australia. DIN fluxes from sediments in south-western Australia are characterised by pulses of high flux rates during weather conditions which generate large waves (Lourey and Kirkman, 2009). This source (and signal) of DIN is rapidly assimilated by pelagic phytoplankton and its signal disappears rapidly as a result. Sponges on the other hand filter continuously, potentially providing a constant source of recycled nitrogen. Indeed, the importance of sponges as a potential source of recycled nitrogen off south-western Australia was recognised by Lourey and Kirkman (2009) who suggested that spatial separation of sponges and benthic primary producers could result in an accumulation of nitrate. Such a situation exists in the deeper, mesophotic waters of south-western Australia where extensive areas of high biomass of sponges in deepwater exists (McEnnulty in press, this study).

On the basis of this study we advance the hypothesis that photosynthetic cyanobacteria-sponge associations have facilitated the high success of sponges in dominating the mesophotic oligotrophic waters of south-western Australia and that these in turn have enabled the high levels of benthic primary production to occur, facilitated by tight recycling of nitrogen on the shelf. Based on published levels of DIN production by sponges and our studies of sponge biomass off SW Australia we contend that it is highly likely that sponges contribute a significant proportion of the new nitrogen deficit required to balance nutrient budgets calculated for the south west of Australia by Feng and Wild Allen (2010).

Key Findings:
This study presents the first record of photosynthetic sponges (sponges having a symbiotic relationship with photosynthetic cyanobacteria) from deepwater temperate habitats. Sponges with high levels of photosynthetic cyanobacteria occurred at depths of up to 50m, medium levels to 75m and low levels at 150m. The proportion of sponges that showed no epifluorescence increased greatly with depth.

Cyanobacterial symbionts sequenced from sponges at 40 m and 50 m belonged to the genera *Synechococcus* and *Synechocystis*. These results verify that the domain of photosynthetic sponges is not just tropical or shallow water temperate environments. Sponges made up the highest biomass of biota across all the sites we sampled from depths of 30-150 m and we hypothesise that sponges play a critical role in pelago-benthic coupling and nutrient recycling. These important ecosystem functions have been demonstrated to be necessary to balance nutrient budgets and explain the productivity of the south-western Australian continental shelf benthic ecosystem.

3.3.8 Modelling of bentho-pelagic coupling

The amount of surface incident sunlight that reaches the seafloor is critical in determining benthic production. Since water molecules restrict the downward propagation of light, illumination of the seafloor is, in part, simply determined by the height of the water-column. However, the disappearance of light with water depth also varies with the concentration of various organic and inorganic substances in the water. Phytoplankton chlorophyll is particularly important in this respect because it is directly related to the phytoplankton biomass, meaning that an increase in phytoplankton production can severely restrict benthic production rates by shading the seafloor (Lavery et al. 1991; Kavanaugh, et al. 2009). Consequently, increased phytoplankton production may lead to a shift in dominance from benthic plants to phytoplankton, reduce the overall productivity and change the ecology of coastal ecosystems. Such changes in the balance between pelagic and benthic biomass can lead to long-term changes in ecosystem function, or phase shifts. An understanding of the threshold

levels for transition from one state to another is necessary in order to establish target levels for important environmental parameters such as water quality, or in order to establish conditions required to restore seagrass beds.

The seawater that covers the Western Australian continental shelf is remarkably clear because of very low concentrations of dissolved nitrogen (and therefore low phytoplankton chlorophyll concentrations), and low levels of coloured organic matter because of limited river discharge. This allows sufficient light to reach the seafloor to support benthic plant production well beyond 50m water depth. However, long term observations at the Rottnest station show a gradual increase in nitrate concentration raising concern that this may fuel an increase in pelagic algal production, reducing the light reaching the seabed, and upsetting the present balance between pelagic and benthic production. The impact of nutrient enrichment on the biogeochemical functioning of the WA shallow-water marine system is not clearly understood. The problem is complicated by spatial differences in substrate and benthic community composition.

For shallow water-columns that overlay soft sediment, the sediment nitrogen biogeochemistry has a large effect on the pelagic nitrogen dynamics. In particular, accumulation and release of nitrogen from the sediment can result in seasonal or inter-annual imbalances in the pelagic-benthic nitrogen budget. This can potentially slow down response to nutrient enrichment (or nutrient reduction) in the water-column (Soetaert & Middelburg, 2009). Sediments may also act as a nitrogen sink via either the burial of refractory organic material or as a result of microbial de-nitrification.

The situation is different when the seafloor substrate is predominantly hard as in the case of limestone reef. This type of seafloor boundary is not considered to possess the ‘buffering’ properties of soft sediment mentioned previously. Even so, benthic filter-feeders that reside on the reef can affect the pelagic nitrogen dynamics by removal of particulate nitrogen and release of dissolved nitrogen at the base of the water-column (Prins et al 1998, Jimenez and Ribes 2007).

The work presented in this section uses a one-dimensional coupled pelagic-benthic model to estimate the impact of water depth, benthic photosynthetic efficiency, seabed substrate and benthic filter-feeding on the balance between benthic and pelagic plant production. The model is used to help understand the impact of nutrient enrichment in a well mixed water column on the biogeochemical functioning of a coupled pelagic-benthic marine system.

Model description

The model couples water-column physics with nitrogen-based pelagic and benthic biogeochemistry. Pelagic and benthic algal production is parameterised as a saturating function of light (I) and dissolved inorganic nitrogen (DIN). Surface incident sunlight (available for photosynthesis) (I_0) and vertical diffusivity are constant in time. Vertical diffusivity is also constant with depth to imitate a well-mixed water-column. Light (I) attenuates as a function of depth (z, negative downwards) and phytoplankton chlorophyll concentration (Chl) according to equation:

$$I_z = I_0 e^{(kw+kp.Chl).z} \quad (1)$$

where kw and kp are the coefficients for the attenuation of light due to water molecules and phytoplankton chlorophyll respectively and are set to 0.04 m^{-1} and 0.025 $(mg\ Chl)^{-1}\ m^{-2}$ (Kirk, 1983). The chlorophyll to nitrogen ratio is assumed to be constant. Phytoplankton sink in the model at a rate of 1.0 m d^{-1} and detrital nitrogen sinks at a rate of 10 m d^{-1}. To represent the soft (sand) seabed type, the pelagic model is coupled to a vertically integrated one-dimensional sediment model. The hard (reef) seabed type is represented by a ‘no flux’ condition at the lower model-boundary (i.e. no sediment model is included). Filter-feeders, when included, are formulated as an additional lower

boundary condition that transfers phytoplankton nitrogen in the bottom pelagic layer to either sediment nitrogen in the soft seabed case, or to pelagic DIN in the hard seabed case.

A single model result is obtained by running the model forward in time from its initial condition until a dynamic equilibrium is reached. Each model parameterisation described below is run 20 times across a range of initial water-column DIN concentrations to record how each model configuration responds to nutrient enrichment. Three sets of experiments are conducted with the model. In the first set, the soft and hard seabed conditions are compared for 27 different parameterisations of the benthic algal production equation by altering the shape of the light response (i.e. 'P versus I') curve (Figure 3.193). In the second set of experiments the addition of a benthic filter-feeding formulation to the hard and soft seabed conditions is tested at four different filtering rates. In the final set of model experiments, the model is run at 5 different water depths between 20 and 100m. The parameterisation of the pelagic model is the same for all model runs.

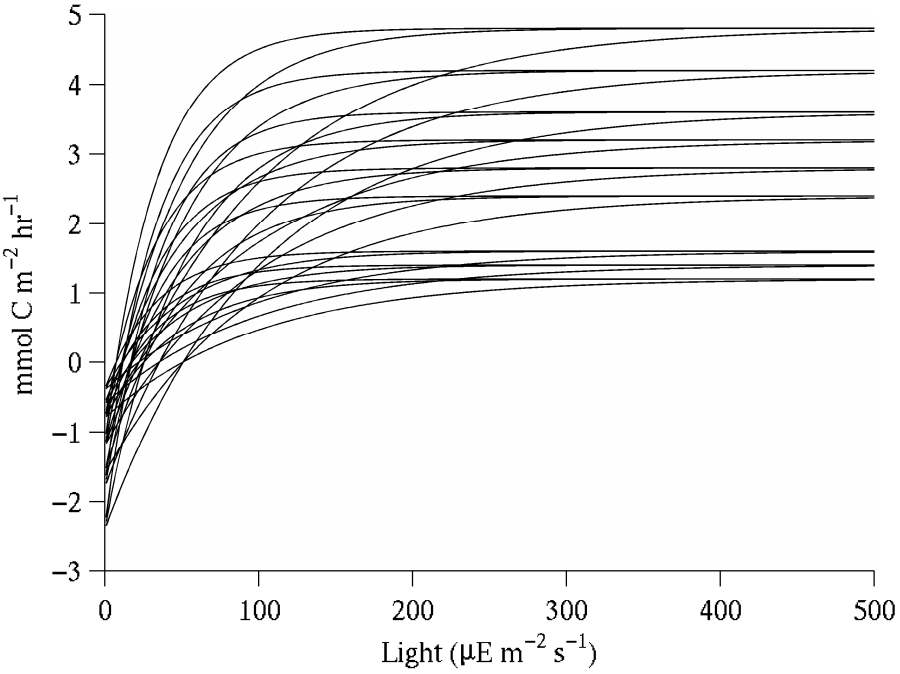

Figure 3.193.The 27 P versus I curves tested in experiment 1. The curve is described by $P=P_{max}(1-e^{-\alpha I} - R)$, where P_{max}, α and R are constants. Values of P_{max} range from 2.08-6.25 hr^{-1}; values of α range from 0.01-0.03 (µmol m^{-2} $s^{-1})^{-1}$; values of R range from 0.1-0.3.

For each different model parameterisation the benthic and pelagic production rate is plotted against the mean water-column DIN concentration recorded when the model reaches equilibrium. The model results highlight a number of important factors that directly affect the resilience of benthic primary producers to water column eutrophication.

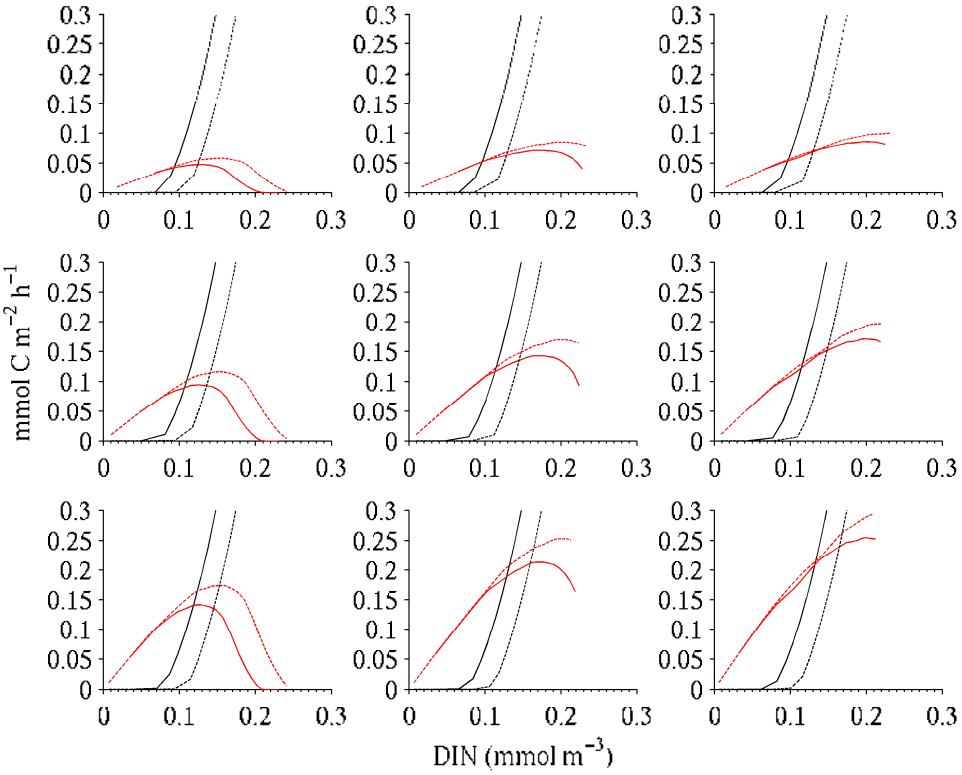

Figure 3.194. Result of model experiment no 1. Pelagic production is shown in black and benthic production is shown in red. Solid lines are used to show result obtained using the 'hard' seabed model configuration, and dashed lines for the 'soft' seabed model configuration. Each panel shows the result obtained for different parameterisations of the P versus I curve used to describe benthic production. α varies by column with values of 0.01 (left), 0.02 (middle) and 0.03 (right). P_{max} varies with row with values of 2 (top), 4 (middle) and 6 (bottom). R is the same in all panels and the value is 0.2.

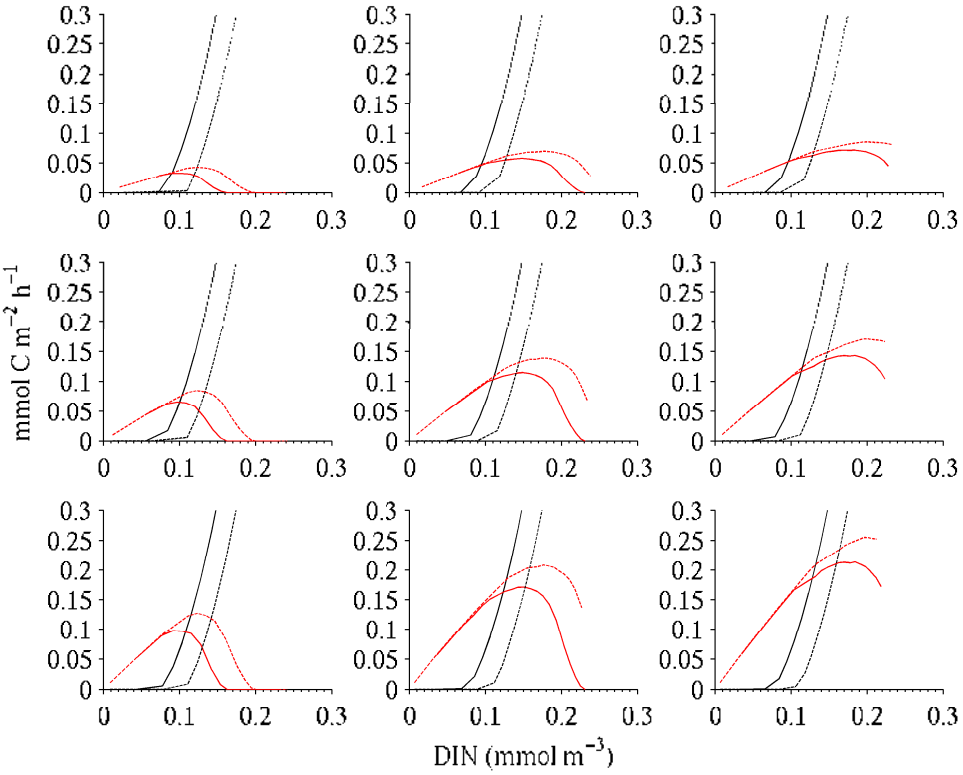

Figure 3.195. Results of model experiment no 1. In this set of results the value of R is 0.3. The value of α and P_{max} for each panel, and the line colours and styles, are the same as identified in Figure 3.194.

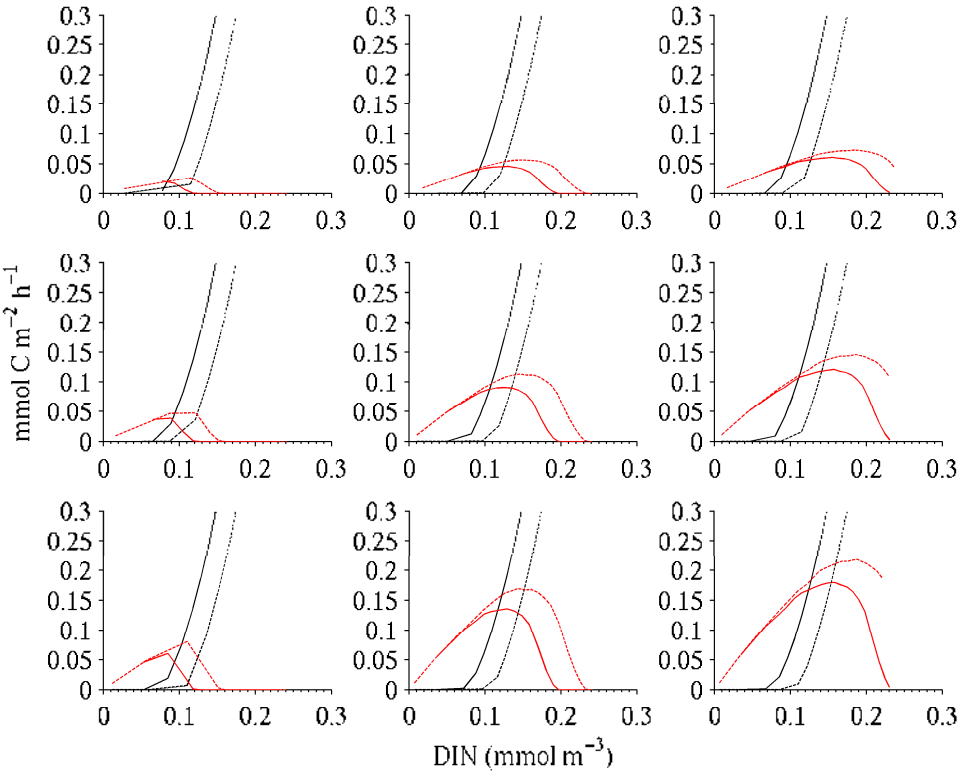

Figure 3.196. Results of model experiment no 1. In this set of results the value of R is 0.4. The value of α and P_{max} for each panel, and the line colours and styles, are the same as identified in Figure 3.194.

Results from the first set of model experiments (Figure 3.194 - Figure 3.196) show two important features. Firstly, comparison of model results obtained with soft and hard substrate parameterisations of the seabed, demonstrate that the presence of a soft seabed (sediment) makes the benthic system more resilient to nitrogen enrichment. Evidence of this is seen in the higher DIN values that are reached at the intersection of the pelagic and benthic production curves for the soft sediment case (Figure 3.194 - Figure 3.196). This finding is consistent with previous work on the role of soft sediments in 'buffering' the effects of nutrient addition to shallow water ecosystems (Soetaert and Middleburg, 2009). Secondly, Benthic algae with greater photosynthetic efficiency (α) and maximum photosynthetic rate (P_{max}) are more resilient to eutrophication. Again, evidence of this is seen in the shift of the intersection between pelagic and benthic production curves toward higher DIN concentrations as the growth parameters Pmax and α are increased in value (Figure 3.194 - Figure 3.196).

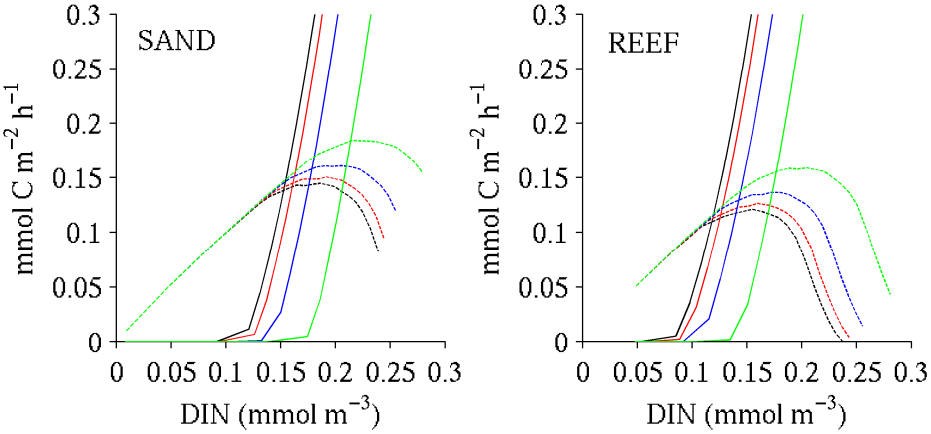

Figure 3.197. Result of model experiment no. 2. Pelagic production is shown with solid lines and benthic production is shown with dashed lines. The result obtained using 4 different filtering rates 10 (black), 20 (red), 40 (blue) and 80 (green) L m^{-2} hr^{-1} are shown. Benthic filtering delays pelagic dominance as the nutrient concentration increases.

Results from the second set of experiments (Figure 3.197) show that benthic filtering 'protects' benthic algae from the detrimental effects of eutrophication. As filtering rate increases the DIN concentration where the pelagic and benthic curves intersect also increases (Figure 3.197). This suggests that greater DIN concentrations can be tolerated by an ecosystem that includes benthic filter feeders, before the pelagic algae start to dominate, than one that does not. This is generally consistent with observations made elsewhere in the world that suggest benthic filter-feeders play an important role in controlling phytoplankton blooms (Peterson et al. 2006).

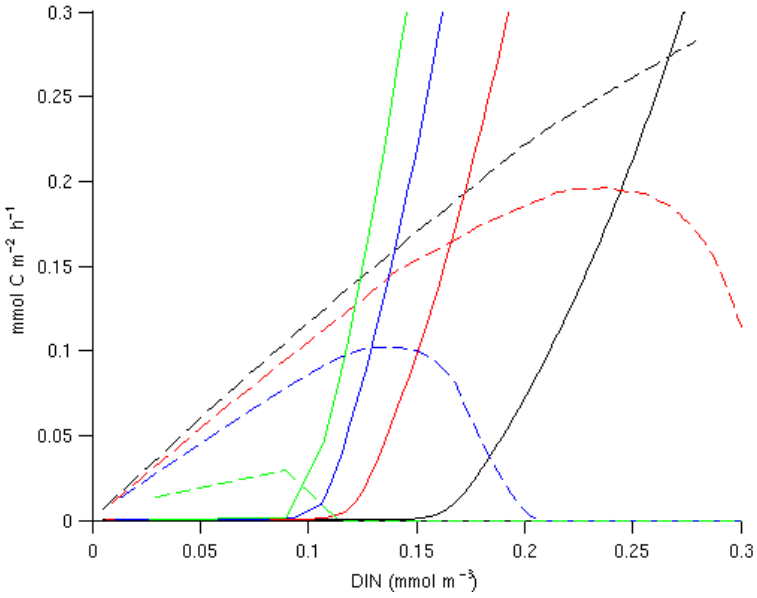

Figure 3.198. Result of experiment no. 3. Solid lines are used to show pelagic production and dashed lines to show benthic production. Colours are used to show the result obtained at different water column depths; black 10 m, red 25 m, blue 50 m, and green 75 m.

Finally, results from the third set of experiments (Figure 3.198) confirm the importance of water depth. The deeper the water the more susceptible the benthic algae are to eutrophication. Evidence of this is seen in the modelled decline (and eventual extinction) of benthic production at increasingly lower DIN concentrations (Figure 3.198). This puts the benthic plant communities living on the

outer-shelf at greatest risk and emphasises the importance of being able to adequately model and predict bottom irradiance. This is dealt with in the section below.

Key Findings:

The model highlights the following important features of benthiopelagic coupling in the system:

The presence of a soft seabed (sediment) makes the benthic system more resilient to nitrogen enrichment

Benthic algae with greater photosynthetic efficiency (α) and maximum photosynthetic rate (P_{max}) are more resilient to eutrophication.

Benthic filtering provides some resistance to benthic algae from the detrimental effects of eutrophication.

The deeper the water the more susceptible the benthic algae are to eutrophication.

3.3.9 Modelling of light (irradiance) at the sea bed

Correctly estimating the irradiance at the sea bed is critical for the modelling or prediction of benthic primary production. Irradiance at the seabed can be relatively easily estimated for pure water as an exponential function of depth. In natural ecosystems, however, it deviates significantly from this relationship for a variety of reasons that are much more difficult to quantify. Only with a detailed examination of a range of factors such as particle load and the nature of the particles can the attenuation coefficient be estimated from first principles. It is known that the attenuation coefficient is significantly greater near shore than offshore and the use of a single value for the coastal domain will result in a considerable error in estimating irradiance at the seabed. Therefore a simple model that allows estimation of the attenuation coefficient from a limited number of easy to obtain parameters would be of benefit to anyone trying to predict benthic or pelagic primary production. This short section describes such a simple model that only requires knowledge of the depth.

From the SS 04/2007 cruise there were a total of 13 vertical profiles of irradiance versus depth were obtained during the near shore work of leg one in Perth coastal waters of the voyage. A few high quality profiles (no shadow from the ship, no cloud cover, during daylight) were selected for detailed analysis. For example, at a location in ~ 100 m deep the irradiance declined exponentially with depth (**Figure 3.199**) or a straight line relationship when replotted as a function of natural logarithm of irradiance. This exponential decline suggests the deviations from classic Beers-Lambert theory are relatively small in Perth's coastal water (Kirk 1994). From these data it is possible to calculate the attenuation coefficient for Perth coastal waters from Kirk (1994) as:

$$I_{dz}=I_0*\exp(-K_d*z) \quad (2)$$

where I_d is irradiance at depth z, I_0 is surface irradiance and K_d is the extinction coefficient.

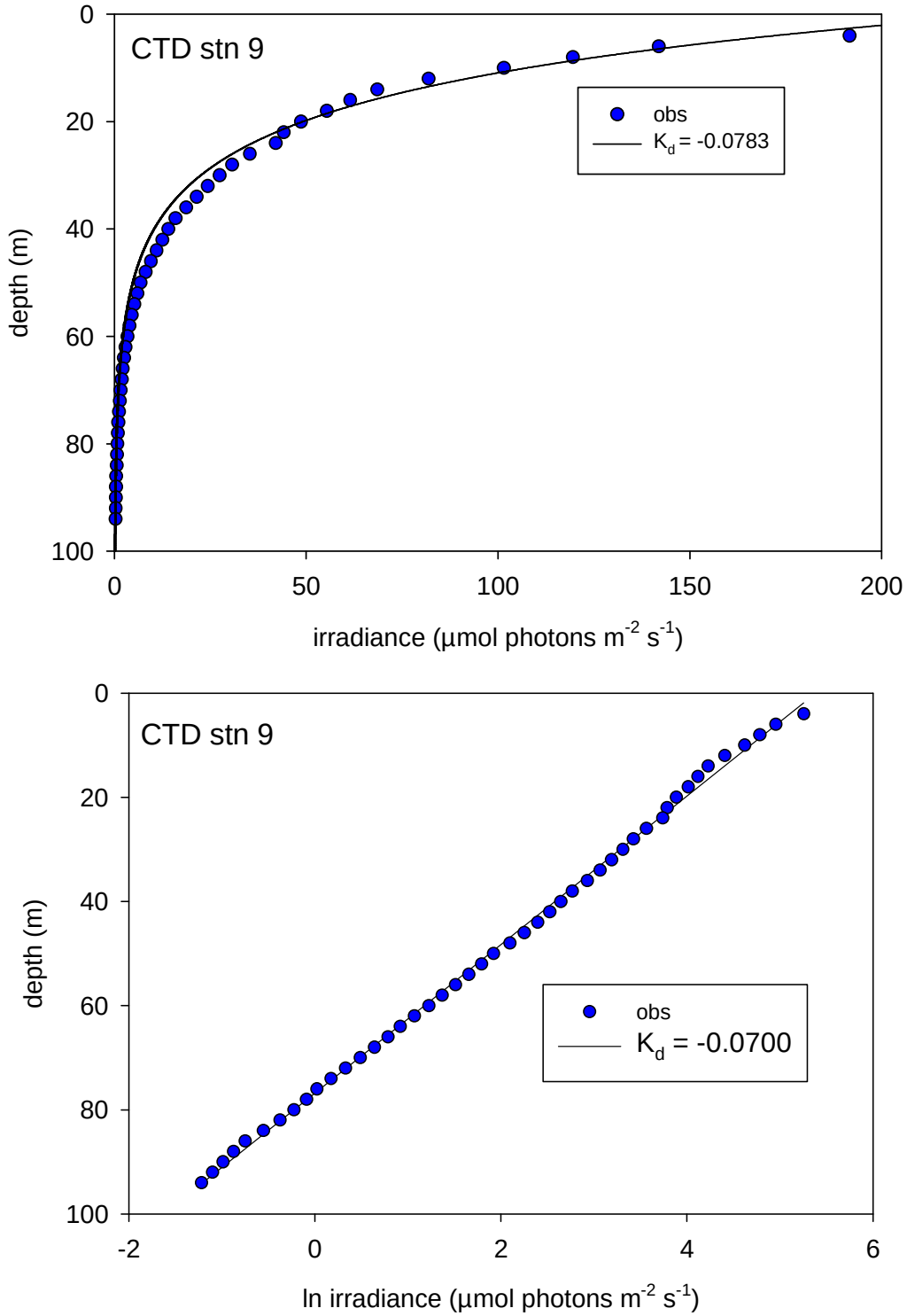

Figure 3.199 Top panel is $I_{dz}=I_0*\exp(-K_d*z)$ where I_d is irradiance at depth z, I_0 is surface irradiance and K_d is the extinction coefficient. The bottom panel is $\ln I_{dz} = -K_d z + \ln I_0$.

Applying this approach to all 4 good profiles (Figure 3.200) showed that attenuation of light through the water column varied from 0.055 m^{-1} to 0.14 m^{-1} (Table 3.43). The factor of 3 variation in K_d represents a serious problem for the estimation of irradiance on the bottom and the capability to predict or model benthic primary production along the West Australian coast.

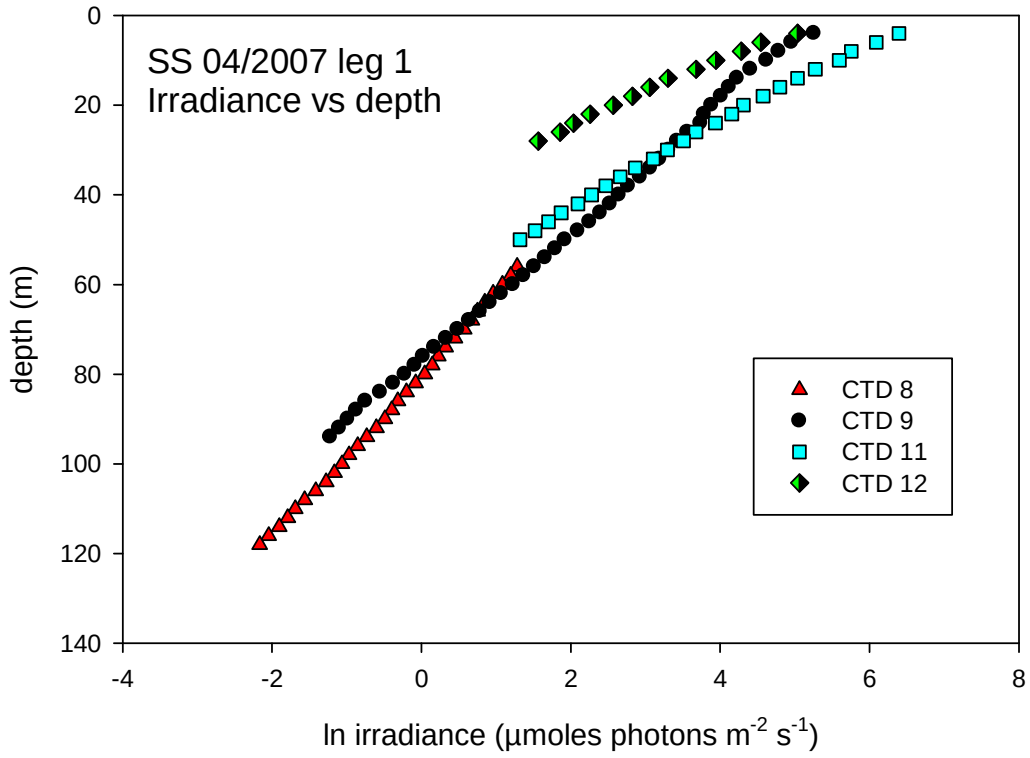

Figure 3.200 Natural logarithm of irradiance as a function of depth for four profiles from the SS 04 voyage in 2007.

Table 3.43 TAttenuation coefficients (K_d) estimated from near shore stations near 32°S durin g the May – June 2007 voyage SS 04/2007.

Cast#	K_d	intercept	r^2	site	approx depth
8	-0.05516	4.420	0.9988	L	150
9	-0.07003	5.381	0.9986	E	100
11	-0.10802	6.596	0.996	C	60
12	-0.14016	5.393	0.9932	A	30

Predicting the attenuation coefficient in shallow (> 200m) water depths in Perth Coastal waters.

Previously reported attenuation coefficients for Perth coastal waters range somewhat depending upon location and season (e.g. Thompson and Waite 2003) but in the shallow (~ 10m) waters of Marmion Lagoon averaged about -0.18 m^{-1} (n = 85, Thompson and Waite 2003). Offshore measurements at similar latitudes are much lower, typically ~ 0.05 m^{-1} (n= 56, Thompson et al. 2007). The data from SS04/2007 showed little deviation from a strict logarithmic irradiance to linear depth relationship such as that might be expected due to differential absorption of longer wavelengths which can make absorption in the top few meters greater than it is lower down (Kirk 1977, Kirk 1994). The model fit here (Table 3.4.3) showed depth explaining > 99% of the variance in irradiance with very modest deviations from linearity.

Using these measurements to constrain a relationship between extinction coefficient and depth as measured on the SS04/2007 cruise provided evidence of an exponential relation between bottom

depth and average light attenuation through the water column (Table 3.44, Figure 3.201). This model provides a considerable improvement (~ factor 4) over the use of a single attenuation coefficient for the waters of the continental shelf. Based on known patterns of phytoplankton biomass for the region (Thompson et al. 2009) and some limited data from shallow waters in Sepia Depression (Thompson and Waite 2003) it is likely that most WA shelf waters will have a seasonal component to K_d. This seasonal component should be obtainable from the IMOS enhancements of the coastal monitoring at Rottnest Island once several years of data are available.

Table 3.44 The relationship between seabed depth and average light attenuation coefficient (-)K_d =0.044 + 0.155exp(-0.0163*z) where z = depth with an r^2 value of 0.997.

parameter	Coefficient	Std. Error	Student's t	P
Minimum value K_d	0.044	0.0043	10.2	0.0020
Constant (a)	0.155	0.0067	22.9	0.0002
Slope (b)	0.0163	0.0017	9.59	0.0024

The relationships (e.g. Table 3.44) between surface irradiance and seabed irradiance as a function of seabed depth emerge from a mixture of factors that impact on light attenuation. These include the nonlinear relationship between chlorophyll *a* concentration and distance from shore (Chapter 1). Chlorophyll *a* and other particulates are the most variable factors determining light attenuation in these waters. Under circumstances where light attenuation is not uniform throughout the water column due to differential absorption of specific wavelengths and scattering (e.g. Kirk 1977) or there is spatial or temporal variation in the concentrations of particles that is not consistent with the particulate load observed during SS04/2007 the use of this equation (Table 3.44) may not be accurate.

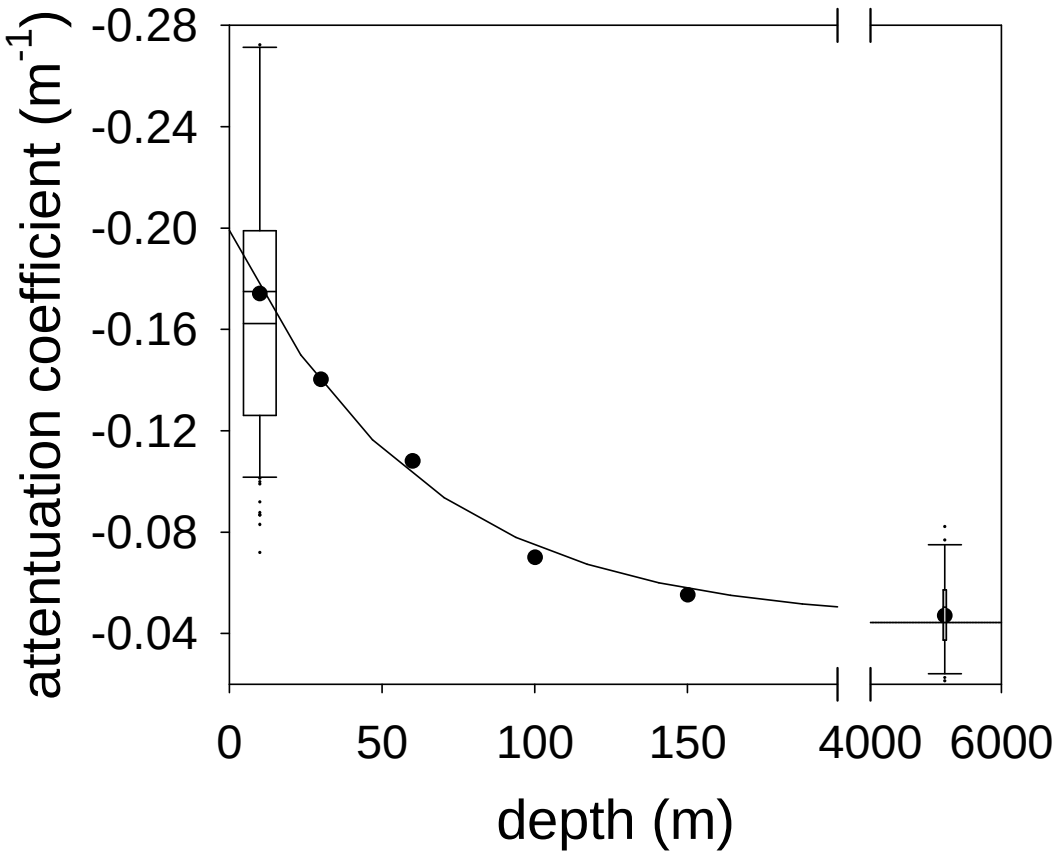

Figure 3.201. A simple model to estimate the average light attenuation as a function of bottom depth for Perth coastal waters.

For the purpose of estimating primary production, especially benthic primary production, from the primary producers quantified during the research voyage SS04/2007 the average irradiance to the ocean surface was determined by the ship borne Biospherical light sensor (Figure 3.202). Results indicated the average daytime high irradiance was ~ 2000 µmoles photons m^{-2} s^{-1} while the average over the voyage was ~ 332 µmoles of photons m^{-2} s^{-1} or about 28.6 moles of photons m^{-2} day^{-1}.

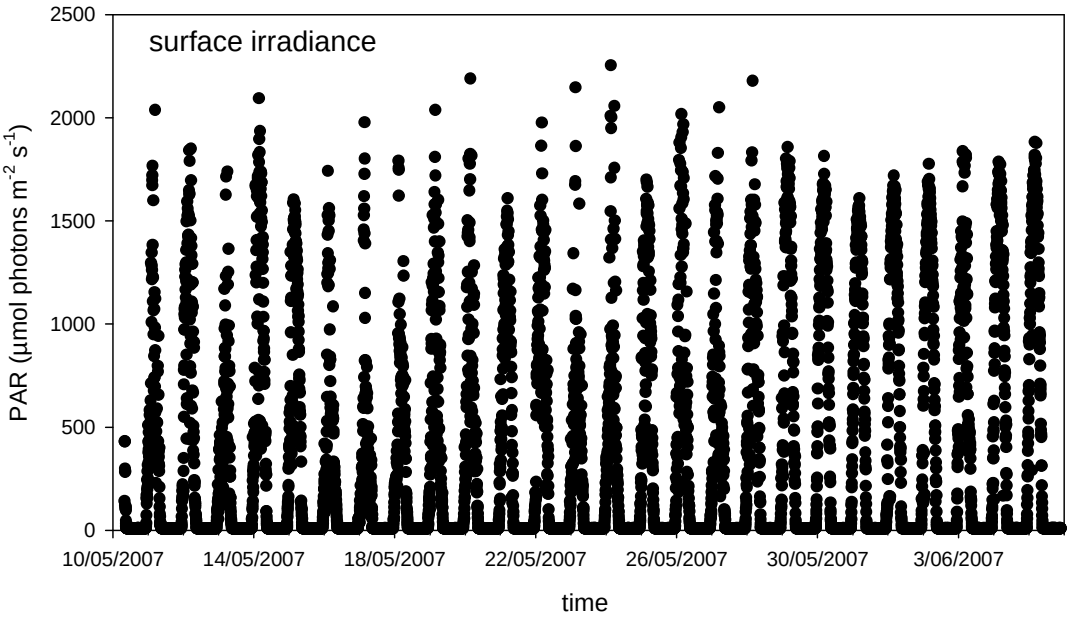

Figure 3.202. Irradiance (5 minute averages) measured at top of the ship's mast during research voyage SS04/2007 with a Biospherical sensor detecting photosynthetically active radiation (400 to 700 nm = PAR).

For the estimate of surface irradiance (insolation) can be measured (as above) or calculated following simple methods outlined below (after Kirk 1994). Incoming irradiance data (Q. = total daily insolation in joules m^{-2} d^{-1}) as measured at Perth Airport can be fitted to a Gaussian curve over an annual cycle. The following relationships (Eqs. 3-6) can be used to calculate surface instantaneous irradiance at any time (t) during any given day: 1) the solar declination can be estimated using the technique of Spencer (1971):

$$\delta = 0.39637 - 22.9133 \cos\Psi + 4.02543 \sin\Psi - 0.3872 \cos 2\Psi + 0.052 \sin 2\Psi \quad (3)$$

where δ = solar declination, and is the date expressed as an angle 360° d/365), where d is the day of the year and converted to daylength (in h) from Kirk (1994):

$$\text{daylength} = 0.133 \cos(-\tan\gamma \tan\delta) \quad (4)$$

where δ is the solar declination (from Eq. 2) and γ is the latitude. The maximum irradiance at solar noon can be calculated from equation (5):

$$E_m = Q_s 2\pi N^{-1} \quad (5)$$

where E_m is the irradiance at solar noon, Q_s is total daily insolation, and N is time in seconds. The irradiance at any given time $E_{(t)}$ is calculated:

$$E_{(t)} = E_m \sin(\pi N^{-1}) \quad (6)$$

where t is time in seconds and other symbols are as above (Kirk 1994). Finally, the instantaneous irradiance can be converted from total energy (all wavelengths) to energy within photosynthetically available radiation (PAR 400-700 nm) using the factor 0.45 from Baker and Frouin (1987) and from joules m^{-2} S^{-1} to µmoles of photons m^{-2} S^{-1} using 2.5 x 10^{18} quanta W^{-1} from Morel and Smith (1974).

Alternatively the irradiance at the surface (isolation) of the ocean can be obtained from a range of remotely sensed observations following methods devised by Frouin et al. (1989) and Frouin and

Chertock (1992). These data can be easily obtained from the Giovanni web site maintained by NASA at http://gdata1.sci.gsfc.nasa.gov/daac-bin/G3/gui.cgi?instance_id=ocean_month.

These satellite data are very useful for extending a limited set of field observations or expanding the geographic range. For example, for the region off Perth the MODIS data from 2002 to 2011 can be used to extend the SS04/2007 data out to a longer time period. Observations from the ship were 28.6 moles of photons m^{-2} d^{-1} well within the MODIS range of 18 to 31 moles of photons m^{-2} d^{-1} for PAR in this region during May 2007 (Figure 3.203).

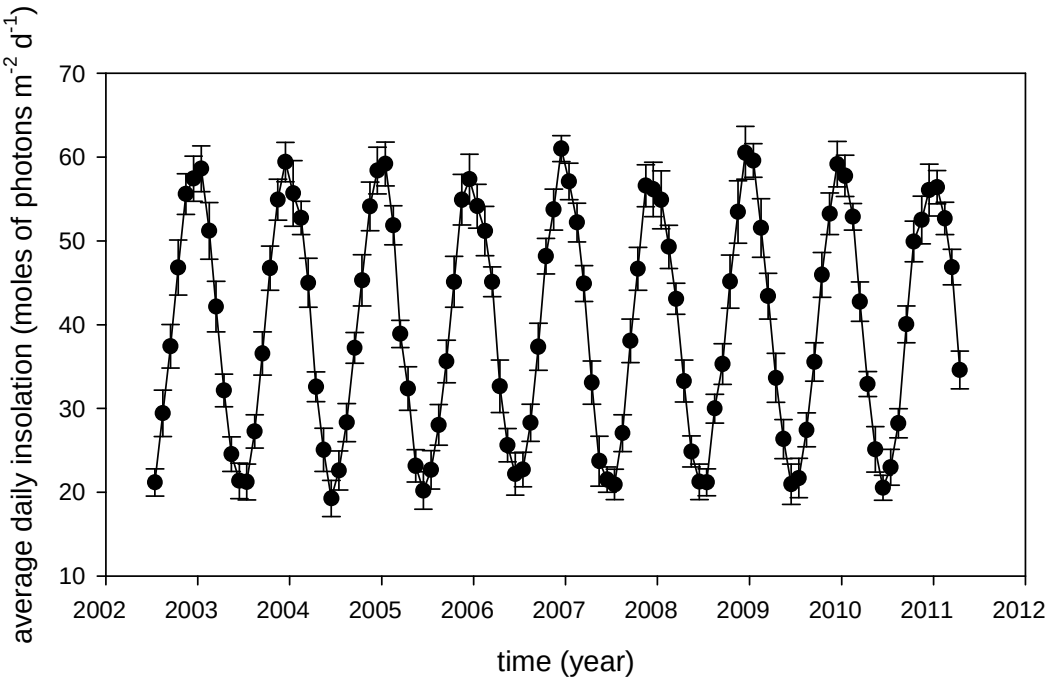

Figure 3.203 Average daily insolation of PAR in the region 28°to 34ºS by 110 to 120ºE obtained from MODIS satellite through the activities of NASA's Science Mission Directorate, and are archived and distributed by the Goddard Earth Sciences (GES) Data and Information Services Center (DISC).

Key Findings:

A simple empirical relationship between the light attenuation coefficient and seabed depth makes it easier to estimate bottom irradiance on the shallow coastal waters off Perth.

3.3.10 Scaling up estimates of biomass distribution and primary production across the continental shelf

This section provides a represention of the distribution and abundance of biomass of animals and plants across the continental shelf off Perth. It has been developed to improve determination of the nitrogen budget for the shelf in the region and to determine the components of the ecosystem at the levels of functional taxa, habitat type and depth zone that are particularly important silos of organic carbon and nitrogen. The latter are particularly relevant as we seek to consider the sources of recycled nitrogen on the shelf and which taxa and habitats are most important in determining the scale of these fluxes.

Methodology

The approach taken was to focus on a section of the continental shelf off metropolitan south western Australia including a section of the Marmion Marine Park where many of our observations have been made and to use our measurements and estimates of habitat type, distribution and abundance and biomass and primary production complemented where necessary with literature values to build a conceptual model of the region overlain with habitat, biomass and productivity estimates in four depth zones. The estimates of primary production were then used to calculate a nutrient budget for the region by revising and scaling down the nutrient budget developed by Feng and Wild-Allen (2010) for the Western Australian coast between Cape Leeuwin and North-West Cape.

Conceptual model domain

The model domain is centred on 23^{o} 45’ and extends eastward from the shore to the 200 m depth contour and 5 km north and south. Thus the model domain is an approximate rectangle 10 km by 67 km (Table 3.45, Figure 3.204) with a total area of 669km^{2}. The bathymetric profile of the region is shown in Figure 3.205. There is a narrow lagoon about 6km wide that extends out to the 20m depth contour, and then a wide gently sloping inner-shelf out to about 50m depth, some 47 km offshore. There is then a steep slope dropping from 50 to 100 m over a distance of just 4.3 km. The bottom then drops away again gently to 200m at 77 km off shore. At this point, the distance between the 100m and 200m isobaths is unusually wide (25.2 km) while on average between Lancelin and Rockingham it is only 15.2 km wide. The model domain for this depth range has been limited to the average distance (15.2 km) to make the model more widely representative of the shelf in this region. The seabed then drops away sharply from 200m, with the 500m depth contour at just 85 km off shore.

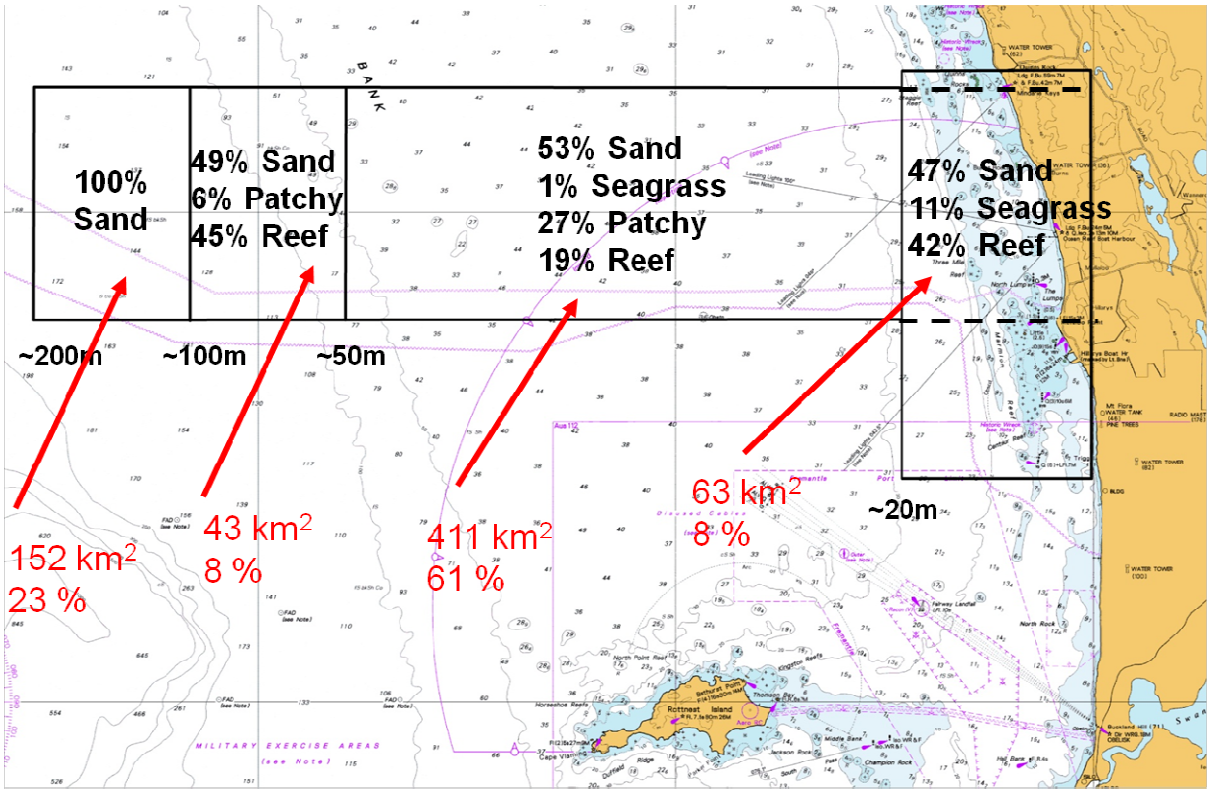

Figure 3.204. Model domain superimposed on AUS754 Navigation Chart (Commonwealth of Australia 2002) showing proportion of habitat types in each of the four depth zones used in the model. The lagoon section referred to in the text is the area inside the 20m bathymetric line.

Table 3.45. Distance and area of each depth zone in the model domain. Distances were calculated using the AUS754 Navigation Chart (Commonwealth of Australia 2002).

Depth zone	Model domain dimensions			
m	naut. mile	km	km^2	%
0-20	3.4	6.3	63.0	8.2
20-50	22.2	41.1	411.1	61.5
50-100	2.3	4.3	42.6	8.2
100-200	8.2	15.2	151.8	22.7
Total	36.1	66.9	668.5	100

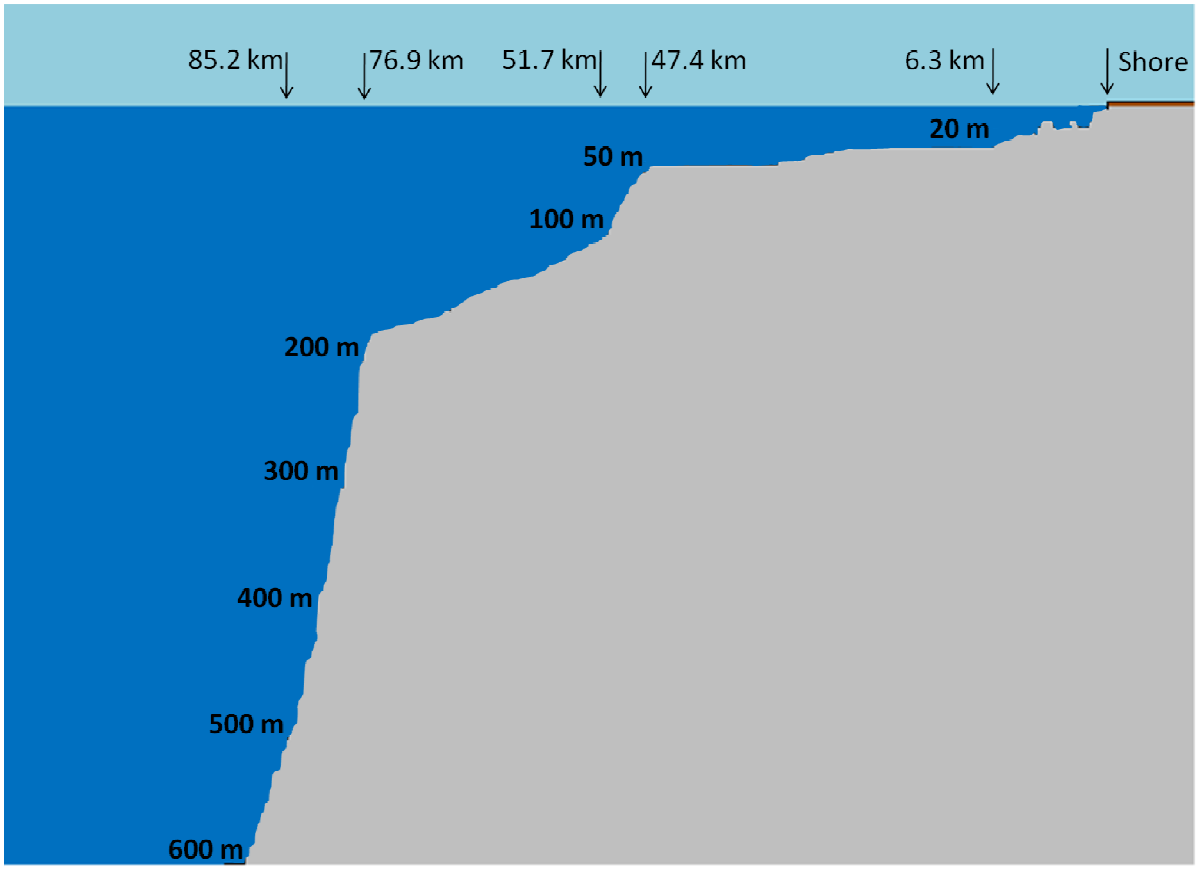

Figure 3.205. Depth profile of the south-west Australian shelf along 31°45'S.

Habitat area and distribution within model domain

The proportion of each habitat type is taken from the acoustic mapping and tow video analysis described above. This is summarised in Table 3.46 below.

Table 3.46. Depth Zones and proportion of Habitat type (from Figure 3.204).

Depth (m)	Depth Zone	Sand/Soft Sediment (%)	Reef/Hard Bottom (%)	Seagrass Meadow (%)	Average Depth of water column (m)	Area of Depth Zone in model domain (km^2)
0-20	Marmion Lagoon	47	42	11	10	63.0
20-50	Shallow shelf	66.5	32.5	1	35	411.1
50-100	Outer Slope	52	48	0	75	42.6
100-200	Deep shelf	100	0	0	150	151.8

Estimating biomass within the model domain Table 3.47 and Table 3.48 show the biomass per m^2 for each type of taxa in each habitat type in each depth zone. Table 3.49 shows the conversion factors used to convert biomass between wet weight, dry weight, organic carbon and nitrogen. Benthic habitat types and animal biomass from 150-200m were assumed to be the same as that from 100-150m where detailed sampling occurred.

Table 3.47. Benthic biomass data and sources. Unless otherwise stated, all biomass is grams wet weight per m^2 except MPB which is grams chlorophyll a per m^2, sediment organic carbon which is gC in top 2cm sediment and sediment nitrogen which is gN in top 2cm of sediment. Sources: [a]This study, this chapter and chapter 4; [b]autumn value of algal biomass from p202 SRFME Final Report volume 2 (Keesing et al. 2006) assuming half kelp/half other algae; [c]benthic sled data this study, this chapter (this method captures drift algae); [d]measured or estimated in his study, this chapter, note sponge, bryozoa and ascidian biomass for seagrass beds and bryozoa biomass on hard bottom/reef is in AFDW ; [e]this study, chapter 4; [f]not measured but assumed to follow[d]out to 50m in the case of sponges, ascidians and bryozoa in seagrass beds and organic carbon and nitrogen follows[e] but is assumed to decline by 25% between 20 and 500m then by 50% between 50 and 100m and by 90% between 100 and 200m;?data gap, probably negligible, model assumes zero; ?? data gap maybe non-negligible, model assumes zero. Notes: MPB is microphytobenthos; Other animals are predominantly molluscs, crustaceans, echinoderms and polychaetes. Note that biomass data for sediment organic carbon and sediment total nitrogen are total. In the model calculations these figures are reduced by subtracting the carbon and nitrogen biomass tied up in MPB.

Parameter	0-20m			20-50m			50-100m		100-200m
	Sand/Soft Sediment	Reef/Hard Bottom	Seagrass Meadow	Sand/Soft Sediment	Reef/Hard Bottom	Seagrass Meadow	Sand/Soft Sediment	Reef/Hard Bottom	Sand/Soft Sediment
MPB	0.040[a]	??	??	0.020 [a]	?	?	0.010 [a]	?	0[a]
Ecklonia	?	2000[b]	?	0.004[c]	144[c]	?	0[c]	240[c]	0[c]
Other algae	?	2000[b]	?	0.041[c]	35.7[c]	?	0.003[c]	26.4[c]	0.002[c]
Seagrass	??	0[d]	263[d]	0.003[c]	2.78[c]	263[d]	0[c]	0[c]	0[c]
Sponges	0[e]	30[d]	0.97[d]	0.002[c]	218[c]	0.97[d]	3.10[c]	325[c]	17.8[c]
Bryozoans	0[e]	0.3[d]	0.09[d]	0.001[c]	0.919[c]	0.09[d]	0.142[c]	6.51[c]	2.23[c]
Ascidians	0[e]	46[d]	3.9[d]	0[c]	5.0[c]	3.9[d]	0.039[c]	0.872[c]	3.4[c]
Other animals	13.2[e]	20 [d]	2 [d]	1.34[c]	15.0[c]	??	0.660[c]	24.2[c]	0.504[c]
Sediment organic carbon	14.2[e]	?	??	10.65[f]	?	??	7.1[f]	?	1.42[f]
Sediment total nitrogen	2.83[e]	?	??	2.12[f]	?	??	1.42[f]	?	0.283[f]

Table 3.48. Water column biomass data used. Sources: zooplankton this study this chapter, 0-20m are averages of summer and winter sampling, other depths are May 2007 samples only 20-50m is from 50m station, 50-100m is average of 50m and 100m stations, 100-200m is average of 100m and 300m stations. Phytoplankton is from annualised estimates based on measurements across the Two Rocks Transect carried out in SRFME (see Keesing et al. (2006). Water column Dissolved inorganic nitrogen (DIN) is based on data in this study, chapter 4 from Marmion Lagoon.

Parameter	0-20m	20-50m	50-100m	100-200m
Zooplankton (350- 1000µm)	0.004215 gDW m^{-3}	0.005044 gDW m^{-3}	0.004003 gDW m^{-3}	0.002426 gDW m^{-3}
Zooplankton (250-350µm)	0.006654 gDW m^{-3}	0.004684 gDW m^{-3}	0.005334 gDW m^{-3}	0.004156 gDW m^{-3}
Zooplankton (<250µm)	0.004878 gDW m^{-3}	0.002040 gDW m^{-3}	0.001735 gDW m^{-3}	0.001177 gDW m^{-3}
Phytoplankton	0.0004 gChla m^{-3} (0.4 mg m^{-3})	0.0003 gChla m^{-3} (0.3 mg m^{-3})	0.0003 gChla m^{-3} (0.3 mg m^{-3})	0.0002 gChla m^{-3} (0.2 mg m^{-3})
Water column DIN	0.000420 gN m^{-3} (0.03 µmol $liter^{-1}$)	0.000280 gN m^{-3} (0.02 µmol $liter^{-1}$)	0.000280 gN m^{-3} (0.02 µmol $liter^{-1}$)	0.000140 gN m^{-3} (0.01 µmol $liter^{-1}$)

Table 3.49. Conversion factors (multipliers) used to convert biomass into different units (refer to Table 3.47 and Table 3.48 for base measurement). [g]phytoplankton and microphytobenthos Carbon to WW and WW to DW from Reilly and Dow in (Link et al. 2006) and AFDW assumed to equal Carbon biomass, [h]calculated from Geiger (1987) C:Chla ratios were 32.5:1 at 10m, 21.3 at 35m, 20.7 at 75m and 20.6 at 150m, [i]estimate based on Duarte (1992), [j]table 4.7 in Postel et al. (2000), [k]actual measured data for zooplankton AFDW used where needed (data not shown), [l]Yamamuro (1999), [m]Thomas Wernberg pers. comm. WW/DW value for kelp 0.1897 and we assumed other algae the same, [n]Vanderklift this study, this chapter, [o]Duarte 1992, [p]Duarte 1990, [q]Ricciardi and Bourget (1998), [r]mid-point of range of 0.14 and 0.34 from Diaz and Ruetzler (2001), [s]Riisgaard et al. (1993), [t]estimate of skeleton free dry weight based on corals from Morton (1980) as no data for bryozoa available, [u]mid range from (Clarke 2008), [v]estimate based on[q], Other animals are predominantly molluscs, crustaceans, echinoderms and polychaetes (for conversions mid-range of values used from cited sources).

	DW to WW *(C to WW)*	WW to DW	DW to AFDW	AFDW to C *(C to AFDW)*	DW to C (*Chla to C*)	AFDW to N	C to N	DW to N
MPB	*(2[g])*	0.2[g]		*(1[g])*	*(20.6 - 32.5[h])*		0.1613[i]	
Phytoplankton	*(2[g])*	0.2[g]		*(1[g])*	*(20.6 - 32.5[h])*		0.1613[i]	
Zooplankton	5[j]	-	[k]	-	0.356[l]	-		0.094[l]
Ecklonia	-	0.1897[m]	-	-	0.369[n]	-		0.015[n]
Other algae	-	0.1144[m]	-	-	0.248[o]	-		0.019[o]
Seagrass	-	0.1[i]	-	-	0.336[p]	-		0.0192[p]
Sponges	-	0.162[q]	0.8[v]	-	0.24[r]	-		0.0305[s]
Bryozoans	-	0.035[t]	0.8[v]	-	0.5[i]	-		0.03[i]
Ascidians	-	0.062[q]	0.8[v]	-	0.22[1]			0.033[l]
Other animals	-	0.2[q]	0.8[q]	0.55[u]	-	0.12[u]		-

Estimating primary production within the model domain

Annual primary production across the model domain was calculated using published or measured values for phytoplankton, microphytobenthos, seagrass, *Ecklonia* and other algae (see Table 3.50). Values for seagrass and algae were calculated such that they could be applied as a function of dryweight biomass.

Table 3.50. outlines the primary production parameters used. Sources: phytoplankton is expressed as mgC per m^2 per day from Koslow unpublished (from fig 4.20, p150, Keesing et al. 2006), MPB in gC per m^2 per year is calculated from Lourey and Thompson unpublished data (elsewhere in chapter 3 this report) using an average net value of 45 millimol O^2 production per m^2 per hour for sediments in shallow lagoon at 5m depth converted to carbon production per year. Estimates for deeper water are based on diminishing the shallow water figure by using the relationship between electron transfer rates for MPB against depth (Thompson unpublished, this chapter). *Ecklonia* 0.1397gC per gWW standing crop per year calculated from a seasonally variable 0.0041 -0.0079 gWW per WWg standing biomass per day (Vanderklift and Bearham this chapter) converted to DW (using WW/DW conversion factor of 18.97% from Thomas Wernberg UWA) and Carbon (as per Table 3.49). Other algae is estimated to be 150% of the measured value for *Ecklonia* based on comparative measurements of productivity from oxygen evolution of *Ecklonia, Sargassum, Hennedya* and *Pterocladia*. These other three genera have much higher levels of productivity 122-306%) compared to *Ecklonia* (see Lourey unpublished elsewhere this chapter). Seagrass is calculated from Duarte and Chiscano (1999) using data for *Posidonia oceanica*. This is likely to be similar to *Posidonia sinuosa* but less than *Amphibolis antarctica*. Both these species are abundant in the study area.

Parameter	0-20m				20-50m				50-100m			100-200m	
	Sand/Soft Sediment	Reef/Hard Bottom	Seagrass Meadow	Water column	Sand/Soft Sediment	Reef/Hard Bottom	Seagrass Meadow	Water column	Sand/Soft Sediment	Reef/Hard Bottom	Water column	Sand/Soft Sediment	Water column
Phytoplankton	-	-	-	100	-	-	-	200	-	-	300	-	300
MPB	165.46	?	??	-	68.97	?	??	-	17.01	?	-	0	-
Ecklonia	-	0.1397	?	-	-	0.1397	?	-	-	0.1397	-	-	-
Other algae	-	0.2095	??	-	-	0.2095	??	-	-	0.2095	-	-	-
Seagrass	-	-	0.2405	-	-	-	0.2405	-	-	-	-	-	-

Results

Patterns of animal and plant biomass

Wet weight

Total animal and plant wet weight biomass in the 669 km^2 model domain was 188,465 tonnes (Table 3.51) or 282 tWW per km^2 or 282 gWW per m^2. Biomass was dominated by kelp (41%), other algae (31)% and filter feeders (23%).

Distribution of wet weight biomass by depth

Relative patterns of wet weight distribution between depth zones are shown in Figure 3.206. Kelp and other algae made up 93% of all biomass in the 0-20 m depth zone while filter feeders made up less than 3%. On the other hand at depths >than 20 m, filter feeders accounted for 53% of all biomass. Fifty-nine percent of all biomass occurred in the 0-20m depth zone which made up only 9% of the area of the model domain while 31% of the biomass was in the 20-50 m depth zone, while the deeper areas 50-200 m made up just 9% of biomass.

Distribution of wet weight biomass by habitat

Reef habitats accounted for 94% of all biomass and between 95% and 98% of biomass in the depth zones less than 100 m (Table 3.52). Sand habitats were the next most important making up 2.4% of all biomass overall and 77% of biomass in the 100-200m depth zone. Water column biomass (phytoplankton and zooplankton) made up 23% of biomass in the 100-200m depth zone but only 1.3% of overall biomass.

Dry weight

Total animal and plant dry weight biomass in the 669 km^2 model domain was 33,869 tonnes (Table 3.53) or 51 tDW per km^2 or 51 gDW per m^2. Biomass was dominated by kelp (43%), other algae (33%) and filter feeders (20%).

Distribution of dry weight biomass by depth

Kelp and other algae made up 97% of all biomass in the 0-20 m depth zone while filter feeders made up just 1.2%. On the other hand at depths >than 20 m, filter feeders accounted for 48% of all biomass. Sixty-one percent of all biomass occurred in the 0-20m depth zone which made up only 9% of the area of the model domain while 29% of the biomass was in the 20-50 m depth zone, while the deeper areas 50-200 m made up just 9% of biomass.

Distribution of dry weight biomass by habitat

Reef habitats accounted for 96% of all biomass and between 96% and 98% of biomass in the depth zones less than 100 m (Table 3.54). Sand habitats were the next most important making up 2% of all biomass overall and 70% of biomass in the 100-200m depth zone. Water column biomass (phytoplankton and zooplankton) made up 30% of biomass in the 100-200m depth zone but only 1.4% of overall biomass. The proportionality of the makeup of biomass distribution did not change greatly in the conversion of wet weight to dryweight.

Organic Carbon

Total mass of organic carbon in animal and plant biomass in the 669 km^2 model domain was 10,670 tonnes (Table 3.55) or 16 tC per km^2 or 16 gC per m^2. Organic carbon biomass was dominated by kelp (51%), other algae (26%) and filter feeders (15%).

Distribution of organic carbon biomass by depth

Relative patterns of wet weight distribution between depth zones are shown in Figure 3.207. Kelp and other algae made up 96% of all biomass in the 0-20 m depth zone while filter feeders made up just 1%. On the other hand at depths >than 20 m, filter feeders accounted for 36% of all biomass. Sixty percent of all biomass occurred in the 0-20m depth zone which made up only 9% of the area of the model domain while 30% of the biomass was in the 20-50 m depth zone, while the deeper areas 50-200 m made up just 9% of biomass.

Distribution of organic carbon biomass by habitat

Reef habitats accounted for 92% of all biomass and between 90% and 98% of biomass in the depth zones less than 100 m (Table 3.56). Sand habitats and the water column were the next most important, each making up 3.2% of all biomass overall and 46% and 54% respectively of biomass in the 100-200m depth zone. Differences in quanta between dry weight and carbon biomass were due to the proportionately higher organic carbon content in macroalgae and seagrass relative to filter-feeders.

Nitrogen

Total mass of nitrogen in animal and plant biomass in the 669 km^2 model domain was 814 tonnes (Table 3.57) or 1.22 tN per km^2 or 1.22 gN per m^2. Nitrogen biomass was dominated by filter feeders (27%), kelp (26%) and other algae (25%).

Distribution of nitrogen biomass by depth

Relative patterns of wet weight distribution between depth zones are shown in Figure 3.208. Kelp and other algae made up 90% of all biomass in the 0-20 m depth zone while filter feeders made up just 2%. On the other hand at depths greater than 20 m, filter feeders accounted for 45% of all biomass. The highest biomass of nitrogen was in the 0-20m depth zone (47%) which comprised 9% of the total model area while 39% of nitrogen biomass occurred in the 20-50m depth zone which made up only 61% of the area of the model domain. Deeper areas 50-200 m made up less than 15% of nitrogen biomass.

Distribution of nitrogen biomass by habitat

Reef habitats accounted for 84% of all biomass and between 83% and 94% of biomass in the depth zones less than 100 m (Table 3.58). The water column (phytoplankton and zooplankton) was the next most important making up 8.6% of all nitrogen biomass overall and 66% of biomass in the 100-200m depth zone. Sand habitats made up 34% of biomass in the 100-200m depth zone but only 6.5% of overall biomass. Differences in quanta between dry-weight and nitrogen biomass were due to the proportionately higher nitrogen content in filter-feeders and phytoplankton relative to macroalgae and seagrass.

Key Findings:

- **The study provides an assessment of the patterns of animal and plant biomass distribution across the shelf showing macroalgae (especially kelp) and filterfeeders (especially sponges) are the dominant biota on the shelf in terms of biomass but important spatial patterns are evident across the shelf.**
- **In the shallow area of the shelf 0-20 m biomass is domated ca >90% by macroalgae and ca. 2-3% by filter feeders.**
- **Beyond 20m filter feeders made up > 50% of biomass**

Incorporating water column dissolved inorganic nitrogen, sediment organic carbon and total nitrogen

In order to provide a more complete representation of the organic carbon and total nitrogen silos in the model domain dissolved inorganic nitrogen in the water column and sediment total nitrogen and sediment organic carbon (less that measured in the MPB) were incorporated from measurements made during the study. The parameters used and their sources are shown in Table 3.47.

Dissolved organic carbon and non-living particulate organic carbon in the water column are not included and maybe non-negligible.

Organic Carbon

Organic carbon tied up in sediment as live animal or plant material, bacteria or detritus comprised 14.2 gC per m^2 in the top 2cm of sediment in the 0-20m habitat zone (Table 3.47). Of this 1.3 gC per m^2 in the top 2 cm in the 0-20m zone is MPB. This figure of 14.2 gC per m^2 compares with a total for all other benthic and pelagic organic carbon of 9.6gC per m^2 (Table 3.55). Incorporating sediment organic carbon into the model increased the total organic carbon load in the model domain to 14,204 t or 21 gC per m^2 (Table 3.60) with 25% of all organic carbon tied up in this source. Standing stock of kelp remains the largest store of organic carbon on the shelf (34%) with sediment stores the next highest (Table 3.59). Figure 3.209 highlights the importance of sediment habitats as a carbon store relative to other sources.

Nitrogen

Nitrogen tied up in sediment as live animal or plant material, bacteria or detritus comprised 2.83 gC per m^2 in the top 2cm of sediment in the 0-20m zone (Table 3.47). This compares with a total for all other benthic and pelagic animal and plant nitrogen of 1.21gC per m^2 (Table 3.55). Incorporating sediment nitrogen of 2.83gC per m2 in sand habitats and water column DIN of 0.01 to 0.03 µmol per litre into the model increased the nitrogen load in the model domain to 1535 t or 2.30 gN per m^2 (Table 3.61) with 46.4% and 0.52% of all nitrogen tied up in sediment and in the water column as DIN respectively. Thus the largest stores of nitrogen on the shelf occur within sediments in the 20-50 m depth zone (562 t or 36.6%) (Table 3.62). Figure 3.210 highlights the importance of sediment habitats as a nitrogen store relative to other sources. The importance of nitrogen resupply facilitated by nitrifciation at the benthos and wave movement of sediments has been highlighted elsewhere in this study (see also Lourey and Kirkman 2007). There is a need to better quantify the levels of sediment nutrients in sediments

beyond the estimates here which are largely based on extrapolation from shallower parts of the domain.

Key Findings:

- **Large stores of organic carbon and total nitrogen exist tied up in sediments on the shelf**
- **These stores provide an important source for nutrient resupply to the water column from the benthos.**
- **There is a need for more empirical measurements of sediment nutrients across the shelf to provide greater rigour to the models presented here.**

Patterns of primary production

Total primary production across in the 669 km^2 model domain was 82,164 tonnes of carbon (Table 3.63) or 122.9 tC per km^2 per year or 122.9 gC per m^2 per year (Table 3.63). Total benthic primary production was 28,568 tonnes of carbon or 42.7 tC per km^2 per year or 42.7 gC per m^2 per year while pelagic (phytoplankton) primary production was 53,597 tonnes of carbon or 80.0 tC per km^2 per year or 80.0 gC per m^2 per year.

Distribution of primary production by depth

Relative patterns of the distribution of primary production between depth zones and plant type are shown in Figure 3.211. Overall, productivity was dominated by phytoplankton (65%) and microphytobenthos (29%) with kelp (2.5)%, other algae (2.8%) and seagrass (0.1%) making up the remainder. Kelp and other algae made up 32% of all primary production in the 0-20 m depth zone but this was still less than that of MPB (45%). At depths >than 20 m, phytoplankton and MPB dominated productivity. As a result of the extensive sand habitats in the 20-50 m zone, MPB made up 38% of primary production in this zone and indeed MPB in this zone accounted for 23% of all primary production within the model domain. At depths beyond 50m primary production was, not surprisingly, almost exclusively dominated by phytoplankton (90% in the 50-100m zone and 100% in the 100-200m zone) but this is only 26% of the total primary production on the shelf. The largest single contribution to primary production (36%) was the phytoplankton in the extensive 20-50m zone.

Distribution of benthic primary production by habitat

Table 3.64 shows that reef habitats make up 5.3% of all primary production on the shelf and 15% of all benthic primary production while comprising 27% of all benthic habitats (35% of benthic habitats <100m).

The revised nutrient budget and its implications

The model of primary production presented here shows total primary production of 122.9 gC per m^2 per year (80.0 gC per m^2 per year pelagic and 42.7 gC per m^2 per year benthic). The nitrogen requirement to fuel this production is estimated to be 18.52 gN per m^2 per year (12.1 gN per m^2 per year pelagic and 6.4 gN per m^2 per year benthic) (Table 3.65). Early in our WAMSI study a preliminary nutrient budget was developed for the entire western Australian coast between NW Cape and Cape Leeuwin (Chapter 1 this study, see also Feng and Wild

Allen (2010). They estimated a nitrogen budget of 16.8 gN per m^2 per year and that 84% of nitrogen used on the shelf for primary production was recycled on the shelf. They attributed a likely imbalance in the budget (about 1 gN per m^2 per year) to an unidentified export flux across the shelf. Their estimates were based in part on much lower rates of benthic primary production than our calculations suggest are the case for the region off Marmion. They also included a significant source of new nitrogen from upwelling in the region north of the Abrolhos which is not relevant to the region we studied. Incorporating our higher levels of benthic primary production requires a higher proportion of recycling on the shelf (90%) and reducing the contribution from upwelling to 0.1 gN per m^2 (see chapter 2 this study) accounts for much of the excess nitrogen identified in the Feng and Wild Allen (2010) model. Our model requires a benthic nitrification flux of 9.53 gN per m^2 per year. This is similar to the flux of 10.9 gN per m^2 per year estimated to occur in this region (see earlier this chapter and Lourey and Kirkman 2009) and is within the range of fluxes of 2 – 10 gN per m^2 per year measured by Rosich et al. (1994). The primary sources of this nitrate are likely to be wave driven resuspension of nitrate from nitrification in sediments (Lourey and Kirkman 2009) and sponges (see discussion earlier in this chapter). The annual production of organic carbon from all primary producer sources is 9 times the living biomass of those primary producers and almost 6 times the total estimate of all organic carbon biomass estimated on the model domain (Table 3.66). Much of this excess production appears to be stored in sediments where it is remineralised and made available as new nitrogen through wave driven resuspension as described early in this chapter (see also Lourey and Kirkman 2009).

Impact of nitrogen input from the Beenyup Waste Water Treatment Plant

The input of nitrogen into this system from the Beenyup Waste Water Treatment Plant (hereafter Marmion outfall) and its affect on the nutrient budget presented is worthy of special consideration. In 2009 the Marmion outfall was adding 816 tonnes of nitrogen into the Marmion Marine Park (Water Corporation Ploom Study). This is the equivalent of 1.29 gN per m^2 per year over the model domain and similar to the amount estimated to be contributed from Leeuwin current advection. It is not possible to estimate how much of this nitrogen is taken up by plants within the model domain and how much is advected from the system. Our study has shown (see chapter 1) that wind driven currents and wave forcing may turn over the water in the lagoon within a day. On the otherhand Thompson and Waite (2003) and Gartner et al (2002) showed that there is a clear signal from the Marmion outfall in phytoplankton and macroalgal primary production. Thus it is difficult to estimate how much of the 1.29 gN per m^2 per year from the Marmion outfall should be included in the supply and export parts of the nutrient budget presented here. Including the full amount on the supply side will have the impact of reducing the estimate of nitrogen supply needed from nitrification at the seabed by 14% (from 9.53 to 8.23 gN per m^2 per year). It would also increase the unaccounted losses of nitrogen (including burial and denitrification) needed to balance the budget from 0.56 to 1.86 gN per m^2 per year. This suggests a significant export of nitrogen not accounted for in the model. One possible mechanism maybe a cross shelf cascade of dense water or near bed gravity current of 0.01–0.02 m s^{-1} taking water off the shelf identified by Pattiaratchi et al. (2011).

Key Findings:

- **Reef habitats accounted for >80% of all animal and plant biomass but the water column and sediment habitats accounted for about 95% of all primary production**
- **Over 1/3rd of all primary production on the shelf is benthic primary production**
- **Primary production by microphytobenthos is very significant highlighting the importance of the large areas of sandy habitat types.**
- **90% of nitrogen used for primary production is recycled on the shelf**
- **Model predictions of the requirment for nitrificant at the sea bed match empirical measurements made elsewhere in this study**
- **The Beenyup WWTP contributes significant nitrogen at the scale of the study region**

Summary

The data and models produced in this part of the study have shown the importance of benthic habitats on the continental shelf and in particular shown that the relevance of the spatially extensive and deeper benthic habitats has been underestimated. Similarly the importance of soft sediment habitats has been underestimated in the past. As such the results have important implications for ecosystem based management of fisheries resources and implications for ecosystem and primary producer habitat protection, with habitats previously regarded as being of low environmental importance now evidently warranting greater protection. It is also clear that our study has demonstrated the need for more extensive studies on the processes which are important in structuring these deepwater habitats and the role they play in primary production and nutrient recycling and resupply. In particular we suggest that the deep water kelp communities warrant study they can tell us about kelp resilience and how to protect kelp resources in shallower eaters in the face of climate change, the role of sponges as nitrifiers and the extent of autotrophy and improved quantification of the contribution of soft sediment habitats to primary production and nutrient resupply functions in southwest Australian ecosystems. Lastly, this study has only looked at a very small section of the western Australian shelf and many of the conclusions are underpinned by assumptions and make use of literature values that should be tested and warrant verifying by targeted investigations. Thus much new work is warranted to quantify the importance of mesotrophic habitats to southwest Australian ecosystems.

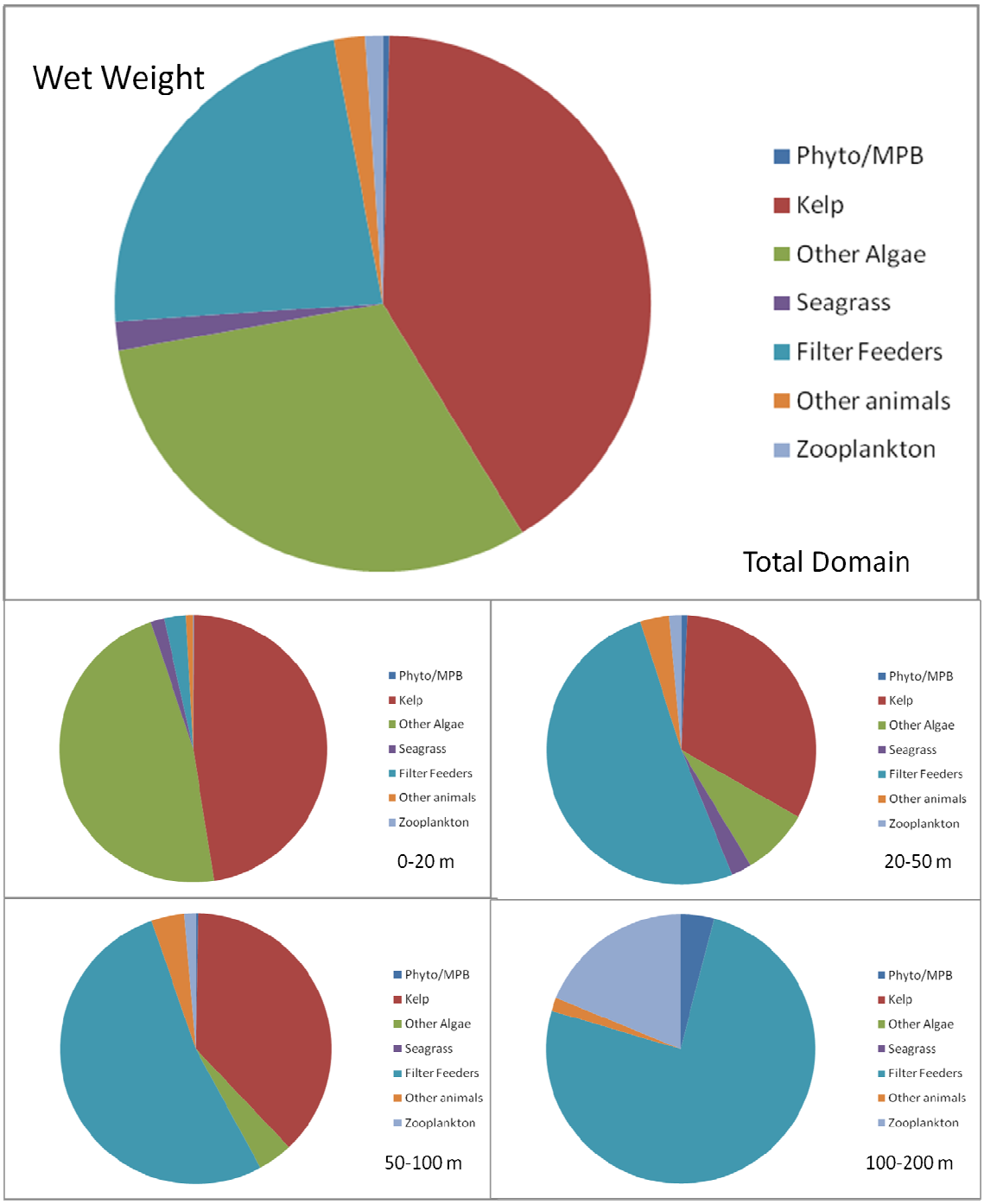

Figure 3.206. Distribution of biomass (wet weight) among depth zones and functional taxonomic groups.

Table 3.51. Wet Weight biomass distribution by animal/plant type and depth zone across the model domain.

tonnes WW	100-200	50-100	20-50	0-20	Total
Phyto/MPB	187.6	35.6	416.8	93.4	733.4
Kelp	0.0	4909.6	19248.5	52920.0	77078.1
Other Algae	0.2	540.0	4782.1	52920.0	58242.3
Seagrass	0.0	0.0	1453.4	1821.9	3275.3
Filter Feeders	3557.4	6862.0	30275.5	2913.5	43608.3
Other animals	76.5	510.2	2049.9	934.2	3570.8
Zooplankton	883.4	176.9	846.7	49.6	1956.5
Total	4705.1	13034.2	59072.9	111652.6	188464.7

tonnes WW	100-200	50-100	20-50	0-20	Total
Phyto/MPB	3.99	0.27	0.71	0.08	0.39
Kelp	0.00	37.67	32.58	47.40	40.90
Other Algae	0.01	4.14	8.10	47.40	30.90
Seagrass	0.00	0.00	2.46	1.63	1.74
Filter Feeders	75.61	52.65	51.25	2.61	23.14
Other animals	1.63	3.91	3.47	0.84	1.89
Zooplankton	18.77	1.36	1.43	0.04	1.04
Total	100.0	100.0	100.0	100.0	100.0

tonnes WW	100-200	50-100	20-50	0-20	Total
Phyto/MPB	25.58	4.86	56.83	12.73	100.00
Kelp	0.00	6.37	24.97	68.66	100.00
Other Algae	0.00	0.93	8.21	90.86	100.00
Seagrass	0.00	0.00	44.37	55.63	100.00
Filter Feeders	8.16	15.74	69.43	6.68	100.00
Other animals	2.14	14.29	57.41	26.16	100.00
Zooplankton	45.15	9.04	43.27	2.54	100.00
Total	2.50	6.92	31.34	59.24	100.00

tonnes WW	100-200	50-100	20-50	0-20	Total
Phyto/MPB	0.10	0.02	0.22	0.05	0.39
Kelp	0.00	2.61	10.21	28.08	40.90
Other Algae	0.00	0.29	2.54	28.08	30.90
Seagrass	0.00	0.00	0.77	0.97	1.74
Filter Feeders	1.89	3.64	16.06	1.55	23.14
Other animals	0.04	0.27	1.09	0.50	1.89
Zooplankton	0.47	0.09	0.45	0.03	1.04
Total	2.50	6.92	31.34	59.24	100.00

Table 3.52. Wet Weight biomass distribution by habitat type and depth zone across the model domain.

t WW biomass in this depth zone	100-200	50-100	20-50	0-20	Total
sand habitat	3634	97	284	468	4482
reef habitat	0	12734	56303	108664	177701
seagrass meadow	0	0	1456	2455	3911
water column	1071	203	1031	66	2371
Total	4705	13034	59073	111653	188465

t WW biomass in this depth zone	100-200	50-100	20-50	0-20	Total
sand habitat	77.2	0.7	0.5	0.4	2.4
reef habitat	0.0	97.7	95.3	97.3	94.3
seagrass meadow	0.0	0.0	2.5	2.2	2.1
water column	22.8	1.6	1.7	0.1	1.3
Total	100	100	100	100	100

t WW biomass in this depth zone	100-200	50-100	20-50	0-20	Total
sand habitat	81.1	2.2	6.3	10.4	100
reef habitat	0.0	7.2	31.7	61.1	100
seagrass meadow	0.0	0.0	37.2	62.8	100
water column	45.2	8.6	43.5	2.8	100
Total	2.5	6.9	31.3	59.2	100

t WW biomass in this depth zone	100-200	50-100	20-50	0-20	Total
sand habitat	1.9	0.1	0.2	0.2	2.4
reef habitat	0.0	6.8	29.9	57.7	94.3
seagrass meadow	0.0	0.0	0.8	1.3	2.1
water column	0.6	0.1	0.5	0.0	1.3
Total	2.5	6.9	31.3	59.2	100

Table 3.53. Dry Weight biomass distribution by animal/plant type and depth zone across the model domain.

tonnes DW	100-200	50-100	20-50	0-20	Total
Phyto/MPB	37.5	7.1	83.4	18.7	146.7
Kelp	0.0	931.3	3651.4	10038.9	14621.7
Other Algae	0.0	102.4	907.2	10038.9	11048.6
Seagrass	0.0	0.0	145.3	182.2	327.5
Filter Feeders	481.6	1092.5	4787.6	256.9	6618.6
Other animals	15.3	102.0	410.0	186.8	714.2
Zooplankton	176.7	35.4	169.3	9.9	391.3
Total	711.2	2270.8	10154.2	20732.4	33868.6

tonnes DW	100-200	50-100	20-50	0-20	Total
Phyto/MPB	5.28	0.31	0.82	0.09	0.43
Kelp	0.00	41.01	35.96	48.42	43.17
Other Algae	0.01	4.51	8.93	48.42	32.62
Seagrass	0.00	0.00	1.43	0.88	0.97
Filter Feeders	67.72	48.11	47.15	1.24	19.54
Other animals	2.15	4.49	4.04	0.90	2.11
Zooplankton	24.84	1.56	1.67	0.05	1.16
Total	100.0	100.0	100.0	100.0	100.0

tonnes DW	100-200	50-100	20-50	0-20	Total
Phyto/MPB	25.58	4.86	56.83	12.73	100.00
Kelp	0.00	6.37	24.97	68.66	100.00
Other Algae	0.00	0.93	8.21	90.86	100.00
Seagrass	0.00	0.00	44.37	55.63	100.00
Filter Feeders	7.28	16.51	72.33	3.88	100.00
Other animals	2.14	14.29	57.41	26.16	100.00
Zooplankton	45.15	9.04	43.27	2.54	100.00
Total	2.10	6.70	29.98	61.21	100.00

tonnes DW	100-200	50-100	20-50	0-20	Total
Phyto/MPB	0.11	0.02	0.25	0.06	0.43
Kelp	0.00	2.75	10.78	29.64	43.17
Other Algae	0.00	0.30	2.68	29.64	32.62
Seagrass	0.00	0.00	0.43	0.54	0.97
Filter Feeders	1.42	3.23	14.14	0.76	19.54
Other animals	0.05	0.30	1.21	0.55	2.11
Zooplankton	0.52	0.10	0.50	0.03	1.16
Total	2.10	6.70	29.98	61.21	100.00

Table 3.54. Dry Weight distribution by habitat type and depth zone across the model domain.

t DW biomass in this depth zone	100-200	50-100	20-50	0-20	Total
sand habitat	497	16	56	94	663
reef habitat	0	2214	9756	20398	32368
seagrass meadow	0	0	135	228	363
water column	214	41	206	13	474
Total	711	2271	10154	20732	33869

%t DW biomass in this depth zone	100-200	50-100	20-50	0-20	Total
sand habitat	69.9	0.7	0.6	0.5	2.0
reef habitat	0.0	97.5	96.1	98.4	95.6
seagrass meadow	0.0	0.0	1.3	1.1	1.1
water column	30.1	1.8	2.0	0.1	1.4
Total	100	100	100	100	100

%t DW biomass in this depth zone	100-200	50-100	20-50	0-20	Total
sand habitat	75.0	2.4	8.5	14.1	100
reef habitat	0.0	6.8	30.1	63.0	100
seagrass meadow	0.0	0.0	37.2	62.8	100
water column	45.2	8.6	43.5	2.8	100
Total	2.1	6.7	30.0	61.2	100

%t DW biomass in this depth zone	100-200	50-100	20-50	0-20	Total
sand habitat	1.5	0.0	0.2	0.3	2.0
reef habitat	0.0	6.5	28.8	60.2	95.6
seagrass meadow	0.0	0.0	0.4	0.7	1.1
water column	0.6	0.1	0.6	0.0	1.4
Total	2.1	6.7	30.0	61.2	100

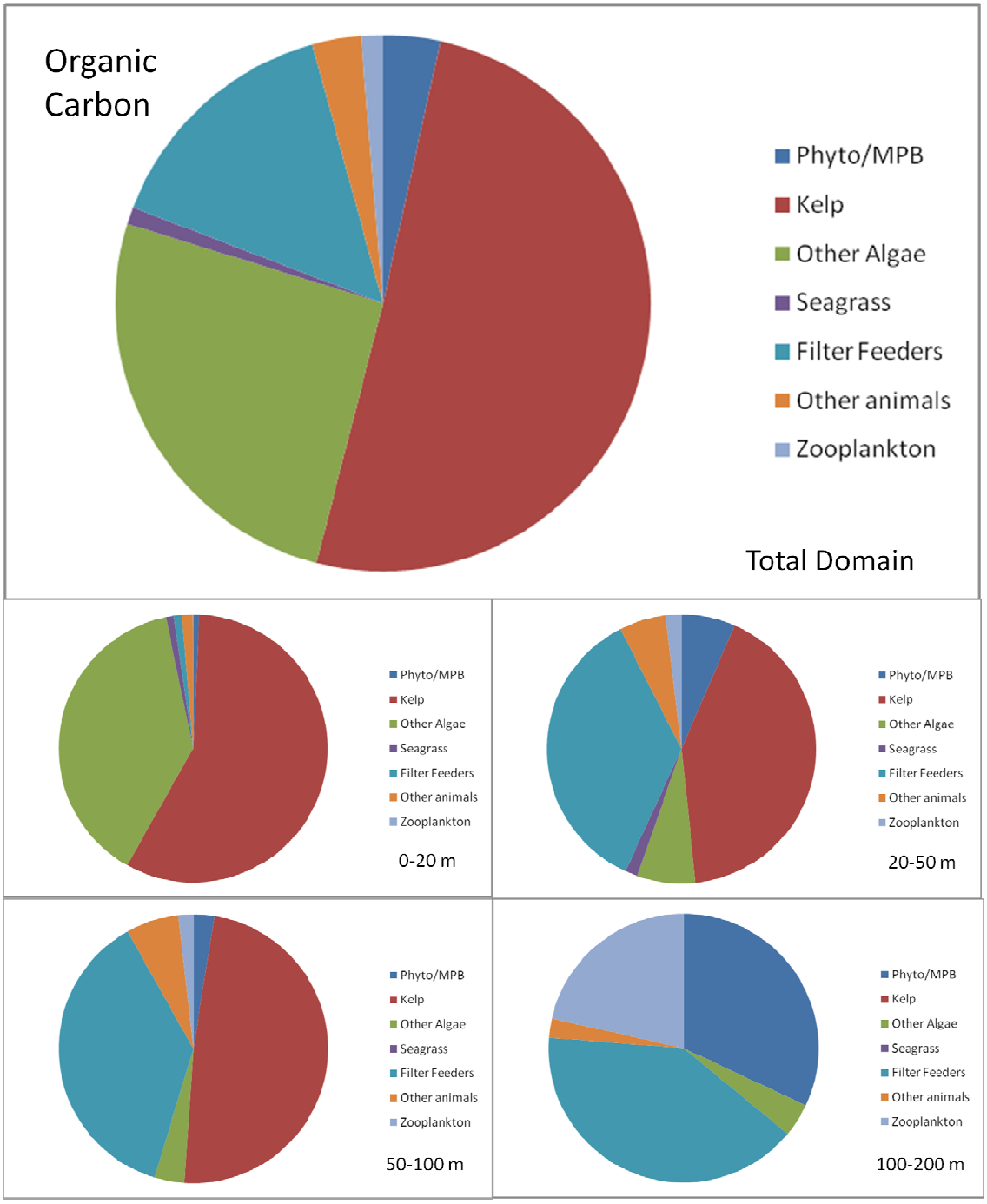

Figure 3.207. Distribution of organic carbon among depth zones and functional taxonomic groups.

Table 3.55. Organic Carbon biomass distribution by animal/plant type and depth zone across the model domain.

tonnes organic C	100-200	50-100	20-50	0-20	Total
Phyto/MPB	93.8	17.8	208.4	46.7	366.7
Kelp	0.0	343.7	1347.4	3704.4	5395.4
Other Algae	11.7	25.4	225.0	2489.7	2751.7
Seagrass	0.0	0.0	48.8	61.2	110.1
Filter Feeders	118.0	263.4	1149.0	62.3	1592.7
Other animals	6.7	44.9	180.4	82.2	314.2
Zooplankton	62.9	12.6	60.3	3.5	139.3
Total	293.2	707.8	3219.3	6449.9	10670.2

tonnes organic C	100-200	50-100	20-50	0-20	Total
Phyto/MPB	32.00	2.52	6.47	0.72	3.44
Kelp	0.00	48.56	41.85	57.43	50.57
Other Algae	3.99	3.59	6.99	38.60	25.79
Seagrass	0.00	0.00	1.52	0.95	1.03
Filter Feeders	40.26	37.22	35.69	0.97	14.93
Other animals	2.30	6.34	5.60	1.27	2.94
Zooplankton	21.45	1.78	1.87	0.05	1.31
Total	100.0	100.0	100.0	100.0	100.0

tonnes C	100-200	50-100	20-50	0-20	Total
Phyto/MPB	25.58	4.86	56.83	12.73	100
Kelp	0.00	6.37	24.97	68.66	100
Other Algae	0.43	0.92	8.18	90.48	100
Seagrass	0.00	0.00	44.37	55.63	100
Filter Feeders	7.41	16.54	72.14	3.91	100
Other animals	2.14	14.29	57.41	26.16	100
Zooplankton	45.15	9.04	43.27	2.54	100
Total	2.75	6.63	30.17	60.45	100

tonnes C	100-200	50-100	20-50	0-20	Total
Phyto/MPB	0.88	0.17	1.95	0.44	3.44
Kelp	0.00	3.22	12.63	34.72	50.57
Other Algae	0.11	0.24	2.11	23.33	25.79
Seagrass	0.00	0.00	0.46	0.57	1.03
Filter Feeders	1.11	2.47	10.77	0.58	14.93
Other animals	0.06	0.42	1.69	0.77	2.94
Zooplankton	0.59	0.12	0.56	0.03	1.31
Total	2.75	6.63	30.17	60.45	100

Table 3.56. Organic Carbon biomass distribution by habitat type and depth zone across the model domain.

t organic carbon total in this depth zone	100-200	50-100	20-50	0-20	Total
sand habitat	136	9	120	73	338
reef habitat	0	673	2904	6293	9870
seagrass meadow	0	0	43	72	115
water column	157	26	152	12	346
Total	293	708	3219	6450	10670

t organic carbon total in this depth zone	100-200	50-100	20-50	0-20	Total
sand habitat	46.5	1.2	3.7	1.1	3.2
reef habitat	0.0	95.1	90.2	97.6	92.5
seagrass meadow	0.0	0.0	1.3	1.1	1.1
water column	53.5	3.6	4.7	0.2	3.2
Total	100	100	100	100	100

t organic carbon total in this depth zone	100-200	50-100	20-50	0-20	Total
sand habitat	40.3	2.5	35.6	21.6	100
reef habitat	0.0	6.8	29.4	63.8	100
seagrass meadow	0.0	0.0	37.2	62.8	100
water column	45.2	7.5	43.9	3.4	100
Total	2.7	6.6	30.2	60.4	100

t organic carbon total in this depth zone	100-200	50-100	20-50	0-20	Total
sand habitat	1.3	0.1	1.1	0.7	3.2
reef habitat	0.0	6.3	27.2	59.0	92.5
seagrass meadow	0.0	0.0	0.4	0.7	1.1
water column	1.5	0.2	1.4	0.1	3.2
Total	2.7	6.6	30.2	60.4	100

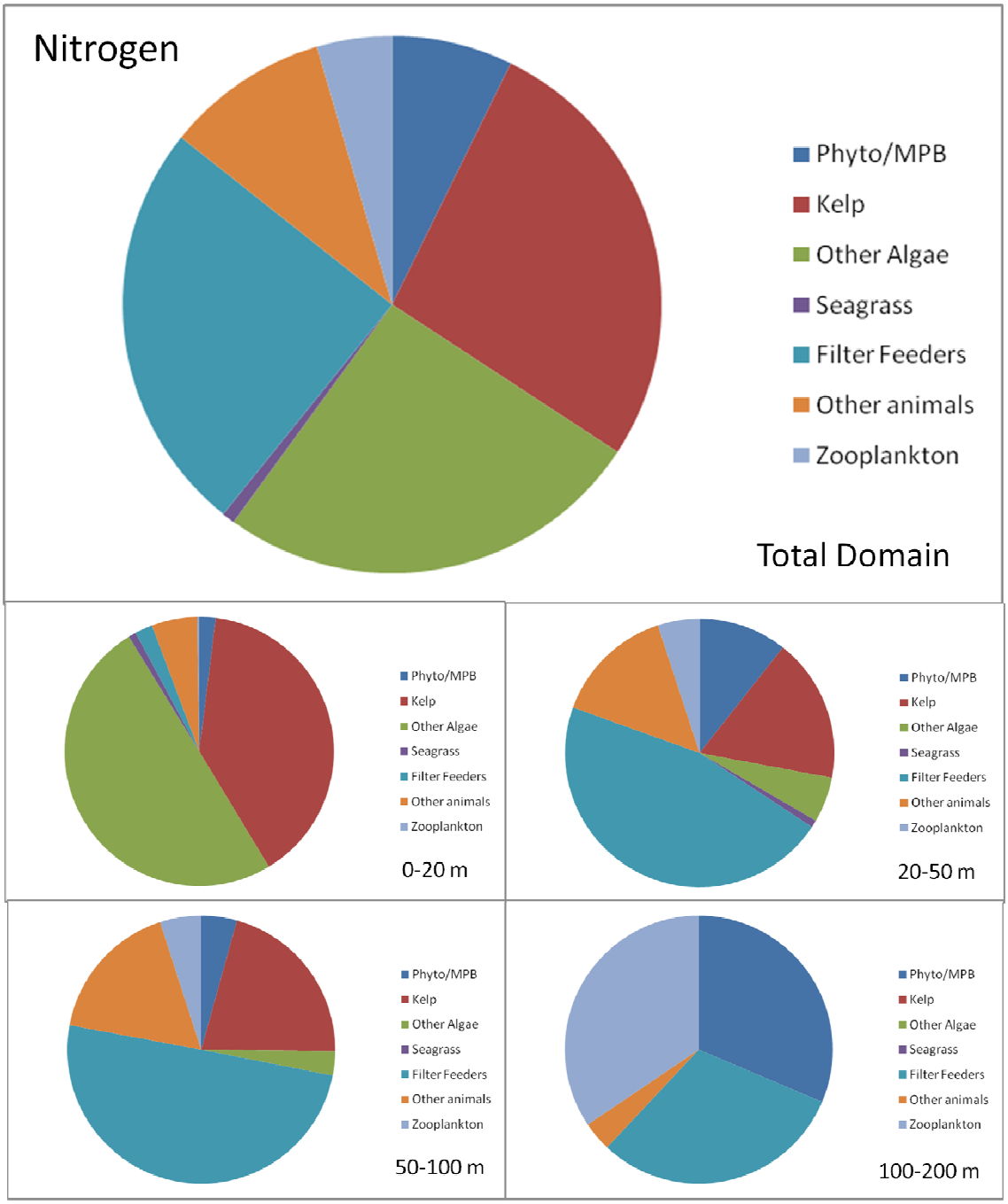

Figure 3.208. Distribution of total nitrogen among depth zones and functional taxonomic groups.

Table 3.57. Nitrogen distribution by animal/plant type and depth zone across the model domain

tonnes N	100-200	50-100	20-50	0-20	Total
Phyto/MPB	15.1	2.9	33.6	7.5	59.2
Kelp	0.0	14.0	54.8	150.6	219.3
Other Algae	0.0	1.9	17.2	190.7	209.9
Seagrass	0.0	0.0	2.8	3.5	6.3
Filter Feeders	14.8	33.3	146.2	8.1	202.4
Other animals	1.7	11.4	45.7	20.9	79.8
Zooplankton	16.6	3.3	15.9	0.9	36.8
Total	48.2	66.9	316.2	382.3	813.6

tonnes N	100-200	50-100	20-50	0-20	Total
Phyto/MPB	31.38	4.30	10.63	1.97	7.27
Kelp	0.00	20.89	17.32	39.39	26.96
Other Algae	0.00	2.91	5.45	49.89	25.80
Seagrass	0.00	0.00	0.88	0.91	0.77
Filter Feeders	30.62	49.83	46.22	2.12	24.87
Other animals	3.55	17.09	14.46	5.47	9.81
Zooplankton	34.44	4.97	5.03	0.24	4.52
Total	100	100	100	100	100

tonnes N	100-200	50-100	20-50	0-20	Total
Phyto/MPB	25.58	4.86	56.83	12.73	100
Kelp	0.00	6.37	24.97	68.66	100
Other Algae	0.00	0.93	8.21	90.86	100
Seagrass	0.00	0.00	44.37	55.63	100
Filter Feeders	7.30	16.47	72.23	4.01	100
Other animals	2.15	14.32	57.31	26.22	100
Zooplankton	45.15	9.04	43.27	2.54	100
Total	5.93	8.22	38.87	46.99	100

tonnes N	100-200	50-100	20-50	0-20	Total
Phyto/MPB	1.86	0.35	4.13	0.93	7.27
Kelp	0.00	1.72	6.73	18.51	26.96
Other Algae	0.00	0.24	2.12	23.44	25.80
Seagrass	0.00	0.00	0.34	0.43	0.77
Filter Feeders	1.81	4.10	17.97	1.00	24.87
Other animals	0.21	1.40	5.62	2.57	9.81
Zooplankton	2.04	0.41	1.96	0.11	4.52
Total	5.93	8.22	38.87	46.99	100

Table 3.58. Nitrogen distribution by habitat type and depth zone across the model domain.

t nitrogen total in this depth zone	100-200	50-100	20-50	0-20	Total
sand habitat	16	1	20	15	53
reef habitat	0	60	263	360	683
seagrass meadow	0	0	3	5	8
water column	32	5	31	2	70
Total	48	67	316	382	814

%t nitrogen total in this depth zone	100-200	50-100	20-50	0-20	Total
sand habitat	34.2	2.1	6.2	3.9	6.5
reef habitat	0.0	89.7	83.1	94.1	83.9
seagrass meadow	0.0	0.0	0.9	1.4	1.0
water column	65.8	8.2	9.7	0.6	8.6
Total	100	100	100	100	100

%t nitrogen total in this depth zone	100-200	50-100	20-50	0-20	Total
sand habitat	31.4	2.7	37.4	28.5	100
reef habitat	0.0	8.8	38.5	52.7	100
seagrass meadow	0.0	0.0	35.8	64.2	100
water column	45.2	7.8	43.8	3.2	100
Total	5.9	8.2	38.9	47.0	100

%t nitrogen total in this depth zone	100-200	50-100	20-50	0-20	Total
sand habitat	2.0	0.2	2.4	1.8	6.5
reef habitat	0.0	7.4	32.3	44.2	83.9
seagrass meadow	0.0	0.0	0.4	0.6	1.0
water column	3.9	0.7	3.8	0.3	8.6
Total	5.9	8.2	38.9	47.0	100

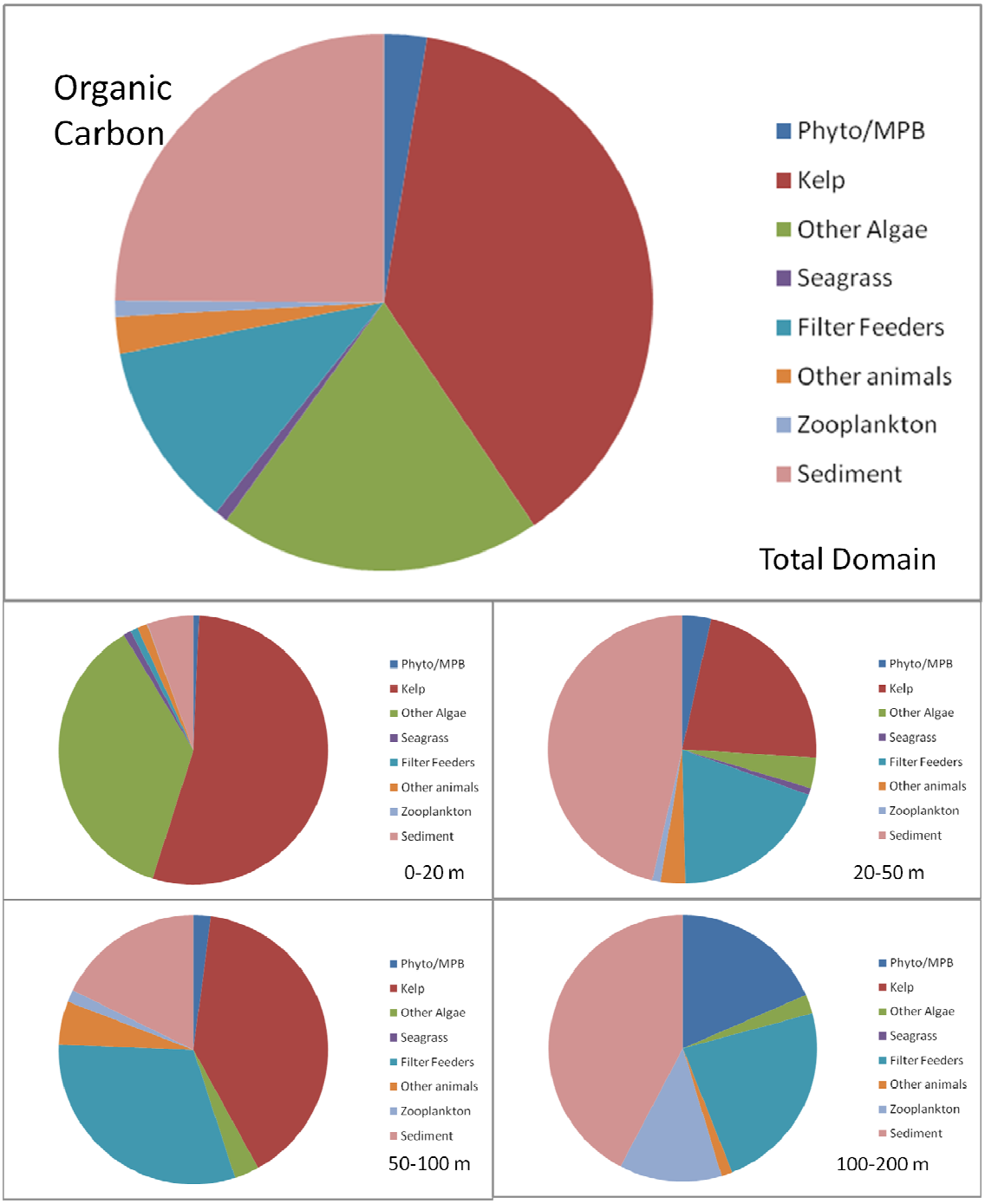

Figure 3.209. Distribution of organic carbon among depth zones and functional taxonomic groups (includes sediment component).

Table 3.59. Organic carbon biomass distribution by animal/plant type and depth zone across the model domain (including organic carbon in top 2cm sediment).

tonnes organic C	100-200	50-100	20-50	0-20	Total
Phyto/MPB	93.8	17.8	208.4	46.7	366.7
Kelp	0.0	343.7	1347.4	3704.4	5395.4
Other Algae	11.7	25.4	225.0	2489.7	2751.7
Seagrass	0.0	0.0	48.8	61.2	110.1
Filter Feeders	118.0	263.4	1149.0	62.3	1592.7
Other animals	6.7	44.9	180.4	82.2	314.2
Zooplankton	62.9	12.6	60.3	3.5	139.3
Sediment	214.9	152.2	2785.7	380.6	3533.3
Total	508.0	860.0	6005.0	6830.5	14203.5

% tonnes organic C	100-200	50-100	20-50	0-20	Total
Phyto/MPB	18.47	2.07	3.47	0.68	2.58
Kelp	0.00	39.96	22.44	54.23	37.99
Other Algae	2.30	2.95	3.75	36.45	19.37
Seagrass	0.00	0.00	0.81	0.90	0.77
Filter Feeders	23.23	30.63	19.13	0.91	11.21
Other animals	1.32	5.22	3.00	1.20	2.21
Zooplankton	12.38	1.46	1.00	0.05	0.98
Sediment	42.29	17.70	46.39	5.57	24.88
Total	100.0	100.0	100.0	100.0	100.0

% tonnes organic C	100-200	50-100	20-50	0-20	Total
Phyto/MPB	25.58	4.86	56.83	12.73	100
Kelp	0.00	6.37	24.97	68.66	100
Other Algae	0.43	0.92	8.18	90.48	100
Seagrass	0.00	0.00	44.37	55.63	100
Filter Feeders	7.41	16.54	72.14	3.91	100
Other animals	2.14	14.29	57.41	26.16	100
Zooplankton	45.15	9.04	43.27	2.54	100
Sediment	6.08	4.31	78.84	10.77	100
Total	3.58	6.05	42.28	48.09	100

% tonnes organic C	100-200	50-100	20-50	0-20	Total
Phyto/MPB	0.66	0.13	1.47	0.33	2.58
Kelp	0.00	2.42	9.49	26.08	37.99
Other Algae	0.08	0.18	1.58	17.53	19.37
Seagrass	0.00	0.00	0.34	0.43	0.77
Filter Feeders	0.83	1.85	8.09	0.44	11.21
Other animals	0.05	0.32	1.27	0.58	2.21
Zooplankton	0.44	0.09	0.42	0.02	0.98
Sediment	1.51	1.07	19.61	2.68	24.88
Total	3.58	6.05	42.28	48.09	100

Table 3.60. Organic carbon distribution by habitat type and depth zone across the model domain (including organic carbon in top 2cm sediment)

t organic carbon total in this depth zone	100-200	50-100	20-50	0-20	Total
sand habitat	351	161	2906	454	3872
reef habitat	0	673	2904	6293	9870
seagrass meadow	0	0	43	72	115
water column	157	26	152	12	346
Total	508	860	6005	6831	14204

%t organic carbon total in this depth zone	100-200	50-100	20-50	0-20	Total
sand habitat	69.2	18.7	48.4	6.6	27.3
reef habitat	0.0	78.3	48.4	92.1	69.5
seagrass meadow	0.0	0.0	0.7	1.1	0.8
water column	30.8	3.0	2.5	0.2	2.4
Total	100	100	100	100	100

%t organic carbon total in this depth zone	100-200	50-100	20-50	0-20	Total
sand habitat	9.1	4.2	75.1	11.7	100
reef habitat	0.0	6.8	29.4	63.8	100
seagrass meadow	0.0	0.0	37.2	62.8	100
water column	45.2	7.5	43.9	3.4	100
Total	3.6	6.1	42.3	48.1	100

%t organic carbon total in this depth zone	100-200	50-100	20-50	0-20	Total
sand habitat	2.5	1.1	20.5	3.2	27.3
reef habitat	0.0	4.7	20.4	44.3	69.5
seagrass meadow	0.0	0.0	0.3	0.5	0.8
water column	1.1	0.2	1.1	0.1	2.4
Total	3.6	6.1	42.3	48.1	100

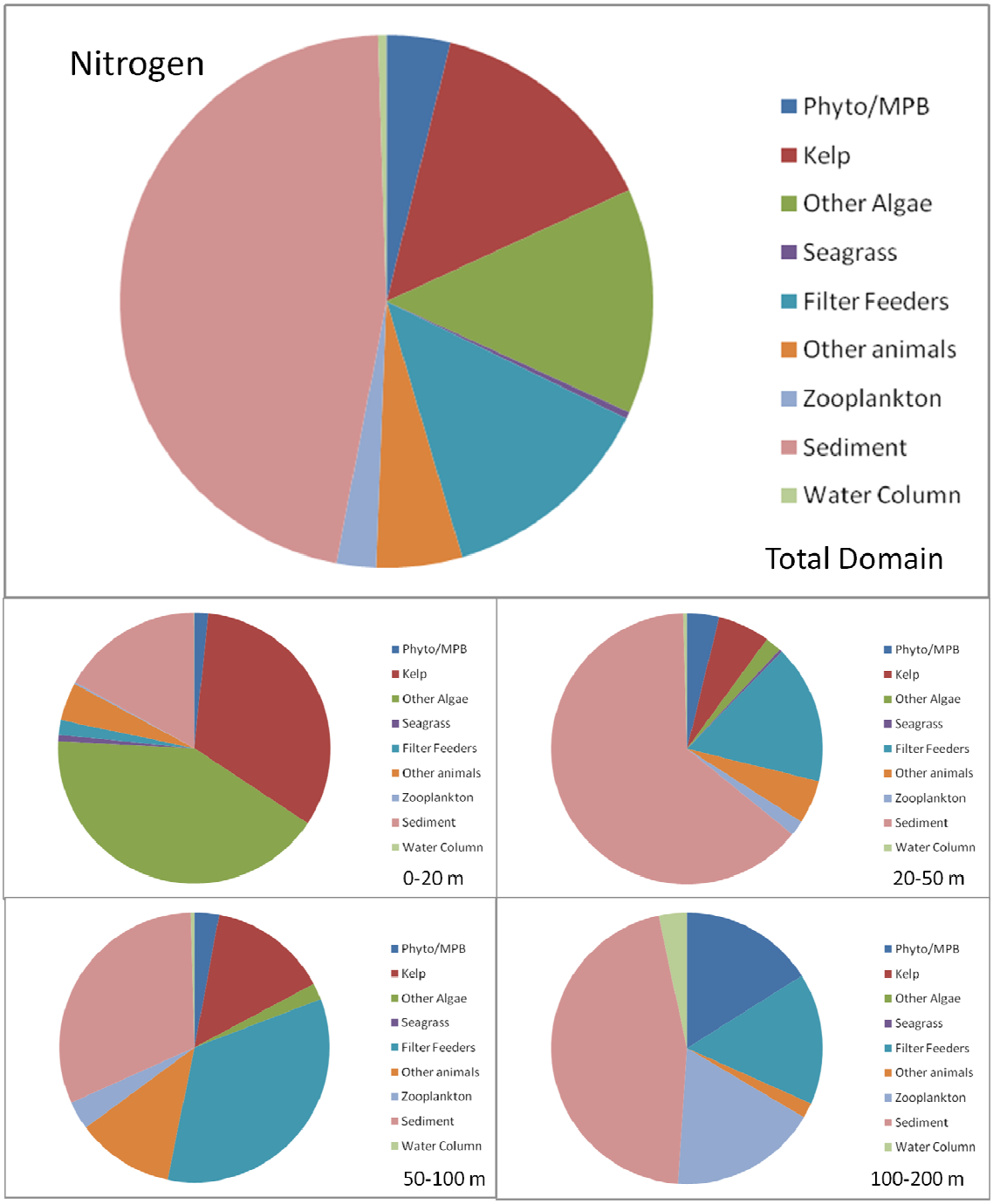

Figure 3.210. Distribution of total nitrogen among depth zones and functional taxonomic groups (includes water column and sediment components).

Table 3.61. Nitrogen distribution by animal/plant type and depth zone across the model domain (including total nitrogen in top 2cm sediment and water column DIN).

tonnes N	100-200	50-100	20-50	0-20	Total
Phyto/MPB	15.1	2.9	33.6	7.5	59.2
Kelp	0.0	14.0	54.8	150.6	219.3
Other Algae	0.0	1.9	17.2	190.7	209.9
Seagrass	0.0	0.0	2.8	3.5	6.3
Filter Feeders	14.8	33.3	146.2	8.1	202.4
Other animals	1.7	11.4	45.9	20.9	80.0
Zooplankton	16.6	3.3	15.9	0.9	36.8
Sediment	43.0	30.6	561.6	77.6	712.8
Water Column	3.2	0.4	4.0	0.3	7.9
Total	94.4	97.9	882.1	460.2	1534.6

% tonnes N	100-200	50-100	20-50	0-20	Total
Phyto/MPB	16.03	2.93	3.81	1.64	3.85
Kelp	0.00	14.27	6.21	32.72	14.29
Other Algae	0.00	1.99	1.95	41.45	13.68
Seagrass	0.00	0.00	0.32	0.76	0.41
Filter Feeders	15.64	34.03	16.57	1.76	13.19
Other animals	1.82	11.67	5.21	4.55	5.21
Zooplankton	17.60	3.40	1.80	0.20	2.40
Sediment	45.53	31.26	63.67	16.87	46.45
Water Column	3.38	0.46	0.46	0.06	0.52
Total	100	100	100	100	100

% tonnes N	100-200	50-100	20-50	0-20	Total
Phyto/MPB	25.58	4.86	56.83	12.73	100
Kelp	0.00	6.37	24.97	68.66	100
Other Algae	0.00	0.93	8.21	90.86	100
Seagrass	0.00	0.00	44.37	55.63	100
Filter Feeders	7.30	16.47	72.23	4.01	100
Other animals	2.14	14.29	57.41	26.16	100
Zooplankton	45.15	9.04	43.27	2.54	100
Sediment	6.03	4.29	78.79	10.89	100
Water Column	40.21	5.64	50.81	3.34	100
Total	6.15	6.38	57.48	29.99	100

% tonnes N	100-200	50-100	20-50	0-20	Total
Phyto/MPB	0.99	0.19	2.19	0.49	3.85
Kelp	0.00	0.91	3.57	9.81	14.29
Other Algae	0.00	0.13	1.12	12.43	13.68
Seagrass	0.00	0.00	0.18	0.23	0.41
Filter Feeders	0.96	2.17	9.53	0.53	13.19
Other animals	0.11	0.74	2.99	1.36	5.21
Zooplankton	1.08	0.22	1.04	0.06	2.40
Sediment	2.80	1.99	36.60	5.06	46.45
Water Column	0.21	0.03	0.26	0.02	0.52
Total	6.15	6.38	57.48	29.99	100

Table 3.62. Nitrogen distribution by habitat type and depth zone across the model domain (including total nitrogen in top 2cm sediment and water column DIN).

t N total in this depth zone	100-200	50-100	20-50	0-20	Total
sand habitat	59	32	581	93	765
reef habitat	0	60	263	360	683
seagrass meadow	0	0	3	5	8
water column	35	6	35	3	78
Total	94	98	882	460	1535

%t N total in this depth zone	100-200	50-100	20-50	0-20	Total
sand habitat	63.0	32.7	65.9	20.1	49.9
reef habitat	0.0	61.3	29.8	78.2	44.5
seagrass meadow	0.0	0.0	0.3	1.1	0.5
water column	37.0	6.0	3.9	0.5	5.1
Total	100	100	100	100	100

%t N total in this depth zone	100-200	50-100	20-50	0-20	Total
sand habitat	7.8	4.2	76.0	12.1	100
reef habitat	0.0	8.8	38.5	52.7	100
seagrass meadow	0.0	0.0	37.2	62.8	100
water column	44.7	7.6	44.5	3.2	100
Total	6.2	6.4	57.5	30.0	100

%t N total in this depth zone	100-200	50-100	20-50	0-20	Total
sand habitat	3.9	2.1	37.9	6.0	49.9
reef habitat	0.0	3.9	17.1	23.5	44.5
seagrass meadow	0.0	0.0	0.2	0.3	0.5
water column	2.3	0.4	2.3	0.2	5.1
Total	6.2	6.4	57.5	30.0	100

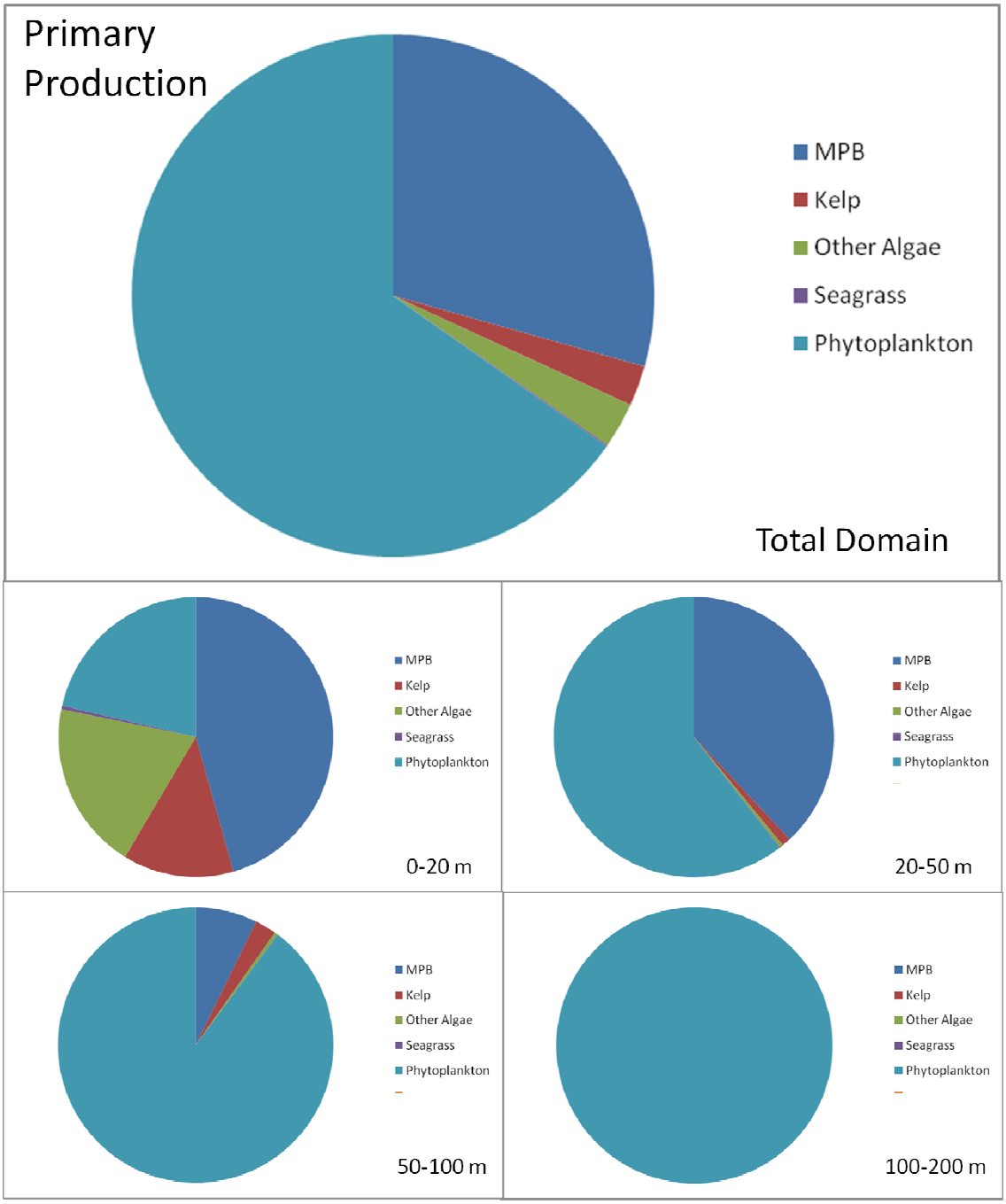

Figure 3.211. Distribution of sources of primary production among depth zones and functional taxonomic plant groups.

Table 3.63. Distribution of primary production (tonnes carbon) by plant type and depth zone across the model domain.

tonnes C per year	100-200	50-100	20-50	0-20	Total
MPB	0.0	376.8	18855.1	4899.3	24131.2
Kelp	0.0	130.1	510.1	1402.4	2042.7
Other Algae	0.0	21.5	190.1	2103.7	2315.2
Seagrass	0.0	0.0	35.0	43.8	78.8
Phytoplankton	16622.1	4664.7	30010.3	2299.5	53596.6
Total	16622.1	5193.1	49600.6	10748.7	82164.4

% tonnes C per year	100-200	50-100	20-50	0-20	Total
MPB	0.00	7.26	38.01	45.58	29.37
Kelp	0.00	2.51	1.03	13.05	2.49
Other Algae	0.00	0.41	0.38	19.57	2.82
Seagrass	0.00	0.00	0.07	0.41	0.10
Phytoplankton	100.00	89.83	60.50	21.39	65.23
Total	100.0	100.0	100.0	100.0	100.0

% tonnes C per year	100-200	50-100	20-50	0-20	Total
MPB	0.00	1.56	78.14	20.30	100.00
Kelp	0.00	6.37	24.97	68.66	100.00
Other Algae	0.00	0.93	8.21	90.86	100.00
Seagrass	0.00	0.00	44.37	55.63	100.00
Phytoplankton	31.01	8.70	55.99	4.29	100.00
Total	20.23	6.32	60.37	13.08	100.00

% tonnes C per year	100-200	50-100	20-50	0-20	Total
MPB	0.00	0.46	22.95	5.96	29.37
Kelp	0.00	0.16	0.62	1.71	2.49
Other Algae	0.00	0.03	0.23	2.56	2.82
Seagrass	0.00	0.00	0.04	0.05	0.10
Phytoplankton	20.23	5.68	36.52	2.80	65.23
Total	20.23	6.32	60.37	13.08	100.00

Table 3.64. Distribution of Primary production (tonnes C per year) by habitat type and depth zone across the model domain.

t C production total in this depth zone	100-200	50-100	20-50	0-20	Total
sand habitat	0	377	18856	4899	24132
reef habitat	0	152	709	3506	4366
seagrass meadow	0	0	26	44	70
water column	16622	4665	30010	2300	53597
Total	16622	5193	49601	10749	82164

% t C production total in this depth zone	100-200	50-100	20-50	0-20	Total
sand habitat	0.0	7.3	38.0	45.6	29.4
reef habitat	0.0	2.9	1.4	32.6	5.3
seagrass meadow	0.0	0.0	0.1	0.4	0.1
water column	100.0	89.8	60.5	21.4	65.2
Total	100	100	100	100	100

% t C production total in this depth zone	100-200	50-100	20-50	0-20	Total
sand habitat	0.0	1.6	78.1	20.3	100
reef habitat	0.0	3.5	16.2	80.3	100
seagrass meadow	0.0	0.0	37.2	62.8	100
water column	31.0	8.7	56.0	4.3	100
Total	20.2	6.3	60.4	13.1	100

% t C production total in this depth zone	100-200	50-100	20-50	0-20	Total
sand habitat	0.0	0.5	22.9	6.0	29.4
reef habitat	0.0	0.2	0.9	4.3	5.3
seagrass meadow	0.0	0.0	0.0	0.1	0.1
water column	20.2	5.7	36.5	2.8	65.2
Total	20.2	6.3	60.4	13.1	100

Table 3.65. Nitrogen budget for continental shelf off Marmion based on benthic model of biomass and primary production presented here compared with budget for entire west coast between North West Cape and Cape Leeuwin (Feng and Wild Allen 2010) All calculations follow the Feng and Wild Allen (2010) model except we adjust the new nitrogen supply from upwelling down from 1.2 gN per m^2 per year to 0.1 gN per m^2 per year to reflect conditions off Marmion (upwelling is more important in the region north of the Abrolhos (which forms part of the Feng and Wild Allen 2010 model domain) than off Marmion, see also Chapter 2 this study).

Nutrient Budget

Calculation of N requirement for PP on the shelf	**From Benthic model**	**From Feng and Wild Allen (2010)**
Refield ratio C:N = 106:16	6.625	6.625
Pelagic PP on shelf (gC per m2 per year)	80	98
N requirement for pelagic PP (gN per m2 per year)	12.08	14.8
Benthic PP on shelf (gC per m2 per year)	42.7	13
N requirement for benthic PP (gN per m2 per year)	6.45	2
Total N requirment (gN per m2 per year)	**18.52**	**16.80**
Model Domain	**Seaward of Marmion to 200m**	**NW Cape to Cape Leeuwin to 200m**
Area (km2)	669	98000
Total tonnes N requirement	**12390**	**1646400**
Sources of Nitrogen for PP (gN per m2 per year)		
f(pelagic)=PP from nitrate/PP total	0.5	0.5
f(benthic)=PP from nitrate/PP total	0.8	0.8
pelagic PP from Nitrate	6.04	7.40
benthic PP from Nitrate	5.16	1.60
pelagic PP from Ammonia	6.04	7.40
benthic PP from Ammonia	1.29	0.40
Sources of N to balance primary production requirement		
Sources of N to shelf (gN per m2 per year)		
Rain	0.02	0.02
N Fixation	0.07	0.07
Terrestrial	0.07	0.07
Upwelling	0.10	1.20
LC Advection	1.40	1.40
Recycled sources (gN per m2 per year)		
Nitrification at benthos required to balance budget	9.53	6.24
Directly recycled ammonia	7.33	7.80
Total sources required (gN per m2 per year)	**18.52**	**16.80**
Fate of N from primary production (gN per m2 per year)		
Directly recycled ammonia	7.33	7.80
To detritus in benthos	10.09	7.90
Losses of N (gN per m2 per year)		
Losses of N from the shelf		

Nutrient Budget		
Eddy export	0.60	0.60
Ekman transport	0.20	0.20
LC Advection	0.30	0.30
Denitrification and burial	0.56	1.66
Proportion nitrogen recycled on shelf	**90%**	**84%**

Table 3.66. Organic carbon biomass and production estimates for the shelf benthic model domain.

	Standing Biomass (t OC)	Productivity (t OC per year)	% of Standing Biomass
Phytoplankton	207	53597	25892
MPB	159	24131	15177
Kelp/Algae/Seagrass	8257	4437	54
Filter Feeders	1593		
Other animals	314		
Sediment	3533		
Total	14063	82165	584

3.3.11 References

Arillo A, Bavestrello G, Burlando B and Sarà M. (1993). Metabolic integration between symbiotic cyanobacteria and sponges: a possible mechanism. Mar Biol 117(1):159-162.

Bayer K, Schmitt S, and Hentschel U. (2007). Microbial nitrification in Mediterranean sponges: Possible involvement of ammonium-oxidizing *Betaproteobacteria*. In: Porifera Research: Biodiversity, Innovation & Sustainability. Custodio M, Lobo-Hajdu G, Hajdu E, Muricy G (eds.) pp. 165-171.

Beer S and Axelsson L. (2004). Limitations in the use of PAM fluorometry for measuring photosynthetic rates of macroalgae at high irradiances. Eur. J. Phycol. 39:1-7

Bergquist PR. (1978). Sponges. Hutchinson London 268pp.

Buchel C and Wilhelm C. (1993). *In vivo* analysis of slow chlorophyll fluorescence induction kinetics in algae: progress, problem and perspective. J. Photochem. Photobiol. B Biol. 58:137-148.

Cahoon LB. (1999). The role of benthic microalgae in neritic ecosystems. Oceanogr. Mar. Biol. Annu. Rev. 37:47–86

Clarke A. (2008). Ecological stoichiometry in six species of Antarctic marine benthos. Mar. Ecol. Prog. Ser. 369:25-37

Corredor JE, Wilkinson CR, Vicente VP, Morell JM, and Otero E. (1988). Nitrate release by Caribbean reef sponges. Limnol Oceanogr 33(1):114-120.

Diaz MC and Ward BB. (1997). Sponge-mediated nitrification in tropical benthic communities. Mar Ecol Prog Ser 56:97–109.

Diaz MC and Ruetzler K. (2001). Sponges: An essential component of Carribbean coral reefs. Bull Mar Sci 69(2):535-546.

Dring MJ. (1981). Chromatic adaptation in benthic marine algae: an examination of its ecological significance. Limnol Oceanogr. 26:271–284.

Duarte CM. (1992). Nutrient Concentration of Aquatic Plants: Patterns Across Species. Limnol Oceanogr 37(4):882-889.

Duarte CM. (1990). Seagrass nutrient content. Mar Ecol Prog Ser 67:201-207

Duarte CM and Chiscano CL. (1999). Seagrass biomass and production: a reassessment. Aquatic Botany 1334:1-16.

Eilers PHC and Peeters JCH. (1988). A model for the relationship between light intensity and the rate of photosynthesis in phytoplankton. Ecol Model 42:199-215

Feng M and Wild-Allen K. (2010). The Leeuwin Current. In: Liu K-K, Atkinson L, Quinones R, Talaue-McManus L. (eds) Carbon and Nutrient Fluxes in Continental Margins: A Global Synthesis. IGBP Book Series. Springer, Berlin. 744 pp.

Figueroa FL, Conde-Álvarez R, and Gómez I. (2003). Relations between electron transport rates determined by pulse amplitude modulated fluorescence and oxygen evolution in macroalgae under different light conditions. Photosynth.Res 75: 259-275.

Forehead HI. (2006). The ecology and biogeochemistry of sandy sediments in the warm coastal waters of Western Australia. Ph.D thesis, University of Western Australia, School of Plant Biology, pp 133.

Franklin L and Badger MR. (2001). A comparison of photosynthetic electron transport rates in macroalgae measured by pulse amplitude chlorophyll fluorescence and mass spectrometry. J. Phycology 37:756-767

Furnas MJ and Crosbie ND. (1999). *In situ* growth dynamics of photosynthetic prokaryotic picoplankters *Synechococcus* and *Prochlorococcus*. In: Charpy L, Larkum AWD (eds) Marine cyanobacteria. Bulletin de l'Institut Océanographique, Monaco, Spécial 19:387–417.

Gail FW. (1922). Photosynthesis in some of the red and brown algae as related to light and depth. Publs Puget Sound Mar. Biol. Stn. 3:177-193

Gartner A, Lavery P, and Smit AJ. (2002). Use of delta N-15 signatures of different functional forms of macroalgae and filter-feeders to reveal temporal and spatial patterns in sewage dispersal. Marine Ecology Progress Series 235, 63–73. doi:10.3354/MEPS235063

Greenwood J. (2010). Evidence that increased nitrogen efflux from wave-influenced marine sediment enhances pelagic phytoplankton production on the inner continental shelf of Western Australia. Mar Freshwat Res 61: 625-632.

Hatcher A. (1994). Nitrogen and phosphorus turnover in some benthic marine invertebrates: implications for the use of C:N ratios to assess food quality. Marine Biology 121:161-166.

Hentschel U, Usher KM and Taylor MW. (2006). Marine sponges as microbial fermenters. FEMS Microbiol Ecol 55(2):167-177.

Heyward A, Fromont J, Schönberg CHL, Colquhoun J, Radford B and Gomez O. (2010). The Sponge Gardens of Ningaloo Reef, Western Australia. The Open Mar Biol J 4: 3-11.

Ilan M, Ben-Eliyahu N and Galil B. (1994). Three deep water sponges from the Eastern Mediterranean and their associated fauna. Ophelia 39:45-54.

Jeffrey SW, Mantoura RFC and Wright SW. (1997). Phytoplankton pigments in oceanography. UNESCO Publishing. Paris. France

Jimenez E and Ribes M. (2007). Sponges as a source of dissolved inorganic nitrogen: Nitrification mediated by temperate sponges Limnol Oceanogr 52(3):948–958.

Kavanaugh MT, Nielsen KJ, Chan FT, Menge BA, Letelier RM and Goodrich LM. (2009). Experimental assessment of the effects of shade on an intertidal kelp: Do phytoplankton blooms inhibit growth of open-coast macroalgae?. Limnol. Oceangr. 54(1):276-288.

Keesing JK, Heine JN, Babcock RC, Craig PD and Koslow JA. (2006). Strategic Research Fund for the Marine Environment Final Report. Volume 2: The SRFME core projects. Strategic Research Fund for the Marine Environment, CSIRO, Australia. 266p.

Kérouel R and Aminot A. (1997) Fluorometric determination of ammonia in sea and estuarine waters by direct segmented flow analysis. Mar. Chem. (57): 265-275.

Kirk JTO. (1977). Attenuation of light in natural waters. Australian Journal of Marine and Freshwater Research 28: 497-508.

Kirk JTO. (1994). Light and photosynthesis in aquatic ecosystems. Cambridge University Press. 509pp.

Larkum AWD, Drew EA, Crossett RN. (1967). The vertical distribution of attached marine algae in Malta. J. Ecol. 55, 361-371.

Lavery PS, Lukatelich RJ, McComb AJ. (1991). Changes in the biomass and species composition of macroalgae in a eutrophic estuary. Estuar. Coast. Shelf. Sci. 33:1-22.

Lemloh M-L, Fromont J, Brummer F, Usher KM. (2009). Diversity and abundance of photosynthetic sponges in temperate Western Australia. BMC Ecology 9(4) doi:10.1186/1472-6785-9-4.

Littler MM, Littler DS, Blair SM, Norris JN. (1986). Deep-water plant communities from an uncharted seamount off San Salvador Island, Bahamas: distribution, abundance, and primary productivity. Deep Sea Res. 33:881-892

Lourey MJ, Dunn JR, and Waring J. (2006). A mixed-layer nutrient climatology of Leeuwin Current and Western Australian shelf waters: Seasonal nutrient dynamics and biomass. J Mar Syst 59(1–2):25-51.

Lourey MJ and Kirkman H. (2009). Short lived dissolved nitrate pulses in a shallow Western Australian coastal lagoon. Mar Freshwat Res 60:1068-1080.

Mackey DJ, Higgins HW, Mackey MD and Holdsworth D. (1998). Algal class ab Algal class abundances in the western equatorial Pacific: Estimation from HPLC measurements of chloroplast pigments using CHEMTAX. Deep Sea Research Part 1: Oceanographic Research Papers 45(9):1441-1468

Markager S. (1993) Light absorption and quantum yield for growth in five species of marine macroalgae. J Phycol 29:54-63

McEnnulty FR, Gowlett-Holmes KL, Williams A, Althaus F, Fromont J, Poore GCB, O'Hara TD, Marsh L, Kott P, Slack-Smith S, Alderslade P, and Kitahara MV. (in press). The deepwater megabenthic invertebrates on the western continental margin of Australia (100–1500 m depths): composition, distribution and novelty. Rec West Aust Mus

Maldonado M and Young CM. (1996). Bathymetric patterns of sponge distribution on the Bahamian slope. Deep-Sea Res I. 43(6): 897-915.

Mohamed NM, Saito K, Tal Y, and Hill RT. (2010). Diversity of aerobic and anaerobic ammonia-oxidizing bacteria in marine sponges. The ISME J 4:38–48.

Morton B. (1980). Some aspects of the biology and functional morphology of *Coralliophaga (Coralliophaga) coralliophaga* (Gmelin 1791) (*Bivalvia: Arcticacea*): a coral associated nestler in Hong Kong. The malacofauna of Hong Kong and southern China, 311-330.

Muenchhoff J, Hirose E, Maruyama T, Sunairi M, Burns BP and Neilan BA. (2007). Host specificity and phylogeography of the prochlorophyte *Prochloron* sp., an obligate symbiont in didemnid ascidians. Environ Microbiol 9:890-899.

Olsen JB and Kellogg CA. (2010). Microbial ecology of corals, sponges, and algae in mesophotic coral environments. FEMS Microbiol Ecol 73:17–30.

Pattiaratchi C, Hollings B, Woo M and Welhena T. (2011), Dense shelf water formation along the south west Australian inner shelf, Geophys. Res. Lett., 38, L10609, doi:10.1029/2011GL046816.

Prins TC, Smaal CS and Dame RF. (1998). A review of the feedbacks between bivalve grazing and ecosystem processes. Aquatic Ecology 31: 349–359.

Reed JK and Pomponi SA. (1997). Biodiversity and distribution of deep and shallow water sponges in the Bahamas. Proc 8th Int Coral Reef Symp 1387-1392.

Ricciardi A and Bourget E. (1998). Weight to weight conversion factors for marine benthic macroinvertebrates. Marine Ecology Progress Series, 163: 245-251.

Ridley CP, Faulkner DJ, and Haygood MG. (2005). Investigation of *Oscillatoria spongeliae*-dominated bacterial communities in four Dictyoceratid sponges. Appl Environ Microbiol 71:7366-7375.

Riisgard HU, Thomassen S, Jakobsen H, Weeks JM, and Larsen PS. (1993). Suspension feeding in marine sponges *Halichondria panicea* and *Haliclona urceolus*: effects of temperature on filtration rate and energy cost of pumping. Mar Ecol Prog Ser 96:177-188

Roberts DE and Davis AR. (1996). Patterns in sponge (Porifera) assemblages on temperate coastal reefs off Sydney, Australia. Marine and Freshwater Research 47: 897–906. doi:10.1071/MF9960897

Roberts DE, Cummins SP, Davis AR, Pangway C. (1999). Evidence for symbiotic algae in sponges from temperate coastal reefs in New South Wales Australia. Mem Queensl Mus 44:493-497.

Rosich RS, Bastyan GR, Pailing EI, and Van Senden DC. (1994). Sediment nutrient processes. Perth Coastal Water Study, project E3.4 (phase 2). Report no. SSB 15/94. Water Authority, Perth

Schmidt EW, Obraztsova AY, Davidson SK, Faulkner DJ, and Haygood MG. (2000). Identification of the antifungal peptide-containing symbiont of the marine sponge *Theonella swinhoei* as a novel dproteobacterium, "*Candidatus Entotheonella palauensis*". Mar Biol 136(6):969-977.

Soetaert K and Middelburg JJ. (2009). Modeling eutrophication and oligotrophication of shallow-water marine systems: the importance of sediments under stratified and well-mixed conditions. Hydrobiol. 629:239-2554

Taylor MW, Radax R, Steger D, and Wagner M. (2007). Sponge associated microorganisms: evolution, ecology, and biotechnological potential. Microbiol Molecular Biol Rev 71:295–347.

Thompson PA and Waite A. (2003). Phytoplankton responses to wastewater discharges at two sites in West Australia. Marine and Freshwater Research 54:721-735

Underwood AJ, Kingsford MJ, and Andrew NL. (1991). Patterns in shallow subtidal marine assemblages along the coast of New South Wales. Aust Ecol, 16(2), 231-49.

Unson MD and Faulkner DJ. (1993). Cyanobacterial symbiont biosynthesis of chlorinated metabolites from *Dysidea herbacea* (Porifera).*vExperientia Basel* . 49(4):349-353.

Usher KM. (2008). The ecology and phylogeny of cyanobacterial symbionts in sponges. Mar Ecol 29:178-192.

van Soest RWM. (1993). Distribution of sponges on the Mauritanian continental shelf. Hydrobiologia 258:95-106.

Watson RJ, Butler ECV, Clementson LA, and Berry KM. (2004). Flow-injection analysis with fluorescence detection of trace levels of ammonium in seawater. Journal of Environmental Monitoring 7: 37–42

Wilkinson CR. (1983). Net primary productivity in coral reef sponges. Science 219: 410-412.

Wilkinson CR. (1987). Interocean Differences in Size and Nutrition of Coral Reef Sponge Populations. Science 236:1654-1657.

Wilkinson CR and Vacelet J. (1979) Transplantation of marine sponges to different conditions of light and current. J Exp Mar Biol Ecol 37: 91–104.

Wright SW, Jeffrey SW, Mantoura, RFC, Llewellyn, CA, Bjørnland T, Repeta D and Welschmeyer N. (1991). Improved HPLC method for the analysis of chlorophylls and carotenoids from marine phytoplankton. Marine Ecology Progress Series 77:183–196.

Yamamuro M. (1999). Importance of epiphytic cyanobacteria as food sources for heterotrophs in a tropical seagrass bed. Coral Reefs. 18:263-271.

4. SIMPLE MODELS FOR ASSESSING IMPACTS OF NUTRIENT ENRICHMENT

Martin Lourey, John Keesing, Peter Thompson, Tennille Irvine, James McLaughlin, Guy Abell, Doug Bearham, Lesley Clementson, Jim Gunson, Peter Hughes, Fiona Graham and Stan Robert.

CSIRO Marine and Atmospheric Research

Objective 4: Develop simple models for assessing and predicting impacts of physical forcing factors, primarily nutrients, on key benthic functional groups/habitats informed by experiments and observations conducted across a range of naturally varying and anthropogenically altered gradients related to nutrient enrichment.

4.1 Introduction

Rapid population growth, combined with associated industrial development and urbanisation has placed increasing pressure on the coastal environment in south Western Australia. There is increasing concern about the effects of anthropogenic nutrients from waste water discharge (Thompson and Waite, 2003), contaminated ground water (Johannes, 1980), riverine discharge (Black et al., 1981) and run off from agricultural drains and canals (McMahon and Walker, 1998) on the WA marine environment. The effects of nutrients discharged into the Western Australian coastal zone are, however, poorly understood. Increased nutrient loadings have the capacity to significantly enhance primary production at the continental shelf scale and cause eutrophication plus hypoxia in some ecosystems (Diaz and Rosenberg, 2008). Benthic plants may be susceptible to such discharge by favouring one group of primary producers over another and could generate regime shift. For example, increased nutrient loadings stimulating enhanced epiphyte growth may have contributed to a large scale reduction in the extent of seagrass beds in Cockburn Sound (Cambridge et al., 1986) and variations in phytoplankton community structure have been identified around metropolitan waste water discharges (Thompson and Waite, 2003). Increased anthropogenic nutrients may also increase detrital loads to the sediments which have the potential to considerably influence soft bottom biogeochemical proceses, infaunal invertebrate communities and macroinvertebrate grazer communities (Pearson and Rosenberg (1978).

Benthic microalgae (BMA) are a major source of primary production in shallow coastal waters (see Chapter 3, this study) and can respond rapidly to increased nutrient loads. Nutrient enrichment can increase BMA biomass (Sundback and Snoeijs 1991) and alter their photosynthetic characteristics (Dizon and Yap, 1999). However, competitive interactions have been observed leading to reduced species diversity in the BMA community (Hilledrand and Sommer, 1997). While nutrient enrichment leads to an increase in BMA biomass, grazing by herbivores can have a strong negative effect on microalgal biomass, species composition and diversity. Grazing of microalgae has been shown to increase with increasing nutrient availability so assessing the functional response of herbivores to nutrient enrichment is a vital component of understanding the effects of nutrient enrichment (Hillebrand et al., 2000). In this chapter we measure a suite of parameters designed to characterise the BMA community response to environmental forcing.

Macroinvertebrate communities can respond to and even modify the magnitude of the autotrophic response to nutrient enrichment (Leibold and Wilber 1992). Grazers may respond to increased sedimentation from stimulated pelagic production or increased benthic algal biomass and enrichment may make fundamental change to food web dynamics. In some cases, the effect of nutrient enrichment of the marine environment may be important in ecological terms but nevertheless subtle and difficult to detect. Differences in species composition, distribution, abundance, biomass and secondary production of infauna and macro-invertebrates can combine yield a sensitive tool for investigating disturbance. One way of assessing ecosystem response to anthropogenic pressure is to compare biological features across existing gradients of one or more variables of interest. By sampling across natural and anthropogenic gradients of sediment nutrient enrichment, soft bottom communities in the Perth and mid-west region were assessed for spatial differences in primary producer and heterotrophy communites and an attempt was made to relate any between site variability to differences in the environmental conditions. Here we compare environmental and biotic attributes along a pre-existing sediment nutrient (Total Organic Nitrogen concentration) gradient. We have sampled a large number of sites with a range of sediment nutrient characteristics designed to provide a gradient of sediment nutrient enrichment in shallow nearshore sediment habitats from low (Marmion lagoon) to high (Cockburn Sound) and a gradient of exposure to physical dynamics from onshore to offshore in both Marmion lagoon and Cockburn Sound. Our goal was to develop an improved capacity to assess, monitor and predict likely changs in nearshore soft sediment habitats in ways that will help manage these coastal environments.

4.2 Methodology

Twenty-nine sites were surveyed (Figure 4.1): 13 in Marmion Marine Park (one near (i.e.<25m) the Ocean Reef sewage outfall (called Marmion Outfall) and the remaining forming transects across a depth gradient with 4 inner lagoon, 4 mid lagoon and 4 outer (outside the lagoon) (see Figure 4.2), 6 in Cockburn Sound (5 forming a transect along a sediment nutrient gradient at the northern end and one at the southern end), 2 sites between these locations at City Beach and Port Beach, one within the Swan River and 7 at Jurien Bay to the north. Some of these sites are considered replicates of a location and have been pooled for analyses while other sites although occurring in proximity to one another are considered individual sites due to differences in natural and anthropogenic stresses. The seven Jurien sites (JV007, Favourite, Dry Lumps, South Bay, Fishermans, Essex and Boullanger North) have been pooled as the Jurien location. Similarly, South Lumps, Whitford Rock, Wreck Rock and Cow Rock make up the Marmion Inner location; MM1, MM2, MM3 and MM4 comprise Marmion Mid; and MM_11, MOF2, M3MRS and M3MRN are Marmion Outer. More intensive investigations of respiration/biological oxygen demand, primary production by BMA, microbial nitrogen dynamics and rates of sediment nutrient efflux were conducted at a subset of six of the above stations distributed evenly across the latitudinal spread of stations (from the Marmion outfall in the North to Southern Flats in the south. The subset of stations included three within Cockburn Sound and three outside of the sound. The exact location of each of the sampling sites is shown in Table 4.1.

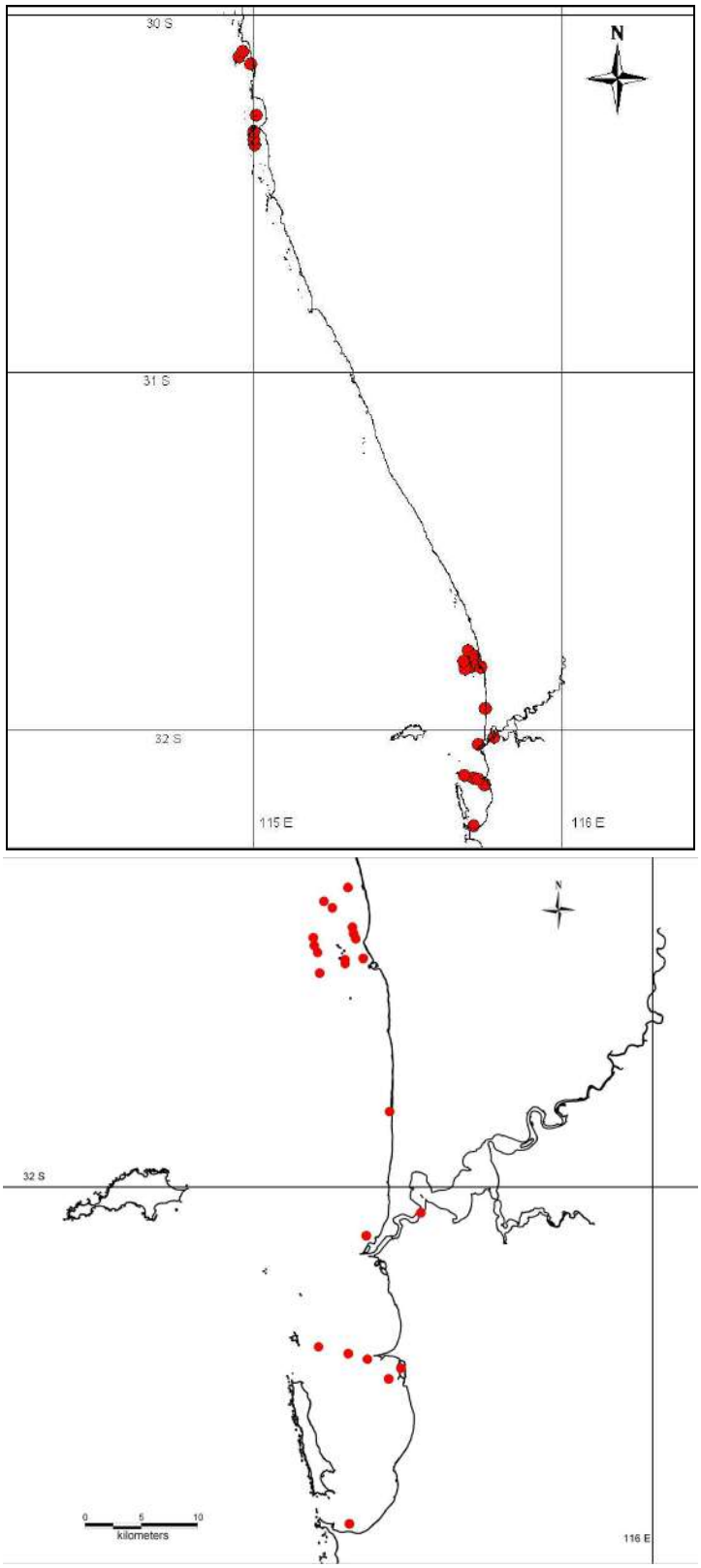

Figure 4.1. Site locations for soft sediment survey. Bottom figure shows detail in the metropolitan area.

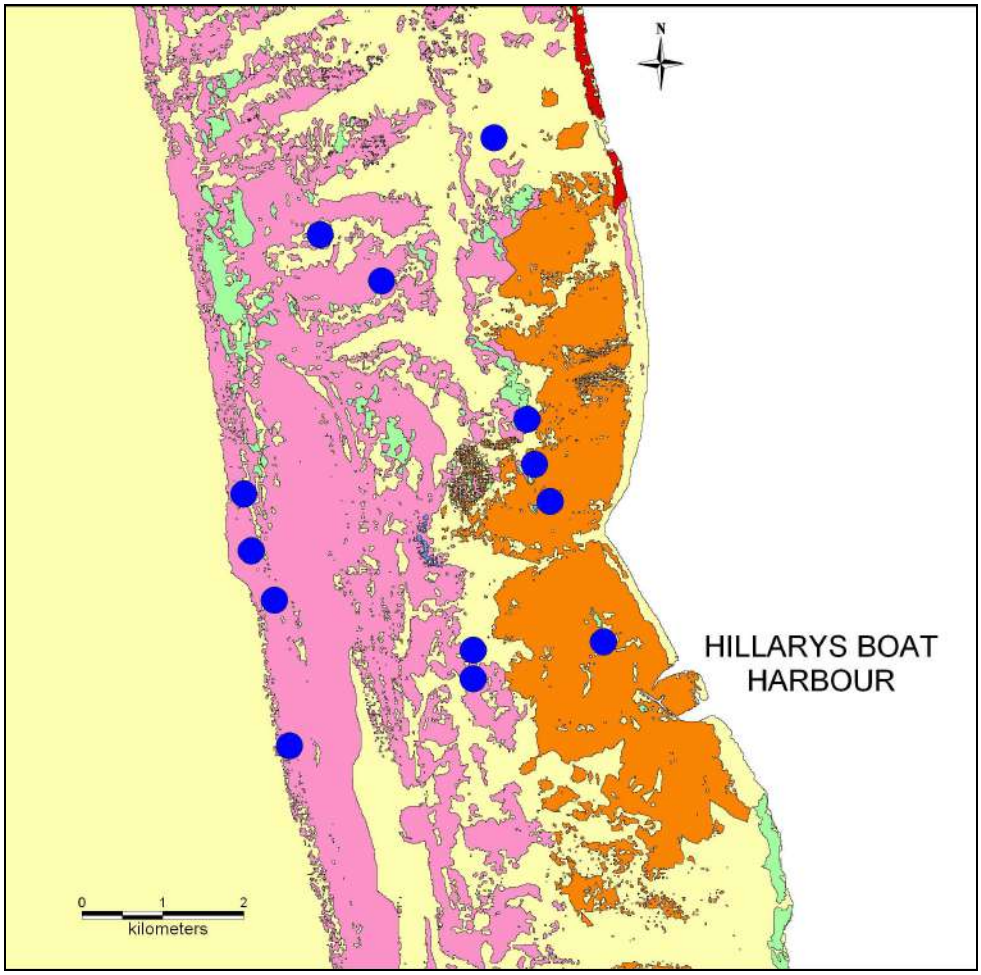

Figure 4.2. Site locations (blue circles) in Marmion Marine Park, shown on Habitat Map (DEC, 2002). The stations are arranged across a depth gradient with 4 inner lagoon, 4 mid lagoon and 4 outer stations (located outside the lagoon).

Table 4.1. List of sites sampled and their exact locations and dates sampled. Note that the Port Beach site is referred to in some figures and tables as "Hall Bank", however the site is not located on the reef off Fremantle known as Hall Bank. ns indicates not sampled.

Location	Site	Latitude	Longitude	Sediment sampling 2008/2009	Sediment sampling 2010	PAM fluorometry and phytopigments	Primary Production and community respiration
Jurien Bay	JV007	-30.3625	115.0042	7/04/2008	ns	ns	ns
Jurien Bay	Favourite	-30.2801	115.0092	7/04/2008	ns	ns	ns
Jurien Bay	Dry Lumps	-30.1188	114.953	8/04/2008	ns	ns	ns
Jurien Bay	South Bay	-30.1035	114.966	8/04/2008	ns	ns	ns
Jurien Bay	Fishermans	-30.138	114.9923	8/04/2008	ns	ns	ns
Jurien Bay	Essex	-30.3489	115.003	9/04/2008	ns	ns	ns
Jurien Bay	Boullanger North	-30.3255	115.0035	11/04/2008	ns	ns	ns
Marmion inshore	Marmion Outfall	-31.7632	115.7112	30/03/2009	30/03/2010	30/03/2009 7/12/2009 2/06/2010	7/12/2009 23/08/2010
Marmion inshore	South Lumps	-31.7935	115.7171	4/03/2008	30/03/2010	27/11/2008 14/12/2009 4/06/2010	ns
Marmion inshore	Whitford Rock	-31.7985	115.7189	7/03/2008	ns	27/11/2008 10/12/2009 4/06/2010	ns
Marmion inshore	Wreck Rock	-31.8027	115.7198	14/03/2008	ns	27/11/2008 10/12/2009 1/06/2010	ns
Marmion inshore	Cow Rock	-31.8184	115.7274	14/03/2008	30/03/2010	26/11/2008 11/12/2009 1/06/2010	ns
Marmion mid	MM1	-31.778	115.6977	13/02/2008	30/03/2010	2/12/2008 10/12/2009 2/06/2010	ns
Marmion mid	MM2	-31.7728	115.6902	13/02/2008	ns	2/12/2008 14/12/2009 2/06/2010	ns
Marmion mid	MM3	-31.8193	115.7096	7/02/2008	ns	26/11/2008 11/12/2009 11/06/2010	ns
Marmion mid	MM4	-31.8225	115.71	7/02/2008	30/03/2010	28/11/2008 14/12/2009 18/06/2010	ns
Marmion mid	AA	-31.835	115.7131	ns	ns	1/12/2008 15/12/2009 18/06/2010	ns
Marmion mid	BB	-31.8278	115.71715	ns	ns	28/11/2008 15/12/2009 18/06/2010	2/12/2009 25/08/2010
Marmion offshore	MM_11	-31.8082	115.6814	17/03/2008	ns	1/12/2008 10/12/2009	ns

Location	Site	Latitude	Longitude	Sediment sampling 2008/2009	Sediment sampling 2010	PAM fluorometry and phytopigments	Primary Production and community respiration
						1/06/2010	
Marmion offshore	MOF2	-31.8137	115.6844	8/02/2008	30/03/2010	1/12/2008 11/12/2009 11/06/2010	ns
Marmion offshore	M3MRS	-31.83	115.6863	14/02/2008	30/03/2010	26/11/2008 11/12/2009 11/06/2010	ns
Marmion offshore	M3MRN	-31.8019	115.6802	17/03/2008	Ns	14/12/2009 4/06/2010	ns
Fremantle location	City Beach	-31.9405	115.7517	3/04/2008	30/03/2010	24/11/2008 16/12/2009 10/06/2010	30/11/2009 11/08/2010
Fremantle location	Port Beach	-32.0393	115.7297	18/03/2008	30/03/2010	24/11/2008 16/12/2009 10/06/2010	ns
Cockburn Sound	Northern Harbour	-32.142	115.7648	31/03/2009	31/03/2010	25/11/2008 17/12/2009 8/06/2010	16/11/2009 18/08/2010
Cockburn Sound	Jervoise Bank	-32.1536	115.7508	19/03/2008	31/03/2010	25/11/2008 17/12/2009 8/06/2010	ns
Cockburn Sound	Cockburn Sound	-32.1378	115.7309	20/03/2008	31/03/2010	25/11/2008 17/12/2009 8/06/2010	11/11/2009 30/08/2010
Cockburn Sound	Parmelia Bank	-32.1333	115.7134	19/03/2008	31/03/2010	ns	ns
Cockburn Sound	Carnac	-32.128	115.6855	2/04/2008	31/03/2010	25/11/2008 17/12/2009 9/06/2010	ns
Cockburn Sound	Southern Flats	-32.269	115.7145	2/04/2008	31/03/2010	25/11/2008 17/12/2009 9/06/2010	23/11/2009 16/08/2010
Swan River	Blackwall Reach	-32.0212	115.7814	21/04/2008	31/03/2010	24/11/2008 16/12/2009 10/06/2010	ns

For ease of reference, the large number of parameters measured in the study are set out in Table 4.2 and the methods used for each are described below.

Table 4.2. Parameters measured or estimated.

Parameter measured	2008/2009	2009/2010	Winter 2010
Physical attributes			
Anaerobic layer depth	yes	yes	
Sand ripple height	yes	yes	
Sediment grain size	yes		
Light attenuation	yes	yes	
Modelled wave climate	yes		
Nutrient load			
Water column nutrients		yes	
Sediment Total Organic Carbon	2 & 5 cm	2 & 10cm	
Sediment δCarbon 13 isotope	2 & 5 cm	2 & 10cm	
Sediment Total Nitrogen	2 & 5 cm	2 & 10cm	
Sediment δNitrogen 15 isotope	2 & 5 cm	2 & 10cm	
Sediment Total Organic content		2 & 10cm	
MPB and microbial community			
Integrated water column chlorophyll *a*	yes	yes	
Sediment chlorophyll *a* and phaeopigments (Fluorometry)	2 & 5 cm	2 & 10cm	
Other phytopigments (HPLC)	yes	yes	yes
Nitrifier/Denitrifier abundance (AOA real time PCR)#	yes	yes	yes
Nirifier/Denitrifier composition (T-FRLP)#	yes	yes	yes
Animal diversity and biomass			
Benthic macrofauna counts and biomass	yes		
Infauna to 0.5mm biomass	yes		
Infauna to 0.5 mm counts	yes		
Polychaete abundance (qPCR) -selected taxa	to 10cm		
Primary production and sediment community metabolism			
Oxygen production and community respiration		yes	yes
Pmax, Ik, alpha	yes	yes	yes
Secondary production			
Infaunal secondary production (to 0.5mm)	yes		

4.2.1 Broad scale assessment

Physical parameters, primary production and characteristics of the sediment infauna and macroinvertebrate populations (see Table 4.2) have been described and quantified. Sampling was conducted to determine species composition, distribution, abundance, biomass and secondary production of infauna and macro-invertebrates. Water column chlorophyll *a*, and nutrients and light attenuation where also measured.

The sampling strategy was designed to overcome small scale (< 10 m) horizontal variability and focus on larger scale (> 100 m) patterns. Five (rarely 4 or 6) transects of 5x1m were established, 10 x 30mm diameter cores to 50mm depth and 3 x 150mm diameter cores to 100mm depth were randomly collected within the transect, and all macrofauna collected using a small rake to search the sediment.

The ten small (30 mm diameter) cores from each of the five transects were vertically sectioned into 0-2cm and 2-5cm depths and the 0-2 or 2-5cm sections from all 10 cores derived from one transect pooled and mixed to homogeneity. Four 20ml subsamples were kept from each of the

0-2cm pooled samples and two from the 2-5cm sections. One of each from both size fractions was analysed for carbon and nitrogen, from the second chlorophyll *a* was determined and the final 2 samples were retained for other analyses including biomass of ammonia oxidizing archaea (AOA) and bacteria (AOB) (Abell et al. 2010) and bacteria abundance and biomass (see below). During the 2010 sampling, at each site, two larger 6cm diameter cores were taken to a depth of at least 10cm and brought vertically and carefully to the surface and extruded and sectioned at 1cm intervals to examine the vertical distribution of organic matter and chlorophyll *a* at different sediment depths. Approximately 4 grams of sediment was subsampled for microphytobenthos pigments (Chl *a* and phaeopigment) analyses and accurately weighed. These were then extracted in 90% acetone overnight and fluorescence measured on a Turner Designs model 10AU fluorometer (detection limit of 0.01 mg chl *a* m^{-3}) following the acidification technique of Parsons et al. (1989). In instances where the chlorophyll *a* content was greater than the upper limit of the fluorometer a serial dilution was implemented. Sediment samples were retained for carbon and nitrogen content and carbon and nitrogen stable isotope abundance. Samples were encapsulatedin tin capsules (samples for carbon isotope abundance were treated with hydrochloric acid (1mol/L) to remove inorganic carbon) and %C, %N, $\delta^{13}C_{POC}$ and $\delta^{15}N_{PN}$ determined using an elemental analyser (ANCA-GSL, Europa, Crewe, United Kingdom) combined with an isotope ratio mass spectrometer (20-20 IRMS, Europa, Crewe, United Kingdom). Reference materials of known elemental composition and isotopic ratios were interspaced with the samples for calibration.

One of the large cores was dry sieved through a set of 15 sieves from 0.063 to 8.0 mm pore size to determine proportions of grain size. One of the remaining cores was washed through 9 sieves from 8.0 to 0.5mm and the phyla composition and biomass of infauna of each size class determined to allow for calculation of daily secondary production as per Edgar (1990). The third core was analysed for relative abundance of enriched sediment indicator guilds of polychaetes using quantitative PCR following (Loo et al. 2006).

At each site, physical factors of bottom water temperature, depth, and water column light attenuation and the structure of sediment such as presence of ripples, depth of anaerobic sand and compactness were recorded. In addition, a water column integrated sample was collected for chlorophyll *a* biomass. Samples for phytoplankton pigment (Chl *a* and phaeopigment) analyses were collected via a tube water sampler which integrates a sample through the water column and then 2 litres was vacuum filtered onto a Whatman 25 mm glass fibre filters (GFF) for total Chl *a* (GFF, 0.7 µm nominal pore size). The 25 mm GFF filters were extracted in 90% acetone overnight and fluorescence measured on a Turner Designs model 10AU fluorometer (detection limit of 0.01 mg chl *a* m^{-3}) following Parsons et al. (1989) acidification technique. A wave height, wave direction and bottom root mean square velocity climatology is available for Marmion Lagoon and is derived from a fine resolution run of the Swan model for the period 2007/2008. These data were used to estimate comparative disturbance by wave forcing at the seabed at each site.

Twice in summer (2008/09 and 2009/10) and once in winter (2010) we collected 12 small 30mm cores from each of the stations. Where present, equal number of cores were collected from peaks and troughs of sand ridges to capture within site variability. The sediment plugs were transferred to small plastic vials and the sediment samples covered with water from the sampling location. The samples were held in the dark for at least 45 minutes to equilibrate and PAM fluorescence measurements performed using a Walz GmbH Phyto-PAM. So called “rapid light curves” were collected and the parameters ETRmax, (the light saturated, maximum rate of photosynthesis), Ik (Light intensity at beginning of saturation) and alpha (slope of the linear section of the P vs I relationship) generated. Light-emitting-diodes in the Phyto-PAM generate

chlorophyll fluorescence at four wavelengths (470, 535, 620 and 650 nm). The output is delineated into "brown" (diatoms), "blue" (cyanobacteria) and "green" (green phytoplankton) from the original 4-channel fluorescence data by comparison to previously stored reference excitation spectra. The data for the dominant group, the browns (diatoms) are presented here. The greens could not be quantified by the software for these samples. Water samples for pelagic nutrients and pelagic chlorophyll *a* were collected in Niskin bottles. Sediments were collected and analysed for grain size isotopic composition and organic C and total N as per the above methods.

Direct cell counts and cell size measurements were obtained from a $1cm^3$ subsample of wet sediment. Each subsample was transferred to a container with 8 ml of a sterile, prefiltered (0.2µm) solution of artificial seawater (ASW) containing 2% formaldehyde. Samples were mixed vigorously and stored at $4^{\circ}C$ in the dark until analysis (see below). Cell counts were made as soon as possible, usually within 2 months and always within 6 months. Cell counts were determined using a dual staining technique with acridine orange and DAPI stains as well as epifluorescence microscopy for marine sediments, as described by Deming et al. (1997). The sample, already diluted five-fold upon fixation was diluted further by 100 fold in ASW, treated with Triton-X detergent, and stained with acridine orange (0.01%) for 3min. The sample was then filtered onto a 25-mm, 0.2µm, prestained black Osmonics polycarbonate membrane filter (area=$200mm^2$), placed on top of a backing filter for support. A DAPI stain (20 $\mu g\ ml^{-1}$) was added after filtering to cover the membrane filter and allowed to stain for 15 minutes. Once the stain was drawn through, the filter was removed to a microscope slide, where it received a drop of high viscosity immersion oil. The slide was then covered by a glass cover slip. Fields were viewed immediately with a Nikon Optiphot microscope fitted with an epifluorescent light source and optical filter sets for acridine orange and DAPI. The microscope was calibrated using an E.R Bogusch measuring slide.

Observed organisms were classified into the following categories based on their differential staining properties and physical characteristics: Single celled autotrophic bacteria, filamentous autotrophic bacteria, phytoplankton, non-photosynthetic protozoa and metazoan and heterotrophic bacteria. The area occupied by organic detritus was also estimated in microns. Heterotrophic bacteria cell counts were made at a magnification of 400 times with a field of view of 0.5 mm^2 while all other counts were made at a magnification of 200 times with a field of view of 1 mm^2. At least four counts were made per slide. All counts were made by the same worker to avoid differences between researchers. Multiple slides from the same sediment sample were used to maintain consistency. One such slide was taken at the start of each counting session for comparison to previous counts. Four counts were made from each section with two sections obtained for each site. All bacterial counts were converted directly to g bacterial cm^{-2} using the factor of $10fg.C.cell^{-1}$(Bjornsen and Kuparinen, 1991; Deming and Carpenter, 2008). Confidence intervals for something were calculated using one way ANOVAs with the software package SPSS 17.0.

All macrofauna were sorted, identified or processed for identification by the Western Australian Museum and total wet weights of each species measured. Additionally, for the abundant large fauna *Archaster angulatus, Ammotropus arachnoides, Peronella lesueuri,* and *Cercodemas anceps* each individual was wet weighed and size measured (diameter of sand dollars, arm length of starfish and total length of holothurians). For these species a subsample of individuals encompassing the size range of the species were used to measure ash free dry weight (AFDW) as the difference between the dried (70ºC) and ashed (500ºC) weights of the individuals and a regression to wet weight and size performed. Regression showed in all cases the better estimate of AFDW was wet weight rather than length/diameter, with r^2 values

ranging 0.83 to 0.97. Hence, the wet weight of individuals of these species was used to calculate AFDW biomass.

4.2.2 Intensive investigations

Intensive investigations into of respiration or biological oxygen demand, primary production by BMA, microbial nitrogen dynamics and rates of sediment nutrient efflux were conducted in summer (November- December 2009) and winter (August 2010). Production by the BMA community was determined by generating production (via oxygen evolution) versus irradiance curves, the P vs I relationship is an important component of our biogeochemical models. At six of the stations, Marmion Outfall (the northern most station), BB (a mid shelf station within Marmion Lagoon), City Beach (located between Marmion lagoon and Cockburn Sound), Cockburn (in the north of Cockburn Sound), Southern Flats (in the south of Cockburn Sound) and Northern Harbour (a small boat harbour in the north of the sound) we collected twenty four 9.3cm ID sediment cores (one station occupied on each day in the filed). The cores were collected from a small area of sea floor location to reduce the effect of spatial variations on larger scales. However, if sand ridges were present, cores were evenly distributed between the ridge peaks and troughs to average out this potential source of variability. Cores were returned to the laboratory and randomly distributed into four tubs (i.e. 6 cores per tub) with a continuous flow of clean ambient seawater (6 litres per minute). The cores in each tub represented replicates of a light intensity treatment. In all, there were 8 intensities investigated at each station (7 different light intensities and one dark incubation) achieved by conducting incubations on sequential days using the same cores.

Each experimental tub was illuminated by a metal halide lamp. Light exposure was varied using neutral density film sufficient to achieve a range of nominal light intensities up to 1200 μmol quanta m^{-2} s^{-1}. Light readings were taken with a Licor PAR meter equipped with at two pi PAR sensor at the beginning and end of each incubation experiment and the irradiance used in the calculations represents the average of these two measurements. Heavy black plastic was wrapped around the tub containing the cores required for the dark treatment.

At the beginning of the incubation, each of the cores was sealed with a clear acrylic lid. The lid had two ports, one for sampling the other to allow the resupply of water from surrounding water as each sample was collected. The water inside the core was stirred gently by a 4cm Teflon coated magnetic stirrer bar suspended under the lid and driven by a small electric motor. Soon after each core was sealed a 30ml sample of water was collected for dissolved oxygen analysis and further 35 ml sample of water was collected from each core for dissolved nutrient analyses. These initial samples represent the starting conditions for the incubation. Two further samples were collected from each core at regular intervals during the incubation. After the incubation was complete the caps were removed and the system left until the next morning when the same routine was repeated for the further light intensity treatments. After the final sampling the length of the sediment plug and overlying water column were measured and the sediment stored frozen for later geochemical analysis (chlorophyll *a*, sediment grain size, sediment moisture content, and sediment POC/PON).

Rates of production and nutrient fluxes were calculated as the slope of the solute versus time relationship, normalised by the overlying water volume. Corrections were made for the replacement water taken from the ambient water tank. Gross rates of oxygen production (production independent of concurrent respiration) were calculated by subtracting the rate of oxygen consumption at zero irradiance (dark flux) from the positive rates of oxygen evolution (light flux). Production by the BMA community was determined by generating production

(expressed as oxygen evolution). A trend line was fitted to the data using nonlinear curve fitting techniques and the equations of Platt et al. (1980) if photoinhibition was evident or Webb et al., (1974) if it was not.

Pathways of nitrogen cycling in sediments across the nutrient gradient were investigated using cutting edge molecular techniques developed by CSIRO (see Abell et al. 2010). By examining the abundance and diversity of different nitrifying (ammonia oxidising archea hereafter AOA and ammonia oxidising bacteria here after AOB) and denitrifying (nirS and nirK) phylotypes we can assess the relationship between the dominant nitrifiers or denitrifiers.

4.3 Results and Discussion

4.3.1 Water column and physical forcing characteristics at sampling sites

Water column nutrients

Water column nutrients at the study sites reflected local influences (see Figure 4.3). Silicate was highest in the estuarine Swan River (12 µM) site while among the marine sites the Marmion Outfall and Northern Harbour sites (both > 2 µM) had the highest silica reflecting high levels of freshwater input. Phosphate was very high at the Marmion Outfall site (0.9 µM) with few other sites above 0.2 µM. The Swan River and Northern Harbour had ammonia levels above 0.3 µM). All other sites were between 0.05 and 0.15 µM). The Marmion Outfall site had the highest nitrate+nitrate level (3.2 µM) while most sites had nitrate+nitrate levels of <0.2 µM). Only two other sites, Northern Harbour and one of the mid lagoon Marmion sites (MM1) had nitrate/nitrate levels above 1 µM. These data represent a comparative snapshot during late summer/early spring in 2010 and it needs to be recognised that water column nutrients and chlorophyll (see below) can vary greatly over time. However the high values of nutrients and chlorophyll at Northern Harbour and Marmion outfall are consistent with regular monitoring undertaken by the the Water Corporation (see http://www.watercorporation.com.au/p/ploom.cfm) and the Cockburn Sound Management Council(see http://portal.environment.wa.gov.au/portal/page?_pageid=513,1&_dad=portal&_schema=PORTAL)

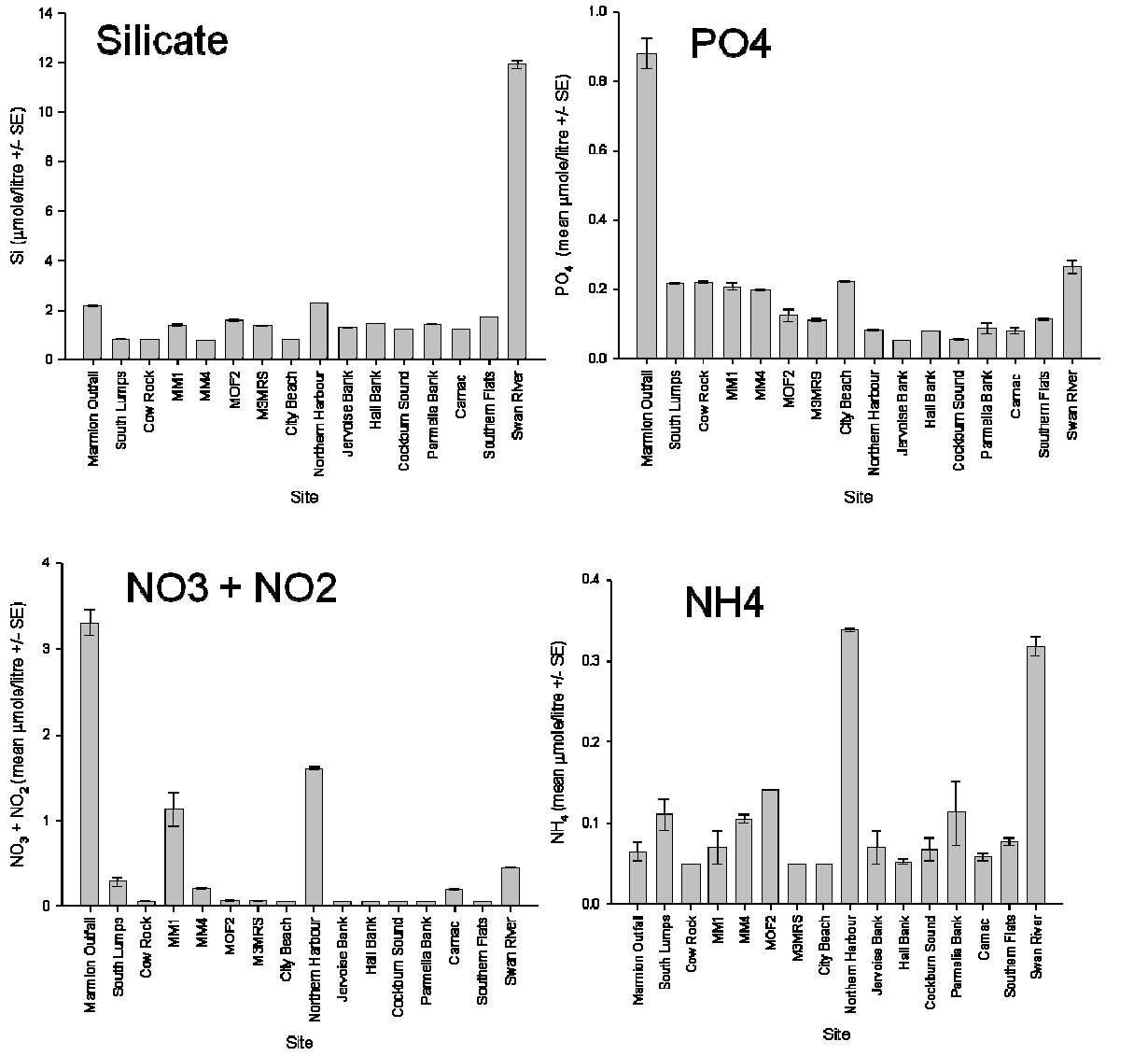

Figure 4.3. Water column nutrients collected at the sampling sites in 2010. Error bars are standard errors from two samples.

Water Column Chlorophyll a

Results of chlorophyll *a* and phaeopigments for water column integrated samples are given in Figure 4.4. Northern Harbour had significantly greater concentrations of both compared to all other ocean sites examined (mostly < 1 mg Chl a per m^3) except Southern Flats in 2010 which was the only other site which exceeded 2 mg chl a per m^3, however levels in the Swan River were also high. In 2010 chlorophyll *a* exceeded 2 mg per m^3 in the Southern Flats site. All locations of Marmion Marine Park had similar pigment concentrations (Table 4.3). Variability in concentrations within the mid location were due to variability between all samples, whereas the variability in chl. *a* in the outer location in 2008 was the result of one site with a much larger concentration (M3MRS).

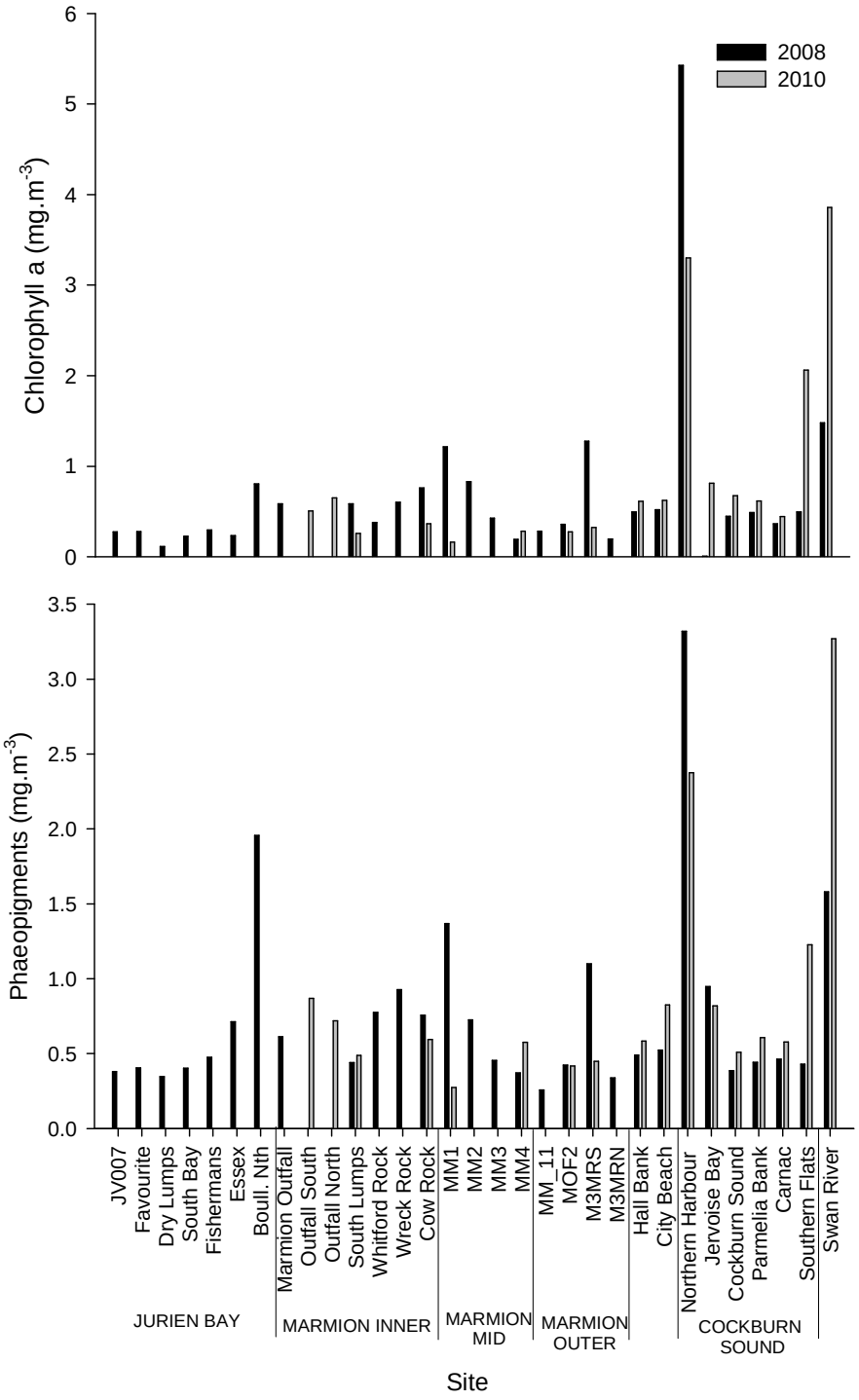

Figure 4.4. Concentrations of chlorophyll a and phaeopigments from water column integrated samples collected from each site in 2008 (dark) and 2010 (light).

Table 4.3. Pigment concentrations within Marmion Marine Park locations (sites pooled) (mean ± S.E.) sampled in 2008 and 2010.

	Chlorophyll *a* (mg.m^{-3})		Phaeopigments (mg.m^{-3})	
	2008	2010	2008	2010
Marmion inner	0.58 ± 0.06	0.45 ± 0.09	0.70 ± 0.08	0.67 ± 0.08
Marmion mid	0.67 ± 0.23	0.22 ± 0.06	0.73 ± 0.23	0.42 ± 0.15
Marmion outer	0.53 ± 0.25	0.30 ± 0.02	0.53 ± 0.19	0.43 ± 0.02

Light attenuation

Figure 4.5 shows that the lowest levels of light attenuation (clearest water, k<-0.15,) were in the offshore sites of MM_11, M3MRS, M3MRN at Marmion and at Carnac Island, while the most turbid sites were Northern Harbour (k=-0.37 and in the Swan River (-0.41). Two sites in the Marmion lagoon had very high levels of light attenuation, Wreck Rock and MM2.

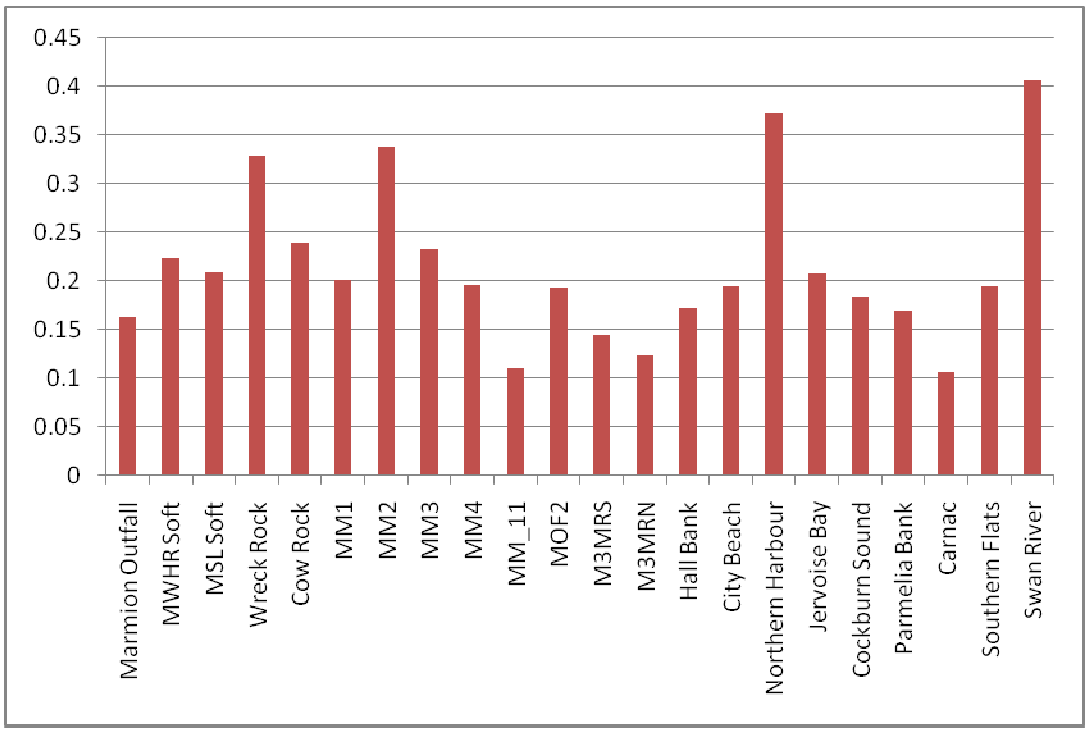

Figure 4.5. Light attenuation coefficients (-k) at each sampling site measured during 2010 sampling trips.

Wave exposure

Wave exposure was estimated at the Marmion sampling sites only using the SWAN model (see model output in Figure 4.6) and the yearly average u_{rms} (root mean square velocity at the seabed) as determined from the Swan model are shown in Table 4.4. The inshore sites had on average the lowest annualised seabed velocity (1.65 m s^{-1}) while the mid (0.24 m s^{-1}) and

offshore (0.23 m s^{-1}) lagoon sites were higher reflecting the relative levels of wave exposure. Estimates were not available for Cockburn Sound.

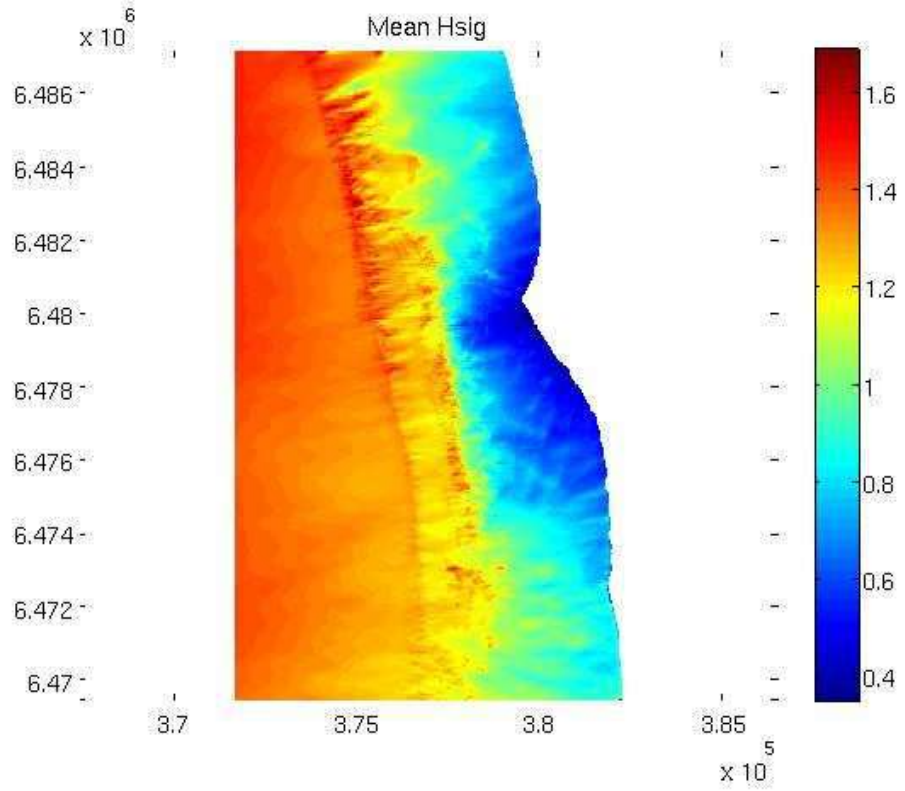

Figure 4.6. Swan model output for the Marmion Region used to estimate relative exposure to bottom forcing from wave forcing at the sampling sites. Hsig is the significant wave height (m) shown in the vertical coloured bar.

Table 4.4. Yearly average urms (root mean square velocity at the seabed) as determined from the Swan model (Figure 4.3) for the sampling sites in the Marmion lagoon.

Location	Site	u_{rms} (m s^{-1})	Location mean u_{rms} (m s^{-1})
Marmion inshore lagoon	SouthLumps	0.174	0.165
	WhitfordRock	0.165	
	WreckRock	0.156	
	CowRock	0.157	
	Outfall	0.171	
Marnion mid-lagoon	MM1	0.205	0.239
	MM2	0.261	
	MM3	0.303	
	MM4	0.185	
Marmion offshore lagoon	MOF2	0.260	0.232
	MM_11	0.205	
	M3MRS	0.229	
	M3MRN	0.236	

Key Findings:

Water column physical and water quality parameters can be summarised as follows:

- **Silicate was highest at the three sites expected to have freshwater influence (>2 micromoles per litre at Northern Harbour and the Marmion outfall and >12 in the Swan River)**
- **Phosphate was four times higher at the Marmion outfall (0.8 micromoles per litre) than any other site except the Swan River (0.3)**
- **Nitrite and nitrate was highest at the Marmion outfall (>3 micromoles per litre). Most sites were less than 0.5 except MM1 in the Marmion lagoon (1.1) and Northern Harbour (1.6)**
- **Ammonia was highest (> 0.3 micromoles per litre) in Northern Harbour and Swan River. Most other sites were about 0.1 or less.**
- **Water column chlorophyll varied between sites but can be generalised as being low (<0.5 mg per m^3)at most of the Jurien Bay and Marmion mid and outer lagoon sites, moderate (0.5 - 1.0) at the Marmion inshore and most Cockburn Sound sites and very high 2.0 – 5.0 in the Swan River, Northern Harbour and at Southern Flats in 2010.**
- **The most modified environments of Swan River and Northern Harbour has the highest levels of light attenuation (>-35) and four of the five offshore sites in Marmion lagoon and Carnac Island had the lowest light attenuation (<-0.15)**
- **Modelling of wave forcing at the seabed showed that the inshore sites were considerably more protected than either the mid or outer lagoon sites**

4.3.2 Sediment characteristics at sampling sites

Sediment Grain Size

Sediments at all sites were dominated by particles in the range of 125µm to 500µm sieve size classes (Table 4.5). At sites within Cockburn Sound and the Swan River sediments were dominated by 250µm grain size class, while at sites in the outer Marmion Marine Park (Marmion Outer) and in the Port Beach and City beach locations sediments were dominated by larger particles in the 500µm sieve size class. Figure 4.7 indicates that samples of the Port Beach/City beach location were composed of more particles at least 8.0mm in size compared to other localities, with a mean of 12% of the overall sample weight. This proportion is a result of the Port Beach samples only, which comprised large rocks (comprising limestone, shell rubble and coral rubble) not found anywhere else.

The size distribution of particles was more heterogeneous at sites in Jurien Bay, and the inner and mid areas of Marmion Marine Park. At the shallower inner Marmion sites sediments were dominated by both 125 and 250µm size classes, while at sites in the mid Marmion location overall had slightly larger overall size with modes of 250 and 355µm. Jurien Bay sediment had the greatest heterogeneity with multimodal distribution across the 125µm to 500 µm size classes.

In general, locations which were more sheltered from swell (e.g. Swan River, Cockburn Sound sites and Marmion inner lagoon sites) had finer grain sizes than more exposed sites (e.g. Marmion outer lagoon) (see Figure 4.5). However at the site level within locations there was

considerable variability and when we compare wave induced turbulence at the seabed as predicted from the SWAN wave model for sites within each of the three Marmion locations (Table 4.4) with the average (between site, within location) sediment grain mode size or the sediment grain mode size for pooled sites within locations there is no significant relationship (regression analysis, r^2=0.134, p=0.218 and r^2=0.125, p=0.236 respectively, n=12).

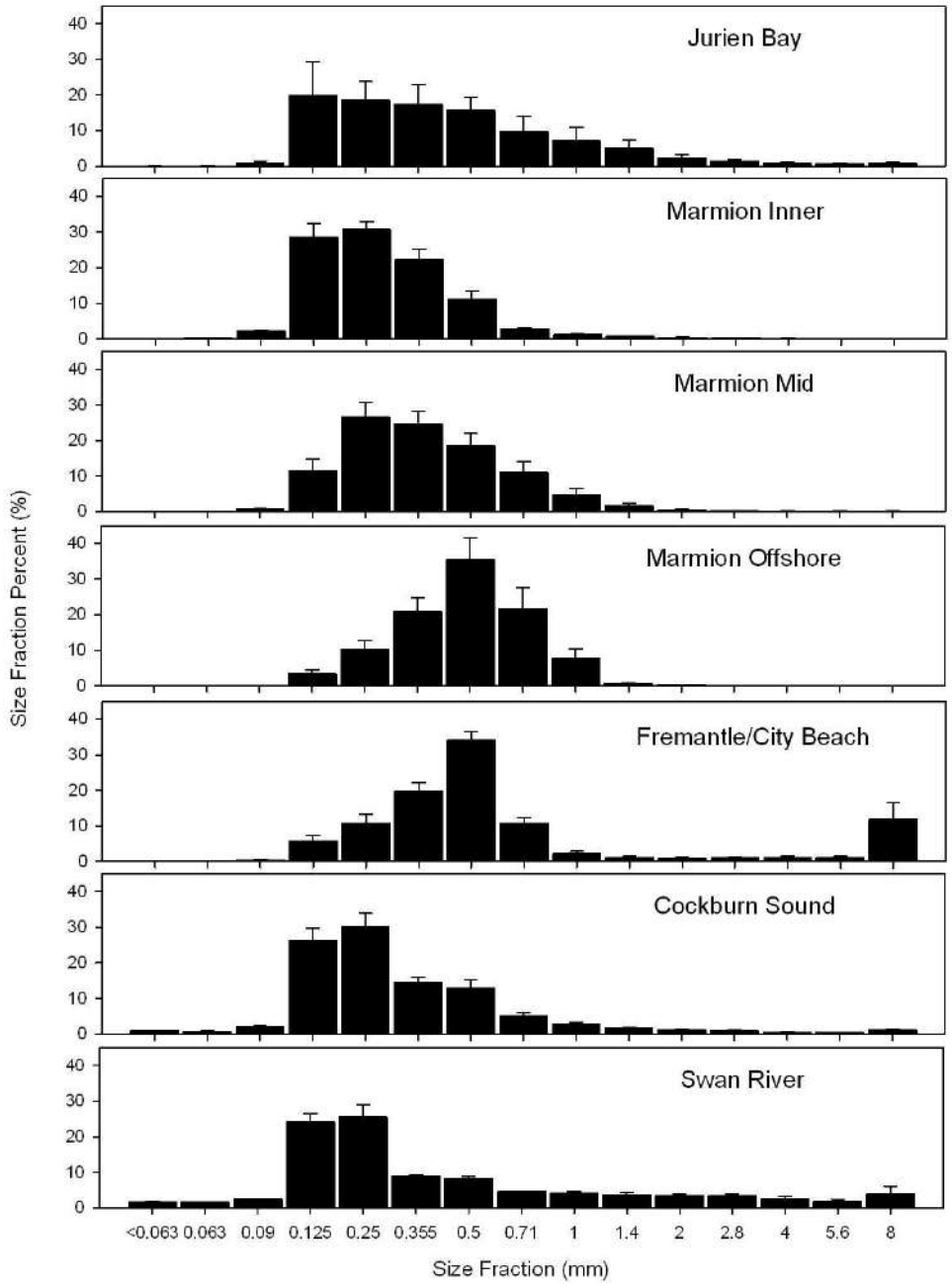

Figure 4.7. Sediment grain size fractionation for grouped sites within locations (5 replicates at each site) sampled in 2008. Means and standard errors are from pooled sites within locations.

Table 4.5. Modes and medians of sediment grain size fractionation. Multiple modes within locations are due to site differences within those locations.

	Mode(s)	Median
Jurien Bay	0.125, 0.25, 0.355, 0.50	0.355
Marmion Inner	0.125, 0.25	0.25
Marmion Mid	0.25, 0.355	0.355
Marmion Offshore	0.50	0.50
Fremantle/City Beach	0.50	0.50
Cockburn Sound	0.25	0.25
Swan River	0.25	0.25

Other characteristics of sites and sediment

The appearance of the sediments from some sites is shown in Figure 4.8 and indicates the range of sediments sampled from coarse and fine sands and high and low organic loads. Measurements of anaerobic layer depth at each site (see Table 4.5) revealed that at the Jurien and Marmion Outer sites the anaerobic layer is absent or deeper than could be detected when the 10 cm core was taken. At Marmion inner sites the anaerobic layer depth was between 3 and 10 cm while at Cockburn Sound sites it was only 1 to 2 cm except at the most offshore site of Carnac Island (>10cm). In the Swan River there were anaerobic sediments almost to the surface layer (<1cm). Sand ripple heights ranged from 0 to 25 cm between sites (see Table 4.6) reflecting the range of wave exposures. As would be expected the well washed sands and exposed sites generally had no anaerobic sediments.

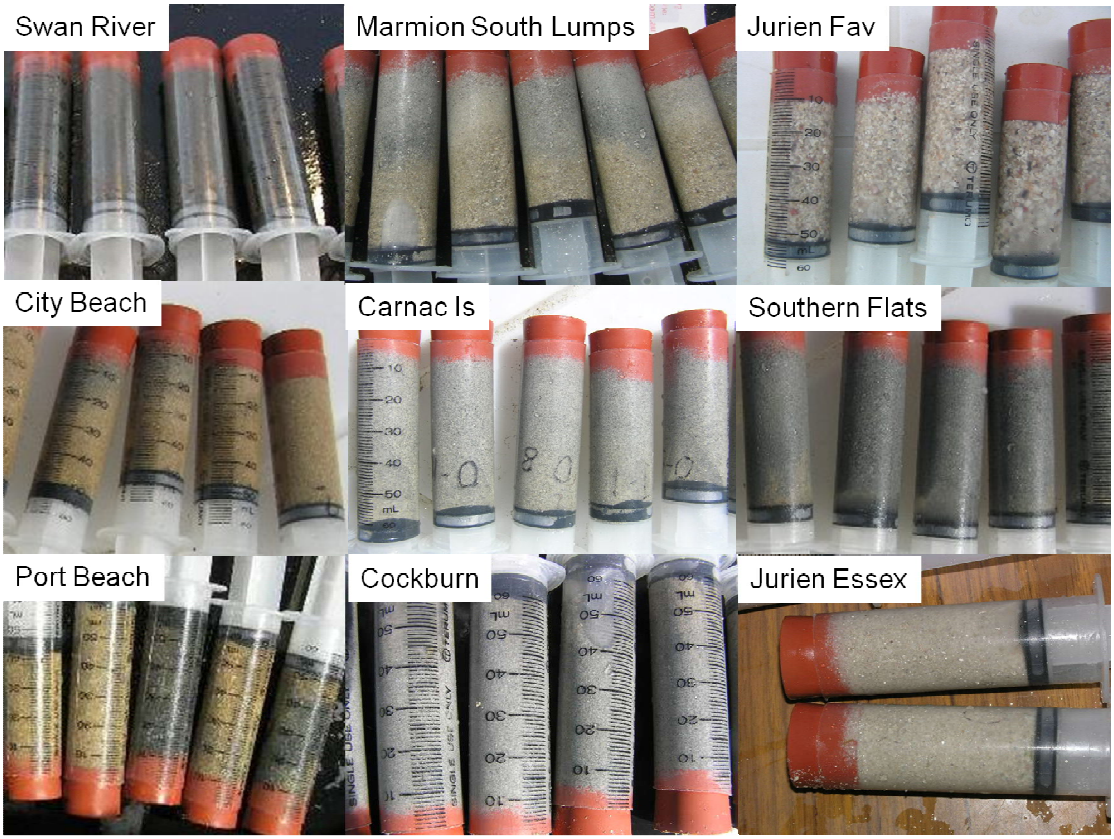

Figure 4.8. Examples of the range of appearance of sediermtns sampled ranging from coarse to fine sands and high and low organic loads.

Table 4.6. Depth and sediment appearance characteristics measured for each site in 2008 and 2009. na denotes not available

Location	Site	Depth (m)	Anerobic sand depth (cm)	Sand ripple height (cm)	Sand compacted?
Jurien Bay	JV007	8.6	none (>10)	3 to 5	yes
Jurien Bay	Favourite	6.2	none (>10)	10 to 15	no
Jurien Bay	Dry Lumps	8.3	none (>10)	10 to 15	no
Jurien Bay	South Bay	5.5	none (>10)	10 to 15	no
Jurien Bay	Fishermans	5.1	none (>10)	2 to 5	slightly
Jurien Bay	Essex	3.5	none (>10)	na	slighty
Jurien Bay	Boullanger North	2.8	none (>10)	na	na
Marmion inner	Marmion Outfall	10	4	5 to 10	no
Marmion inner	South Lumps	7	3	2 to 5	yes
Marmion inner	Whitford Rocks	8	none (>10)	3 to 5	yes
Marmion inner	Wreck Rock	6.5	some none (>10) , some from 3	0 to 2	yes
Marmion inner	Cow Rock	6	5	2 to 5	no
Marmion mid	MM1	11	5	0 to 2	yes
Marmion mid	MM2	8	10	2 to 5	slightly
Marmion mid	MM3	4	3	5 to 10	no
Marmion mid	MM4	9	none (>10)	10 to 15	no
Marmion outer	MM_11	14	none (>10)	20 to 25	no
Marmion outer	MOF2	15	none (>10)	2 to 5	no

Location	Site	Depth (m)	Anerobic sand depth (cm)	Sand ripple height (cm)	Sand compacted?
Marmion outer	M3MRS	14	none (>10)	10 to 15	no
Marmion outer	M3MRN	15	none (>10)	15 to 20	no
Fremantle	Hall Bank	9	2	0 to 2	no
Fremantle	City Beach	8	10	7 to 10	no
Cockburn Sound	Parmelia Bank	7	?	0 to 2	no
Cockburn Sound	Northern Harbour	6	1	none (0)	na
Cockburn Sound	Jervoise Bank	8	1.5	none (0)	yes
Cockburn Sound	Cockburn Sound	7	2	0 to 2	no
Cockburn Sound	Carnac Island	7	none (>10)	3 to 5	yes
Cockburn Sound	Southern Flats	7	1	0 to 2	slightly
Swan River	Swan River	6	<1	none (0)	slightly

Organic matter content of sediment

The organic matter content of sediments varied from 3mg per gram of sediment dry weight at one of the offshore Marmion sites to 47mg/g at Northern Harbour (Figure 4.9). In general the Cockburn Sound Sites (excluding Northern Harbour) were significantly more enriched (21-40 mg/g) when compared to Marmion offshore lagoon (4-17 mg/g), Marmion mid lagoon (20-27 mg/g) and Marmion inshore (9-20 mg/g). The Marmion outfall and Swan River sites site had high organic matter contents of 27mg/g and 30 mg/g respectively.

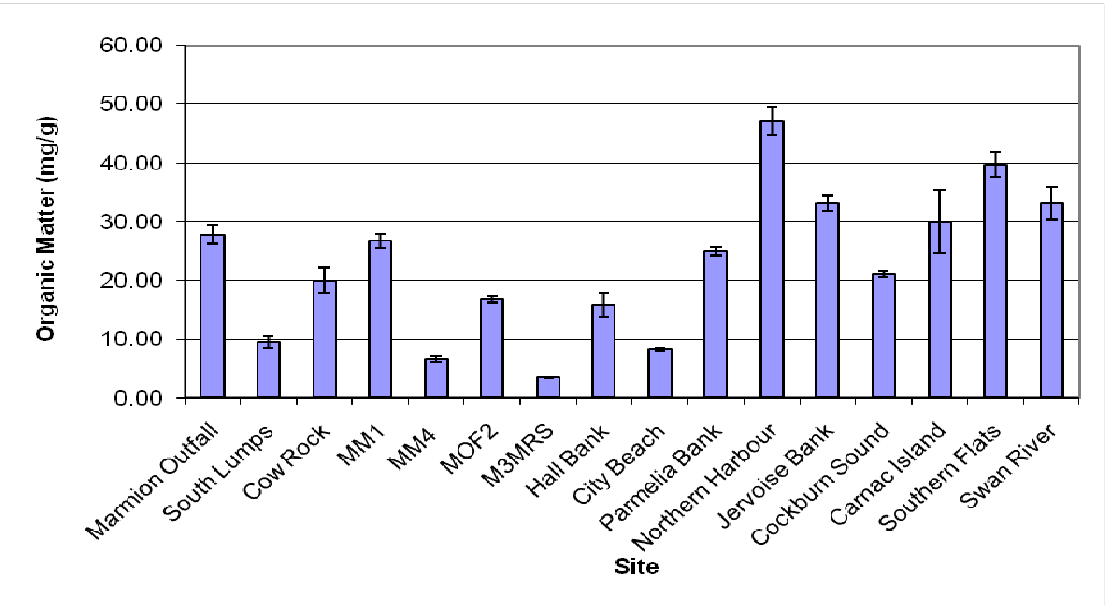

Figure 4.9. Organic content of sediment from each site sampled in 2010. Means and error bars are from 2 samples per site.

Total sediment nitrogen

The nitrogen content is given in Figure 4.10 and nitrogen isotope ratios (relative to N_2 in air) are given in Figure 4.11. For both measures, quantities in the two sediment depth layers (0-2 and 2-5cm) were similar. Jervoise Bank, Southern Flats and Northern Harbour (2010) in Cockburn Sound and the site in the Swan River all had much greater nitrogen concentrations (0.06 to 0.12 %) than other sites. Port Beach, City Beach and some of the outer sites in Marmion Marine Park all had less nitrogen content than other sites. The remaining sites had nitrogen contents of approximately 0.02 to 0.04%.

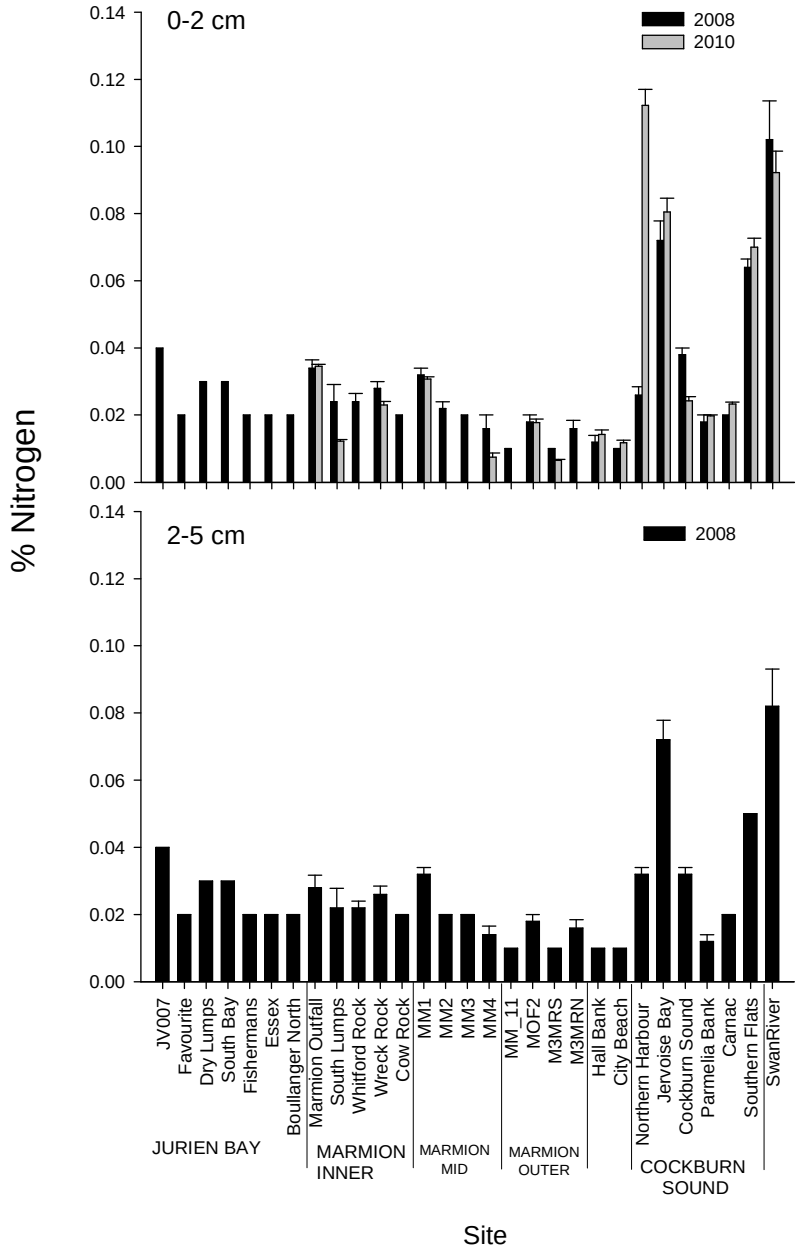

Figure 4.10. Percent nitrogen in sediment samples collected in 2008 and 2010.

Nitrogen isotopes

$\delta^{15}N$ in the 0-2cm sediment layer ranged from 4.4 at Fishermans, Jurien in 2008 to 8.9 at City Beach in 2008 (Figure 4.11). For most locations studied, there were similar amounts of variation between sites. However, sites in the Marmion Outer location showed little variation. Low $\delta^{15}N$ at Jurien Bay are likely to relatively low input of anthropogenic nitrogen, which tends to have higher $\delta^{15}N$ (e.g. sewage sources have δN^{15} values of +8 to +20 and agricultural fertilisers have values of -1 to +2, e.g. Kendall 1998). Treated sewage effluent from the Marmion outfall has been measured to produce $\delta^{15}N$ of as high as 25 (range 13-25) by Gartner et al. (2002). $\delta^{15}N$ in marine sediments can be expected to reflect the $\delta^{15}N$ of the source of detritus in the sediment and any fractionation that occurs as the detritus is recycled and broken down. The high value at the city beach site in 2008 is probably indicative of an anthropogenic source, perhaps derived from stormwater drains in the area.

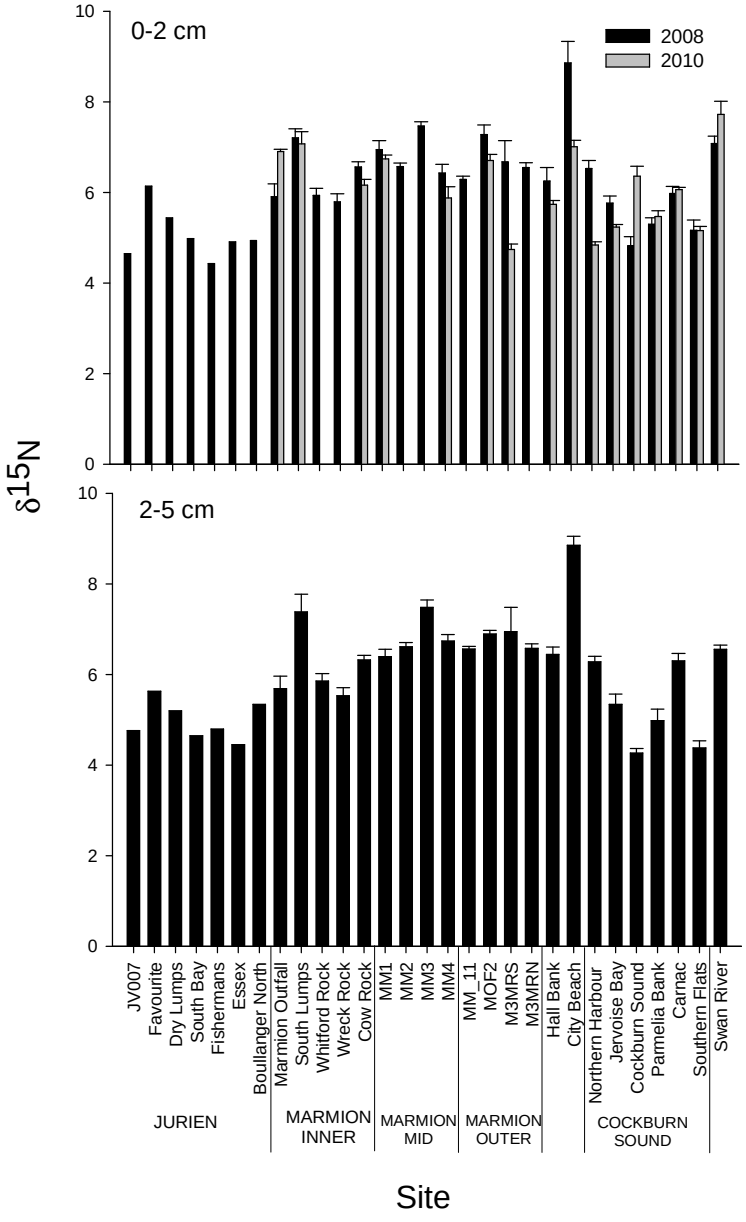

Figure 4.11. δNitrogen 15 stable isotope analysis of sediment samples collected in 2008/2009 and 2010

Sediment organic carbon

Organic carbon levels varied between sites and between years (Figure 4.12). The lowest levels, generally <0.1% were at Jurien Bay. The Swan River and Northern Harbour sites were the highest (0.6-1% and 0.3-0.7 % respectively). The only other sites to exceed 0.2% organic carbon content were Southern Flats and Jervoise Bank in Cockburn Sound, Port Beach and one site in each of the Marmion mid lagoon and Marmion offshore lagoon locations.

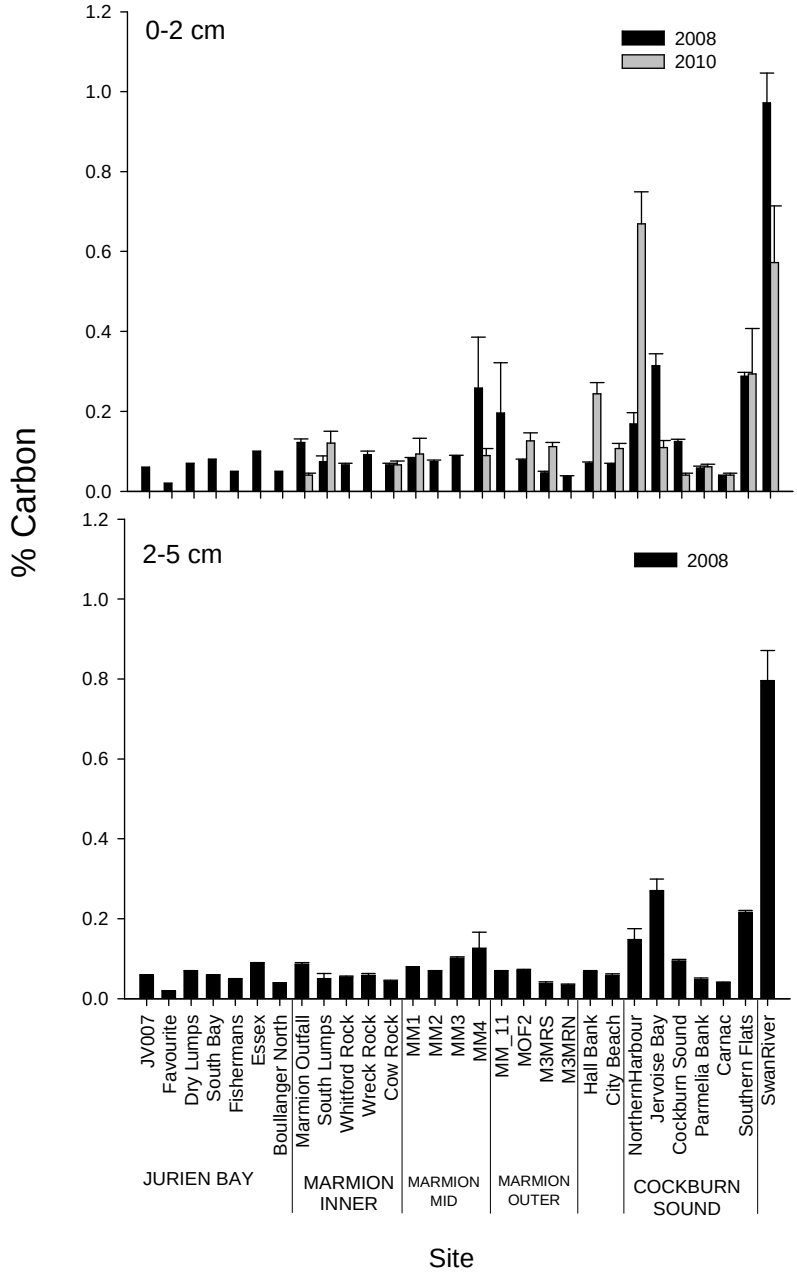

Figure 4.12. Organic carbon content of sediment (calculated as a percentage of dry weight) sampled in three times, once in the summer of 2008 and again in summer 2009 and then in winter 2010. Error bars are standard error n = 3.

Sediment carbon isotopes

There was little variation in $\delta^{13}C$ ($\delta^{13}C$ = [(13C/12C in sample)/(13C/12C standard)]*1000 relative to a standard with 13C:12C ratio (0.0112372 or ~ Pee Dee Belemnite) content of sediment between sites and within sites between years (Figure 4.13). The $\delta^{13}C$ values were mostly -20 to -25‰ suggesting that macroalgae is an important source of carbon stored in sediments rather than seagrass or phytoplankton which typically have $\delta^{13}C$ signatures less than -20 (O'Leary 1988). However, little is known of the diagenesis of primary producer derived carbon in sediments (Macko and Estep 1984), and so this inference is relatively weak. Indeed the $\delta^{13}C$ value for sediment deeper than 2cm was on average 3.5% less (X= -21.09) than shallower sediment (X= -20.34). This is a statistically significant difference (paired t-test=4.587, p=0.0001), suggesting that burial and the diagenetic process may alter $\delta^{13}C$ values in marine sediments.

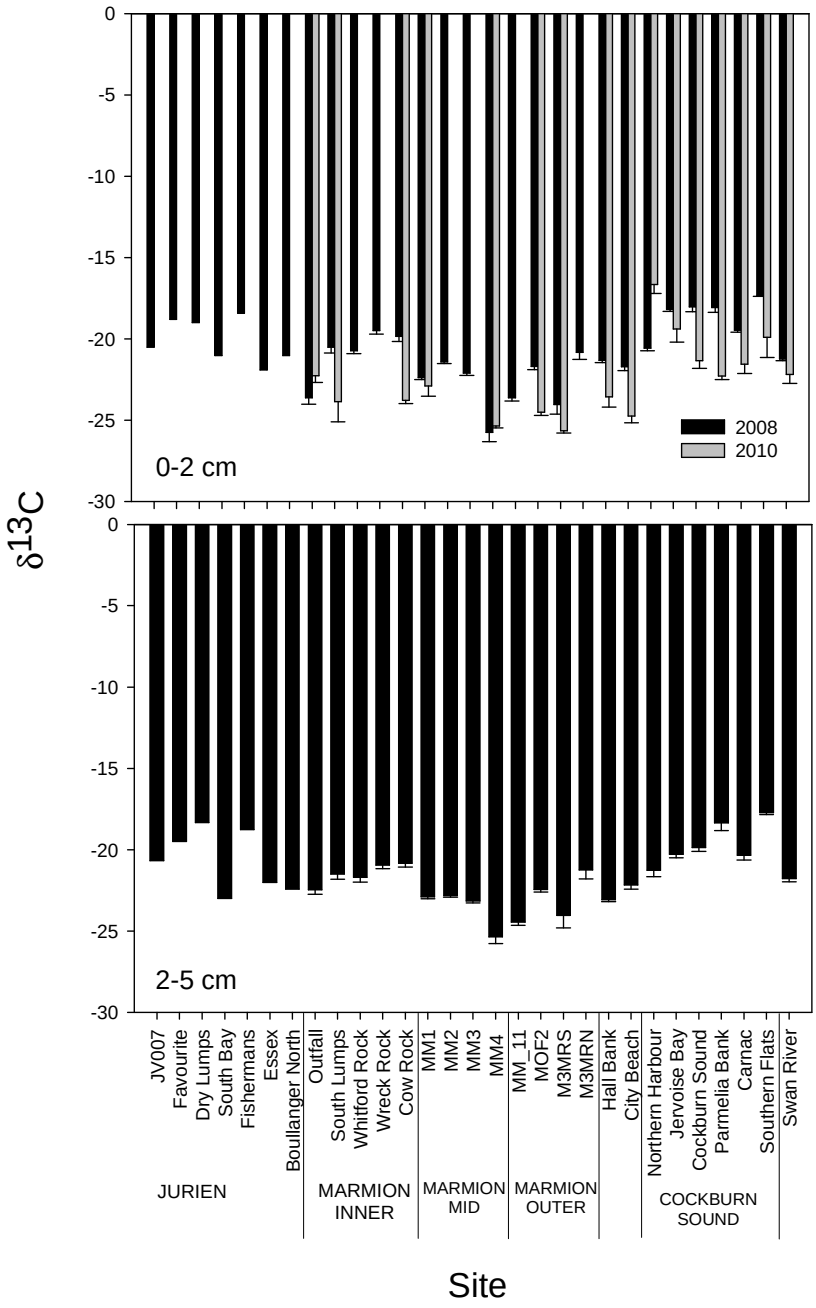

Figure 4.13. Carbon 13 isotope ($\delta^{13}C$) content (‰) of sediments sampled in 2008/2009 and 2010.

Benthic Microalgae (BMA)

The chlorophyll *a* content for all sites sampled in 2008/9 has been determined, as shown in Figure 4.14 and Figure 4.15 (see Figure 4.19 and Figure 4.22 for 2010 data). The mean chlorophyll *a* concentrations in the surface 0-2 cm deep samples ranged from 4 $mg.m^{-2}$ to 126 $mg.m^{-2}$, while in the deeper 2-5cm deep samples chlorophyll *a* ranged from 1 $mg.m^{-2}$ to 97 $mg.m^{-2}$. These values are consistent with those observed in sediments across a range of other studies (see Cahoon 1999). Results demonstrate that over this shallow depth range most of the variability in *a* biomass was not associated with water column depth (Figure 4.16) in contrast to comparisons across much greater depth ranges (e.g. see chapter 3). From this we conclude that

different processes are important in determining BMA biomass in near shore regions of the continental shelf. In south-western Australia BMA biomass has also been associated with water column nutrients and shelter/wave impact (Kendrick et al. 1998, Forehead 2006). Our study was conducted over a much wider range of locations and water column nutrient levels and we did not find this relationship (see Figure 4.17 in a regression analysis with $r^2<0.001$, p=0.919. We did however find a significant relationship between BMA biomass and wave forcing estimates at the seabed as estimated from the SWAN model for the Marmion sites (see Figure 4.18) $r^2=0.429$, p=0.015. We do have wave forcing estimates for the non-Marmion sites. Both these findings show what might be expected, that a range of factors are important in determining BMA biomass in shallow coastal waters.

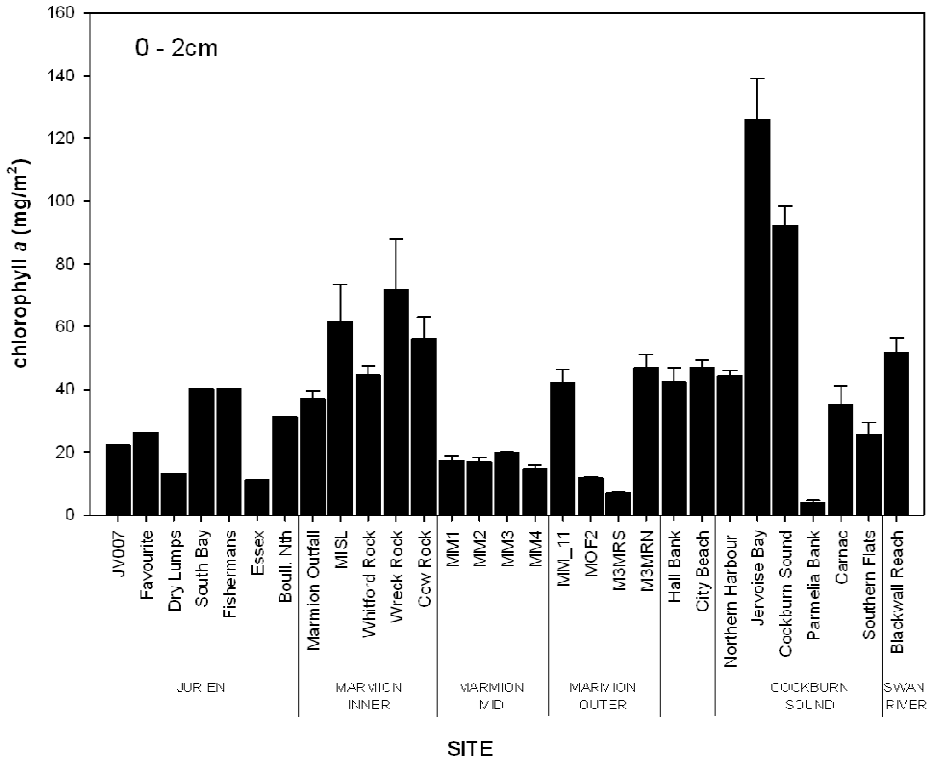

Figure 4.14. Chlorophyll *a* concentration of 2008/2009 sediment samples 0-2cm depth (mean ± S.E. n = 5).

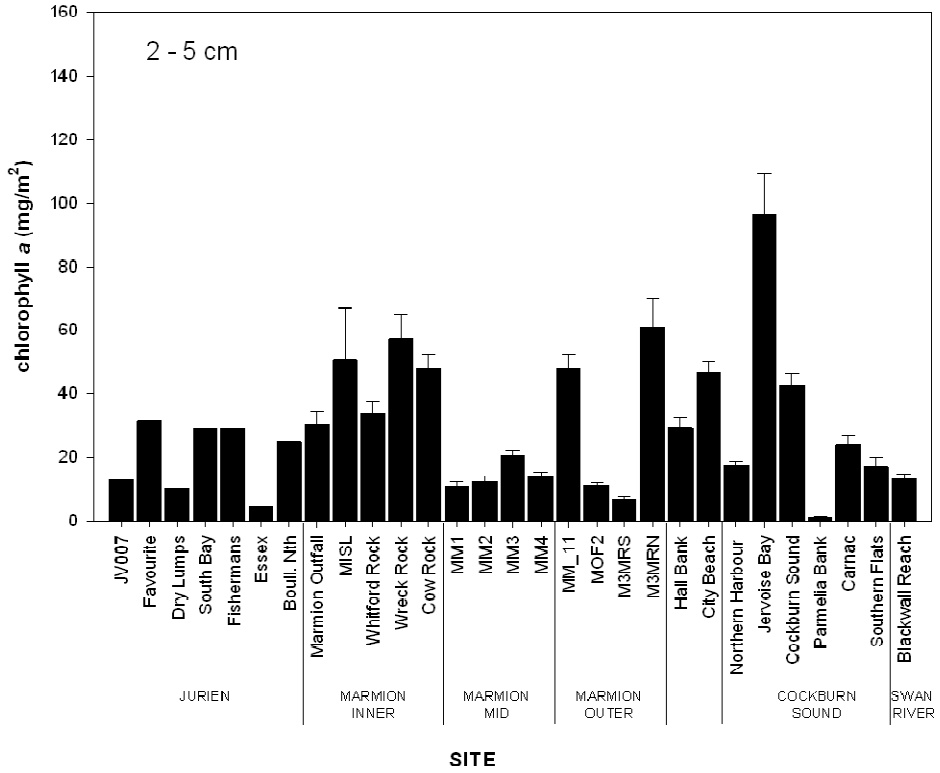

Figure 4.15. Chlorophyll *a* concentration of 2008/2009 sediment samples 2-5cm depth (mean ± S.E.).

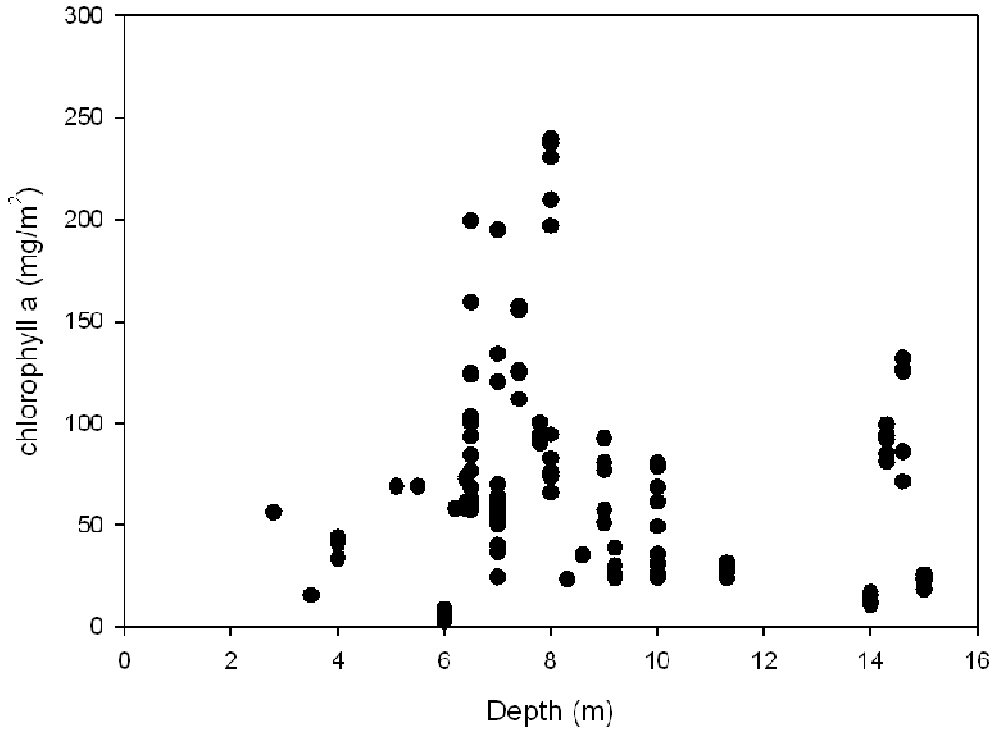

Figure 4.16. Chlorophyll *a* biomass (0-5 cm sediment depth) as a function of water column depth from samples taken in 2008.

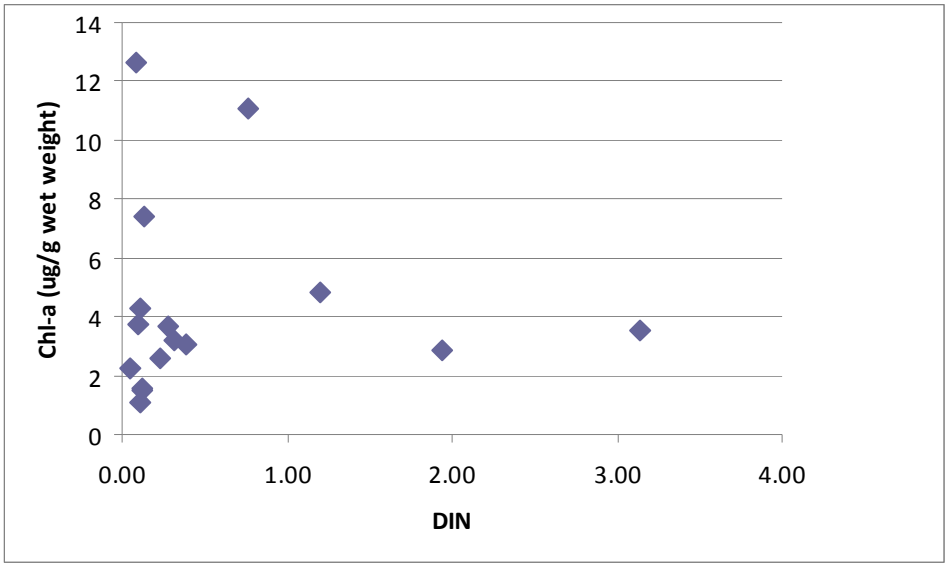

Figure 4.17. Relationship between water column nutrients and BMA biomass for sites sampled in 2010 DIN is micromoles per liter.

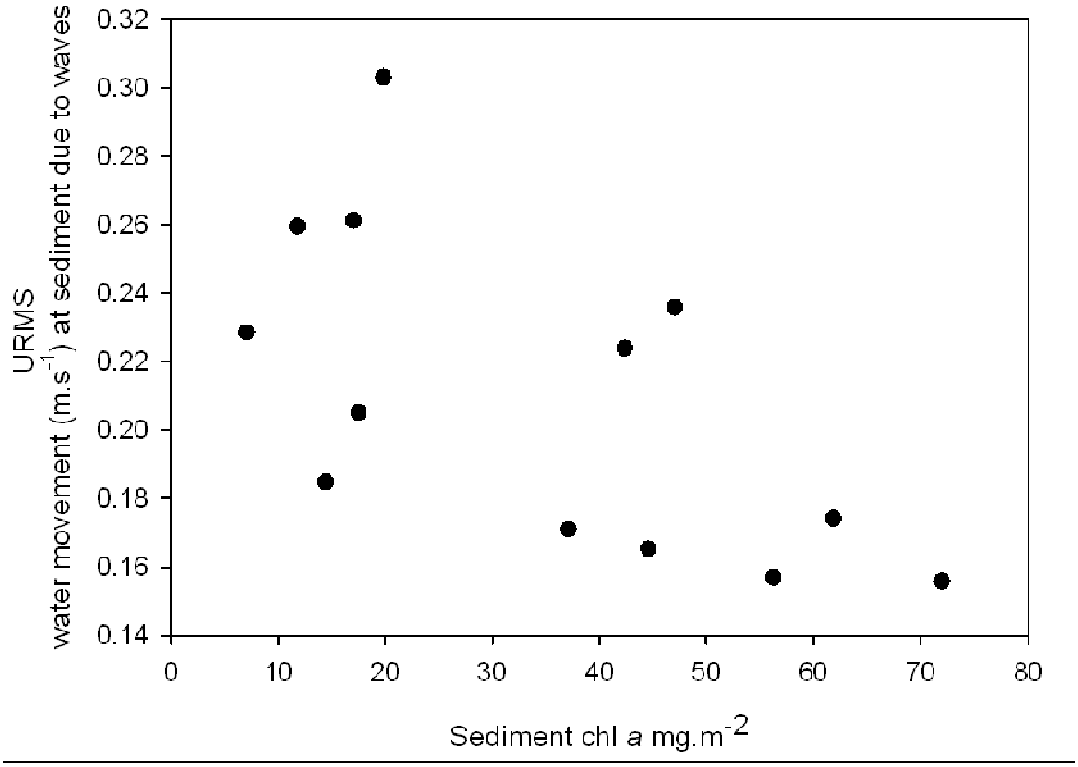

Figure 4.18. Relationship between wave forcing at the seabed and BMA biomass for sites sampled in 2008.

Sediment chlorophyll a as a function of sediment depth

We found somewhat surprisingly that photosynthetic pigments could be detected deep within the sediment. This is very different from conventional literature on BMAs which are mostly from the much different sediments found in the northern hemisphere (eg. Cahoon 1990). The deeply buried BMA biomass has a range of implications for primary production potential and raises questions about the mobility of microalgae in sediments. Chlorophyll *a* and Phaeopigment concentrations generally fell with increasing depth from 0-1cm to 3-4cm. From 3-4cm concentrations of chlorophyll *a* were relatively stable. There were some exceptions to this pattern and a general description of the profile at each site is given below.

At Marmion Outfall chlorophyll *a* concentrations remained relatively high with increasing depth. Average chlorophyll *a* concentrations were 3.44 ug/g at 0-1cm compared to 2.04 ug/g at 9-10cm. Average phaeopigment concentrations were 2.43 ug/g at a depth of 0-1cm and 1.19 ug/g at a depth 9-10cm (Figure 4.19). Chlorophyll *a* and phaeopigment concentrations at South Lumps followed the observed pattern falling from 2.23 ug/g and 1.24ug/g at 0-1cm to 3-4cm with stable concentrations from 4-5 cm to 9-10cm at approximately (Figure 4.19). Like South Lumps, Cow Rock followed a pattern of a fall in chlorophyll *a* and phaeopigment concentrations from 0-1cm (chl-a: 2.86 ug/g, phae: 1.80 ug/g) to 3-4cm (chl-a: 1.96 ug/g, phae: 0.93ug/g) followed by a stable concentration from 4-5cm to 9-10cm (chl-a: 0.93ug/g and phae: 0.64ug/g) (Figure 4.19). Sediment chlorophyll *a* and phaeopigment concentrations at MM1 fell sharply from 4.68 ug/g and 2.40 ug/g at 0-1cm to 2.19 ug/g and 0.83 ug/g at 4-5cm. From 4-5cm to 9-10cm concentrations were generally stable (Figure 4.19). Average concentrations of chlorophyll *a* were 1.70 ug/g at 9-10cm while for phaeopigments average concentrations were 0.95 ug/g at the same depth.

At MM4 average chlorophyll *a* and phaeopigment concentrations fell from 2.30 ug/g and 1.41 ug/g at 0-1cm to 2.18 ug/g and 0.51 ug/g at 3-4cm. From 4-5cm to 9-10cm average concentrations were stable at approximately 1.28 ug/g and 0.76 ug/g at a sediment depth of 9-10cm (Figure 4.20). Only one replicate was obtained from MOF2. However, chlorophyll *a* and phaeopigment concentrations followed a general pattern observed at other sites. Maximum chlorophyll *a* and phaeopigment concentrations were observed at the 0-1cm depth at 2.36 ug/g for chlorophyll *a* and 1.29 ug/g for phaeopigments. Concentrations fell to 0.87 ug/g for chlorophyll *a* and 0.55 ug/g for phaeopigments at a depth of 4-5cm. From 4-5cm to 9-10cm they were stable with a final concentration of 1.25 ug/g for chlorophyll *a* and 0.85 ug/g for phaeopigments (Figure 4.20). Chlorophyll *a* and phaeopigment concentrations at M3MRS decreased with depth from 1.48 ug/g and 1.13 ug/g at 0-1cm to 0.79 ug/g and 0.63 ug/g at 9-10cm.

At Hall Bank concentrations varied but followed a general falling trend with the exception of the 2-3cm sample in Rep 1 which was sharply higher at 5.77 ug/g (Figure 4.20). At City Beach Chlorophyll *a* concentrations were 2.74 ug/g at 0-1cm, 3.86 ug/g at 2-3cm, 0.89 at 4-5cm and finally 0.17 ug/g at 9-10cm. Phaeopigment concentrations were 2.66 ug/g at 0-1cm, 2.00 ug/g at 2-3cm, 0.79 ug/g at 4-5cm and finally 0.26 ug/g at 9-10cm. Sediment chlorophyll *a* concentrations fell slightly from 2.97ug/g at 0-1cm to 2.26 ug/g at 9-10cm. Phaeopigment concentrations fell more steeply from 1.73 ug/g at 0-1cm to 0.77 ug/g at 9-10cm (Figure 4.21).

Moving south to the Cockburn Sound location, Parmelia Bank sediment chlorophyll *a* concentrations fell from an average of 1.13 ug/g at 0-1cm to 0.09 ug/g at 9-10cm. Phaeopigment concentrations fell from 1.00 at 0-1cm to 0.16 ug/g at 9-10cm. There was a sharp

rise in concentrations of 1.59 ug/g at 4-5cm in rep2 and 1.05 ug/g at 7-8cm in rep 1 (Figure 4.21). At Northern Harbour chlorophyll *a* concentrations fell from an average of 2.73 ug/g at 0-1cm to 0.61 ug/g at 9-10cm. Phaeopigment concentrations were relatively high at 6.48 ug/g at 0-1cm. These concentrations fell to an average of 2.13 ug/g at 9-10cm (Figure 4.21). Chlorophyll *a* concentrations were relatively high at Jervoise Bank with an average of 9.82 ug/g at a depth of 0-1cm. These concentrations fell to an average of 1.65 ug/g at 9-10cm. Phaeopigment concentrations were lower at an average of 4.70 ug/g at 0-1cm falling to an average of 1.25 ug/g at 9-10cm (Figure 4.21). At Cockburn Sound chlorophyll *a* and phaeopigment concentrations fell uniformly from an average of 1.98 ug/g at 0-1cm for chlorophyll *a* and 1.09 ug/g for Phaeopigments to 0.30 ug/g for both chlorophyll *a* and Phaeopigments at 9-10cm (Figure 4.22). At Carnac Island chlorophyll *a* concentrations fell sharply from 4.56 ug/g at 0-1cm to 1.76 at 3-4cm. Concentrations were stable at this level through to 9-10cm where they were 1.28 ug/g. Phaeopigment concentrations exhibited less of a depth gradient compared to chlorophyll *a* concentrations. Average phaeopigment concentrations were 1.15 ug/g at 0-1cm while they were 0.81 ug/g at 9-10cm (Figure 4.22). Chlorophyll *a* and phaeopigment concentrations followed a uniform pattern at Southern Flats. Average pigment concentrations fell sharply from 5.93 ug/g and 5.65 ug/g at 0-1cm to a low of 0.55 ug/g and 1.11 ug/g at 9-10cm (Figure 4.22). At Blackwall Reach in the Swan River, concentrations of chlorophyll *a* and phaeopigment concentrations fell from an average of 12.5 ug/g and 7.63 ug/g at 0-1cm to 0.43 ug/g and 1.73 ug/g at 9-10cm (Figure 4.22).

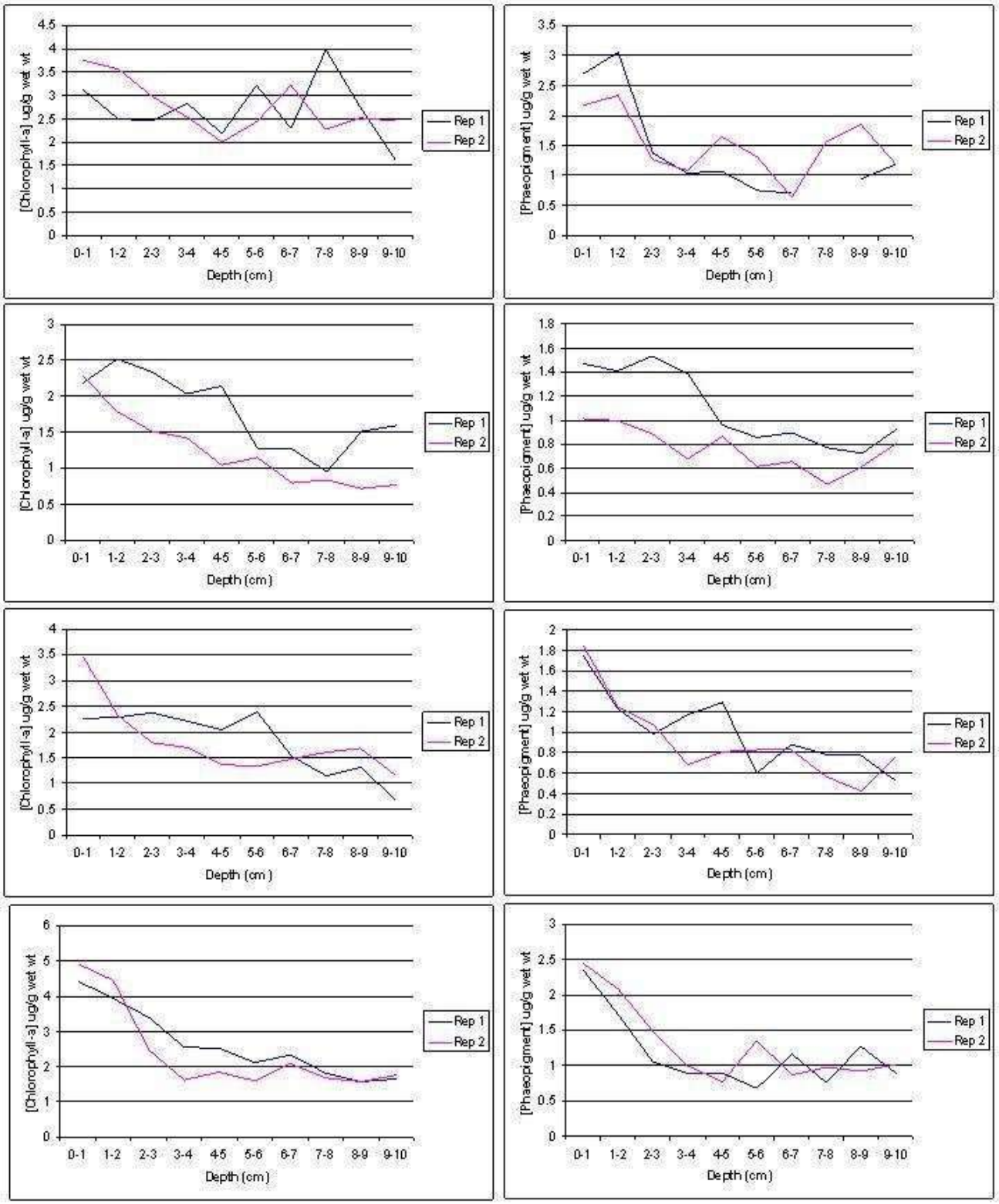

Figure 4.19. Chlorophyll *a* (left) and Phaeopigment (right) concentrations at Marmion Outfall (top) South Lumps (second top), Cow Lumps (third) and MM1 (bottom) for all core depths and for both repetitions.

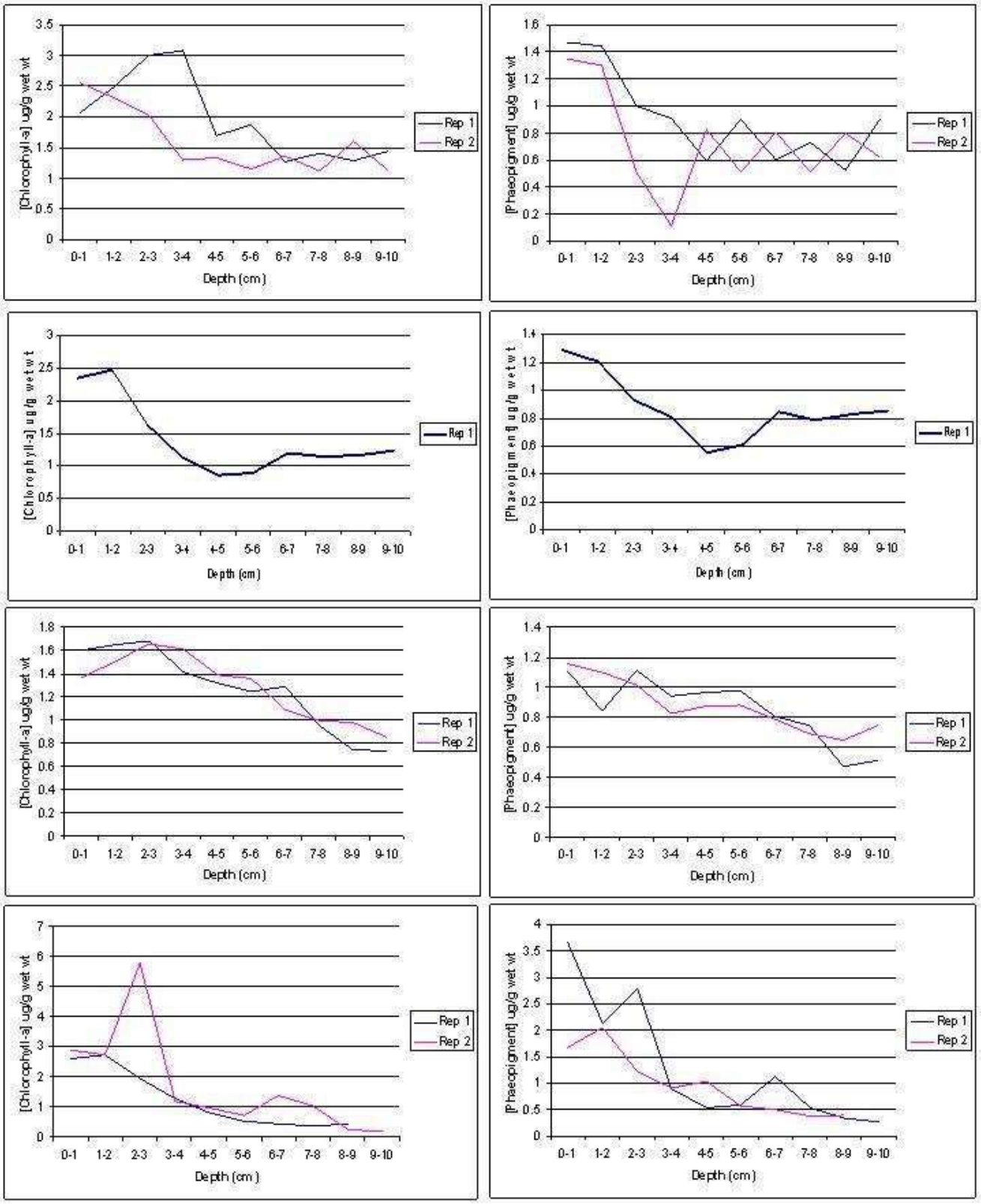

Figure 4.20. Chlorophyll *a* (left) and Phaeopigment (right) concentrations at MM4 (top), MOF2 (second top), M3MRS (third) and Hall Bank (bottom) Lumps for all core depths and for both repetitions.

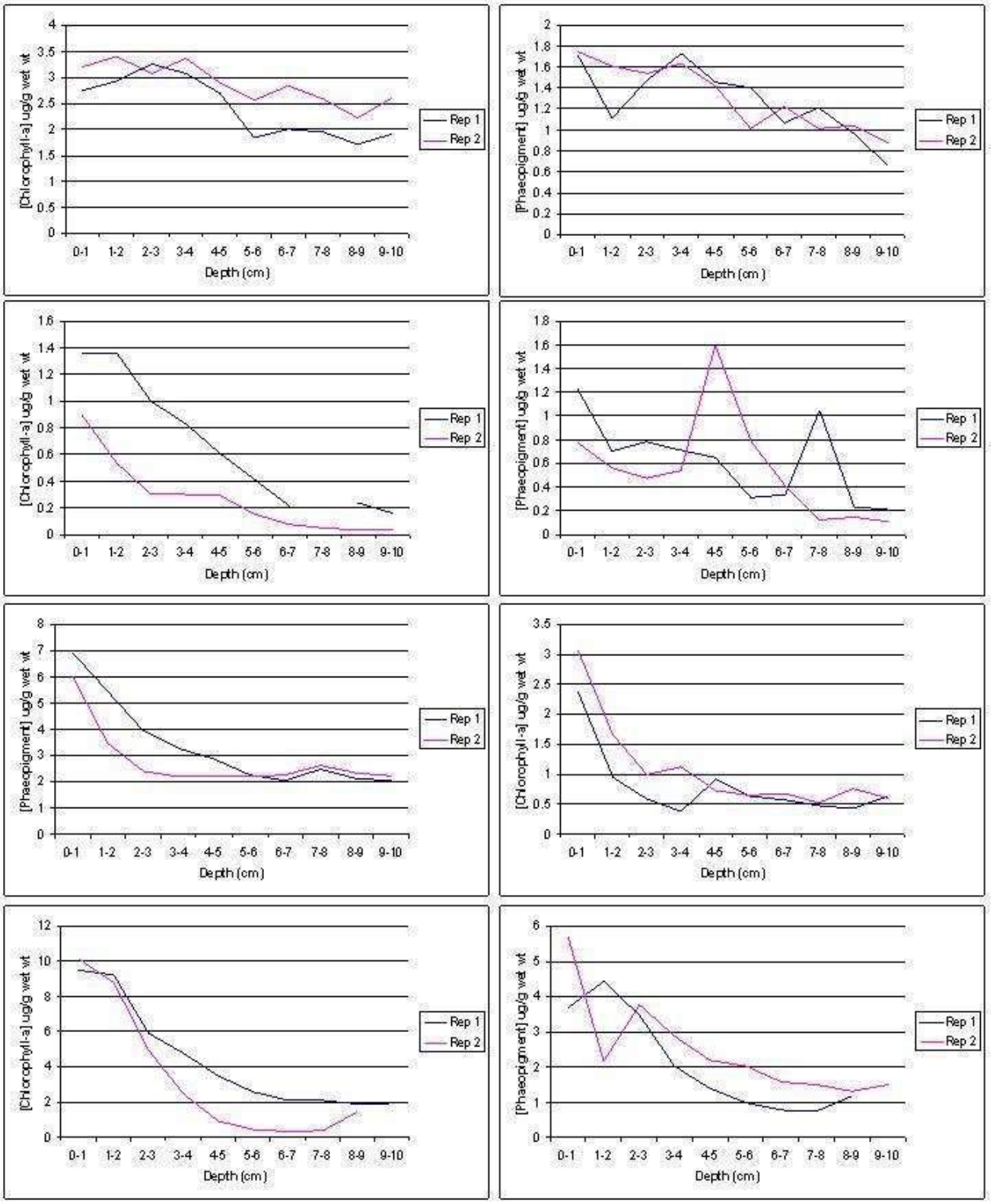

Figure 4.21. Chlorophyll *a* (left) and Phaeopigment (right) concentrations at City Beach (top), Parmelia Bank (second top), Northern Harbour (third), and Jervoise Bank (bottom) for all core depths and for both repetitions.

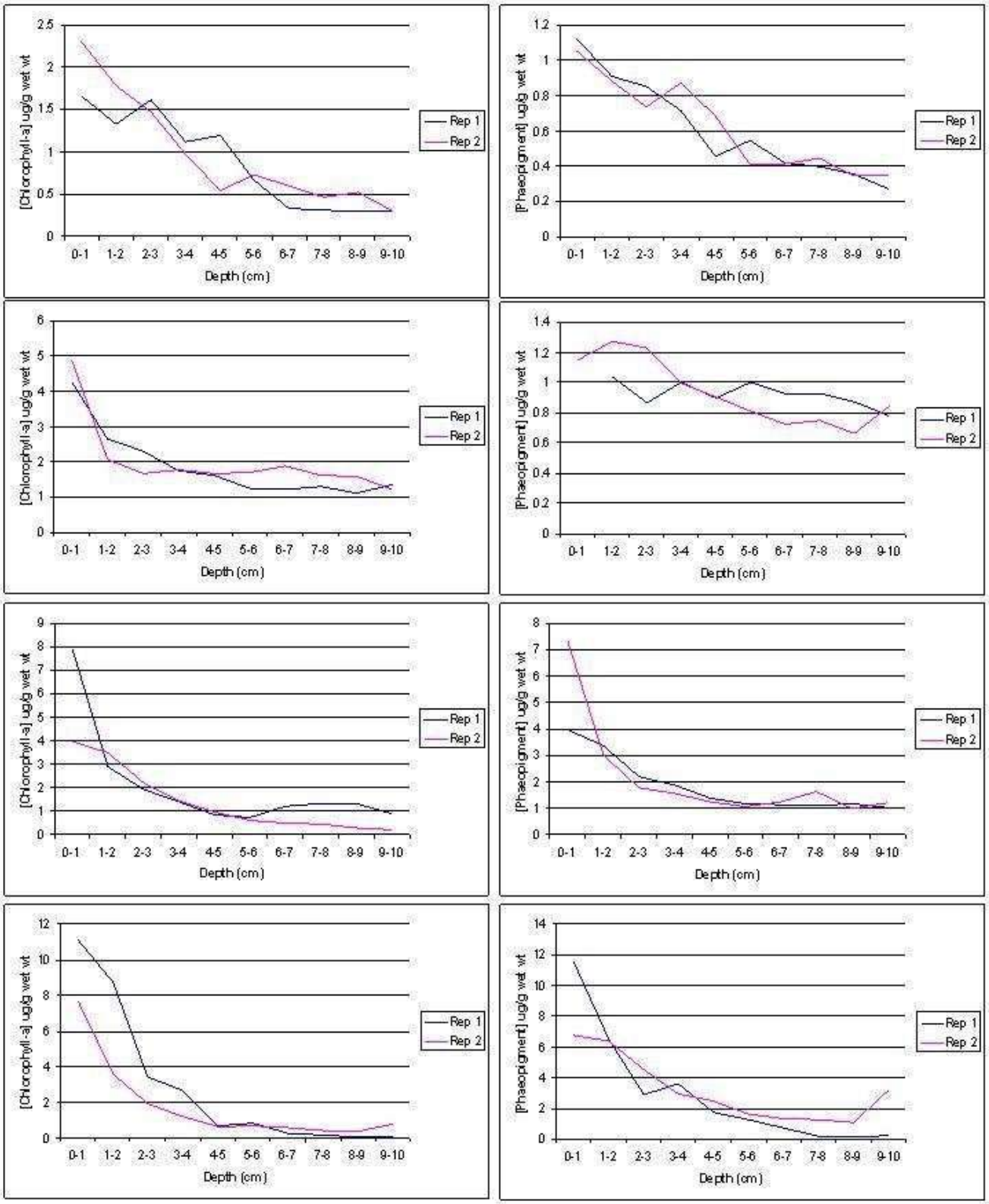

Figure 4.22. Chlorophyll *a* (top) and Phaeopigment (bottom) concentrations at Cockburn Sound (top), Carnac Island (second top), Southern Flats (Third) and Swan River (bottom) for all core depths and for both repetitions.

Sediment microalgae type derived from phytopigments

At all stations in both seasons the MPB community was dominated by diatoms (~fucoxanthin) (Figure 4.23). Fucoxanthin amounted for between 40% (Swan River during winter) and almost 100% (MOF2 in winter) of the normalised pigment compliment (Figure 4.23). The ratio of fucoxanthin to chlorophyll *a* was > 0.8 at 90% of the stations. In the marine samples and the Swan River during summer small amounts of zeaxanthin, lutein and chlorophyll *b* (prasinophytes) were generally present in addition to the dominant fucoxanthin (Figure 4.23). The highest concentrations of these additional pigment groups was at station AA, (both seasons), MM 4 (in summer) and the (Swan River in summer) (Figure 4.23). The Swan River in winter had a different and more diverse assemblage than the marine stations. Here almost all the pigment classes are represented. butanoyloxyfucoxanthin (chrysophytes), prasinoxanthin (prasinophytes), Zeaxanthin Lutein and chorophyll *b* (chlorophytes and possibly cyanobacteria) and hexanoyloxyfucoxanthin (haptophytes) (Figure 4.23).

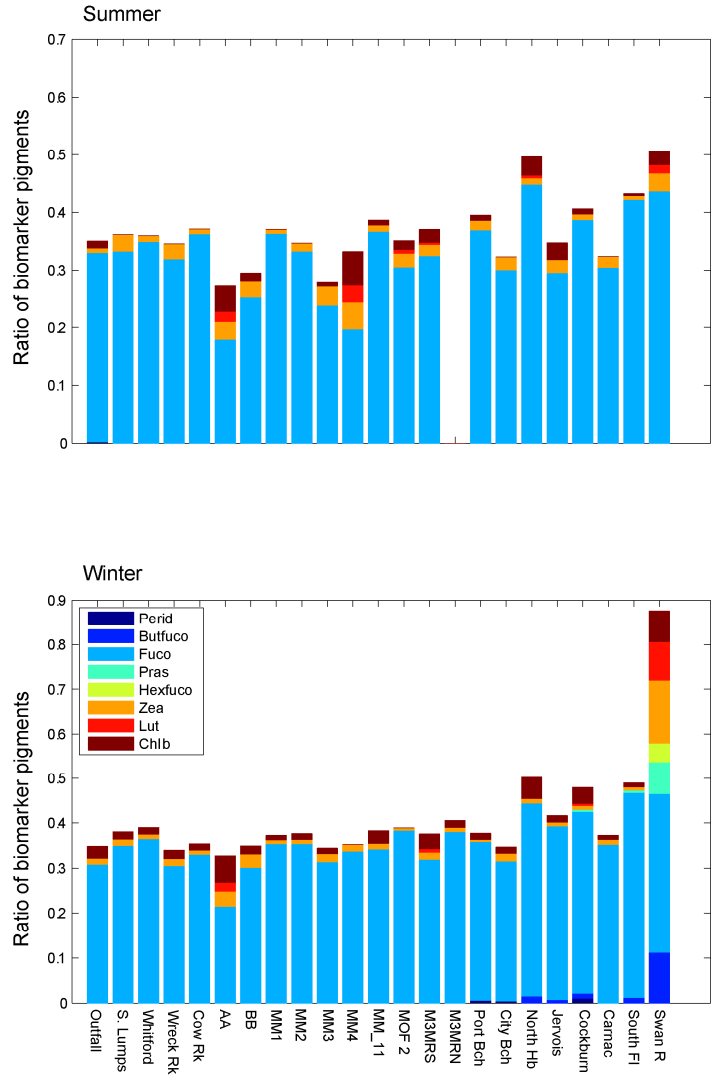

Figure 4.23. Accessory pigment:chl a ratios of major pigments detected in surface sediment in summer (top) and winter (bottom) from a series of stations located between the Marmion Outfall and Southern Flats in the south of Cockburn Sound (including one station in the Swan River).

Sediment bacteria counts

A high amount of variability was observed both between sites and within locations indicating a dynamic system. However, some trends were evident. Northern Harbour, Jervoise Bank, Swan River and Port Beach had significantly higher counts of autotrophic bacteria, phytoplankton, organic detritus and heterotrophic bacteria than other sites (Figure 4.24). These differences were not present in non-photosynthetic protozoa and metazoan where only Jervoise Bank was significantly higher than other sites mainly due to the presence of microscopic gastropod spat (Figure 4.24). The highest concentrations of autotrophic bacteria were observed at Port Beach (Figure 4.24 and Figure 4.25). Significantly higher cell counts of autotrophic bacteria were observed in sediments from Northern Harbour, Jervoise Bank, Swan River and Port Beach compared to all other sites. Within this group, Port Beach had significantly higher counts than Jervoise Bank but not Northern Harbour or Swan River. No filamentous autotrophic bacteria were observed at any sites. The highest cell counts of phytoplankton were observed at Port Beach which was significantly higher than all other sites (Figure 4.26). Of the remaining sites, Northern Harbour, Jervoise Bank and Swan River were significantly higher than all other sites. The highest cell counts for non-photosynthetic protozoa were observed at Jervoise Bank which was significantly higher than all other sites (Figure 4.27). This result was due to the presence of microscopic gastropod spat in the sediments. The Swan River had significantly higher amounts of organic detritus than all other sites (Figure 4.28). Jervoise Bank, Northern Harbour and Port Beach were also significantly higher than other sites. Concentrations of heterotrophic bacteria were significantly higher at Northern Harbour and Swan River compared to all other sites (Figure 4.29 and Figure 4.30). Cell counts were also higher at Jervoise Bank and Port Beach compared to the remaining sites.

Measurements of chlorophyll *a* and phaeopigment concentrations were consistent with results obtained from cell counts. Northern Harbour and Blackwall Reach (Swan River) had the highest concentrations of chlorophyll *a* and phaeopigments in 2008 (Figure 4.4). These two sites also had high biomass estimates for autotrophic and heterotrophic bacteria (Figure 4.25 and Figure 4.29) as well as phytoplankton (Figure 4.26) and high amounts of organic matter (Figure 4.28).

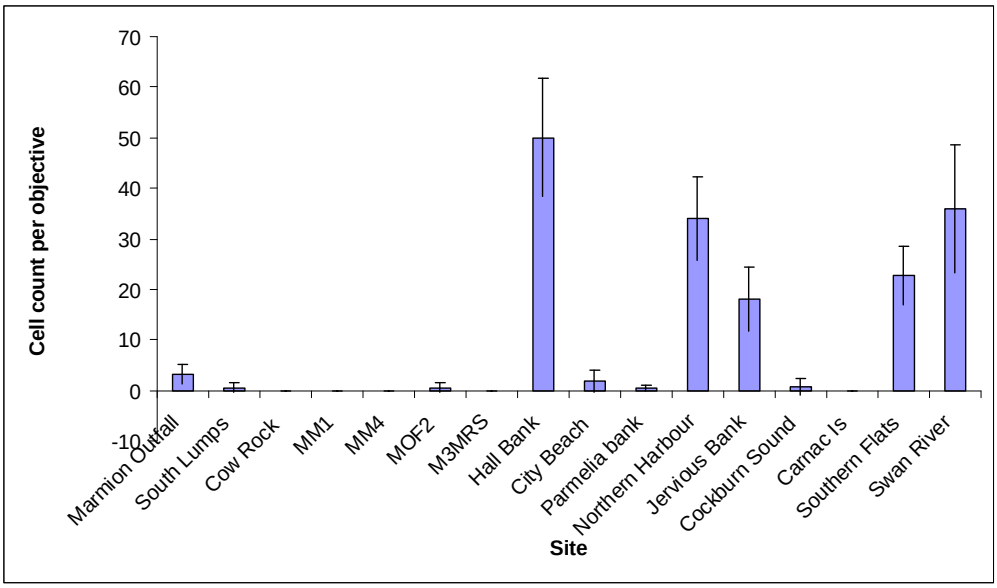

Figure 4.24. Average number of autotrophic bacteria observed per objective at 200 times magnification. Error bars indicate 95% confidence interval.

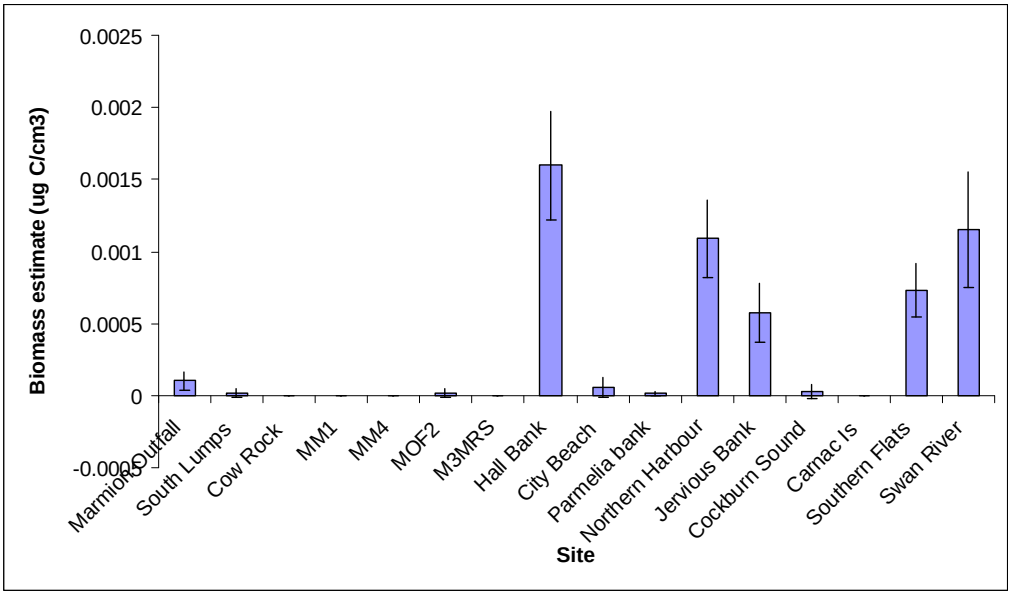

Figure 4.25. Estimated biomass of autotrophic bacteria observed per cm^3 of sediment at each of the study sites. Error bars indicate 95% confidence interval. Estimated biomass assumes a factor of 10fg Carbon per bacterial cell.

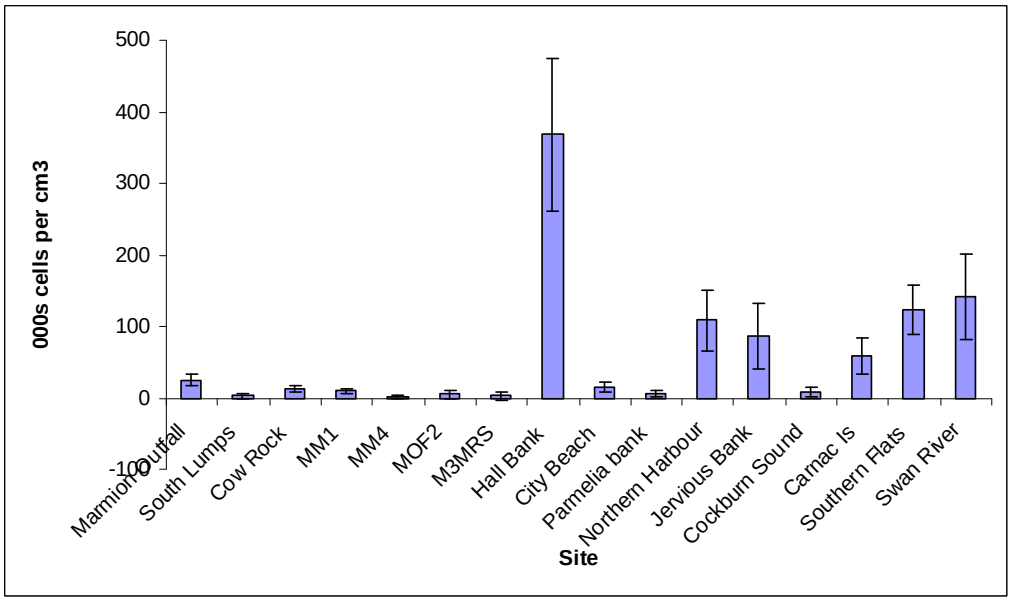

Figure 4.26. Average number of phytoplankton cells in a cm^3 of sediment. Error bars indicate 95% confidence interval.

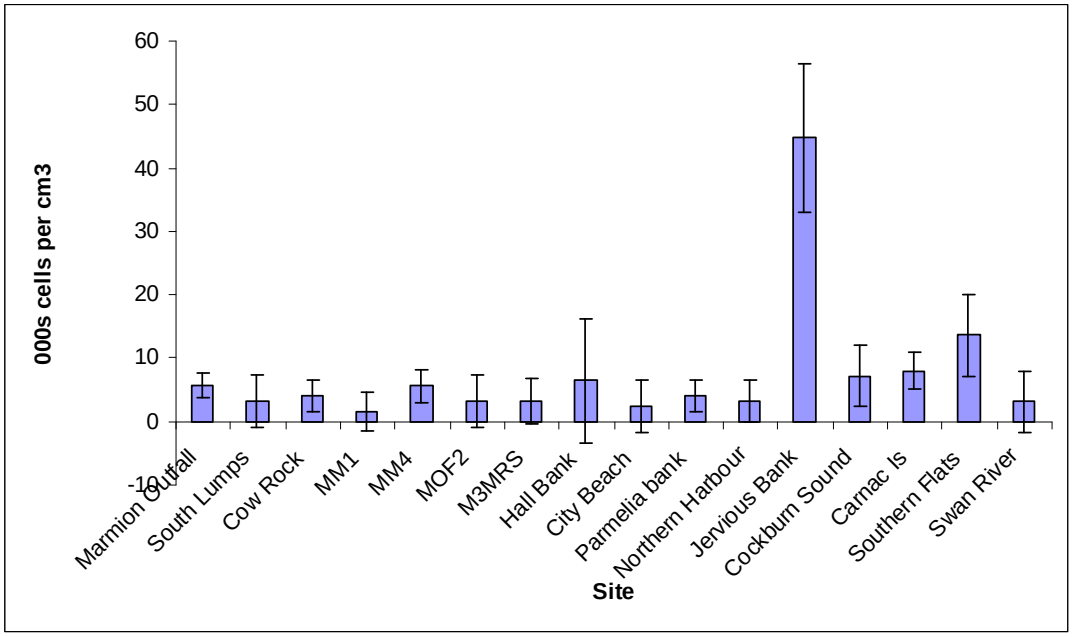

Figure 4.27. Average number of non-photosynthetic protozoa cells in a cm^3 of sediment. Error bars indicate 95% confidence interval.

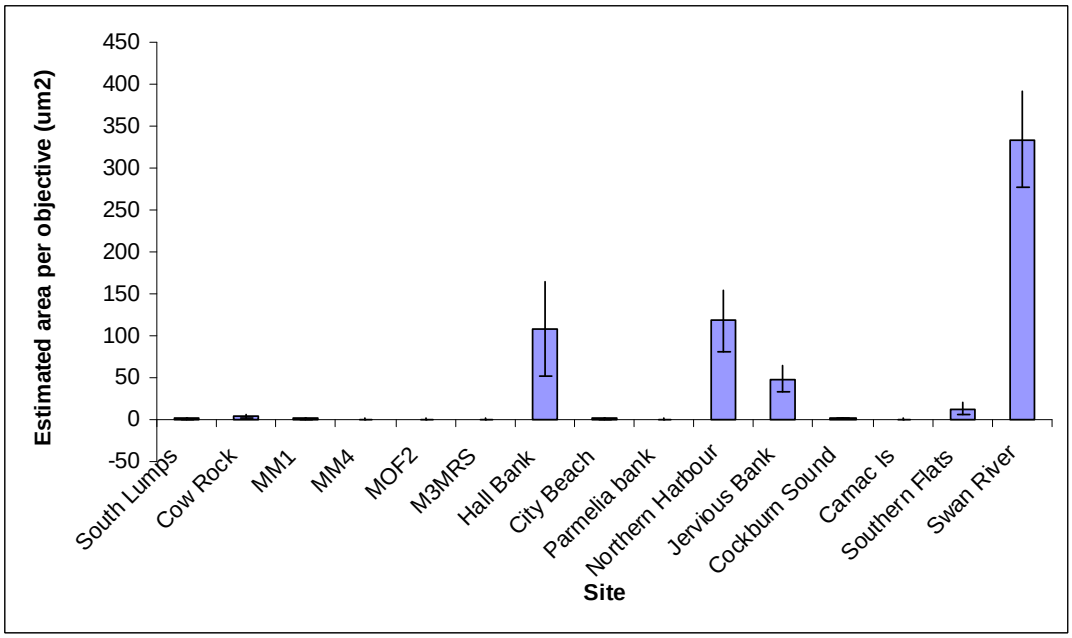

Figure 4.28. Estimated area of objective occupied by organic detritus in um^2 at 200 times magnification. Error bars indicate 95% confidence interval.

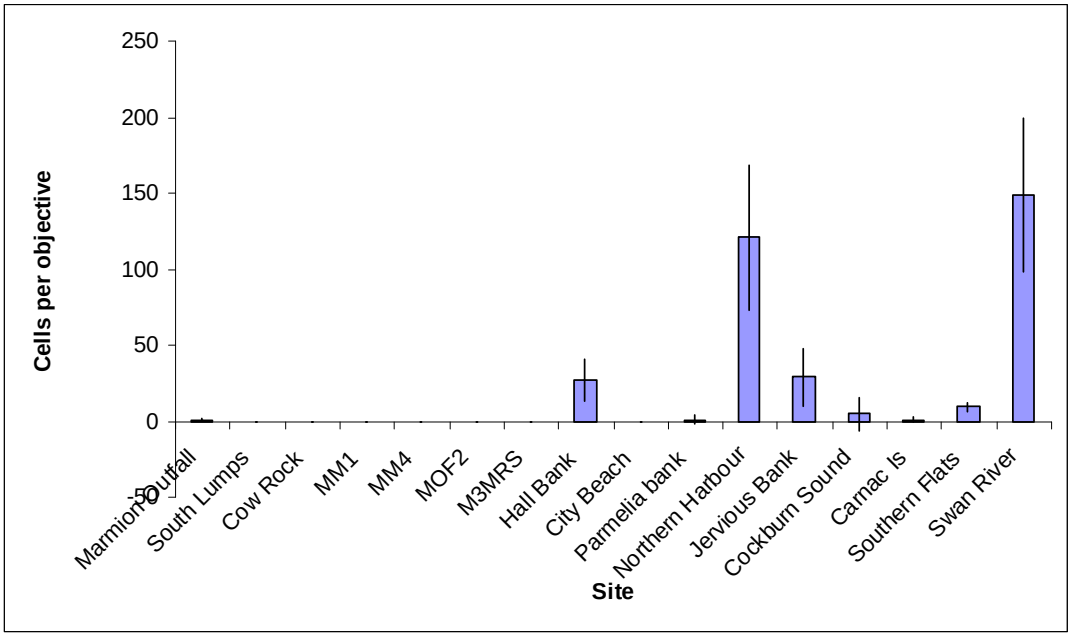

Figure 4.29. Number of heterotrophic bacteria observed at 400 times magnification. Error bars indicate 95% confidence interval.

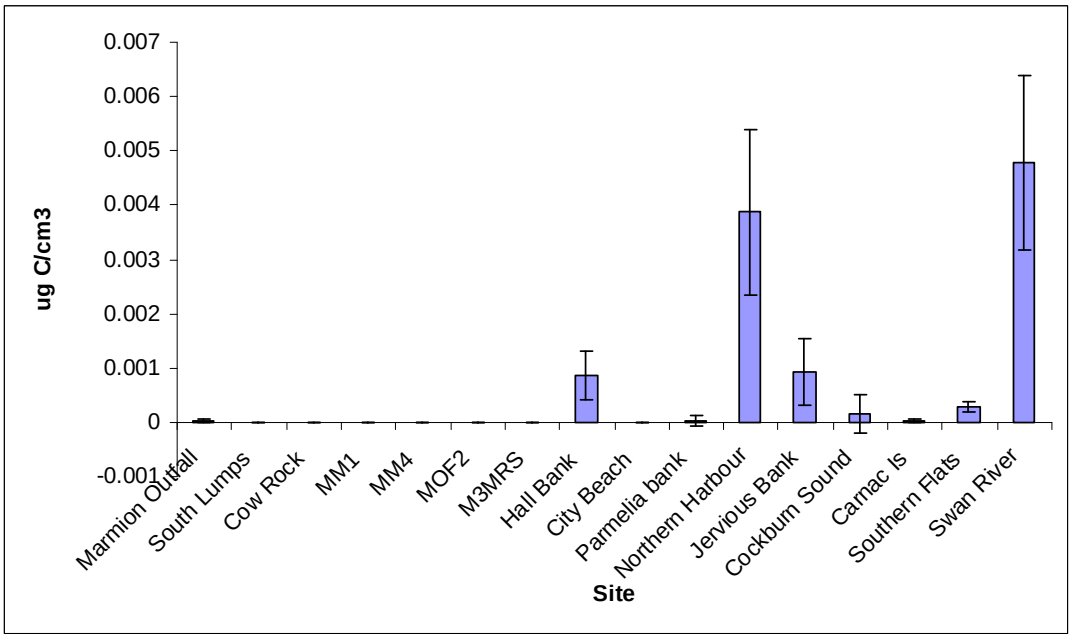

Figure 4.30. Estimated biomass of heterotrophic bacteria per cm^3 of sediment at each of the study sites. Error bars indicate 95% confidence interval. Estimated biomass assumes a factor of 10fg carbon per bacterial cell.

Abundance of Nitrifying Archea and Bacteria determined by DNA probes

The abundance of ammonia oxidizing archaea (AOA) and bacteria (AOB) was measured in sediment samples from each site to help determine the potential of these marine sediments to resupply nitrogen from sediment to the water column by nitrification within the sediments. The most enriched sites of Northern Harbour, Southern Flats and Swan River had the highest levels of both. Next highest was the Marmion outfall site (Figure 4.31 and Figure 4.32). The Marmion

offshore lagoon site MOF2 also had a high AOB density (Figure 4.31). The ratio of AOA to AOB shows that at all sites AOA were 10 to 80 times more abundant that AOB (Figure 4.33). High AOA:AOB ratios are typical of other studies (e.g. Abell et al 2010) and is thought to occur because AOA are considered more competitive than AOB for low levels of nitrogen (Herrmann et al.2011).

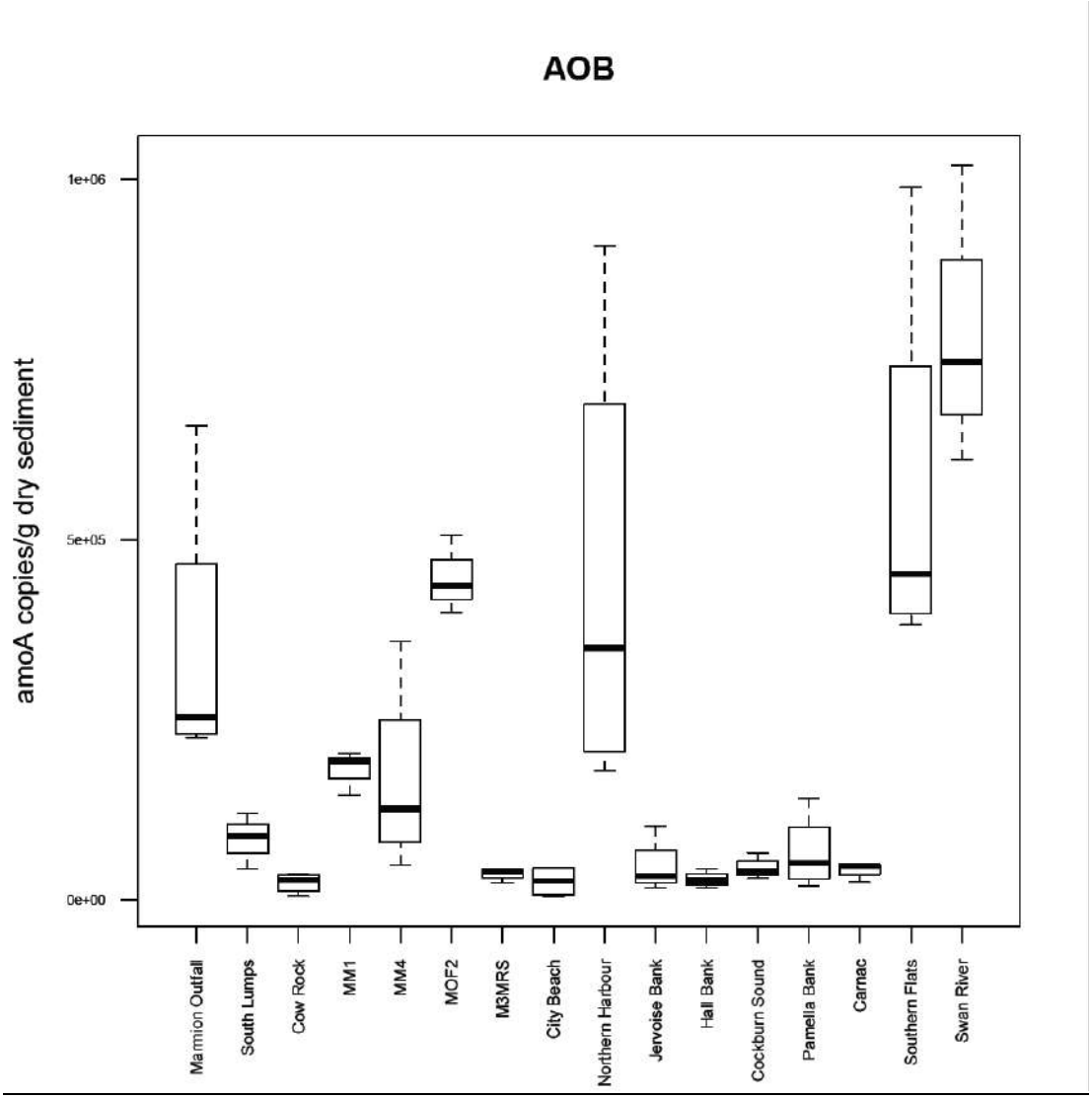

Figure 4.31. Abundance of ammonia oxidising bacteria (AOB) at each sampling site.

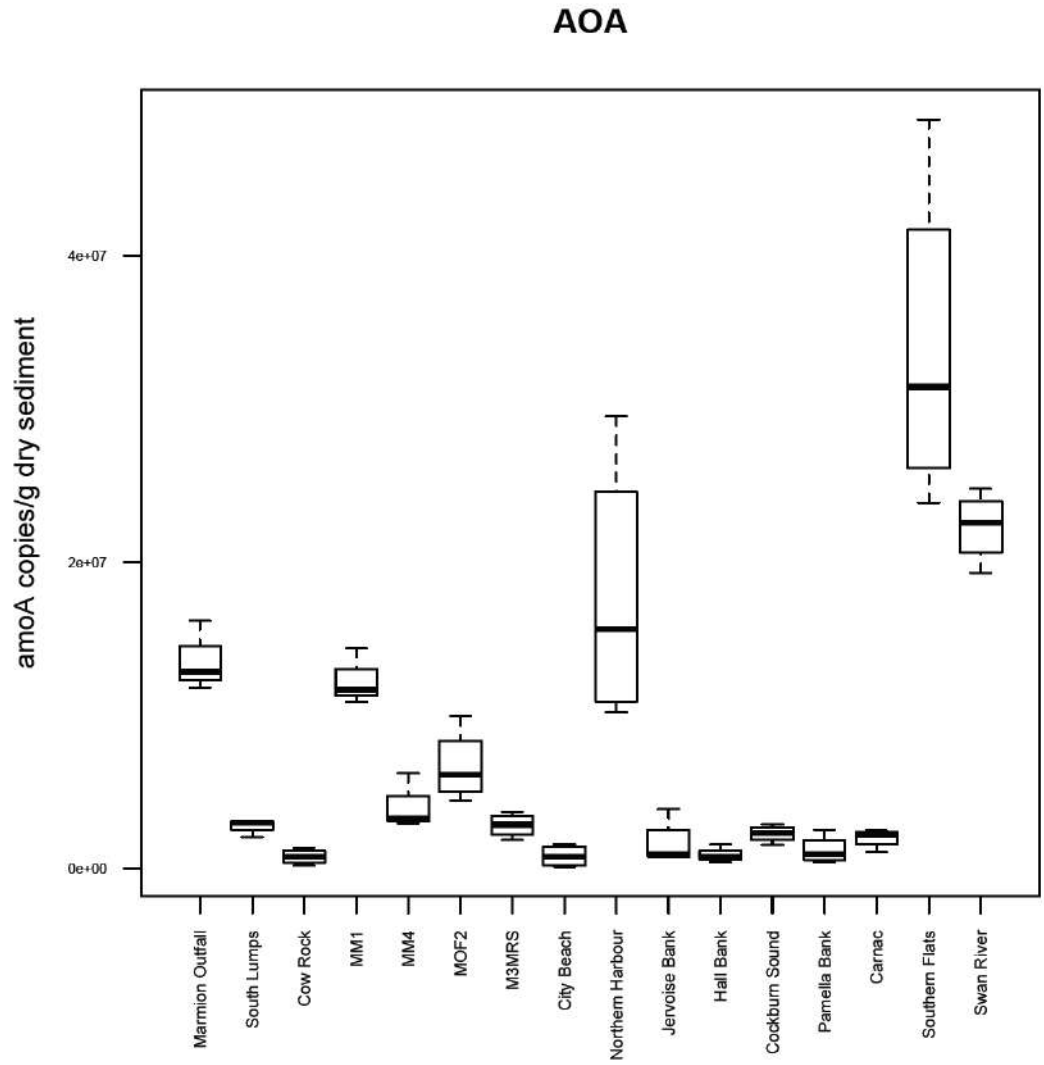

Figure 4.32. Abundance of ammonia oxidising archaea (AOA) at each sampling site

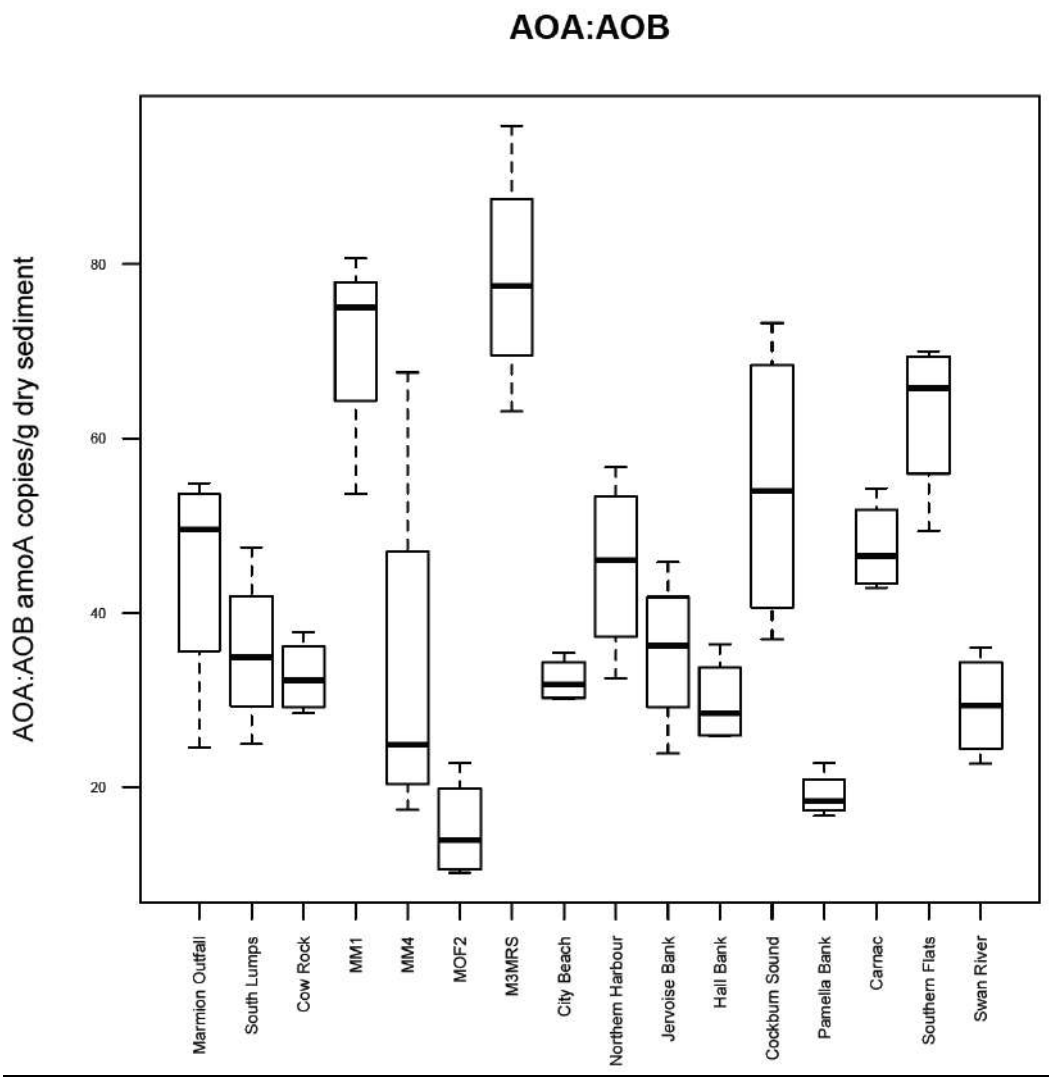

Figure 4.33. Ratio of Abundance of ammonia oxidising archea (AOA) to ammonia oxidising bacteria (AOB) at each sampling site

Key Findings

- **Median sediment grain sizes varied from 0.125- 0.250 mm to 0.500 mm across the onshore to offshore gradient at Marmion lagoon. Fine sediments were also a feature of Cockburn Sound and Swan River sites**
- **Organic matter content of sediments varied from 3mg per gram of sediment dry weight at one of the offshore Marmion sites to 47mg/g at Northern Harbour. Other Cockburn Sound Sites were significantly more enriched (21-40 mg/g) when compared to Marmion offshore lagoon (4-17 mg/g), Marmion mid lagoon (20-27 mg/g) and Marmion inshore (9-20 mg/g). The Marmion outfall and Swan River sites site had high organic matter contents of 27mg/g and 30 mg/g respectively.**
- **Organic carbon levels varied between sites and between years. The lowest levels, were at Jurien Bay (<0.1%). The Swan River and Northern Harbour sites were the highest (0.6-1% and 0.3-0.7 % respectively).**
- **$\delta^{13}C$ values of sediment were mostly -20 to -25‰ suggesting that macroalgae is an important source of carbon stored in sediments.**
- **Most sites had sediment total nitrogen contents of approximately 0.02 to 0.04%. Jervoise Bank, Southern Flats and Northern Harbour (2010) in Cockburn Sound and the site in the Swan River all had greater nitrogen concentrations (0.06 to 0.12 %).**
- **$\delta^{15}N$ in sediments were lowest at Jurien Bay (4 – 5). Other sites were more variable (5 – 7). The most elevated levels were at City Beach in 2008 (ca. 9) suggestive of an anthropogenic source.**
- **Sediment chlorophyll *a* biomass in the surface (0-2 cm deep) samples averaged 4 to 126 mg Chl a per m^2 across all sites, Although variable across sites, the following applied generally: with two exceptions outer and mid Marmion lagoon biomass was 10 to 20 mg Chl a per m^2, inner lagoon Marmion sites were 40 to 80 mg Chl a per m^2 and Cockburn Sound sites were generally higher 40 to 130 mg Chl a per m^2.**
- **Benthic microalgae (BMA) biomass was correlated with wave forcing at the seabed but not with water column nutrients or depth.**
- **Surprisingly we found sediment chlorophyll quite deep in sediments at many sites. In particular the well flushed Marmion sites often had 50% of surface chlorophyll still present at 5cm depth. This has implications for how benthic microalgae (BMA) biomass is measured.**
- **Benthic microalgae (BMA) were dominated at all sites by diatoms as indicated by fucoxanthin pigments in both summer and winter (mostly greater than 90% diatoms). Only the Swan River in winter had significant non-diatom flora present (60%) with pigments indicating the presence of prasinophytes, chrysophytes and chlorophytes**
- **Biomass of heterotrophic bacteria was highest at Northern Harbour and in the Swan River (both >0.004 micrograms per cm^3 of sediment)**
- **Levels of ammonia oxidizing archaea (AOA) and bacteria (AOB) are an indication of sediment nitrification potential and were highest in the most enriched sites of Northern Harbour, Southern Flats and Swan River. They were also elevated at the Marmion outfall site.**

4.3.3 Sediment invertebrate fauna

Infaunal biomass and secondary production

Biomass of sediment infauna has been calculated for each transect at each site using the total ash-free dry weight (AFDW) biomass of infauna retained by sieves of differing mesh size and formula established in Edgar (1990).

The biomass of animals in the various sieve size classes used in secondary production calculations can be measured directly, or by a formula given in Edgar (1990) based on the number of individuals and the sieve size they are contained in; the latter saving time and effort. All transects at two Marmion Marine Park sites and two Cockburn Sound sites were employed to conduct a pilot study to establish which of these methodologies was most applicable to this study.

Edgar's (1990) work discerned equations for each phyla separately, concluding that there was no statistical difference between the equations, with the exception of caprellid amphipods due to their elongate morphology. A combined equation for all fauna unless dominated by long thin animals was established as an accurate and rapid method of determining biomass for each sieve size.

The equations established by Edgar (1990) are as such:

mean biomass of animals in a particular sieve size is calculated as:

$$\log B = a + b*\log S \quad (1)$$

(where B = mean AFDW (mg); S = sieve size (mm))

this is then used to calculate total biomass of animals as:

$$B = \Sigma n_i * B_i \quad (2)$$

(where n_i = abundance of animals in sieve size i; B_i = mean biomass of animals in sieve size i (as calculated from above regression equation)

Table 4.7 shows the coefficients in Equation 1 for both Edgar (1990) and those calculated from the actual measured AFDW biomass in this study. The work of Edgar (1990) showed strong correlation between sieve size and AFDW in all phyla and when pooling all fauna, as shown by high r^2 values. As mentioned, the combined equation adequately estimates total biomass of all fauna, thus the formula of log B = -1.01 + 2.64*logS can be used. In contrast, with the exception of platyhelminthes (which comprised only a small sample size) none of the regressions in this study were strong (as shown by very minimal r^2 in Table 4.7). Thus, neither the equations for individual phyla or the combined equation can be accurately used to measure mean biomass for a sieve size class.

Table 4.7. Coefficients and regression strengths for Eqn 1, comparing results of Edgar (1990) and this study.

	Edgar (1990)				This Study			
	a	**b**	**r^2**	**n**	**a**	**b**	**r^2**	**n**
Mollusc	-1.02	2.76	0.99	17	-0.15	0.47	0.13	24
Echinoderm	-	-	-	-	-0.54	0.48	0.09	3
Crustacean	-1.04	2.67	0.99	16	-0.95	-0.13	0.01	7
Polychaete	-0.99	2.49	0.98	18	-0.85	-0.19	0.01	22
Platyhelminth	-0.96	2.64	0.98	12	-1.74	2.96	0.99	4
Caprellids	-1.21	1.90	0.98	14	-	-	-	-
Foramifera	-	-	-	-	-0.19	0.87	0.28	11
Combined	-1.01	2.64	0.98	63	-0.55	0.43	0.04	71

Without being able to calculate mean biomass in this way, abundance data can be converted to biomass data using equation 2 as in Edgar (1990). As a result, biomass can only be measured directly as AFDW, the difference between the dried (80ºC for 48 hr) and ashed (500 ºC for 2 hr) weights of the fauna retained by each sieve. This direct measurement method was applied to all cores in order to determine infaunal biomass present. We were unable to calculate secondary production using the method of Edgar (1990).

AFDW biomass of infauna is shown in Figure 4.34. Blackwall Reach in the Swan River had the greatest infaunal biomass. This is attributed to the presence of hermit crabs, polychaetes and molluscs all in high numbers and in a range of sizes. In addition, 3 hermit crabs greater than 8mm contributed 0.21g AFDW in one core and 1 hermit crab and 2 molluscs > 8mm in another core contributed 0.14g AFDW. Port Beach, Jervoise Bank and Southern Flats all had significantly greater infaunal biomass than other marine sites. At Port Beach this was simply the result of one large mollusc weighing 0.23g AFDW, hence the large standard error associated with this mean. At Jervoise Bank, the large AFDW was the result of 2 large molluscs (>8mm) in one core with a total weight of 0.10g and a large number of polychaetes found in all size fractions up to 5.6mm. At Southern Flats, also in Cockburn Sound, the biomass was not the result of a small number of individuals but rather large numbers of molluscs (3607 - 4540 per core in 3 of 5 transects) and forams (8443 – 10875 per core in the same 3 of 5 transects) found in a range of size, with smaller ones more abundant than larger.

Within Marmion Marine Park, the outer sites contained less biomass (0.17 ± 0.03 g.m^{-2}) than the inner (0.49 ± 0.07 g.m^{-2}, excluding the Marmion Outfall site) and mid sites (0.66 ± 0.21 g.m^{-2}).

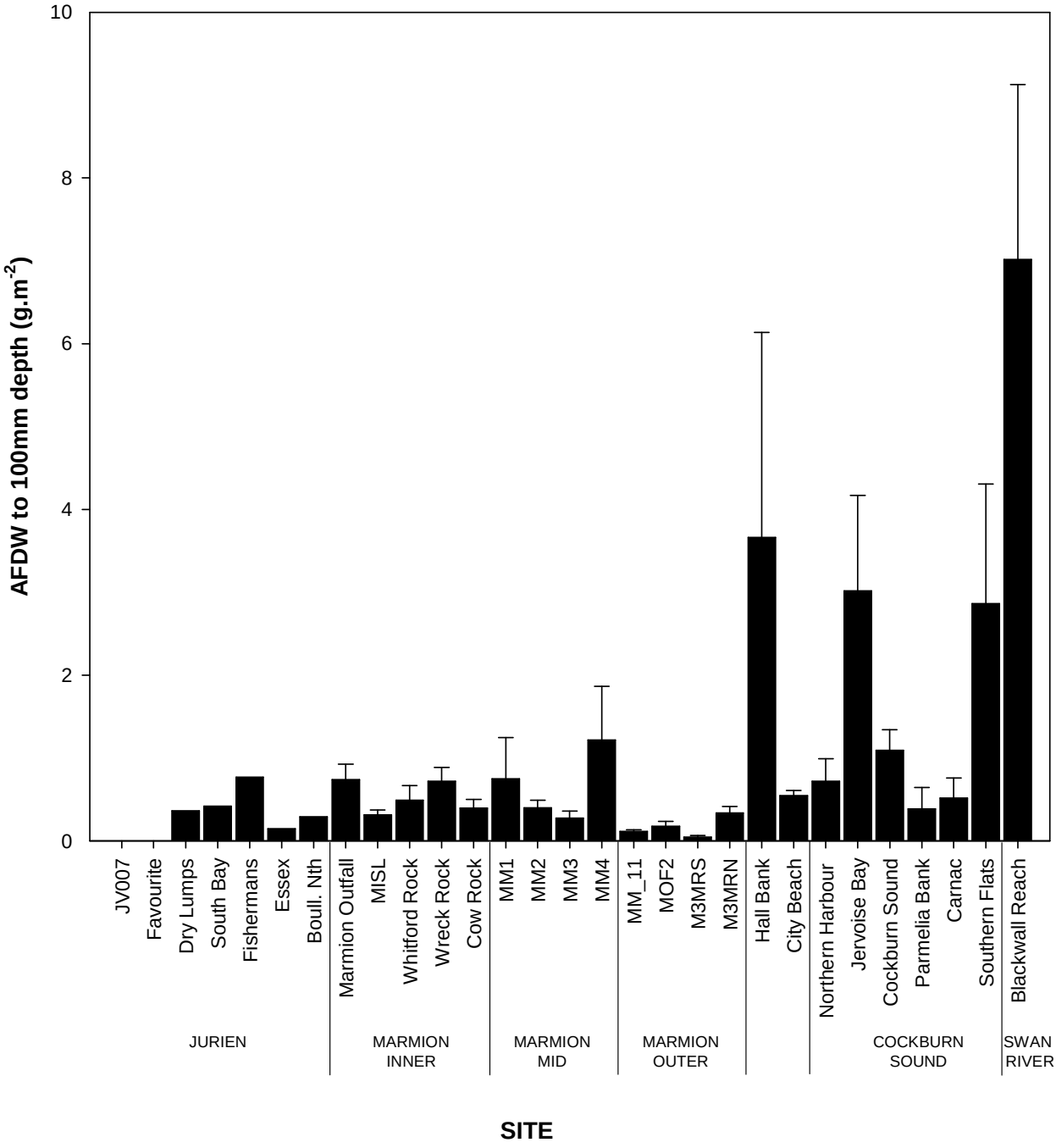

Figure 4.34. AFDW biomass of infauna to 100mm depth at each site sampled in 2008/2009 (mean ± S.E., except Jurien sites where only one core per site was sampled).

Secondary production was calculated from infaunal biomass as described by Edgar (1990) with the following equation:

$$\text{Production } (\mu g.day^{-1}) = 0.0049 \times B^{0.80} \times T^{0.89}$$

where B = AFDW biomass (μg)

T = mean monthly water temperature (ºC)

Secondary production values have been calculated with available temperature information from Pearce *et al.* (1999) for marine sites and from Water Corporation (pers. comm.) for the Swan River (Table 4.8).

Table 4.8. Infauna AFDW biomass, temperature and secondary production values of soft sediment sites or locations.

Location/Site	Mean AFDW Biomass ± SE ($g.m^{-2}$)	Mean Annual Temperature (ºC)	Production ± SE ($g.m^{-2}.yr^{-1}$)
Jurien Bay	0.28 ± 0.10	20.4	1.25 ± 0.41
Marmion Outfall	0.74 ± 0.18	19.4	2.74 ± 0.62
Marmion Inner	0.49 ± 0.07	19.4	1.97 ± 0.23
Marmion Mid	0.66 ± 0.21	19.4	2.31 ± 0.58
Marmion Outer	0.17 ± 0.03	19.4	0.81 ± 0.14
City Beach	0.54 ± 0.06	19.4	2.20 ± 0.21
Port Beach	3.66 ± 2.47	19.4	9.03 ± 5.01
Northern Harbour	0.72 ± 0.27	19.3	2.63 ± 0.82
Jervoise Bank	3.02 ± 1.15	19.3	8.25 ± 2.60
Cockburn Sound	1.09 ± 0.25	19.3	3.80 ± 0.69
Parmelia Bank	0.38 ± 0.26	19.3	1.46 ± 0.83
Carnac	0.52 ± 0.24	19.3	1.97 ± 0.76
Southern Flats	2.86 ± 1.44	19.3	7.79 ± 3.09
Swan River	7.02 ± 2.11	19.1	16.35 ± 4.04

Secondary production was almost twice as high in the Swan River compared to the next highest value. Port Beach, Jervoise Bank and Southern Flats had the greatest secondary production of the marine sites. As temperature values did not vary much between sites or locations, secondary production is tightly linked to AFDW biomass.

Sediment infauna abundance

The abundance of the different taxa recovered from the infauna cores is summarised in Table 4.9. Molluscs and polychaetes were the most abundant taxa with mollusc densities very high (ca >2400 per core). At all other sites infauna numbers were lower. Sites at Jurien Bay had very low numbers of infauna.

Table 4.9. Abundance of the different taxa recovered from the infauna cores. Values are mean + 1standard error based on 4-6 samples per site. Each sample consists of a 15cm diameter core inserted in the sediment to 10cm.

Site	Molluscs	Echino.	Crustacea	Polychaete	Platyhelm.	Caprell.	Nemat.
Boull. Nth	0	0	0	44	0	0	0
Dry Lumps	6	0	0	15	0	0	0
Essex	3	0	0	8	0	1	0
Favourite	0	0	0	0	0	0	0
Fishermans	1	0	0	16	0	0	0
JV007	0	0	0	0	0	0	0
South Bay	3	0	0	4	0	0	0
Marmion Outfall	24.00±5.39	0	5.60±2.77	17.80±3.46	0	0	0.80±0.58
Cow Rock	9.00±1.84	0	1.00±0.55	16.80±3.60	0.60±0.40	0	0.80±0.80
MISL (South Lumps)	9.25±2.87	0	0.75±0.25	10.00±5.21	0	0	0
MWHR (Whitford Rock)	8.20±3.07	0	2.20±0.73	28.80±4.63	0.40±0.24	0	0
Wreck Rock	67.80±9.05	0.20±0.20	0.60±0.40	2.20±0.86	0.20±0.20	0	0
MM1	1.20±0.73	0.20±0.20	4.20±2.08	4.60±2.04	0.40±0.40	0	1.60±0.81
MM2	3.80±1.07	0	1.00±0.55	9.40±2.42	0	0	1.40±0.75
MM3	1.17±0.40	0	8.33±2.74	8.67±3.05	0.17±0.17	0	1.83±1.17
MM4	3.00±1.29	0	1.00±0.71	3.20±1.10	0.60±0.55	0	3.80±2.49
MM_11	0.40±0.24	0	0.80±0.37	3.20±0.80	0	0	0
MOF2	1.00±0.55	0	1.60±0.81	2.40±0.68	0	0	0
M3MRS	1.00±0.82	0	4.00±1.00	0.83±0.40	0	0.33±0.33	1.00±0.37
M3MRN	2.75±0.63	0	2.00±1.68	5.25±0.85	0	0	0
City Beach	16.60±5.10	0	10.40±3.06	6.40±2.29	0.20±0.20	0	0
Port Beach	17.80±3.44	0.40±0.24	1.60±0.81	8.80±1.98	0.20±0.20	0	0
Carnac	21.40±10.85	1.20±0.58	0.40±0.40	6.40±4.17	0	0	0
Parmelia Bank	3.00±1.76	0	0.40±0.24	3.20±1.07	0	0	0
Cockburn Sound	31.75±8.44	0.25±0.25	0.50±0.50	27.75±1.44	6.25±4.39	0	0.25
Jervoise Bank	4.40±2.50	1.60±0.68	0	55.00±15.31	1.00±0.55	0	0.4
Northern Harbour	20.80±3.31	0	0	44.20±9.67	0	0	1.80±1.11
Southern Flats	2409.60±949.19	0.80±0.80	0	4.20±2.62	2.60±2.14	0	0.40±0.40
Swan River	21.40±4.25	2.00±1.76	11.80±7.58	35.60±13.47	3.60±1.50	0.60±0.40	0

Quantitative PCR assays for polychaete indicators of sediment enrichment

Figure 4.35 shows the results of quantitative DNA analyses on DNA extracted from the sediment cores using probes designed for different groupings of polychaete species used as indicators of sediment nutrient enrichment from pollution. Cirratulid polychaetes are mostly deposit feeders and have a high tolerance for hypoxic sediments (Loo et al. 2006). Lumbrinerid polychaetes are often carnivorous and are associated with low pollutant loads and semi-healthy sediments. Nephytid polychaetes are mostly carnivorous and favour habitats with high prey abundance, often associated with moderately enriched sediments. Spionid polydorids are deposit feeders and rapid colonisers and are often abundant in enriched sites. Capitellids are opportunistic rapid colonisers and tolerant of a wide range of environmental conditions. More detail on the characteristics of these and the other different indicator polychaete groups can be found in Loo et al. (2006). The sites with the highest total biomass of indicator polychaetes were Northern Harbour and Southern Flats. These are the most sheltered sites in our study while exposed sites such as those from Jurien Bay and the mid and offshore lagoon sites at Marmion had zero or low indicator polychaete biomass. It is important to note that these probes have been developed to assess the health of sediments and the level of impact by tuna farms in Spencer Gulf in South Australia (Loo et al. 2006). In general, the higher the levels of these taxa, the greater the impact on the sediment from the addition of nutrients which derive from from fish faeces and uneaten food. Thus the probes cannot be used as an indicator of total polychaete abundance as they do not target species which in habit healthy sediments, nor do they target estuarine species, which may explain why the probes detected few polychaetes in Swan River sediments despite them being among the most organic carbon and nitrogen enriched sites in our study. The fact that the probes cannot be used as an indicator of total polychaete abundance also explains why, when we compared abundance of polychaetes in the samples (Table 4.9) with the indicator polychaete DNA biomass only CIRR and NEPH showed weak correlations with abundance ($p=0.032$, $p=0.033$ respectively). Nevertheless there are indications that the probes are a useful indicator of nutrient enrichment in our region. For example our Northern Harbour site which is heavily enriched had 10 times the biomass of Cirratulid polychaetes than the next highest site (Cockburn Sound) and 50 times higher than the inshore sites at Marmion. They were not detected at all in the Marmion mid and offshore sites. In addition the contrast in abundance of groups such as the Capitellids which are higher in the inshore Marmion sites and largely absent from the mid and offshore sites at Marmion and all but the Fishermans site at Jurien Bay is worthy of further investigation to determine if this may be providing some early indication of sediment (and thus habitat) modification at these sites. It would be worthwhile to develop probes which a specifically suited to our region for use in environmental impact assessment to be able better interpret these results and for application in environmental impact studies in our region.

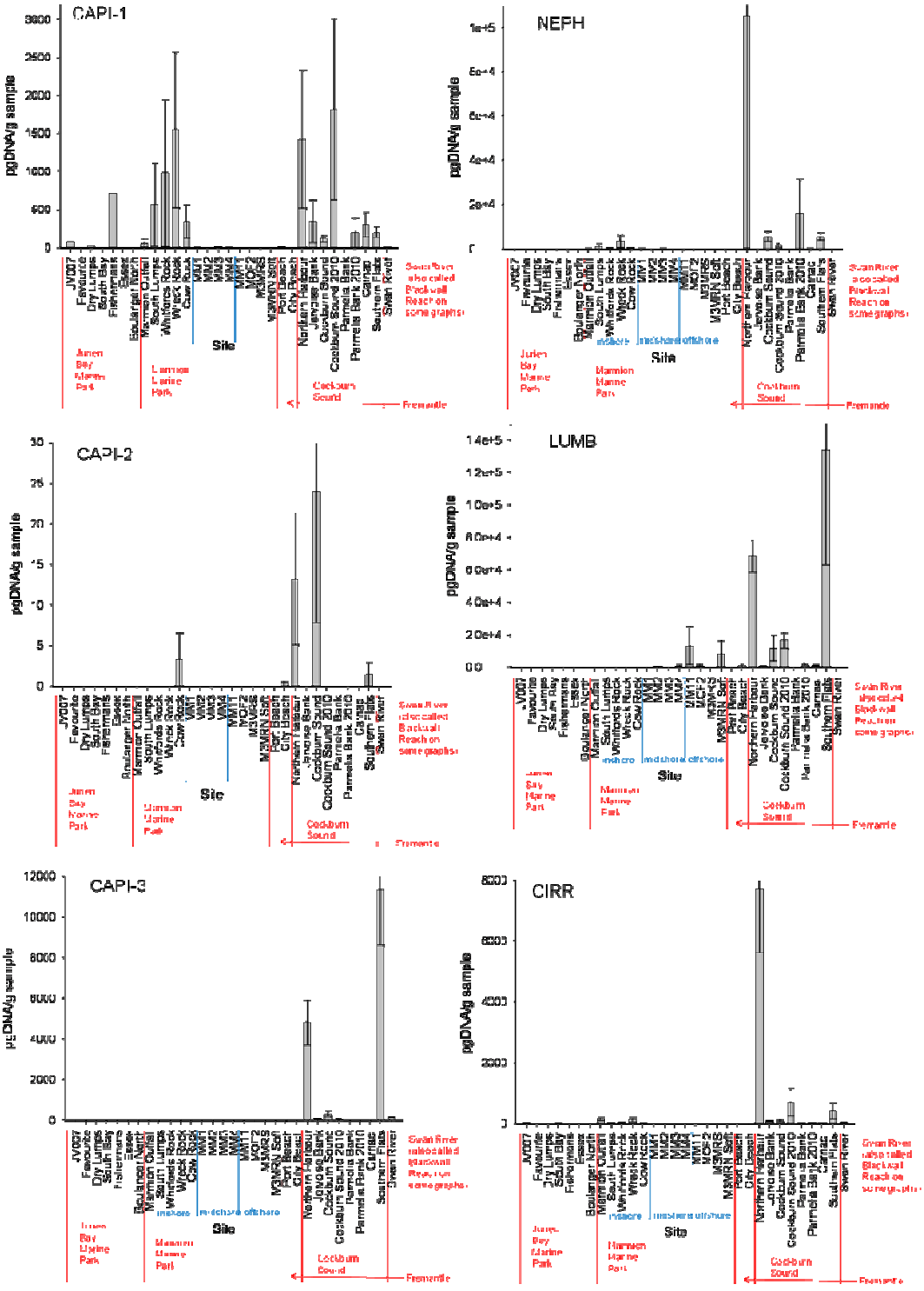

Figure 4.35. Top and bottom panels are quantitative DNA profiles for polychaete taxa from survey sites. All data are from 2008 except the two sites labelled from 2010.

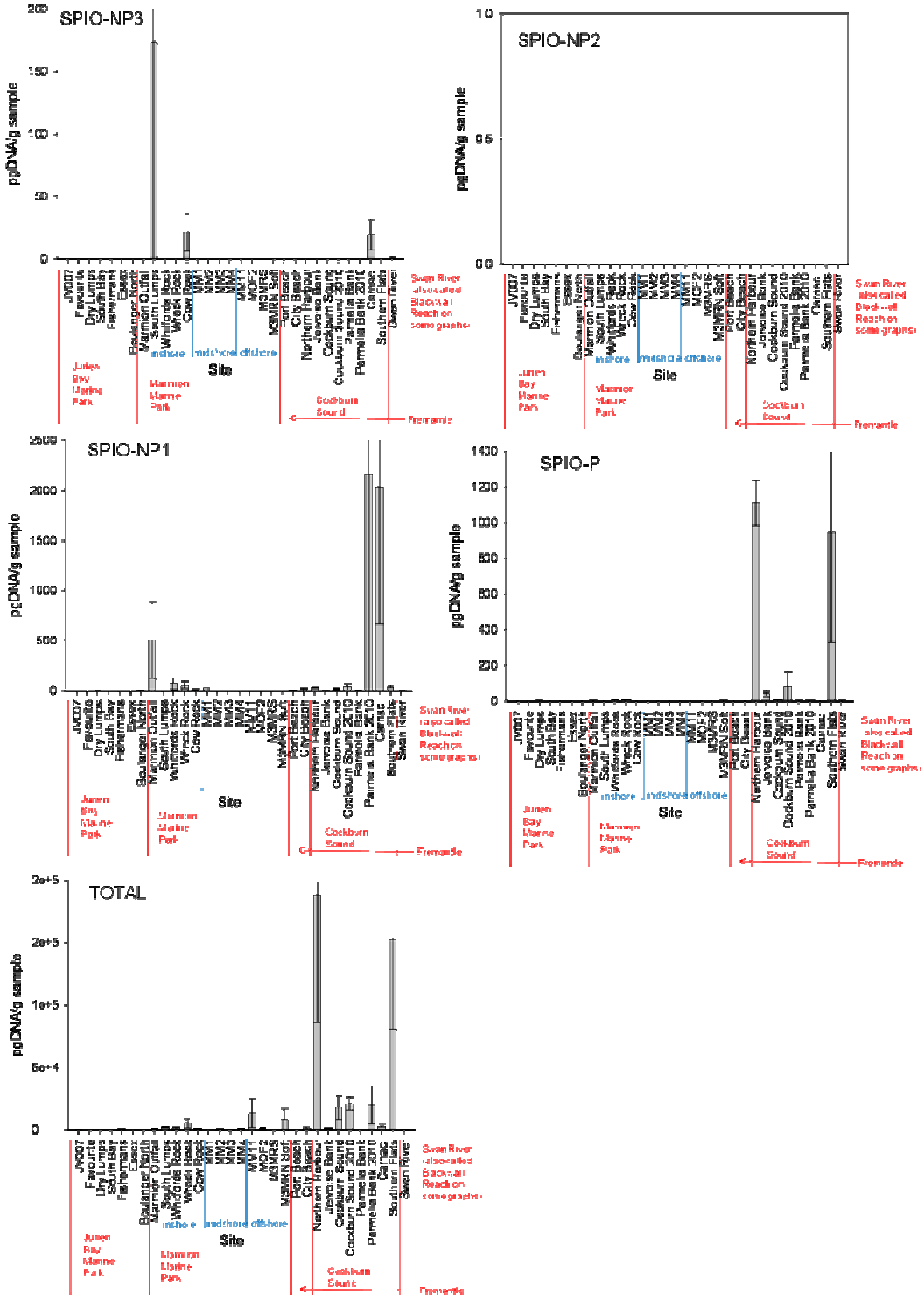

Figure 4.35. Continued. Top and bottom panels are quantitative DNA profiles for polychaete taxa from survey sites. All data are from 2008 except the two sites labelled from 2010.

Epibenthic macrofauna abundance and biomass

The mean number of individuals, species and total wet weights are given in Table 4.10. Figure 4.36 demonstrates the animals which contribute to each site and Figure 4.37 the animals which contribute to biomass. The greatest density of animals was found in the Swan River, where hermit crabs were measured at 7.04 ± 2.45 individuals per m^2 and ophiuroids at 3.16 ± 2.67 individuals per m^2 (Figure 4.36). This site also had the greatest species diversity, with a range of species encompassing all animal groups found in the study except for Crinoidea and Cephalopoda. In addition to having greatest quantities of infauna biomass of the marine sites, Port Beach, Jervoise Bank and Southern Flats had some of the greatest densities of macrofauna, with City Beach also having high numbers. With the exception of Southern Flats, these Cockburn Sound location sites also had some of the highest species diversities.

Fewer individuals, fewer species and less biomass were found in the deeper outer location of Marmion Marine Park than the inner and mid locations (Table 4.10). The heavily impacted site of Marmion Outfall had animal densities, diversity and biomass similar to other sites in the area. However, the other heavily impacted site of Northern Harbour had less individuals, species and biomass compared to its nearby sites. The Parmelia Bank site is worthy of special mention given its low biomass and diversity. This site was surveyed before realised that it was a dredge spoil site from the sand mining for Cockburn Cement. Recent work in the area had created a large area of fine sand spoil which had very little biota associated with it. The sediment grain size profile for this site varied little from that at the Cockburn Sound site.

The greatest biomass was found at Jervoise Bank and Southern Flats (Table 4.10) at both sites this was the result of echinoids (Figure 4.37) *Peronella lesueuri* and *Ammotropus arachnoides* at Jervoise Bank and *Peronella lesueuri* at Southern Flats. Similarly, the biomass in the Swan River and Cockburn Sound was also due to *Peronella lesueuri.* At Port Beach and Marmion Inner sites, biomass was composed mainly of the seastar *Archaster angulatus*. All other sites had less than 6g wet biomass per m^2 (Figure 4.37). Given the importance, and likely habitat structuring influence of both *Archaster angulatus* and *Peronella lesueuri* the ecology of both species was examined in greater detail with the assistance of PhD students, visiting scientists and volunteers (see description of Sharon Yeo's PhD study elsewhere in the WAMSI final report and Lawrence et al. (in press) and Keesing et al. (in press).

Table 4.10. Characteristics of macrofauna assemblage at sites or locations (mean ± SE).

Location/ Site	Density (no. indiv. per m^2)	Species Diversity (no. per m^2)	Wet Wt Biomass (g per m^2)
Jurien	0.43 ± 0.12	0.19 ± 0.03	2.36 ± 0.85
Marmion Outfall	1.88 ± 0.77	0.72 ± 0.08	5.79 ± 3.84
Marmion Inner	1.60 ± 0.25	0.86 ± 0.10	43.52 ± 9.15
Marmion Mid	1.88 ± 0.31	0.86 ± 0.12	3.35 ± 1.08
Marmion Outer	0.30 ± 0.08	0.22 ± 0.06	0.18 ± 0.06
Port Beach	3.44 ± 0.51	1.52 ± 0.37	47.92 ± 10.03
City Beach	4.36 ± 1.14	1.48 ± 0.22	6.01 ± 1.43
Northern Harbour	0.64 ± 0.22	0.32 ± 0.05	0.58 ± 0.20
Jervoise Bank	5.08 ± 0.60	1.56 ± 0.44	231.69 ± 19.88
Cockburn Sound	2.04 ± 0.94	0.56 ± 0.23	96.69 ± 27.46
Parmelia Bank	0.20 ± 0.09	0.12 ± 0.05	0.16 ± 0.13
Carnac	0.76 ± 0.17	0.72 ± 0.15	5.44 ± 3.42
Southern Flats	3.44 ± 1.26	0.48 ± 0.08	252.49 ± 87.15
Swan River	14.72 ± 3.34	2.36 ± 0.39	130.46 ± 25.41

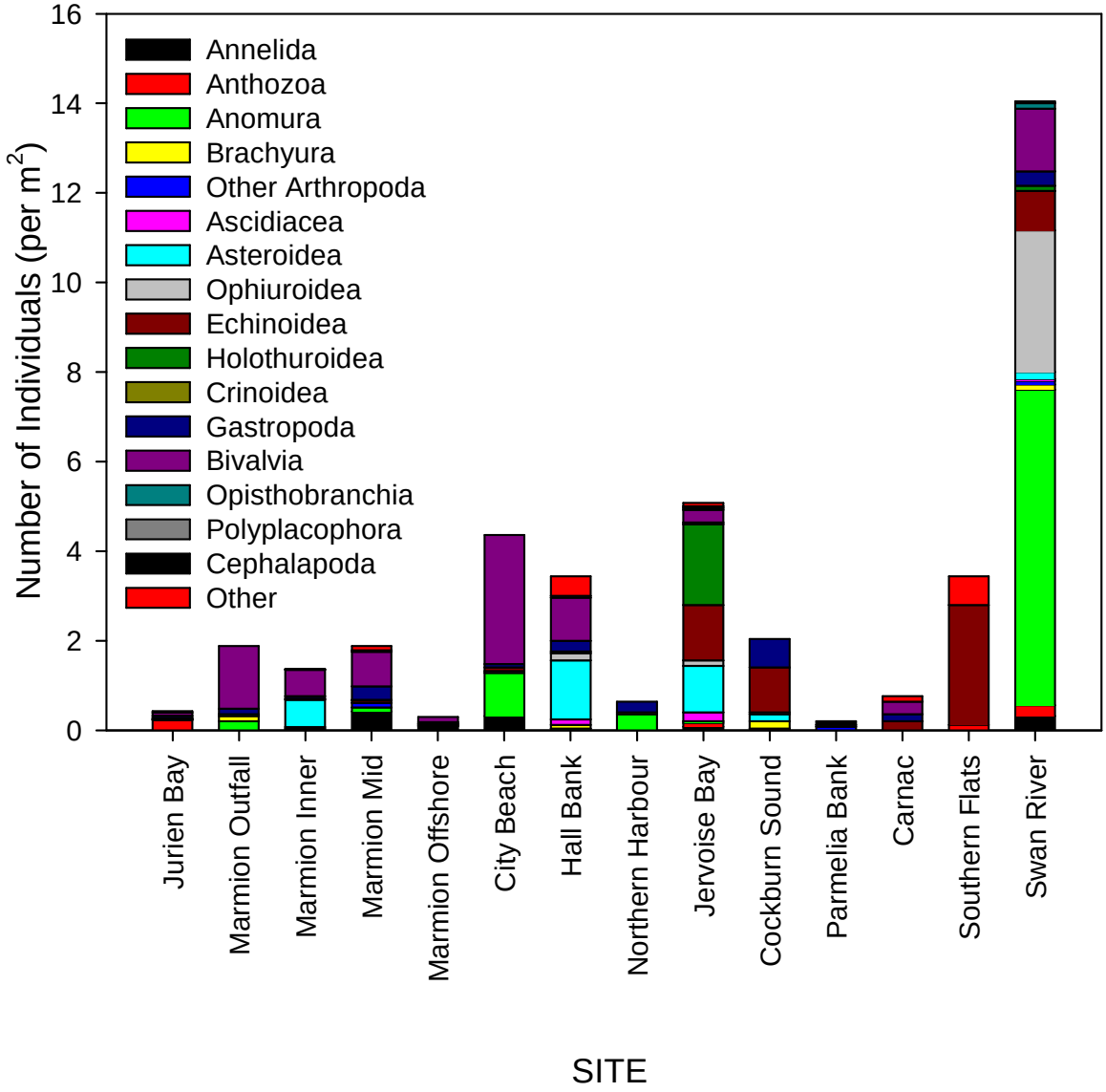

Figure 4.36. Number of individuals of various phylum and classes present in soft sediment sites and locations sampled in 2008.

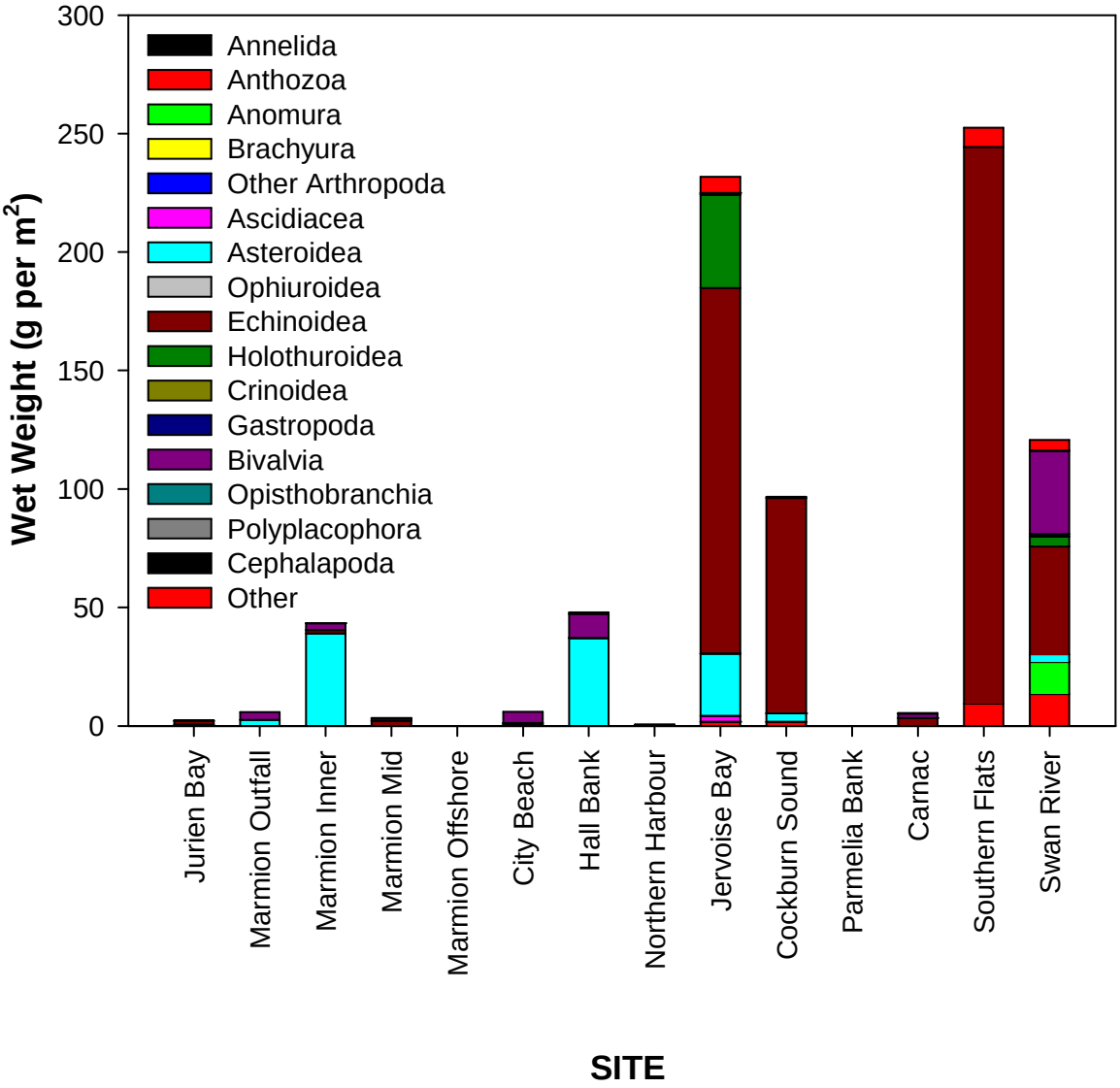

Figure 4.37. Wet weight of various phylum and classes present in soft sediment sites and locations sampled in 2008.

Key Findings

- **Molluscs and polychaetes were the most abundant infauna and the sites with the highest abundances and biomass of these animals were in Cockburn Sound and the Swan River. Low numbers and biomass of infauna were recorded at Jurien and Marmion.**
- **Polychaete taxa that are indicators on enriched sediments were measured as being most abundant at Northern Harbour and Southern Flats using quantitative DNA analyses**
- **Jurien Bay the Marmion sites and Carnac Island had low macrofauna biomass (0-45 g wet weight per m^2) Biomass of the inshore Cockburn Sound and Swan River sites were high (100 – 250 g) except Northern Harbour (<1g)**
- **Macrofauna species diversity was lowest (<0.22 species per m^2) at the Jurien Bay, Offshore Marmion sites and the Parmelia Bank (dredge spoil) site and highest (ca. 1.5 species per m^2) at Parmelia Bank, Port Beach and City Beach.**

4.3.4 Relationships between biotic and abiotic parameters measured along the gradient

We used multiple regression analyses and principal component analyses to assess which relationships between the range of parameters measured were important. These are used to present some simple models to show which parameters are associated with each others and may provide useful predictors of sediment characteristics relative its biogeochemistry and ecology

Multiple regression models

A linear multiple regression with a forward stepwise algorithm was used to assess which environmental factors had the most influence on the various measures of productivity at the study sites. These data don't meet the requirements for a regression analysis since the non-assessed environmental factors could not be held constant while variation in the assessed factor was determined. Nonetheless, these analyses can still provide a valuable assessment of the environmental factors that best predict productivity. Selections of models of different sizes yielded statistically significant ($p<0.05$) models for each growth factor except protozoa (Table 4.11).

Percentage carbon content in the sediment was the first factor to be added to the candidate model for sediment chlorophyll *a* concentrations with an adjusted R^2 of 0.498 (Table 4.11). Dissolved silicate was the only other significant factor to be added to the chlorophyll *a* model for a final R^2 of 0.601 ($p=0.001$, Table 4.11).

For phaeopigments, light attenuation was the first factor to be added ($R^2=0.767$; $p<0.0001$;Table 4.11). Like the sediment chlorophyll *a* model, silicate concentration was the second significant factor to be added to the model ($R^2=0.906$, $p<0.0001$, Table 4.11). The final significant factor to be added to the model for phaeopigments was sediment nitrogen content to produce a model with a final adjusted R^2 of 0.93 ($p<0.0001$,Table 4.11).

The candidate model for percentage organic matter contained only percentage nitrogen content as a significant factor. The adjusted R^2 for this model was 0.698 ($p<0.0001$, Table 4.11).

The candidate models for each of the cell data factors featured mode grain size as an important predictor of microbial community dynamics. Mode grain size was the first factor to be added to the candidate model for autotrophic bacteria (R^2=0.422). Sediment nitrogen content was found to be almost as important for autotrophic bacteria growth with a final adjusted R^2 for the model of 0.842 (p<0.0001,Table 4.11).

Like the model autotropic bacteria, the model for filamentous bacteria also added mode grain size as the first environmental factor (R^2=0.422, p=0.004). The next (and final) significant factor to be added to this model was ammonia concentration for a final R^2 of 0.859 (p<0.0001,Table 4.11). The candidate model for sediment phytoplankton counts also added mode sediment grain size as the most important factor with a R^2 of 0.65. The next most important predictor to be added was percentage nitrogen content (R^2=0.745, p<0.0001, Table 4.11).

The most important predictor of organic detritus area counts were the presence of the nutrient dissolved silica. This factor alone produced a model with an adjusted R^2 of 0.837 (p<0.0001,Table 4.11). Model grain size was found to be the next most important factor (R2= 0.896,) followed by light attenuation (R^2=0.968, Table 4.11) and Ammonia concentrations (R^2=0.973, p=0.031,Table 4.11). The model for heterotrophic bacteria contained ammonia concentration as the first factor (R^2=0.823, p=0.001, Table 4.11). Like the model for organic detritus mode grain size was the second factor to be added to the candidate model (R^2=0.887, p=0.011, Table 4.11) followed by light attenuation (R^2=0.931, p=0.037,Table 4.11). The fourth significant environmental predictor for heterotrophic bacteria cell counts was percentage nitrogen content (R^2=0.931, p=0.041,Table 4.11) while dissolved silica was added as the final factor (R^2=0.949, p=0.049, Table 4.11). For number of infauna species, number of infauna individuals and ash free dry weight (AFDW) percentage carbon content was the most important predictor (R^2=0.365 and 0.846; Table 4.11). For number of infauna species and AFDW mode grain size was the only other factor to be added to the model (#species: R^2=0.494,p=0.008 and AFDW:R^2=0.904,p<0.0001; Table 4.11). For number of infauna individuals, Ammonia was the only other factor to be added (R^2=0.867,p=0.008; Table 4.11). The most important predictor of macrofauna biomass was percent nitrogen content (R^2=0.222) followed by Ammonia concentration (R^2=0.53, p=0.003; Table 4.11). Percentage carbon content was the next factor to be added to the model (R^2=0.704, p<0.0001) followed by Nitrate and Nitrite concentrations. The final adjusted R^2 for the model was 0.77 (p<0.0001; Table 4.11).

Multiple linear regression analyses indicated that percentage carbon and the presence of silicate were the best predictors for chlorophyll *a* concentrations. This differed from phaeopigments where light attenuation, silicate and percentage nitrogen content were identified as important covariates. The importance of silicates in both models is consistent with diatoms being the dominant benthic micro alga in these sediments (see analysis of phytopigments above). Mode grain size was identified as an important predictor in biomass estimates of autotrophic bacteria, heterotrophic bacteria and filamentous bacteria as well as for cell counts of phytoplankton and organic detritus content. Previous studies have identified sediment grain surface area has the strongest correlate of bacterial abundance in coastal sediments (Schmidt et al 1998). For example, the numbers of bacteria were found to be inversely proportional to grain size in sediments on the tidal flat of Nova Scotia (Dale, 1974).

Table 4.11. Candidate models obtained from linear multiple regressions in SPSS 17.0 comparing sediment biomass data to environmental parameters at each site. Only statistically significant models are included in the table.

No	Model	Adj R^2	(p)
[Chlorophyll *a*]			
1	%Carbon Content	0.498	0.001
2	%Carbon Content + Silicate	0.601	0.001
[Phaeopigment]			
1	Light Attenuation	0.767	<0.0001
2	Light Attenuation + Silicates	0.891	<0.0001
3	Light Attenuation + Silicates + %Nitrogen Content	0.963	<0.0001
% Organic Matter			
1	% Nitrogen Content	0.35	0.016
Autotrophic Bacteria (Biomass)			
1	Mode Grain Size	0.544	0.001
2	Mode Grain Size + Nitrogen Content	0.867	<0.0001
Filamentous Bacteria (Biomass)			
1	Mode Grain Size	0.628	<0.0001
2	Mode Grain Size + Ammonia	0.892	<0.0001
Phytoplankton (Cell Count)			
1	Mode Grain Size	0.716	<0.0001
2	Mode Grain Size + % Nitrogen Content	0.758	<0.0001
Protozoa			
1	No significant environmental factors		
Organic Detritus (Area counts)			
1	Silicates	0.837	<0.0001
2	Silicates + Mode Grain Size	0.925	<0.0001
3	Silicates + Mode Grain Size + Light Attenuation	0.977	<0.0001
Heterotrophic Bacteria			
1	Ammonia	0.823	<0.0001
2	Ammonia + Mode Grain Size	0.884	<0.0001
3	Ammonia + Mode Grain Size + Silicates	0.920	<0.0001
4	Ammonia + Mode Grain Size + Silicates + % Nitrogen content	0.949	<0.0001
Number of Infauna species			
1	% Carbon Content	0.365	0.008
2	% Carbon Content + Mode Grain Size	0.449	0.008
Number of Infauna individuals			
1	% Carbon Content	0.846	<0.0001
2	% Carbon Content + Ammonia	0.867	<0.0001
Macrofauna Biomass (wet weight)			
1	% Nitrogen Content	0.222	0.037
2	% Nitrogen Content + Ammonia	0.530	0.003
3	% Nitrogen Content + Ammonia + % Carbon Content	0.704	<0.0001
4	% Nitrogen Content + Ammonia + % Carbon Content + Nitrate and Nitrite	0.770	<0.0001
Infauna Ash Free Dry Weight (AFDW)			
	% Carbon Content	0.753	<0.0001
	% Carbon Content + Mode Grain Size	0.904	<0.0001

Principal Component Analyses

A PCA analysis comparing water quality characteristics and environmental factors with the study sites was also performed. The analysis comparing all sites found:

- Marmion Sites grouped together along with some Cockburn Sound sites (Figure 4.38).
- Swan River and Northern Harbour separated from the other sites on the basis of bacterial content, % Carbon and Nitrogen content, light attenuation, and percentage organic matter.
- Hall Bank and Jervoise Bank separated from other sites on the basis of Mode grain size and Phytoplankton cell counts.

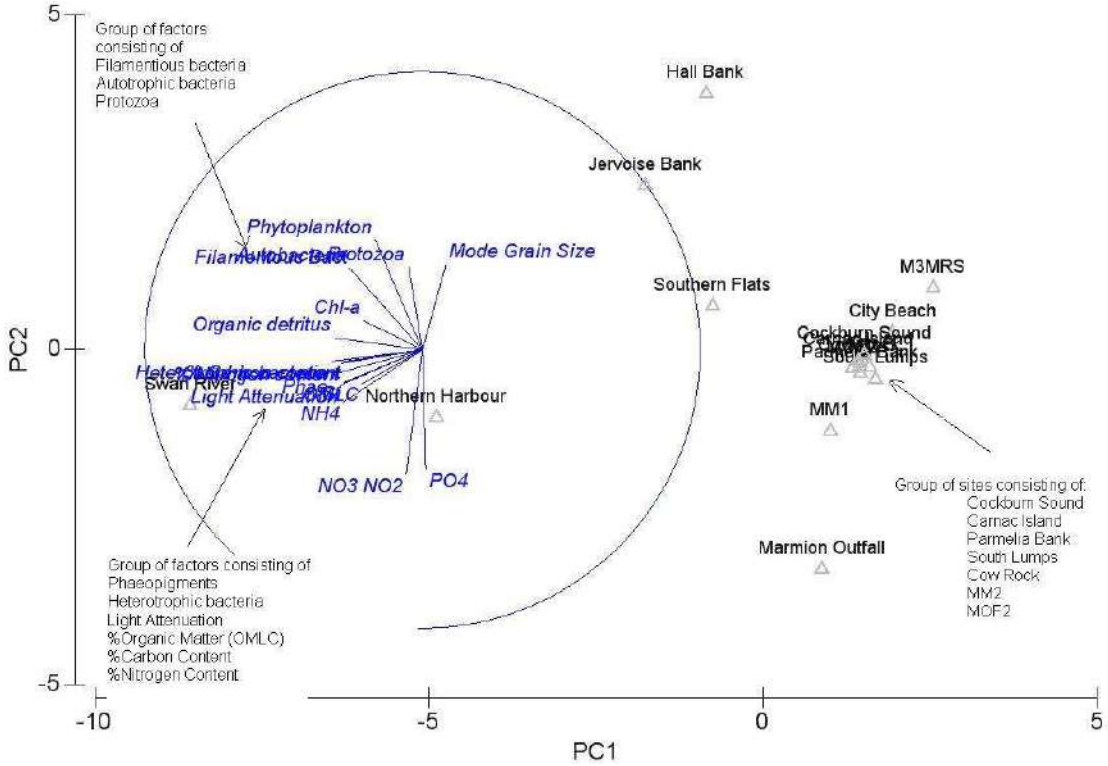

Figure 4.38. PCA analyses comparing water quality and environmental factors from all of the study sites in 2008/9 and 2010.

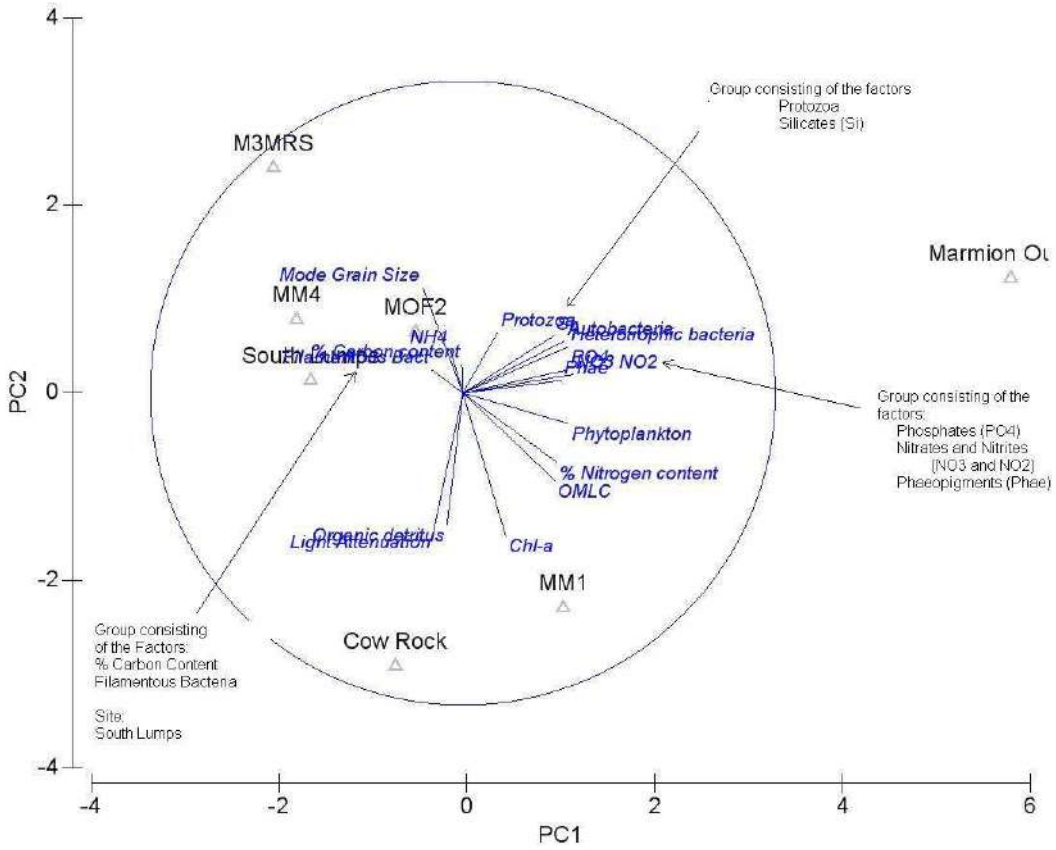

Figure 4.39. PCA analyses comparing water quality and environmental factors from the Marmion sites in 2008/9 and 2010.

At the Marmion locations sites, Marmion Outfall was an outlier on the basis of the nutrients Nitrate and Nitrite, Phosphate, and the presence of heterotrophic and autotrophic bacteria, and phaeopigment concentrations (Figure 4.39). Other sites were separated by mode grain size (M3MRS) and Chlorophyll *a* concentrations (MM1 and Cow Rock seeFigure 4.39).

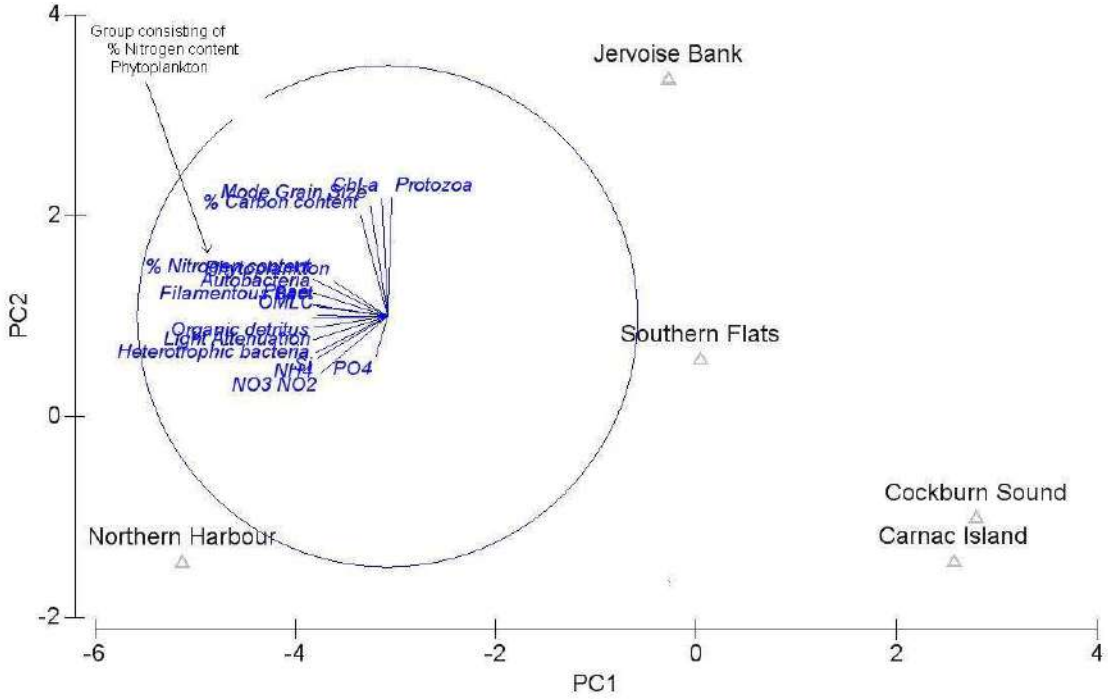

Figure 4.40. PCA analyses comparing the water quality and environmental factors present in just the Cockburn Sound sites in 2008/9 and 2010.

At the Cockburn Sound sites, Northern Harbour was removed from the other sites due to the nutrients ammonia, nitrate and nitrate, and phosphate and the presence of heterotrophic bacteria (Figure 4.40). Jervoise bank was separated from other Cockburn Sound Sites due to chlorophyll *a* concentrations and the presence of protozoa. Southern Flats was separated from Cockburn Sound and Carnac Island by percentage nitrogen content and phytoplankton counts (Figure 4.40).

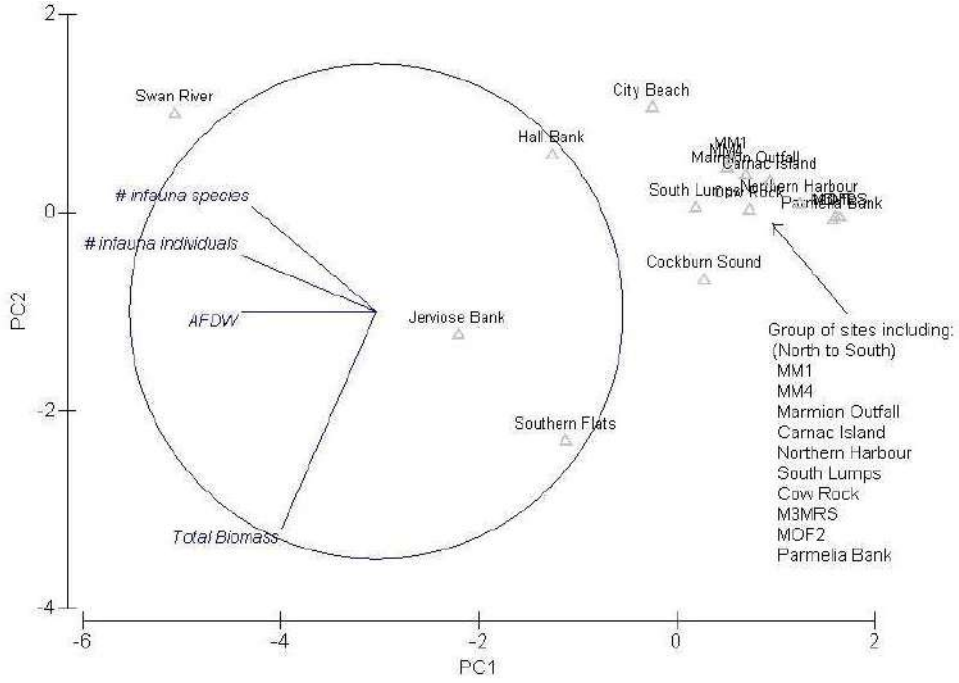

Figure 4.41. PCA analyses comparing the water quality and environmental factors present to the Infauna data for all sites in 2008/9 and 2010.

The Swan River, Jervoise Bank, Southern Flats and Hall Bank sites were separated from the main group of sites consisting of the Marmion Lagoon sites and remaining Cockburn Sound site (Figure 4.41).

The Swan River was separated from the main group on the basis of number of infauna species and individuals as well as AFDW. Jerviose Bank was separated from the main group by AFDW while Hall Bank was separated from the main group by number of infauna species, individuals and AFDW. Southern Flats differed from the other sites due to the total biomass present at the site (Figure 4.41).

Key Findings

- **The multiple regression analyses showed that as expected the indicators of sediment enrichment like %carbon, % nitrogen were strongly associated with a range of other biogeochemical parameters but that when coupled with factors such as sediment grain size provide a useful predictor of infaunal biomass**
- **Principal Components Analysis revealed how at Cockburn Sound there was a clear separation of Northern harbour and the Cockburn Sound (Woodman's Point) and Carnac site on the axis related to range of nutrient enrichment indicator parameters with Southern Flats and Jerviose Bank intermediate to these groups**
- **Principal Components Analysis for the Marmion sites revealed a strong separation of the Marmion outfall site from the others based on water column nutrients and heterotrophic bacteria levels.**

Summary of relationships

Interrelationships between the range of parameters measured show that sediment habitats are complex and a range of responses were observed. However it is clear from the analyses, that nutrients drive much of the response and that both physical and ecological interactions mediate the response of the sediment biogeochemistry to the enrichment. The characteristics of sediments across a nearshore gradient of sediment enrichment (high in Cockburn Sound and low at Marmion) and an onshore-offshore gradient of sheltered nearshore to exposed offshore at both Cockburn Sound and Marmion) offer an insight into the responses of sediment habitats to nutrient enrichment. A conceptual model can be developed to describe these states and responses in a way which should be useful for managers to both assess the state of nearshore sediment habitats and also predict their trajectory should habitat modification or changed nutrient loading occur.

Sites that are exposed tend to have better water quality, light availability at the seabed and lower levels of sediment nutrient enrichment. These sites have sediment chlorophyll biomass similar to more enriched sites but, as is shown later in this chapter, higher levels of photosynthetic potential. These sites could be regarded as having healthy sediments and typify much of the soft sediment habitats which occur along the mid- and south-west Australian coast. In these habitats natural levels of sediment nutrients is due to the natural incorporation of

organic matter derived from the excess production of seagrass and macroalgal production (this is discussed in Chapter 3).

Sites that are sheltered are more susceptible to enrichment as a result of greater water residence times from comparably less flushing and less physical disturbance of the seabed from waves. As a result of this enrichment and less physical disturbance, the sediment can support a greater biomass and diversity of heterotrophic organisms and subsequently a complex interaction of biogeochemical and ecological interactions come to define these habitats.

When the combination of degree of shelter and level of enrichment reach levels where biological and ecological processes mediating the enrichment are reduced, the habitat advances to the degraded state such as observed at Northern Harbour where reduced water clarity reduces BMA primary production and heterotrophic bacteria cause the sediment to become anoxic reducing the biomass and diversity of animals to only species which are highly tolerant to reduced oxygen.

The three states described were observed in this study however most sites are a variant or transitionary phase between these condition states.. Figure 4.42 below illustrates the changes observed when we compare natural, altered and severely degraded sediment habitats and Figure 4.43 shows a conceptual model of how changes in shelter and anthropogenic nutrient enrichment might set otherwise healthy sediment habitats on a trajectory to altered and degraded states. This model is similar to that proposed by Pearson and Rosenberg (1978) who specified Normal, Transitionary and Polluted states based on changes in infauna abundance, diversity and biomass. Our Principal Component Analyses above also support the presenece of a transitory state between normal and degraded at least at Cockburn Sound.

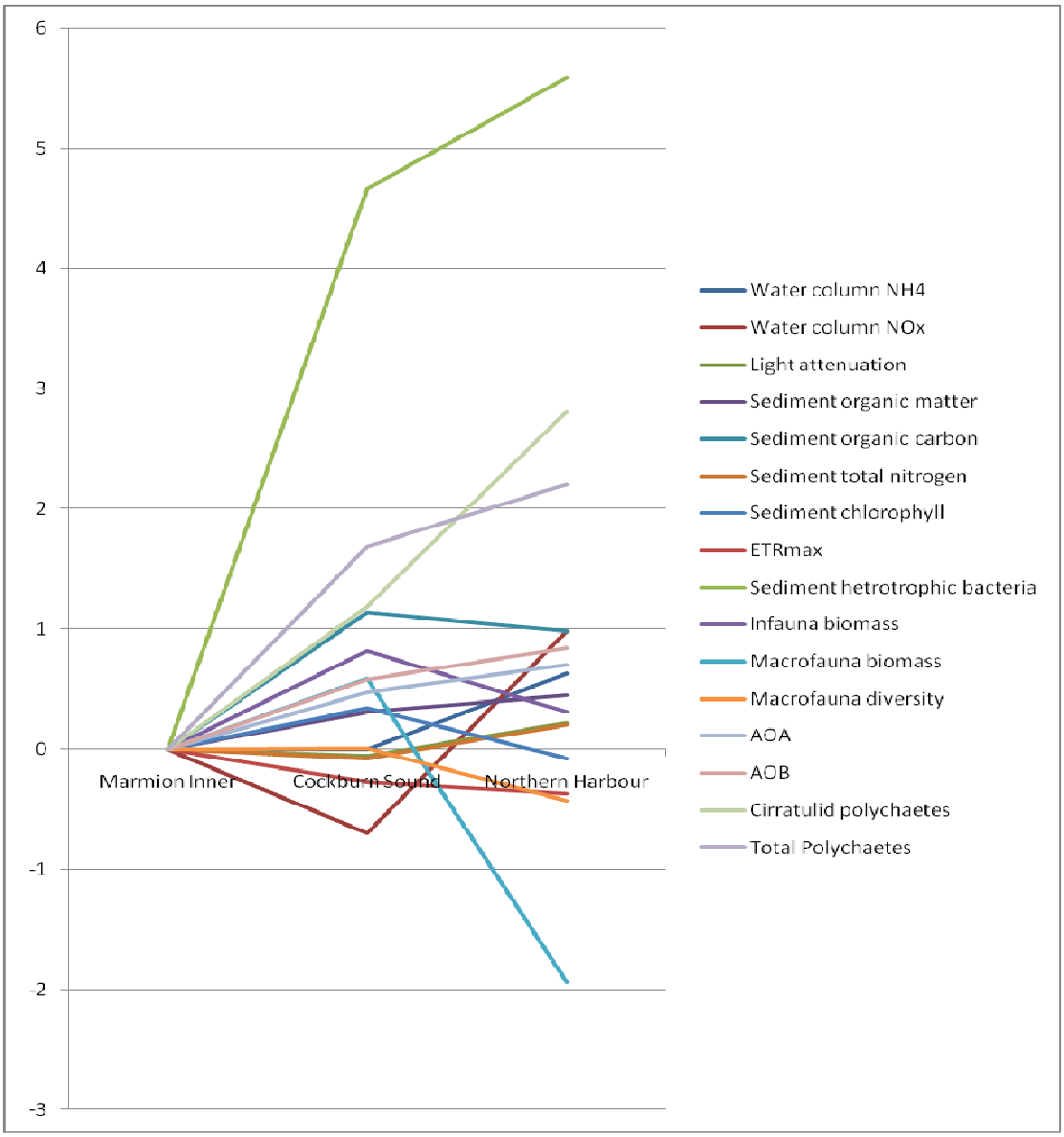

Figure 4.42. Comparison of sediment parameters at Northern Harbour site, other Cockburn Sound sites (except Carnac Island and Parmelia Bank) relative to Marmion inshore sites (Cow Rock and South Lumps – other sites were excluded because data for all parameters was not available from all sites in all years) Y axis is the natural log of the ratio of each site and Marmion inshore (hence all value for Marmion inshore are 1).

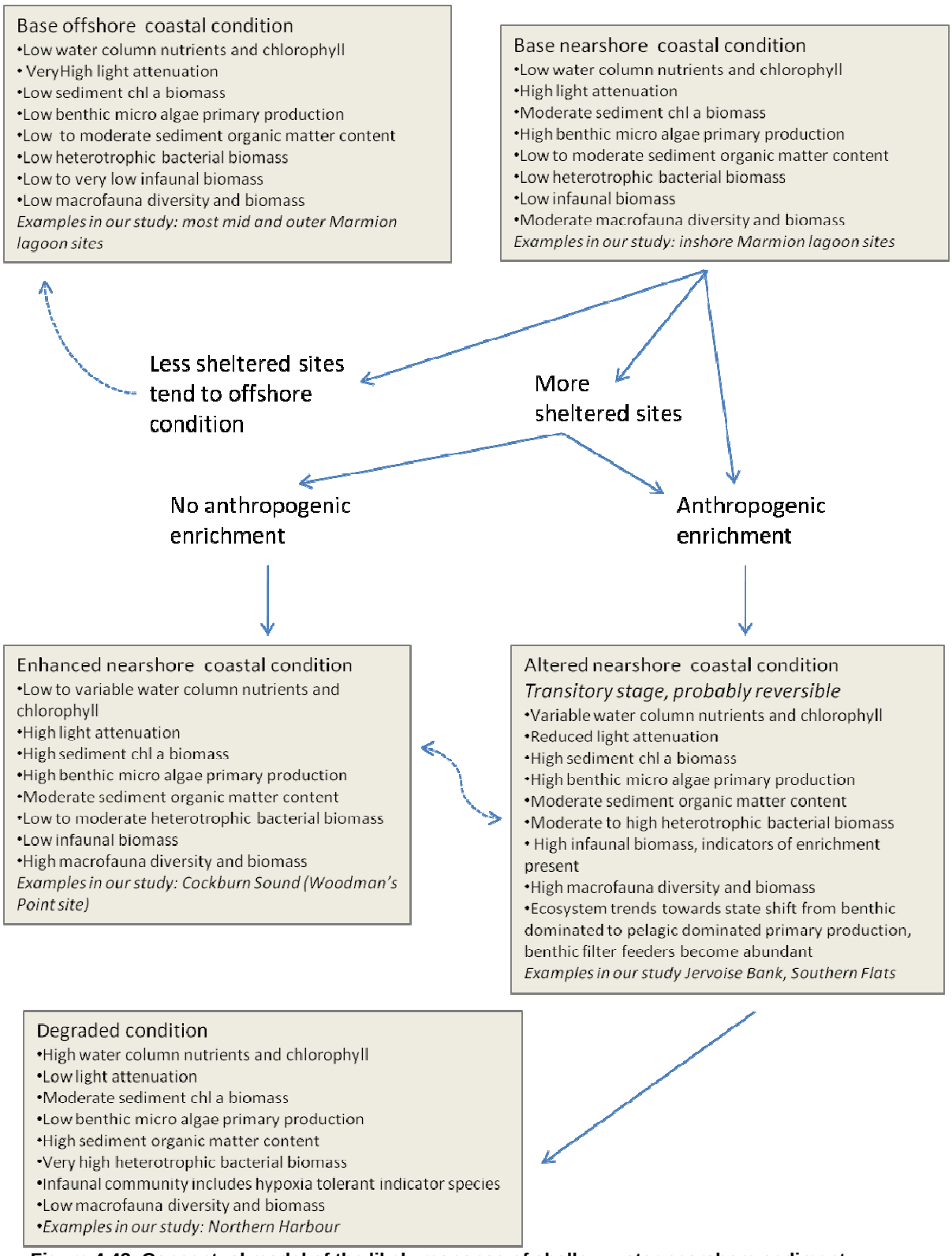

Figure 4.43. Conceptual model of the likely response of shallow water nearshore sediment habitats to increased nutrient enrichment.

Key Findings

- **A hypothesis and conceptual model of soft sediment habitat condition or state is proposed based on the parameters we measured. It suggests that biogeochemical and ecological attributes of sediments can reveal the degree of alteration of sediments between a base state of "typical" or "healthy" sediment habitats and the degraded condition state. Some aspects of the model are simplistic and require qualification but it does present a practical approach to assessing habitats, designing and carrying out monitoring and for predicting the trajectory of sediment habitats where there is concern about the potential for anthropogenic enrichment.**

4.3.5 Process Studies

Process studies: PAM Fluorometry

The lowest average ETR_{Max} was in the Swan River during the second summer (4.8 ± 1.1 μmol electrons m^{-2} s^{-2}) (Figure 4.44). Next lowest was Northern Harbour (both summers) or Southern Flats (winter) (Figure 4.44). Increased nutrient loadings have long been recognised as a stressor to Cockburn Sound and the Swan River and increased epiphyte growth competing for resources has been blamed for reduction in the extent of seagrass beds in the sound (Cambridge et al., 1986). Similar competitive impact on benthic micro-algae (i.e. increased biomass of pelagic species would reduce light penetration) may be reflected by a reduction in photosynthetic efficiency (ETRMax).There appears to be a gradient in the PMax values moving away from one of the high sediment nutrient stations along a gradient of reducing sediment nutrient concentrations. There was a gradual increase in ETR_{Max} values across stations located between Northern Harbour at the northeast of Cockburn Sound and Carnac Island at the north west (Northern Harbor, Jervoise Bank, Cockburn Sound and Carnac Island) with each being significantly higher than the previous (Figure 4.44). ETR_{Max} values at Carnac Island were not significantly different to the open ocean City Beach station in any of the three sampling trips (Figure 4.44) suggesting that production conditions at the Carnac Island station are similar to those at City Beach. However, ETR_{Max} at the station located near the mouth of the Swan River (Port Beach) was universally lower than the City Beach and Carnac Island stations (Figure 4.44) suggesting that the influence of the river may extend into the surrounding ocean.

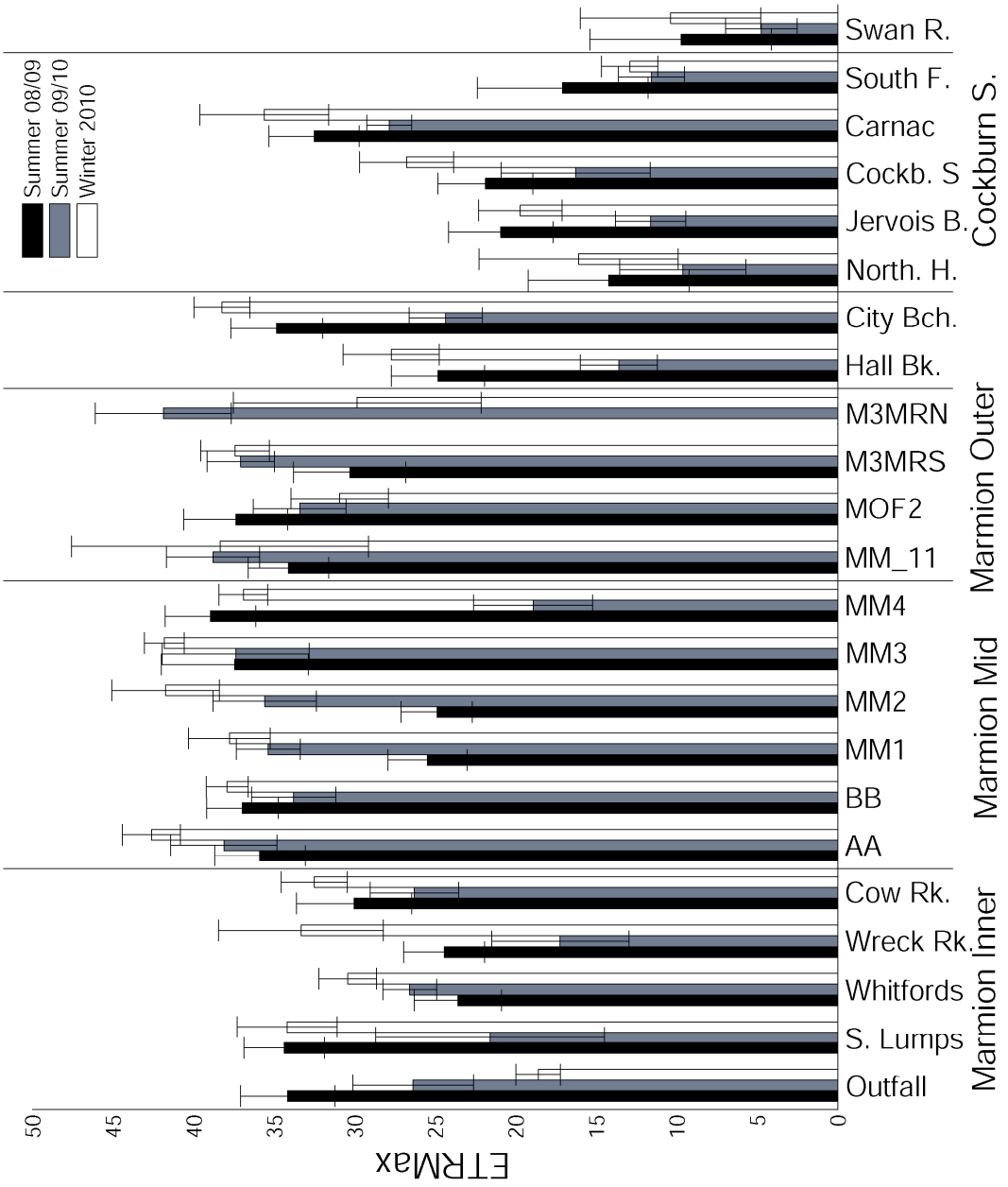

Figure 4.44. ETRMax derived from PAM flourometer "rapid light curves" collected twice in summer and once in winter from a series of stations located between Marmion Outfall north of Marmion lagoon and Southern Flats in the south of Cockburn Sound (including one station in the Swan River).

We tested for correlation among the environmental parameters (biomass, wave energy, depth and temperature. that are most likely to have an effect on ETRMax values Marmion Lagoon. In this case, ETRMax was not well correlated with chlorophyll *a* suggesting other environmental processes such as disturbance by waves have more influence here Table 4.12. PMax and chlorophyll *a* were both positively correlated to wave energy (Table 4.12), suggesting that waves stimulate production and biomass. Previous investigations in this region were biomass and production of BMA tended to be inversely proportional to natural and simulated disturbance (Forehead 2006). However, wave energy likely releases nutrients in the upper water column (Lourey and Kirkman 2009) and the positive correlation between

PMax/chlorophyll *a* and waves may be a community response to the release of those nutrients (Greenwood 2010). A correlation between ETRMax and depth has been observed in samples collected from a large range of depths (see chapter 3). There was no correlation between PMax and depth across the much smaller range of depths investigated here (6 – 15 m) (Table 4.12). This lack of correlation between PMax and depth suggests that the stations were effectively part of one functional depth zone (Forehead and Thompson 2010). The significant correlation between wave energy and temperature is a cross correlation reflecting seasonal effects on both those parameters (Table 4.12).

Table 4.12. Pearson correlation coefficients and p values (in brackets) for the correlation between PMax with chlorophyll *a* content, wave energy, depth and temperature. P values < 0.05 are highlighted in bold and n=28.

	Chlorophyll *a*	Bottom velocity	Depth	Temperature
PMax	0.197 (0.32)	**0.390 (0.040)**	-0.072 (0.72)	-0.024 (0.90)
Chlorophyll *a*		**0.440 (0.019)**	-0.223 (0.26)	-0.218 (0.27)
u_{bot} (m s^{-1})			0.154 (0.43)	**-0.501 (0.007)**
Temperature				-0.112 ((0.57)

The Swan river station had the lowest average alpha values (0.065 ± 0.011 to 0.105 ± 0.010 μmol electrons μmol $photons^{-1}$ depending on sampling trip), which were significantly lower than all the other the other stations in the corresponding year (Figure 4.45). The next lowest alpha values tended to be at the Northern Harbour station (in the first summer and winter samplings) although tended not to be universally different to surrounding stations (Figure 4.45). The rest of the stations were similar (Figure 4.45).

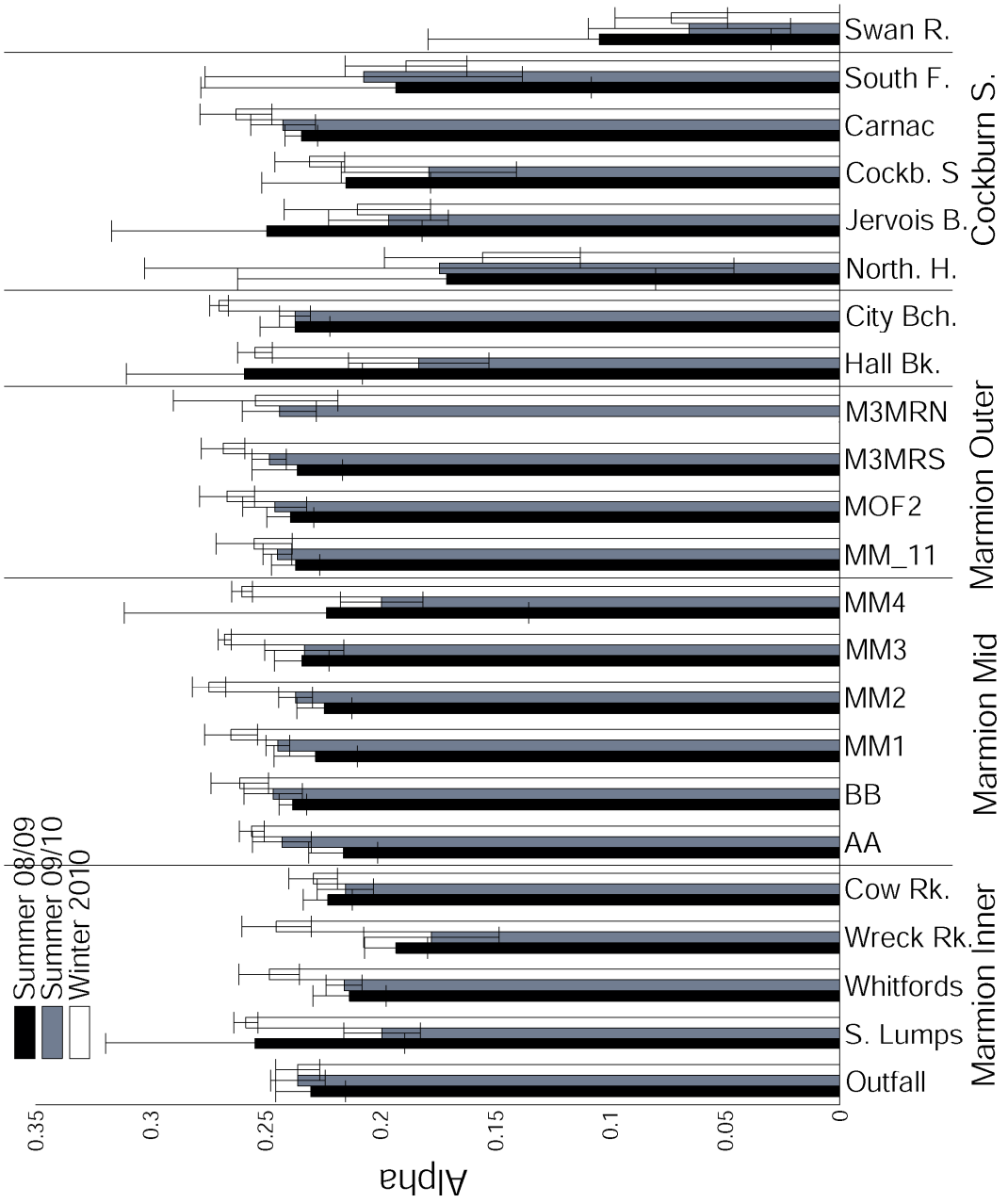

Figure 4.45. Alpha derived from PAM fluorometer "rapid light curves" collected twice in summer and once in winter from a series of stations located between Marmion Outfall and Southern Flats in the south of Cockburn Sound (including one station in the Swan River).

The highest Ik values were typically measured at the open ocean stations. The lowest Ik values tended to be in Cockburn Sound, for example Jervoise Bank (58.9 ± 6.8 µmol photons m^{-2} s^{-1} in the second summer) and Southern Flats (57.8 ± 7.2 µmol photons m^{-2} s^{-1} in the second summer and 69.3 ± 7.5 µmol photons m^{-2} s^{-1} in the winter) (Figure 4.46) presumably in response to lower levels of ambient light reaching the sediments. These spatial variations in IK are broadly consistent with the spatial variations in PMax with one important exception. PMax (and alpha) in the Swan River were the lowest recorded while Ik at that station was equivalent to the highest values measured.

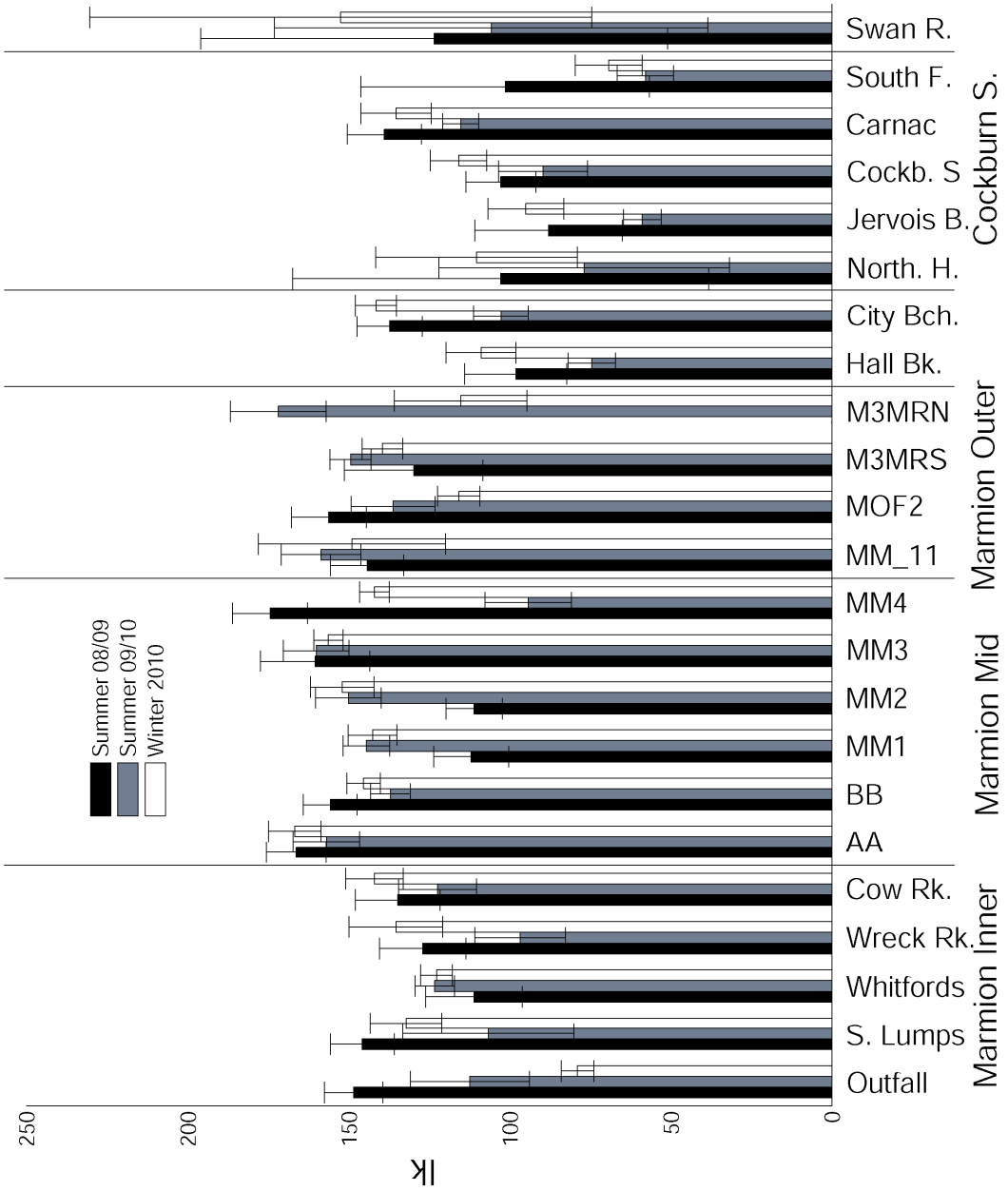

Figure 4.46. Ik derived from PAM flourometer "rapid light curves" collected twice in summer and once in winter from a series of stations located between Marmion Outfall north of Marmion lagoon and Southern Flats in the south of Cockburn Sound (including one station in the Swan River).

Seasonal variations in ETRMax were varied. In some situations ETRMax in winter was significantly lower than one or both summers (Marmion Outfall and MOF2) (Figure 4.44). However, in most situations where there was a significant trend, ETRMax in the winter was either higher than one (South Lumps, Whitford Rock, AA, MM1, MM2, MM4, M3MRN, Port Beach, City Beach, Northern harbour, Jervoise Bank, Cockburn, Southern Flats) or both summers (Wreck Rock) (Figure 4.44). At Marmion Outfall, Ik in the first summer (148.5 ± 6.8 µmol photons m^{-2} s^{-1}) was significantly higher than in the winter (79.0 ± 7.9 µmol photons m^{-2} s^{-1}) (Figure 4.46). At MM4, Ik in the first summer (174.4 ± 6.8 µmol photons m^{-2} s^{-1}) and the

winter (142.0 ± 7.5 μmol photons m^{-2} s^{-1}) were higher than the second summer (94.3 ± 6.8 μmol photons m^{-2} s^{-1}) (Figure 4.46). At Southern Flats, the first summer Ik (101.4 ± 6.8 μmol photons m^{-2} s^{-1}) was higher than the second (57.8 ± 7.15μmol photons m^{-2} s^{-1}) and at Swam River, winter Ik (152.5 ± 7.9μmol photons m^{-2} s^{-1}) was higher than the second summer Ik (105.8 ± 7.5 μmol photons m^{-2} s^{-1}) (Figure 4.46).

There were few significant seasonal variations in alpha. At Wreck Rock the second summer (0.178 ± 0.010 μmol electrons μmol $photons^{-1}$) was significantly lower than in the winter (0.245 ± 0.010 μmol electrons μmol $photons^{-1}$) (Figure 4.45). The first summer (0.193 ± 0.011 μmol electrons μmol $photons^{-1}$) was lower than the winter but the difference was not significant (Figure 4.45). At Port Beach the second summer (0.183 ± 0.010 μmol electrons μmol $photons^{-1}$) was lower than the first (0.259 ± 0.010 μmol electrons μmol $photons^{-1}$) and the winter (0.254 ± 0.011 μmol electrons μmol $photons^{-1}$) (which were not different to each other) (Figure 4.45).

Key Findings:

- **In Marmion Lagoon ETRMax was lowest inshore, while mid lagoon and outer rates were similar. Unlike other studies ETRMax was not well correlated with biomass but this gradient is at least partly explained by differences in exposure to wave generated bottom stresses.**
- **In Cockburn Sound, ETRMax lowest in what we consider to be our most "impacted" sites (Northern Harbour, Southern Flats and Swan River).**
- **There was an ETRMax gradient along a series of stations distributed along a transect between a high sediment nutrient (Northern Harbour) and low sediment nutrient (Carnac Island) station. These three stations are on a east-west transect running out of Cockburn S. ETRMax at the Carnac Island site is similar to City Beach an oceanic site well removed from Cockburn Sound.**
- **The Port Beach located at the mouth of the Swan River has a lower ETRMax than its nearest stations (Carnac Island and City Beach), possibly reflecting the influence of the Swan River mouth.**

Process Studies: Benthic Primary Production

PMax was higher in summer than winter at all stations except Southern Flats, although in many cases these seasonal differences were not statistically significant (Figure 4.47 and Figure 4.48). The highest average Pmax measured was during summer at Cockburn Sound (96.7 ± 18.0 mmol O2 m-2 hr-1) with the second highest measured at Northern Harbor during summer (86.2 ± 13.0 mmol O2 m-2 hr-1) (Figure 4.47 and Figure 4.48). The lowest summer PMax values were at Marmion Outfall and Southern Flats stations (34.9 ± 12.9 and 33.1 ± 5.9 mmol O2 m-2 hr-1, respectively) (Figure 4.47 and Figure 4.48). Summer PMax was significantly higher than winter PMax (i.e. 95% confidence intervals do not overlap) at City Beach, Cockburn Sound and Northern Harbour (Figure 4.48). Winter Pmax was significantly higher than summer PMax at the Southern Flats station.

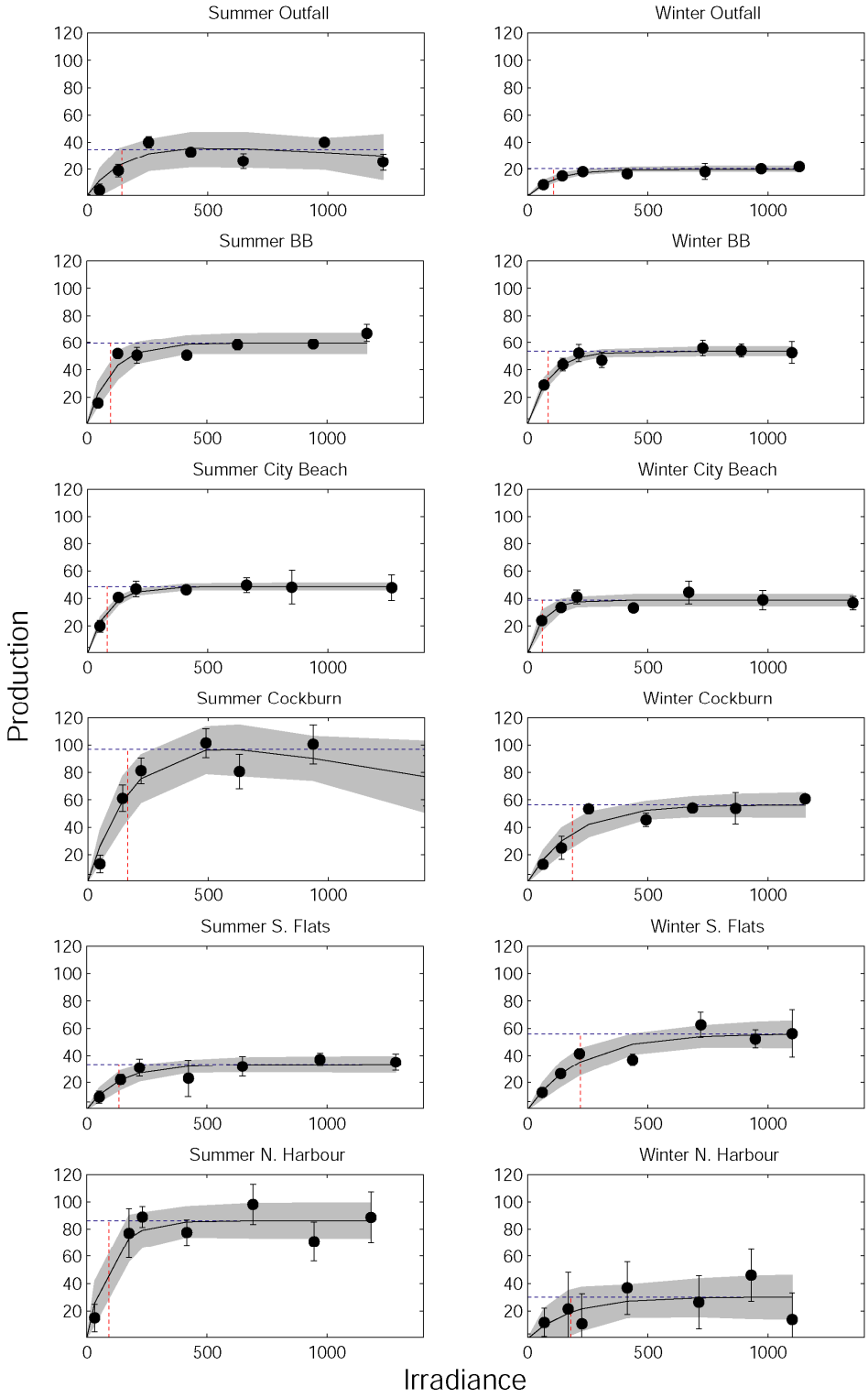

Figure 4.47. Production (mmol O_2 m^{-2} h^{-1}) versus irradiance (µmol photons m^{-2} s^{-1}) curves collected during summer (left) and winter (right) from six stations across our disturbance gradient. The blue dotted line is PMax and the red dotted line is Ik. The shaded area is the 95% confidence interval for the fitted curve.

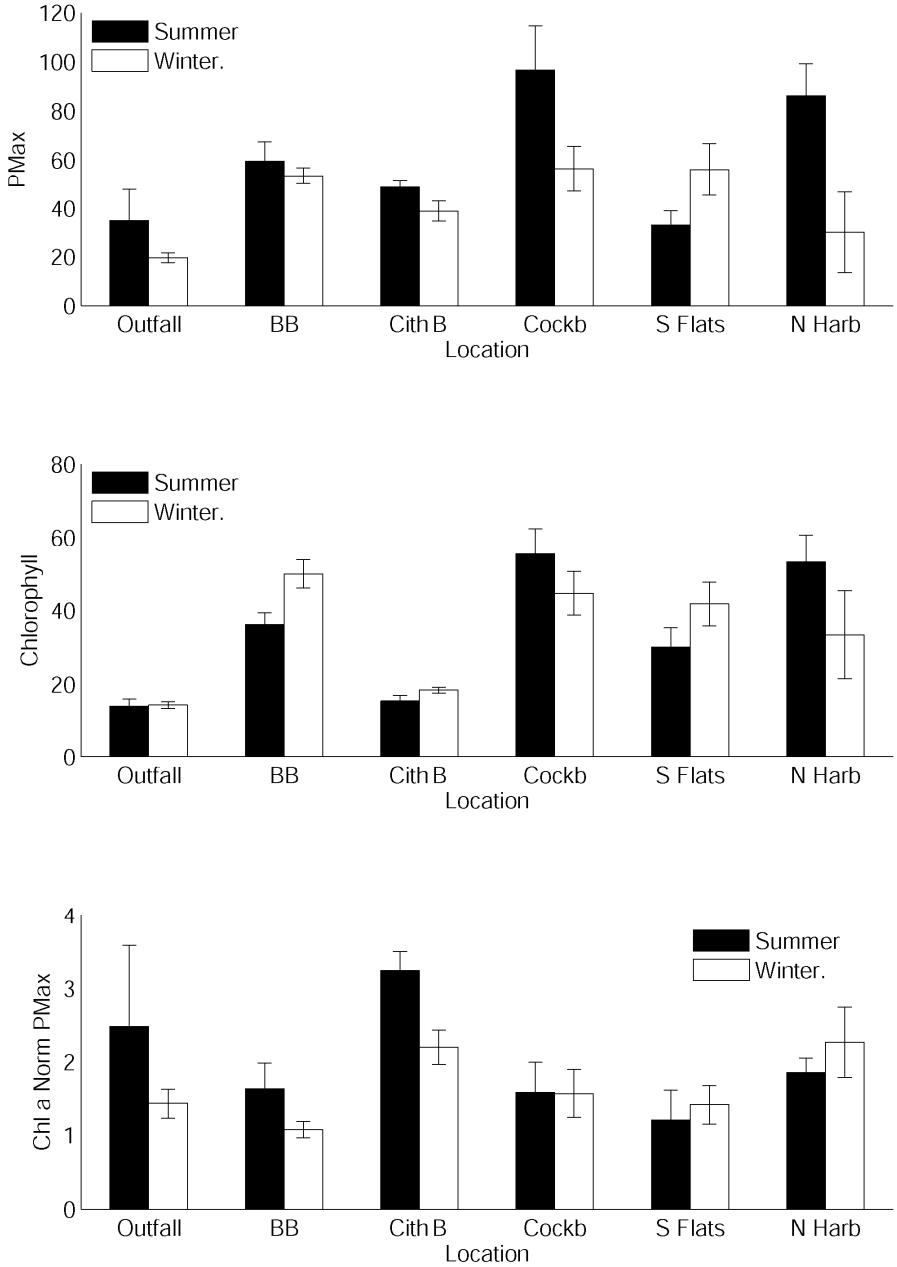

Figure 4.48. Mean (and 95% confidence intervals) of (top) PMax (mmol O_2 m^{-2} h^{-1}), (centre) Chlorophyll *a* concentration (mg m^{-2}) and (bottom) PMax calculated from Chlorophyll *a* normalised oxygen flux data (mmol O_2 m^{-2} h^{-1}/mg m^{-2}) collected in summer and winter from the six stations across the disturbance gradient.

Biomass generally has a strong influence on production rates and this study is no exception. Around 63% of the variation in Pmax is explained by variations in biomass (Figure 4.49). The spatial variations in biomass were very similar to and generated the majority of spatial PMax variations. For example, the Cockburn and Northern Harbour stations had the highest summer concentrations of chlorophyll *a* (55.4 ± 6.9 and 53.2 ± 7.4 mg m^{-2} respectively) (Figure 4.48). Similarly, the large summer winter differences in PMax at the three Cockburn Sound stations (Cockburn, Southern Flats and Northern Harbour) were mirrored by similar variations in biomass (Figure 4.48).

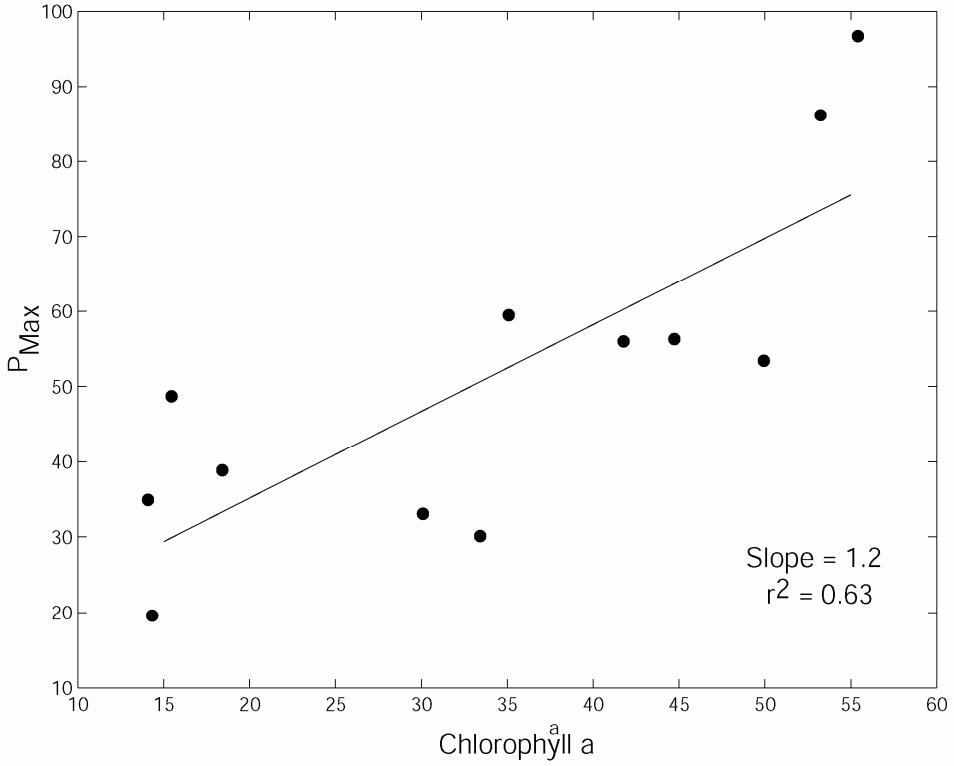

Figure 4.49. The relationship between sediment chlorophyll *a* content and PMax.

PMax in the absence of the contribution made by differences in biomass (i.e production data normalised according to chlorophyll *a* content or Pb) tends to be higher outside Cockburn Sound than within. In summer, PbMax (a measure of production efficiency) was highest in the open at City Beach (3.2 ± 0.3 mmol O_2 m^{-2} h^{-1}/mg m^{-2}) and lowest at Southern Flats in Cockburn Sound (1.2 ± 0.4 mmol O_2 m^{-2} h^{-1}/mg g^{-1}) (Figure 4.48). This suggests that production efficiency is suppressed in Cockburn Sound. Most of the seasonal variations in PMax observed above were due to the seasonal differences in biomass and only City Beach displayed a significant summer to winter difference (a decrease) in PbMax (Figure 4.48).

While IK appeared to be greater in Cockburn Sound (Cockburn, Southern Flats and Northern Harbour) than at stations outside the sound (Out fall, BB and City Beach), None of these differences were statistically significant (Figure 4.50). There were no significant seasonal differences in Ik at any of the stations (Figure 4.50). Similarly, there were also no significant spatial or seasonal differences in alpha across the six stations (Figure 4.50).

Respiration rates (oxygen consumption in dark treatments) were variable although tended to be higher in Cockburn Sound than at stations to the north (Figure 4.50) possibly reflecting higher organic carbon loadings in the sound. This north-south difference was particularly evident in summer where the difference between the Cockburn Sound and the northern stations was most pronounced (Figure 4.50) presumably reflecting temperature related differences in microbial activity. Seasonally, the summer to winter differences in respiration were only significant at the Northern Harbour station (Figure 4.50).

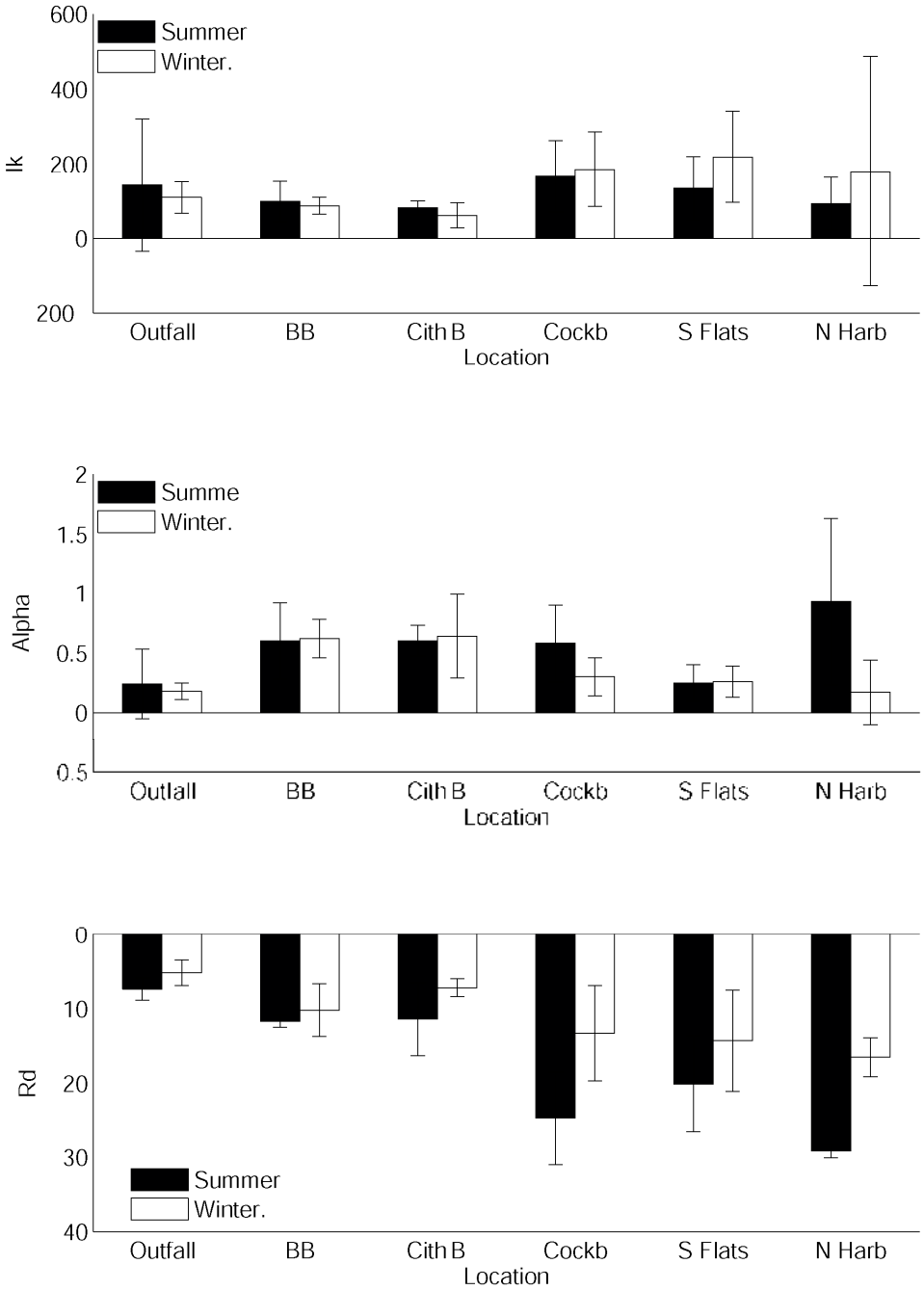

Figure 4.50. Mean (and 95% confidence intervals) of (top) Ik (µmol photons m-2 s-1), (centre) alpha (mmol O2 µmol quanta-1) and (bottom) Rd (mmol O2 m-2 h-1) for data collected in summer and winter from six stations across the disturbance gradient.

Key Findings:

- **Biomass has a strong influence on seasonal and spatial variations in primary production (variations in biomass explain 63% of the variability in production rates).**
- **PbMax (production assessed independently of the effect of biomass = production efficiency) was generally higher at open stations than in Cockburn Sound, suggesting that production efficiency is suppressed in Cockburn Sound.**
- **Respiration rates (oxygen consumption in dark treatments) tended to be higher in Cockburn sound than at open ocean stations to the north possibly reflecting higher organic carbon loadings in the sound.**
- **This north-south difference in respiration rates was generally most evident in the summer, presumably reflecting temperature related constraints on microbial activity.**

Process Studies: Nutrient Fluxes

The majority of mean nutrient fluxes encountered outside Cockburn sound were negative suggesting that consumption of nutrients by microphytobenthos is greater than supply from the sediments. Presumably, with little pelagic nutrients available (Lourey et al., 2006) nutrients released by the sediments are rapidly consumed to sustain the production. For example, silicate was universally consumed outside Cockburn Sound, while on average it was released inside the sound (Figure 4.51). Within Cockburn Sound the magnitude of the silicate fluxes was lowest at the Cockburn station where they were positive but not significant to zero, next highest was at Southern Flats and highest of all at Northern Harbour (Figure 4.51). Seasonal differences were generally not large and the difference between light and dark treatments generally not significant (Figure 4.51).

Phosphate fluxes were a mix of production and consumption, and often these variations were not significantly different to zero (Figure 4.51). There were no consumption/production patterns that were specific to stations within the sound or outside (on average both consumption and production was evident in both locations see Figure 4.51). Average nitrate fluxes were generally strongly negative (consumption) in both the illuminated and dark experimental treatments and in both summer and winter seasons (Figure 4.51). The Southern Flats station was a notable exception to the general consumption trend (Figure 4.51). Nitrate was strongly consumed in dark and light treatments during summer but released during winter sampling (Figure 4.51). Ammonium was universally consumed outside Cockburn Sound, in both seasons and in both light and dark experimental treatments (Figure 4.51). Inside the Sound the situation is quite different. There was pronounced summer time ammonium release from sediments in the dark treatments (Figure 4.51).

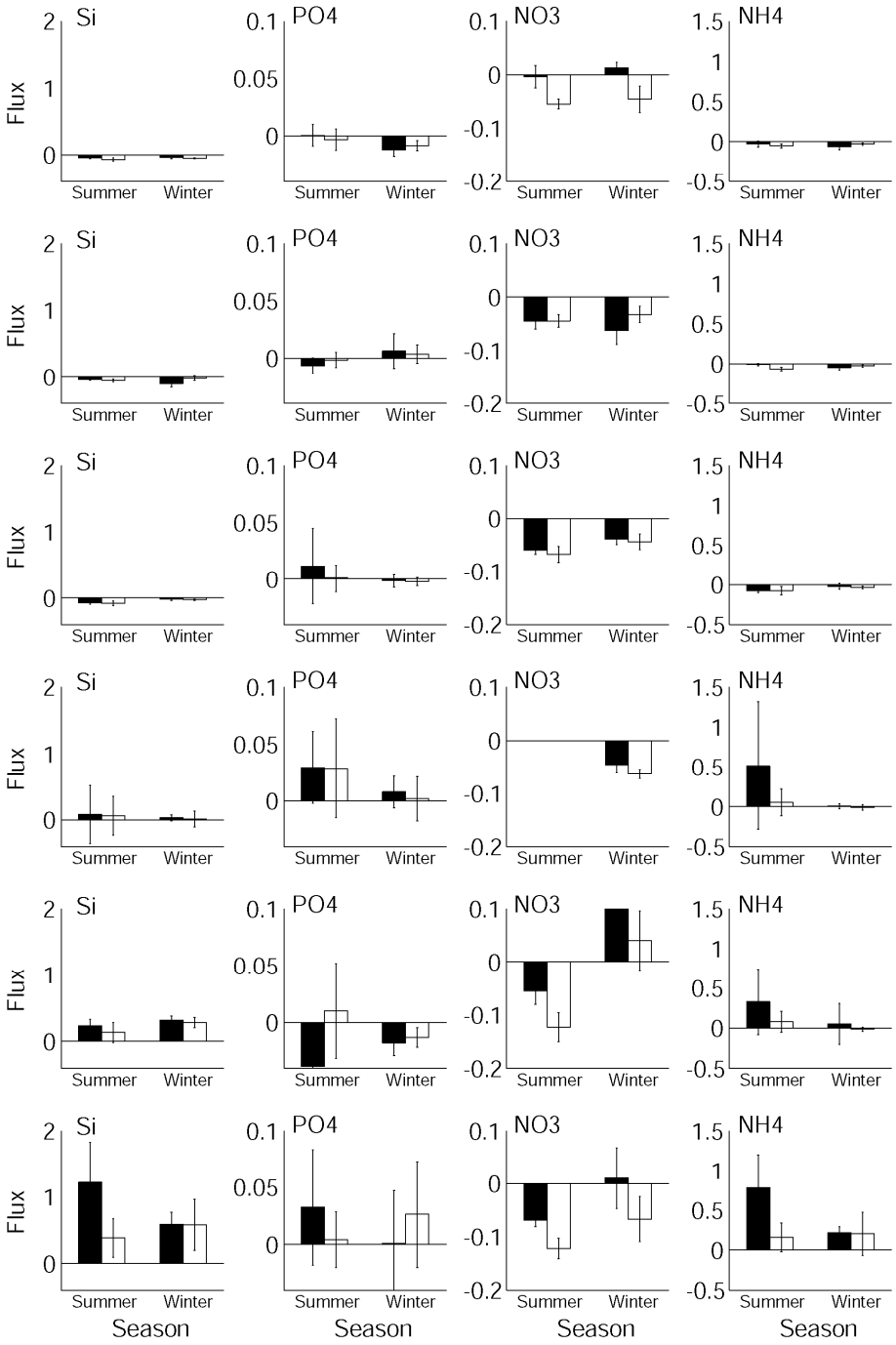

Figure 4.51 Summer and winter sediment nutrient fluxes (mmol nutrients m-2 hr-1) at six stations along the disturbance gradient. The stations arranged from top to bottom are the Marmion Outfall, BB (in Marmion Lagoon) City Beach, Cockburn, Southern Flats and Northern Harbour. The dark bars are dark fluxes (respiration) and the light bars represent the average of all the irradiated treatments.

Conceptually, we expect a negative relationship between dissolved oxygen and nutrient fluxes. Strong bacterial activity is expected to consume oxygen and release nutrients (particularly ammonium) as organic matter is consumed and broken down. In contrast high levels of primary production would produce oxygen and consume nutrients. In general, the relationships between

dissolved oxygen and nutrient concentration for each of the nutrient species were negative (Figure 4.52). Particularly in instances where benthic respiration dominates (i.e. where there was net dissolved oxygen consumption). The highest rates of silicate, phosphate and ammonium production were in situations where the oxygen fluxes were negative (Figure 4.52). The gradient of the relationship between the dissolved oxygen and nutrient fluxes was also steepest where flux rates were less than zero (Figure 4.52). For the dissolved inorganic nitrogen fluxes (i.e. NH_4 plus NO_3) the steeper relationship between dissolved oxygen consumption and nutrient flux starts around -15 mmol DO m^{-2} hr^{-1} (Figure 4.53) suggesting that dark nutrient uptake by phytoplankton dominated production up until that point.

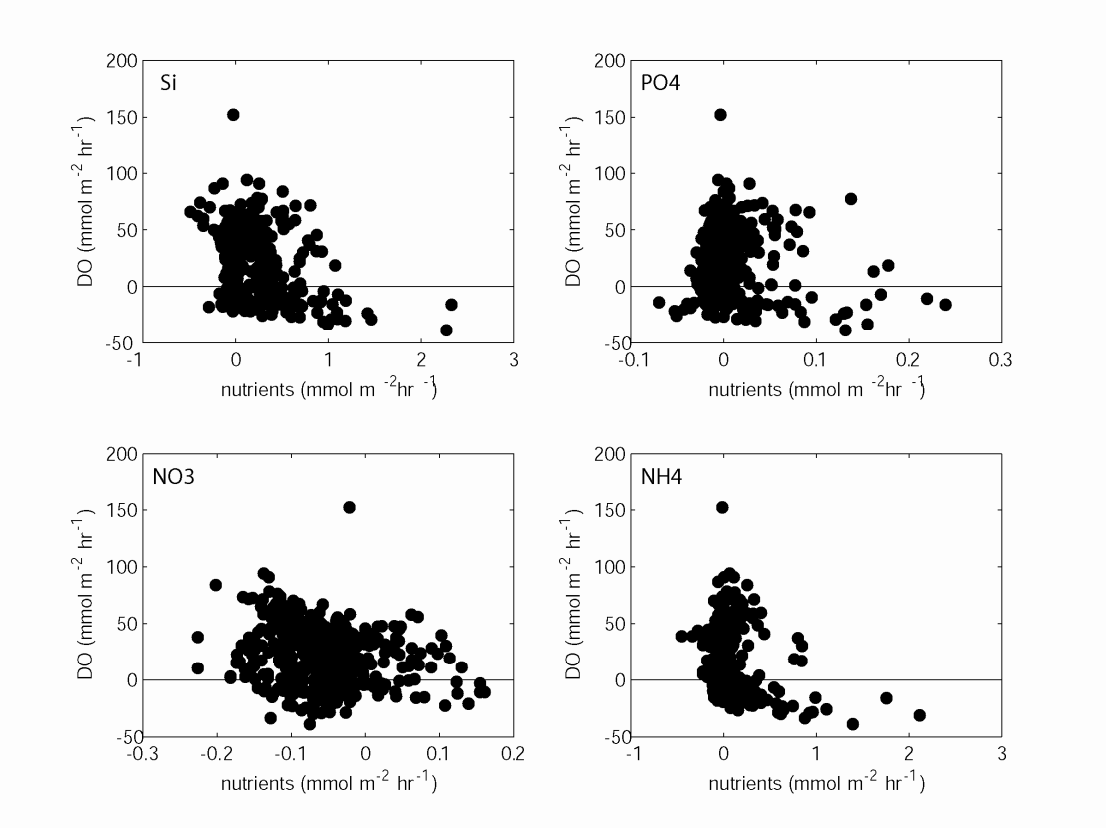

Figure 4.52. Relationship between oxygen production/consumption and sediment nutrient flux.

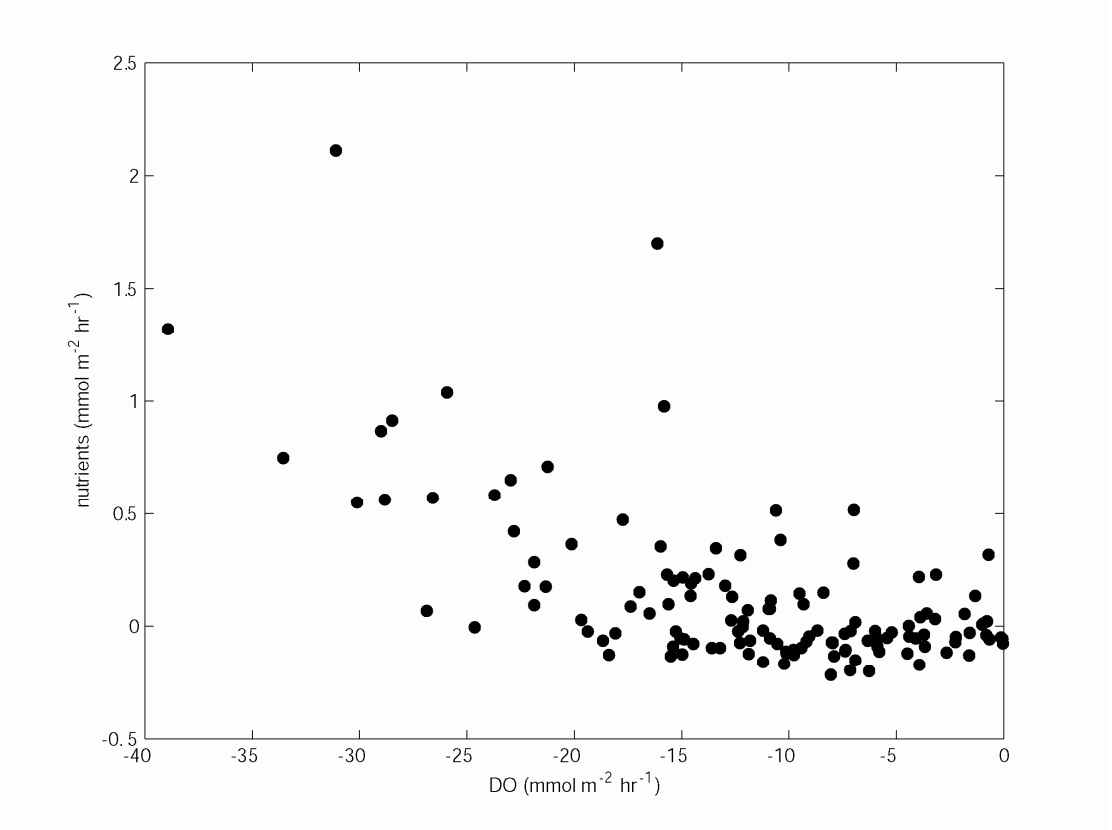

Figure 4.53. Relationship between oxygen production consumption and sediment dissolved inorganic nitrogen flux for situations where respiration dominates production (i.e., the dissolved oxygen flux is less than zero).

In situations where production dominates respiration, the nutrient fluxes were generally centered around zero (e.g. Forehead and Thompson 2010) despite large variations in the magnitude of the oxygen flux (Figure 4.52). These nutrient fluxes represent a small proportion of what would be expected from the rates of oxygen production and Redfield requirements of phytoplankton. These lower than Redfield nutrient flux rates suggest that rapid uptake by microphytobenthos dominates the nutrient dynamics in these sediments. Presumably, with little pelagic nutrients available nutrients released from the sediments are rapidly consumed to sustain the production Nitrate fluxes were an order of magnitude smaller than the ammonium fluxes (i.e., up to ~0.2 mmol m^{-2} hr^{-1} for nitrate compared to >2 mmol m^{-2} hr^{-1} for ammonium see Figure 4.51). This large efflux of ammonia relative to nitrate suggests nitrification may have been inhibited (possibly by low dissolved oxygen) and conversion of ammonium to nitrate is small. Alternately nitrate generated by nitrification may have been lost via coupled denitrification. However, as previously measured rates of denitrification in Cockburn Sound sediments were low (Forehead 2006) the loss of significant nitrate through that process (or annamox) is perhaps unlikely.

Key Findings:

- **The majority of mean nutrient fluxes encountered outside Cockburn sound were negative suggesting that consumption of nutrients by microphytobenthos out strips supply from the sediments.**
- **Ammonium was universally consumed outside Cockburn Sound, in both seasons and in both light and dark experimental treatments suggesting that there is dark uptake by microphytobenthos at these stations.**
- **Inside the Sound there was pronounced summer time ammonium release from sediments in the dark treatments suggesting that remineralisation of organic matter during summer is greater than the capacity of dark uptake by MPB to consume released nutrients.**
- **Large efflux of ammonia relative to nitrate suggests nitrification may have been inhibited (possibly by low dissolved oxygen) or that nitrate generated by nitrification may be lost via coupled denitrification or anammox.**

Nitrogen gene community

Total DNA extracted from the samples was higher in winter than summer at the Cockburn Sound and Southern Flats stations (Figure 4.54) it is likely that this DNA comes from a range of organisms including microbes and MPB.. The abundance of both the ammonia oxidising archaea (AOA) and the ammonia oxidising bacteria (AOB) was higher in winter than summer at all of the stations sampled (Figure 4.54). As a result, AOA and AOB are a higher proportion of the total DNA in winter than summer at all but the Southern Flats station (Figure 4.55). The ratio of AOA to AOB was greater in summer than winter at four of the stations (Figure 4.55). Seasonal variations in the abundance of the nirS gene were only significant at the Marmion Outfall station (higher in winter than summer, see Figure 4.1) and mostly varied in concert with changes in total DNA (Figure 4.55).

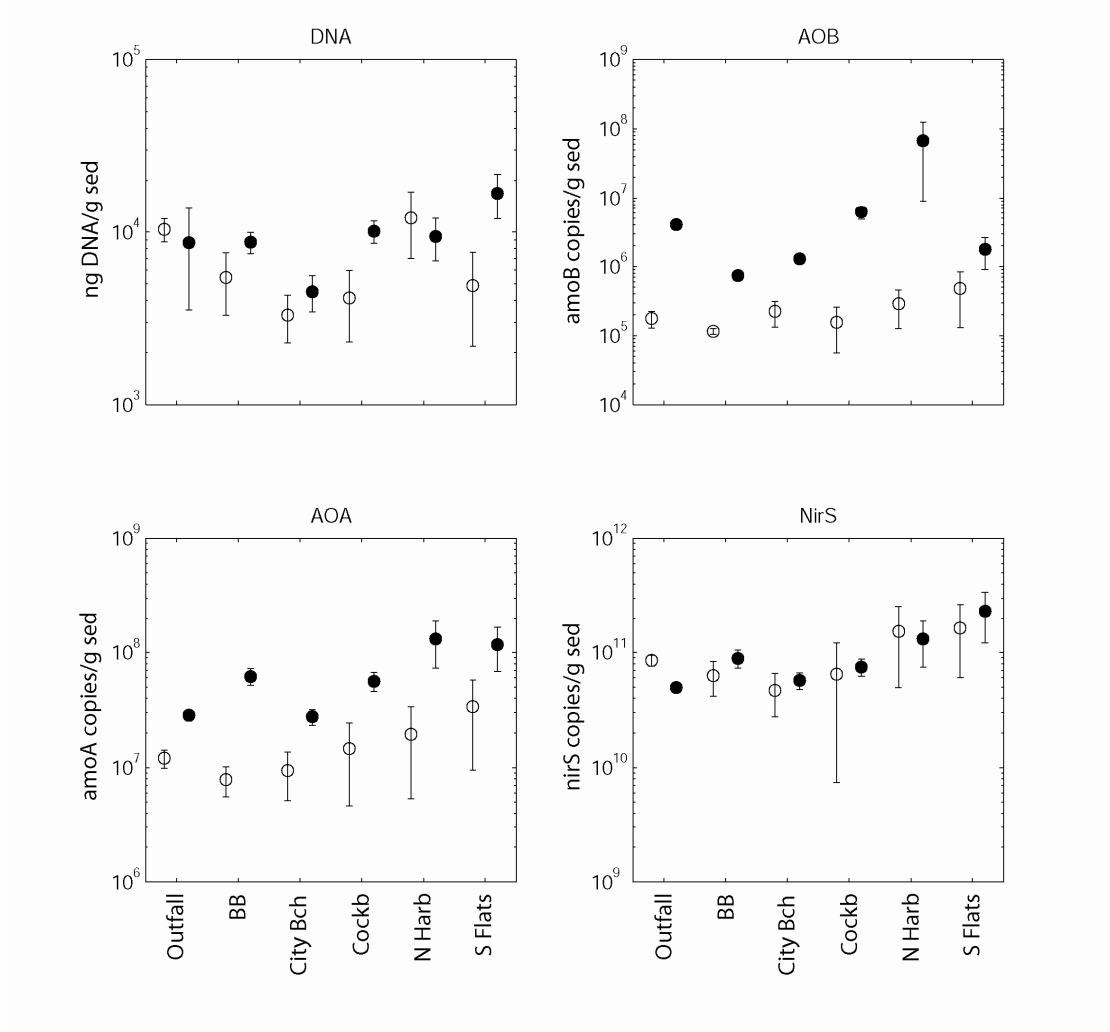

Figure 4.54. The abundance of total DNA, ammonia oxidising bacteria (AOB), ammonia oxidising archaea (AOA) and *nir*S genes from six stations along the disturbance gradient. The solid symbols are samples collected in winter and the open symbols are samples collected in summer.

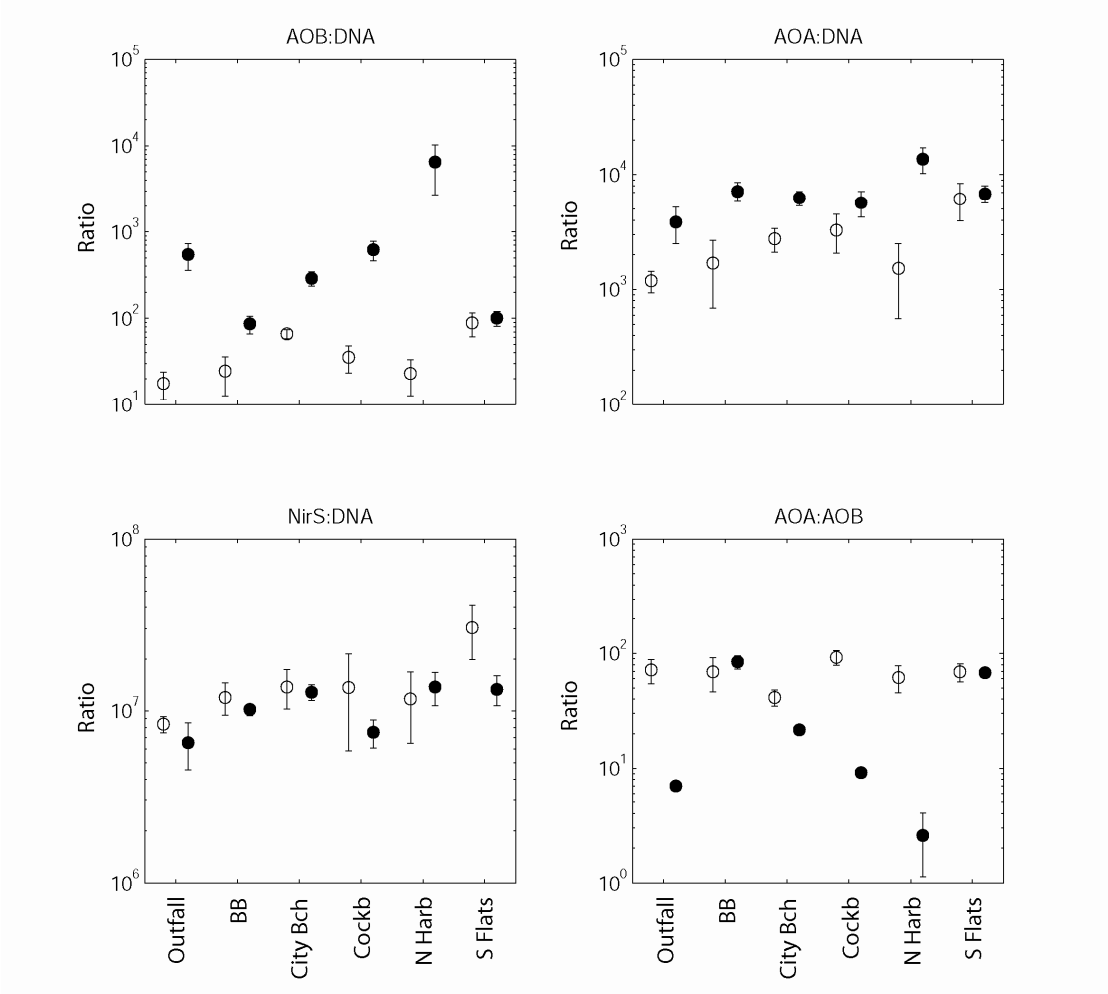

Figure 4.55. Relative abundance of ammonia oxidising bacteria (AOB), ammonia oxidising archaea (AOA) and nirS denitrifier genes to the total DNA. as well as the relative abundance of AOA to AOB genes from six stations along the disturbance gradient. The solid symbols are samples collected in winter and the open symbols are samples collected in summer.

The abundance of AOA and AOB were similar at all the stations in summer (Figure 4.54). In winter, AOA abundance was highest at the Northern Harbour and Southern Flats stations (both in Cockburn sound) while AOB abundance was highest at the Northern Harbour station (Figure 4.54). The ratio of AOB to AOA was similar at all the stations in summer, while in winter AOB was more abundant relative to AOA at the Marmion Outfall, City Beach, Cockburn Sound and Northern Harbour stations (Figure 4.55). Spatial variations in total DNA and the nirS denitrifier gene were small (Figure 4.54).

Both the AOA and AOB phylotypes are present in sediments in both seasons and at all six stations. Both phylotypes no doubt contribute to nitrification in these sediments. Seasonally, both the AOA and AOB distributions are very similar with greater numbers in winter than summer and form a larger percentage of the total DNA in that season. Understanding these seasonal trends in AOA and AOB abundance is difficult because multiple interacting factors influence the distribution. However, similar seasonal variations in suggests that the factors that control the distribution of AOA also control AOB. The higher abundance of nitrifiers in winter compared to summer coincides with decreased efflux of ammonia at the corresponding sites, suggesting that and increase in nitrifier biomass may effect an increase in nitrification rate.

The nirS genes were detected in both seasons and at all stations at high abundance compared to similar studies, suggesting genomic potential for denitrification. These genes were distributed evenly between stations and between seasons. However, the detection of the *nir*S gene here does not necessarily correspond to denitrifying activity as the gene is present in the majority of heterotrophic microorganisms. Previous studies in these (Cockburn Sound) sediments have found very low rates of denitrification (Forehead 2006). Conditions in WA sediments may not sufficiently anoxic to generate high rates of denitrification. In the presence of O_2 the denitrifying bacteria present may effectively function as heterotrophs.

Key Findings:

- **Seasonally, both the AOA and AOB are more numerous in winter than summer and form a larger percentage of the total DNA in that season. The higher abundance of nitrifiers in winter compared to summer coincides with lower efflux of ammonia at the corresponding sites, suggesting that this winter increase in nitrifier biomass may also generate an increase in nitrification rate.**

- **The nirS genes were detected in both seasons and at all stations at high abundance, suggesting genomic potential for denitrification. However, previous studies in these (Cockburn Sound) sediments have found very low rates of denitrification. Conditions in WA sediments may not sufficiently anoxic to generate high rates of denitrification and the denitrifying bacteria may effectively function as aerobic heterotrophs.**

4.4 Summary

The motive for the research contained within this chapter was to develop a conceptual understanding of ecosystem responses to forcing factors (primarily sediment nutrient load) with the ultimate aim of improving our capacity to predict the impacts of sediment nutrient enrichment. The wide range of parameters measured in this study across a gradient of nutrient enrichment together with studies of the biogeochemical processes have provided an insight in the function of these habitats and their response to nutrient enrichment, A number of simple regression models are used to describe these responses and a conceptual model of transition states for soft sediment habitats subject to nutrient enrichment is provided as an aid to monitoring and managing impacts to these habitats.

4.5 References

Abell GCJ, Revill AT, Smith C, Bissett AP, Volkman JK and Robert SR (2010) Archeaal ammonia oxidisers and nirS-typr dentrifiers dominate sediment nitrifying and denitrifying populations in a subtropical macrotidal estuary. The ISME Journal 4: 286-300

Bjornsen PK, Kuparinen J (1991) Growth and herbivory by heterotrophic dinoflagellates in the Southern Ocean, studied by microcosm experiments. Marine Biology 109(3): 397-405

Bjornsen PK, Kuparinen J (1991) Determination of bacterioplankton biomass, net production and growth efficiency in the Southern Ocean. Marine Ecology Progress Series 71(2): 185-194

Black RE, Lukatelich RJ, McComb AJ, Rosher JE (1981) Exchange of water, salt, nutrients and photoplankton between Peel Inlet, Western Australia, and the Indian Ocean. Australian Journal of Marine and Freshwater Research 32(5): 709-720

Cambridge ML, Chiffings AW, Brittan C, Moore L, McComb AJ (1986) The loss of seagrass in Cockburn Sound, Western Australia. II. Possible causes of seagrass decline. Aquatic Botany 24(3): 269-285

Dale NG (1974) Bacteria in intertidal sediments: factors related to their distribution. Limnology and Oceanography 19: 509-518

Deming JW, Reysenbach AL, Macko SA, Smith CR (1997) Evidence for the microbial basis of a chemoautotrophic invertebrate community at a whale fall on the deep seafloor: Bone-colonizing bacteria and invertebrate endosymbionts. Microscopy Research and Technique 37(2): 162-170

Deming JW, Carpenter SD (2008) Factors influencing benthic bacterial abundance, biomass, and activity on the northern continental margin and deep basin of the Gulf of Mexico. Deep-Sea Research II 55: 2597-2606

Diaz RJ, Rosenberg R (2008) Spreading dead zones and consequences for marine ecosystems. Science 321(5891): 926-929.

Dizon RM, Yap HT (1999) Short-term responses of coral reef microphytobenthic communities to inorganic nutrient loading. Limnology and Oceanography 44, 1259-1267.

Edgar GJ (1990) The use of the size structure of benthic macrofaunal communities to estimate faunal biomass and secondary production. J. Exp. Mar. Biol. Ecol., 137: 195-214

Forehead HI (2006) The ecology and biogeochemistry of sandy sediments in the warm temperate coastal waters of Western Australia. PhD Thesis, University of Western Australia, School of Plant Biology

Forehead HI, Thompson PA (2010) Microbial communities of subtidal shallow sandy sediments change with depth and wave disturbance, but nutrient exchanges remain similar. Marine Ecology Progress Series 414: 11–26

Johannes RE (1980) The ecological significance of the submarine discharge of groundwater. Marine Ecology-Progress Series 3(4): 365-373

Gartner A, Lavery P, Smit AJ (2002) Use of δ15N signatures of different functional forms of macroalgae and filter-feeders to reveal temporal and spatial patterns in sewage dispersal. Mar. Ecol. Prog. Ser. 235: 63–73

Herrmann M, Scheibe A, Avrahami S, Kusel K (2011). Ammonium Availability Affects the Ratio of Ammonia-Oxidizing Bacteria to Ammonia-Oxidizing Archaea in Simulated Creek Ecosystems. Applied and Environmental Microbiology 77(5): 1896–1899.

Hillebrand H, Sommer U (1997) Response of epilithic microphytobenthos of the Western Baltic Sea to in situ experiments with nutrient enrichment. Marine Ecology Progress Series 160, 35-46.

Hillebrand H, Worm B, Lotze HK (2000) marine microbenthic community structure regulated by nitrogen loading and grazing pressure. Marine Ecology Progress Series 204, 27-38.

Keesing JK, Graham F, Irvine T, Crossing R (2011) Synchronous aggregated pseudocopulation of the sea star *Archaster angulatus* Muller and Troschel, 1842 (Echinodermata: Asteroidea) and its reproductive cycle in south-western Australia. Marine Biology 158: 1163-1173

Kendall C (1998) Tracing sources and cycling of nitrate in catchments. In: Isotope Tracers in Catchment Hydrology; Kendall, C., McDonnell, J. J., Eds.; Elsevier: Amsterdam

Kendrick GA, Langtry S, Fitzpatrick J, Griffiths R, Jacoby CA (1998). Benthic microalgae and nutrient dynamics in wave-disturbed environments in Marmion Lagoon, Western Australia, compared with less disturbed mesocosms Journal of Experimental Marine Biology and Ecology, 228:83–105

Lawrence JM, Keesing JK, Irvine TR (in press). Population characteristics and biology of two populations of *Archaster angulatus* (Echinodermata: Asteroidea) in different habitats off the central-western Australian coast. Journal of the Marine Biological Association UK Doi:10.1017/s0025315410000871

Leibold MA, Wilber HM (1992). Interactions between food-web structure and nutrients on pond organisms. Nature 360, 341 - 343

Loo MGK, Ophel-Keller K, Cheshire A (2006) Development of novel methodologies for cost effective assessment of the environmental impact of aquaculture. AquaFin CRC, FRDC and SARDI (Aquatic Sciences), Adelaide. 116p. SARDI Publication No. RD03/0036-4

Lourey MJ, Dunn JR, Waring J (2006) A mixed-layer nutrient climatology of Leeuwin Current and Western Australian shelf waters: Seasonal nutrient dynamics and biomass. Journal of Marine Systems 59(1-2): 25-51

Macko SA and Estep MLF (1984) Microbial alteration of stable nitrogen and carbon isotopic compositions of organic matter. Org. Geochem. 6, pp. 787–790.

O'Leary MH (1988) Carbon Isotopes in Photosynthesis. BioScience 38 (5): 328–336. doi:10.2307/1310735.

McMahon K, Walker DI (1998) Fate of seasonal, terrestrial nutrient inputs to a shallow seagrass dominated embayment. Estuarine Coastal and Shelf Science 46(1): 15-25

Parsons TR, Maita Y, Lalli CM (1989) A Manual of Chemical and Biological Methods for Seawater Analysis. Pergamon Press, Toronto

Pearce AF, Rossbach M, Tait M, Brown R (1999) Sea temperature variability off Western Australia 1990 to 1994. Fisheries WA Research Report 111. 45pp

Pearson TH, Rosenberg R (1978) Macrobenthic succession in relation to organic enrichment and pollution of the marine environment. Oceanography and Marine Biology an Annual Review. 16:229-311.

Platt T, Gallegos CL, Harrison WG (1980) Photoinhibition of photosynthesis in natural assemblages of marine phytoplankton. Journal of Marine Research 38(4): 687-701

Schmidt JL, Deming JW, Jumars PA, Keil RG (1998) Constancy of Bacterial Abundance in Surficial Marine Sediments. Limnology and Oceanography 43: 976-983

Sundback K, Snoeijs P (1991) Effects of nutrient enrichment on microalgal community composition in a coastal shallow-water sediment system: an experimental study. Botanica Marina 34, 241-358.

Thompson PA, Waite A (2003) Phytoplankton responses to wastewater discharges at two sites in West Australia. Marine and Freshwater Research 54:721-735

Webb WL, Newton M, Starr D (1974) Carbon Dioxide Exchange of *Alnus rubra*. A Mathematical Model. Oecologia 17(4): 281-291

Contact Us
Phone: 1300 363 400
+61 3 9545 2176
Email: enquiries@csiro.au
Web: www.csiro.au

Your CSIRO

Australia is founding its future on science and innovation. Its national science agency, CSIRO, is a powerhouse of ideas, technologies and skills for building prosperity, growth, health and sustainability. It serves governments, industries, business and communities across the nation.